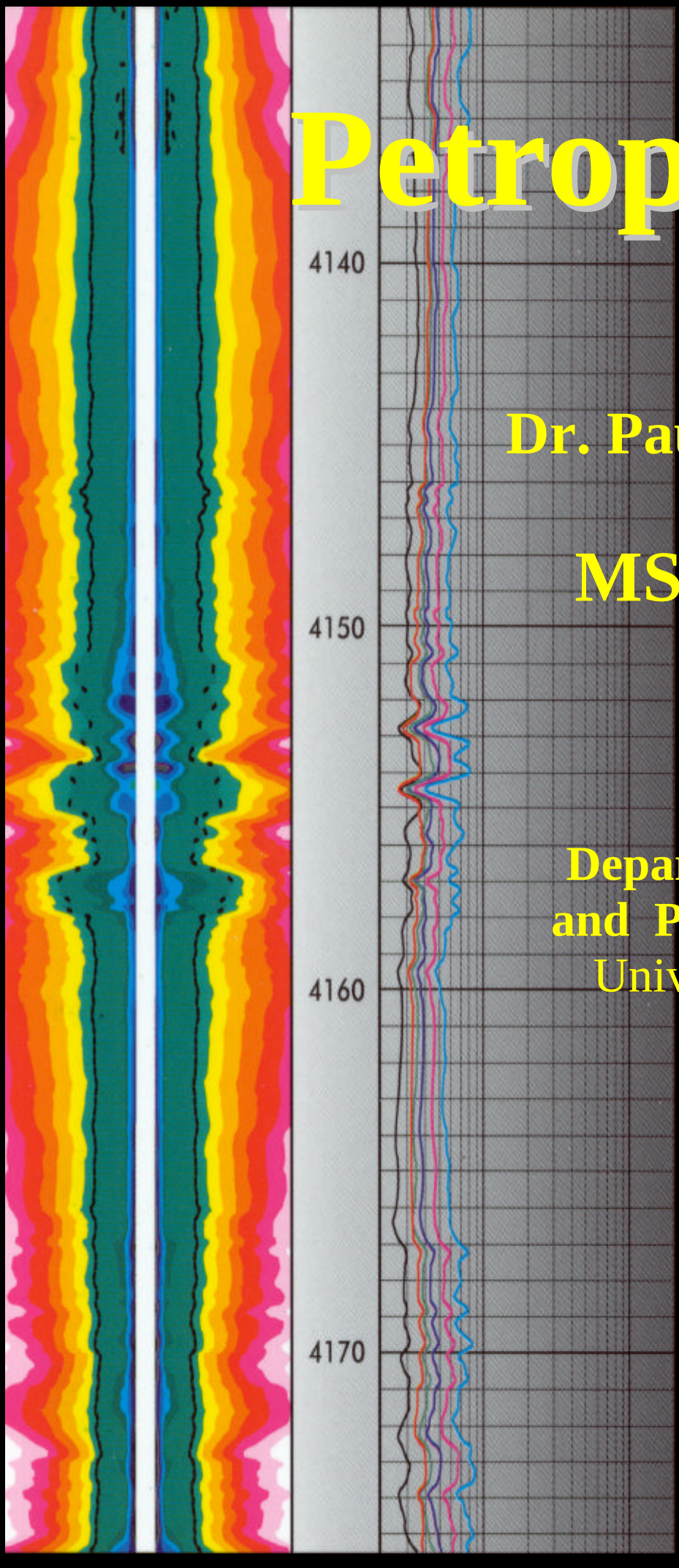

Petrophysics

Dr. Paul W.J. Glover

MSc Petroleum Geology

Department of Geology and Petroleum Geology
University of Aberdeen
UK

Contents

Contents

1. INTRODUCTION TO PETROPHYSICS AND FORMATION EVALUATION

1.1 Introduction

The search or economic accumulations of oil and gas starts with the recognition of likely geological provinces, progresses to seismic surveying, and the drilling of one or more wild-cat wells. If one is lucky, these wells may encounter oil, and if that is the case, measurements made down the hole with wireline tools are used to assess whether sufficient oil is present, and whether it can be produced. Clearly, the evaluation of sub-surface formations requires the combined efforts of geologists, petrophysicists, drilling engineers and even geophysicists. However, it is the geologist and petrophysicist that has the most influence.

The geologist is interested in the lithology, stratigraphy and depositional environment of the sub-surface strata penetrated by the drilling bit. The *exploration geologist* uses wireline tool responses in a number of wells to create a large scale image of the sub-surface geology by correlating wireline responses that are characteristic of a given formation or horizon between formations. This picture is very useful when carrying out initial reservoir modelling and in the decision where to drill new wells. Later the *production geologist* carries out much the same process with much more well information, and adds any extra information that has been gathered to produce a detailed geological model of the reservoir and related sub-surface formations. This model will be the basis of reservoir modelling, and all major reservoir management decisions from primary drainage through to enhanced oil recovery and shut-down.

The *petrophysicist's* job is to use all available information to analyze the physical and chemical properties of the rocks in the sub-surface, and their component minerals, with particular emphasis given to the amount and distribution of those fluid minerals that we know of as water, oil, and gas. The petrophysicist will use extensively wireline log data and data from experiments done on cores extracted from the well, and will occasionally use other sources of information such as engineering and production logs, as well as mud logging data. Initially, it is the aim of the petrophysicist to differentiate between oil, gas and water bearing formations, estimate the porosity of the formations and the approximate amount of hydrocarbons present in each formation. Ultimately, the petrophysicist also uses laboratory data to estimate how easy it will be to extract the hydrocarbons in place, and to design reservoir management strategies to optimize long term oil recovery.

There is a large database of information available to both the geologist and the petrophysicist, and as time passes the amount and variety of information increases. Table 1.1 summarizes a few of the main measurement that a geologist or petrophysicist will have access to, arranged in approximate chronological order. It is the responsibility of the wellsite geologist or engineer to ensure that all this data is properly collected and recorded.

This course is designed to introduce you to wireline logs and the simple analysis of the data that they provide. The following sections cover the theory behind the operation of each tool, how each tool operates, its advantages and limitations, and its main applications. There is a huge number of tools available in the industry, many too many to be covered individually. However, all are variations on a small number of generic tool types, which will be described.

Table 1.1 Main sources of data concerning sub-surface rocks.

Source	**Data Type**
Drilling (Mud logging)	Rate of penetration of drill bit (ROP) Analysis of drill cuttings Analysis of drilling mud Shows of gas, oil or water Gains or losses of drilling mud
Wireline Logs	Mechanical logs (e.g., calipers) Electrical logs (e.g., laterologs, induction logs, SP logs) Natural radiation logs (e.g., simple and spectral gamma ray logs) Acoustic logs (e.g., sonic logs) Pressure and temperature logs Artificial radiation logs (e.g., density and neutron logs) Imaging logs (e.g., dipmeter and various other types) Special logs (e.g., NMR logs)
Cores	Lithology Hydrocarbon shows Heterogeneity and fracturing Porosity Permeability (Klinkenberg, liquid and relative permeability) Wettability and capillary pressure Grain and pore size distributions
Production Logs	Formation testing (e.g., RFT –Repeat Formation Tester) Drill stem tests Production tests Pressure build-up and spinner tests

It should be remembered at all times that the main job of the petrophysicist is to evaluate the amount of hydrocarbons in place in the reservoir. Hence, the evaluation sequence for a straightforward reservoir will be as follows:

For any given well interval:

1. **Distinguish between reservoir and non-reservoir rock**
   (Reservoir rock contains a reasonably high connected porosity.)

2. **For the reservoir intervals only, distinguish between hydrocarbons and water filling the pores, hence calculate water saturation in reservoir rocks**
   (Hydrocarbons are electrical insulators, while water conducts.)

3. **For the hydrocarbon fraction, distinguish between oil and gas, hence calculate gas and oil saturations in reservoir rocks**
   (Gas has a much lower density than oil.)

1.2 Conditions Allowing the Accumulation of Hydrocarbons in a Reservoir

Oil and gas reservoirs have come into being over large periods of time as the result of geological processes. The gasses and oils have been formed from organic remains, have migrated into the reservoir rock, and then have been trapped there by overlying rock formations with very low permeability. Hence, for a hydrocarbon reservoir to exist we need the following to be available at the same location:

1. A *source rock* containing the original organic remains.
2. Pressure and temperature conditions suitable to convert the organic remains into oil and gas.
3. A *porous, permeable reservoir rock* where the hydrocarbon can accumulate.
4. A migration pathway from the source rock to the reservoir rock for the hydrocarbons.
5. A suitable *trap* to keep the hydrocarbons in the reservoir rock until we wish to exploit it.

These processes can take extremely long periods of time. Most formations that contain reservoirs are sedimentary rocks, where the deposition of organically rich material has been followed by clean sandstones that form high porosity well connected pore systems, and are subsequently capped by shales with very low permeabilities. Here the burial of the initial deposition provides the pressures and temperatures to produce hydrocarbons. The hydrocarbons are less dense than water, so migrate upwards into the sandstones, replacing the water that originally occupied the reservoir sandstone, where the hydrocarbons are constrained from rising further by the shale cap. The hydrocarbon then waits until we decide to produce it.

The depositional and post-depositional history of the reservoir rock, and particularly its diagenetic history (compaction, cementation and dissolution), all contribute to the mineralogical composition of the rock, and hence its grain size distribution, porosity, pore size distribution and the connectivity of its pores. Note that in the process of migration the hydrocarbon replaces water in the reservoir rock because it is less dense than water. In practice, the replacement is almost never complete, with some water associated with even the best oil accumulations. The reason for the remaining water is that the grains comprising the reservoir rock are usually *water-wet*, i.e., having a chemical preference to be covered in water rather than hydrocarbon, hence they retain a thin film of water when the hydrocarbon replaces most of the water in the pores. *Oil-wet* rocks do exist, and the ability to distinguish between oil and water wet rocks is extremely important in reservoir management, especially in the final stages of reservoir production. In general, any given reservoir rock the pore space will be occupied by a *water saturation* S_w, a *gas saturation* S_g, and an *oil saturation* S_o.

Since gas is less dense than oil, which is less dense than water, the fluids separate in hydrocarbon reservoirs with the gas occurring just below the trapping lithology, oil a little deeper, and water at the bottom. The fluids are commonly immiscible and so we can define a *gas-oil contact* (GOC) and an *oil-water contact* (OWC). Since, gravity is the force that separates the fluids into these layers, the GOC and OWC are horizontal providing that horizontal and vertical permeability is good in the reservoir and there are no complicating structures or fractures. Note that it is not compulsory to have all three fluids occurring together. Hence in gas reservoirs the oil is missing and there is a *gas-water contact* (GWC). Similarly, oil reservoirs can exist without a *gas cap*.

1.3 Calculating Hydrocarbon Volumes in a Reservoir

We can define a *reservoir rock* as one that has a porosity and permeability that allows it to contain a significant amount of extractable hydrocarbon, AND contains hydrocarbons. A non-reservoir rock may have a porosity that is too low, a permeability that is too low, or a low or zero hydrocarbon saturation. The major control is often the basic lithology. For example, shales often contain hydrocarbon with high saturations, but have porosities and permeabilities that are much too low for the hydrocarbon to be extractable. Shales are considered to be non-reservoir rock. In contrast a high porosity, high permeability sandstone could be a reservoir rock providing that the hydrocarbon saturations are sufficiently high, i.e., above the oil water contact.

The calculation of hydrocarbon volume requires us to know the volume of the formations containing the hydrocarbons, the porosity of each formation, and the hydrocarbon saturation in each formation. In practice each reservoir will be made up of a number of *zones* each with its own thickness, areal extent, porosity and hydrocarbon saturation. For example, reservoir sandstones may alternate with non-reservoir shales, such that each zone is partitioned. Such zonation is mainly controlled by lithology. Hence, it is an early requirement to identify the lithologies in a particular well, identify which formations have the required porosity to enable it to be a reservoir rock, and determine whether the formation contains hydrocarbons. Reservoir rocks containing hydrocarbons are allocated a zone code.

The volume of reservoir rock in a single zone depends upon the area of the zone A, and the thickness of reservoir rock in the zone h. The area is obtained usually from seismic data (from the reservoir geologist), and is the only data used in the calculation of hydrocarbon volumes in place that is not derived from petrophysical techniques. The thickness of reservoir rock is derived from the zonation of the reservoir based upon an initial lithological interpretation and zonation of the reservoir from the wireline logs. The bulk volume of the reservoir $V_{bulk}=A \times h$.

The majority of this volume is occupies by the solid rock matrix, and the remainder is made up of the pore space between the minerals. The relative amount of pore space to the bulk volume is denoted by the porosity f, where the *porosity* is the fraction of the bulk volume occupied by pore volume, and is expressed as a fraction or as a percentage; $f=V_{pore}/V_{bulk}$. However, note that the fractional form is used in ALL calculations. The pore volume in any given zone is therefore $V_{pore}=f \times A \times h$.

In general the porosity is completely occupied by either water and hydrocarbon, where the saturation of the water is S_w, and that of the hydrocarbon is S_h, and $S_w + S_h = 1$. In most reservoirs the hydrocarbon has replaced all the water that it is possible to replace, and under these conditions the water saturation is termed the irreducible water saturation S_{wi}. Now we can write the hydrocarbon saturation as $S_h = (1 - S_w)$. Hence the volume of hydrocarbons in place can be written as

$$V_h = Ahf\ (1-S_w) \qquad \textbf{(1.1)}$$

The determination of this value is the **primary** job of the petrophysicist, and requires a lithological assessment and zonation of the reservoir. At a later stage the petrophysicist may also be called upon to assess the permeability of the reservoir under various conditions. However, the primary function of the petrophysicist is to assess the amount of hydrocarbons initially in place.

All the parameters in Eq. (1.1) except the area are derived from measurements made in the borehole using wireline tools or increasingly using data obtained from tools that measure the rock formations during drilling (measurement/logging while drilling: MWD/LWD).

Figure 1.1 illustrates the derivation of Eq. (1.1) diagrammatically.

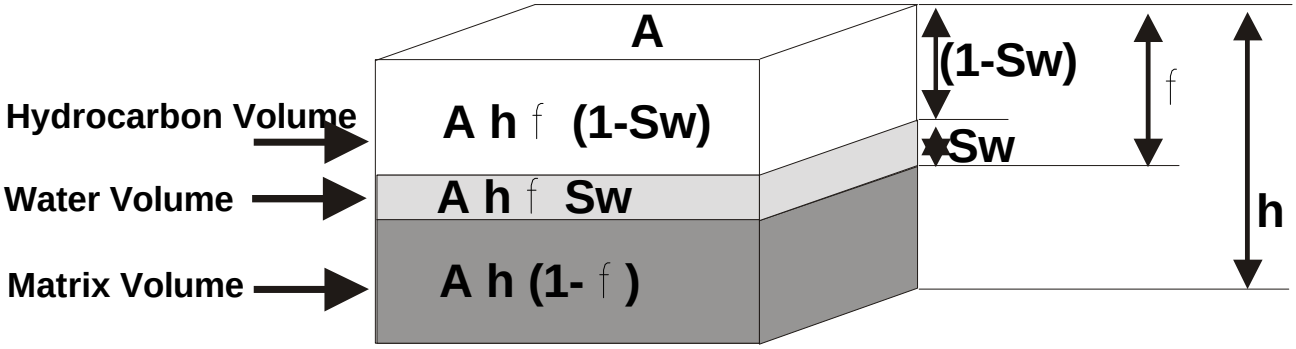

Figure 1. Volume of hydrocarbons in place

Equation (1.1) gives the volume of hydrocarbons in m^3, and the calculated values are often unwieldy. The oil industry uses a range of industry standard units, in which all calculations should be carried out. The volume of oil is measured in barrels, the amount of gas in cubic feet, thickness in feet, and area in acres. Conversions for these are given in Table 1.2 below.

Table 1.2 Common oil-field units.

Unit	**Equivalent in foot-units**	**SI Equivalent**
1 acre	43560 sq.ft	4047 m^2
1 barrel (bbl)	5.6154 cu.ft	159 litres
1 acre foot	43560 cu.ft	1233522 litres = 7758 bbl

Hence, for an oil reservoir zone of *A* acres and *h* feet thickness, the volume of oil in place (OIP) is

$$\text{OIP} = 7758\ Ahf\ (1-S_w) \quad bbl. \tag{1.2}$$

and for a gas reservoir of the same dimensions, the volume of gas in place (GIP) is

$$\text{GIP} = 43560\ Ahf\ (1-S_w) \quad cu.ft. \tag{1.3}$$

Note that sometimes these values are phrased as the amount of oil originally in place (OOIP) and gas initially in place (GOIP).

If the area is not known, the amounts of oil or gas are quoted in bbl/acre or cu.ft/acre respectively, and if the reservoir zone thickness is also not known, the values are given in bbl/acre.foot and cu.ft/acre.ft respectively.

These calculations are done for *reservoir zones*, which are thicknesses of formation of the same lithology, with similar cleanness (i.e., containing little clay), porosity, permeability, and hydrocarbon saturation (i.e., deep resistivity). The zonation of a reservoir is a qualitative exercise that often depends upon the individual petrophysicist. There will often be a minimum thickness for a zone that depends upon the study, however zones are rarely defined less than 5 ft. thick.

The thickness of the reservoir zone used in this calculation is the *net sand*. The *net sand* is the thickness of clean, permeable, hydrocarbon-containing sand in the reservoir zone. The *gross sand* is

the thickness of sand in the reservoir zone irrespective of whether it is clean, its permeability or its fluid saturation. The *net to gross ratio* (thickness of net sand divided by the thickness of gross sand) is often used to represent the quality of a reservoir zone.

Also note that the oil and gas will be at raised temperature and pressure in the reservoir. The compressibility of oil and especially gas, and their coefficients of expansion with temperature means that they will occupy different volumes at surface pressure and temperature conditions, or those present in the stock tank at the surface. For this reason reserves are often quoted corrected for the changes in temperature and pressure at the conditions of the stock tank. If this has been done the stock tank oil and gas originally in place is given as STOOIP and STGOIP.

The expansion or reduction in volume undergone by oil and gas as its temperature and pressure conditions change from that in the reservoir to that in the stock tank depend upon the changes in pressure and temperature and the composition of the oil or gas. The change is expressed by what are called *formation volume factors*. The *oil formation volume factor* B_o is the ratio of the volume of a standard mass of oil at reservoir conditions to that at stock tank conditions, and has no units. Hence, we can calculate now the amount of oil originally in place in the reservoir when measured at the pressure and temperature conditions prevailing in the stock tank (i.e., during production).

$$\text{STOOIP} = \frac{7758\ Ahf\ (1-S_w)}{B_o} \quad bbl. \tag{1.4}$$

Similarly, the *gas formation volume factor* B_g is the ratio of the volume of a standard mass of gas at reservoir conditions to that at stock tank conditions, and also has no units. Hence, we can calculate now the amount of gas originally in place in the reservoir when measured at the pressure and temperature conditions prevailing in the stock tank (i.e., during production).

$$\text{STGOIP} = \frac{43560\ Ahf\ (1-S_w)}{B_g} \quad cu.ft. \tag{1.5}$$

Oil Field Example

Area of zone, A	2000 acres
Thickness, h	150 ft
Porosity, f	15%
Water saturation, S_w	30%
Oil formation volume factor, B_o	1.65 (reservoir bbl per stock tank bbl)

Note that B_o>1, hence the volume of oil is less at the surface than at depth. This is because the effect compressibility of oil with pressure for the range of pressures usually found in reservoirs is less than the effect of thermal expansion of the oil caused by reservoir temperatures. Therefore, when hot, pressurized oil at depth is brought to the cooler, lower pressure stock tank it contracts due to the lowering of temperature more than it expands due to the lowering of pressure.

Using Eq. (1.4) gives

$$\text{STOOIP} = \frac{7758 \times 2000 \times 150 \times 0.15 \times (1-0.3)}{1.65} \quad = \quad 148.10727 \quad \textit{Mbbl}$$

Whereas, the calculation for reservoir OOIP from Eq. (1.2) would have given 244.377 *Mbbl.*

Gas Field Example

Area of zone, A	2000 acres
Thickness, h	150 ft
Porosity, f	15%
Water saturation, S_w	30%
Gas formation volume factor, B_g	0.0035 (reservoir cu.ft per stock tank cu.ft)

Note that B_g<<1, hence the volume of gas is much greater at the surface than at depth. This is because the effect compressibility of gas with pressure for the range of pressures usually found in reservoirs is enormous compared to the effect of thermal expansion of the gas caused by reservoir temperatures. Therefore, when hot, pressurized gas at depth is brought to the cooler, lower pressure stock tank it expands considerably more due to the lowering of pressure more than it contracts due to the lowering of temperature. This is the opposite of the case for oil.

Using Eq. (1.5) gives

$$\text{STGOIP} = \frac{43560 \times 2000 \times 150 \times 0.15 \times (1-0.3)}{0.0035} \quad = \quad 392.04 \quad \textit{billion cu. ft}$$

Whereas, the calculation for GOIP from Eq. (1.3) would have given 1.372 *billion cu.ft.* The huge difference in the volume of the gas at stock tank conditions compared with that at depth indicates the importance of taking full account of the formation volume factor for gas.

It should, however, be noted that gas and oil cannot usually be taken as independent as in the two examples above. In practice, gas is dissolved in oil, and comes out of solution as the oil is brought to the surface. This results in additional shrinkage in the apparent oil volume, and this is taken into account in quoted figures for the oil formation volume factor. The reservoir then also produces gas, and the exsolved gas adds to the volume of the gas produced.

The complex interplay between gas and oil phase behaviours will be covered in formation evaluation course later in the MSc.

1.4 Uncertainties

Note that errors in any of the measurements leads to errors in the final value, and that the porosity and water saturation are in some ways inter-dependent, which can lead to larger error than might otherwise be expected.

The error in the area of a reservoir zone is usually quite small because seismic surveys can delineate the extent of reservoirs with great accuracy now. A greater error can be introduced from petrophysical measurements. These values are derived from a small number of wells that intersect the reservoir. There arises, therefore, the possibility that the well information is nit representative of the reservoir as a whole. Clearly, the greater the number of wells, the smaller the possible errors from this source. However, early in the development of a field, when the result of reservoir management decisions can have a large impact upon the reserves and life of a field, the amount of petrophysical data is small, and the resulting errors can be quite large. It is therefore, always important to realize the impact that uncertainty in the knowledge of the petrophysical parameters can have in the final value of STOOIP.

Table 1.3 shows the impact that a 10% variation in the petrophysical parameters can have in the calculation of STOOIP.

Table 1.3 Propagation of errors in calculations of STOOIP.

Parameter	**Base Case**	**Possibility 1**	**Possibility 2**
Area, acres	2000	2000	2000
Thickness, ft	150	135	165
Porosity, %	15	13.5	16.5
Water saturation, %	30	33	27
Oil formation volume factor	1.65	1.815	1.485
STOOIP, Mbbl	**148**	**104**	**208**
Percentage relative difference, %	**0**	**-30**	**40**

These errors can be analyzed statistically to give a probability curve from which the most likely value of STOOIP can be judged. As more and better quality data become available, we can reduce the possible error on the STOOIP analysis, generating probability curves with less variation. Figure 1.2 shows an example of probability curves for an initial appraisal, followed by two other curves made 8 and 15 years later. Note that there has been great improvement in the first 8 years, when appraisal drilling added much more data to the data base, followed by less improvement in the subsequent 7 years, when appraisal drilling was reduced significantly, and hence there was less new data added to the database. As with all things, there is an economic balance between added value generated from new data and the cost of obtaining the new data.

Figure 1.2 is read by taking the ordinate (y-axis) and reading across. For example in 1972 there was 100% probability that the reservoir contained greater than 80 Mbbl, and 75% probability that it contained more than 250 Mbbl. By 1980 there was 100% probability of the reservoir containing greater than 220 Mbbl and 75% probability of it containing greater than 310 Mbbl of oil. Thus, as time progresses the range of possible STOOIP decreases from a possible range of 80 Mbbl<STOOIP<600 Mbbl in 1972 to 260 Mbbl <STOOIP<470 Mbbl in 1987.

The data represented by Fig. 1.2 is shown in the Table 1.3 below.

Table 1.3 Probability vs. STOOIP data for Fig. 1.2

Probability (%)	**STOOIP Greater Than (Mbbl)**		
	1972	**1980**	**1987**
100	80	220	260
75	250	310	320
50	350	360	360
25	450	420	400
0	600	500	470

Most critical financial and reservoir management decisions usually have to be made early in the life of a field when data is at a premium and errors in the estimated STOOIP are greatest. This is particularly true of offshore fields, where the cost of top-side production structures is a significant factor in the economic viability of the field. For example, globally, the Norway and UK sectors of the North Sea are the two most expensive oil provinces to produce from due to their deep off-shore nature combined with inhospitable conditions. In these cases it is critical to obtain as much high quality data as possible from the first few appraisal wells in each prospective reservoir.

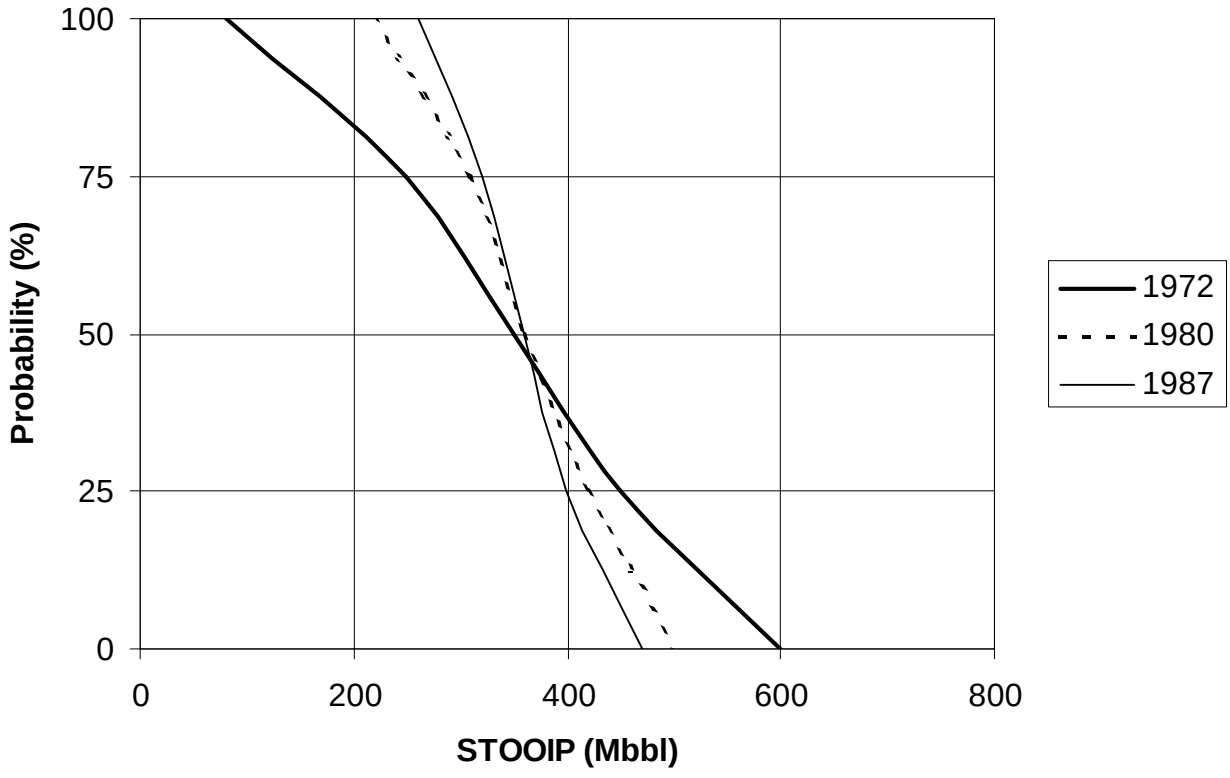

Figure 1.2 STOOIP Probability Curve

Since it is clear that the main interests of petrophysicists are porosity and permeability, the following few chapters (Chapters 2 and 3) will deal with these parameters. Fluid saturations are also critical, and these depend upon capillary pressure, which is described in Chapter 4.

2. POROSITY

2.1 Theory

The *porosity* of a rock is the fraction of the volume of space between the solid particles of the rock to the total rock volume. The space includes all pores, cracks, vugs, inter- and intra-crystalline spaces. The porosity is conventionally given the symbol f, and is expressed either as a fraction varying between 0 and 1, or a percentage varying between 0% and 100%. Sometimes porosity is expressed in 'porosity units', which are the same as percent (i.e., 100 porosity units (pu) = 100%).

However, the fractional form is **ALWAYS** used in calculations.

Porosity is calculated using the relationship

$$f = \frac{V_{pore}}{V_{bulk}} = \frac{V_{bulk} - V_{matrix}}{V_{bulk}} = \frac{V_{bulk} - \left(W_{dry} / r_{matrix}\right)}{V_{bulk}}, \qquad \textbf{(2.1)}$$

where: V_{pore} = pore volume
V_{bulk} = bulk rock volume
V_{matrix} = volume of solid particles composing the rock matrix
W_{dry} = total dry weight of the rock
r_{matrix} = mean density of the matrix minerals.

It should be noted that the porosity does not give any information concerning pore sizes, their distribution, and their degree of connectivity. Thus, rocks of the same porosity can have widely different physical properties. An example of this might be a carbonate rock and a sandstone. Each could have a porosity of 0.2, but carbonate pores are often very unconnected resulting in its permeability being much lower than that of the sandstone. A range of differently defined porosities are recognized and used within the hydrocarbon industry. For rocks these are:

(i)	Total porosity	Defined above.
(ii)	Connected porosity	The ratio of the connected pore volume to the total volume.
(iii)	Effective porosity	The same as the connected porosity.
(iv)	Primary porosity	The porosity of the rock resulting from its original deposition.
(v)	Secondary porosity	The porosity resulting from diagenesis.
(vi)	Microporosity	The porosity resident in small pores (< 2 μm) commonly associated with detrital and authigenic clays.
(vii)	Intergranular porosity	The porosity due to pore volume between the rock grains.
(viii)	Intragranular porosity	The porosity due to voids within the rock grains.
(ix)	Dissolution porosity	The porosity resulting from dissolution of rock grains.
(x)	Fracture porosity	The porosity resulting from fractures in the rock at all scales.
(xi)	Intercrystal porosity	Microporosity existing along intercrystalline boundaries usually in carbonate rocks.
(xii)	Moldic porosity	A type of dissolution porosity in carbonate rocks resulting in molds of original grains or fossil remains.
(xiii)	Fenestral porosity	A holey ('bird's-eye') porosity in carbonate rocks usually associated with algal mats.
(xiv)	Vug porosity	Porosity associated with vugs, commonly in carbonate rocks.

2.2 Controls on Porosity

The initial (pre-diagenesis) porosity is affected by three major microstructural parameters. These are grain size, grain packing, particle shape, and the distribution of grain sizes. However, the initial porosity is rarely that found in real rocks, as these have subsequently been affected by secondary controls on porosity such as compaction and geochemical diagenetic processes. This section briefly reviews these controls.

2.2.1 Grain Packing

The theoretical porosities for various grain packing arrangements can be calculated. The theoretical *maximum* porosity for a cubic packed rock made of spherical grains of a uniform size is 0.4764, and is independent of grain size. The maximum porosity of other packing arrangements is shown in Table 2.1 and Figure 2.1.

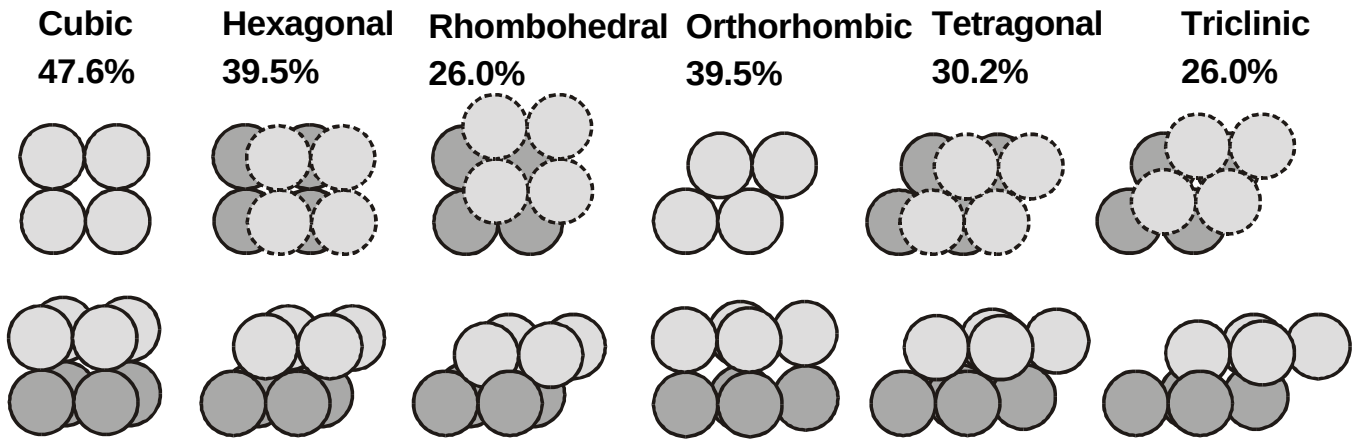

Figure 2.1 Ordered packing arrangements.

Table 2.1 Maximum porosity for different packing arrangements

Packing	**Maximum Porosity (fractional)**
Random	≥0.399 (dependent on grain size)
Cubic	0.476
Hexagonal	0.395
Orthorhombic	0.395
Rhombohedral	0.260
Tetragonal	0.302
Triclinic	0.260

The calculations of these ideal porosities is relatively simple. For example, taking the cubic arrangement of identical spheres of radius *r* occupying a cubic unit cell of length *L*, as shown in Fig. 2.2, the following calculation is possible.

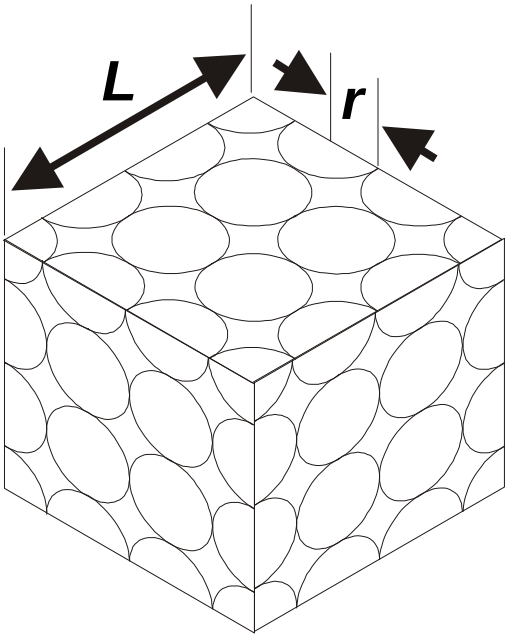

Figure 2.2 Cubic packing of identical spheres.

The bulk volume of the cell $V_{bulk} = L^3$, and the number of spheres in the cell $n = (L/2r)^3$. Hence the volume of the matrix $V_{matrix} = (4\ np\ r^3)/3 = (L/2r)^3\ (4p\ r^3)/3 = (p\ L^3)/6$. The porosity can now be calculated from Eq. (2.1) as

$$f = \frac{L^3 - (p\ L^3/6)}{L^3} = (1 - p\ /6) = 0.4764 \qquad \textbf{(2.2)}$$

which is independent of the sphere size. Most of the other values in Table 2.1 can be calculated similarly, although with a little more difficulty as a result of their different packing geometries. There are 6 different ways that identical spheres can be packed, and these are shown in Fig. 2.1.

2.2.2 Grain Size

It was noted above that the ordered cubic packing of identical sphere leads to a porosity that is grain size independent. This is also true for the other ordered packing lattices, but not true for the random arrangement of spheres. In real depositional environments, ordered packings are not formed because they are energetically unstable, and the grains become randomly distributed.

The equilibrium porosity of a porous material composed of a random packing of spherical grains is dependent upon the stability given to the rock by frictional and cohesive forces operating between individual grains. These forces are proportional to the exposed surface area of the grains. The specific surface area (exposed grain surface area per unit solid volume) is inversely proportional to grain size. This indicates that, when all other factors are equal, a given weight of coarse grains will be stabilized

at a lower porosity than the same weight of finer grains. For a sedimentary rock composed of a given single grain size this general rule is borne out in Figure 2.3. It can be seen that the increase in porosity only becomes significant at grain sizes lower than 100 μm, and for some recent sediments porosities up to 0.8 have been measured. As grain size increases past 100 μm, the frictional forces decrease and the porosity decreases until a limit is reached that represents random frictionless packing, which occurs at 0.399 porosity, and is independent of grain size. No further loss of porosity is possible for randomly packed spheres, unless the grains undergo irreversible deformation due to dissolution-recrystallisation, fracture, or plastic flow, and all such decreases in porosity are termed *compaction*.

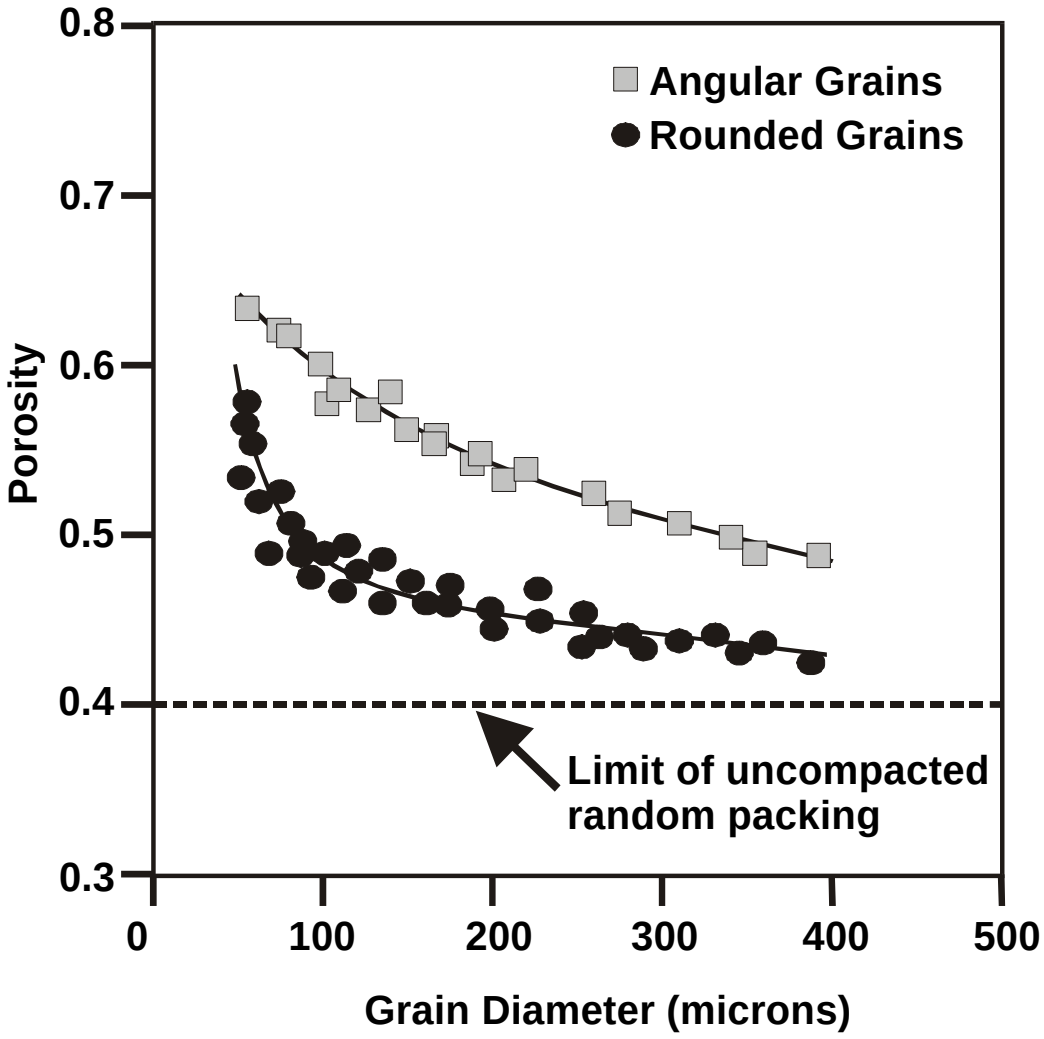

Figure 2.3 Relation between porosity, grain size and grain shape

Rarely, in borehole petrophysics do we need to look at accurate grain size determinations as many of the tools that we use have minimum vertical resolutions of the order of tens of centimetres. However, as well logs are correlated to core logging it is well to bear in mind the agreed semi-quantitative classifications for grain size in siliclastic and carbonate rocks (Tables 2.2 and 2.3).

Table 2.2 Siliclastic grain size definitions

Category	Median Grain Size (mm)
Gravel	2000
Very Coarse	1000
Coarse	500
Medium	250
Fine	125
Very Fine	62
Silt	

Table 2.3 Carbonate grain size definitions

Category	Median Grain Size (mm)
L	400
M	200
F	100
VF	50
EF	
Symbol	**Pore Size (mm)**
B	<100
C	100-200
D	>200
Matrix Code	Texture
I	Compact
II	Chalky
III	Sucrose

2.2.3 Grain Shape

This parameter is not widely understood. Several studies have been carried out on random packings of non-spherical grains, and in all cases the resulting porosities are larger than those for spheres. Table 2.4 shows data for various shapes, where the porosity is for the frictionless limit. Figure 2.3 shows data comparing rounded and angular grains, again showing that the porosity for more angular grains is larger than those that are sub-spherical.

Table 2.4 The effect of grain shape on porosity

Grain Shape	Maximum Porosity (fractional)
Sphere	≥0.399 (dependent on grain size)
Cube	0.425
Cylinder	0.429
Disk	0.453

2.2.4 Grain Size Distribution

Real rocks contain a distribution of grain sizes, and often the grain size distribution is multi-modal. The best way of understanding the effect is to consider the variable admixture of grains of two sizes (Figure 2.4). The porosity of the mixture of grain sizes is reduced below that for 100% of each size. There are two mechanisms at work here. First imagine a rock with two grain sizes, one of which has 1/100th the diameter of the other. The first mechanism applies when there are sufficient of the larger grains to make up the broad skeleton of the rock matrix. Here, the addition of the smaller particles reduces the porosity of the rock because they can fit into the interstices between the larger particles. The second mechanism is valid when the broad skeleton of the rock matrix is composed of the smaller grains. There small grains will have a pore space between them. Clearly, if some volume of these

grains are removed and replaced with a single solid larger grain, the porosity will be reduced because both the small grains and their associated porosity have been replaced with solid material. The solid lines GR and RF or RM in Figure 2.4 represent the theoretical curves for both processes. Note that as the disparity between the grain sizes increases from 6:3 to 50:5 the actual porosity approaches the theoretical lines. Note also that the position of the minimum porosity is not sensitive to the grain diameter ratio. This minimum occurs at approximately 20 to 30% of the smaller particle diameter. In real rocks we have a continuous spectrum of grain sizes, and these can give rise to a complex scenario, where fractal concepts become useful.

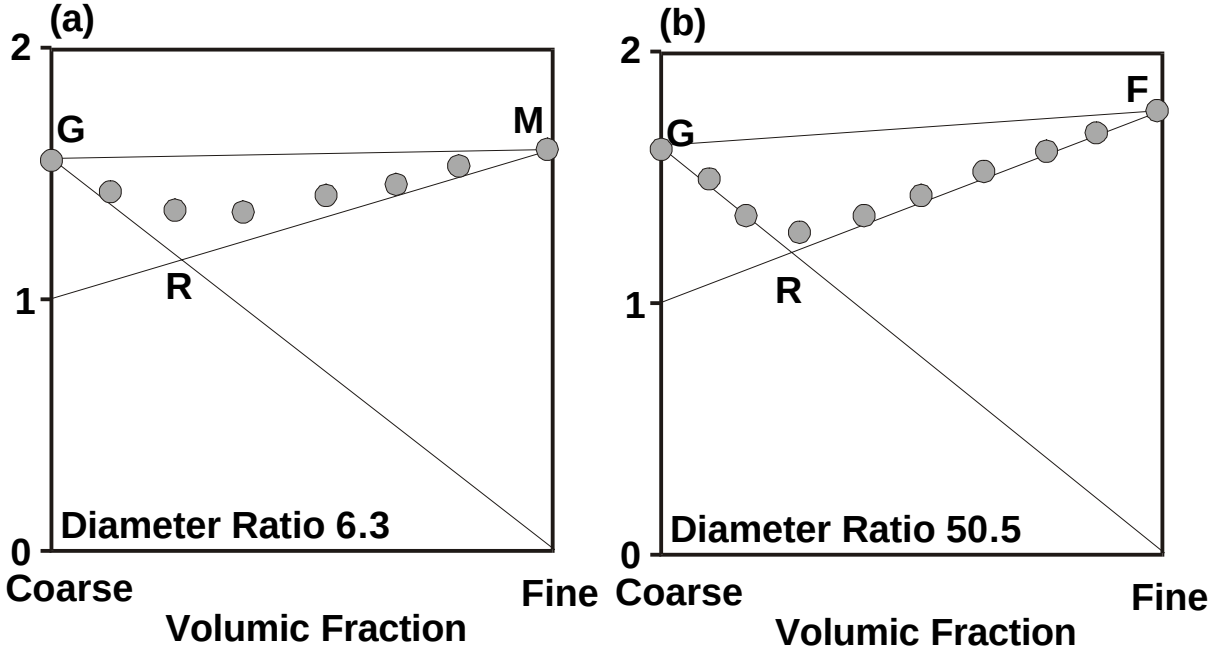

Figure 2.4 Apparent volume for assemblages of spheres of different diameter ratios.

In practice such detail is rarely entered into. Grain size distributions can be inferred from mercury porisimetry measurements that will be studied later in the MSc course, or by direct sieving of a disaggregated sample. In the sieving technique, the dried, weighed and disaggregated sample is placed in the topmost of a stack of sieves with decreasing mesh size *D*. A motor vibrates the stack such that given particle sizes remain in each of the sieves. The cumulative percentage weight of these remains are plotted against the mesh size of the sieves *D*, resulting in a distribution curve similar to that in Fig. 2.5. The degree of sorting (grain size distribution) is expressed by the *Trask Coefficient* s_o, which is expressed as

$$s_o = \sqrt{\frac{D_{25}}{D_{75}}}, \qquad \textbf{(2.3)}$$

where: D_{25} = mesh size (grain diameter) at 25% of sample weight (larger grain fraction).
D_{75} = mesh size (grain diameter) at 75% of sample weight (all but smallest grain fraction).

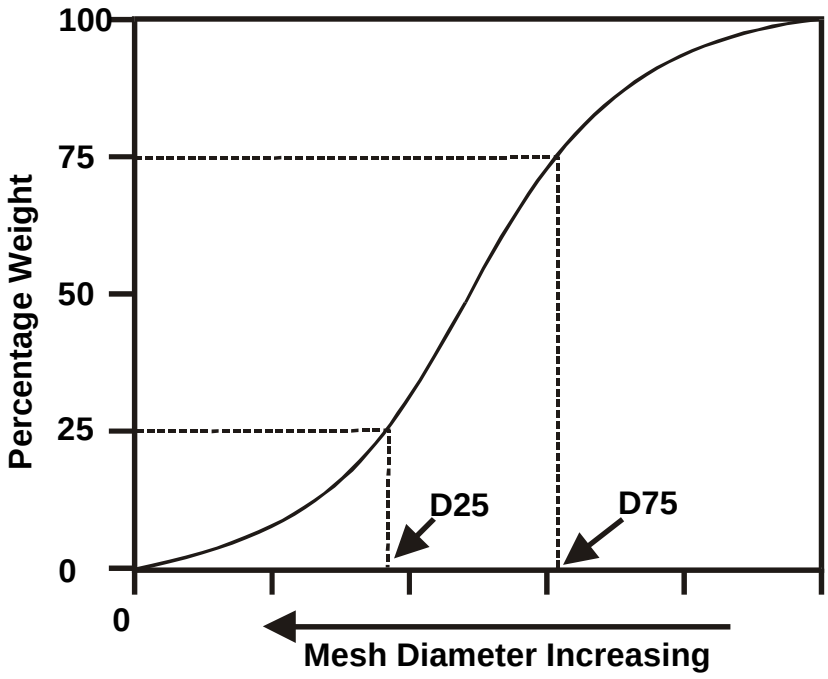

Figure 2.5 Cumulative grain size distributions by sieved weight.

In general the porosity of a sandstone decreases as the degree of sorting decreases, where the degree of sorting is expressed as a Trask coefficient or classified according to Table 2.5.

Table 2.5 The Trask sorting classification

Sorting Classification	Trask Coefficient
Extremely well	1.00
Very well	1.10
Well	1.20
Moderately	1.40
Poorly	2.00
Very poorly	2.70
	5.70

2.2.5 Secondary Controls on Porosity

Porosity is also controlled by a huge range of secondary processes that result in compaction and dilatation. These can be categorized into (i) mechanical processes, such as stress compaction, plastic deformation, brittle deformation, fracture evolution etc., and (ii) geochemical processes, such as dissolution, repreciptation, volume reductions concomitant upon mineralogical changes etc. The description of these process will be examined in the sedimentary techniques courses.

2.2.6 The Range of Porosity Values in Nature

In recently deposited, unconsolidated sediments, such as those that you might find on the floor of a lake, porosity may be very high (values up to 80% have been recorded). However, more common materials, such as loose sands, can have porosities as high as 45% that are either extremely unstable or stabilized by cements. High porosities can also occur when the porosity is due to dissolution (secondary porosity), particularly in carbonates. In the case of carbonates the total porosity may be very high, but their permeability can be very low as the pores and vugs that make up the pore structure are unconnected. Similarly, porosities can be very low. In massive fractured carbonates it can commonly be as low as 1%, and igneous and metamorphic rocks almost always have porosities less that 1%. Sandstones, generally, lie in the range 5% to 20%. Table 2.6 gives approximate ranges of porosities for some common lithologies.

Table 2.6 The range of porosity values for rocks.

Lithology	Porosity Range (%)
Unconsolidated sands	35-45
'Reservoir' Sandstones	15-35
Compact Sandstones	5-15
Shales	0-45
Clays	0-45
Massive Limestones	5-10
Vuggy Limestones	10-40
Dolomite	10-30
Chalk	5-40
Granite	<1
Basalt	<0.5
Gneiss	<2
Conglomerate	1-15

2.3 Porosity Determination

The best way of determining porosity is to carry out experiments on core extracted from the well. These techniques will be examined in detail in the Formation Evaluation course later in the MSc. However, the basic techniques will be described here. It should be noted that core determined porosities have a much higher degree of accuracy than porosities determined from down-hole tools, but suffer from sampling problems. Taken together core and borehole determined porosities optimize accuracy and high resolution sampling.

There are at least 4 common methods of measuring the porosity of a core. These are:

- **Buoyancy**
- **Helium porisimetry**
- **Fluid saturation**
- **Mercury porosimetry**

The first three will be described here, and the last will be described in Chapter 4.

2.3.1 Saturation Method

This method only measures the effective (connected) porosity of the rock as it depends on the saturation of the rock with a fluid.

- Clean and dry the rock.
- Weigh the rock in its dry state to give the dry weight, W_{dry}.
- Fully saturate the rock in a wetting fluid. Conventionally toluene or dichloroethene were used, but now it is more common to saturate the rock with a brine that has been made to mimic that in the reservoir, i.e., contain the same concentrations of major dissolved salts (a *synthetic brine*).
- Weigh the saturated sample after drying any excess fluid from its surface to give its saturated weight, W_{sat}.
- Determine the bulk volume of the rock, V_{bulk}. This can be done using measuring calipers and assuming the core to be cylindrical, but is prone to large errors even if the core is almost cylindrical. Another method is to immerse the sample in mercury, which is a non-wetting fluid and will not enter the pores of a rock at atmospheric pressure, and measure the volume of the mercury displaced. This method used to be common, but the sample can then no longer be used for experiments and must be safely disposed of. Archimedes method is preferred, which will be described in the Formation Evaluation course.
- Determine the density r_{fluid} of the saturating fluid by weighing a known volume of it.

The porosity is then

$$f = \frac{V_{bulk} - V_{matrix}}{V_{bulk}} = \frac{(W_{sat} - W_{dry}) / r_{fluid}}{V_{bulk}} \quad \textbf{(2.4)}$$

Note that the mean grain density of the sample can also be calculated from this data using the relationship

$$r_{ma} = \frac{W_{dry}}{V_{matrix}} = \frac{W_{dry}}{V_{bulk} - \left((W_{sat} - W_{dry}) / r_{fluid}\right)} \quad \textbf{(2.5)}$$

2.3.2 Buoyancy Method

This method is somewhat similar to the saturation method, and also measures the effective (connected) porosity.

- Clean and dry the rock.
- Weigh the rock in its dry state to give the dry weight, W_{dry}.
- Fully saturate the rock in a wetting fluid as before.
- Weigh the saturated sample suspended in a bath of the same fluid with which it was saturated to give its suspended weight, W_{sus}. This is shown in Fig. 2.6. Note that a cradle is needed to suspend the sample in the fluid, and this has a weight W_{cradle} when in the fluid. So the actual measured weight when the sample and cradle are suspended in the fluid is (W_{sus} + W_{cradle}). The effect of the cradle must be taken away, hence the weight of the cradle when suspended in the fluid (up to the same level), W_{cradle}, must be taken account of in the final calculation
- Determine the bulk volume of the rock, V_{bulk} as before.

- Determine the density r_{fluid} of the saturating fluid by weighing a known volume of it.

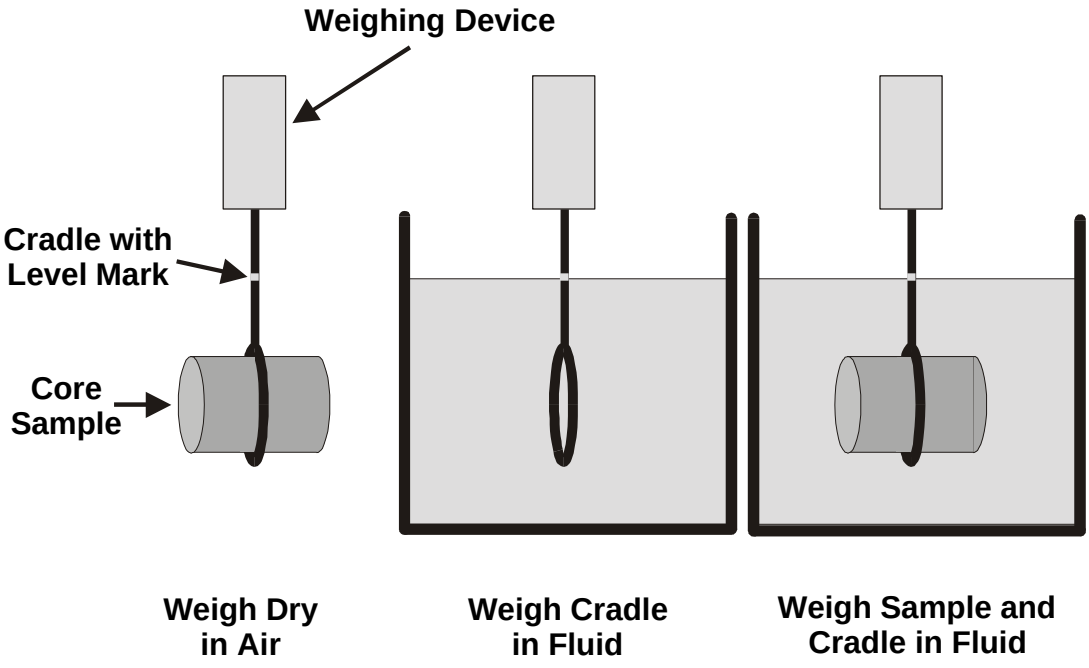

Figure 2.6 The buoyancy method for porosity determination.

The porosity is given by the relationship

$$f = \frac{V_{bulk} - V_{matrix}}{V_{bulk}} = \frac{V_{bulk} - (W_{dry} - (W_{sus} + W_{cradle}) + W_{cradle}) / r_{fluid}}{V_{bulk}} \quad \textbf{(2.6)}$$

Again, the mean grain density can also be calculated as

$$r_{ma} = \frac{W_{dry}}{V_{matrix}} = \frac{W_{dry}}{(W_{dry} - (W_{sus} + W_{cradle}) + W_{cradle}) / r_{fluid}} \quad \textbf{(2.7)}$$

2.3.3 Helium Porisimetry

This method relies on the expansion of helium gas, and also measures the effective porosity of the rock. However, since helium is a slippery little molecule, it can penetrate pores which are much smaller than those that the fluid used in the two previous methods can. Hence, this method provides slightly higher porosity measurements on any given rock sample.

This method uses the apparatus shown in Fig. 2.7, together with the following procedure.

- Clean and dry the core sample.
- Obtain the bulk volume of the sample as in the previous methods.

- Ensure Valve 2 is closed.
- Gas is introduced into Chamber A of the apparatus using Valve 1 until a pressure P_i is reached, when Valve 1 is closed. This pressure is arbitrary, and commonly about 100 psi.
- Insert the sample into Chamber B, which is at atmospheric pressure, P_{atm}, and ensure Valve 3 is closed.
- Slowly open Valve 2 to let the gas equilibrate through the entirety of both chambers. The gas will penetrate into the pores of the rock sample. During this process the pressure will decrease to a new stable level, P_f.

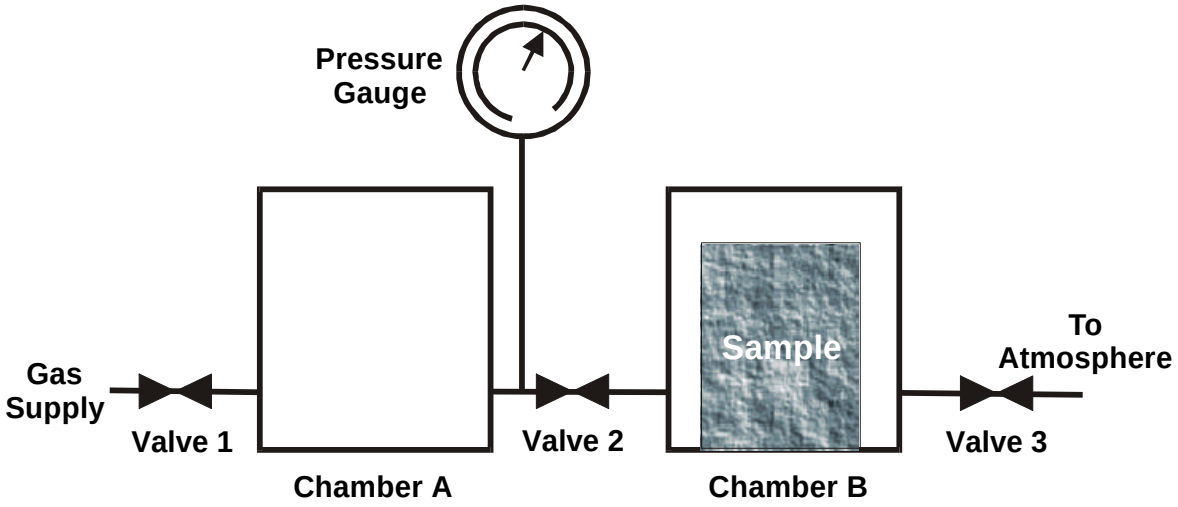

Figure 2.7 Helium expansion porisimeter.

The drop of pressure depends upon how much space there is in Chamber B, and that depends on how much of Chamber B is occupied by solid rock particles. The measured gas pressures P_i, P_{atm} and P_f alone are not sufficient to obtain the volume of the sample rock matrix. However, we can calibrate the system by putting a range of metal cylinders of accurately known volume into Chamber B and repeating the experiment. When this is done, the calibration constant, and the pressures allow the volume of the rock matrix V_{matrix} to be obtained. The porosity is then calculated using

$$f = \frac{V_{bulk} - V_{matrix}}{V_{bulk}} \quad . \tag{2.8}$$

3. PERMEABILITY

3.1 Theory

The *permeability* of a rock is a measure of the ease with which the rock will permit the passage of fluids.

The fundamental physical law which governs this is called the Navier-Stokes equation, and it is very complex. For the purposes of flow in rocks we can usually assume that the flow is laminar, and this assumption allows great simplification in the equations.

It should also be noted that the permeability to a single fluid is different to the permeability where more than one fluid phase is flowing. When there are two or more immiscible fluid phases flowing we use relative permeability, which will be introduced in this section, but covered in much more detail on the Formation Evaluation course later in the MSc.

The fluid flow through a cylindrical tube is expressed by Poiseuille's equation, which is a simplification of Navier-Stokes equation for the particular geometry, laminar flow, and uncompressible fluids. This equation can be written as

$$Q = \frac{p\ r^4\ (P_i - P_o)}{8\ m\ L} \qquad \textbf{(3.1)}$$

where: Q = the flow rate (cm^3/s or m^3/s)
r = the radius of the tube (cm or m)
P_o = the outlet fluid pressure ($dynes/cm^2$ or Pa)
P_i = the inlet fluid pressure ($dynes/cm^2$ or Pa)
m = the dynamic viscosity of the fluid (poise or Pa.s)
L = the length of the tube (cm or m)

About 150 years ago Darcy carried out simple experiments on packs of sand, and hence developed an empirical formula that remains the main permeability formula in use in the oil industry today. Darcy used the apparatus shown in Fig. 3.1, where he used a vertical sand pack through which water flowed under the influence of gravity while measuring the fluid pressures at the top and bottom of the pack by the heights of manometers. Here the difference in fluid pressures can be calculated from $h_1–h_2$ providing the density of the fluid is known. It has since been validated for most rock types and certain common fluids. Darcy's formula can be expressed as

$$Q = \frac{k\ A\ (P_i - P_o)}{m\ L} \qquad \textbf{(3.2)}$$

where: Q = the flow rate (cm^3/s or m^3/s)
P_o = the outlet fluid pressure ($dynes/cm^2$ or Pa)
P_i = the inlet fluid pressure ($dynes/cm^2$ or Pa)
m = the dynamic viscosity of the fluid (poise or Pa.s)
L = the length of the tube (cm or m)
k = the permeability of the sample (darcy or m^2)
A = the area of the sample (cm^2 or m^2)

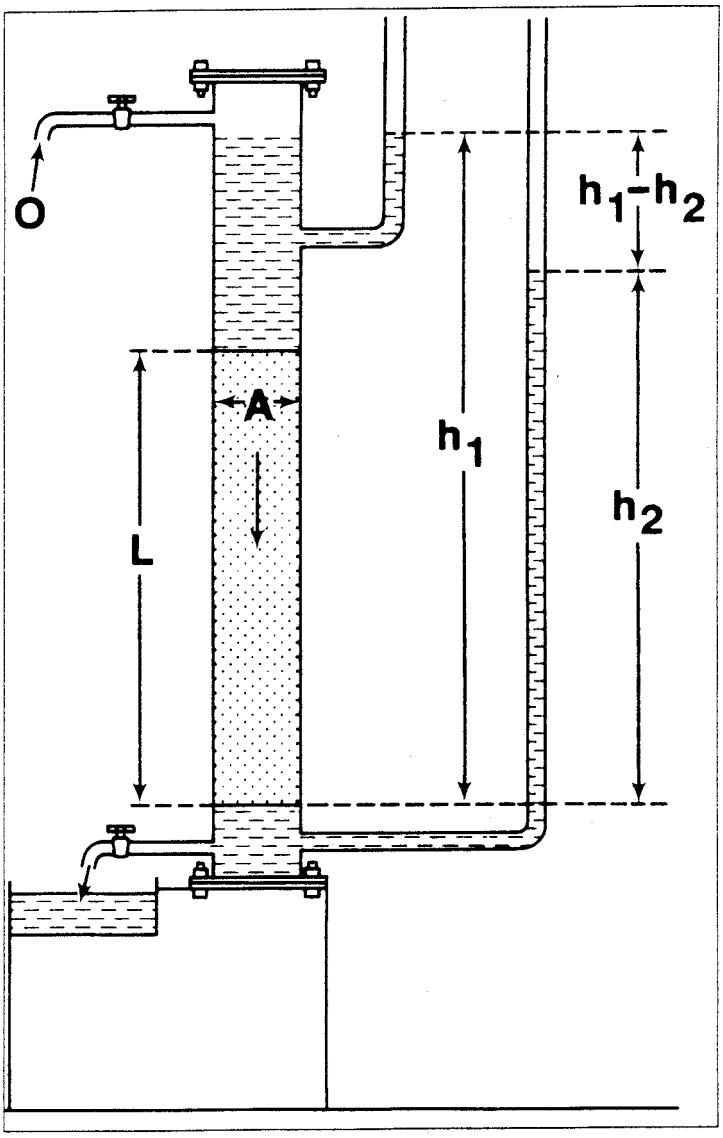

Figure 3.1 The Darcy apparatus (after Hubert, 1953).

Note, either the first set of quoted units can be used (c.g.s system) as in the oil industry, or the second set (S.I. units) as in academic research, but one must use the units consistently.

The units of permeability are the darcy, D, and m^2, where 1 D = 0.9869×10^{-12} m^2. One darcy is the permeability of a sample 1 cm long with a cross-sectional area of 1 cm^2, when a pressure difference of 1 dyne/cm^2 between the ends of the sample causes a fluid with a dynamic viscosity of 1 poise to flow at a rate of 1 cm^3/s (Fig. 3.2). In geological applications the darcy is commonly too large for practical purposes, so the millidarcy (mD) is used, where 1000 mD = 1D.

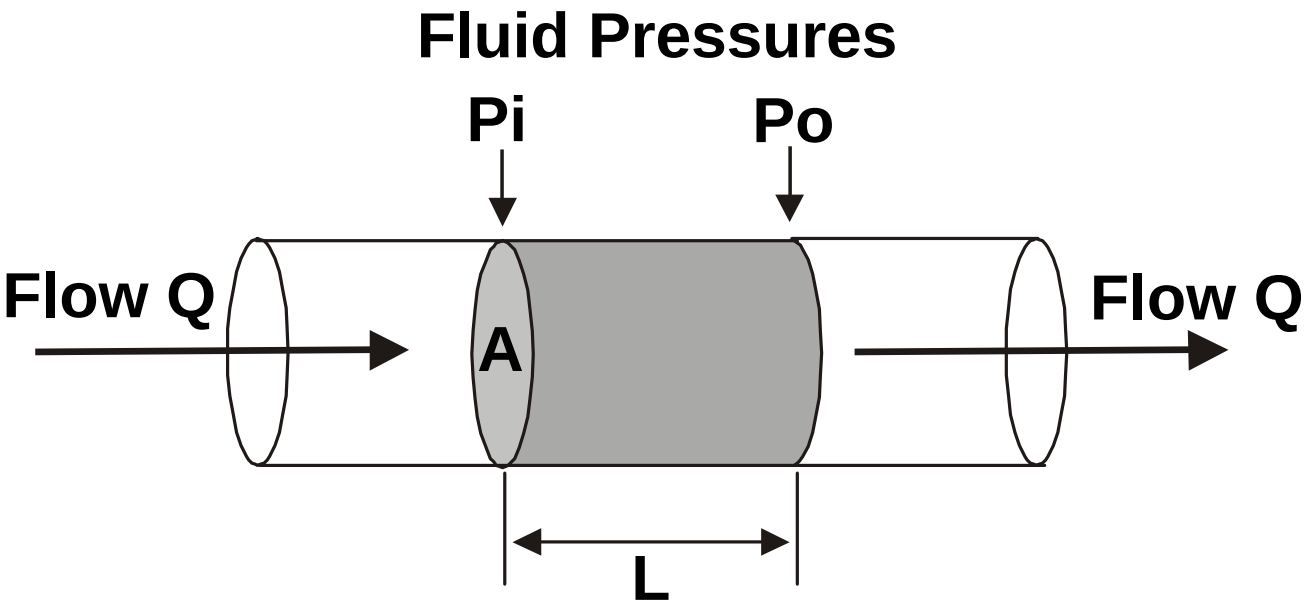

Figure 3.2 Permeability definition.

For practical calculations the following rearranged equations are used

For liquids (oil and water):

$$k = 1000 \frac{L}{A} m \ \ Q \frac{1}{(P_o - P_i)} = 1000 \frac{L}{A} m \frac{\Delta V}{\Delta T} \frac{1}{(P_o - P_i)} \qquad \textbf{(3.3)}$$

where: DV = the volume of liquid flowed in time DT (cm^3)
DT = the time period over which flow is measured (s)
Q = the flow rate = DV/DT (cm^3/s)
P_o = the outlet fluid pressure (atmospheres absolute, atma)
P_i = the inlet fluid pressure (atmospheres absolute, atma)
m = the dynamic viscosity of the fluid (centipoise, cP)
L = the length of the sample (cm)
k = the permeability of the sample (millidarcy, mD)
A = the area of the sample (cm^2).

For gasses (hydrocarbon gasses or nitrogen):

$$k = 2000 \frac{L}{A} m \ \ Q \frac{P_{atm}}{\left(P_o^2 - P_i^2\right)} = 2000 \frac{L}{A} m \frac{\Delta V}{\Delta T} \frac{P_{atm}}{\left(P_o^2 - P_i^2\right)} \quad ` \qquad \textbf{(3.4)}$$

where: DV = the volume of gas flowed in time DT measured at atmospheric pressure (cm^3)
DT = the time period over which flow is measured (s)

Q = the flow rate = DV/DT (cm^3/s)
P_o = the outlet fluid pressure (atmospheres absolute, atma)
P_i = the inlet fluid pressure (atmospheres absolute, atma)
P_{atm} = The atmospheric pressure (atmospheres absolute, atms, =1)
m = the dynamic viscosity of the fluid (centipoise, cP)
L = the length of the sample (cm)
k = the permeability of the sample (millidarcy, mD)
A = the area of the sample (cm^2).

3.2 Controls on Permeability and the Range of Permeability Values in Nature

Intuitively, it is clear that permeability will depend on porosity; the higher the porosity the higher the permeability. However, permeability also depends upon the connectivity of the pore spaces, in order that a pathway for fluid flow is possible. The connectivity of the pores depends upon many factors including the size and shape of grains, the grain size distribution, and other factors such as the operation of capillary forces that depend upon the wetting properties of the rock. This is a complex subject that will be covered in more detail in the Formation Evaluation course later in the MSc.

However, we can make some generalizations if all other factors are held constant:

- The higher the porosity, the higher the permeability.
- The smaller the grains, the smaller the pores and pore throats, the lower the permeability.
- The smaller the grain size, the larger the exposed surface area to the flowing fluid, which leads to larger friction between the fluid and the rock, and hence lower permeability.

The permeability of rocks varies enormously, from 1 nanodarcy, nD (1×10^{-9} D) to 1 microdarcy, μD (1×10^{-6} D) for granites, shales and clays that form cap-rocks or compartmentalize a reservoir, to several darcies for extremely good reservoir rocks. In general a cut-off of 1 mD is applied to reservoir rocks, below which the rock is not considered as a reservoir rock unless unusual circumstances apply (e.g., it is a fractured reservoir). For reservoir rocks permeabilities can be classified as in Table 3.1 below.

Table 3.1 Reservoir permeability classification.

Permeability Value (mD)	Classification
<10	Fair
10 – 100	High
100 – 1000	Very High
>1000	Exceptional

3.3 Permeability Determination

Permeability is measured on cores in the laboratory by flowing a fluid of known viscosity through a core sample of known dimensions at a set rate, and measuring the pressure drop across the core, or by setting the fluid to flow at a set pressure difference, and measuring the flow rate produced.

At this point we must make a distinction between the use of gaseous fluids and the use of liquids. In the case of liquids the measurement is relatively straightforward as the requirement for laminar flow and incompressibility of the fluid are almost always met at surface geological conditions. If one wants to use gas as the fluid, as is commonly done in the industry, there are two complications:

Gas is a compressible fluid, hence if gas is flowing at the same mass per unit time through the core, it will actually be travelling more slowly when measured in volumes per time at the input (high pressure) end of the sample because it is compressed into a smaller volume, than at the output end (low pressure) where it expands. The equation used to calculate the permeability value from the measured parameters has to be modified to take the gas compression into account.

At low gas pressures, there can be very few molecules of gas occupying some of the smaller pores. If this happens, the laws that we are using breakdown, and their use causes an overestimation in the permeability. This is known as *gas slippage* or the *Klinkenberg Effect*. The problem becomes smaller as the pressure is increased because the gas is compressed and there are more gas molecules per unit volume, and does not arise in liquids because liquids are very much denser than gasses.

Gas slippage is corrected for by making permeability measurements with gas at multiple pressure differences and constructing a graph of the measured apparent permeability against the reciprocal of the mean pressure in the core. If the input gas pressure is P_i and the output pressure is P_o, then the permeability is plotted as a function of $1/P_{av} = 2/(P_i + P_o)$, as in Fig. 3.3. The points should now lie on a straight line, which intersects the y-axis at $1/P_{av} = 0$. This value is called the Klinkenberg permeability, and effectively represents the permeability at which the gas (which is near to a perfect gas) is compressed by infinite pressure and becomes a near perfect liquid. It is because of this that the klinkenberg permeability is often given the symbol k_L.

The klinkenberg permeability is very commonly used within the oil industry, and should approximate very well to the permeability of the sample measured with liquid flowing through it. It should be noted that the correction cannot be ignored, especially in tight rocks, as it can lead to corrections of up to 100%. In general, the correction is smaller for higher permeability rocks containing larger pores.

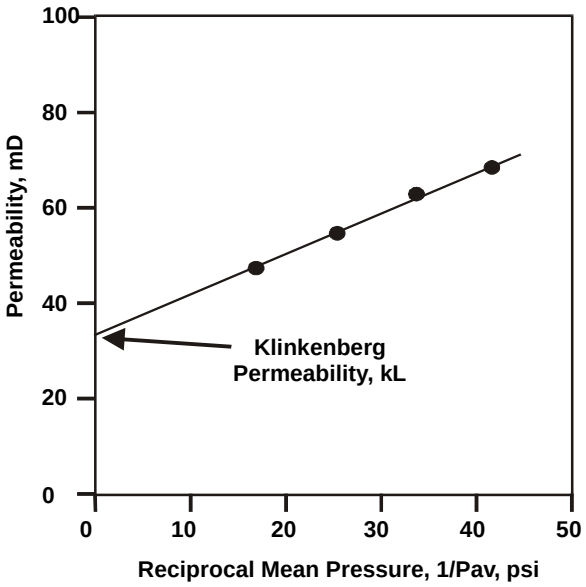

Figure 3.3 The klinkenberg correction plot.

Permeability is generally anisotropic in a rock, partly because of depositional effects, and partly because of the *in-situ* stress field in the crust. To account for this, permeability measurements are made both parallel to and perpendicular with bedding. The permeability perpendicular to bedding will be about a third to half of that parallel to bedding. Clearly this has implications for extracting oil from a reservoir, as oil would usually much rather travel laterally than vertically.

3.4 Relative Permeability

As indicated in Section 3.2, permeability depends upon many factors. Perhaps not surprisingly, one of those factors is the degree to which the available pore space is saturated with the flowing fluid. The pore space may not be completely saturated with one fluid but contain two or more. For, example, there may be, and generally is, both oil and water in the pores. What is more, they may both be flowing at different rates at the same time. Clearly, the individual permeabilities of each of the fluids will be different from each other and not the same as the permeability of the rock with a single fluid present. These permeabilities depend upon the rock properties, but also on the saturations, distributions, and properties of each of the fluids.

If the rock contains one fluid, the rock permeability is maximum, and this value is called the *absolute permeability*.

If there are two fluids present, the permeabilities of each fluid depend upon the saturation of each fluid, and can be plotted against the saturation of the fluid, as in Fig. 3.4. These are called *effective permeabilities*. Both effective permeabilities are always less than the absolute permeability of the rock and their sum is also always less than the absolute permeability of the rock. The individual effective permeabilities are most often expressed as a fraction of the absolute permeability of the rock to either of the two fluids when present at 100% saturation, and these are called *relative permeabilities*.

Hence, if 100% water occupies the rock, the absolute permeability to water is k_{aw}, and the same applies for 100% saturations with oil (k_{ao}), and gas (k_{ag}). If any two, or all three, of these fluids are present together in the rock at some partial saturation S_w, S_o and S_g, we can measure their *effective permeabilities*, which are k_{ew}, k_{eo}, and k_{eg}, which will all be less than their absolute values. We can define and calculate the relative permeability values by expressing the effective permeabilities as a fraction of some base permeability, which is arbitrary but usually the absolute permeability of one of the fluids present. For example, if we take k_{ao} as the base permeability, the relative permeabilities are:

$$k_{rw} = k_{ew} / k_{ao}$$
$$k_{rg} = k_{eg} / k_{ao,} \text{ and}$$
$$k_{ro} = k_{eo} / k_{ao.}$$

Note that the precise value of the relative permeabilities depends upon the base permeability with which they are calculated, and this should always be quoted whenever relative permeabilities are used.

Referring to Fig. 3.4, it can be seen that the effective and hence relative permeability of a given fluid decreases as the saturation of that fluid decreases, and that there is a threshold value of saturation of any given fluid that needs to be present before that fluid will move. This last point is on the one hand intuitive, as one would expect the need for sufficient of a given fluid to be present before a connected, flowable pathway could come into being, and on the other hand critical, because it implies that fluids become trapped (unmovable) in a rock when they are still present in significant amounts. In the figure, oil is immobile until its saturation is about 20%, indicating that we cannot produce from zones that

contain less than 20% oil, and that we will not be able to produce the last 20% of oil from zones which initially have higher oil saturations. This is known as the *residual oil saturation, S_{or}*.

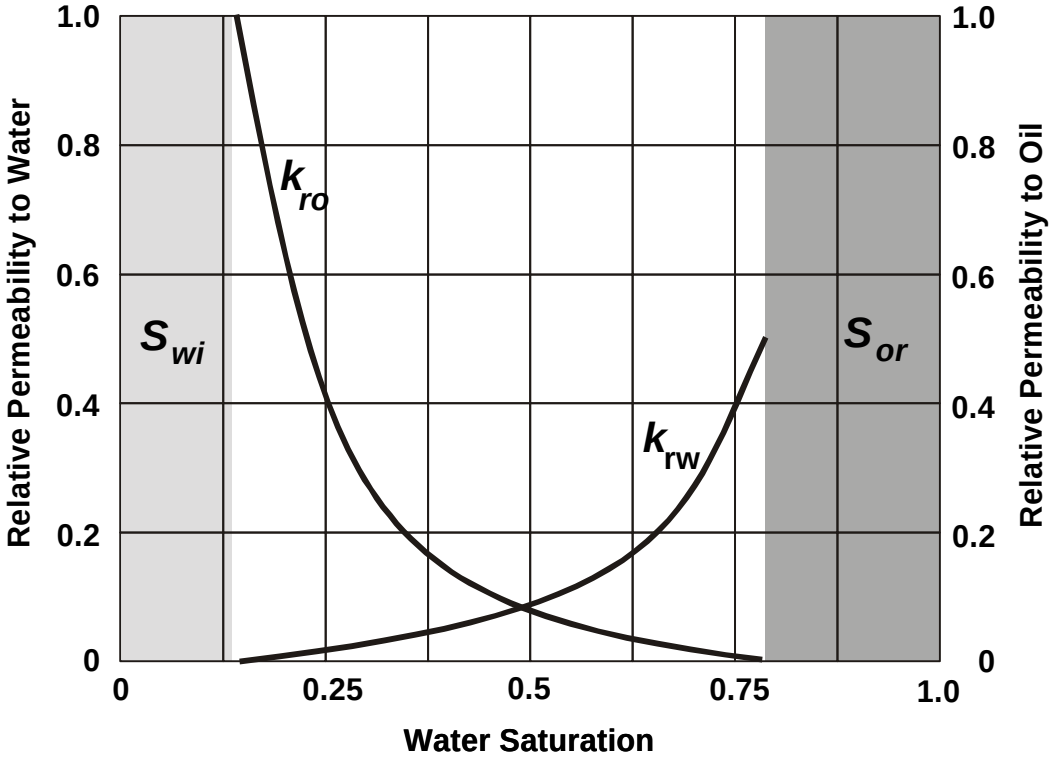

Figure 3.4 Relative permeability curves for an oil/water system that is water wet.

The same applied to the water, whose immobile fraction is termed the *irreducible water saturation, S_{wi}*, and gas, whose immobile fraction is termed the *trapped gas saturation, S_{gt}*.

There is a point on the plot where the curve intersect. Here the permeability to each fluid is the same, and both fluids are equally easily produced. As the oil saturation increases, the permeability to oil increases, and that to water decreases, and *vice versa*. Hence it is apparent that in oil reservoirs it is important to avoid the production of water as not only does it not make money, but an increasing *water cut* reduces the permeability of the reservoir to the oil, making oil more difficult to produce.

3.5.1 Well Productivity

As we have just seen, the permeability is an extremely important parameter because it controls the well's productivity. The productivity of a well is related both to the permeability and to the interval of the borehole open for production (i.e., the interval where the well casing is *perforated*).

For the arrangement shown in Fig. 3.5, we can write the flow equation

$$Q = \frac{k\,A\,(P_f - Pw)}{m\;L} = \frac{k\,2p\;\;r_w\,h\;\;(P_f - Pw)}{m\;\;L} = C\,k\,h \qquad \textbf{(3.3)}$$

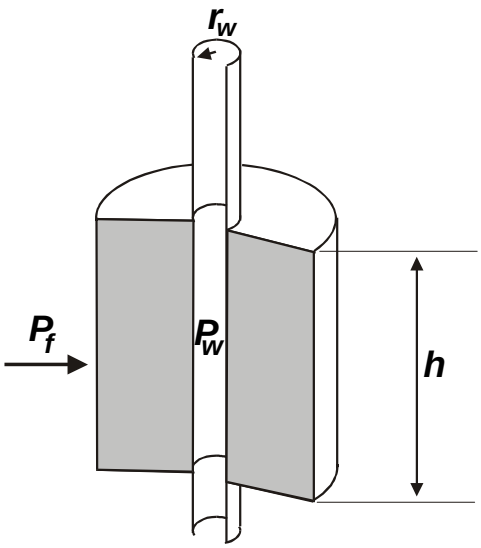

where, the internal area of the borehole has been substituted for the area *A*. It can be seen that for any instant in time, when the formation pressure P_f and the well pressure P_w are constant, and for constant fluid viscosity, m, the productivity of the well will be proportional to the permeability and the interval of production, *h*, with *C* being the coefficient of proportionality.

Figure 3.5 Well productivity.

3.6 PoroPerm Relationships

The most obvious control on permeability is porosity. This is because larger porosities mean that there are many more and broader pathways for fluid flow. Almost invariably, a plot of permeability (on a logarithmic scale) against porosity for a formation results in a clear trend with a degree of scatter associated with the other influences controlling the permeability. For the best results these poroperm cross-plots should be constructed for clearly defined lithologies or reservoir zones. If a cross-plot is constructed for a whole well with widely varying lithologies, the result is often a disappointing cloud of data in which the individual trends are not apparent. Figure 3.6 shows a poroperm cross-plot for a clean sandstone and a carbonate.

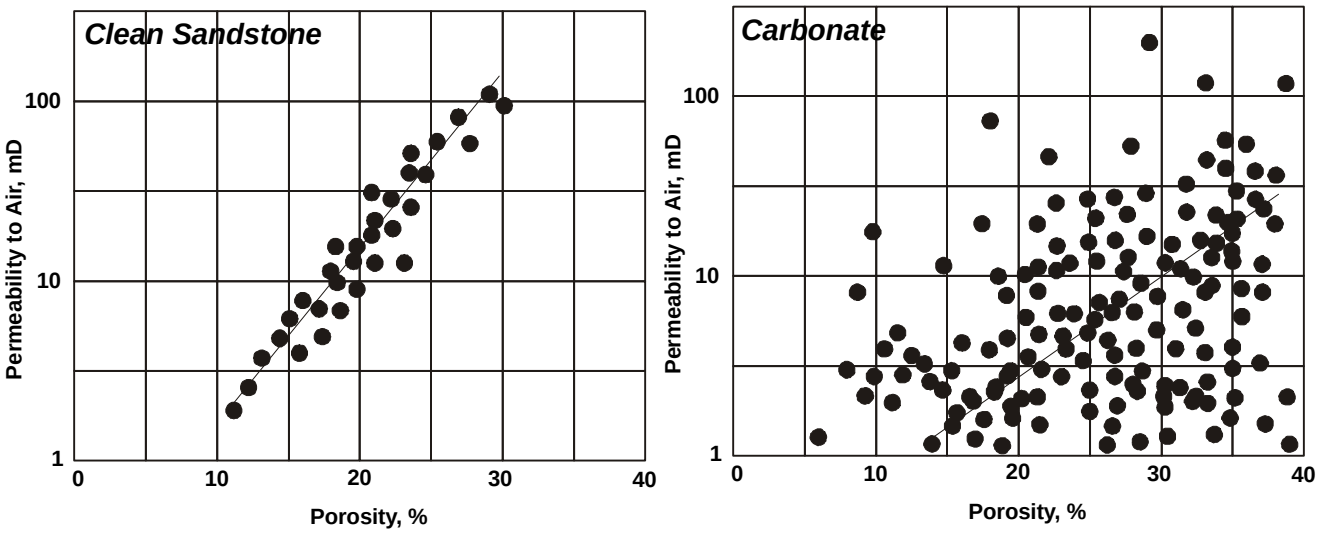

Figure 3.6 Typical poroperm cross-plots.

It is clear from this figure that the permeability of the sandstone is extremely well controlled by the porosity (although usually there is more scatter than in this figure), whereas the carbonate has a more diffuse cloud indicating that porosity has an influence, but there are other major factors controlling the permeability. In the case of carbonates (and some volcanic rocks such as pumice), there can exist high porosities that do not give rise to high permeabilities because the connectivity of the vugs that make up the pore spaces are poorly connected.

Poroperm trends for different lithologies can be plotted together, and form a map of poroperm relationships, as shown in Fig. 3.7.

It would be time consuming to describe the figure in detail, but interpretation is not difficult. For example, fractured rocks fall above the sandstones because their porosity (fracture porosity) is very low, yet these fractures form very connected networks that allow the efficient passage of fluids, and hence the permeability is high. Such permeability may be directional because of preferred orientations of the fractures. By comparison, clay cemented sandstones have high porosities, but the porosity is mainly in the form of micro-porosity filled with chemically and physically (capillary) bound water which is immobile. This porosity does not take place in fluid flow, so the permeability is low.

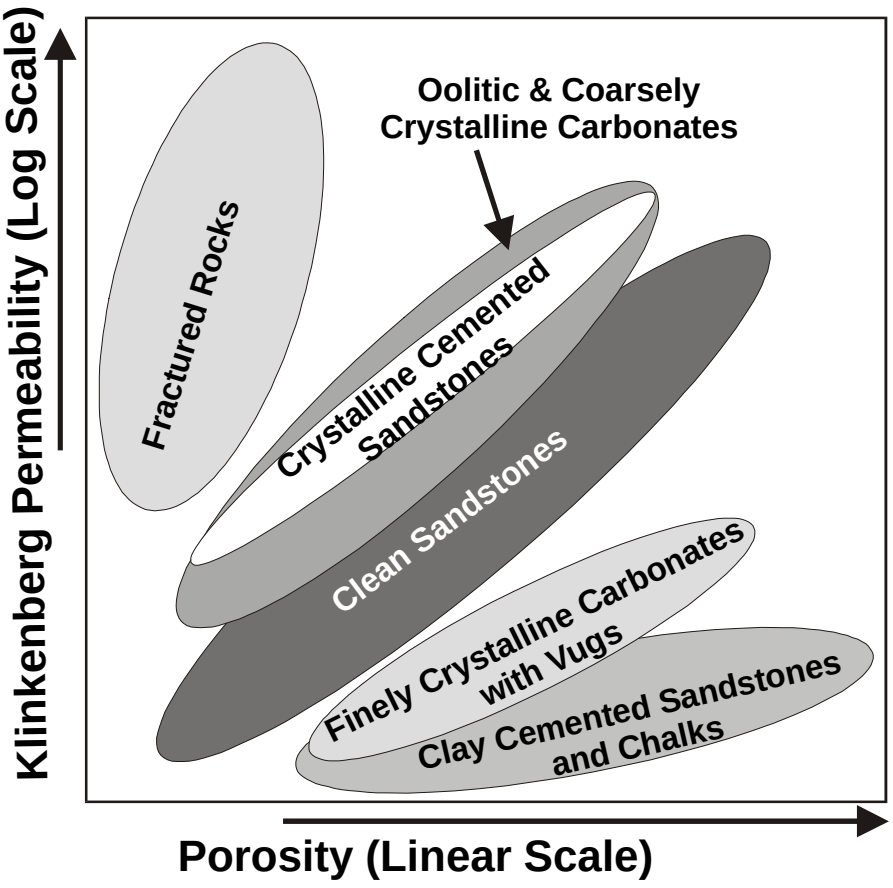

Figure 3.7 Poroperm relationships.

It might be expected that grain size also has some control on permeability. Figure 3.8 shows a poroperm cross-plot for a well in a carbonate reservoir where the grain size, porosity and permeability were measured for each core taken. Taking the data as a whole, there is little in the way of a clear trend. However, trends emerge when the individual grain size fractions are considered. Now it is clear that rocks with smaller grain sizes have smaller permeabilities than those with larger grain sizes. This is because smaller grain sizes produce smaller pores, and rather more importantly, smaller pore throats, which constrain the fluid flow more than larger grains which produce larger pore throats.

In summary, permeability:

- Depends upon porosity.
- Depends upon the connectivity of the flow paths in the rock.
- Depends, therefore, in a complex way upon the pore geometry of the rock.
- Is a directional quantity that can be affected by heterogeneous or directional properties of the pore geometry.
-

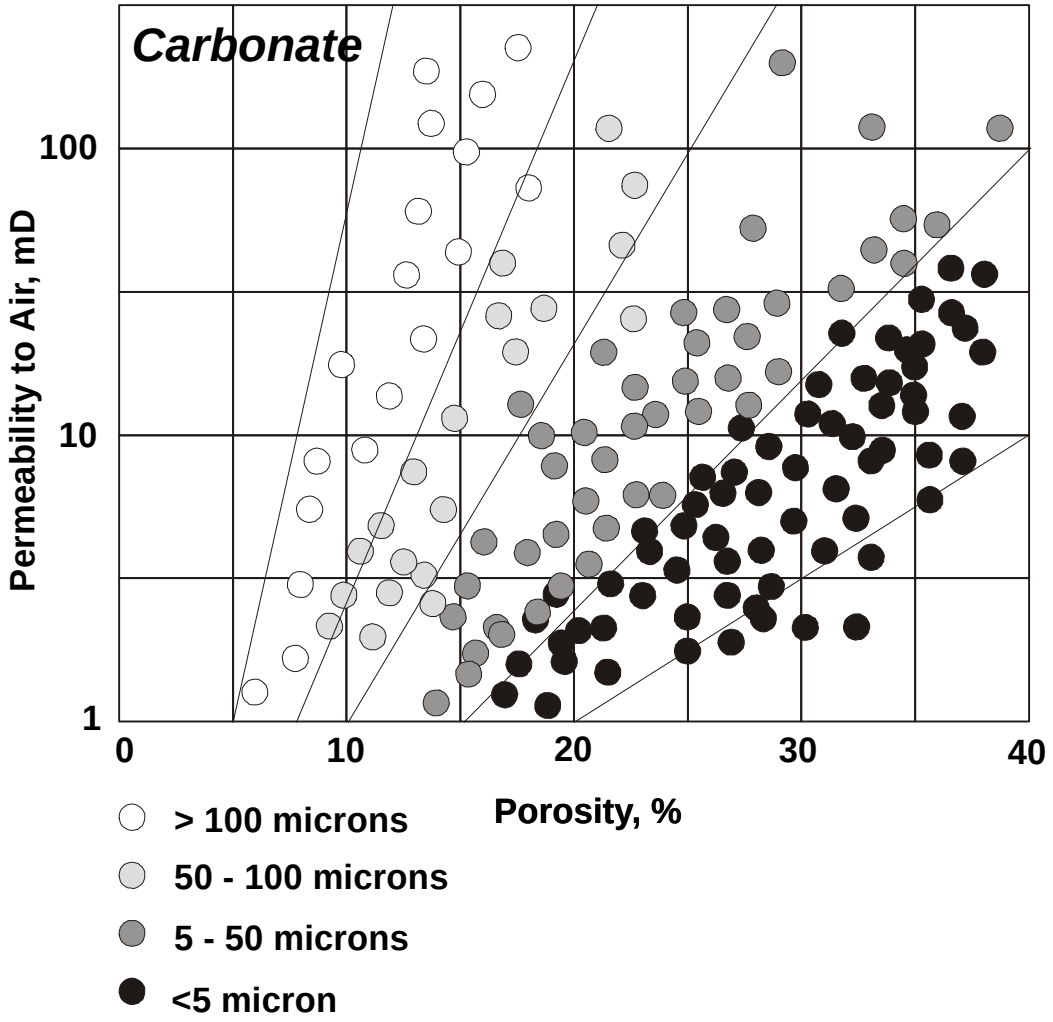

Figure 3.8 Poroperm cross-plots and the influence of grain size.

3.7 Permeability Relationships

The complexity of the relationship between permeability and pore geometry has resulted in much research. No fundamental law linking the two has been found. Instead, we have a plethora of empirical approximations for calculating permeability, some of which are given in Table 3.2.

Table 3.2 Permeability relationships (modified from Grouping's list).

Name	**Equation**	**Notes**
Solution Channel	$k = 0.2 \times 10^8 \times d^2$	k = permeability (D) d = channel diameter (inches)
Fractures	$k = \frac{0.544 \times 10^8 \times w^3}{h}$	k = permeability (D) h = fracture width (inches) w = fracture aperture (inches)
Wyllie and Rose equations I	$k = \left(\frac{100\, f^{2.25}}{S_{wi}} \right)^2$	k = permeability (mD) f = porosity (fraction) S_{wi} = irreducible water saturation (fraction)
Wyllie and Rose equations II	$k = \left(\frac{100\, f^2\, [1 - S_{wi}]}{S_{wi}} \right)^2$	k = permeability (mD) f = porosity (fraction) S_{wi} = irreducible water saturation (fraction)
Timur equation	$k = \frac{0.136\, f^{4.4}}{S_{wi}^2}$	k = permeability (mD) f = porosity (%) S_{wi} = irreducible water saturation (%)
Morris and Biggs equation	$k = \left(\frac{C\, f^3}{S_{wi}^2} \right)$	k = permeability (mD) f = porosity (fraction) S_{wi} = irreducible water saturation (fraction) C = constant; oil=250; gas=80
Slichter equation	$k = \frac{10.2\, d^2}{K_s}$	k = permeability (mD) d = median grain size (microns) K_s = packing correction; slope of line when plotting median grain size vs. permeability.
Kozeny-Carman equation	$k = \frac{c\, d^2\, f^3}{(1-f)^2}$	k = permeability (mD) f = porosity (fraction) c = constant d = median grain size (microns)
Berg equation	$k = 8.4 \times 10^{-2} \times d^2\, f^{5.1}$	k = permeability (mD) f = porosity (fraction) d = median grain size (microns)
Van Baaren equation	$k = 10\, D_d^2\, f^{(3.64+m)}\, C^{-3.64}$	k = permeability (mD) f = porosity (fraction) D_d = modal grain size (microns) C = sorting index m = Archie cementation exponent.
RGPZ equation	$k = \frac{1000\, d^2\, f^{3m}}{4\, a\, m^2}$	k = permeability (mD) d = weighted geometric mean grain size (microns) ϕ = porosity (fraction) m = Archie cementation exponent. a = grain packing constant

4. FLUID SATURATION AND CAPILLARY PRESSURE

4.1 Fluid Saturations

We have seen that the viability of a reservoir depends upon three critical parameters. The first two of these are the porosity of the reservoir rock, which defines the total volume available for hydrocarbon saturation, and the permeability, which defines how easy it is to extract any hydrocarbons that are present. The final critical parameter is the hydrocarbon saturation, or how much of the porosity is occupied by hydrocarbons. This, and the related gas and water saturations are controlled by capillary pressure.

The pore space in a rock is occupied by fluids. In hydrocarbon reservoirs these fluids are hydrocarbon gasses, oil and an aqueous brine. We define the pore fraction of each of these as S_g, S_o and S_w, respectively. Hence, $S_g + S_o + S_w = 1$.

The amount of each of these fluids present at a given level in the reservoir depends upon gravity (buoyancy) forces, which tend to stratify the reservoir fluids according to their density, external hydrodynamic forces such as flow from a remote aquifer, and interfacial forces that act between the various reservoir fluids and between the fluids and the rock matrix.

The interfacial forces either take the form of (i) forces on the interface between two fluids, or (ii) between the fluid and the solid matrix of the rock. Both effects rely upon differences in the relative strength of inter-molecular forces between gasses, liquids and solids.

- Liquid-gas or liquid-vapour forces result from the differences in molecular attraction of each of the gas and liquid molecules for molecules of the same fluid compared to the molecular attraction for molecules of the other fluid.

- The liquid-liquid forces result from the differences in molecular attraction of each of the liquid molecules for molecules of the same liquid compared to the molecular attraction for molecules of the other liquid.

- The fluid-solid forces result from the preference for fluid molecules to be attracted to the solid mineral surface rather than to molecules of the same fluid.

The interfacial forces give rise to what is known as a capillary pressure. *Capillary pressure* is the difference in fluid pressure across an interface between two fluids in a confined volume.

In the discussion of capillary pressure, we will first examine surface energy and wettability, and then go on to derive a general expression for capillary pressure.

4.2 Fluid-Fluid Interactions (Surface Tension)

The fundamental property of that state of matter that we call a fluid is that its molecules are free to move. In gasses the freedom is great, but in liquids the freedom is constrained by relatively strong *cohesive* (attractive) forces that operate between the molecules. Imagine a drop of liquid suspended in a gas. In the interior of the liquid drop, a molecule is completely surrounded by other liquid molecules. On average it is equally attracted to the molecules surrounding it in every direction. By contrast, a molecule that occupies the surface of the drop is strongly affected by the attractive forces of

its fellow molecules inside the drop, but only weakly attracted to molecules outside the drop. This is because there are much fewer molecules in the vapour phase that surrounds the drop. Hence, the molecules on the surface of the drop experience net inward attraction. Figure 4.1 illustrates this schematically.

This attraction ensures that the drop attains the shape with least surface area in any given environment. For example, in zero gravity, the drop will float and will be perfectly spherical; the sphere being the geometry with the least surface area per volume.

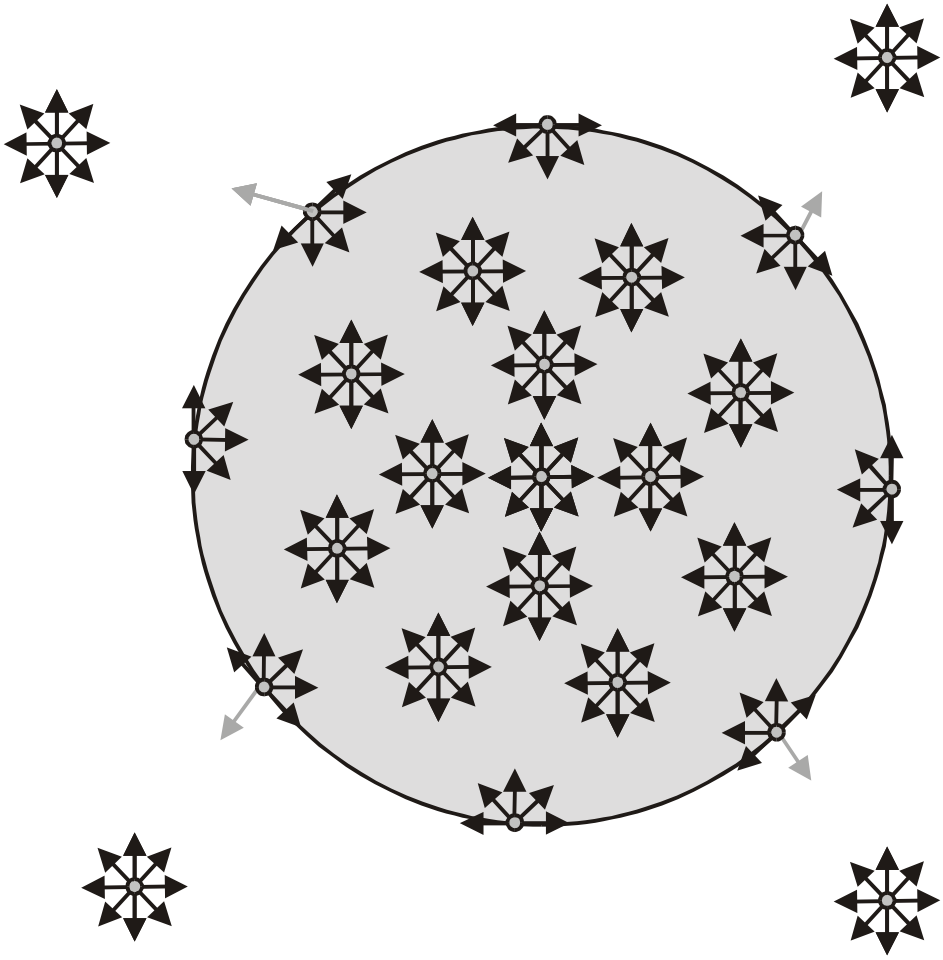

Figure 4.1 Schematic illustration of surface energy.

To summarize; in the drop there are attractive forces between the molecules. The molecules inside the drop are surrounded by balanced attractive forces. The molecules at the surface experience a net inward force, which results in the drop contracting to the smallest surface area. The fluid pressure inside the drop is higher than that outside it, therefore the drop behaves as though it was contained in a skin.

If we have a drop of liquid suspended in a gas, and we want to increase the surface area of the drop, we must do *work* to move molecules from the interior of the drop to the surface. This is equivalent to saying that the surface possess *free surface energy*.

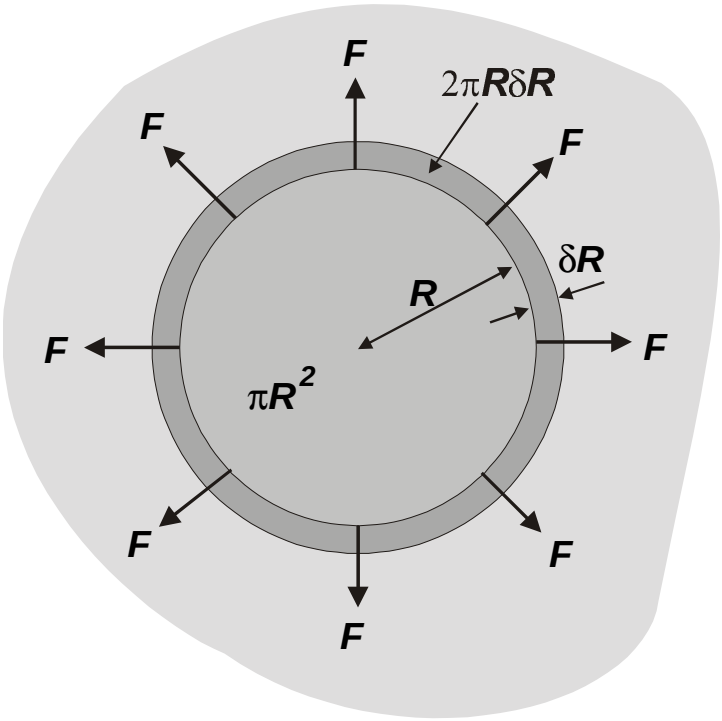

Figure 4.2 Calculation of surface energy and surface tension.

Take the surface of any liquid droplet, and imagine that a circle is drawn on this surface with radius *R*. The area of the circle is pR^2 (Fig. 4.2). To increase the surface area of this drop by one unit of surface area, work must be done to move molecules from the interior of the drop to its new surface. The surface energy s is equivalent to the work done W per unit surface area increase dA, i.e., $s = W/dA$. But the work done W is the force operating to make the change F multiplied by the distance the force moves, so in the case of an imaginary circle on the surface of the liquid drop which increases its diameter from R to R + dR, we can see that $W = FdR$ and hence, $s = FdR/dA$. When the droplet expands the surface area of the droplet and the area of the circle also expand. If the change in the radius of the circle is dR, the expanded circle has area $p(R+dR)^2$, and the change in area has been $dA = 2pRdR$ (Fig. 4.2). Hence, $s = FdR/2pRdR = F/2pR = F/L_p$, where L_p is the perimeter of the original circle. Hence we can see that surface energy s has the dimensions of [force]/[length], and is therefore a form of tension. Hence, the surface energy of a fluid interface is also called the *surface tension* of the fluid interface. Note therefore, that the surface tension is the force operating perpendicular to a line on a fluid interface divided by the length of that line. In our case the force was uniform around the circle, and the length of the circle (perimeter) was $2pR$.

We can write:

$$s = \frac{F}{L} \qquad \textbf{(4.1)}$$

where: s = the surface tension (≡surface energy) in dynes/cm or N/m
F = the force operating on the surface (dynes or N)
L = the length of the line that the force operates on perpendicularly (cm or m).

The surface tension of a fluid-fluid interface is commonly measured by using a loop of wire. If loop of wire is placed upon a fluid-fluid interface, it will be held in place by surface tension. Figure 4.3 shows the general arrangement. In this case we will be assuming that the lower fluid has the greater forces of attraction between its molecules. If we apply a small upward force to the loop it tries to leave the surface, but the surface tension hold the loop down (Fig. 4.3). There are two fluid interfaces that contribute to this, the outer circle and the inner circle. Both need to be overcome to remove the loop from the interface. The force required (from Eq. (4.1)) is $F = F_{inner} + F_{outer} = 2\pi\sigma R_{inner} + 2\pi\sigma R_{outer} = 4\pi\sigma R_{mean}$. Hence;

$$\sigma = \frac{F}{4\pi R_{mean}} \qquad \textbf{(4.2)}$$

where, F = the force required to lift the loop from the surface interface (dynes or N)
σ = the surface tension (dynes/cm or N/m)
R_{mean} = the mean radius of the loop (cm or m).

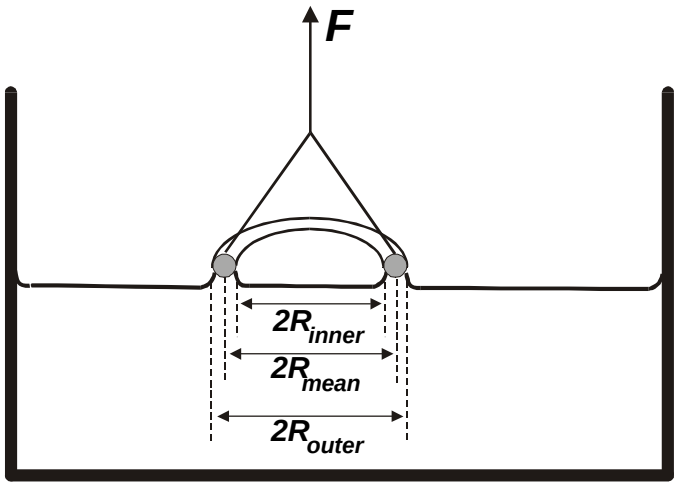

Figure 4.3 Calculation of surface energy and surface tension.

Table 4.1 shows the surface tensions of some common fluid-fluid interfaces.

Table 4.1 Surface tensions of some common fluid interfaces.

Interface	**Surface Tension @ 20°C**	
	(N/m)	**(dynes/cm)**
Water-Air	0.0726	72.6
Benzene-Air	0.0289	28.9
Cyclohexane-Air	0.0253	25.3
n-Hexane-Air	0.0184	18.4
n-Octane-Air	0.0218	21.8
Water-Oil	Approx. 0.0350	Approx. 35.0
Mercury-Air	0.3680	368.0
Units: 1 N/m = 1000 dynes/cm		

Note that the liquid drop cannot exist in isolation. The arguments put forward so far have considered a single fluid in a gas. In practice both the fluid in the droplet and the fluid in which the droplet exists contribute to the interfacial effects. It is the *relative* attractions of the molecules of each fluid for themselves and each other that are important. In the case of a liquid drop in a gas, the effect of the gas can usually be ignored. This is because the cohesion forces operating between the molecules in the fluid are much greater than those in the gas because the fluid has a much higher density (number of molecules per unit volume).

The interfacial tension of an interface is a fundamental property of that interface. If a liquid has an interface with a gas, then some molecules of the liquid will be found in a vapour phase in the gas above the interface. These molecules reduce the surface tension. As temperature increases the concentration of the vapour phase increases, and the surface tension decreases. At the critical point there are as many molecules in the gas phase as in the liquid phase, the interface effectively disappears, and the surface tension becomes zero.

4.3 Fluid-Solid Interactions (Wettability)

We have seen that a fluid has a preferential attraction to itself, and the relative strengths of such cohesive forces result in surface tension that develops on a fluid-fluid interface. However, the molecules of a fluid may also have a preferential attraction to solid interfaces. If two fluids occupy a solid surface, the fluid whose molecules display the greatest attraction for the atoms that compose the solid will be the fluid that occupies most of the surface, displacing the other fluid.

The *wettability* of a surface is the type of fluid which is preferentially attracted to that surface.

Figure 4.4a shows the general case of a single solid immersed in two immiscible fluids at an unstable initial state. Now, imagine that the molecules of Fluid A are attracted to the solid molecules more than those from Fluid B are. Fluid A will then displace Fluid B on the surface. However, the molecules of Fluid A and Fluid B are contemporaneously also experiencing attractions from their fellow molecules and, to a smaller extent, the molecules of the other fluid. Consequently, Fluid A cannot displace all of Fluid B from the surface unless the attraction between the molecules on the surface of the solid and those in Fluid A is very great. In the general case a stable state will be encountered where Fluid A occupies the majority of the surface. At this equilibrium state, the *contact angle q* characterizes the balance between the various cohesive forces (Fig. 4.4b).

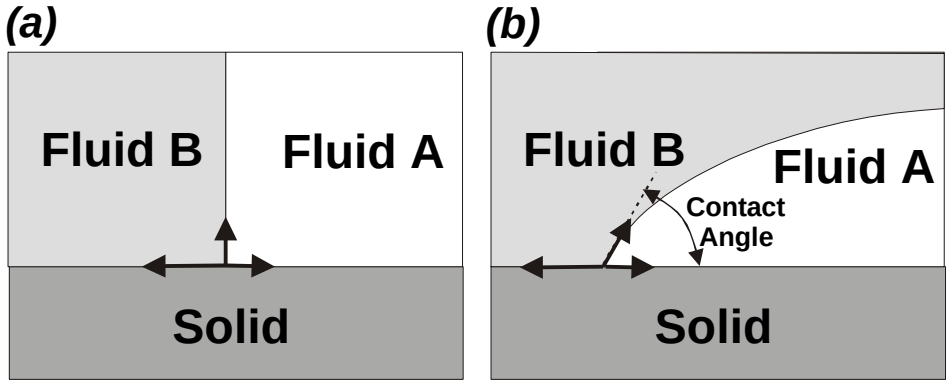

Figure 4.4 Surface wettability.

Clearly, the contact angle can be used as a measure of wettability. Figure 4.5 and Table 4.2 show three possible scenarios.

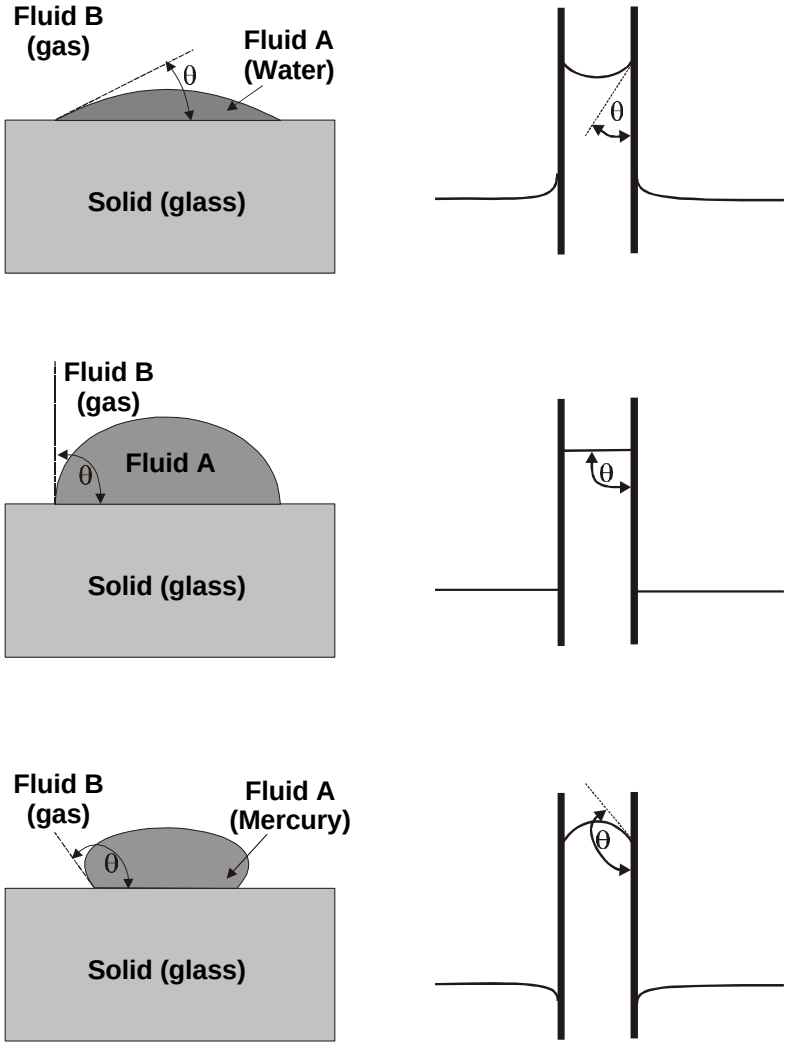

Figure 4.5 Contact angles for different wettabilities.

Table 4.2 Contact angles for different wettabilities.

Contact Angle relative to Fluid A, q (degrees)	Description
0	Extremely Fluid A wet
0-30	Significantly A wet
30-60	Moderately Fluid A wet
60-90	Weakly Fluid A wet
90	Neutrally wet
90-120	Weakly Fluid B wet
120-150	Moderately Fluid B wet
150-180	Significantly B wet
180	Extremely Fluid B wet

4.4 Capillary Pressure

4.4.1 Derivation of the Capillary Pressure Equation

Take a spherical droplet of fluid, of radius R. Its surface area is $4\pi R^2$.

If the sphere is increased in size by increasing its radius from R to $R+dR$, the increase in surface area dA is $4\pi(R^2+rdR+dR^2)-4\pi R^2$, which as $dR^2 \rightarrow 0$ is $dA=8\pi RdR$.

To increase the radius of the sphere from R to $R+dR$ requires work to be done moving molecules from the inside of the droplet to the surface. As work done W is the product of the surface tension σ, and the change in surface area dA, we can say $W = \sigma\, dA = 8\pi\, \sigma\, RdR$.

But the work done is also the force operating to cause the change multiplied by the distance the force moves. By definition any pressure P is equal to the force F operating per unit area A, perpendicular to that area. Hence, $F = PA$. The force operating on the spherical surface of the droplet is therefore equal to the nett pressure $(P_{in} - P_{out})$ multiplied by the area of the spherical droplet $4\pi R^2$, i.e., $F = 4\pi R^2(P_{in} - P_{out})$. Since $P_{in} > P_{out}$, the net pressure $(P_{in} - P_{out})$ is positive, and the net pressure and resulting force is outward. The distance the force moves is also outward , and its value is clearly dR. Hence, the work done is $W = F\, dR = 4\pi R^2(P_{in} - P_{out})\, dR$.

Equating these relationships to eliminate W, gives

$$(P_{in} - P_{out}) = \frac{2\,\sigma}{R}\,. \qquad \textbf{(4.3)}$$

Note that the derivation equates the work done. This type of derivation does not rely on the interface of the spherical droplet being static, as it is based upon the conservation of work (energy). It is also independent of direction because work is a scalar quantity.

The *capillary pressure* is defined as the difference between the pressures in each of the two fluids forming an interface. Hence Eq. (4.3) is an equation for capillary pressure.

The capillary pressure is proportional to the surface tension. Note that the greater of the two pressures is developed in the fluid which contains the centre of curvature of the curved fluid interface.

The geometry of pore systems in rocks is complex, but can be approximated by a bundle of capillary tubes. If the pore throat is represented by a capillary tube such as that shown in Fig. 4.6, we can note that the radius of the capillary tube R_{tube} can be expressed in terms of the radius of curvature of the surface of the fluid-fluid interface R by $R_{tube} = R\cos\theta$, where θ is the contact angle defined in the previous section. Hence, we can write the equation

$$P_{cap} = (P_{in} - P_{out}) = \frac{2\,\sigma\,\cos\theta}{R_{tube}} \qquad \textbf{(4.4)}$$

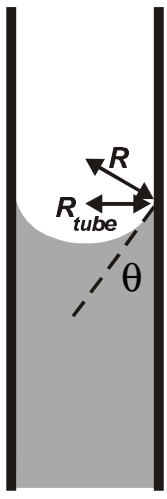

Figure 4.6 Capillary pressure in a tube (pore throat).

Note that the pressure is proportional to the surface tension and cos$q$, but inversely proportional to the radius of the tube. Hence, as the radius of the tube increases, the capillary pressure decreases.

The difference in pressure (the capillary pressure) causes the interface to rise up the capillary tube until the weight of the suspended column of fluid balances the capillary force that is associated with the capillary pressure. Hence Eq. (4.4) can be used to describe the rise of fluids in a capillary tube.

4.4.2 Capillary Force

The capillary force acting on the periphery of the meniscus is, according to Eq. (4.1) $F = s\ L = 2\pi s R_{tube}$.

A proportion of this force acts up the capillary tube $F_{up} = F \cos\theta = 2\pi s R_{tube} \cos\theta$.

At equilibrium (i.e., the meniscus is static), the upward capillary force is balanced by an equal and opposite force due to the weight of the suspended column of fluids.

The weight of the suspended column of fluids is $\pi R^2_{tube}\, h\, g\, (\rho_{liquid} - \rho_{vapour})$, where h is the height of the fluid column, g is the acceleration due to gravity, and ρ_{liquid} and ρ_{vapour} are the densities of the liquid phase below the meniscus and the vapour phase above the meniscus, respectively.

Hence, we can write $2\pi s R_{tube} \cos\theta = \pi R^2_{tube}\, h\, g\, (\rho_{liquid} - \rho_{vapour})$, and by rearrangement

$$h = \frac{2\, s\, \cos\theta}{R_{tube}\, g\left(\rho_{liquid} - \rho_{vapour}\right)} = \frac{P_{cap}}{g\left(\rho_{liquid} - \rho_{vapour}\right)} \qquad \textbf{(4.5)}$$

Hence, the height to which the fluid rises depends inversely upon the tube radius (pore throat radius); the larger the tube (pore throats) the less the fluid rises.

The capillary pressure in a simple system of glass tubes of different radii can be calculated from Eq. (4.5) by measuring the height of the capillary rise, while knowing g, and the densities of the liquid and the vapour. In practice the density of the vapour is small at surface conditions and can be ignored. It cannot, however, be ignored at down-hole conditions, where its density may approach the density of the fluid.

4.4.3 Reservoir Scenarios

There are two scenarios that are of particular importance in a hydrocarbon reservoir. These are the gas/water and oil/water systems. In these scenarios, it should be noted that the *free water level* is defined as the level at which $P_{cap} = 0$, i.e., the pressure in the two fluids forming the interface is the same.

Gas/Water System. A model of the capillary pressure in a gas/water system is shown in Fig. 4.7. The free water level is the height of the interface when the radius of the capillary tube tends to infinity (i.e., the capillary pressure is zero and h=0). In Fig. 4.7, this is approximated by a wide bath of fluid. The interface at the free water level may exist at any given absolute pressure P_{FWL}. Capillary forces exist inside the restricted capillary tubing that result in the rise of the water to a height h above the free water level.

The pressure in the gas phase above the meniscus in the capillary tube is P_{gas}, where $P_{gas} = P_{FWL} - r_{gas}\, g\, h$.

The pressure in the water phase below the meniscus in the capillary tube is P_{water}, where $P_{water} = P_{FWL} - r_{water}\, g\, h$.

Hence the capillary pressure is $P_{cap} = P_{gas} - P_{water} = (r_{water} - r_{gas})\, g\, h$, which is consistent with Eq. (4.5).

Using Eq. (4.4), the height to which the water rises can be obtained by rearranging this equation to give

$$h = \frac{P_{cap}}{g\left(r_{water} - r_{gas}\right)} = \frac{2\, s\, \cos q}{R\, g\left(r_{water} - r_{gas}\right)} \qquad \textbf{(4.6)}$$

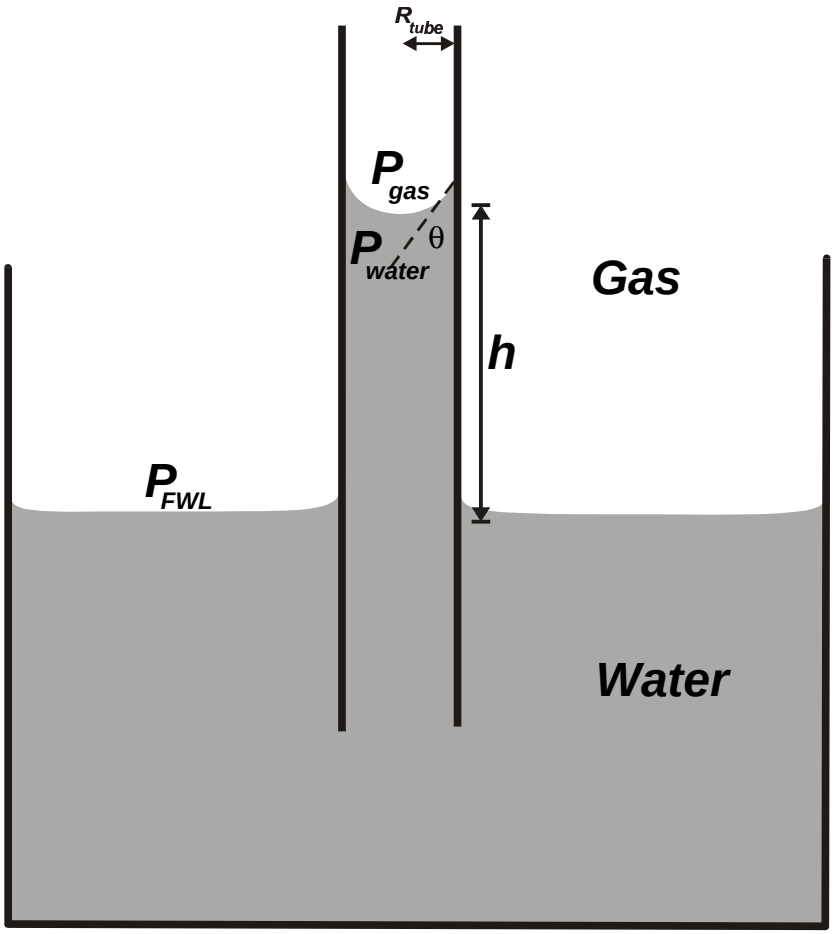

Figure 4.7 Capillary pressure in a gas/water system.

Oil/Water System. A model of the capillary pressure in a oil/water system is shown in Fig. 4.8. The free water level is the height of the interface when the radius of the capillary tube tends to infinity (i.e., the capillary pressure is zero and h=0) as before. This interface exists at a given absolute pressure P_{FWL}. Capillary forces exist inside the restricted capillary tubing that result in the rise of the water to a height h above the free water level.

The pressure in the oil phase above the meniscus in the capillary tube is P_{oil}, where $P_{oil} = P_{FWL} - r_{oil}\, g\, h$.

The pressure in the water phase below the meniscus in the capillary tube is P_{water}, where $P_{water} = P_{FWL} - r_{water}\, g\, h$.

Hence the capillary pressure is $P_{cap} = P_{oil} - P_{water} = (r_{water} - r_{oil})\, g\, h$, similarly to the last case.

Using Eq. (4.4), the height to which the water rises can be obtained by rearranging this equation to give

$$h = \frac{P_{cap}}{g\left(r_{water} - r_{oil}\right)} = \frac{2\, s\, \cos q}{R\, g\left(r_{water} - r_{oil}\right)} \qquad \textbf{(4.7)}$$

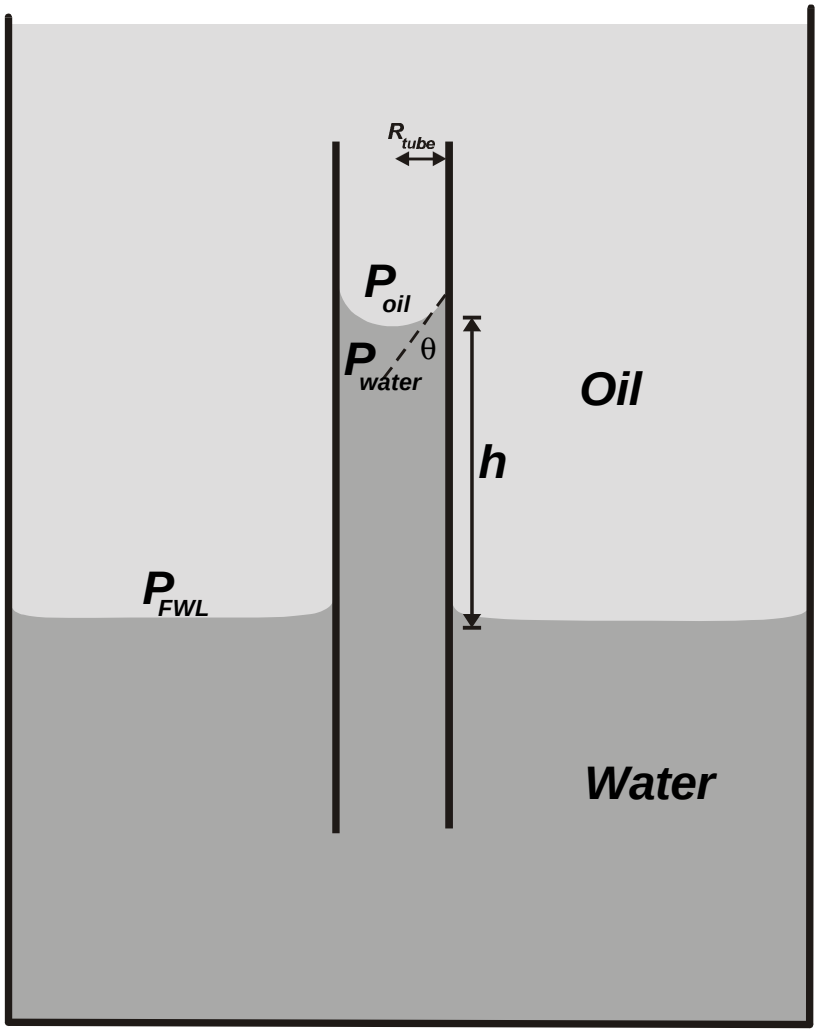

Figure 4.8 Capillary pressure in a oil/water system.

Knowledge of Parameters. The capillary pressure depends most critically upon the interfacial tension and the wetting angle. These parameters change with pressure and temperature for any given fluid/fluid/solid system. Measurements can be made accurately in the laboratory in simplified systems

such as the capillary tube, but are very difficult to carry out in the rock itself. The result is that we use a range of values which are generally considered to be standard, but should not be considered to be accurate. These are given in Table 4.3.

Table 4.3 Standard interfacial tension and wetting angle values for common mixtures of reservoir fluids and solids.

System	**Wetting Angle, *q* (degrees)**	**cos *q***	**Interfacial Tension at 20°C, *s* (dynes/cm [N/m])**
Water/Gas/Mineral	0	1	72 [0.072]
Water/Oil/Mineral	0	1	35 [0.035]
Air/Mercury/Mineral	0	1	368 [0.368]

The mercury/air. solid system is included because it is used in mercury porisimetry for obtaining porosity, capillary pressure, and pore size distributions. This technique will be described later.

4.5 Implications of Capillary Pressure in Reservoirs

So far we have restricted ourselves to a simple single capillary tube. Real rocks contain an array of pores of different sizes connected together by pore throats of differing size. Each pore or pore throat size can be considered heuristically to be a portion of a capillary tube. Real rocks may be completely water-wet, and indeed are commonly so. They may, however be oil-wet or neutrally wet or have a mixed wettability, where some mineral grain surfaces are water-wet and some are oil-wet. For the purposes of this discussion we will consider only water-wet rocks.

4.5.1 Capillary Rise and Reservoir Fluid Pressures

Assume that the pores of the rock are water-wet and can be represented by capillaries of five sizes: very small, small, medium, large and very large. The capillary rises in each of these pores will be as shown in Fig. 4.9. The capillary pressure at each of these menisci is the difference between the pressure in Fluid A above the menisci (say gas) and the pressure in Fluid B below the menisci (say water), as defined earlier (Eq. 4.3).

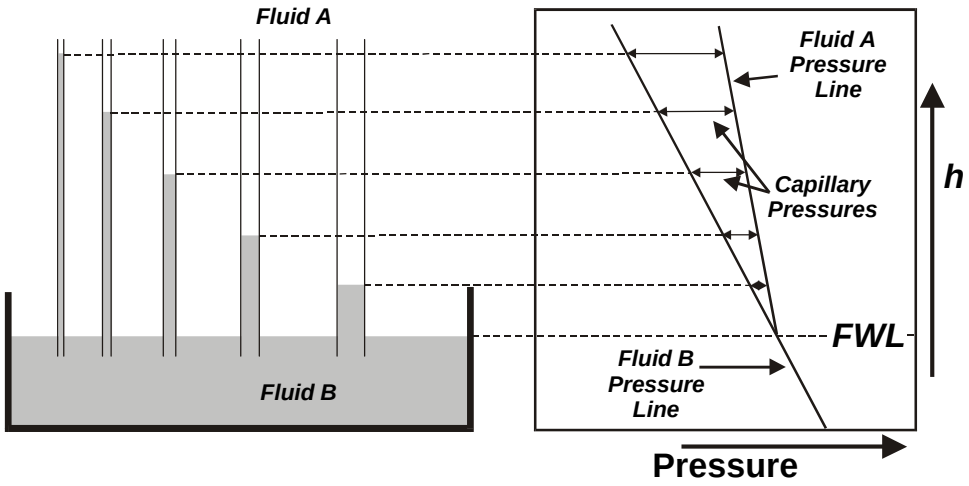

Figure 4.9 Capillary rise and capillary pressures.

The capillary pressures are shown in the graph in Fig. 4.9. We can see that Fluid A (gas) has increasing pressure with depth due to the column of Fluid A above it, and this is described by the line labeled 'Fluid A Pressure Line', which has a gradient $r_{FluidA}\ g\ h$. Fluid B (water) has increasing pressure with depth due to the column of Fluid B above it, and this is described by the line labeled 'Fluid B Pressure Line', which has a gradient $r_{FluidB}\ g\ h$. Fluid A sits above Fluid B because it is less dense. Its lower density results in it having a steeper gradient. Where the two line intersect, the pressures in both fluids are the same and the capillary pressure is therefore zero. This is the free water level.

4.5.2 Displacement Pressure

If we have a capillary tube or a rock that contains 100% saturation of a non-wetting fluid (e.g. gas) and we introduce a wetting fluid (e.g. water) to one end, the capillary pressure will draw the wetting fluid into the tube or the pores of the rock spontaneously. If the pathway is down or horizontal this process can continue as long as there is more tube or rock for the wetting fluid to fill. If the pathway is upward or vertical, the process will continue until the capillary force pulling the fluid into the tube or rock pores is balanced by the gravitational force acting on the suspended column of fluid (Fig. 4.10).

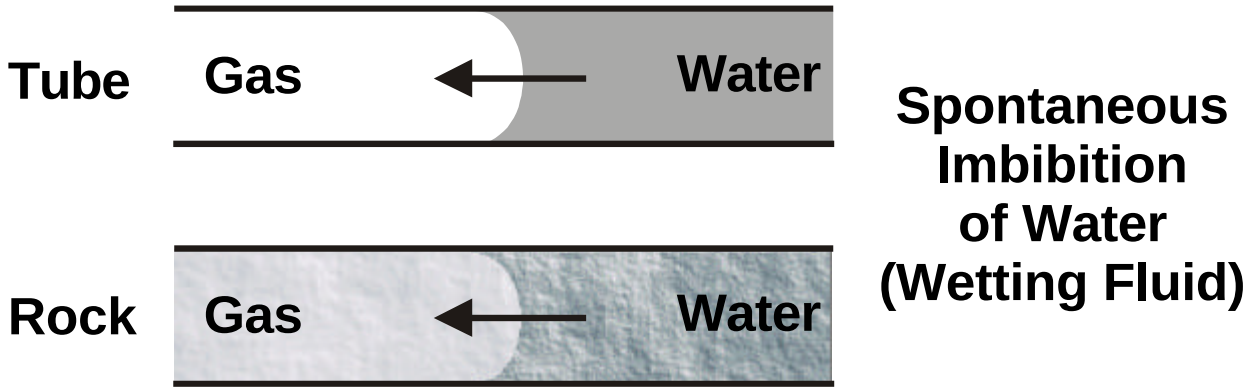

Figure 4.10 Capillary pressure spontaneously drawing up a wetting fluid..

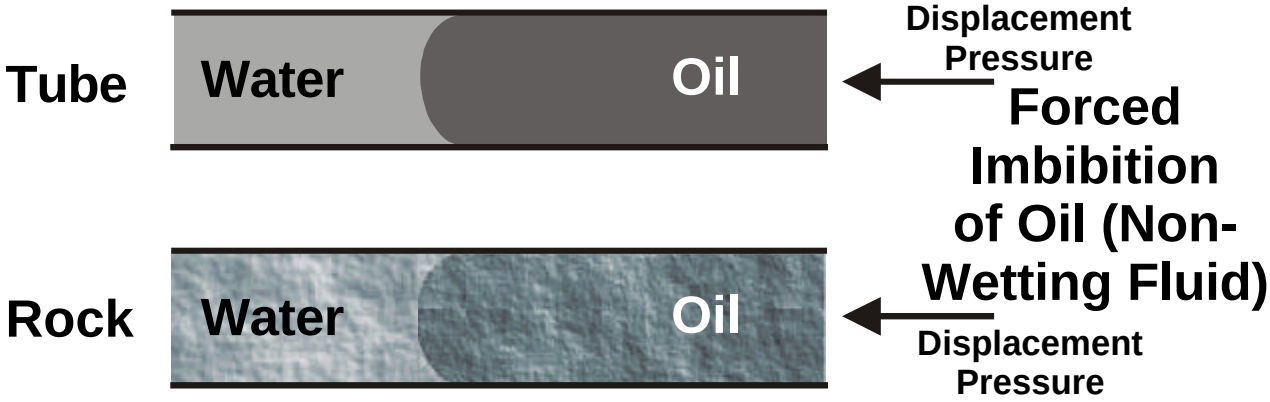

Figure 4.11 A force is needed to overcome the capillary pressure to displace a wetting fluid with a non-wetting fluid.

If we have a capillary tube or a rock that contains 100% saturation of a wetting fluid (e.g. water) and we introduce a non-wetting fluid (e.g. oil) to one end, the non-wetting fluid will not be spontaneously drawn up into the tube or the pores of the rock. This is because the wetting fluid is held inside the tube or the rock by the capillary force. To introduce the non-wetting fluid into the tube or the rock, we must apply an external force to overcome the capillary force holding the wetting-fluid in place (Fig. 4.11). This is called the *displacement force* or *displacement pressure*, and is equal in magnitude, but opposite in sign (direction) to the capillary force and capillary pressure respectively.

IMPORTANT: In oil reservoirs, the reservoir rock initially contains water and is water-wet. Oil migrates into the reservoir rock displacing the water. A displacement force is required to overcome the capillary forces in the water saturated water-wet reservoir rock. This force is supplied by gravity operating upon the differential buoyancy of the two fluids that results from their different densities. There is a level at which oil cannot replace water further because the driving force is insufficient to overcome the capillary force. This does not occur at the free water level, but at some height above the free water level defined by the displacement pressure. Thus, in reservoirs, the oil/water contact (*OWC*) is above the free water level (*FWL*).

Hence, if we have a number of capillary tubes of different radii arranged horizontally and containing a wetting fluid (e.g., water) (Fig. 4.12), and we wish to force a non-wetting fluid into the tubes (e.g., oil), a lower displacement pressure will be required to replace the water in the larger tubes than to replace the water in the thinner tubes. One can use the analogy with rocks, but remember that the pore space in rocks is composed of pores of different sizes connected by pore throats of varying size that are smaller than the pores. Hence the displacement force or pressure required to force a non-wetting fluid into a rock saturated with a wetting fluid will be controlled by the size of the pore openings.

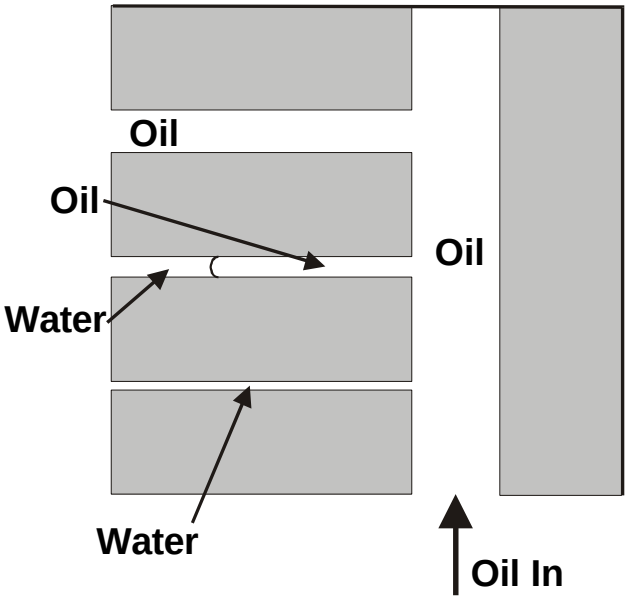

Figure 4.12 Displacement pressure.

An Example. Assume that a rock is composed of five sizes of pore in equal number, and for the sake of simplicity, these pores are connected by pore throats of the same size as the pores. The rock is completely saturated with a wetting fluid. Table 4.4 shows the size, number and volume of pores together with their respective displacement pressures.

Table 4.4 Pore size and displacement pressure example.

Pore Radius [mm]	Individual Pore Volume [mm^3]	Pore Number [-]	Volume of Pores [mm^3]	Contribution to Total Pore Volume [%]	Displacement Pressure [Pa ´10^3]
1	3.1415	10000	31415	0.132	70
2.5	19.6349	10000	196349	0.825	28
5	78.5498	10000	785398	3.301	14
10	314.1593	10000	3141593	13.206	7
25	1963.4954	10000	19634954	82.535	2.8

The data given in Table 4.4 can be plotted as a displacement versus pressure plot (Fig. 4.13). In this rock the pressure required to begin to displace water by oil is the initial displacement pressure (2800 Pa in this case). The level in the reservoir at which this is the case is called the *100% water level* which should be the same as the *OWC*, and is above the *FWL* by a height related to the size of the displacement pressure and controlled by the largest pore openings in the rock. If the rock was composed of 100% of pores of 25 micron size, this would be the level above which there would be 100% oil saturation and below which there would be 100% water saturation. However, the rock also contains smaller pores, with higher displacement pressures. Thus there will be a partial water saturation above the 100% water level occupying the smaller pores, and this water saturation will reduce and become confined to smaller and smaller sized pores as one progresses to higher levels above the 100% water level. Water will only be displaced from a given pore size if there is a sufficiently large force to overcome the capillary force for that size of pore. Commonly, the force driving the oil into the reservoir rock (due to differential buoyancy) is insufficient to overcome the capillary forces associated with the smallest pores. Hence, the smallest pores in an oil zone remain saturated with water, and there is an *irreducible water saturation* (S_{wi}) in the reservoir.

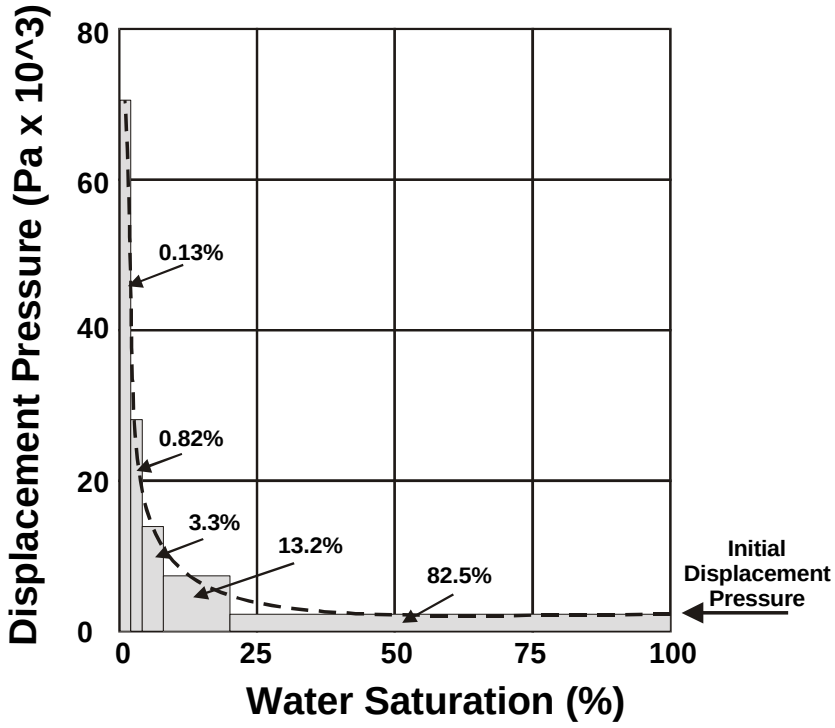

Figure 4.13 Displacement/pressure curves.

Note that once oil is in place, the operation of temperature and pressure may geochemically alter the properties of the mineral surfaces such that they become oil-wet. This occurs only in the presence of oil, so it can be imagined that a mature reservoir may have a mixed wettability, with water-wet small pores containing water and oil-wet larger pores containing oil. This has implications when we want to move oil and water through the rock during production.

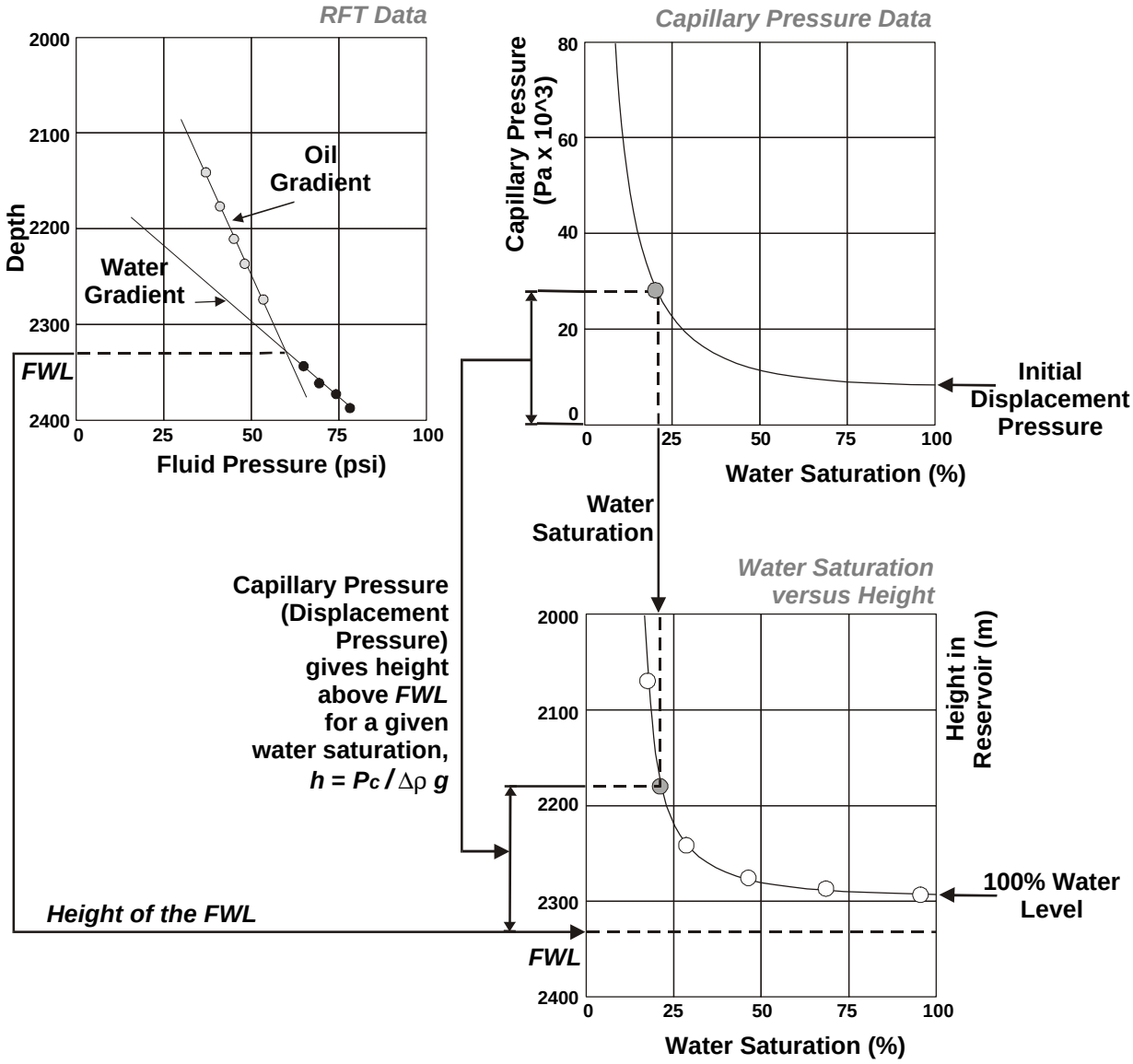

Figure 4.14 Calculation of water saturation in a reservoir.

The curve shown in Fig. 4.13 is continuous for a reservoir rock because the rock contains a continuous pore size distribution. This curve is called the *capillary pressure curve*. The capillary pressure curve describes the pressure required to displace from the rock a wetting fluid at initially 100% saturation to a given saturation.

The capillary pressure is related to the height above the *FWL* by the relationship

$$P_c = \Delta r \; g \; h \tag{4.8}$$

So, if the capillary pressure curve is known, and the *FWL* is known, we can calculate the water saturation at any point in the reservoir as in Fig. 4.14. If this water saturation agrees with the water saturations obtained from wireline tools and core in a given well, the wireline water saturation data can be used with confidence as a predictor of water saturation in the uncored sections of other wells in the same field.

4.6 The Measurement of Capillary Pressure Curves for Rocks

There are many ways of measuring capillary pressure curves in rocks. The most common are described below. A detailed description of these will be given in courses given later in the MSc course.

4.6.1 Porous Plate

The sample is saturated completely with a wetting fluid (usually water), and its effective porosity is measured. It is then placed on a porous plate in a pressure vessel. Gas or oil is introduced into the vessel around the sample at a low pressure (Fig. 4.15). The porous plate is constructed so that it will only let through water. The pressurized oil or gas displaces some of the water from the sample (throughout the whole sample) and the displaced water passes through the porous plate, whereupon it is collected and its volume is measured. The vessel is left at the set pressure until no more water evolves, which may take several days. The pressure of the gas or oil is then increased, and more water evolves and is measured. The procedure is repeated usually about 7 times at increasing pressures (e.g., 1, 2, 4, 8, 16, 32, 64 psi). A capillary curve can then be constructed with pressure versus the water saturation in the sample (Fig. 4.16).

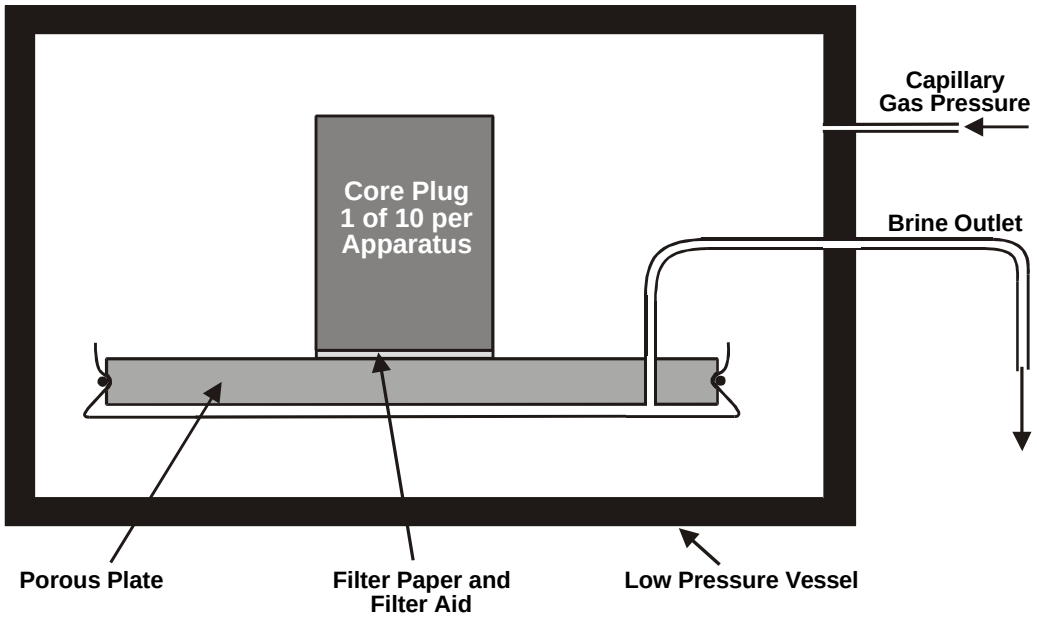

Figure 4.15 Porous plate capillary pressure measurement.

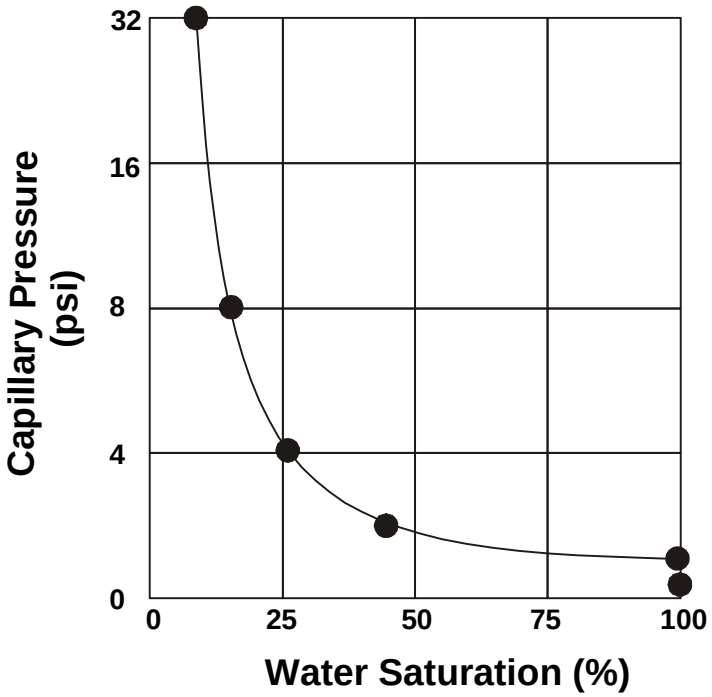

Figure 4.16 Capillary press curve from porous plate measurements.

The maximum pressure is limited by the pressure at which the porous plate begins to let the gas or oil pass through with the water.

There is also a range of specialized dynamic and semi-dynamic versions of the porous plate technique that can be used on confined cores together with direct measurement of sample fluid saturations using X-Ray, CT and gamma radiometric imaging techniques.

Advantages: Can use actual reservoir fluids for the measurements.
Accurate.

Disadvantages: Slow.
Only provides a few data points on the capillary pressure curve.

4.6.2 Centrifuge

The sample is saturated completely with a wetting fluid (usually water), and its effective porosity is measured. It is placed in a centrifuge and rotated at progressively higher speeds. The speed of rotation generates a centripetal force that displaces the wetting fluid from the sample replacing it with air or oil (if an oil reservoir is attached to the inside of the rotating sample). The volume of the evolved fluid is measured by collecting it in a graduated vial attached to the outside of the spinning arrangement, and read using a stroboscope. At slow rotation speeds, the force is only sufficient to displace water from the largest pores. At higher speeds the force is able to displace water from smaller and smaller pores in the sample. The pressures on the fluids can be calculated from an equation based upon the rotary motion of the centrifuge. This is plotted against the water saturation in the sample calculated from the measured volume of evolved fluids for each spin speed (Fig. 4.17).

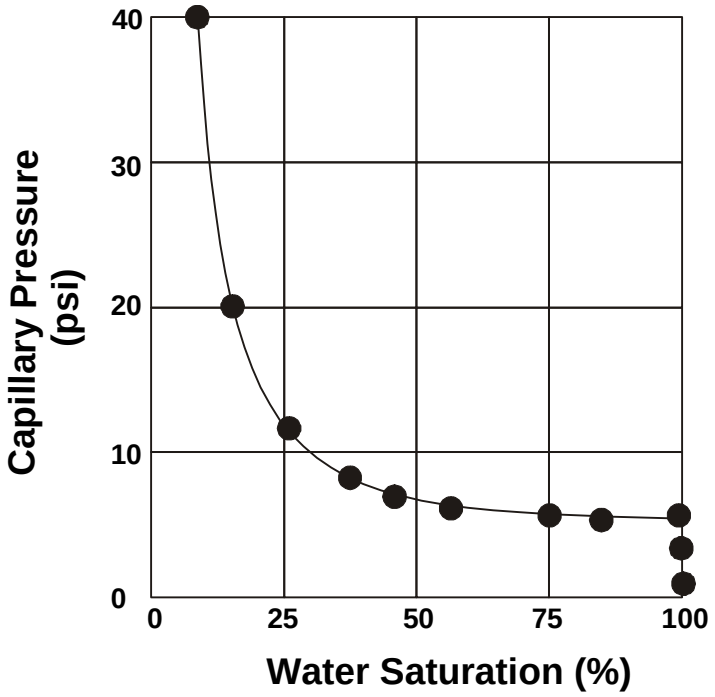

Figure 4.17 Capillary pressure curve from centrifuge measurements.

Advantages: Fast.

Disadvantages: Commonly only used with air as the displacing fluid.
Only provides a few data points on the capillary pressure curve.
As pressure is a function of distance from the spin centre, the fluid saturation across the sample varies, and the measured values are taken as the mean value.

4.6.2 Mercury Porosimetry

A dry sample of any shape, but of known weight, is placed in a chamber which is filled with mercury. The mercury is a non-wetting fluid and does not spontaneously enter the pores of the rock. This the bulk volume of the rock can be measured. The pressure on the mercury is increased in a step-wise fashion. At each step, the mercury enters smaller and smaller pores overcoming the capillary pressure operating against the non-wetting fluid (Fig. 4.18). At each stage the amount of mercury intruded is measured. A graph can be constructed of mercury pressure at each step against volume of mercury intruded. This is the capillary pressure curve. This data can also be inverted to provide the pore size and grain size distributions of the rock, and the raw data also provides a rough estimate of the connected porosity of the rock.

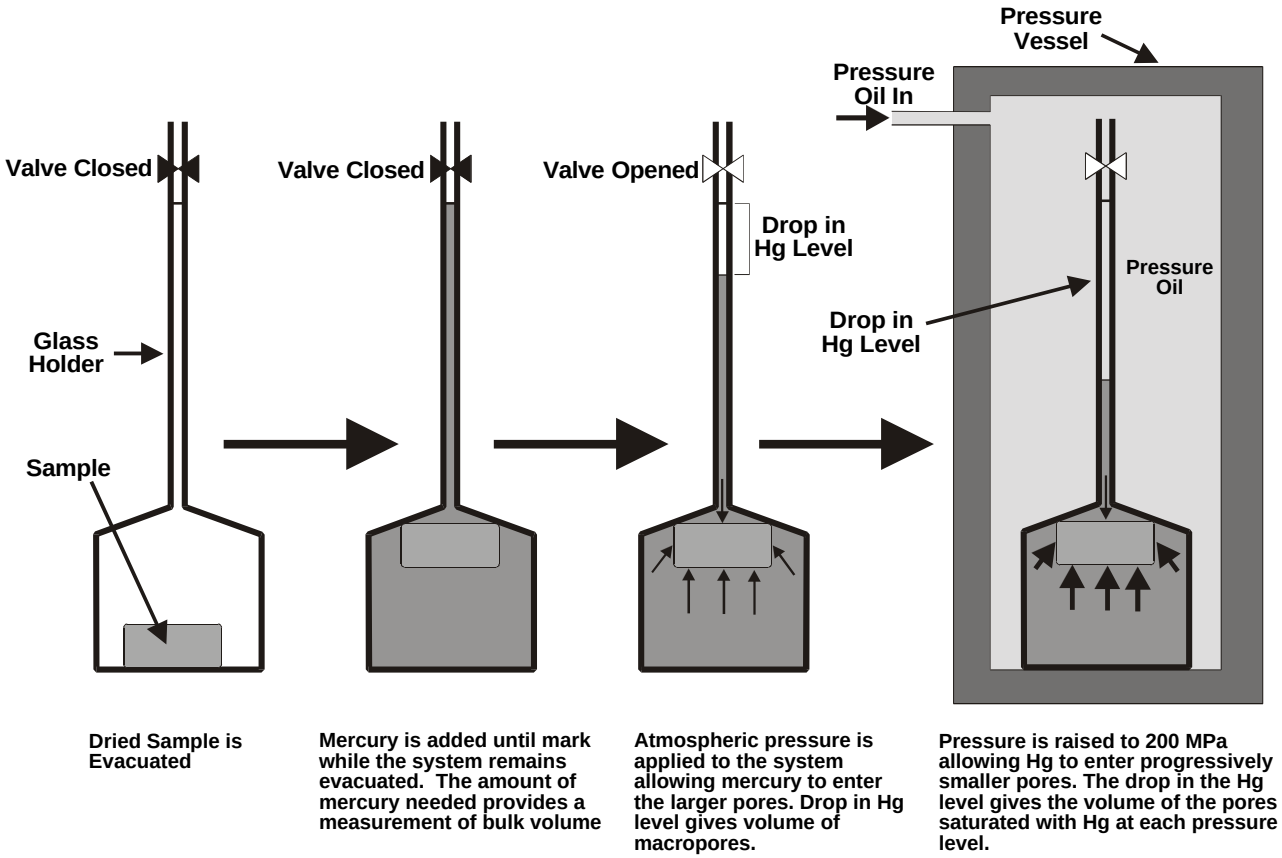

Figure 4.18 Mercury porisimetry.

Advantages: Fast.
Provides porosity of sample.
Provides pore size distribution.
Provides grain size distribution.
Can be used on small, irregular samples, such as cuttings.
Gives many data points for intrusion.

Disadvantages: Cannot be used with reservoir fluids.
Data must be corrected to give reservoir values.
Can only be used in imbibition cycle.

4.7 Capillary Pressure Data Correction

We require the capillary pressure curve for the reservoir fluids and the reservoir rock. Measurements, however, are generally made with other fluids. We must, therefore have a method for correcting the data to give the capillary pressure for the reservoir fluids. The corrections are simple and take account of the different interfacial tensions and wetting angles for different fluid combinations at 20°C only.

The measured capillary pressure for a mercury/air/sample system P_c(Hg/air/rock) is

$$P_c(\text{Hg/air/rock}) = \frac{2s\cos q}{R} = \frac{2\times 368\times 1}{R} \qquad \textbf{(4.9)}$$

The required capillary pressure for a oil/water/sample system P_c(oil/water/rock) is

$$P_c(\text{oil/water/rock}) = \frac{2s\cos q}{R} = \frac{2\times 35\times 1}{R} \qquad \textbf{(4.10)}$$

In both cases the values for interfacial tension and wetting angle come from Table 4.3. Since the value of R is the same whatever the fluids are, we can equate and rearrange Eqs. (4.9) and (4.10) to give

$$\frac{P_c(\text{Hg/air/rock})}{P_c(\text{oil/water/rock})} = \frac{368}{35} = 10.5; \quad \text{and} \quad \frac{P_c(\text{oil/water/rock})}{P_c(\text{Hg/air/rock})} = \frac{35}{368} = 0.09524 \qquad \textbf{(4.11)}$$

Similarly,

$$\frac{P_c(\text{Hg/air/rock})}{P_c(\text{gas/water/rock})} = \frac{368}{72} = 5.1; \quad \text{and} \quad \frac{P_c(\text{gas/water/rock})}{P_c(\text{Hg/air/rock})} = \frac{72}{368} = 0.1960 \qquad \textbf{(4.12)}$$

and,

$$\frac{P_c(\text{oil/water/rock})}{P_c(\text{gas/water/rock})} = \frac{35}{72} = 0.4861; \quad \text{and} \quad \frac{P_c(\text{gas/water/rock})}{P_c(\text{oil/water/rock})} = \frac{72}{35} = 2.057 \qquad \textbf{(4.13)}$$

Hence, to convert P_c(Hg/air/rock) to P_c(oil/water/rock) we should divide by 368 and multiply by 35 (i.e, multiply by 0.09524). Table 4.5 summarizes the conversions.

Table 4.5 Capillary pressure conversions.

From	To	Multiply by
Mercury/Air/Rock	Oil/Water/Rock	0.09524
Mercury/Air/Rock	Gas/Water/Rock	0.19608
Oil/Water/Rock	Mercury/Air/Rock	10.5
Oil/Water/Rock	Gas/Water/Rock	2.057
Gas/Water/Rock	Mercury/Air/Rock	5.1
Gas/Water/Rock	Oil/Water/Rock	0.4861
Note: This is only valid for 20°C		

These conversions are valid for the values of interfacial tension and wetting angle measured at 20°C and given in Table 4.3. However, these parameters change with pressure and temperature, and are therefore different in the sub-surface. Values of interfacial tension and wetting angle are very difficult to obtain for sub-surface conditions, and one might commonly have to make do with those at 20°C. However, sub-surface values should always be used when available as the interfacial angle is particularly sensitive to changes in temperature, with values as low as 10 dynes/cm for oil/water systems, and as low as 25 dynes/cm for gas water systems.

Many of the values in Table 4.5 are given to 4 significant figures accuracy. However, it is common for only two significant figures to be used (i.e., 10 for 10.5 and 5 for 5.1). This is often justified on the grounds that our knowledge of the values of interfacial tension and wetting angle is not accurate. The lack of accurate data introduces errors in any final calculations. However, noting that these inaccuracies occur is no excuse for introducing further voluntary inaccuracies by making such assumptions as using 10 instead of 10.5. The error introduced by this assumption can result in errors of millions of dollars on the bottom line.

Now we can convert mercury derived capillary pressure data to the capillary pressure for the reservoir fluids, we can write Eq. (4.8) in terms of the mercury capillary pressure.

$$P_c\left(Hg/air/rock\right) = 10.5 \times P_c\left(oil/water/rock\right) = 10.5 \times \Delta r\ g\ h \qquad \textbf{(4.14)}$$

and

$$P_c\left(Hg/air/rock\right) = 5.1 \times P_c\left(oil/water/rock\right) = 5.1 \times \Delta r\ g\ h \qquad \textbf{(4.15)}$$

These equations are very useful, because they allow the height in the reservoir for a given saturation to be calculated from capillary curves measured by mercury porisimetry, which is the most common capillary pressure technique practiced in the industry.

4.8 Fluid Distributions in Reservoirs

Capillary pressure curves can tell us much about the variation of saturations across a reservoir. The following example is taken from the personal notes of Theo. Grupping, and is a particularly good example.

In deltaic-type deposition sands may be laid down in fan-like bodies. The current that is responsible for the deposition is fast in the proximal region and becomes progressively slower as one progresses distally or laterally. Hence, in the proximal region the grain size of the resulting rocks is large (only large grains have time to fall from the fast current). Distally and laterally the grain size of the resulting rocks becomes finer as smaller sand particles have time to fall out of the slower current. Eventually, at the extreme edges of the fan, the current is so slow that very fine clay particles are also deposited, becoming interspersed with the fine sand grains.

- The proximal large grained clean sands have large pores and large pore throats. Therefore, they have small initial displacement pressures, and their water can easily be displaced by migrating oil.

- The distal fine grained clean sands have small pores and consequently small pore throats. They have higher initial displacement pressures, and their water cannot be displaced by migrating oil as easily as for the coarser grained rocks.

- The distal fine grained shaly sands (containing interspersed clay) have the smallest pores and consequently the smallest pore throats, and these pores and pore throats are blocked by the clay particles. They have very high initial displacement pressures; the great majority of their water is immobile and cannot be displaced by migrating oil. Figure 4.19 shows the results of 5 wells drilled progressively more distally in the same sub-marine fan.

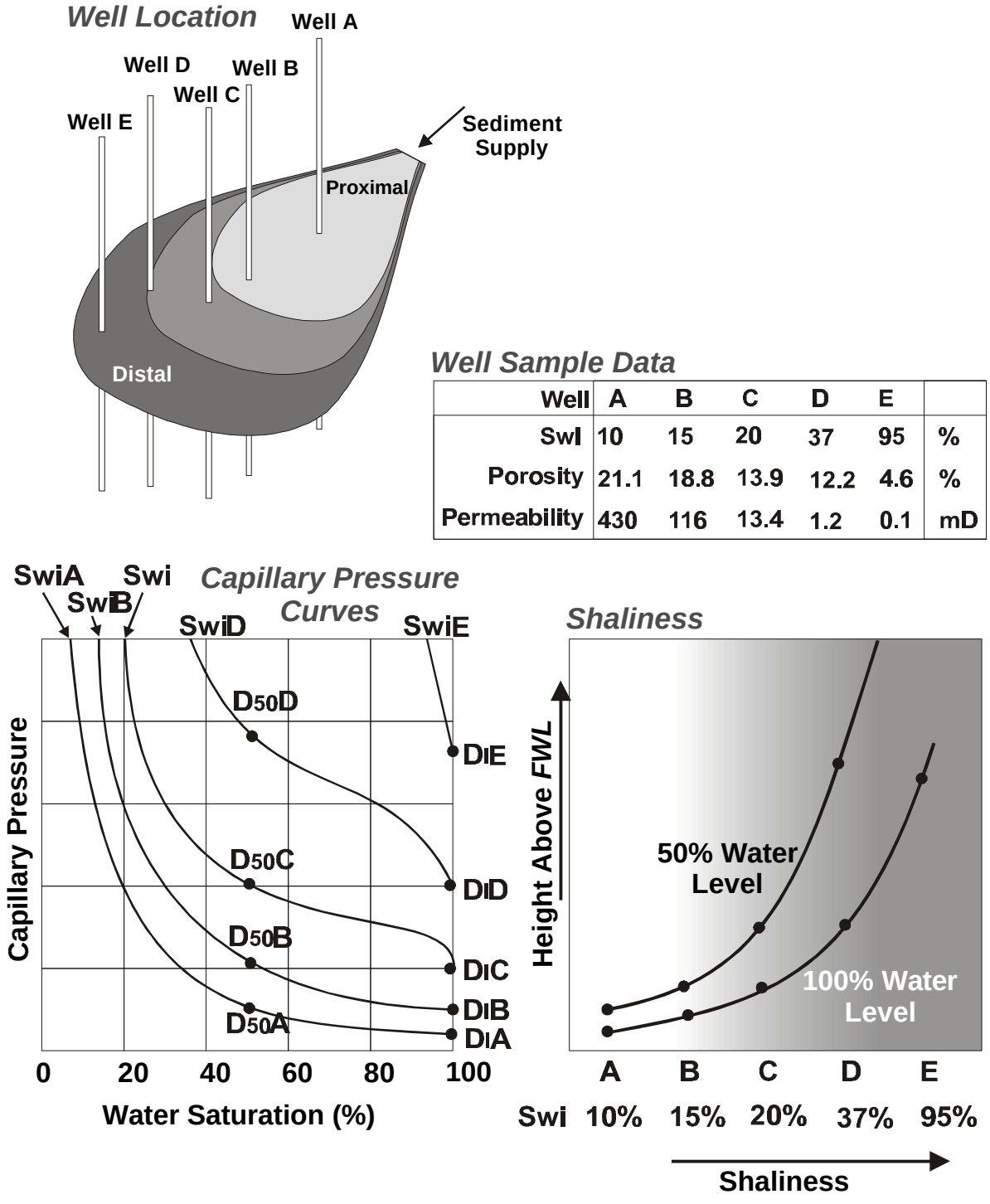

Well	A	B	C	D	E	
Swi	10	15	20	37	95	%
Porosity	21.1	18.8	13.9	12.2	4.6	%
Permeability	430	116	13.4	1.2	0.1	mD

Figure 4.19 Capillary pressure curves and facies.

The first part shows the fan geometry and position of the wells (labeled A to E). The second part shows the capillary pressure curves for each of 5 samples taken from each of the wells with the 100% water point labeled $S_{100}A$ to $S_{100}E$, the initial displacement pressure labeled D_IA to D_IE, the 50% water point labeled as $S_{50}A$ to $S_{50}E$, and the irreducible water saturation labeled $S_{wi}A$ to $S_{wi}E$. The third part shows the height above the free water level as a function of facies and water saturation, with the same saturation labels as in part 2. Note the following:

- The initial displacement pressure becomes greater as the sample becomes more shaly (finer grained) as one moves distally.
- The irreducible water saturation becomes greater as the sample becomes more shaly (finer grained) as one moves distally.
- The capillary pressure curve for the proximal samples are quite flat from 100% water to about 60% water indicating that only low pressures are required to replace about the first 40% of water with oil (in the largest pores with the largest and most accessible pore throats).
- At any given capillary pressure, more water is retained as the sample becomes more shaly (finer grained) as one moves distally.
- The height above the free water level of 100% water saturation increases as the sample becomes more shaly (finer grained) as one moves distally.
- The height above the free water level of 50% water saturation increases as the sample becomes more shaly (finer grained) as one moves distally.

So, the grain size controls the height of the 100% water saturation level. Now imagine four layers of sand that have different grain sizes, porosities and permeabilities, and that have become folded (Fig. 4.20). Each layer has its own capillary pressure characteristics associated with its grain size, and that capillary pressure is related to the height of the 100% water level above the free water level as shown. It can be seen that it is possible to drill through layers which are 100% water zones existing between oil or gas zones from the same reservoir. In this case Well C has two oil water contacts. It is the bottom one that is the true *OWC*. Because multiple *OWC*s are confusing, we tend to talk about *oil down to* (*ODT*) and *gas down to* (*GDT*) levels when there are multiple hydrocarbon/water contacts.

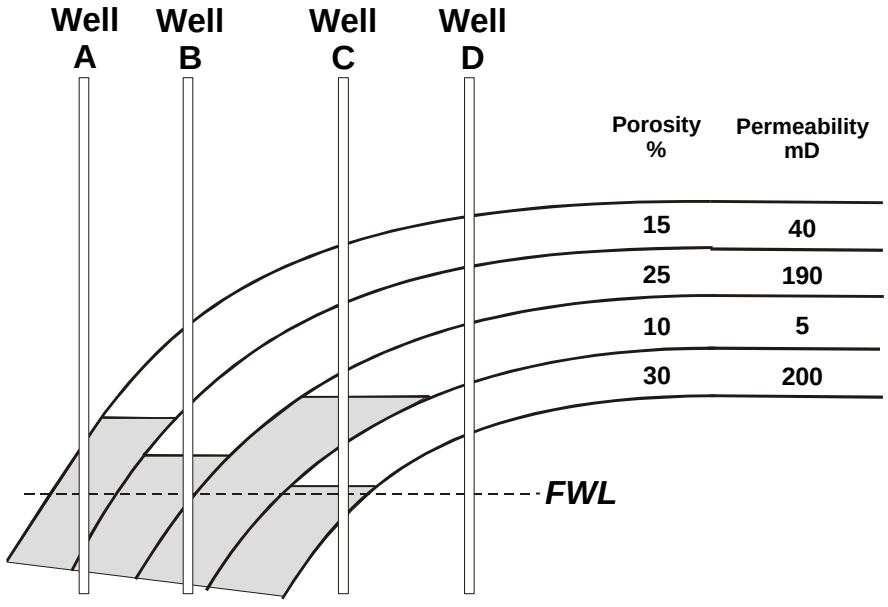

Figure 4.20 Suspended water zones.

5. WIRELINE LOGGING

5.1 What is a Wireline Log

A *log* is a continuous recording of a geophysical parameter along a borehole.

Wireline logging is a conventional form of logging that employs a measurement tool suspended on a cable or wire that suspends the tool and carries the data back to the surface. These logs are taken between drilling episodes and at the end of drilling. Recent developments also allow some measurements to be made during drilling. The tools required to make these measurements are attached to the drill string behind the bit, and do not use a wire relying instead on low band-width radio communication of data through the conductive drilling mud. Such data is called *MWD* (*measurement while drilling*) for simple drilling data, and *LWD* (*logging while drilling*) for measurements analogous to conventional wireline measurements. MWD and LWD will not be covered by this course, although the logs that are produced in this way have very similar characteristics, even though they have been obtained in a completely different way.

Figure 5.1 shows a typical wireline log. In this case it is a log that represents the natural gamma radioactivity of a formation. Note that depth is arranged vertically in feet or metres, and the header contains the name of the log curve and the range. This example shows a single *track* of data. Note also that no data symbols are shown on the curve. Symbols are retained to represent discrete core data by convention, while continuous measurements, such as logs, are represented by smooth curves. Figure 5.1 shows only 50 m of borehole, but real logs are often much longer (thousands of metres), and contain multiple curves on a single track such as this, and multiple tracks.

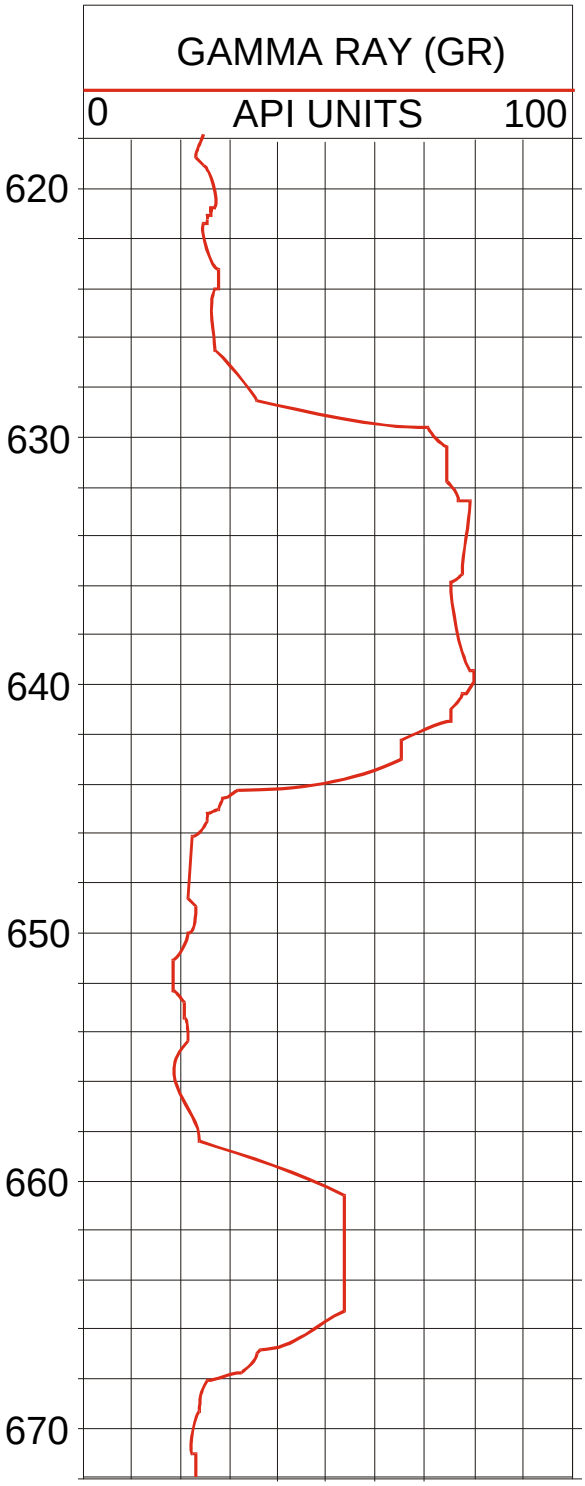

Fig. 5.1 Example of a Gamma Ray Log

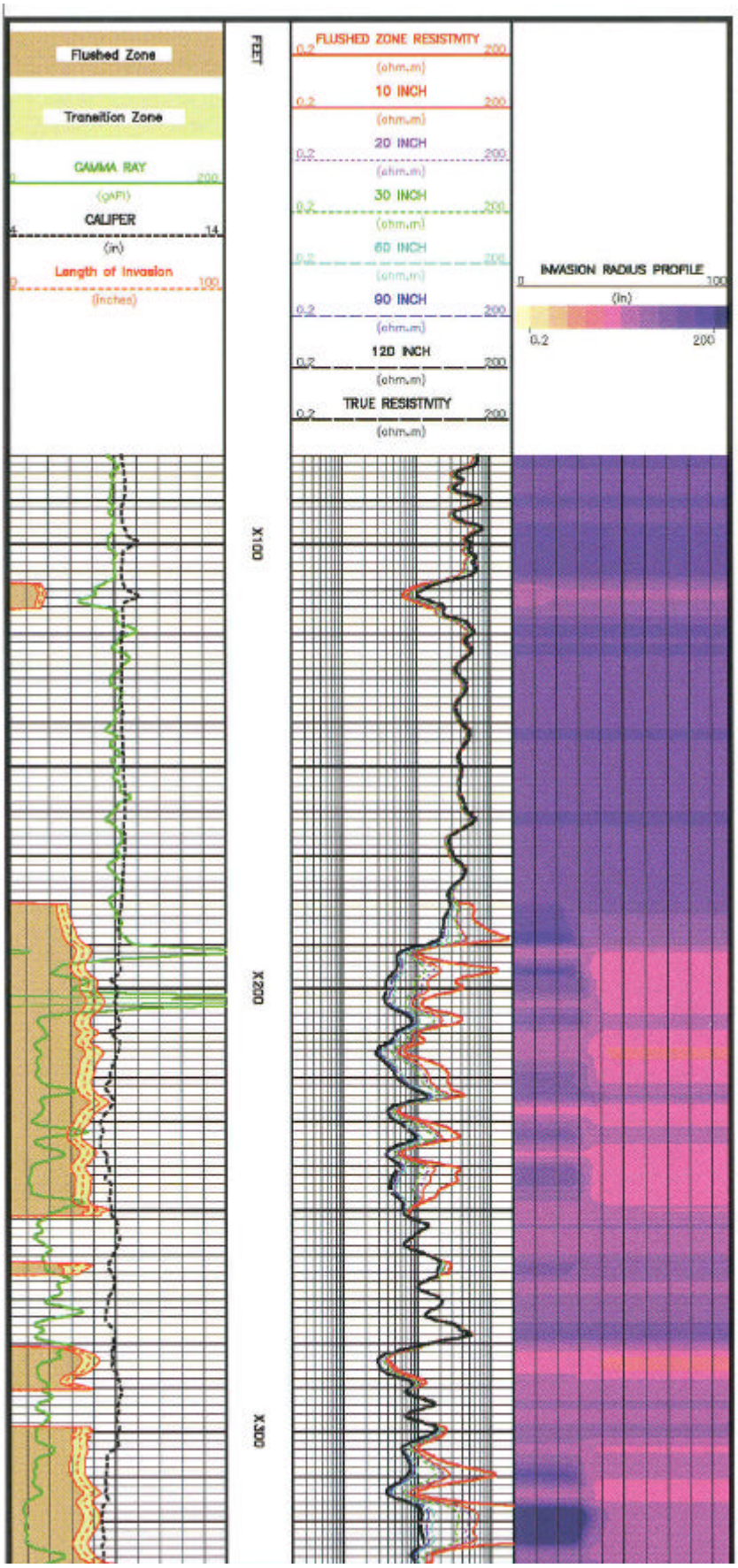

Figure 5.2 A typical log set

An example of a more usual log is given as Fig. 5.2. This log contains 3 tracks and many different sets of log data. There is a very large range of basic logs that can be run in a well, and an even greater number of derived logs, i.e., data that can be plotted in log form that is calculated from the basic logs.

Examples of the basic physical parameters that can be measured down-hole with logs include (a) the size of the borehole, (b) the orientation of the borehole, (c) temperature, (d) pressure, (e) the natural radioactivity of the rocks, (f) the acoustic properties of the rocks, (g) the attenuation offered by the rocks to radioactivity generated from the tool, (h) the electrical properties of the rocks, (i) the NMR characteristics of the rocks, and so on.

Examples of derived logs include (a) porosity derived from the sonic or density log, (b) water saturation calculated from the porosity and the electrical logs.

5.2 Running a Wireline Log

Oil companies require log data to assess the reservoirs that they are interested in. As with drilling, the oil companies contract out the job of making the wireline measurements to specialist companies, and increasingly these companies also complete much of the processing of the measured data. The two largest wireline companies are Schlumberger and Halliburton, although there is a range of smaller specialist companies too.

Wireline logs are made when the drill-bit is removed from the borehole. This can be either between drilling episodes, before casing is laid, or at the end of drilling. Wireline logging can be done when the newly drilled rock formations form the wall of the borehole (*open-hole logs*) or after a concrete lining or casing has been inserted to stabilize the well bore (*cased-hole logs*). However, as may be guessed, the quality of data from the rock is best from open-hole logs, and some measurements cannot be done at all through casing. Cased-hole logging requires special tools to optimize measurement through the casing, and is a specialist subject not covered by this course.

A wireline logging set-up consists of the wireline tool, the wire itself, a winching gear, and a vehicle containing data analysis and recording equipment. The vehicle is usually a large lorry (Fig. 5.3) for land-based measurements, or a transportable cabin for use on rigs (Fig. 5.4). All data recording and processing is now done digitally using powerful computers and array processors (Fig. 5.5).

The required tool is attached to the wire and lowered into a cleaned and stable borehole from which the drill string and bit has been extracted. When it reaches the bottom of the interval to be logged, it is slowly withdrawn at a predetermined speed. Log measurements are made continually during this process. The wire is made from a bundle of cables, the outermost ones of which are steel and carry the load, and the innermost of which are insulated copper and carry the electrical signals. The wireline is winched up the borehole by a motorized drum at speeds between 0.3 to 1.8 km/hr (1000 to 6000 ft/hr). It should be noted that all logs except one are run during their withdrawal from the borehole. The exception is the temperature log, which must be run on the way into the borehole because its presence in the hole disturbs the temperature reading.

The tension in the wire and the speed of the wire is constantly monitored using magnetic markers attached to the wire so that intermittently stuck tools can be detected. This information is used together with knowledge about the natural elasticity of the wire that causes it to stretch under its own weight to calculate the instantaneous depth throughout the logging phase.

Figure 5.3 Land logging vehicle

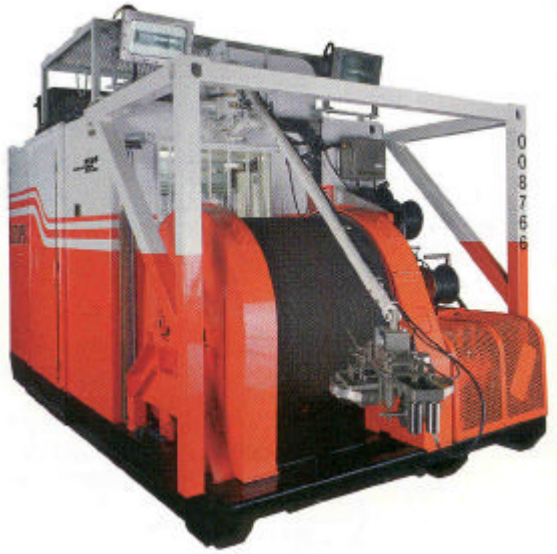

Figure 5.4 Offshore logging cabin

Figure 5.5 Inside the logging unit

Data is transmitted to the surface through the wire and recorded digitally. Modern tools sample the formation at intervals from 2.5 mm for the high definition imaging tools to about 15 cm for the simpler tools, so for a combination tool with several different logs, there may be as many as 100,000 individual measurements per metre over a log run of up to say 2000 m. Depending on the logging speed, data transmission rates may be as high as 200 kbits per second. This data is subjected immediately to a rudimentary analysis by powerful processors and displayed so that the quality of the measurements can be checked. The data is also recorded onto digital (DAT) tape and transmitted to the controlling office of the logging company by satellite for in-depth analysis.

A typical drilling and logging history for a well might be as shown in Table 5.1. Note that the logs are run in each section before casing takes place. When each log is run, the operator ensures that some measurements are included opposite the previously cased section above the log run as a test that the log tools are working correctly and to provide a local depth fixed point to help tie the depths for each tool together. Whenever a borehole is logged in sections the operator also ensures that there are overlap sections so that the logs can be tied together accurately, and repeat sections to check log quality and consistency.

Table 5.1 A typical drilling and logging history.

Procedure	**Drill Bit Size (inches)**	**Casing Diameter (inches)**	**Depth (m sub sea surface)**	**Tools**
Drill	25	-	300-400	
Case		20	300-400	
Drill	17.5	-	400-700	
Log	-	-	700-400	ISF-Sonic-GR/1
Case	-	13.375	300-690	
Drill	12.25	-	700-1400	
Log	-	-	1400-680	ISF-Sonic-GR/2
Log	-	-	1400-680	FDC-CNL/1
Log	-	-	1400-680	HDT/1
Case	-	9.625	690-1390	
Drill	8.5	-	1400-2100	
Log	-	-	2100-1380	ISF-Sonic-GR/3
Log	-	-	2100-1380	FDC-CNL/2
Log	-	-	2100-1380	HDT/2
Log	-	-	2100-1380	DLL/1

Note in Table 5.1 that the logs are recorded during the withdrawal of the tools from the well, that some tools were run several times at different depth intervals and that these runs have been coded consecutively, that there is an overlap of data, and that the lower log runs include part of the previous casing at their top. Note also that the most tools are run in the area that is expected to be of greatest interest (i.e., the reservoir). For tool codes see wireline operators manuals.

Efforts are made at all times to ensure that the logs are of the highest quality. Methods of ensuring that logging quality is high include (a) making repeat sections of log measurements over short sections that contain both low and high measured values, (b) making overlap measurements of the previous

(shallower) run of the same tool, (c) making measurements opposite the casing at the top of the run, (d) local calibration of all logging tools both before and after the survey, and (e) ensuring that a 'master' calibration of the tools has been carried out recently at the wireline service company's workshop (particularly for sensitive and important 'porosity' tools).

5.3 The Presentation of Log Data

Conventionally, logs are presented on a standard grid defined by the American Petroleum Institute (API). This grid consists of 3 tracks and a depth column as shown in Fig. 5.6.

Track 1 on the leftmost side is always linear and is often reserved for drill bit size, caliper and gamma ray tool information.

Moving to the right, there is a depth column that may be in feet or metres. A range of depth scales are used depending upon the resolution required for a particular analysis. In Europe and The East scales of 1:1000 and 1:500 are often used for large scale correlations between wells, while 1:200 is optimum for petrophysical evaluation, 1:40 for correlation with core information, and 1:20 for detailed dipmeter analysis. In the USA they use 1:1200. 1:600 and 1:240. However, the digital recording of logs now ensures that they can be displayed and printed at any required scale.

Moving once more to the right, there are tracks 2 and 3, which may have either a linear or a logarithmic scale and may be combined into one. These tracks traditionally were reserved for density, porosity and electrical tool data.

All tracks can take multiple log curves, and the code for the curve, its style (i.e., green dashed line), and the scale units are given in a stack at the top of the log. The curves are arranged in such a way that they can wraparound (i.e., if the curve slips of the top of the scale it appears again at the bottom, and the reader must make the required scale adjustments to read the wrapped-around data).

The fundamental basis of the API standard is still used, but the advent of computer analysis has made the presentation of logs rather easier. The modern log data is not first presented as hardcopy, but will come to you on a tape or CD-ROM. The arrangement of this data in the form of logs on a display or a printout is now likely to have as many tracks as 8 (its up to you!). Each will be linear or logarithmic, or even use a core image or a coloured array to represent the data. However the depth track is usually retained between tracks 1 and 2.

Electrical data is almost always presented on a logarithmic track because it can vary over many orders of magnitude.

There are numerous little markers and 'grace notes' present on logs that require to be learnt. The majority of these will be described with their particular log type. However, one general mark is that which records the time on the log. On Schlumberger logs, the right-hand margin of track 1 will often be seen to be punctuated by gaps. The distance between these gaps represents one minute and indirectly allows you to tell the logging speed. If these gaps are of uniform spacing, the logging speed is constant. If there is a non-uniformity, then there is a problem such as a temporarily stuck tool that could affect the data quality. Other companies use ticks or spikes along the margin as a time marker.

The main section of logs will have a comprehensive header sheet that contains a plethora of information about how the log was run. Some of this information also appears at the end of the logs, together with repeat or overlap sections and information on tool calibration.

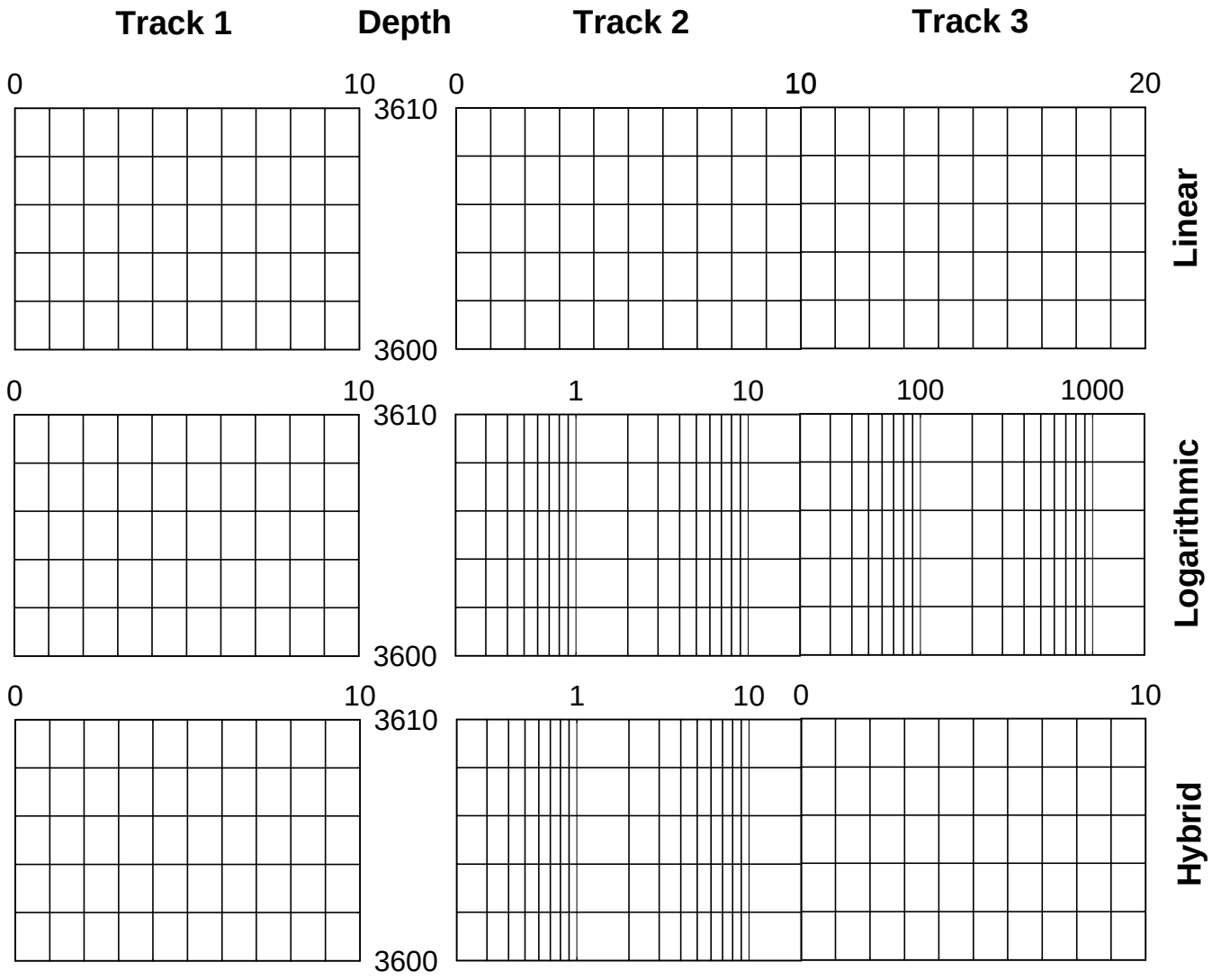

Figure 5.6 Log presentation grids. Note that the API format defines particular dimensions for each track, and an overall width of 8.25 inches.

5.4 Tools

There are a plethora of logging tools now available in the oil industry. There can be split into the following types:

- **Standard open-hole tools (diameter 3 to 4 inches)**
  These range from the simplest caliper tool to the sophisticated imaging and NMR tools and have vertical resolutions from 2.5 mm to over 30 cm.
- **Slim hole tools (diameter 1.6875 to 2 inches)**
  These are slimmer versions of the standard tools, and are used where standard tools are too thick. Applications of these tools are in specialist logging through drill-pipe or coiled tubing, and in small scale holes used in the water industry.

- **Cement-logging tools**
  These are special versions of those tools that work through cement casing that are optimized to work under these conditions.
- **Production tools**
  These are specialist tools for running during the production of hydrocarbons for measuring pressure and flow rate, and are always of the slim-hole variety to facilitate their insertion into a producing well.
- **LWD tools**
  These tools are designed to connect into the drill string and communicate data to the surface through the drilling mud.

A summary of some of the main standard open-hole tools is given in Table 5.2.

Drilling rigs are expensive and can often amount to almost 10% of the total drilling costs. The time required to run wireline logs effectively delays the drilling operation leading to greater expense. To minimize this expense tools are bolted together for lowering down the borehole. All wireline tools are designed to be combined in this way and there are many possible combinations, some which are as long as 30 m. Each tool in the combination has its own measurement-sensitive region, which measures a given formation at a specific depth at different offset times. The data has to be depth shifted to account for this. This is done in the data acquisition vehicle with information about the instantaneous speed and dimensions of the tool combination. Even using combinations, it is common for as many as three log runs to be made in the same section of the borehole with different combinations of tools. If this is the case, one tool is included in all combinations to act as a reference to which the others might be compared for depth matching purposes. This tool is commonly the gamma ray tool (GR).

Figure 5.7 shows an example standard open-hole logging tool. Note that it is a neutron porosity tool, which is combined with a gamma ray tool. The loops at each end cover screw threads to enable it to be combined with other tools of similar design.

On land, where the general geology is well known and drilling is cheaper, only a few logs may be run. This is because expense can be spared as information concerning the subsurface is not hard to come by. However, and perhaps counter-intuitively, offshore a full set of logs is often carried out even when there are no hydrocarbon shows. This is because drilling is so expensive that relatively fewer wells will be drilled, and hence the maximum data must be squeezed out of each well regardless almost of the cost. If there are no hydrocarbon shows, the well data will still be very useful for correlation with other wells that do show hydrocarbons, will help to constrain the extent of neighbouring reservoirs, as well as adding to the information about the general geological structure of the area.

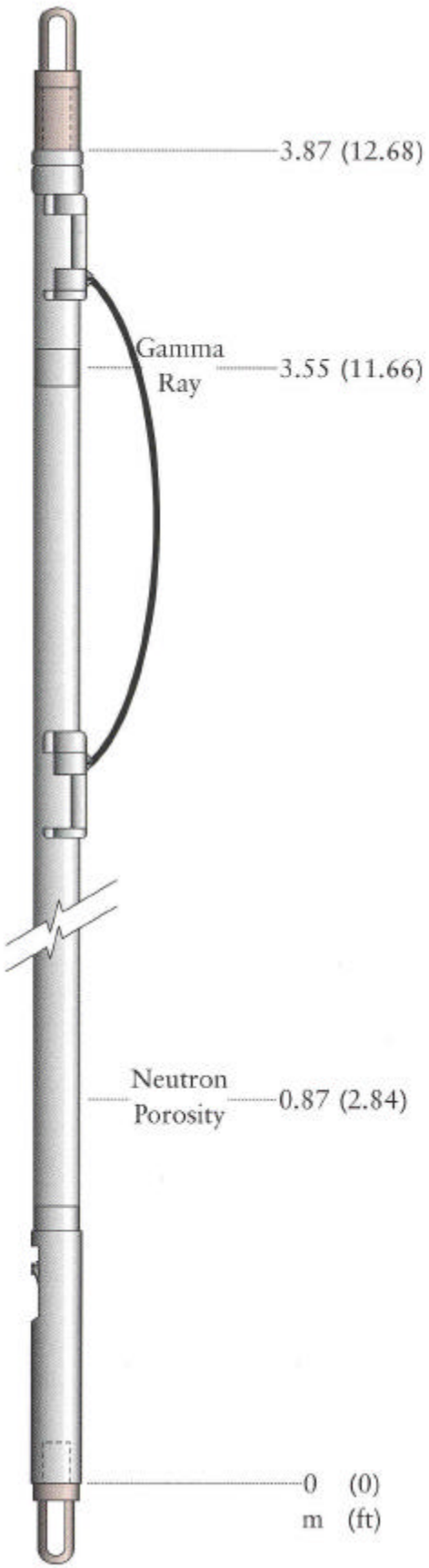

Figure 5.7 A Compensated Neutron Sonde (CNS)

Length	3.87 m (12.68 ft)
Diameter	95 mm (3.74 in)
Weight in air	109 kg (240 lb)
Range	-3 to 100 lpu
f Resolution	Better than 0.05 pu at 20 pu
Vert. Resolution	750 mm (30 in)
Investigation Depth	260 mm (10.2 in)

Table 5.2 Common open-hole tools and their uses

Tool	Physical Measurement	Use	Comments
Logging conditions			
Temperature (BHT)	Temperature	Borehole temperature for resistivity calculations.	Corrected with Horner plot
Pressure (PRESS)	Fluid pressure	Fluid pressure for formation volume factor calculations.	Incorporated in RFT
Caliper (CAL)	Borehole diameter	Data quality, in situ stress tensor, lithology and permeability indicator	Available in 2, 4, or multi-arm versions.
Lithology			
Gamma Ray (GR)	Natural radioactivity of the formation.	Shale indicator and depth matching	Can read through casing.
Spontaneous Potential (SP)	Sand/shale interface potential.	Permeable beds Resistivity of formation water	Does not work in conductive muds, or offshore.
Porosity			
Sonic (BHC, LSS)	Velocity of an elastic wave in the formation.	Effective (connected) porosity	Compaction, gas and vugs, calibration of seismic data.
Density (FDC, LDT)	Bulk density of the formation.	Total porosity	Used to calculate synthetic seismograms.
Neutron (SNP, CNL)	Hydrogen concentration in the formation.	Total porosity (shale increases measured porosity, gas reduces measured porosity)	Can read through casing.
Resistivity			
Simple electric log (SN, LN, Lat)	Resistivity of flushed, shallow and deep zones respectively.	Used in water saturation calculations.	Now obsolete, not focussed, can't be used in oil based muds, prone to invasion.
Induction Logs (IES, ISF, DIL, DISF, ILm, ILd)	Conductivity of the formation.	Conductivity and resistivity in oil based muds, and hence calculation of water saturation.	Focussed devices. Use in oil based and fresh water muds. Range of depths of investigation. (Vertical resolution 5-10 ft.)
Laterologs (LL3, LL7, DLL, LLs, LLd)	Resistivity of the formation.	Resistivity in water based muds, and hence calculation of water saturation.	Focussed devices. Use in salt water based muds. Range of depths of investigation. (Vertical resolution 2-4 ft.)
Microlog (ML)	Resistivity of mudcake and flushed zone.	Indicator of permeability. Detector of thin beds.	(vertical resolution about 1 ft.)
Micro-laterolog (MLL)	Resistivity of flushed zone.	Measures R_{XO}	Not good with thick mudcakes.
Proximity Log (PL)	Resistivity of flushed zone.	Measures R_{XO}	Not good if invasion is small.
Micro-spherically focussed log (MSFL)	Resistivity of flushed zone.	Measures R_{XO}	Part of DLL-R_{XO} tool.
Imaging Logs There is a range of imaging logs based upon sonic, visual, electrical and NMR measurements that are beyond the scope of this course.			

6. THE BOREHOLE ENVIRONMENT

6.1 Introduction

Wireline logging has a single clearly defined purpose: to give accurate and representative data on the physical properties of the rock formations and fluids encountered in a borehole.

The tools used to take these readings have to cope with extremely tough conditions downhole, particularly, high temperatures and pressures, inhospitable chemical conditions and the physical constraints imposed by the physics of the measurements and the borehole geometry. It should also be remembered that we are interested in the properties of the rocks in undisturbed conditions, and the act of drilling the borehole is the single most disturbing thing that we can do to a formation.

6.2 Overburden Pressures

The formations in the sub-surface are at raised pressure, and are occupied by fluids which are also at high pressure.

The pressure that a rock is subjected to at a given depth is determined by the weight of the rock above it, and hence the density of that rock. This is called the *overburden pressure* or sometimes the *lithostatic pressure* (note that, to a first approximation, the overburden pressure is the same in all directions (*isotropic*)). We can write an equation to describe the overburden pressure

$$P_{over} = \rho_{rock}\ g\ h \tag{6.1}$$

where, P_{over} = the overburden pressure at depth h
ρ_{rock} = the mean rock density above the depth in question
g = the acceleration due to gravity
h = the depth to the measurement point.

Clearly the rock above a given depth will have a varied lithology and porosity and hence a varying density. A more accurate determination of the overburden pressure can be obtained by summing the pressure contributions for each density by writing Eq. (6.1) for i different rock densities, each with thickness h_i.

$$P_{over} = \sum_i (\rho_i\ g\ h_i) \tag{6.2}$$

The overburden pressure/depth curve is called the *geobar* or *lithostat*. An example is given in Fig. 6.1.

It should be noted that in actuality this pressure is not isotropic but operates vertically. The pressures horizontally depend upon the overburden pressure, but are modified by additional large scale sub-horizontal tectonic forces (in tension and compression), and are affected by local inhomogeneities in the crust, such as fractures. However, to a first approximation the pressure at depth can often be considered to be isotropic (hydrostatic).

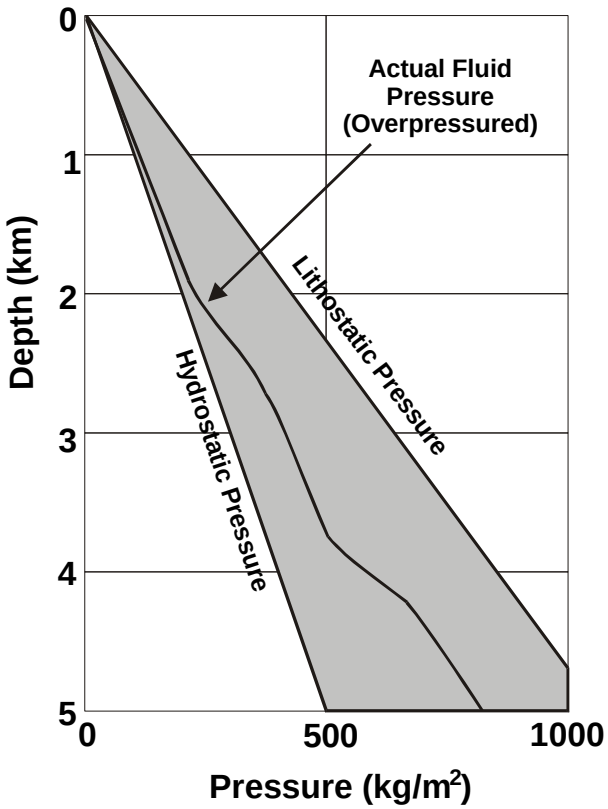

Figure 6.1 Lithostatic, hydrostatic and overpressures.

6.3 Fluid Pressures

The pressure in a fluid occupying a formation depends upon many forces. If there is a continuously connected pathway of fluid from the surface to the depth in question, the fluid pressure depends primarily upon the weight of the fluid above it, in a direct analogy to the situation for rocks. As the density of fluids is approximately one third of that for rocks, the fluid pressure will be approximately one third of the overburden pressure at any given depth.

$$P_{fluid} = r_{fluid}\, g\, h \qquad \textbf{(6.3)}$$

where, P_{fluid} = the fluid pressure at depth h
r_{fluid} = the mean rock density above the depth in question
g = the acceleration due to gravity
h = the depth to the measurement point.

Clearly the fluid in the rock above a given depth may have a varying density, hence a summed equation may be better at describing the fluid pressure at depth. The connected fluid pressure is called the *hydrostatic pressure* and is shown in Fig. 6.1.

Clearly, the fluids will not always be in good connection with the surface, and indeed this will generally not be the case in reservoirs, where a seal is required to stop the hydrocarbons escaping. In these conditions the fluid pressure may be much higher than that predicted by Eq. (6.3). These fluids are called *overpressured* fluids (Fig. 6.1). Overpressurization is caused by a trap to stop fluids escaping, and a process that will raise the fluid pressure such as compaction of the rock.

However, the fluid pressure is also affected by other forces. These are capillary pressure, buoyancy forces (if the fluid is dynamically driven by a density gradient), and externally imposed fluid flow forces from aquifers.

6.4 Effective Pressure

The overburden pressure acts upon a rock to crush it. The fluids in the pore spaces would then be compressed. Hence, the fluid pressure acts on the rock to stop the rock crushing. The fact that the rock does not crush under the overburden pressure, is the combined result of the inherent strength of the rock grains and any cementation, and the strengthening effect of the fluid pressure. A total effective pressure may be defined, therefore, as the pressure that the rock effectively experiences. The *effective pressure* is the overburden pressure minus the fluid pressure. (Note there is increasing evidence that it is better to define effective pressure as the overburden pressure minus about 80% of the fluid pressure.)

The extraction of hydrocarbons in a reservoir ultimately lowers the fluid pressure, and hence raises the effective pressure experienced by the rock. Thus there may be occasions where, what was once stable reservoir rock, now is exposed to a greater effective pressure, and begins to crush and compact. This is currently occurring in several reservoirs in the North Sea, and causes huge problems for wellbore and platform stability.

6.5 Drilling Muds

Drilling muds are used for at least three reasons:

- To lubricate the drill bit.
- To remove drilled material away from the drill bit and transport them to the surface.
- To counteract the fluid pressure in the rock.
- Stabilize the wellbore.

If a well could be drilled without a drilling fluid, formation fluids, which are under their fluid pressure, would spurt out of the borehole (*blow-out*). The density of the drilling fluid used in a particular borehole is designed to generate a drilling mud pressure (due to the weight of the drilling mud in the borehole above a given depth) that counteracts the fluid pressure in the formation and prevent blow-outs. This is usually successful, but because sudden increases in overpressure can be encountered the drilling mud pressure is kept higher than necessary as a safety feature. When the mud pressure is greater than the formation fluid pressure, the well is said to be *over-balanced*.

Note that varying the drilling mud weight also helps to protect the wellbore from crushing by the high lithostatic forces, especially in deviated and horizontal wells.

The drilling mud is a suspension of mud particles (a slurry) in an aqueous or oil-based medium. Each of these will be discussed in more detail later in this section.

6.6 Invasion

6.6.1 Introduction

The drilling mud is at a pressure greater than the fluid pressure in the formation. When the drilling mud encounters a porous and permeable formation, the drilling mud will flow into the formation under the influence of this difference in fluid pressures. This is called *invasion*. However, the particulates in the mud will be left at the surface, with the rock acting as an efficient filter. Thus, there is a build-up of mud particles on the inner wall of the borehole, and this is called the *mud cake*. The remaining liquid part of the drilling mud enters the formation, pushing back the reservoir fluids. This part of the drilling mud is called the *mud filtrate*. The zone where the mud filtrate has replaced the reservoir fluids is called the *flushed zone* and there is a zone further into the rock where the replacement of reservoir fluids with mud filtrate is incomplete, which is called the *transition zone*. The Virgin reservoir fluids occupy the *uninvaded zone* further into the formation.

Figure 6.2 shows the general borehole environment with invasion.

Note that invasion only occurs for porous and permeable formations, and is a self limiting process because the mud cake is an efficient block to further filtration and flow. However, there is a qualitative relationship between low porosity and high permeability, and larger depth of invasion and thicker mud cake. High permeability formations admit the mud filtrate easily, so the invasion is deep and the mudcake builds up quickly to thick layers. High porosity formations allow the storage of more mud filtrate per invasion distance, therefore the depth of invasion is smaller than for low porosity formations of the same permeability.

The different fluid types in each of the zones, and hence the formations that they occupy, will have different physical properties. Only the deepest zone contains the circumstances of the undisturbed rock, while the wireline tools occupy the borehole. Thus, to get good readings of the true sub-surface properties of the rock, the tool has to either, (i) measure accurately through the borehole mud, mud cake flushed zone and transition zone, or (ii) make readings closer to the tool (i.e., in the flushed zone) that can be reliably corrected to represent the values in the uninvaded zone.

All wireline companies provide correction graphs for their various tools. However, the accuracy of the correction diminishes as the diameter of the borehole, the thickness of mud cake, and the depth of invasion increase. Effort is therefore made to ensure that these are minimized by (i) ensuring the mud is sufficiently saline to avoid wash-outs increasing the borehole diameter, (ii) ensuring that the mud is not so low salinity that it causes the swelling of formation clays, (iii) minimize mud filtrate, and (iv) set the mud weight such that the mud pressure is only slightly greater than the formation pressures (only slightly *over-balanced*).

One simple method of checking for invasion is by measuring the loss of drilling fluids. This is done regularly at the wellsite for water-based drilling muds by forcing samples of drilling mud through filter paper with a 100 psi pressure for 30 minutes and measuring the volume of the mud filtrate. For oil-based muds a high temperature apparatus is required as the filtration of oil-based muds is low at surface temperatures. While mudcake is a useful indicator of porous and permeable formations, it can cause the drill-bit, drill-pipe and wireline tools to stick in the hole, and the associated deep invasion causes problems for accurate wireline data acquisition.

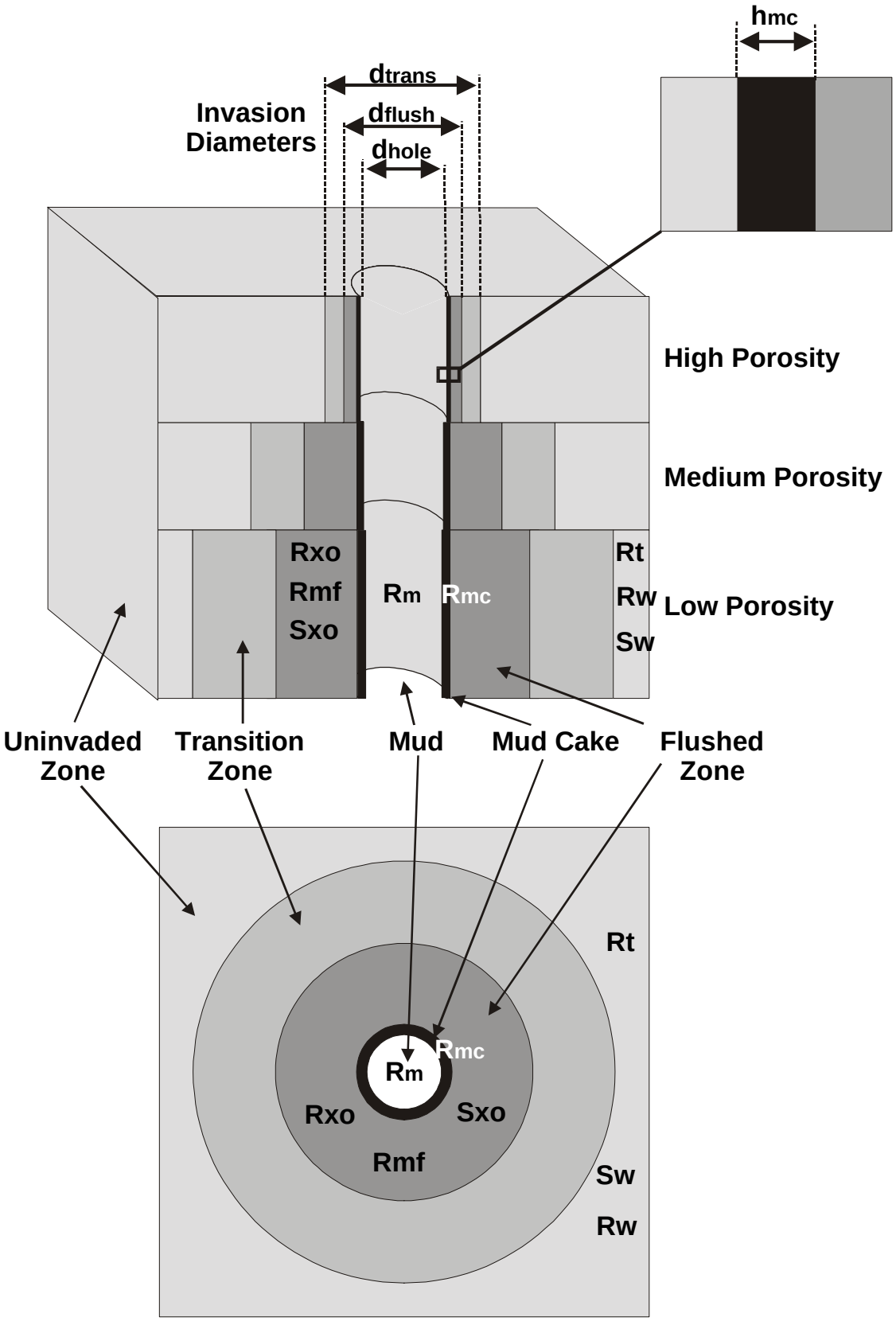

Figure 6.2 The borehole environment.

6.6.2 Invasion with Water-Based Drilling Muds

The depth of invasion is related to the permeability of the rock. The water-based mud filtrate diffuses into the formation water in the rock at a rate that depends upon the pore size distribution and hence the permeability of the rock. This diffusion can be faster than the rate of filtration at the borehole wall in highly permeable formations. Thus the invasion is limited by the rate of filtration, and the build-up of mudcake stops the process limiting the depth of invasion. For lower permeability formations, the diffusion is slower but reaches a greater depth (Fig. 6.3). The replacement of oil by the water-based mud filtrate is by pressure driven displacement.

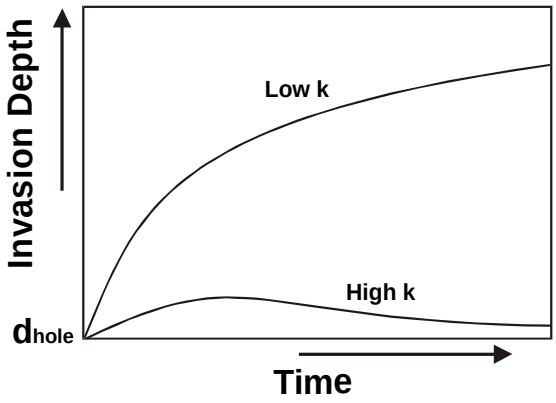

Figure 6.3 Effect of time and permeability on invasion depth for water-based muds.

In water-bearing formations the mud filtrate replaces all of the formation water close to the borehole (Fig. 6.4) and this decreases with depth of invasion. In oil-bearing formations the mud filtrate replaces all the formation water and most of the oil close to the borehole wall, again decreasing with distance into the formation (Fig 6.4).

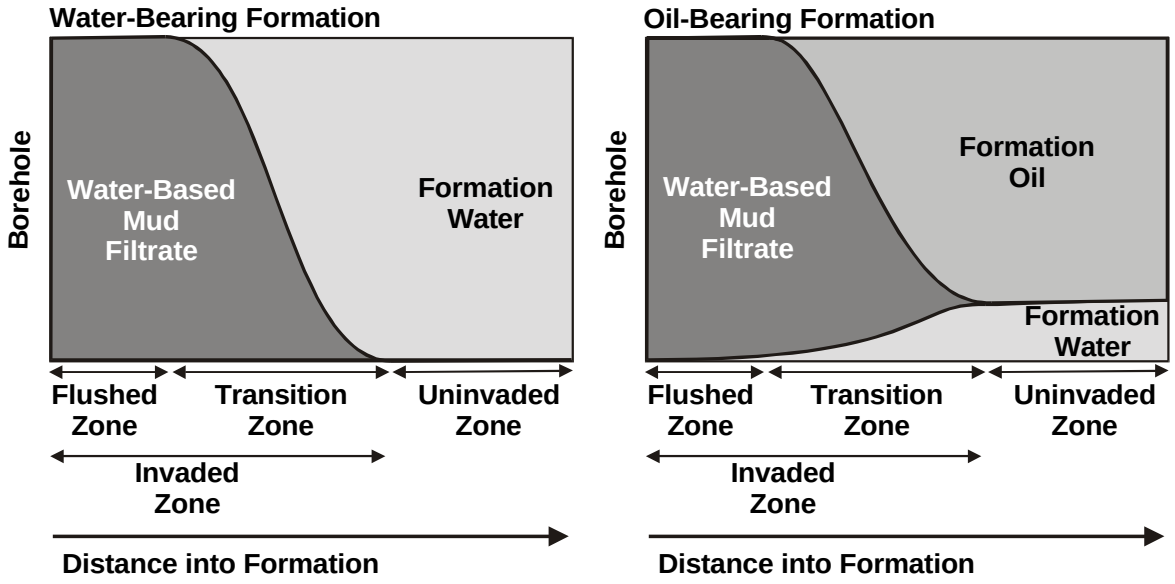

Figure 6.4 Invasion profiles for water-based muds in water and oil bearing formations.

6.6.3 Invasion with Oil-Based Drilling Muds

Oil-based mud filtrates replace the fluids in the invaded zone by pressure driven displacement alone. The resulting invasion profiles are shown in Fig. 6.5. Note that in water-bearing formations the oil-based mud filtrate does not replace all the formation water even close to the borehole wall, and that in oil-bearing formations the oil-based mud filtrate only replaces the oil in the formation, leaving the formation water in place.

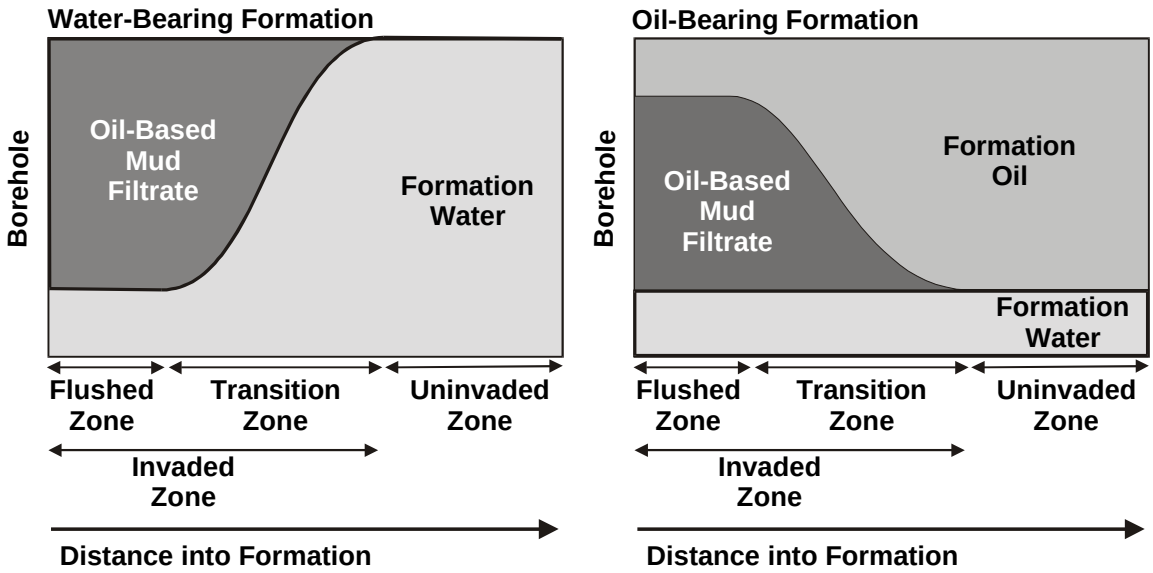

Figure 6.5 Invasion profiles for oil-based muds in water and oil bearing formations.

6.6.4 Fluid Segregation

In general, the fluids in the invaded zone are formation water, water or oil-based mud filtrate and oil in various saturations. These have different densities, and so may undergo gravity driven fluid segregation resulting from their relative buoyancies, if the vertical permeability of the formation is sufficiently high. While this may seem like a subtle effect, it is not uncommonly seen on wireline log data. The effect is well developed in the following two scenarios, which are shown in Fig. 6.6.

Drilling oil-bearing formations with salt saturated water-based muds. The high density salty mud filtrate accumulates at the bottom of the formation resulting in a resistivity profile that has lower resistivities at the base of the formation than at the top.

Drilling water-bearing formations with oil-based drilling muds. The low density oil-based mud filtrate accumulates at the top of the formation, again resulting in a resistivity profile that has lower resistivities at the base of the formation than at the top.

These effects usually disappear with time after the casing is set and cemented, remaining only if the permeability of the formation is very low.

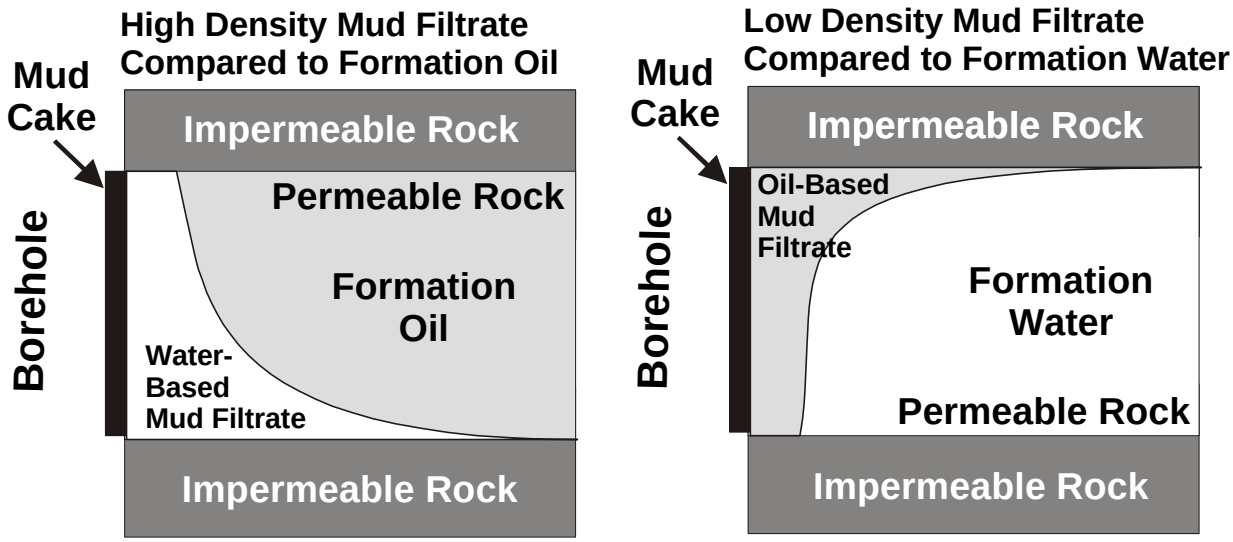

Figure 6.6 Gravity segregation during invasion.

6.7 Logging Tool Characteristics

Each of the logging tools has particular characteristics that depend upon the physics of the measurement of their particular parameters, and upon the borehole environment. These will be covered in the sections on the individual logging tools.

The main characteristics affecting log quality are:

Depth of Investigation. Most tools have a shallow depth of investigation, resulting in the measurement of the formation in the flushed or transition zones. Most radiation tools have an investigation depth of less than 0.5 m because they rely on measuring natural or induced radiations that are adsorbed by the rock or the fluids they contain. Electrical tools come in various versions with a wide range of investigation depths, from the micro-tool, which measure only the mud cake (a few centimetres), to the deep penetration tools (up to 5 m). The depth of investigation often depends upon the density/porosity of the formation.

Vertical (Bed) Resolution. This is closely related to the depth of investigation and to the logging speed. In general a tool with a large depth of investigation, has a low vertical resolution. The true parameters of the rock formation can only be measured if the bed is larger than at least the source-detector distance of the tool. An electrical log with a source-detector distance of 2.5 cm, has a bed resolution of about 7.5 cm, while a deeply penetrating induction log with a source-detector distance of 1 m can resolve usually only down to about 3 m. It is a reasonable rule of thumb to triple the source-detector distance on the tool to get the minimum bed resolution in ideal conditions. If the beds are thinner than the bed resolution for the tool, then the measured parameter is underestimated. This is the *thin-bed effect*.

Investigation Geometry. This depends upon the tool. Some tools have a pseudo-hemispherical zone of sensitivity (the radiation logs), some toroidal (the induction logs), some tubular (acoustic logs), and some focussed planar (the laterologs). The raw data that is measured depends very much upon the geometry of the measurement, but these effects are corrected for by the wireline logging company as standard.

Logging Speed. The speed at which the logs are run has an effect upon the quality of the data as a result of statistical fluctuations in the measured radiation in the case of radiation tools, and as a function of the measurement (sampling) interval in other tools. It can therefore be seen that logging speed, data quality and vertical resolution are linked.

7. FLUID TESTING AND PRESSURE LOGS

7.1 Introduction

Formation fluid testing involves taking fluid samples from the formation and measuring their pressures. It gives information on the types and properties of fluids in the formation, indicates the presence of hydrocarbons, and provides information on the pressures of the fluids within the formation.

There are three generic types of test, the second of which will be examined in detail as it is a wireline method. The three measurement types are as follows, and are described in the order that they are performed, in their complexity, and therefore their cost.

Drillstem testing. This is carried out during the drilling of the well. A portion of perforated drill pipe and one or two devices for sealing the interval of the well of interest off (*packers*) are lowered down the well to the required depth. The packer is then expanded to make a seal between the borehole wall and the drill pipe. If the bottom of the well is being tested, only one packer is needed. If an interval further up the well is being tested, two packers are needed, one above the interval and one below. A valve is then opened to reduce the pressure within the drill stem and the packed-off interval to surface pressures. Fluids will flow from the formation into the packed-off interval and hence to the surface through the perforations in the drill pipe and up the pipe. These fluids may be sampled and analyzed. Note that this procedure is the equivalent of a temporary completion of the well. (Fig. 7.1).

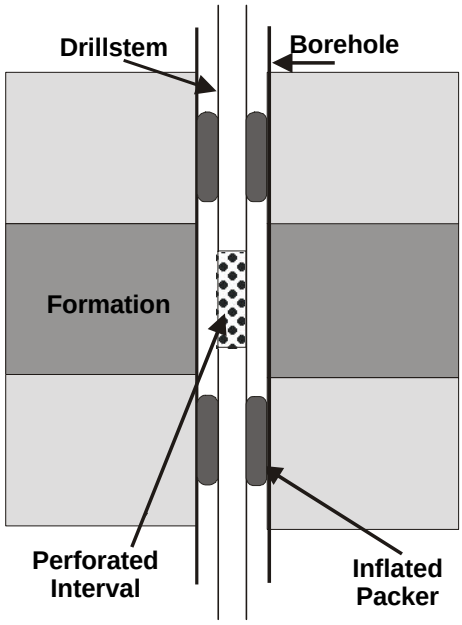

Figure 7.1 The drillstem test.

Wireline formation testing (*RFT*). This operation is carried out in an open hole during wireline logging operations. The wireline tool is lowered down the uncased hole to the point of interest. It is then jacked and sealed against the borehole wall. Samples of fluids and measurements of the fluid pressures are then taken. Note that this form of logging is not continuous, and is carried out at a few previously defined depths in the reservoir zone of the well only (Fig. 7.2).

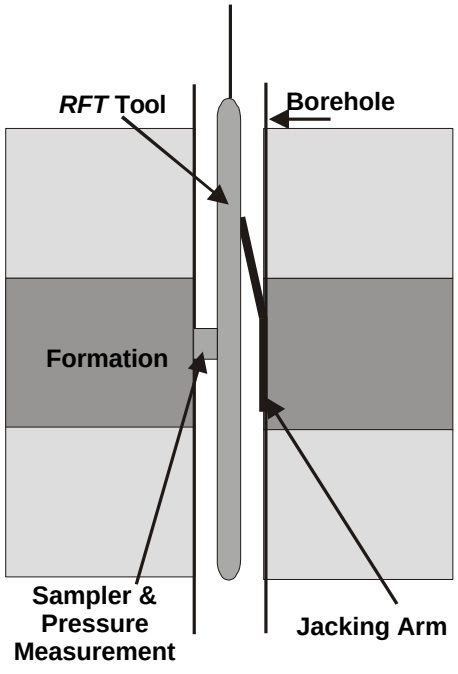

Figure 7.2 The RFT test.

Production Testing. This is carried out in a cased hole and completed hole with a packer that has been set in place and a production pipe. The casing is perforated using a wireline perforation gun. As the pressure inside the production pipe is held at a value that is lower than the formation pressure, the formation will produce fluids, which by this stage in the well completion, should be hydrocarbons. If the test produces sufficient hydrocarbons, the production may be allowed to continue as a fully completed well (Fig. 7.3).

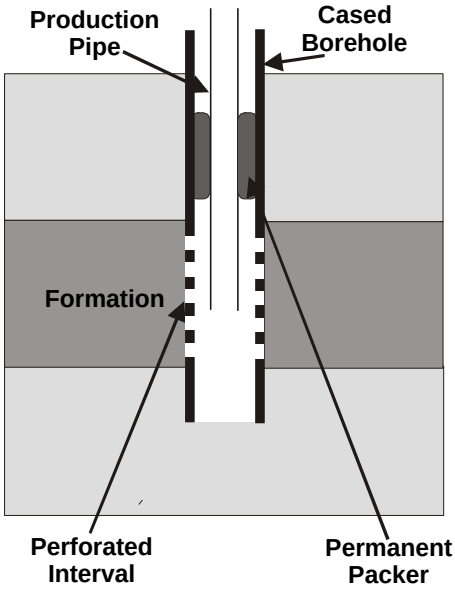

Figure 7.3 The production test.

7.2 Wireline Formation Testing

There are a range of wireline formation testing tools now available, such as the *Repeat Formation Tester* (*RFT*), *Repeat Formation Sampler* (*RFS*), shown in Fig. 7.4, and the *Formation Multi-Tester* (*FMT*). These tools are capable of taking multiple samples of fluids and pressure measurements in the borehole without withdrawal. These testers can mix the fluids sampled from several *settings* in one chamber, or take two separate samples and keep them separate. Fluids can be maintained at high pressure, which is important in some volatile oils as a sudden pressure drop causes a change in the composition of the oil. Time is saved by the tools incorporating a pre-test facility, where the seal between the probe and the rock formation is tested and an adequate flow of fluids for sampling is checked. If either of these is not the case, the tool can be reset at another depth for another try. This facility also enables the first part of the sample (mud filtrate) to be stored separately from the latter part of the fluid sample (reservoir fluids), or enable the first part to be ignored, so that the sample reliably samples only the reservoir fluid. The tools can cope with consolidated and unconsolidated formations, and provide very accurate fluid pressure readings. The tools also require very little time between runs for *re-dressing* the tool, i.e., unloading the sampled fluids and preparation for the next run.

By comparison, older tools (the *Formation Interval Testers, FIT*) had a range of problems including low pressure accuracy, bad sealing, mixed sampling of mud filtrate and reservoir fluids, were not operable in unconsolidated formations, and required one run per sample with a long re-dressing time between runs.

It should be noted that even with the newer tools, the RFT is expensive to use if many fluid samples are required, as only two separate samples can be obtained on each run. Hence, RFT fluid samples are expensive.

7.3 Operation

The tool is run into the well to the depth required, which is recognized by comparing the gamma ray readings from a gamma ray sensor attached to the tool with previously taken logs. In this way an

accurate depth may be fixed. Initially the tool takes a reading of the drilling mud pressure. The tool is then attached securely to the wall of the borehole, by a jacking device known as a *back-shoe* on one side of the tool. Opposite the back-shoe is the measurement and sampling head. This consists of an annular seal or packer surrounding a sampling probe which contains a piston. Figure 7.5 shows details if the back-shoe and sampling head for the *RFT* device. A similar, although much more cleanly designed arrangement applies in the case of the *RFS* in Fig. 7.4. The packer seals the sampling head from the drilling mud and mud-cake surrounding the tool (Fig. 7.6a). The probe containing the piston is then pressed through the mud-cake into the formation (Fig. 7.6b). The piston is withdrawn, allowing fluids to pass from the formation into the tool (Fig. 7.6c). This fluid is made to enter a chamber (first pre-test chamber) through a special valve that limits the flow rate to about 60 cm^3/min. The sampling pressure is measured. When the first chamber is full, it is closed-off and a second pre-test chamber is filled at a higher rate (150 cm^3/min), while measuring the fluid pressure. When this chamber is full the flow-line fluids are at the same pressure as the fluids in the formation, and this pressure is measured. Figure 7.7 shows the internal piping of the tool.

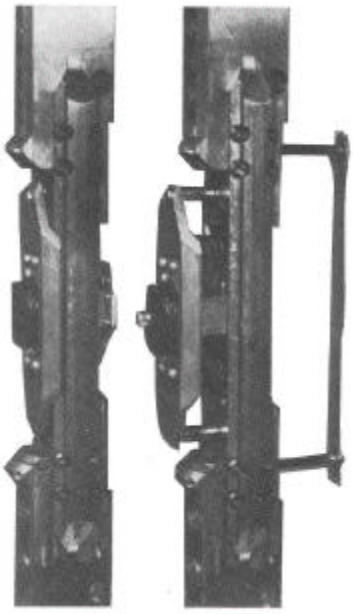

Figure 7.5 The *RFT* tool. (Courtesy of Schlumberger)

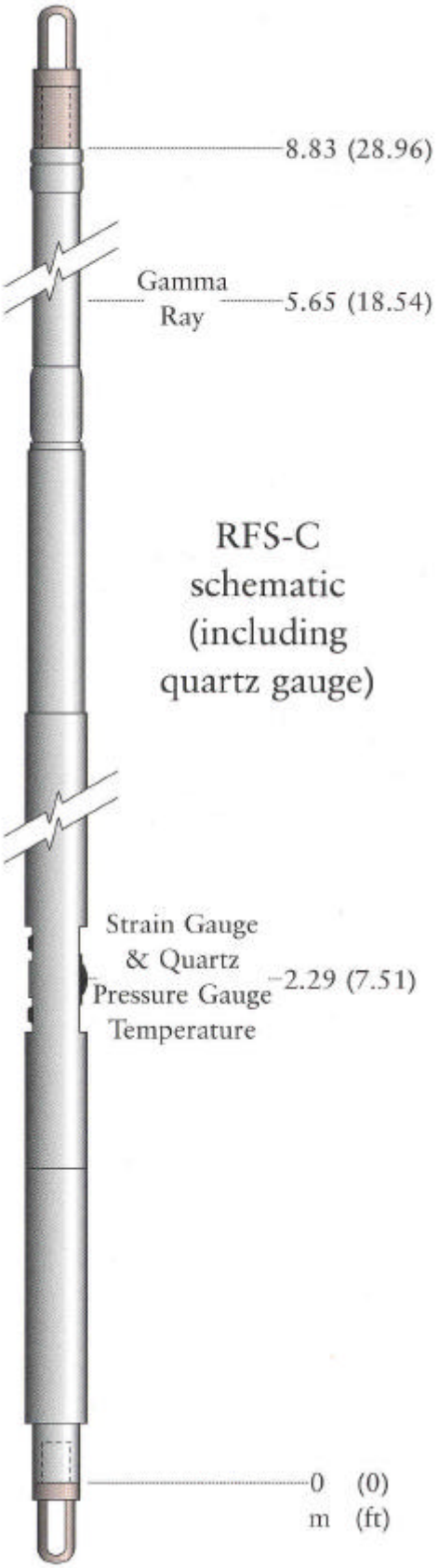

Figure 7.4 The *RFS* tool. (Courtesy of Reeves Wireline Ltd.)

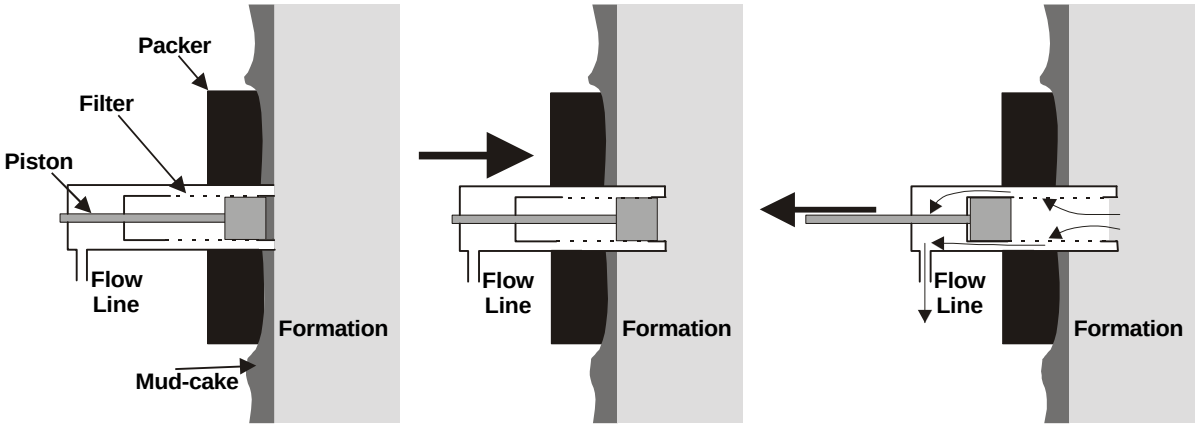

Figure 7.6 RFT operation.

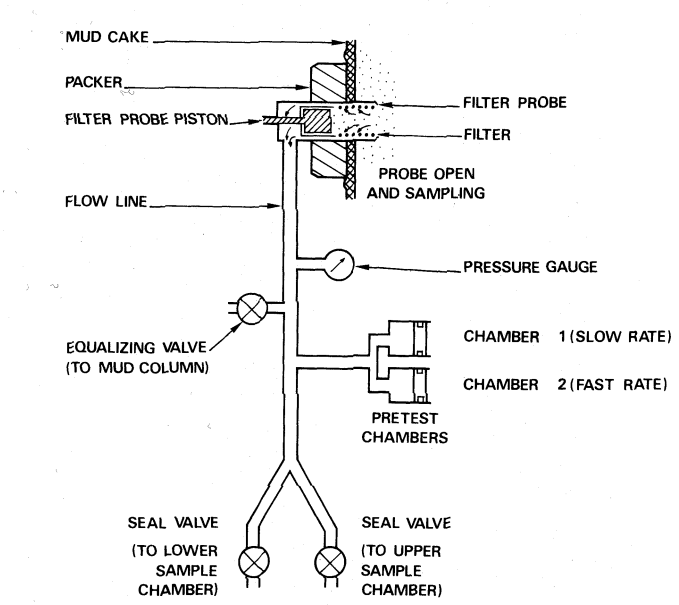

Figure 7.7 RFT internal piping.

Up to now, only pressures have been measured, and there are two pre-test samples in the pre-test chambers. The measured pressures give an indication of the productivity of fluids from the test depth. Since, there are only two main sampling chambers in the tool for operational samples, these samples are precious. It may therefore be decided that the tool should not take an operational sample, but move on to another depth. If this is the case, the pre-test chambers are emptied into the borehole, the back-shoe is retracted, the drilling mud pressure is re-recorded, and the tool moves on to another depth. If an operational sample is required, one of two valves to two chambers is opened so that fluid flows into a chamber. The fluid sample is commonly between 5 and 20 litres. Once the sampling chamber is full, the valve is closed. Note that the fluids are sealed in the sampling chamber at reservoir pressures. If another sample or more pressure data is required from further depths, the pre-test chambers are emptied and the tool progresses. Finally, the tool is removed with both its sampling chambers full, and having taken a number of pressure readings at sampled or unsampled depth points.

The samples are usually sent to a specialist laboratory where the compositions, physical properties and relative volumes of oil, gas, mud filtrate, and formation water can be measured.

7.4 Analysis of Pressure Measurements

A typical *RFT* recording of pressures from one depth is shown in Fig. 7.8.

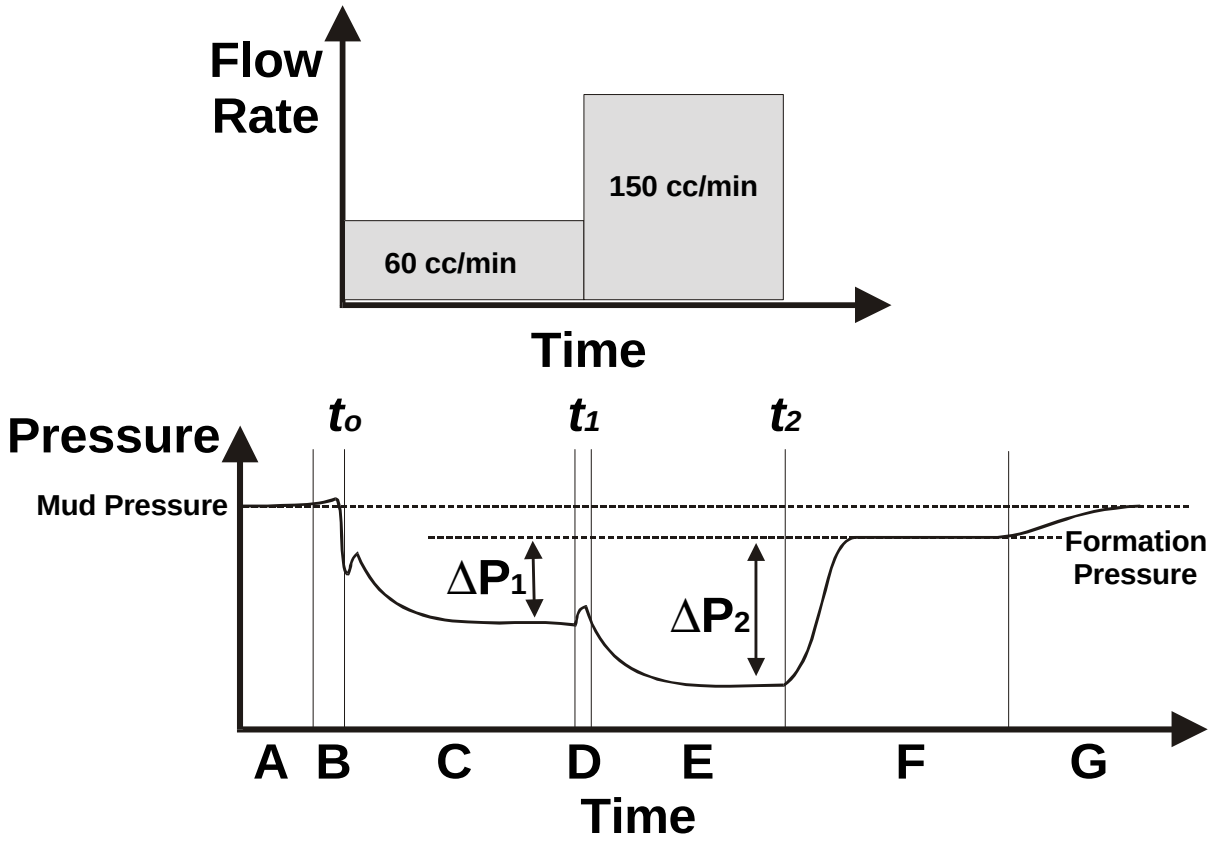

Figure 7.8 RFT pressure data.

The hydrostatic pressure is that of the drilling mud, and is recorded while the tool is at the required depth, but has not been pressed against the wall by the packer (A). This is constant for a given depth in the borehole, and depends upon the weight of the column of mud above it. As the mud density is generally known, this value can be calculated and compared with the measured value.

When the probe penetrates the mud-cake, some mud is compressed between the probe and the formation wall, leading to a transient pressure increase (B).

The piston is open, and fluid flows into pre-test chamber 1 at 60 cm^3/min. The pressure drops because an additional volume has been added to the system (the chamber). The pressure pushing the fluid into the chamber is ΔP_1 (C). There may be some variation in the pressure behaviour here as the flowing fluid is a mixture of mud-cake particles, mud filtrate, and formation fluids of different flow characteristics. When the chamber is approaching full the measured pressure begins to increase towards the formation pressure again (D).

However, the second chamber is opened up, and the pressure once again drops because fluid now flows at 150 cm^3/min into the second chamber. The pressure pushing the fluid into the chamber is ΔP_2 (E).

When both chambers are full the measured pressure increases towards the formation pressure, which may take some time for low permeability formations (F).

After the pressure measurement, the back-shoe is retracted and the mud pressure is measured again (G).

Note that the pre-test chambers have a low volume (about 20 cm^3). Hence, the fluid flowing into these chambers is most likely mud filtrate. However, the pressure that is recorded is the true formation pressures, as this is the pressure driving the mud filtrate into the chambers.

Several problems may occur. The most common are:

A Tight Test. If the sample is very impermeable the sampling pressure drops to near zero. In this case it will take too long to obtain a pressure reading and the tool may stick in the borehole.

Stuck Tool. Usually when the tool has been set at a given depth for some time.

Plugging. Sand grains from the formation may enter the tool and block the flow lines, especially in unconsolidated samples. This problem is reduced by the filter in the sampling probe, but fine grains may still get through.

Seal Failure. If the packer fails, the drilling mud will be sampled and the mud pressure will be recorded.

7.5 Log Presentation

The pressures are given in analogue and digital form. Track 1 usually contains the analogue pressure data. Tracks 3 and 4 are divided into 4 sub-tracks that contain the pressure data in exploded form:

Subtrack 1. Pressures from 0 to 10000 psi in 1000 psi increments.
Subtrack 2. Pressures from 0 to 1000 psi in 100 psi increments.
Subtrack 3. Pressures from 0 to 100 psi in 10 psi increments.
Subtrack 4. Pressures from 0 to 10 psi in 1 psi increments.

The sum of all four digital tracks is the same as the analogue data. A typical RFT log for one depth is given as Fig. 7.9. Note that the vertical scale is in TIME not in DEPTH.

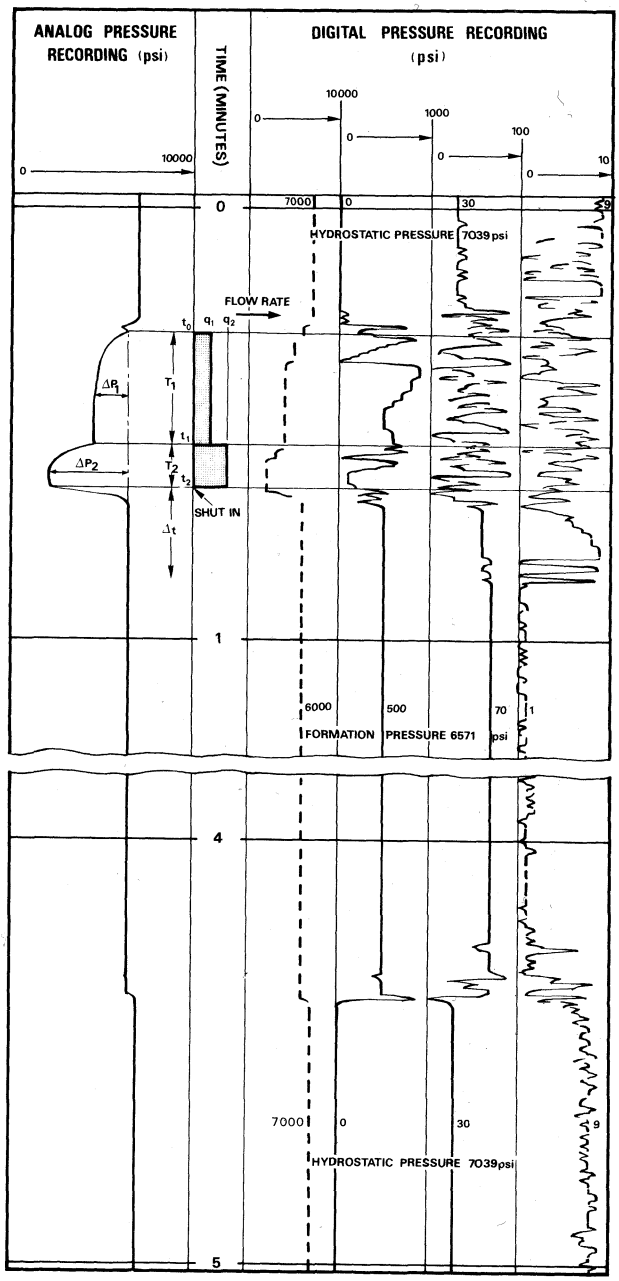

Figure 7.9 An example RFT pressure log. (Courtesy of Schlumberger.)

7.6 *RFT* Data Interpretation

The pressure data obtained from *RFT*s are very useful as they enable judgements to be made about the position of the free water level (*FWL*), oil-water contact (*OWC*), and the gas-oil contact (*GOC*). Additionally, it gives information about compartmentalization, or whether the various fluids in a reservoir are separated physically by an impermeable barrier.

If we have several (>4 say) fluid pressure measurements at different depths in an fluid-bearing sand, where the fluid is in good connection throughout the interval, we can calculate the pressure gradient in the formation fluid. All the pressures should lie on the straight line which defines the pressure at a given depth as a function of the depth and the density of the fluid.

$$P = P_o + r_{fluid}\, g\,(z - z_o) \quad \textbf{(7.1)}$$

where: P_o = the fluid pressure at depth z_o
P = the fluid pressure at depth z
r_{fluid} = the density of the fluid
g = the acceleration due to gravity.

This is applicable to all fluids (gas, oil or water) providing that the fluid in question is continuously connected throughout the interval.

A plot of pressure on the *x*-axis against depth on the *y*-axis is used to interpret reservoir pressures as shown in the following sections. This simple equation and the pressure versus depth plot allows us to examine a large range of possibilities that might occur in a reservoir. It can be seen from the pressure depth plot that the gradient of the line $G = 1/r_{fluid}\, g$, hence the density of the fluid represented by a line $r_{fluid}=1/(9.81\times G)$.

7.6.1 Oil and Water

Referring to Fig. 7.10, the four oil pressures in Sand A determine the oil pressure line according to Eq. (7.1), and by fitting this equation to this pressure depth data, we can calculate the density of the oil.

The six water pressures in Sand B determine the water pressure line according to Eq. (7.1), and by fitting this equation to this pressure depth data, we can calculate the density of the water.

Note that the gradient of the lines is steeper for fluids of lower density. If one has pressure data, but does not know the type of fluid, then one may infer it from the relative gradients on the pressure/depth plot, or calculate the densities (gas very low, oil 0.5 to 0.9 g/cm^3, water about 1 g/cm^3). The intersection of the two lines is the likely free water level, providing Sand A and Sand B are connected. Sand B may be oil-bearing up-dip.

7.6.2 Gas, Oil and Water

Referring to Fig. 7.11, the four gas pressures in Sand A determine the gas pressure line according to Eq. (7.1), and by fitting this equation to this pressure depth data, we can calculate the density of the gas.

The data in Sand B do not form one straight line, but two. The higher is for oil and the lower for water. The densities of each can be calculated as above. The intersection of the water and oil lines is the free water level, as in the previous example. Note that this is about 2.5 m below the known oil water contact *OWC*.

If Sand A and Sand B are in communication, the intersection of the gas line with the oil line gives the gas oil contact (*GOC*). If they are not in communication, the *GOC* is controlled by the impermeable barrier, and might be anywhere between the two sands.

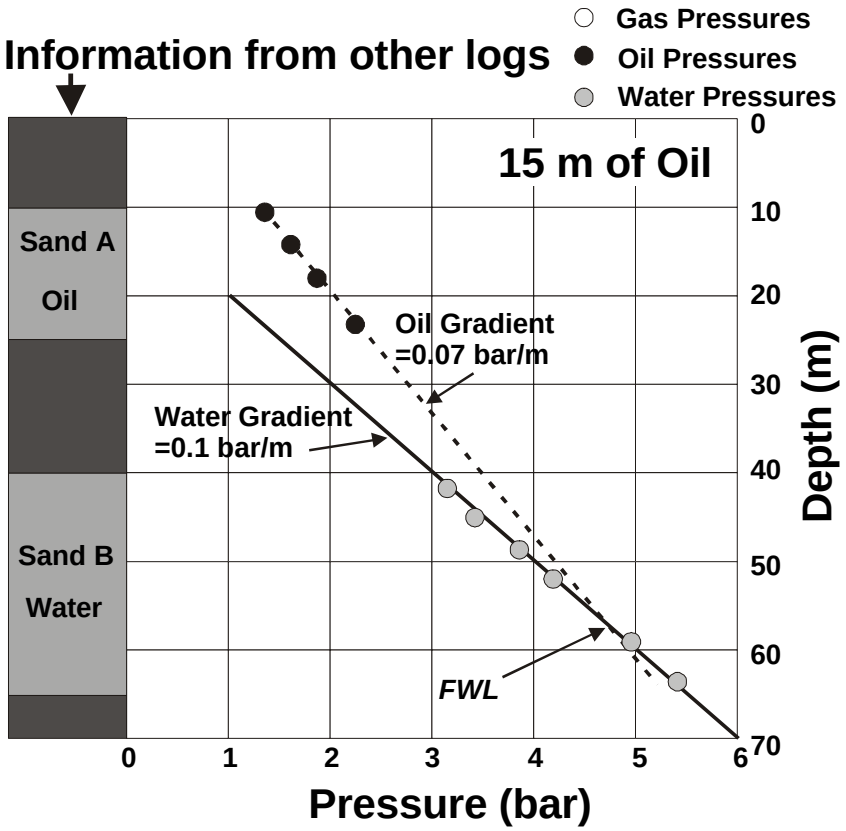

Figure 7.10 Pressure versus depth plot 1.

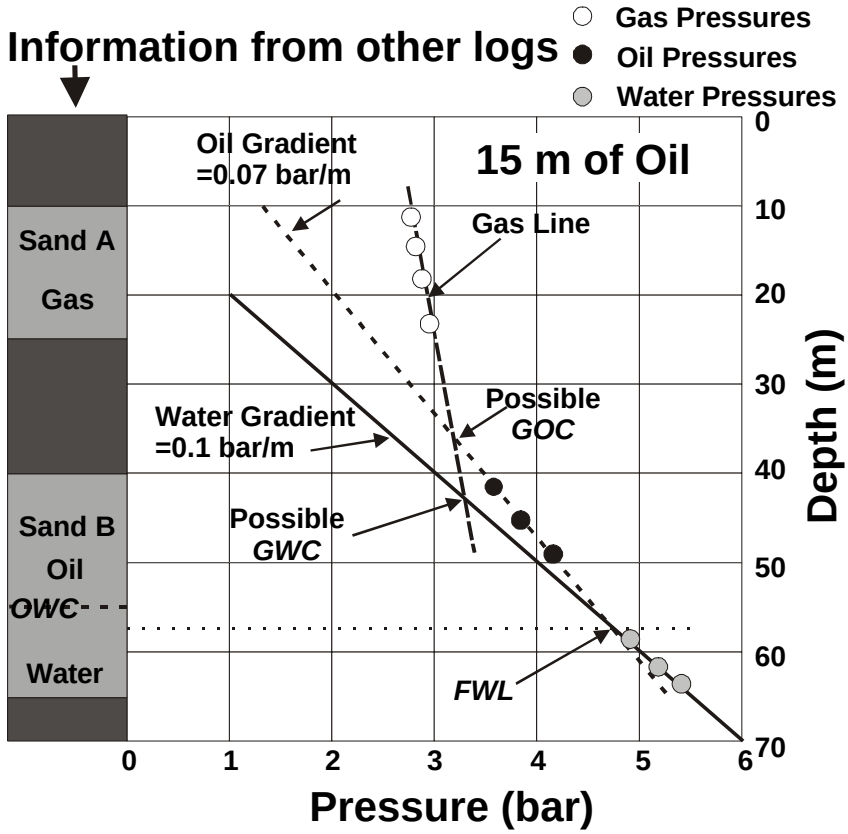

Figure 7.11 Pressure versus depth plot 2.

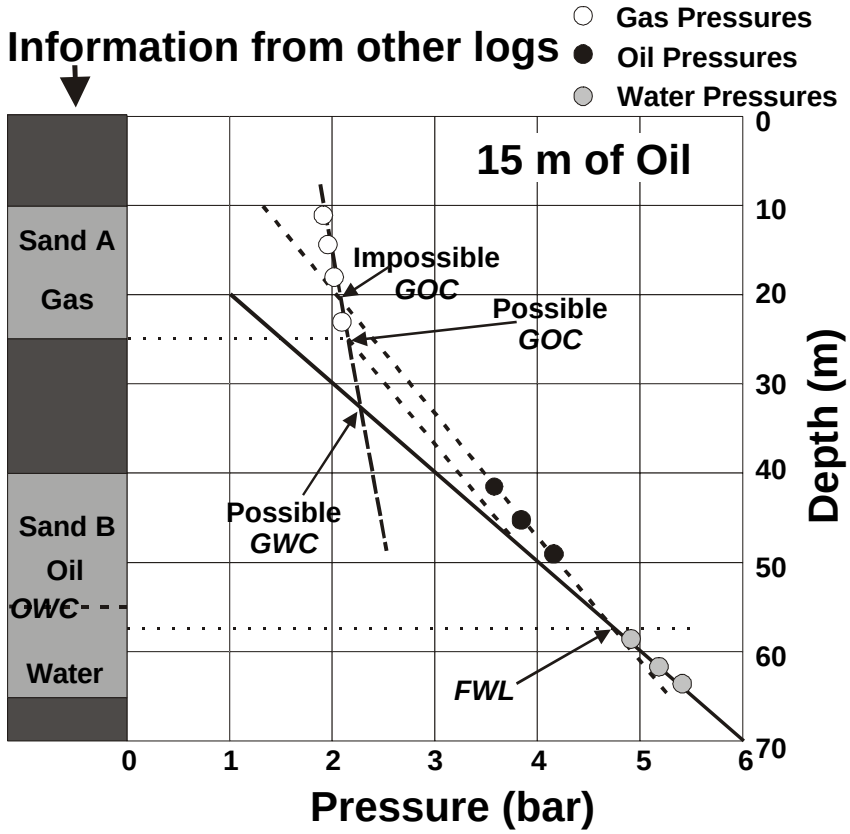

Figure 7.12 Pressure versus depth plot 3.

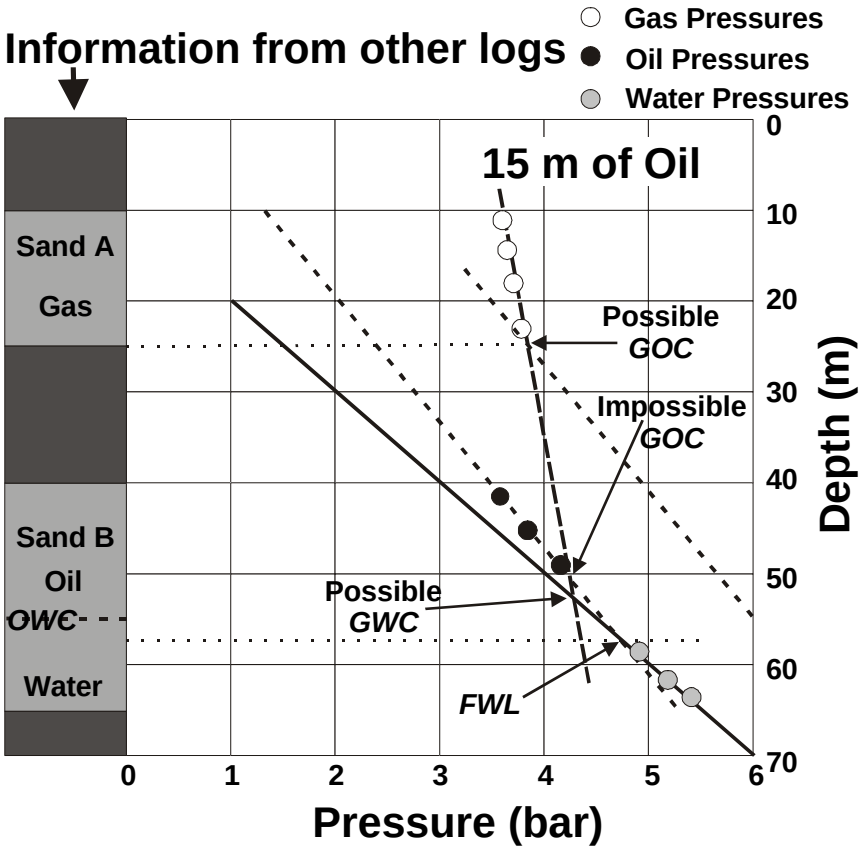

Figure 7.13 Pressure versus depth plot 4.

If oil is missing in the column, then the likely gas water contact (*GWC*) would be where the gas and the water lines intersect, again providing there is good communication between the two sands.

If the recorded gas pressures are lower (Fig. 7.12), the assumption that the sands are in communication implies a *GOC* in Sand A, which is contrary to the log evaluation shown on the left of the figure. Hence, the sands are not in communication.

If the recorded gas pressures are higher (Fig. 7.13), the assumption that the sands are in communication implies a *GOC* in Sand B, which again is contrary to the log evaluation shown on the left of the figure. Hence, the sands are not in communication.

8. TEMPERATURE LOGS

8.1 Introduction

The *Temperature Log* is a tool for measuring the borehole temperature. Temperature sensors are attached to every tool combination that is run in a well for the measurement of the maximum temperature (assumed to be at the bottom of the well), and a few modern tools exist that can continuously measure temperature as the tool travels down the well.

Readings from a number of the maximum thermometers attached to different tool combinations and run at different times are analyzed to give the corrected temperature at the bottom of the borehole (*bottom hole temperature*, *BHT*).

The borehole temperature is an important parameter in the analysis of resistivity logs, but also for the detection of fluid movement, the analysis of fluid pressures and in geochemical modelling of formations and the maturity of hydrocarbons.

8.2 Theory

Temperature in the sub-surface increases with depth. The rate at which it does so is called the *geothermal gradient* or *geotherm*. Typical geotherms for reservoirs are about 20 to 35^{o}C/km, although significantly higher values (up to 85^{o}C/km) can be found in tectonically active areas, and lower ones (0.05^{o}C/km) in stable continental platforms. Hence, the bottom hole temperature (*BHT*) for a 3000 m well with a geotherm of 25^{o}C and a surface temperature of 15^{o}C is 90^{o}C.

Note that this assumes that the geothermal gradient is constant. In practice this is rarely the case because of differences in the thermal conductivities of rocks between the bottom of the hole and the surface, and fluctuations in the surface temperature which penetrate the sub-surface and perturb the sub-surface temperature. Low thermal conductivity rocks, such as shale, act as a thermal insulator and have a large temperature gradient across them, while high thermal conductivity rocks, such as salt, permit the conduction of heat efficiently, and have a small temperature gradient across them.

8.3 Borehole Temperature Measurement

Each tool combination is equipped with a temperature sensor. Temperature measurements are always made at the bottom of the well (highest temperature) and sometimes at intervals up the well. The temperature measuring devices can be as simple as a number of maximum temperature monitors that are attached to the outside of a tool string, and this was commonly the case until recently. In this case only the highest temperature (assumed to be at the bottom of the borehole) is measured. Recently a several special temperature logging sondes have been developed (the *AMS* of Schlumberger and the *Temperature Survey* of Western Atlas), which read temperature continuously up the well using a thermistor, and sometimes also read the temperature difference between two probes spaced along the tool.

The absolute accuracy of temperature measurements is low (±2.5^{o}C), but the resolution is good (0.025^{o}C).

It should be noted that the temperature logs are the only logs to be measured while the sensor is being lowered into the well. This is to reduce any temperature perturbations caused by the logging tool itself.

8.4 Borehole Temperature Corrections

The actual temperature measured is that of the drilling fluid not the formation. The drilling mud is circulated during drilling and prior to inserting the wireline tool, and this drilling mud is cold compared to the formation. The cold drilling fluid invades the formation and cools it down very efficiently *via* heat convection. During circulation of drilling fluid the temperature of the borehole reaches an equilibrium defined by the cooling effect of the drilling fluid and the heating effect of the formation. When the circulation of the drilling mud stops (for example, in preparation for the insertion of a wireline tool), the borehole gradually regains the true formation temperature, because the large mass of formation around the borehole heats the drilling fluid up to its ambient temperature. This process is slow because it occurs *via* heat conduction which is less efficient than heat convection. Equilibrium may only be attained after several months after stopping the circulation of the drilling fluid.

Hence, temperature measurements made during drilling (MWD and LWD) consistently underestimate the formation temperature because drilling mud is being circulated. Temperature measurements made on wireline logs sometime after the drilling fluid circulation has stopped also underestimate the formation temperature, but less than the MWD/LWD case as the formation is now in the process of reheating the borehole. Measurements of temperature made by wireline logs at increasing times after fluid circulation has stopped are closer and closer to the real formation temperature.

Various methods have been adopted in the past to correct the logged BHT to real formation temperatures. The most common method is the Horner plot. The Horner method, plots the measured temperature (at a given depth) from each of several logging runs, against $\log(T/(t+T))$, where T is the time since circulation of the drilling fluid was stopped (usually in hours), and t is the length of time of circulation of drilling fluid prior to this. The parameter t represents the length of time that the borehole was subjected to the cooling effects of the fluid, and T represents the time after circulation that the borehole has had to partially reheat. This plot is a straight line that intersects $T/(t+T)=1$ at the formation temperature.

For example, Table 8.1 gives the drilling, logging, and temperature data for three tool combinations that were run in a single hole one after another.

Table 8.1 Horner plot example.

Time	**Operation**	**Temperature (^{o}C)**	***T*** **(hours)**	***t*** **(hours)**	***T*/(*t*+*T*)** **(-)**
00:00	Circulation started	-	-	6	
06:00	Circulation stopped	-	0	6	
13:00	Run IEL log	100	7	6	0.538
17:30	Run Sonic log	105	11.5	6	0.671
01:30	Run FDC-CNL log	108	19.5	6	0.765

Figure 8.1 shows the Horner plot generated with this data, and the resulting formation temperature.

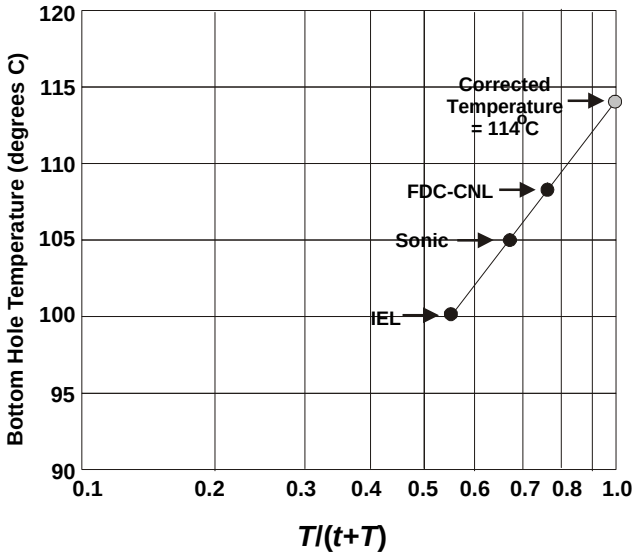

Figure 8.1 The Horner plot for correction of *BHT* at 3200 m in a well using data in Table 8.1.

8.5 Uses of Temperature Logs

Table 8.2 shows the main uses of the temperature log data.

Table 8.2 Uses of the temperature log.

Use	**Comment**
Correction of other tools	The sensors of other logging tools are sensitive to temperature. The temperature measurement can be used to correct for this, or to recognize temperatures that are outside the operating range of the tool and likely therefore to be erroneous..
Correction of measurements	Some parameters measured by other tools are sensitive to temperature. The best example is resistivity logs. The temperature data is used to correct ALL resistivity data to a standard 24°C (75°F) so they are not depth dependent and can be compared.
Hydrocarbon maturation	The maturity of hydrocarbons depends upon the maximum temperature that the organic remains have been subjected to, as well as time and pressure.
Correlation	Continuous temperature logs record differences in thermal gradient that result from differences in the thermal conductivity of the formations. These difference can be used for correlation.
Fluid movement	Continuous logs can observe intervals of raised (or lowered) temperature caused by the influx of hotter (or colder) fluids into the borehole through the rock matrix, or more usually, through patent fractures. This effect may also be due to cold drilling fluid escaping into the rock.
Overpressured zones	Continuous logs also note the presence of overpressured zones, where the hot overpressured fluids escape into the borehole and are noted by a rise in the measured temperature.

9. CALIPER LOGS

9.1 Introduction

The *Caliper Log* is a tool for measuring the diameter and shape of a borehole. It uses a tool which has 2, 4, or more extendable arms. The arms can move in and out as the tool is withdrawn from the borehole, and the movement is converted into an electrical signal by a potentiometer.

In the two arm tool (Fig. 9.1), the borehole diameter is measured. This is shown in track 1 of the master log together with the bit size for reference. Borehole diameters larger and smaller than the bit size are possible. Many boreholes can attain an oval shape after drilling. This is due to the effect of the pressures in the crust being different in different directions as a result of tectonic forces. In oval holes, the two arm caliper will lock into the long axis of the oval cross-section, giving larger values of borehole diameter than expected. In this case tools with more arms are required.

In the 4 arm (dual caliper) tool, the two opposite pairs work together to give the borehole diameter in two perpendicular directions. An example of a 4 arm tool is the Borehole Geometry Tool (BGT). This has 4 arms that can be opened to 30 inches (40 inches as a special modification), and give two independent perpendicular caliper readings. The tool also calculates and integrates the volume of the borehole and includes sensors that measure the direction (azimuth) and dip of the borehole, which is useful in plotting the trajectory of the borehole.

In the multi-arm tools, up to 30 arms are arranged around the tool allowing the detailed shape of the borehole to be measured.

Some of the other tools in this course have sensors attached to pads that are pressed against the borehole wall. The pressing device is also a form of caliper, and so caliper information can sometimes also be obtained from these tools.

Figure 9.1 The Reeves 2 arm caliper tool.

9.2 Log Presentation

The caliper logs are plotted in track 1 with the drilling bit size for comparison, or as a differential caliper reading, where the reading represents the caliper value minus the drill bit diameter (Fig. 9.2). The scale is generally given in inches, which is standard for measuring bit sizes.

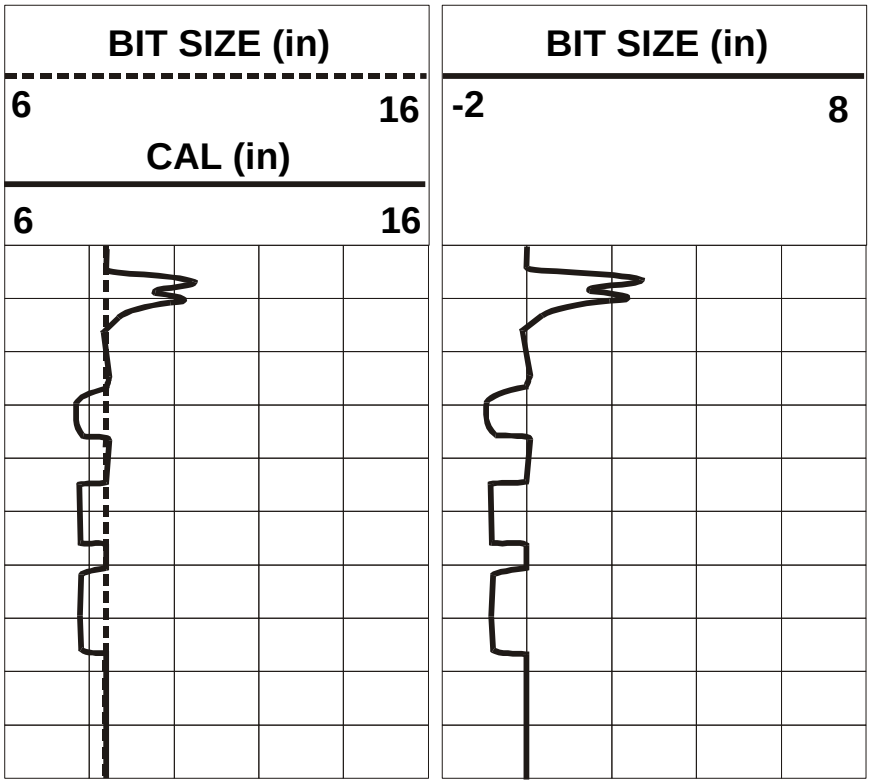

Figure 98.2 Presentation of 2 arm caliper log data.

The 4 arm (or dual caliper) tools are presented in a range of formats, an example of which is given in Fig. 9.3. Note that data from the caliper pairs are shown together, and that they are different indicating an oval hole. Also the tool rotates in the hole (the pad 1 azimuth P1AZI changes). The hole azimuth is reasonably constant at HAZI≈180^{o}, and the dip is almost vertical (DEVI is about 0^{o}).

The ticks represent borehole volume. This information is useful to estimate the amount of drilling mud in the borehole, and to estimate the amount of cement required to case the hole. There are engineering approximation formulas to calculate both of these from caliper data.

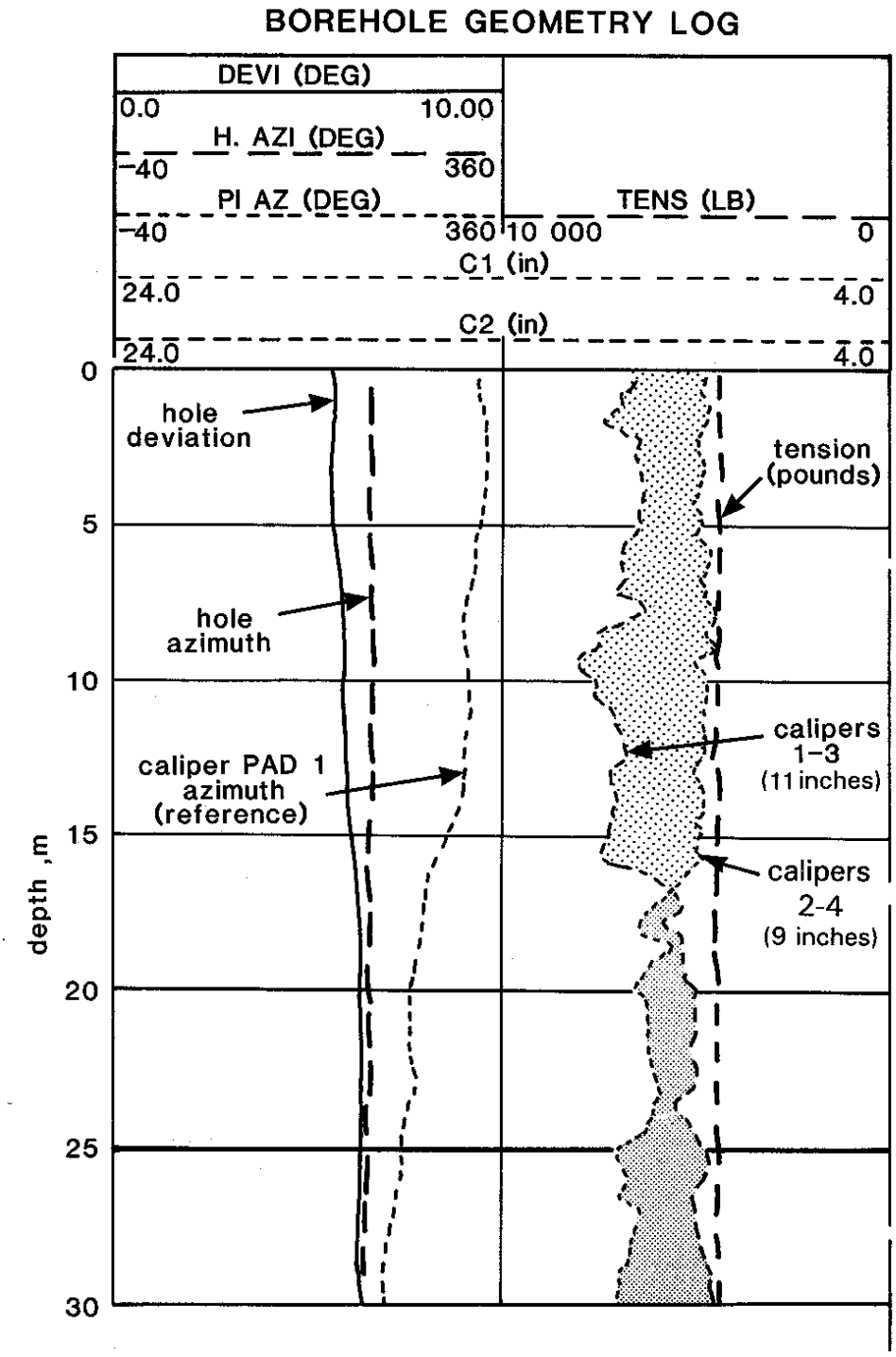

Figure 9.3 Presentation of 4 arm caliper log data (After Rider, 1996).

9.3 Simple Caliper Interpretation

Figure 9.4 shows a schematic hole with caliper information, and Table 9.1 describes the main influences on caliper values. Note that when a hole is the same diameter as the bit-size it is called *on gauge*.

Table 9.1 Factors influencing caliper responses.

Hole Diameter	**Cause**	**Possible Lithologies**
On Gauge	Well consolidated formations Non-permeable formations.	Massive sandstones Calcareous shales Igneous rocks Metamorphic rocks
Larger than Bit Size	1. Formation soluble in drilling mud. 2. Formations weak and cave in.	1. Salt formations drilled with fresh water. 2. Unconsolidated sands, gravels, brittle shales.
Smaller than Bit Size	1. Formations swell and flow into borehole. 2. Development of mudcake for porous and permeable formations.	1. Swelling shales. 2. Porous, permeable sandstones.

9.4 Uses of the Caliper Log

The commoner uses of the caliper log are as follows:

- Contributory information for lithological assessment (see Table 9.1 and Fig. 9.4).
- Indicator of good permeability and porosity zones (reservoir rock) due to development of mudcake in association with gamma ray log.
- Calculation of mudcake thickness, $h_{mc} = (d_{bit} - d_h)/2$, where h stands for the hole, in inches.
- Measurement of borehole volume, $V_h = (d_h^2/2)+1.2\%$, in litres per metre.
- Measurement of required cement volume, $V_{cement} = 0.5 \times (d_h^2 - d^2_{casing}) + 1\%$, in litres per metre.
- Indication of hole quality for the assessment of the likely quality of other logs whose data quality is degraded by holes that are out of gauge. Other log data can often be corrected for bad hole conditions using the caliper readings, but the larger the correction, the less reliable the final data will be. Centralized tools are designed to be about 4 inches in diameter for a standard 8.5 inch hole, and they are designed to work with 2.25 inches of drilling mud between them and the formation. If the hole caves to 14 inches, which is not uncommon, the distance to the formation becomes 5 inches and the tool responses are degraded. This can be corrected for to some extent if the caliper value is known. Tools that work by being pressed up against the side of the borehole wall have even greater problems because the irregularity of the borehole wall makes it impossible to obtain reliable readings. In both cases the recognition that a borehole has bad caving or thick mudcake can help us judge the reliability of other tool's readings.
- Selection of consolidated formations for wireline pressure tests, recovery of fluid samples, for packer seating for well testing purposes, and for determining casing setting depths.

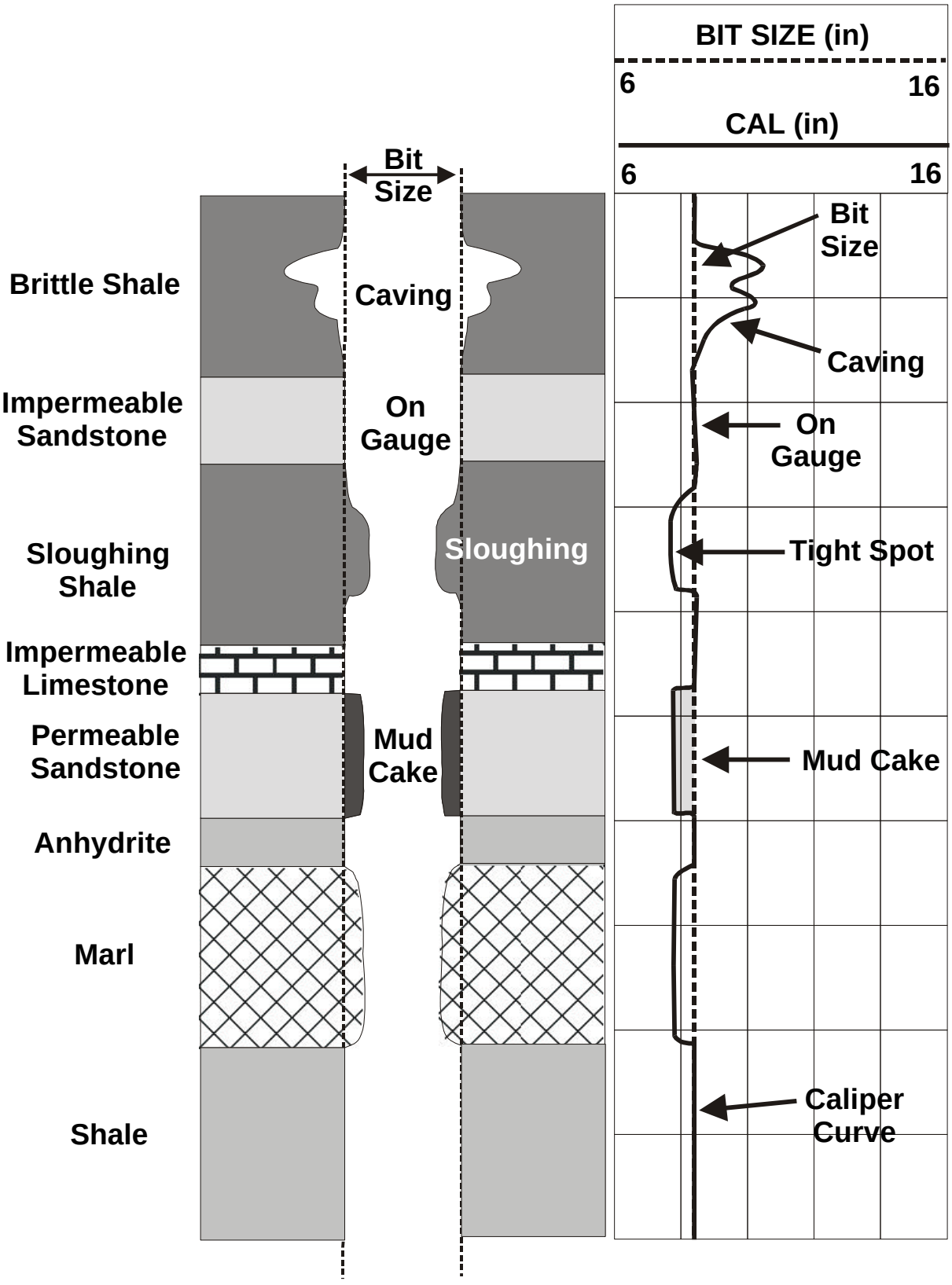

Figure 9.3 Typical caliper responses to various lithologies.

10. RADIOACTIVITY LOGGING

10.1 Introduction

Radioactivity is used in several different types of logging tool. There are those that measure the natural radiation generated by the formation, such as the total and spectral gamma ray logs, and those that measure the response of the formation to radiation generated by the tool, such as the neutron, density and litho-density logs. This chapter will cover the total gamma ray log and the following one will examine the spectral gamma ray log.

10.2 Radioactivity Theory

Radioactivity is a fundamental property of the structure of all matter. The atoms of all elements have a *nucleus* which contains different numbers of *protons* and *neutrons*, which is surrounded by a sheath of *electrons* that are arranged in different energy levels. Each element is defined by the number of positively charged protons its nucleus contains. This is called the *atomic number Z.* Each nucleus also contains a number of neutrally charged neutrons, and the sum of the number of protons and neutrons in the nucleus is called the *atomic mass number, A.* There are a number of negatively charged electrons surrounding the nucleus equal to the number of protons within it, and their charge balances the positive charge of the protons. Since the mass of electrons is insignificant compared to the mass of the protons and neutrons, the atomic mass number is a measure of the mass of the atoms of each element. Although the number of protons and electrons for a given element is characteristic of that element, the number of neutrons is not. An element may have several *isotopes* which are atoms with different numbers of neutrons in their nucleus. Thus any given atom of an element will have a fixed atomic number, and a atomic mass number that depends upon which isotope it is. Most natural materials are a mixture of different isotopes.

Each isotope of each element is given a code ${}_{Z}X^{A}$, where X is the elemental code. For example, carbon has an atomic number Z=6, but 7 isotopes containing between 4 and 10 neutrons. These are ${}_{6}C^{10}$ to ${}_{6}C^{16}$. Carbon-12, ${}_{6}C^{12}$, is the most common isotope, and it is stable. Most of the other isotopes are not stable energetically, and decay to more stable elements by various processes whereby they lose energy by expelling particles or photons. Carbon-14, ${}_{6}C^{14}$, is one of these, and its decay process can be used to date archaeological remains.

There are five main methods whereby an unstable isotope can gain stability by losing energy. These are:

- Emission of an α particle, which is a helium nucleus ${}_{2}He^{4}$, and carries two positive charges.
- Emission of a β^{-} particle, which is a negatively charged high energy electron originating in the nucleus together with an anti-neutrino, $\underline{\nu}$.
- Emission of a β^{+} particle, which is a positively charged high energy positron originating in the nucleus together with an neutrino, ν.
- Emission of a gamma rays, γ, which are high energy photons (electro-magnetic waves) and have no mass and carry no charge.
- Electron capture, which involves an electron being captured by the nucleus.

Under some circumstances neutrons may also be expelled from a material, but this is not a spontaneous decay.

Gamma rays are the most important in petrophysical logging because they have the highest penetration of all the radiations except neutrons. Their penetration ability means that they can be detected through several centimetres of cement casing. Alpha and beta particles have very limited penetration ability, being stopped immediately by any solid material.

Most isotopes found naturally in rocks are either stable, present in insignificant amounts, or generate insignificant amounts of radiation. There are, however, a few which are significant. These are:

- The potassium isotope $_{19}K^{40}$ (the stable forms are $_{19}K^{39}$ and $_{19}K^{41}$).
- The Thorium series isotopes.
- The Uranium-Radium series isotopes.

The first is a single gamma emission at a single energy (1.46 MeV). The last two are mixtures of unstable elements that generate each other in a series of radioactive emissions involving gamma radiation. Hence, there is a spectrum of energies produced over the range 0 MeV to 3 MeV. The energy spectra from the three gamma sources is shown in Fig. 10.1.

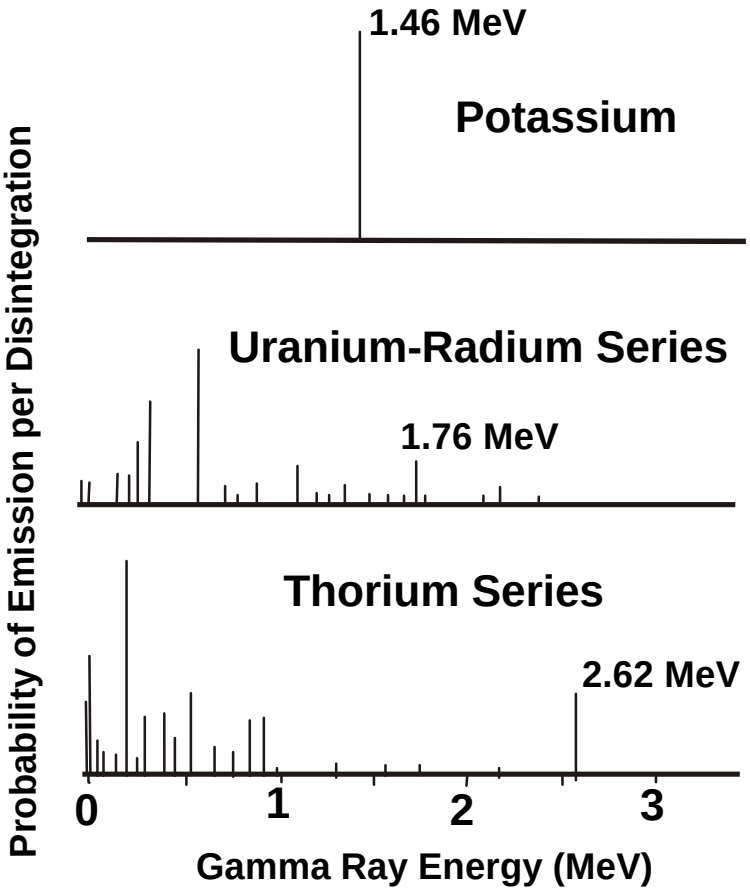

Figure 10.1 Gamma ray emission energy spectra.

The three gamma ray sources also produce different intensities of radiation per gram per second. The U-Ra series produces 26000 photons per gram per second, the Th series produces 12000 photons/g/s, and $_{19}K^{40}$ produces 3 photons/g/s. One might think that the potassium would be insignificant. However, the potassium is much more abundant than the isotopes in the other two series, which makes

its contribution to the overall radioactivity of a formation significant. Potassium is common in most clays and some evaporites.

The most common gamma emitting lithology is shale. This is because shales are ultimately derived from igneous rocks which have significant amounts of gamma emitting isotopes. Igneous rocks are composed of quartz, feldspars and micas, the last two of which contain significant amounts of potassium and occasionally also U-Ra and Th-series isotopes. The feldspars and micas alter to clay minerals whose open lattice structure facilitates the inclusion of the larger radio-isotopes. These clays form the principle components of shales. Hence, shales can contain up to 0.3% radio-potassium and up to 0.01% of each of the U-Ra and Th-series isotopes. Unsurprisingly, potash beds are also highly radioactive.

The gamma radioactivity from minerals in petrophysical logging are measured on the API scale, described later. Table 10.1 shows typical API values for some common minerals. Note particularly that shale and some evaporites have high gamma ray values, while sandstone and limestone have low values.

Table 10.1 Gamma radiation from common minerals and lithologies (after Pirson, 1963).

Mineral or Lithology	**Composition**	**Gamma Radiation (API Units)**
Pure Mineral		
Calcite	$CaCO_3$	0
Dolomite	$CaMg(CO_3)_2$	0
Quartz	SiO_2	0
Lithology		
Limestone	-	5-10
Dolomite	-	10-20
Sandstone	-	10-30
Shale	-	80-140
Evaporites		
Halite	NaCl	0
Anhydrite	$CaSO_4$	0
Gypsum	$CaSO_4(H_2O)_2$	0
Sylvite	KCl	500
Carnalite	$KCl\ MgCl_2(H_20)_6$	220
Langbeinite	$K_2SO_4(MgSO_4)_2$	290
Polyhalite	$K_2SO_4MgSO_4(CaSO_4)_2(H_2O)_2$	200
Kainite	$MgSO_4KCl(H_2O)_3$	245
Others		
Sulphur	S	0
Lignite	$CH_{0.849}\,N_{0.015}\,O_{0.221}$	0
Anthracite	$CH_{0.358}\,N_{0.009}\,O_{0.022}$	0
Micas	-	200-350

Figure 10.2 shows the range of gamma ray values generated by common lithologies. Note the particularly high values for potash beds, which contain a large amount of potassium-40, and organic shales, which contain enhanced uranium associated with their organic nature.

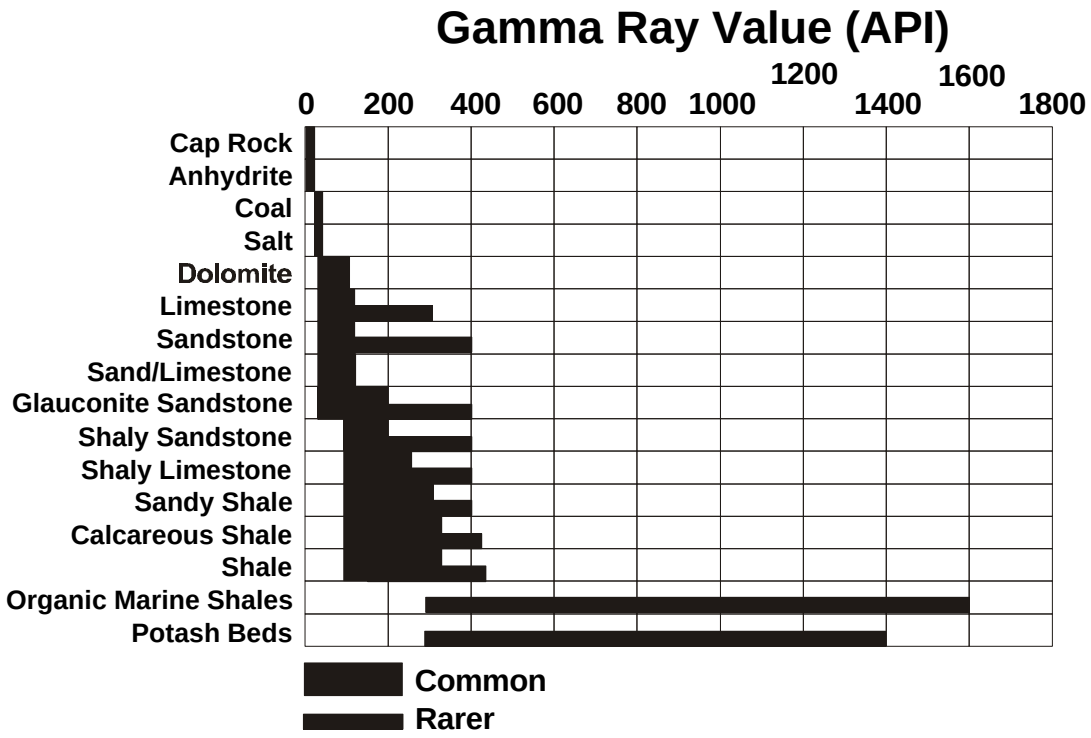

Figure 10.2 Gamma ray values from common lithologies.

10.3 Scattering and Attenuation

Once the gamma rays have been emitted they travel through materials (formation, fluids, mud cake and drilling mud) and interact with them. There are three processes that occur, and each is applicable to gamma rays with a given energy range. These are:

- **Gamma rays with energy >3 MeV.** These interact with the nucleus of the materials that they are travelling through and are converted into an electron and a positron in the process (*pair production*). The efficiency of the process is low, so these gamma rays may be measured by a sensor. However, they contribute only small amounts to the overall signal.

- **Gamma rays with energy 0.5 to 3 MeV.** These gamma rays undergo *compton scattering*, where a gamma ray interacts with the electrons of the atoms through which they are passing, ejecting the electron from the atom, and losing energy in the process. A gamma ray in this range may undergo several of these collisions reducing its energy from its initial value to an energy of less than 0.5 MeV in a stepwise fashion.

- **Gamma rays with energy <0.5 MeV.** These gamma rays collide with electrons of the atoms through which they are passing, and are adsorbed. The gamma ray energy is either used to promote the electron to a higher energy level or to eject it from the atom. This process is called *photo-electric adsorption*, and is important in the Litho-Density tool.

Thus, gamma rays start with a given energy, and are either lost through pair production, or undergo compton scattering until their energy is sufficiently low for them to be adsorbed by photo-electric absorption.

The number of collisions, hence the reduction in gamma ray energy, and the number of gamma rays adsorbed is directly related to the number of electrons in the materials through which the gamma rays pass. High count rates are observed for materials with low electron densities, and low count rates for high electron densities. The electron density is, of course, related to the mean atomic number and bulk density of the material.

Figure 10.3 shows the processes of scattering and absorption schematically.

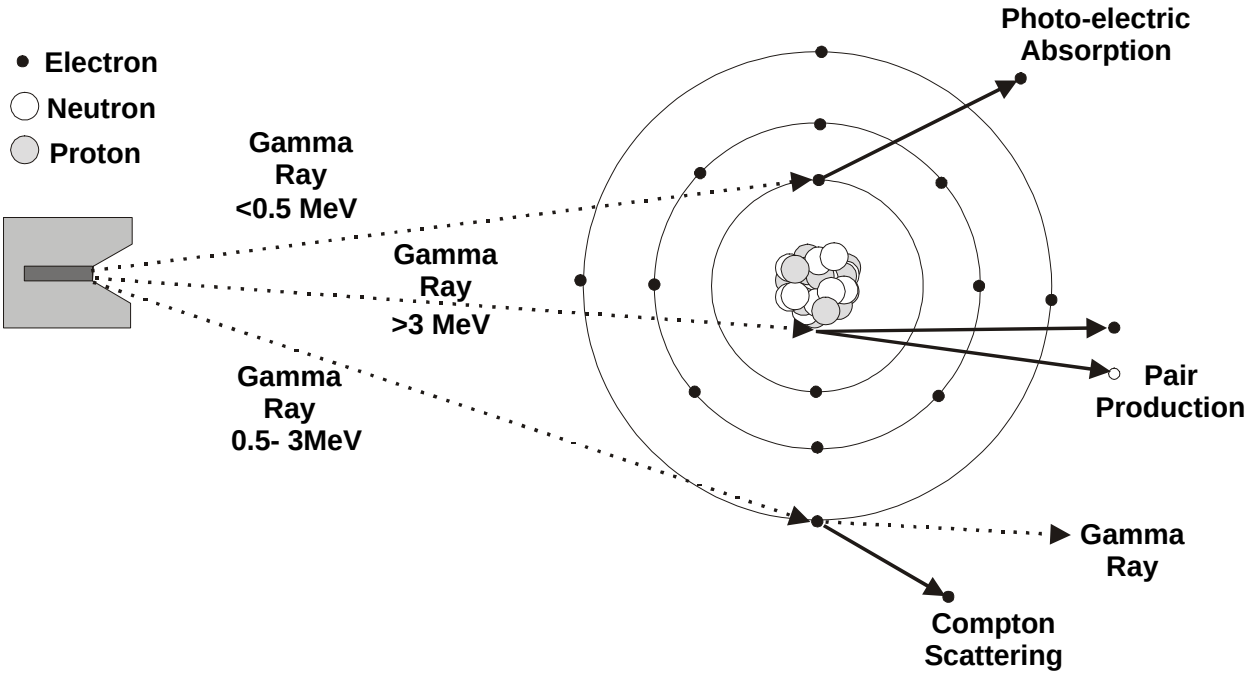

Figure 10.3 Processes of gamma ray scattering and absorption.

11. THE TOTAL GAMMA RAY LOG

11.1 Introduction

The *gamma ray* log measures the total natural gamma radiation emanating from a formation. This gamma radiation originates from potassium-40 and the isotopes of the Uranium-Radium and Thorium series. The gamma ray log is commonly given the symbol *GR*.

Once the gamma rays are emitted from an isotope in the formation, they progressively reduce in energy as the result of collisions with other atoms in the rock (*compton scattering*). Compton scattering occurs until the gamma ray is of such a low energy that it is completely absorbed by the formation.

Hence, the gamma ray intensity that the log measures is a function of:

- The initial intensity of gamma ray emission, which is a property of the elemental composition of the rock.
- The amount of compton scattering that the gamma rays encounter, which is related to the distance between the gamma emission and the detector and the density of the intervening material.

The tool therefore has a limited depth of investigation.

Note that the gamma ray measurement device accepts gamma rays from almost a hemisphere that includes the formation and the drilling mud between the formation and the sensor. Gamma rays may therefore come from the formation at any angle from horizontal to almost vertically, and indeed may come from the drilling mud itself (beware: some drilling muds are very radioactive!).

The gamma ray log is combinable with all tools, and is almost always used as part of every logging combination run because of its ability to match the depths of data from each run.

11.2 Principles

The tool consists simply of a highly sensitive gamma ray detector in the form of a scintillation counter. The scintillation counter is composed of a thalium activated single sodium iodide crystal backed by a photomultiplier. When a gamma ray strikes the crystal a small flash of light is produced. This flash is too small to be measured using conventional electronics. Instead, it is amplified by a photomultiplier, which consists of a photocathode and a series of anodes held at progressively higher electrical potentials, all of which are arranged serially in a high vacuum. The flash of light hits the photocathode and causes a number of *primary electrons* to be produced. These few electrons still represent too small a signal to be measured. The primary electrons are accelerated towards the first anode. For every electron that hits the anode, a number of *secondary electrons* are emitted (between 4 and 8 usually). These electrons are accelerated towards the next anode, where each of the secondary electrons produce even more secondary electrons. This process is repeated for each of say 10 anodes. If 6 electrons are emitted at each anode for each incident electron, we can see that a single incident gamma ray ultimately produces 6^{10} = 60,466,176 electrons, which represents a current that can be amplified further by conventional amplifiers.

The whole process takes an extremely short time, but during this time the photomultiplier is *saturated* and is insensitive to further gamma rays. However, the small incident flux of gamma rays produced from rocks ensures that saturation is rarely if ever reached for down-hole tools. Since the flash of light and the number of primary electrons is proportional to the energy of the gamma ray, the final current from the scintillation counter is also proportional to the energy of the incident gamma ray. Hence, there will be a threshold gamma ray energy below which the scintillation counter is insensitive to gamma rays.

Scintillation counters are relatively small devices, which means that the gamma ray tool can have a high vertical resolution.

11.3 Calibration

Intuitively, we might expect the units for gamma ray logging to be in gamma counts per second. However, this results in extremely unwieldy values. Conventionally, the gamma ray log is reported in pseudo-units called API units. The API unit is defined empirically by calibration to a reference well at the University of Houston. This reference well is an artificial one that is composed of large blocks of rock of accurately known radioactivity ranging from very low radioactivity to very large radioactivity. The API unit is $1/200^{th}$ of the difference between the highest activity formation in the reference well, and the lowest.

Tools are run in the Houston well (*test pit*), and are used as standards to calibrate further tools at local test pits. A further calibration check is also carried out at the well-site before and after the log is run, by using a radioactive source of accurately known radioactivity a fixed distance from the tool.

It should be noted that logs from the USSR and its satellite countries used counts per second as its gamma ray logging units until recently. As with all USSR logs, the interpretation and correction of these logs to API units is not straightforward.

11.4 Log Presentation

The total gamma ray log is usually recorded in track 1 with the caliper log, bit size and SP log. In this case, the other tracks most often include resistivity, density, neutron or sonic logs (Fig. 11.1).

Although the API scale goes from 0 to 200 API, it is more common to see 0 to 100 API and 0 to 150 API used in log presentations, as data greater than 150 API is not common, and can always be handled by the use of wrap-around.

When gamma ray logging is carried out through the cement casing, a scale of 0 to 50 API is most often used, as a result of the lower values measured due to the attenuation of the gamma count rate by the casing.

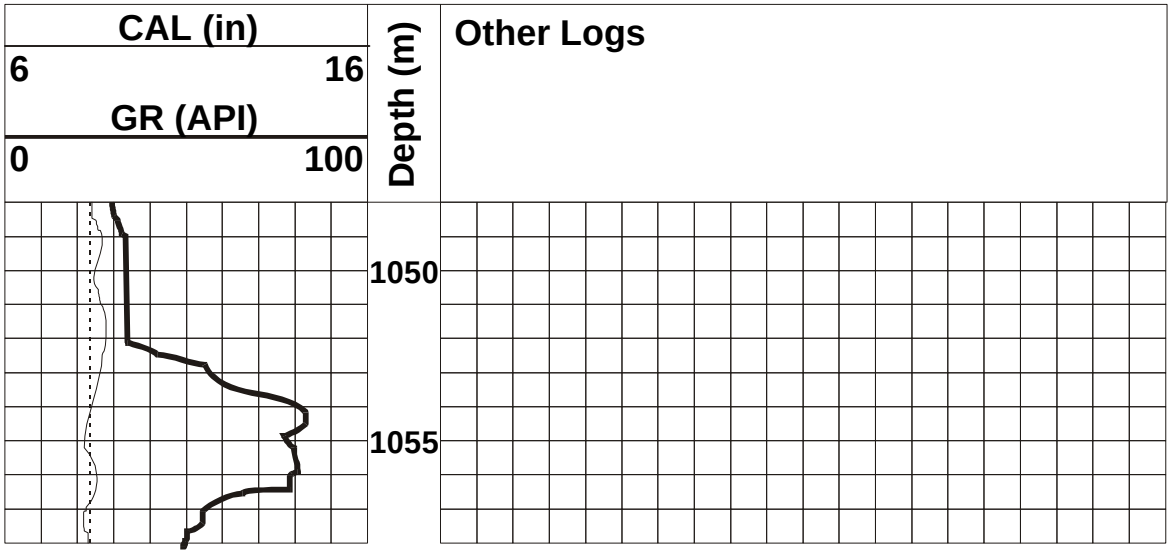

Figure 11.1 Gamma log presentation.

11.5 Depth of Investigation

The gamma rays are attenuated by compton scattering by all materials between the atom that emitted the gamma ray and the detector, which includes the rock itself and the drilling mud. The degree of attenuation depends upon the number density of atoms in the material, and this is related to the density of the material. As we have seen in Chapter 10, there is a distribution of gamma ray energies, but at distance from the emitting atom increases, the energy of the gamma rays decreases but compton scattering until they are too low to be measured by the scintillation counter. Clearly, therefore, there is a maximum depth of investigation for the tool that depends upon formation and mud density.

For average values of drilling mud and formation density, we can say that approximately 50% of the gamma ray signal comes from within 18 cm (7 inches) of the borehole wall, increasing to 75% from within 30 cm (1 foot). Hence, the depth of investigation, if defined at 75% of the signal, is 30 cm. However, this will decrease for denser formations of the same radioactivity, and increase for less dense formations of the same radioactivity.

Note that the zone of sensitivity is almost hemispherical, so the 30 cm depth of investigation applies both horizontally (perpendicular to the borehole wall) and sub-vertically (sub-parallel with the borehole wall). This has implications for the vertical resolution of the tool.

11.6 Logging Speed

Radioactive emissions are random, and hence fluctuate in an unpredictable way with time. If the count rates are high, this causes no real problems as there are sufficiently many counts in a reasonable time interval for the fluctuations to average out. In gamma ray logging, the count rate is low so the fluctuations have to be taken into account. For each measurement depth, the tool must linger long enough to measure enough count in order to obtain good quality data. In gamma ray logging a time averaging procedure is adopted to minimize the statistical fluctuations. The output from the detector is measured as a gamma ray count rate, which is averaged over a time defined by a *time constant* T_c.

In order to increase the quality of the log data T_c should be as large as possible. However, as the logging tool is constantly moving, a large T_c will result in the bluring of bed boundaries, which as implications for the vertical resolution of the tool. As there are large costs associated with running logs slowly, thee is a compromise to be reached between logging speed and log quality. In practice, the product of logging speed in feet per second and T_c in seconds is conventionally held constant at 1 foot. Hence, the gamma ray measurement is averaged over this one foot interval, and the log data is shifted down by 1 foot to compensate. Note that the log data is therefore recorded at the bottom of the one foot interval over which it is averaged.

Table 11.1 illustrates the effect of the interplay between the statistical fluctuations, the gamma count rate and T_c for a single formation with a constant radioactivity. In this example we assume that the logging speed is 1 foot per second $\times$ T_c. If the time constant is set to one third of a second, there are 9 measurements with an apparent vertical resolution of 4 inches, but these measurements fluctuate wildly between 9 and 18 counts per second. If the time constant is one second, there are 3 measurements covering the logged interval with an apparent vertical resolution of 12 inches, but a much smaller error in the measurements themselves (i.e., the range has dropped to 12 to 14 counts per second). If the time constant is any higher, the measured value of counts per second becomes very well constrained, but the vertical resolution degrades rapidly, 3 foot in this case. Clearly the T_c = 1 s case is a good balance between logging variability (error) and resolution.

Table 11.1 Variations in count rate in gamma ray logging.

Counts	**No. of Counts**	**Period (s)**	**Count Rate (per second)**	**No. of Counts**	**Period (s)**	**Mean Count Rate**	**No. of Counts**	**Period (s)**	**Mean Count Rate**
	T_c = 0.333 s			**T_c = 1 s**			**T_c = 3 s**		
• • • •	4	0.333	12	14	1	14	39	3	13
• • • • • •	6	0.333	18						
• • • •	4	0.333	12						
• • • • •	5	0.333	15	12	1	12			
• • •	3	0.333	9						
• • • •	4	0.333	12						
• • • • •	5	0.333	15	13	1	13			
• • •	3	0.333	9						
• • • • •	5	0.333	15						
Mean Count Rate (per second)	-	-	13	-	-	13	-	-	13
Range of Count Rate (per second)	-	-	9 -18	-	-	12-14	-	-	13-13
Standard Deviation (per second)	-	-	3	-	-	1	-	-	-

Note that the apparent vertical resolution is not the one encountered in practice because of the geometry of the sensor arrangement. In practice one must add about 2 feet to the apparent vertical resolution to obtain the real one.

Figure 11.2 shows gamma ray log data across a boundary between two formations of different radioactivity for various values of logging speed *V* in ft/hr and for a time constant of 2 s. Note that even at *V*=0 there is a gradual change from the gamma ray count in one formation and that in the next due to the finite sensor size and the geometry of its sensitive zone. Increasing logging speeds show an increased bluring of the boundary.

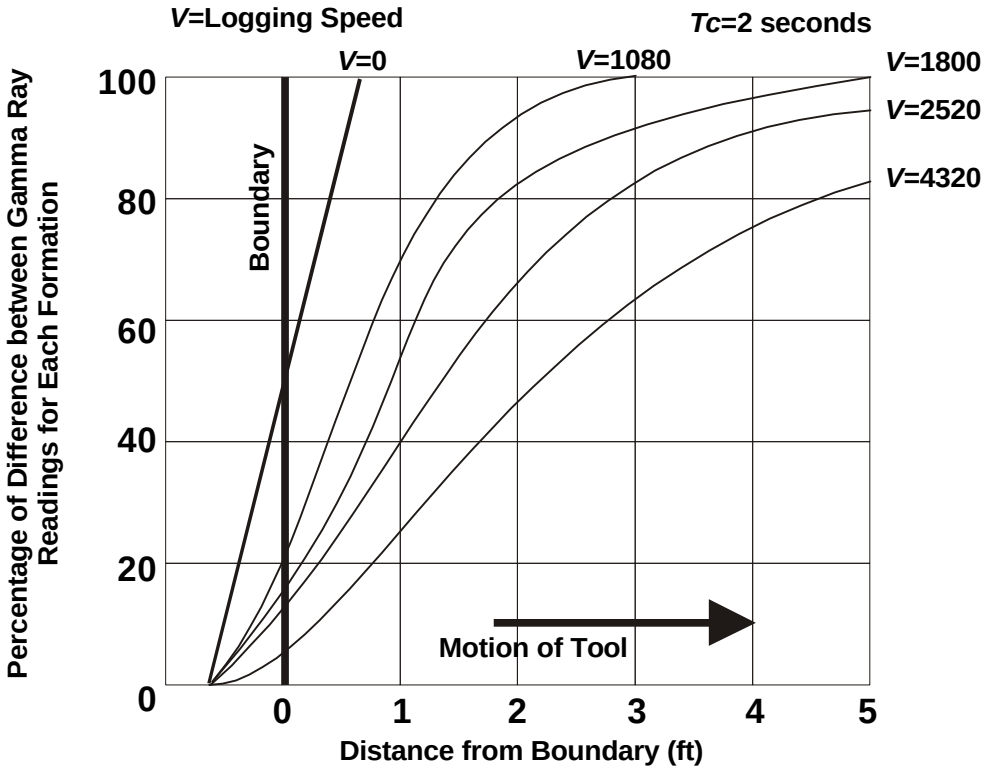

Figure 11.2 Effect of logging speed in bed boundaries.

11.7 Vertical Resolution

There are three factors governing the vertical resolution:

- The size of the detector, which is quite small (about 5-10 cm diameter).
- The effect of the time constant as described in Section 10.6. For conventional logging, with the product of logging speed and time constant set to 1 foot, the contribution to degradation in the vertical resolution from his cause is 1 foot.
- The hemispherical zone of sensitivity of the sensor. As the sensor is sensitive to gamma rays from a hemispherical zone, and its approximate depth of investigation of about 30 cm (1 foot) for formations of average density, we can see that the degradation in vertical resolution from this source will be about 2 foot.

Hence, the vertical resolution of the tool is just over 3 foot (90 cm).

This is quite a high vertical resolution for an open-hole tool, and so the gamma ray tool is good at defining thin beds, for fine correlation, and for depth matching between logging runs.

11.8 Borehole Quality

The gamma ray log usually runs centered in the borehole. If the borehole suffers from caving, the gamma ray log can be badly affected. In intervals that suffer from caving, there is more drilling mud between the formation and the gamma ray detector to attenuate the gamma rays produced by the formation. Hence, the log is underestimated, as shown in Fig. 11.3.

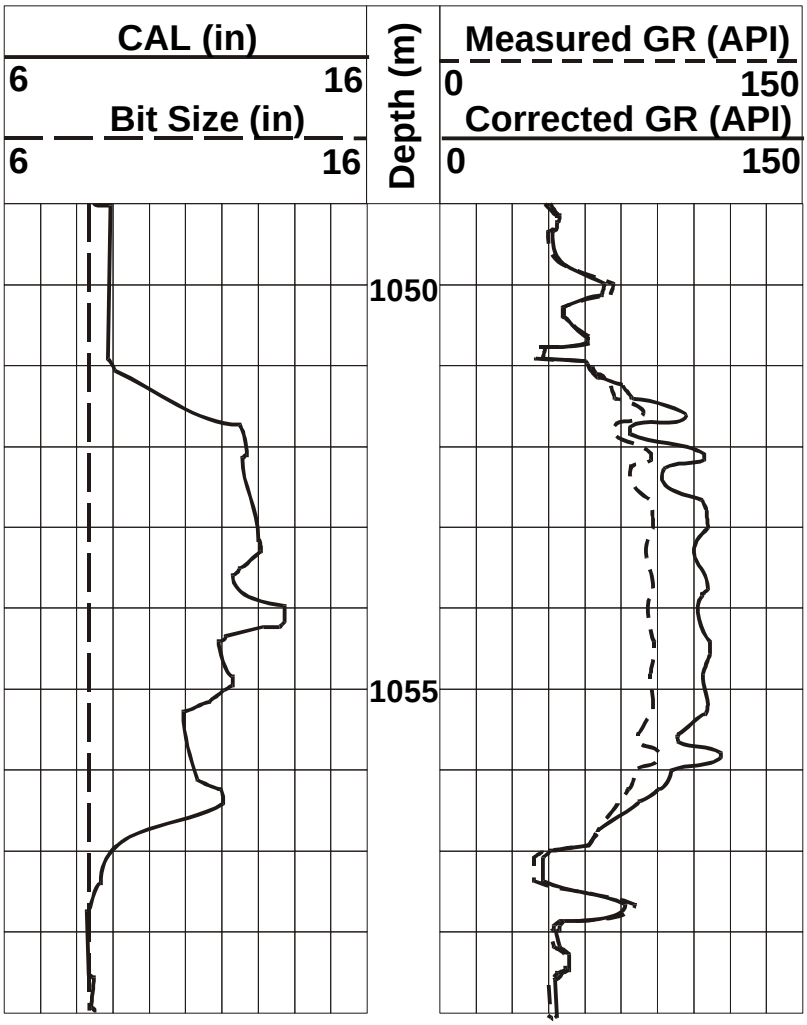

Figure 11.3 Effect of caving on the gamma ray log.

Note that the denser the mud used, the greater the underestimation will be, because of increased compton scattering in the drilling mud. Barite muds are a particular problem as barite is very efficient at absorbing gamma rays.

The measured overestimation may usually be corrected if the caliper log for the well is known. Figure 11.3 also shows the corrected gamma ray log. Comparison of the two show the degree to which the

caving has affected the gamma ray reading. Corrections are carried out using correction charts supplied by the logging tool company. Each tool design has its own set of charts, which are drawn up for a range of drilling fluids and tool geometries. Figure 11.4 shows an example of such a correction chart. Note that the tool can also be run in eccentred mode (pressed up against the borehole wall). When run in eccentred mode the corrections are much smaller as the drilling mud contributes less to the gamma ray signal, and has less opportunity to attenuate the gamma rays.

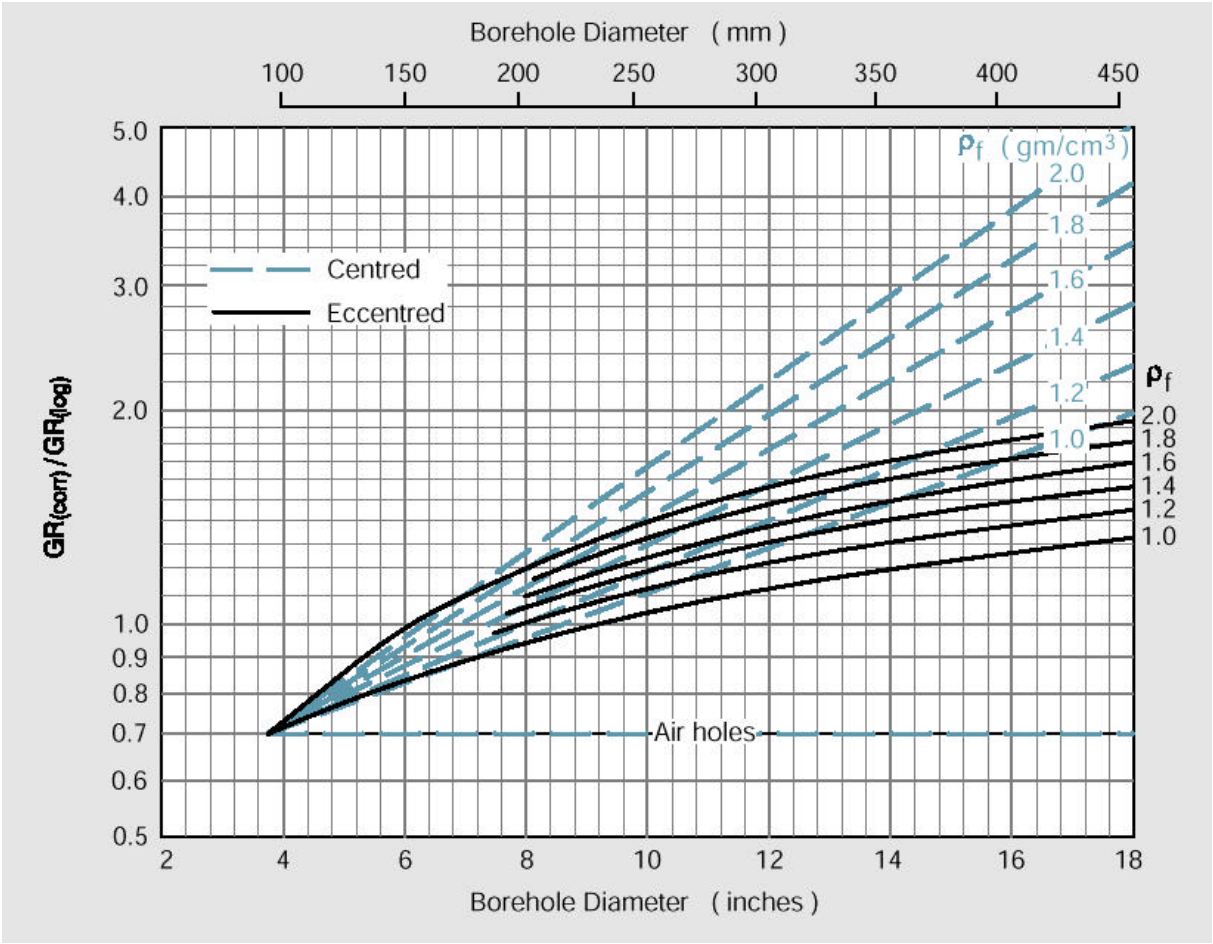

Figure 11.4 Gamma ray log correction chart for a 3.75 inch tool in an 8 inch hole with a KCl-free drilling mud with a mud weight of r_f g/cm^3 as a function of borehole diameter (courtesy of Reeves Wireline Ltd.).

11.9 Mud Type

The density of the drilling mud (*mud weight*) effects the signal because higher density muds attenuate gamma rays more. This effect is taken account of by the borehole correction done in the previous section. However, extra care should be taken with barite drilling muds, as barite is very efficient at attenuating gamma rays and will give an anomalously low gamma ray reading.

In the discussion so far, we have assumed that the drilling mud attenuates the gamma ray signal, but does not contribute to it. While this is true of many drilling muds, it is not generally true. Potassium

chloride-based drilling muds are not uncommon. These muds have a natural gamma radioactivity associated with potassium-40. The radiation from KCl drilling muds contributes to the total gamma ray count rate measured, increasing it considerably.

In good quality 'on-gauge' boreholes the gamma ray log is consistently increased by a constant amount. This is not a significant problem as a glance at the log header information would tell us that KCl mud was used and we should expect slightly higher values of the gamma ray log than usual.

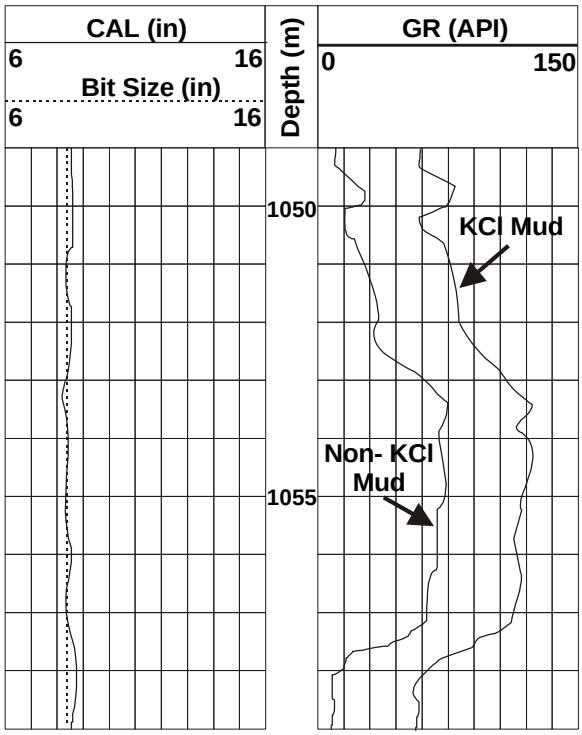

Figure 11.5 Effect of KCl drilling mud on the gamma ray log in an on-gauge borehole.

Problems may arise if the borehole diameter varies, leading to varying amounts of drilling-fluid between the formation and the sensor with depth. In caved holes in radioactive formations there is usually no effect observed as the caving effectively replaces a radioactive formation with radioactive drilling fluid. However, a significant local increase in the gamma ray log can be observed where very low radioactivity formations, such as some evaporites, have been washed out.

11.10 Uses of the Total Gamma Ray Log

The gamma ray log is an extremely simple and useful log that is used in all petrophysical interpretations, and is commonly run as part of almost every tool combination. Consequently, every well may have as many as 5 independent sets of gamma ray log data. The high vertical resolution of the gamma ray log makes it extremely useful for depth matching and fine scale correlation. The main uses of the gamma ray log are outlined in the following sections. The first three applications are by far the most important.

11.10.1 Determination of Lithology

The gamma ray log is an extremely useful tool for discrimination of different lithologies. While it cannot uniquely define any lithology, the information it provides is invaluable when combined with information from other logs.

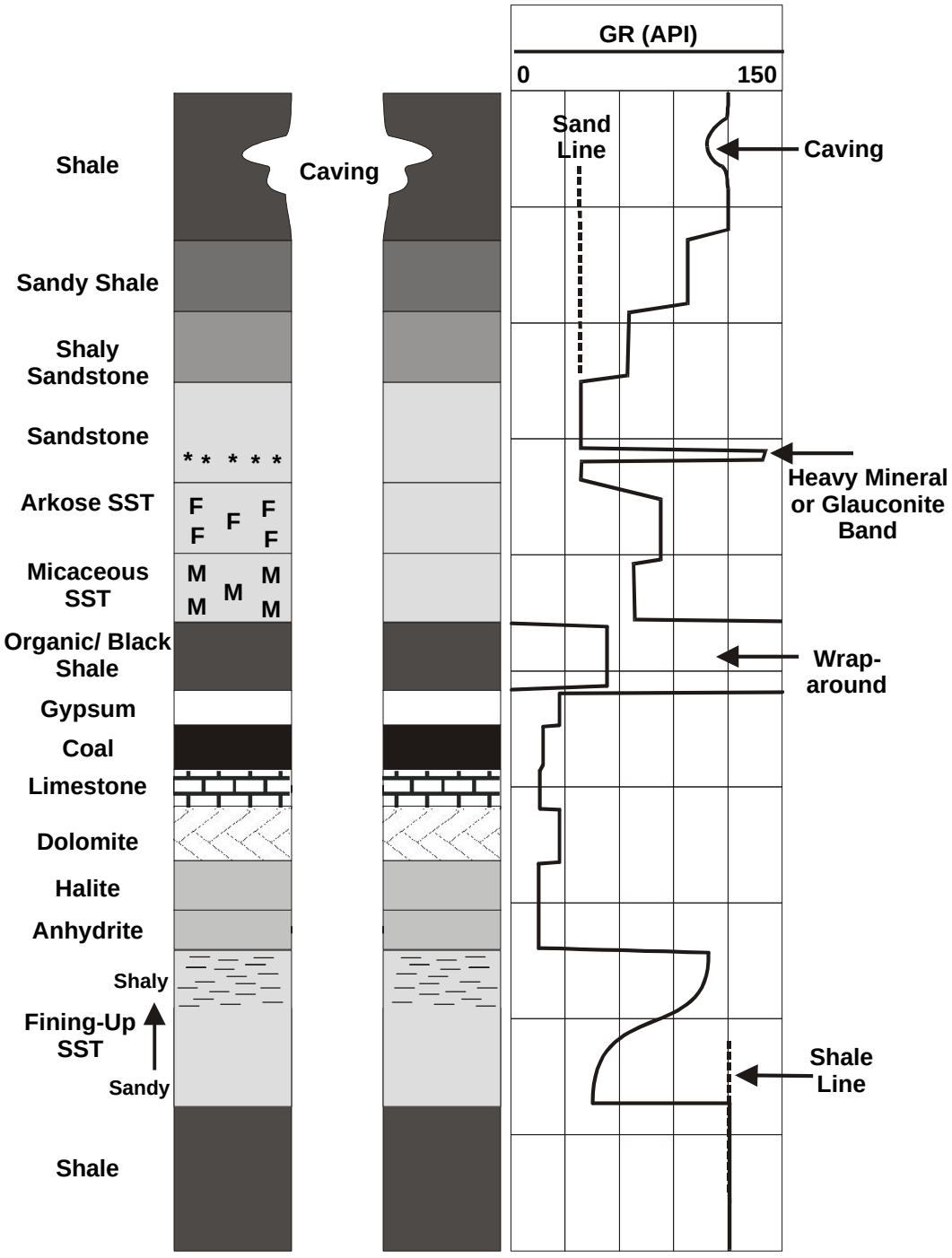

Figure 11.6 Effect of different lithologies on the gamma ray log.

Its main use is the discrimination of shales by their high radioactivity. Figure 11.6 shows how different lithologies affect the total gamma ray log. Note that shales, organic rich shales and volcanic ash show the highest gamma ray values, and halite, anhydrite, coal, clean sandstones, dolomite and limestone have low gamma ray values. Care must be taken not to generalize these rules too much. For example a clean sandstone may contain feldspars (arkose sandstones), micas (micaceous sandstones) or both (greywackes), or glauconite, or heavy minerals, any of which will give the sandstone higher gamma ray values than would be expected from a clean sandstone.

11.10.2 Determination of Shale Content

In most reservoirs the lithologies are quite simple, being cycles of sandstones and shales or carbonates and shales. Once the main lithologies have been identified, the gamma ray log values can be used to calculate the shaliness or *shale volume* V_{sh} of the rock. This is important as a threshold value of shale volume is often used to help discriminate between reservoir and non-reservoir rock.

Shale volume is calculated in the following way: First the *gamma ray index* I_{GR} is calculated from the gamma ray log data using the relationship

$$I_{GR} = \frac{GR_{\log} - GR_{\min}}{GR_{\max} - GR_{\min}} \qquad \textbf{(11.1)}$$

where: I_{GR} = the gamma ray index
$GR_{\log}$ = the gamma ray reading at the depth of interest
$GR_{\min}$ = the minimum gamma ray reading. (Usually the mean minimum through a clean sandstone or carbonate formation.)
$GR_{\max}$ = the maximum gamma ray reading. (Usually the mean maximum through a shale or clay formation.)

Many petrophysicists then assume that $V_{sh} = I_{GR}$. However, to be correct the value of I_{GR} should be entered into the chart shown as Fig. 11.7, from which the corresponding value of V_{sh} may be read.

It should be noted that the calculation of shale volume is a 'black art' as much depends upon the experience of the petrophysicist in defining what is the minimum (*sand line*) and the maximum (*shale line*) values, noting that the sand line and/or shale line may be at one gamma ray value in one part of the well and at another gamma ray value at deeper levels.

Once the shale volume has been calculated, a threshold shale volume may be defined which will divide the well into a number of reservoir and non-reservoir zones. This zonation is combined with the zonation that will also take place on the basis of porosity, permeability and hydrocarbon saturation.

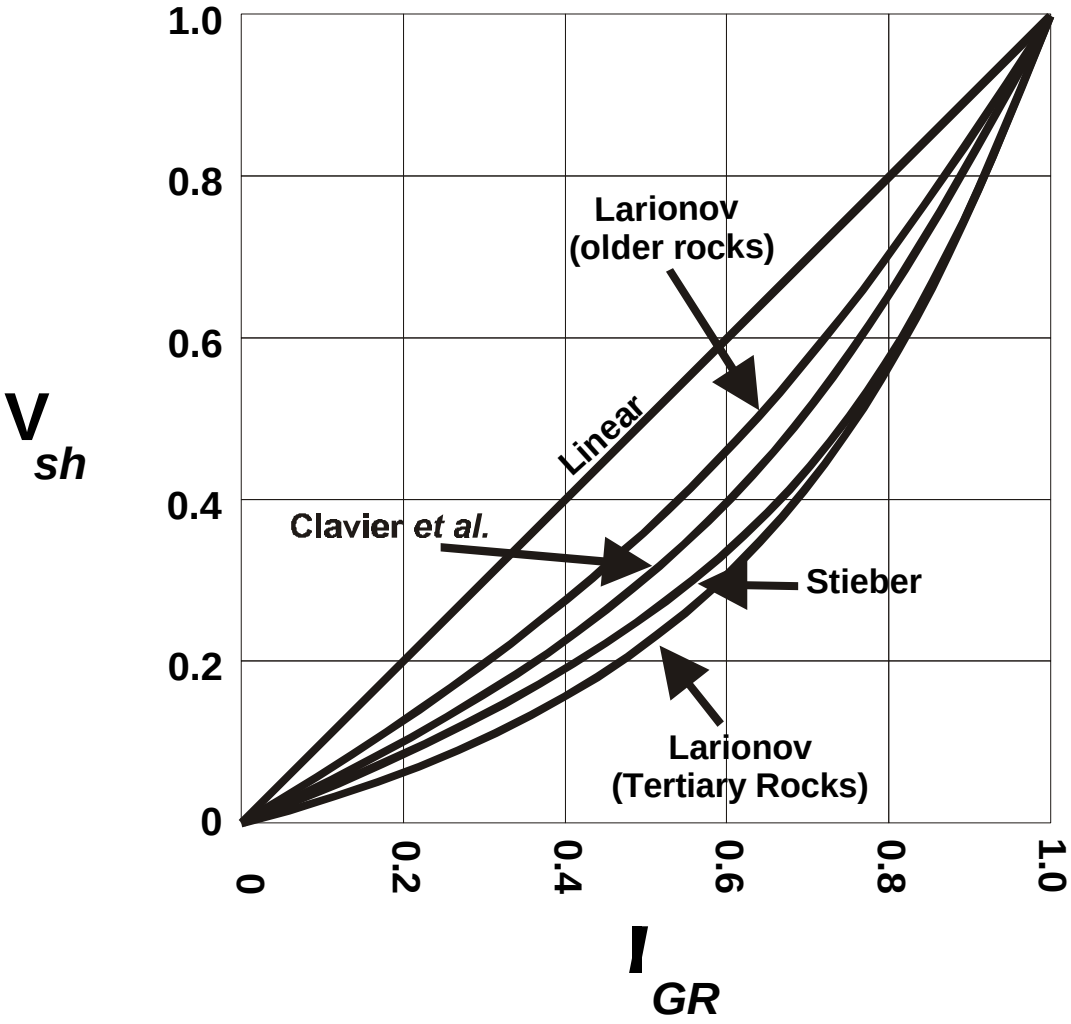

Figure 11.7 Calculation of shale volume.

10.10.3 Depth Matching

The gamma ray tool is run as part of almost every tool combination. It has a high reliability and a high vertical resolution. The tool will also show a useful decrease when opposite casing. For all these reasons, the tools is commonly used to match the depths of data from a given depth interval made at different times with different tool combinations. The depth matching may rely on the characteristic sudden reduction in gamma ray values when the tool encounters the casing of the section of borehole above the interval of interest, but more usually relies on matching the patterns in the gamma ray response from the gamma ray tools run with each tool combination.

10.10.4 Cased Hole Correlations

A different type of depth matching relates open hole measurements to cased hole and production logging measurements. Clearly, we would want to match accurately the depths at which open-hole data are taken and the depths at which cased-hole or production logging data are taken. The gamma ray log and the Casing Collar Locator allow this matching to be performed, ensuring that accurate

depth control is maintained during cased-hole logging, and while perforating the correct depths. Note that the gamma ray readings will be less in the cased holes due to the attenuation of gamma rays by the cement casing.

11.10.5 Recognition of Radioactive Mineral Deposits

The gamma ray log can be used to recognize certain radioactive deposits, the most common of which are potash deposits and uranium ores.

Potassium-40 emits gamma rays with the single energy of 1.46 MeV. This results in there being a linear relationship between the gamma ray count rate and the content of potassium in the formation. In potash deposits, the gamma ray reading after hole size correction gives approximately 15 API units per 1%wt. K_2O.

There is no simple relationship between the gamma ray reading and the abundance of uranium in a formation, because the energy spectrum also includes radiation from other elements in the uranium-radium series.

11.10.6 Recognition of Non-Radioactive Mineral Deposits

Particular deposits have a very low natural radioactivity. The gamma ray log can also be used to indicate these. Formations with extremely low natural radioactivities are the non-radioactive evaporites (salt, anhydrite and gypsum), and coal beds. Note that some evaporites have a large concentration of potassium and can be very radioactive. These rare evaporites are given in Table 10.1.

11.10.7 Radio-isotope Tracer Operations

Deliberate doping of fluids with radioactive tracers is sometimes carried out to find the location of pipe leaks, thief zones and channeling behind the casing. The gamma ray log is sometimes employed as a detector in these cases.

11.10.8 Facies and Depositional Environment Analysis

We have seen that the gamma ray log is often used to measure the shaliness of a formation. In reality the shaliness often does not change suddenly, but occurs gradually with depth. Such gradual changes are indicative of the litho-facies and the depositional environment of the rock, and are associated with changes in grain size and sorting that are controlled by facies and depositional environment as well as being associated with the shaliness of the rock. Figure 11.8 analyses the shape of gamma ray log responses for various depositional environments.

All possible combinations of these shapes may be encountered.

Shape	Smooth	Environments	Serrated	Environments
Cylinder Represents uniform deposition.	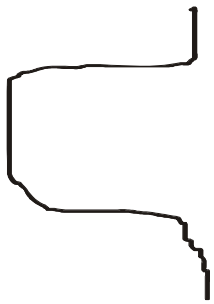	Aeolian dunes Tidal sands Fluvial Channels	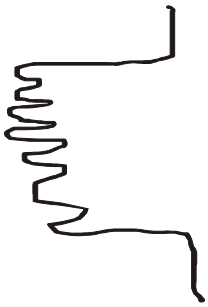	Deltaic distributaries Turbidite channels Proximal deep-sea fans
Bell Shape Fining upwards sequences.	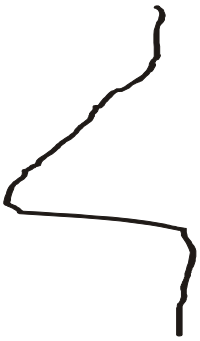	Tidal sands Alluvial sands Braided streams Fluvial channels Point bars	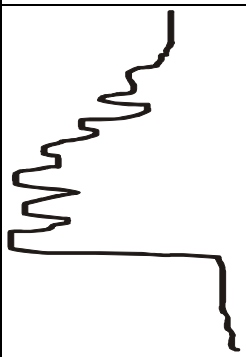	Lacustrine sands Deltaic distributaries Turbidite channels Proximal deep-sea fans
Funnel Shape Coarsening upward sequences.	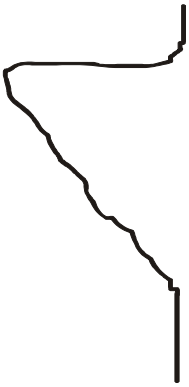	Barrier bars Beaches Crevasse splays	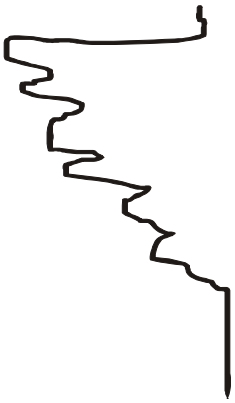	Distributary mouth bars Delta marine fringe Distal deep-sea fans

Figure 11.8 The gamma ray log and depositional environments.

12. THE SPECTRAL GAMMA RAY LOG

12.1 Introduction

The *spectral gamma ray* log measures the natural gamma radiation emanating from a formation split into contributions from each of the major radio-isotopic sources. Analysis of the sources of the natural gamma radiation give us added information concerning the composition and likely lithology of the formation.

The spectral gamma ray log is commonly given the symbol *SGR*.

A typical spectral gamma ray tool is shown in Fig. 12.1.

12.2 Principles

It will be remembered that the amplitude of the output from the gamma ray sensor is proportional to the energy of the incident gamma ray. We can use this information to measure the proportion of the total gamma radiation coming from each of potassium-40, the uranium-radium series, and the thorium series for a particular formation.

Figure 10.1 shows that the energy distributions from each of the major contributors to the natural gamma radiation from a formation are different. The labeled peaks in Figure 10.1 are the energies that are dominant (most gamma rays have this energy). When the radiation has traveled through the rock and drilling fluid to the sensor, the energy distributions shown in Figure 10.1 are added together because the rock contains different amounts of each of radio-isotopes. The energy distributions are also spread out in energy space as the result of compton scattering. However, the energy peaks from each of the major contributors to the gamma radiation are still recognizable (Fig. 12.2).

Figure 12.1 The Spectral Gamma Ray Sonde (SGS). (Courtesy of Reeves Wireline Ltd.)

The spectral gamma ray tool uses the same sensor as the total gamma ray tool. The output from the sensor is fed into a multi-channel analyzer that calculates the amount of radiation coming from the energies associated with each of the major peaks. This is done by measuring the gamma ray count rate for 3 energy windows centred around the energies 1.46 MeV for potassium-40, 1.76 MeV for the uranium-radium series, and 2.62 MeV for the thorium series. These readings represent the gamma ray radioactivity from each of these sources. Their sum should be the same as the total gamma ray value measured by the total gamma ray tool, and is coded *SGR* if measured with a spectral gamma ray tool. Any combination of the three components can be summed and analyzed. However, the most important is the sum of the potassium-40 and thorium radiation, which is called the *computed gamma ray* response (*CGR*).

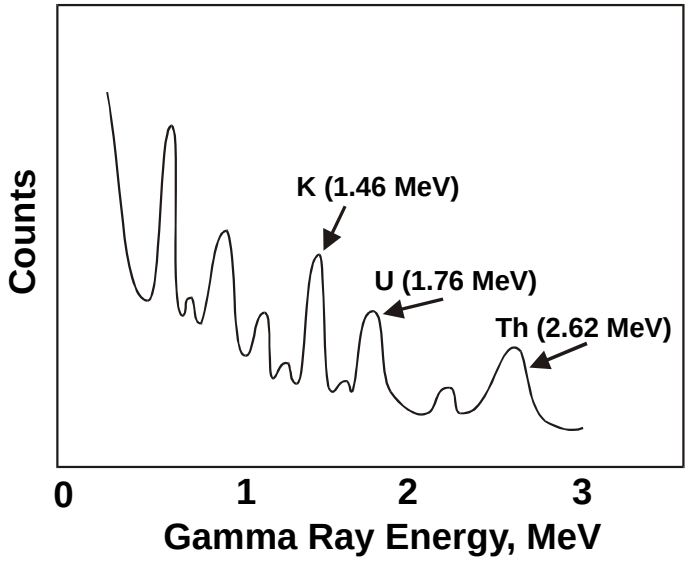

Figure 12.2 Measured gamma ray energy spectrum from a formation after compton scattering.

12.3 Calibration

The spectral gamma ray tool is calibrated using 4 sources of accurately known composition, one each containing only K^{40}, U^{238}, and Th^{232}, and one containing a mixture. Each of the sources is placed next to the detector and the tool is used to make a measurement. The calibration is designed such that the calibrated readings of the tool accurately report difference in the amount of radiation from each of the radiation sources, and the total count rate is calibrated to the Houston test pit.

12.4 Log Presentation

The format for reporting the spectral gamma ray data is more complex than for the total gamma ray log because it contains much more detailed information.

Track 1 is used to record the derived total gamma ray log (*SGR*), which is a sum of all the radiation contributions, as well as the computed gamma ray log (*CGR*), which is the sum of the potassium and thorium responses, leaving out the contribution from uranium.

Tracks 2 and 3 are used to record the calculated abundances associated with the radiation from the individual contributions from each of K^{40}, U^{238}, and Th^{232}. It should be noted that potassium is reported as a percentage, while U^{238} and Th^{232} are reported in parts per million (ppm).

Figure 12.3 shows a typical spectral gamma ray log.

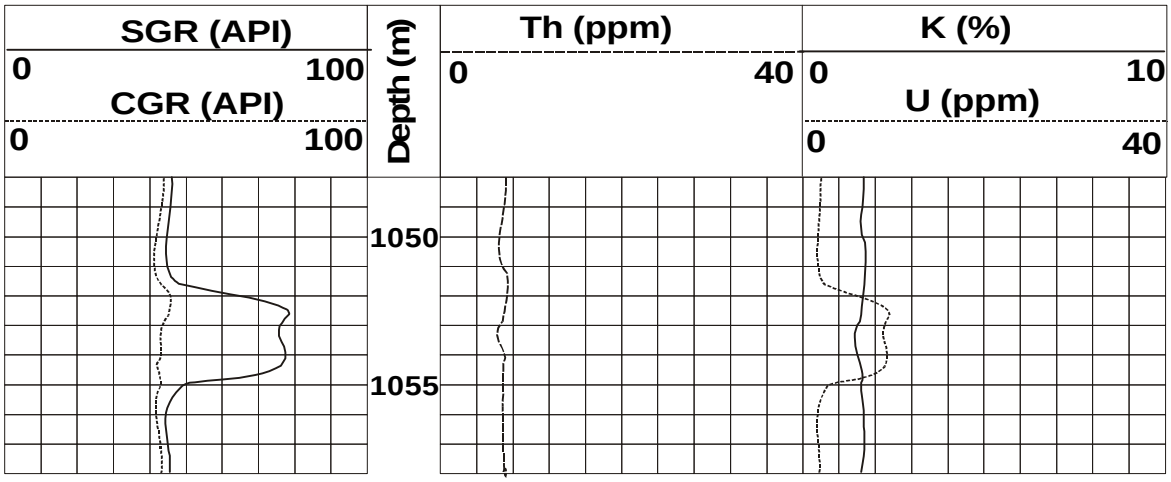

Figure 12.3 The presentation of the spectral gamma ray log.

12.5 Depth of Investigation

The depth of investigation is controlled by the same fundamental physics as for the total gamma ray tool, and is identical to the total gamma ray tool (i.e., about 1 ft).

12.6 Logging Speed

While all the arguments concerning logging speed for the total gamma ray tool are also appropriate for the spectral tool, the statistical fluctuations must now be applied to proportions of the total gamma count rate. If good quality data for each of K^{40}, U^{238} and Th^{232} are to be obtained, the logging speed must consequently be lower. In practice, the log is usually run 2 to 3 time more slowly that the total gamma ray log. However, this results in very high quality *SGR* logs.

12.7 Vertical Resolution

The vertical resolution is often better than the total gamma ray tool as a consequence of the slower logging speeds. Resolutions as low as 1 foot have been obtained with some tools.

12.8 Borehole Quality

As with the total gamma ray log, the spectral tool can be run centered in the borehole or pushed up against the borehole wall (eccentred). If the borehole suffers from caving, the spectral gamma ray log can be badly affected in the same way as the total gamma ray tool, although the effect is not as bad for

the eccentred version. Correction charts for the spectral gamma ray tools are also supplied by the logging tool company for centred and eccentred configurations.

12.9 Mud Type

The density of the mud has a bearing on the detection rate, as a higher density mud absorbs the gamma rays more efficiently and reduces count rate. This is taken into account by the borehole correction, which is done for a given drilling mud density (mud weight). The worst effects are seen when barite mud is used, as barite is efficient at adsorbing gamma rays. Again, the eccentred version is less susceptible to mud weight.

The problem with KCl-based drilling mud is also apparent with the spectral tool. However, the effect of the KCl mud will only be apparent in the *SGR*, *CGR* and potassium logs. Again, the eccentred version is less susceptible to KCl mud.

12.10 Uses of the Spectral Gamma Ray Log

The spectral gamma ray log is an extremely useful log, especially for subtle lithological and compositional analysis, which benefits from its high vertical resolution. In the analysis of spectral gamma ray data, use is commonly made of the ratios of the abundances of the main radioactive sources. For example the Th/K ratio. It should be noted, however, that this is not a dimensionless ratio as the Th is measured in ppm and the K is measured in percent. Thus Th=12 ppm and K=4%, gives Th/K=3, where the units are usually not mentioned, but are actually parts per ten thousand (ppm/%).

12.10.1 Determination of Lithology

12.10.1.1 Discriminating between Sands, Shales and Accessory Minerals

It was seen in the discussion concerning the total gamma ray log that clean sands can sometimes produce high gamma ray readings which would confuse them with shales. Such sandstones include those containing feldspars, micas, glauconite, and heavy minerals including uranium-bearing ores. The extra information supplied by the spectral gamma ray tool can, in most cases, help recognize these situations, and calculate the amount of the particular radioactive minerals present.

Radioactive sandstones fall into one of six main groups, which are classified below, and may be recognized using Figs. 12.4 and 12.5.

Clay-Bearing Sandstones. If clay minerals are known to be present in the rock, they may be identified using Fig. 12.5.

Arkose sandstones. These contain feldspars, which have a significant potassium content, but a low thorium content. The Th/K ratio will therefore be low (<1 ppm/%), as shown in Fig. 12.4.

Micaceous sandstones. These contain mica, which has a potassium composition that is less than feldspars and a thorium content that is higher. The Th/K ratio is usually between 1.5 and 2.5 ppm/%.

Graywackes. These contain both feldspars and micas, and give Th/K ratios intermediate between 1 and 2.5 ppm/%.

Greensands. These contain glauconite, which is a mica group mineral containing iron, magnesium and potassium. It has Th/K ratios between 1 and 1.5 ppm/%.

Heavy mineral-bearing sandstones. The heavy minerals are often abundant in either U or Th or both. The U and Th values are usually sufficiently high to ensure high U/K and Th/K ratios even if the sandstones also contains potassium in the form of feldspars, micas or glauconite. Typically Th/K values will be above 25 ppm/%, and U/K values will be above 20 ppm/%.

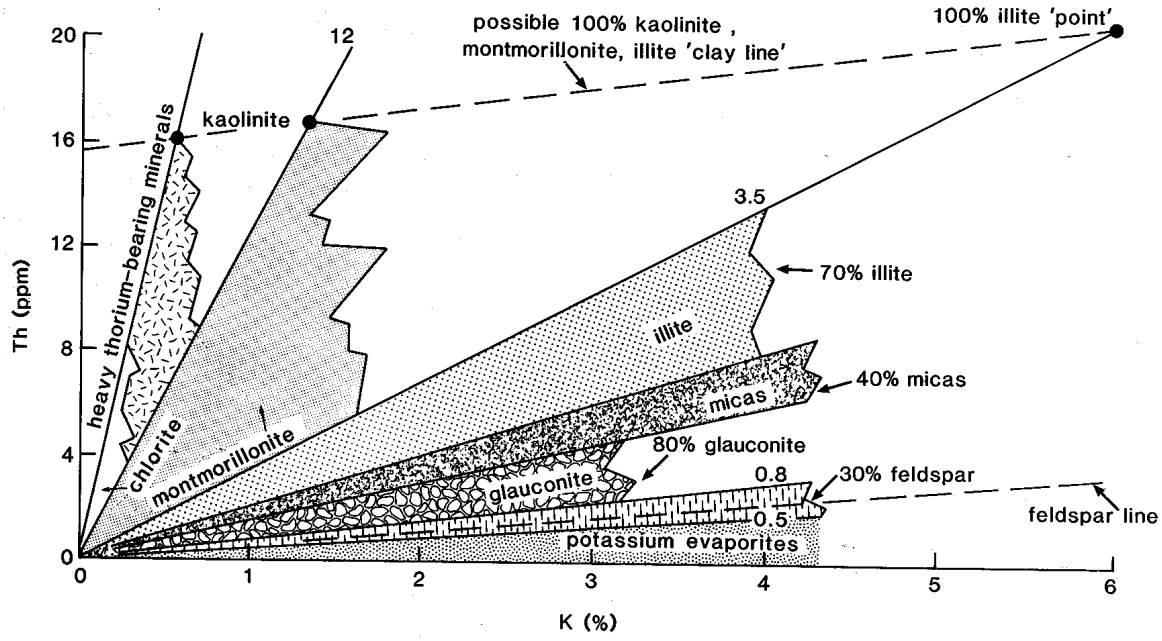

Figure 12.4 Thorium/potassium cross-plot for mineral identification using spectral gamma ray data.

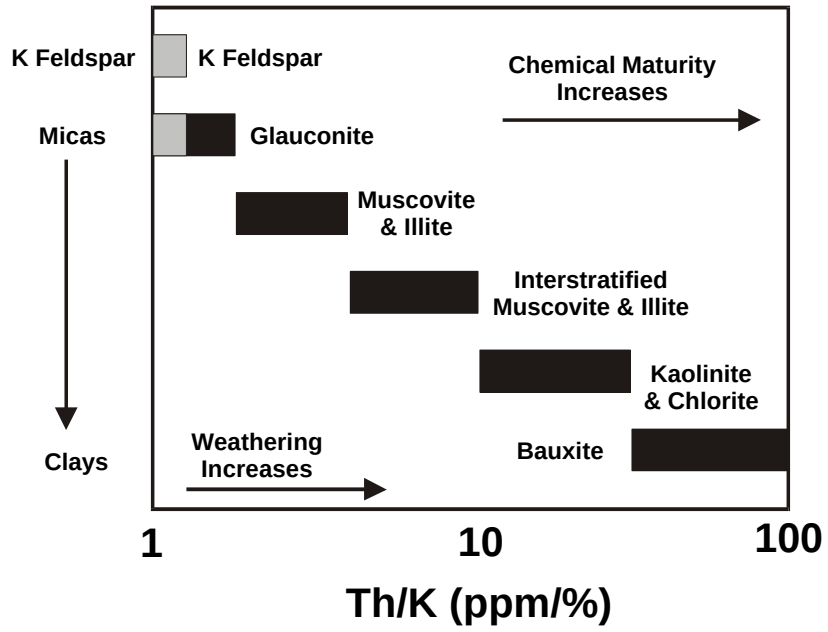

Figure 12.5 Thorium/potassium ratio plot for mineral identification using spectral gamma ray data.

The fact that sands that do not contain clays are sometimes radioactive, as seen above, indicates that there will be occasions when the shale volume calculated from the total gamma ray log (*GR*) or the total gamma ray log from the spectral tool (*SGR*) will be misleading. However, we can calculate the shale volume from the individual readings of the spectral gamma ray log (K, Th, and U), and from the computed gamma ray log (*CGR*).

$$V_{sh}\big|_{CGR} = \frac{CGR - CGR_{\min}}{CGR_{\max} - CGR_{\min}} \quad \textbf{(12.1)}$$

$$V_{sh}\big|_{K} = \frac{K - K_{\min}}{K_{\max} - K_{\min}} \quad \textbf{(12.2)}$$

$$V_{sh}\big|_{Th} = \frac{Th - Th_{\min}}{Th_{\max} - Th_{\min}} \quad \textbf{(12.3)}$$

$$V_{sh}\big|_{U} = \frac{U - U_{\min}}{U_{\max} - U_{\min}} \quad \textbf{(12.4)}$$

Equations (12.1) to (12.3) are better shale indicators than Eq. (11.1), since the random contribution of U is eliminated. Equation (12.4), is almost never used.

12.10.1.2 Carbonate Formations

In pure carbonates, thorium will usually be absent because the common thorium ions are insoluble, and potassium will also be negligible. So we can say that, if the formation has very low Th and K abundances, the rock may be a pure carbonate. The rock, however, may contain uranium. Uranium usually indicates material of an organic origin as organisms are extremely good at concentrating and storing uranium. Uranium ions are either soluble or insoluble depending upon their oxidation state. Highly oxidized uranium ions, from oxidizing environments (such as deserts) are insoluble. Thus a carbonate, which also has low U abundance, comes from an oxidizing (maybe desert) environment. Conversely, non-oxidized uranium ions from sub-surface depositional environments are more soluble, and hence can be present in carbonates.

It should be noted that oxidizing environments are not conducive to the conservation of organic material, while reducing environments not only favour the conservation of organic material, they aid the conversion of the organic material to hydrocarbons. The source organic material for hydrocarbons in carbonate rocks is often algal mats that are incorporated in the deposited rocks in a sub-sea (reducing) environment and contain a significant amount of uranium.

In clay-bearing carbonate rocks high total gamma readings are not related only to the clay fraction, but are also due to the presence of uranium-radium series isotopes of organic origin. High total gamma ray readings are therefore not a reliable indicator of the shaliness of a carbonate. However, if the spectral gamma ray log indicates the presence of K and Th together with the U, it may be said that the K and Th contributions are associated with the clay content of the shaly carbonate, while the U is associated with some organic source which was deposited in a reducing environment that favours the

conservation of organic material. Similarly, high K and Th values together with low U indicates a shaly carbonate, deposited in an oxidizing environment which is not a favourable environment for the conservation of organic material.

Note that K and Th must be present **together** for a clay to be indicated. The presence of K and no Th (with or without U) is usually an indicator of the remains of algal mats in the carbonate, or of glauconite. Thus, when calculating the shaliness of a carbonate, it is better to use the *CGR* (Eq. 12.1) as in the case of sandstones in 12.10.1.1 above.

The actual values of K and Th in the shaly carbonate will depend upon the type of clay present, as shown in Fig. 12.4.

Note that isolated intervals of any combination of high U, K and Th in carbonate rocks may correspond to stylolites, which tend to concentrate uranium, organic matter, and clay minerals.

Table 12.1 shows the main interpretations of the spectral gamma ray data for carbonate rocks.

Table 12.1 Interpretation of spectral gamma ray data in carbonates.

K	Th	U	Explanation
Low	Low	Low	Pure carbonate, no organic matter or oxidizing environment.
Low	Low	High	Pure carbonate, organic matter, reducing environment.
Low	High	Low	Not a carbonate, or shaly carbonate with rarer low K high Th clay minerals, no organic matter or oxidizing environment.
Low	High	High	Not a carbonate or shaly carbonate with rarer low K high Th clay minerals, organic matter, reducing environment.
High	Low	Low	Glauconite carbonate, no organic matter or oxidizing environment. Also consider K-bearing evaporites.
High	Low	High	Algal carbonate, or glauconite present, organic matter, reducing environment.
High	High	Low	Shaly carbonate, no organic matter or oxidizing environment.
High	High	High	Shaly carbonate, organic matter, reducing environment.
Note: Stylolites can locally concentrate U, clays and organic matter.			

12.10.1.3 Evaporites

Large total gamma ray values are commonly associated with shales and certain types of potassium-bearing evaporite. We can discriminate between these because the potassium-bearing evaporites have much larger potassium abundances and zero thorium resulting from the insolubility of thorium ions in

water. Evaporites are deposited in oxidizing environments, so the uranium is usually also very low or zero. Some K-bearing evaporites are shown in Table 12.2.

Table 12.2 Potassium-bearing evaporites.

Name	**Composition**	**K (wt%)**	**Density [FDC] (g/cm^3)**	**Pe [LFDC] (b/e)**	**Porosity [CNL] (%)**	**DT [Sonic] (ms/ft)**
Sylvite	KCl	52.44	1.86	8.51	-3	74
Langbeinite	$K_2SO_4(MgSO_4)_2$	18.84	2.82	3.56	-2	52
Kainite	$MgSO_4\ KCl(H_2O)_2$	15.7	2.12	3.5	>60	-
Glaserite	$(K\ Na)_2SO_4$	24.7	2.7	-	-	-
Carnalite	$KCl\ MgCl_2(H_2O)_6$	14.07	1.57	4.09	>60	83
Polyhalite	$K_2SO_4\ MgSO_4\ (CaSO_4)_2\ (H_2O)_2$	13.37	2.79	4.32	25	57.5

12.10.2 Unconformity Detection

The mean Th/K ratio of large intervals of formations is usually approximately constant. This is because it depends ultimately upon the depositional conditions. Hence any sudden changes in the mean Th/K ratio can act as an indicator of sudden change in depositional environment, such as at an unconformity.

12.10.3 Inter-well Correlation

Volcanic ashes (bentonitic intervals) are considered to be deposited at exactly the same time over a wide area. They can therefore be used to correlate between wells. Peaks in the thorium abundance log are generally considered the best signature in this correlation.

12.10.4 Recognition of Igneous Rocks

The values of Th and U from the spectral gamma ray log are used together with the density from the density log and the sonic wave travel time from the sonic log to identify and discriminate between igneous rocks. Most igneous rocks show a Th/U ratio close to 4, as shown in Fig. 12.6. The exception is syenite (Th/U=0.52). Note the progression from low values of both Th and U for ultramafic rocks to higher values as the rocks become more acidic, but with constant Th/U.

12.10.5 Diagenesis

Diagenesis is studied using the Th/K ratio derived from spectral gamma ray logs.

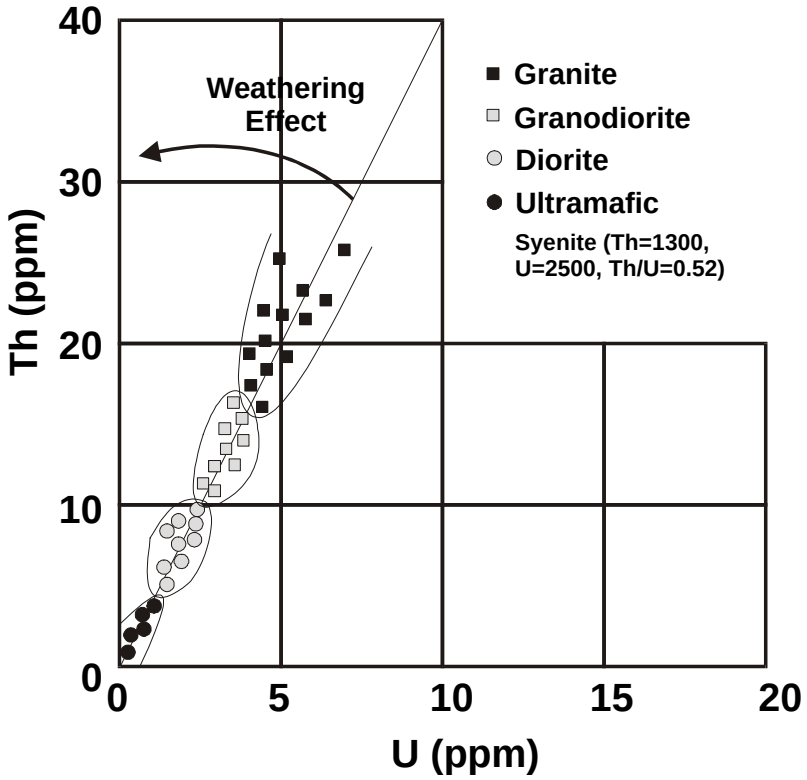

Figure 12.6 Thorium-Uranium cross-plot for igneous rocks. (Courtesy of Schlumberger).

12.10.6 Sedimentology

The spectral gamma ray log provides a large amount of data that can help discriminate between depositional environments and allow grain size and mineralogical composition to be constrained. Some of the more important sedimentologically relevant data are shown in Table 12.3.

Table 12.3 Sedimentological inferences from spectral gamma ray data.

SGR Observation	**Sedimentological Inference**
Presence of glauconite	Marine, mainly continental shelf origin.
Phosphatic deposits	Marine, mainly continental shelf origin, with warm water in a reducing environment.
Uranium	Low energy, reducing conditions
Clay type	Analysis of depositional environment.
Bauxite	Warm, humid, continental environment with good drainage.
Feldspars	Indicator of the degree of evolution of sand facies, only found in abundance close to the igneous source.

12.10.7 Estimation of Uranium Potential

Direct measurement of the amount of uranium present in the rocks, and its variation.

12.10.8 Cation Exchange Capacity

The cation exchange capacity of the rock may be calculated by knowing the type and quantity of clays present in the rock from spectral gamma ray data.

12.10.9 Radioactive Scaling

Unusually raised U contents are frequently observed in the perforated intervals of old wells due to the build-up of uranium salts.

12.10.10 Hydrocarbon Potential

Organic matter is good at concentrating uranium. If this is deposited in a reducing environment it can be preserved and transformed to hydrocarbons. Hence, there is a correlation between the presence of uranium and hydrocarbons. It is possible to evaluate the total organic carbon content of rocks from the uranium content derived from the spectral gamma ray log providing the relationship is calibrated using core data. The hydrocarbon potential of the rock may then be derived from the total organic carbon content.

12.10.11 Fracture Detection

Uranium is soluble in reducing conditions. Dissolved uranium salts may then be precipitated along fractures, causing local peaks in the uranium spectral gamma ray log. However, local uranium peaks do not unambiguously indicate fractures, so their presence must be checked on image logs.

12.10.12 Stylolite Detection

Stylolites concentrate clay minerals, organic matter and uranium, and can be compacted into thin bands which show up as thin peaks in the uranium spectral gamma ray log.

12.10.13 Phosphate Detection

Uranium is also associated with phosphates, which are encountered with evaporites.

13. THE FORMATION DENSITY LOG

13.1 Introduction

The *formation density* log measures the bulk density of the formation. Its main use is to derive a value for the total porosity of the formation. It s also useful in the detection of gas-bearing formations and in the recognition of evaporites.

The formation density tools are induced radiation tools. They bombard the formation with radiation and measure how much radiation returns to a sensor.

13.2 Theory

The tool consists of:

- **A radioactive source.** This is usually caesium-137 or cobalt-60, and emits gamma rays of medium energy (in the range 0.2 – 2 MeV). For example, caesium-137 emits gamma rays with a energy of 0.662 MeV.

- **A short range detector.** This detector is very similar to the detectors used in the natural gamma ray tools, and is placed 7 inches from the source.

- **A long range detector.** This detector is identical to the short range detector, and is placed 16 inches from the source.

The gamma rays enter the formation and undergo compton scattering by interaction with the electrons in the atoms composing the formation, as described in Section 9.3. Compton scattering reduces the energy of the gamma rays in a step-wise manner, and scatters the gamma rays in all directions. When the energy of the gamma rays is less than 0.5 MeV they may undergo photo-electric absorption by interaction with the atomic electrons. The flux of gamma rays that reach each of the two detectors is therefore attenuated by the formation, and the amount of attenuation is dependent upon the density of electrons in the formation.

- A formation with a high bulk density, has a high number density of electrons. It attenuates the gamma rays significantly, and hence a low gamma ray count rate is recorded at the sensors.

- A formation with a low bulk density, has a low number density of electrons. It attenuates the gamma rays less than a high density formation, and hence a higher gamma ray count rate is recorded at the sensors.

The density of electrons in a formation is described by a parameter called the *electron number density*, n_e. For a pure substance, number density is directly related to bulk density, and we can derive the relationship in the following way.

- The number of atoms in one mole of a material is defined as equal to Avagadro's number N ($N \approx 6.02 \times 10^{23}$).

- The number of electrons in a mole of a material is therefore equal to NZ, where Z is the atomic number (i.e., the number of protons, and therefore electrons per atom).

- Since the atomic mass number A is the weight of one mole of a substance, the number of electrons per gram is equal to NZ/A.

- However, we want the number of electrons per unit volume, and we can obtain this from the number of electrons per gram by multiplying by the bulk density of the substance, ρ_b. Hence, the electron number density is

$$n_e = \frac{N\,Z}{A}\,\rho_b \qquad \textbf{(13.1)}$$

where: n_e = the number density of electrons in the substance (electrons/cm^3)
N = Avagadro's number ($\approx 6.02\times10^{23}$)
Z = Atomic number (no units)
A = Atomic weight (g/mole)
ρ_b = the bulk density of the material (g/cm^3).

Thus, the gamma count rate depends upon the electron number density, which is related to the bulk density of a substance by Eq. (13.1). The bulk density of a rock depends upon the solid minerals of which it is composed, its porosity, and the density of the fluids filling that porosity. Hence, the formation density tool is useful in the determination of porosity, the detection of low density fluids (gasses) in the pores, and as an aid in lithological identification.

13.3 Operation

A radiation emitter and one detector are all that is necessary for a simple measurement. The early tools had only one detector, which was pressed against the borehole wall by a spring-loaded arm. Unfortunately, this type of tool was extremely inaccurate because it was unable to compensate for mudcake of varying thicknesses and densities through which the gamma rays have to pass if a measurement of the true formation is to be achieved.

All the newer tools have two detectors to help compensate for the mudcake problem. The method of compensation is described in subsequent sections. The newer two detector tools are called compensated formation density logs, an example of which is Schlumberger's FDC (formation density compensated) tool.

Compensated formation density tools have one focussed (collimated) radiation source, one short spacing detector at 7 inches from the source, and one long spacing detector 16 inches from the source (Fig. 13.1). The source and both detectors are heavily shielded (collimated) to ensure that the radiation only goes into the mudcake and formation, and that detected gamma rays only come from the mudcake or formation. The leading edge of the shield is fashioned into a plough which removes part of the mudcake as the tool is pulled up the well. The tool is pressed against one side of the borehole using a servo-operated arm with a force of 800 pounds force. Under this pressure and the pulling power of the wireline winch the plough can make a deep impression in the mudcake. The large eccentering force also means that there is much wear of the surface of the tool that is pressed against the borehole wall. The heavy shielding also doubles as a skid and a wear plate that protects the source and detectors and can be replaced easily and cheaply when worn down.

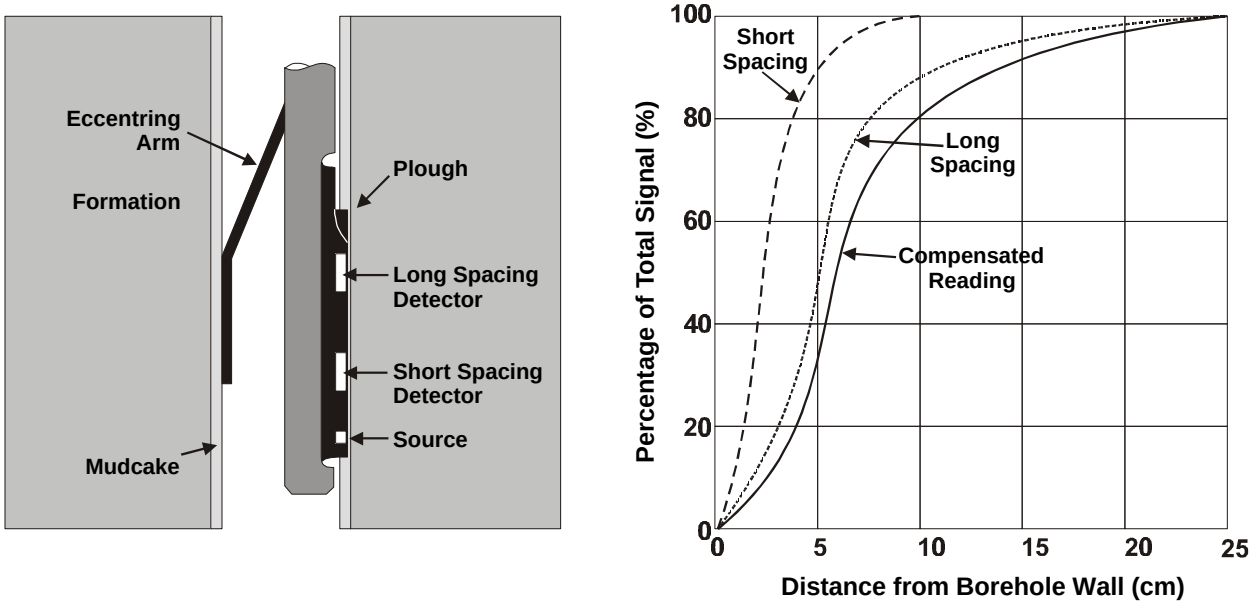

Figure 13.1 Schematic diagram of a formation density tool.

The operation of this tool depends upon the detection of gamma rays that have been supplied to the formation by the source on the tool and have undergone scattering. Clearly the natural gamma rays from the formation confuses the measurement. A background gamma ray count is therefore carried out so that the gamma rays coming from the formation can be removed from the measurement.

Note in Fig. 13.1 that for the short spacing detector over 80% of its signal comes from within 5 cm of the borehole wall, which is commonly mainly mudcake. About 80% of the long spacing signal comes from within 10 cm of the borehole wall. Therefore the tool has a shallow depth of investigation. We wish to remove the mudcake signal from the measurement, and the procedure to do this is described in Section 13.4. When the mudcake compensation has been carried out, one can see from Fig. 13.1 that the depth of investigation has been improved, and less signal comes from the first 5 cm region.

13.4 Mudcake Compensation

Gamma rays detected by the short spacing detector have penetrated only a short way into the mudcake and formation before being scattered back to the detector. Readings from the short spacing detector are therefore a measure of attenuation in the near-borehole region (i.e., mudcake and very shallow in the formation). By comparison, gamma rays detected by the long spacing detector have penetrated through the mudcake and deeper into the formation before being scattered back to the detector. Readings from the long spacing detector are therefore a measure of attenuation in the formation that has been perturbed by the gamma rays having to pass through the mudcake twice.

The compensation scheme described below effectively takes the effect of the near-borehole region (short spaced detector) away from the formation plus near-borehole region (long spacing detector). This sounds easy but is not straightforward.

For any given borehole and tool geometry there are eight independent parameters that affect the reading of the tool. These are:

Z_b = the mean atomic number of the formation
A_b = the mean atomic weight of the formation
r_b = the bulk density of the formation
Z_{mc} = the mean atomic number of the mudcake
A_{mc} = the mean atomic weight of the mudcake
r_{mc} = the bulk density of the mudcake
h_{mc} = the thickness of the mudcake

The influence of changing Z_b, A_b and A_{mc} are small, and so these parameters can be considered to be constant. Unfortunately we cannot assume that Z_{mc} is constant as the drilling mud (and hence mudcake) may or may not contain barite in very significant quantities.

The number of variable parameters is reduced to three by the incorporation of r_{mc} and Z_{mc} into a single parameter, the effective mudcake density r_{mc}* , which combines the influences of both r_{mc} and Z_{mc}. The remaining three parameters are r_b, r_{mc}* and h_{mc}.

These three parameters are represented as a function of the readings from the short and long spacing detectors by a single and rather clever graph. The *y*-axis (ordinate) of the graph is the reading from the long spacing detector, and the *x*-axis (abscissa) of the graph is the reading from the short spacing detector. Points plot on this graph in different ways depending upon the various values of r_b, r_{mc}* and h_{mc}.

Imagine that there is no mudcake. The short spaced detector will make a reading of gamma count rate that is dependent upon the short path between the source and the detector through the formation. The long spaced detector will also make a reading, which will be lower because of the greater distance of this detector from the source.

The readings from the long and short spaced detectors will fall on a straight line (Fig. 13.2). The higher the readings, the less dense the formation and *vice versa*. So we can calibrate the straight line to be read in terms of the bulk density of the formation. This line is called the *spine* of the plot.

Now imagine that a mud of variable thickness and r_{mc}*=1.5 g/cm^3 is present on the borehole wall, and the formation density is 2.5 g/cm^3. If the mudcake does not exist the detector values plot at point A in Fig. 13.3 as expected. If the mudcake thickness increases, the short spaced detector sees more of the less dense mudcake, and so gives a higher count rate. The long spaced detector also give a higher count rate due to the lower density mudcake that is present, but the increase is initially marginal because the long spaced detector is sensitive to a region which the mudcake only forms a small part. The result is the curve shown in Fig. 13.3. Note that this curve leaves the spine at 2.5 g/cm^3, when h_{mc}=0, forms an arc to the right of the spine, and rejoins the spine at 1.5 g/cm^3 as $h_{mc}\rightarrow\infty$. The rejoining represents the state where the thickness of the mudcake is greater than the depth of investigation of the tool, so that both the long and short spaced detectors read only mud. The curved part of the graph therefore represents the complete range of mudcake thicknesses.

If the effective mudcake density remains at 1.5 g/cm^3, but the formation density changes, the bottom point where the curved part of the line joins the spine slides up and down the spine, as shown in Fig. 13.4 for formation densities of 2.0, 2.5 and 3.0 g/cm^3. Each of the curved lines represents a different formation density, leaving the spine at the formation density value for h_{mc}=0, and rejoining the spine together at the effective mudcake density of 1.5 g/cm^3.

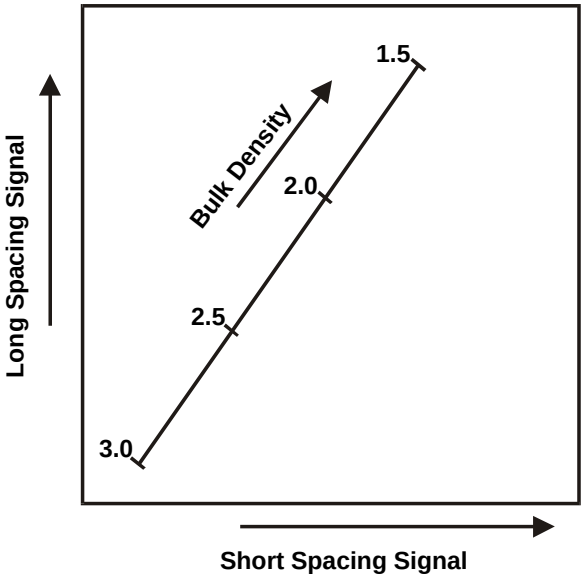

Figure 13.2 Formation density tool mudcake correction plot (spine and ribs) with no mudake present.

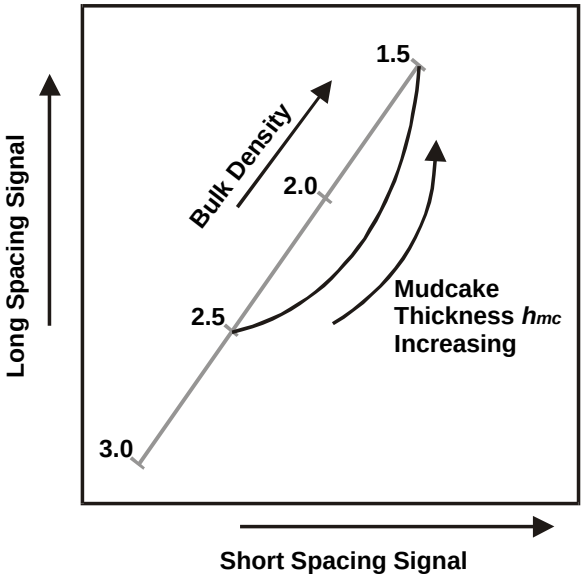

Figure 13.3 Formation density tool mudcake correction plot (spine and ribs) with r_b=2.5 g/cm^3, r_{mc}*=1.5 g/cm^3, and variable thickness mudake.

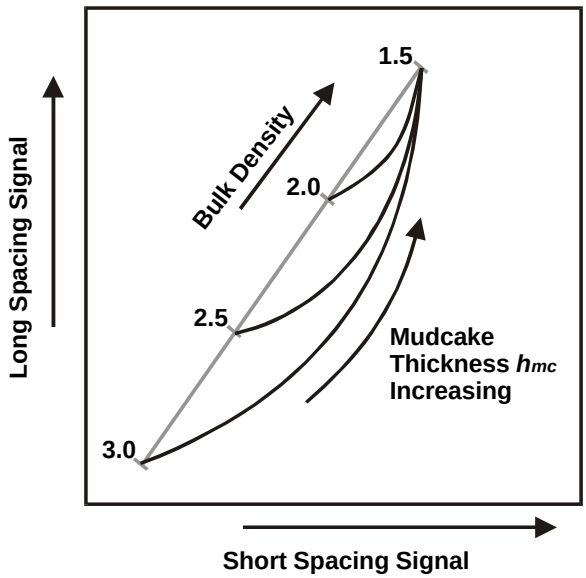

Figure 13.4 Formation density tool mudcake correction plot (spine and ribs) with r_b=2.0, 2.5 and 3.0 g/cm^3, r_{mc}*=1.5 g/cm^3, and variable thickness mudake.

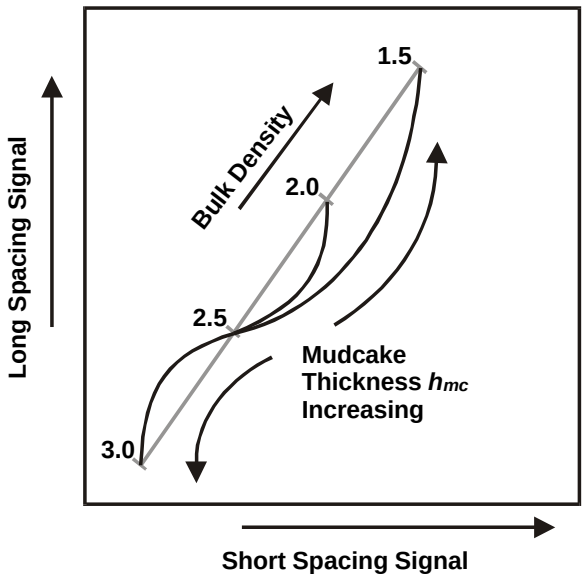

Figure 13.5 Formation density tool mudcake correction plot (spine and ribs) with r_b=2.5 g/cm^3, r_{mc}*=1.5, 2.0 and 3.0 g/cm^3, and variable thickness mudake.

If the formation density remains fixed at 2.5 g/cm^3 the point where the curved portion of the line leaves the spine is fixed at 2.5 g/cm^3. Now, if the effective mudcake density changes, the point where the curved part of the line rejoins the spine slides up and down the spine, as shown in Fig. 13.5 for effective mudcake densities of 1.5, 2.0 and 3.0 g/cm^3. Each of the curved lines represents a different effective mudcake density, leaving the spine at the formation density value of 2.5 g/cm^3 for h_{mc}=0, and rejoining the spine together at the relevant effective mudcake density, which may be above or below the formation density on the spine.

Note that if the effective mudcake density is the same as the formation density, the curved portion of the line does not exist, and the tool interprets the mudcake as formation.

In practice, only portions of the curved lines are relevant to wellbore conditions. Over the practical range, the combination of the curves and the spine is reminiscent of a rib-cage. This type of plot is therefore called a *spine and ribs plot*.

Figure 13.6 shows a spine and ribs plot for the formation density tool during a well controlled laboratory study of the tool. Note that the data on each rib is practically independent of effective mudcake density and composition, and that as mudcake becomes thicker, the data points lie further up or down the rib from the spine as expected.

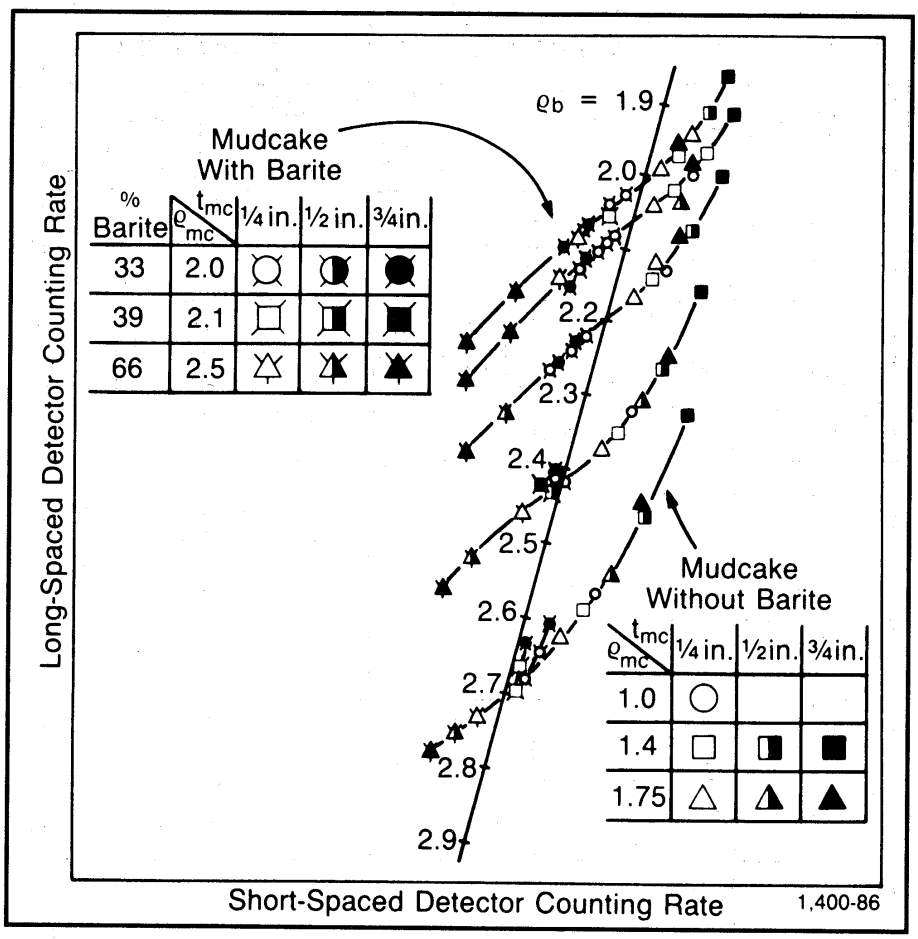

Figure 13.6 Formation density tool mudcake correction plot (spine and ribs) from laboratory derived calibration data.

The spine and ribs plot therefore has the advantages that (i) the variation in effective mudcake density and mudcake thickness can be described by a single parameter (the distance up a given rib), (ii) for each formation density, all ribs leaving one side of the graph coincide on the spine at a single point (the effective mudcake density), and (iii) knowing the spine and ribs plot for a given tool, the long and short detector readings can be used to obtain the corrected value of formation density without explicit measurement of either the effective mudcake density or the mudcake thickness. The correction procedure is automated in modern tools.

13.5 Calibration

The direct relationship between electron number density and bulk density indicates that no calibration is necessary. However, hydrogen is anomalous, and its presence perturbs the direct relationship. For this reason the formation density tools are calibrated. The primary calibrations are made by inserting the tool into a block of pure limestone saturated with fresh water of accurately known density. Secondary (check) calibrations are made in the wireline tool workshop by inserting the tool into large blocks of aluminium, sulphur and magnesium of known density. Sleeves of varying thickness are put around the tool to simulate mudcake thickness to check the operation of the automatic mudcake compensation process. A portable radiation source is used at the wellsite to check the responses of the two detectors before and after the tool has been run.

The relationship between electron number density and the bulk density is given by Eq. (13.1). Note that there is a linear relationship between the electron number density and the bulk density, and the remaining parameters in the equation are either constant for a given element (A and Z), or universally constant (N). Table 13.1 shows the values of A, Z, Z/A and $2Z/A$ for common elements in the crust.

Table 13.1 Atomic number and mass data for common elements in the crust.

Element	***Z***	***A***	***Z/A***	**2*Z/A***
H	1	1.0079	0.99215	1.9843
C	6	12.0111	0.4995	0.999
O	8	15.9994	0.5	1.000
Na	11	22.9898	0.47845	0.9569
Mg	12	24.3120	0.4936	0.9872
Al	13	26.9815	0.4818	0.9636
Si	14	28.086	0.49845	0.9969
S	16	32.064	0.499	0.9980
Cl	17	35.453	0.4795	0.9590
K	19	39.102	0.4859	0.9718
Ca	20	40.080	0.499	0.9980

Note that Z/A is close to 0.5 for all elements except hydrogen, which is almost unity.

We define a new parameter called the effective number density r_e, where $r_e = 2\, n_e/N$. Hence, Eq. (13.1) becomes

$$r_e = \frac{2Z}{A} r_b \quad \textbf{(13.2)}$$

For rocks that are composed of more than one element, Eq. (13.2) is valid providing that Z is the mean atomic number and A is the mean atomic mass.

For most elements, the constant term is almost unity giving a one to one calibration. For hydrogen the equation breaks down. We can examine the effect of the hydrogen on Eq. (13.2) by carrying out a calibration of the tool in limestone saturated with fresh water, where its density is accurately known. This calibration provides the relationship

$$r_a = 1.07 \times r_e - 0.188 \quad \textbf{(13.3)}$$

where r_a is the apparent density (that read by the tool). For water-filled sandstones, limestones and dolomites the tool reading is almost identical to the actual bulk density. Table 13.2 compares the apparent density read by the tool against the actual bulk density.

Table 13.2 Comparison of apparent density measured by the formation density tool with the actual bulk density for common mineralogies and fluids.

Compound	**Composition**	**Actual Bulk Density, ρ_b**	**2 *Z*/*A***	**Effective Electron Density, ρ_e**	**Apparent Bulk Density, ρ_a**
Quartz	SiO_2	2.654	0.9985	2.650	2.648
Calcite	$CaCO_3$	2.710	0.9991	2.708	2.710
Dolomite	$CaCO_3.MgCO_3$	2.870	0.9977	2.863	2.876
Anhydrite	$CaSO_4$	2.960	0.9990	2.957	2.977
Sylvite	KCL	1.984	0.9657	1.916	1.863
Halite	NaCl	2.165	0.9581	2.074	2.032
Gypsum	$CaSO_4.2H_2O$	2.320	1.0222	2.372	2.351
Anthracite (low)		1.400	1.030	1.442	1.355
Anthracite (high)		1.800	1.030	1.852	1.796
Coal (Bituminous)		1.200	1.060	1.272	1.173
Coal		1.500	1.060	1.590	1.514
Pure Water	H_2O	1.000	1.1101	1.110	1.000
Salt Water	200,000 ppm NaCl	1.146	1.0797	1.237	1.135
Oil	$(CH_2)_n$	0.850	1.1407	0.970	0.850
Methane	CH_4	ρ_m	1.247	$1.247\rho_m$	$1.335\rho_m$-0.188
Gas	$C_{1.1}H_{4.2}$	ρ_g	1.238	$1.238\rho_g$	$1.325\rho_g$-0.188

The density in some formations such as anhydrite, sylvite and halite must be corrected, as do readings in gas-bearing formations. Figure 13.7 shows the corrections that need to be made.

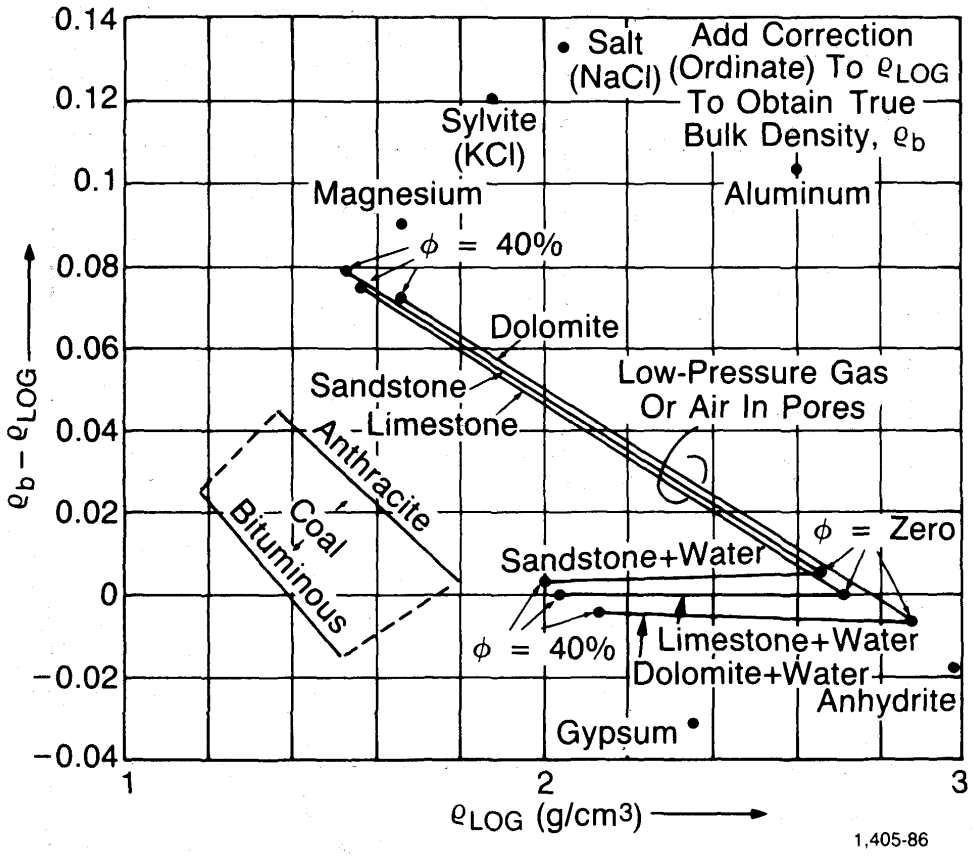

Figure 13.7 Formation density tool mineral correction plot.

Corrections also need to be made if the borehole is larger than 10 inches in diameter. The correction curve for one tool is given in Fig. 13.8.

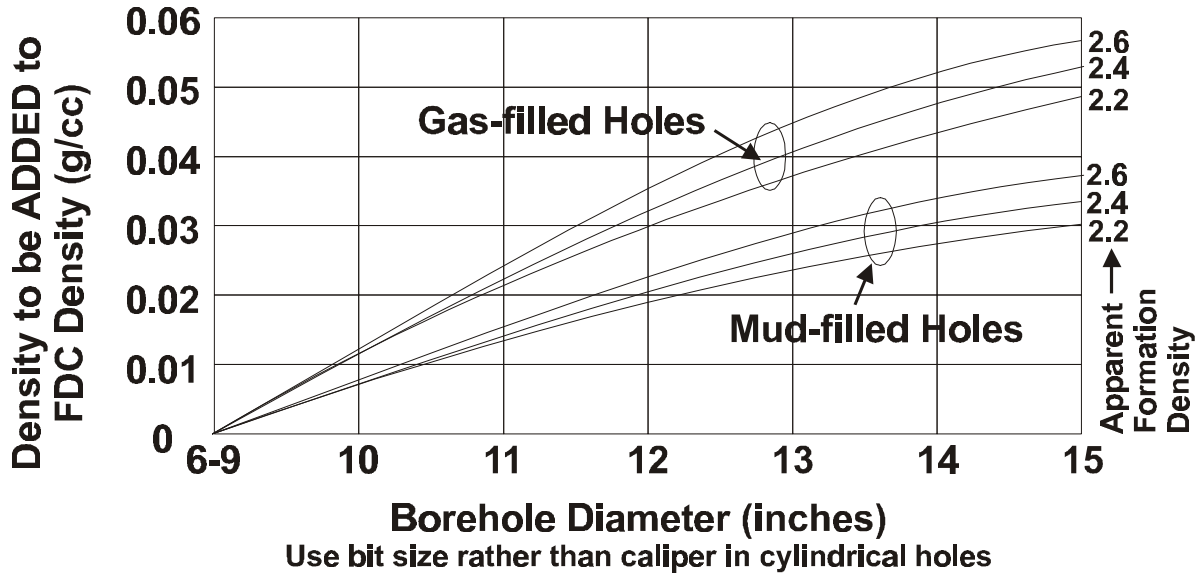

Figure 13.8 Formation density tool hole diameter correction plot.

13.6 Log Presentation

The formation density log is recorded in tracks 2 and 3 of the standard API log presentation on a linear scale. The scale is in g/cm^3, and usually spans 1.95 to 2.95 g/cm^3 as this is the normal range for rocks (Fig. 13.9).

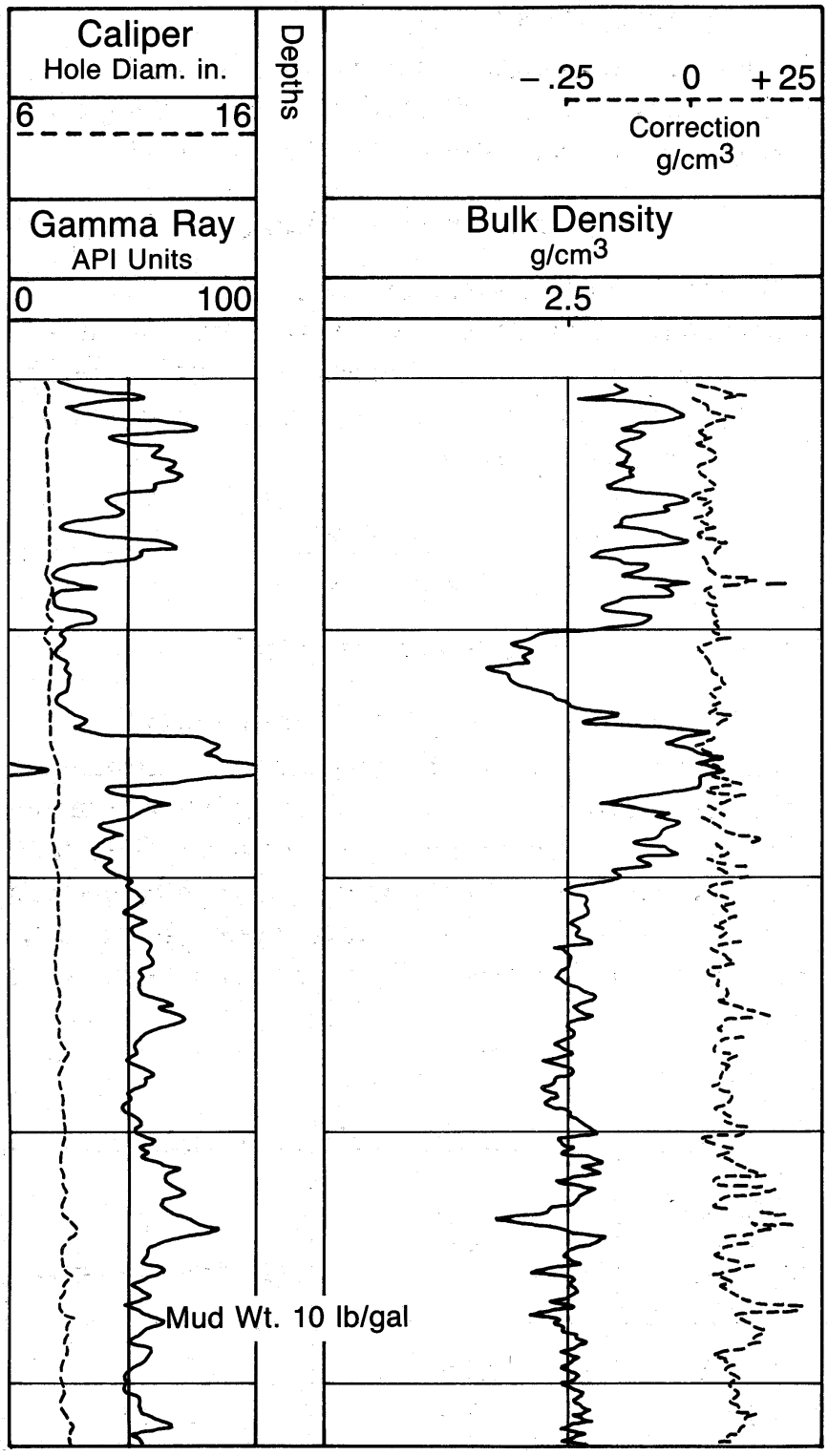

Figure 13.9 Formation density tool log presentation.

The automatic compensation (correction) for mudcake is often shown in either track 2 or track 3 on a linear scale. This curve is included as a quality control curve. If the correction curve is greater than ± 0.15 g/cm^3, the data in the main curve will not be very reliable.

As the formation density tool is a log that is commonly used to calculate porosity, a pseudo-porosity that has been calculated from the density data may be shown together with the bulk density curve and correction curve. This is a pseudo-porosity curve because it will assume a matrix and fluid density to be constant throughout the logged interval. Matrix densities of 2.65 g/cm^3 (for quartz) and fluid densities of 1.1 g/cm^3 (for salt water) are often used.

A wireline tension curve is often also included in the record, because the formation density tool is prone to getting stuck in holes as a result of its ploughing in sticky mudcake.

The formation density tool is most often run in combination with (i) a gamma ray log, for depth matching, (ii) a caliper log, for borehole quality control, and (iii) a neutron log, because the interpretation of the formation density tool together with the results from the neutron log provide one of the two best lithological assessment techniques for a reservoir.

13.7 Depth of Investigation

The depth of investigation of the tool is very shallow. For Schlumberger's FDC tool 90% of the response comes from the first 13 cm (5 inches) from the borehole wall for a 35% porosity sandstone (which has low density compared with most reservoir rocks). In higher density rocks the depth of investigation is even less, and a value of about 10 cm (4 inches) can be taken as an average value for reservoir rocks. Figure 13.1 shows the percentage of the signal that comes from different depths into the formation.

The shallow depth of investigation of the tool makes it sensitive to borehole quality, and it is therefore necessary to interpret the formation density log together with the caliper log to ensure that the measured values is not an artifact of bad hole quality.

The shallow depth of investigation also implies that in porous and permeable formations, where its main use lies, it only measures the invaded zone. This should be taken into consideration when deciding on a fluid density (mud filtrate density) to use for porosity calculations. The fact that the tool only measures the invaded zone in porous formations makes the tool little use for distinguishing between formation oil and formation water. However, gas may still be detected because (i) the greater difference in density between gas and oil or water, and (ii) the fact that mud filtrate invasion into gas-bearing zones is never complete, and always leaves a significant amount of gas behind in the invaded zone.

13.8 Logging Speed

The typical logging speed for the tool is 1300 ft/hr (400 m/hr), although it is occasionally run at lower speeds to increase the vertical resolution. The log quality is not as effected by logging speed as the natural gamma ray logs because much higher count rates are obtained with the radioactive source on the tool.

13.9 Vertical Resolution

The vertical resolution at the typical logging speed (1300 ft/hr) is good (about 26 cm, 10 inches), which is defined by the distance between the two detectors. The measurement point is taken to be half way between the two detectors. Beds can be resolved down to about 60 cm (2 ft) with the density tool reading the true density value of the bed. Even better resolutions are possible with slower logging speeds. Partial reaction of the logging tool to very thin beds of anomalously high or low density is sometimes encountered. For example, thin (5 – 10 cm thick) layers of calcareous nodules.

The high vertical resolution means that the log is useful for defining formation boundaries.

13.10 Borehole Quality

The log is run eccentred in the borehole, and therefore is prone to caving and rough borehole walls where the detectors or the source may not be pressed against the borehole wall. In this case the readings will be erroneous due to radiation leakage along the borehole between the detectors and bad measurement geometry. The sensitivity to bad hole quality is exacerbated by the shallow depth of investigation that the tool has. The formation density log should, therefore be run with a caliper tool, and the caliper reading should be used to judge the likely quality of the formation density log data.

13.11 Mud Type

Drilling muds with high density or that absorb gamma rays efficiently, such as barite filled muds, will effect the detector readings. However, the effect of these muds is compensated for automatically by the spine and ribs correction.

13.12 Uses of the Formation Density Log

The main use of the formation density log is to determine porosity. It has numerous other uses, the main ones being the recognition of gas-bearing zones, and the identification of minerals (particularly evaporites). The combination of formation density log data with neutron log data gives one of the best ways of identifying lithologies in a borehole. This will be described in Chapter 15.

13.12.1 Determination of Porosity

The porosity f of a formation can be obtained from the bulk density if the mean density of the rock matrix and that of the fluids it contains are known.

The bulk density r_b of a formation can be written as a linear contribution of the density of the rock matrix r_{ma} and the fluid density r_f, with each present is proportions (1- f) and f, respectively :

$$r_b = (1-f)\, r_{ma} + f\ r_f \qquad \textbf{(13.4)}$$

When solved for porosity, we get

$$f = \frac{r_{ma} - r_b}{r_{ma} - r_f} \quad \textbf{(13.5)}$$

where: r_b = the bulk density of the formation
r_{ma} = the density of the rock matrix
r_f = the density of the fluids occupying the porosity
f = the porosity of the rock.

The fluid densities are usually available from RFT sampling, but values of 1.0 g/cm^3 for fresh water and 1.1 g/cm^3 for salt water are often used. Remember that the tool measures the invaded zone, so the relevant fluid is the mud filtrate in most circumstances. If available, the fluid densities should be corrected to borehole temperature conditions. If the formation is hydrocarbon-bearing the fluid density can be calculated by

$$r_f = r_{mf} S_{XO} + r_{hc}(1 - S_{XO}) \quad \textbf{(13.6)}$$

where: S_{XO} = the saturation of the mud filtrate in the invaded zone
r_{mf} = the density of the mud filtrate
r_{hc} = the density of the hydrocarbon
r_f = the fluid density.

The value of the matrix density taken depends upon the lithology of the interval under question. For sandstones, the density of quartz is 2.65 g/cm^3, and for limestones, the density of calcite is 2.71 g/cm^3. Clay minerals have varied grain densities. Often core data is used to provide accurate matrix densities for particular intervals.

Table 13.3 gives the matrix densities of some common minerals.

Table 13.3 Grain (matrix) densities of some common rock forming minerals.

Mineral	Grain Density (g/cm^3)	Mineral	Grain Density (g/cm^3)
Quartz	2.65	Halite*	2.16
Calcite	2.71	Gypsum*	2.30
Dolomite	2.87	Anhydrite*	2.96
Biotite	2.90	Carnalite*	1.61
Chlorite	2.80	Sylvite*	1.99
Illite	2.66	Polyhalite*	2.78
Kaolinite	2.594	Glauconite	2.30
Muscovite	2.83	Kainite	2.13

*Evaporites

Care must be taken within some lithological intervals because the composition of the matrix may change. For example, the grain density for a clean sandstone is that of quartz (2.65 g/cm^3). However, if there is a variable amount of biotite present mixed in with the sand, the bulk density of the rock can rise to 2.84 g/cm^3 because biotite has a density of 2.9 g/cm^3. This scenario is encountered in some North Sea reservoirs. Analysis of Eq. (13.3) shows that an error of 0.01 g/cm^3 in the matrix density gives an error of 0.5% in the calculated porosity, which gives an error of almost 10% if a matrix

density of 2.65 g/cm^3 is assumed for a sand that has an actual density of 2.84 g/cm^3 due to additional biotite.

The Effect of Fluid Density. The porosity may also be in error if the fluid density is misjudged. The fluid existing in the zone of the rock measured by the formation density tool is usually mud filtrate. The density of these fresh and salt waters is approximately 1.0 g/cm^3 and 1.1 g/cm^3, respectively. However, these vary with temperature and composition, so accurate values for the actual reservoir formation water at the relevant reservoir temperatures should be used wherever possible. Such data can be obtained from samples of reservoir fluid from RFT analysis, or from the analysis of mud filtrate, bearing in mind that the tool measures the invaded zone, so the relevant fluid density to use in the porosity calculations is most often the mud filtrate density. Mud filtrate densities are now corrected automatically for temperature and pressure in most petrophysical software. However, the correction used to be carried out with the aid of a nomogram.

The Effect of Gas. If gas is present in the formation, porosities can be overestimated. The density of gasses is very low (approximately 0.0001 g/cm^3) compared to aqueous fluids. If the formation is gas-bearing a significant amount of gas is always left in the invaded zone. This gas will reduce the mean fluid density of the invaded zone, and will cause overestimations of the porosity if a fluid density of 1.0 or 1.1 g/cm^3 is used as shown in Fig. 13.10.

The Effect of Oil. The density of oil (approximately 0.7 g/cm^3) is less than that of aqueous fluids. However the presence of oil-bearing formations rarely causes problems in porosity calculation because both the oil and water in the invaded zone, which the tool measures, is replaced by mud filtrate.

The Effect of Shale. The density of shales varies greatly, and if present as a proportion of a lithology (such as a shaly sandstone of shaly limestone) can make the derivation of a reliable porosity inaccurate. If we have zones of clean lithology and zones of shale with a shaly sandstone in between (or a full fining-up or coarsening-up sequence), we can use the bulk densities in the shale and clean sandstone together with V_{sh} to obtain a corrected density for the shaly sandstone at any given depth.

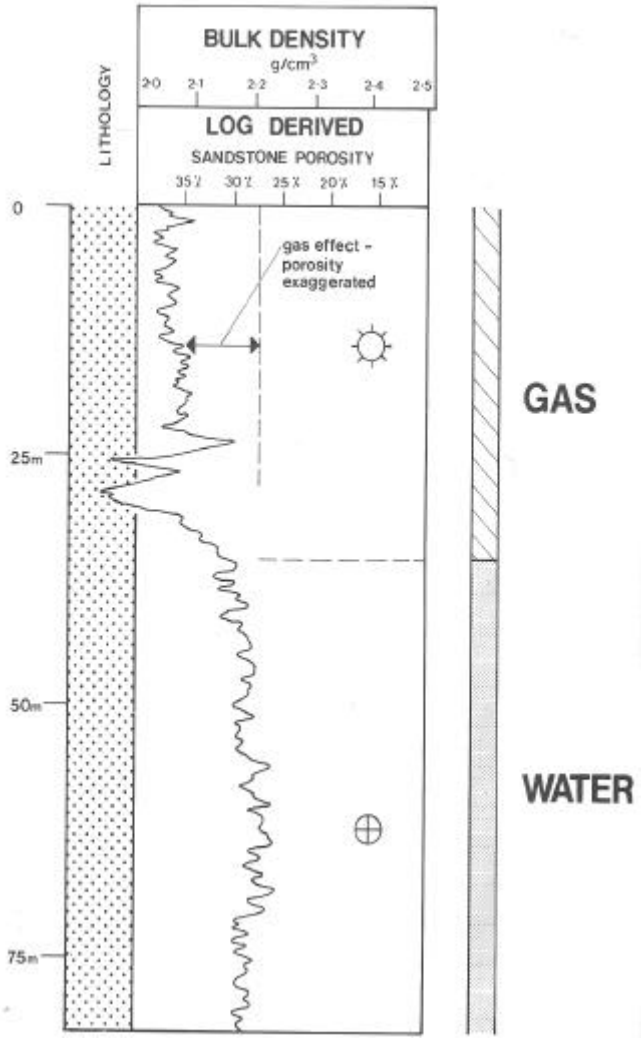

Figure 13.10 The effect of gas on the formation density log.

This corrected value of density may then be used in Eq. (13.5) to obtain a porosity which takes account of the shaliness of the sandstone (or limestone). The corrected bulk density of the shaly lithology is given by

$$(r_b)_{corr} = (r_b)_{clean}(1-V_{sh}) + (r_b)_{shale} V_{sh} \qquad \textbf{(13.7)}$$

Calibration with Core Porosities. The most accurate porosity determinations are obtained from laboratory measurements on cores. If there is a database of core porosities for a given well, it is often advantageous to plot the core porosity against the formation density log derived porosity or (better) the bulk density from the formation density log. The first type of plot should show the points lying on a 1:1 straight line. The second type of plot also gives a straight line with a negative gradient (Fig. 13.11). Non-linearity in the second type of plot indicates problems with the formation density log, while the first type of plot can be used to indicate that there is a better matrix or fluid density to use to transform the measured bulk density data to reliable porosity values.

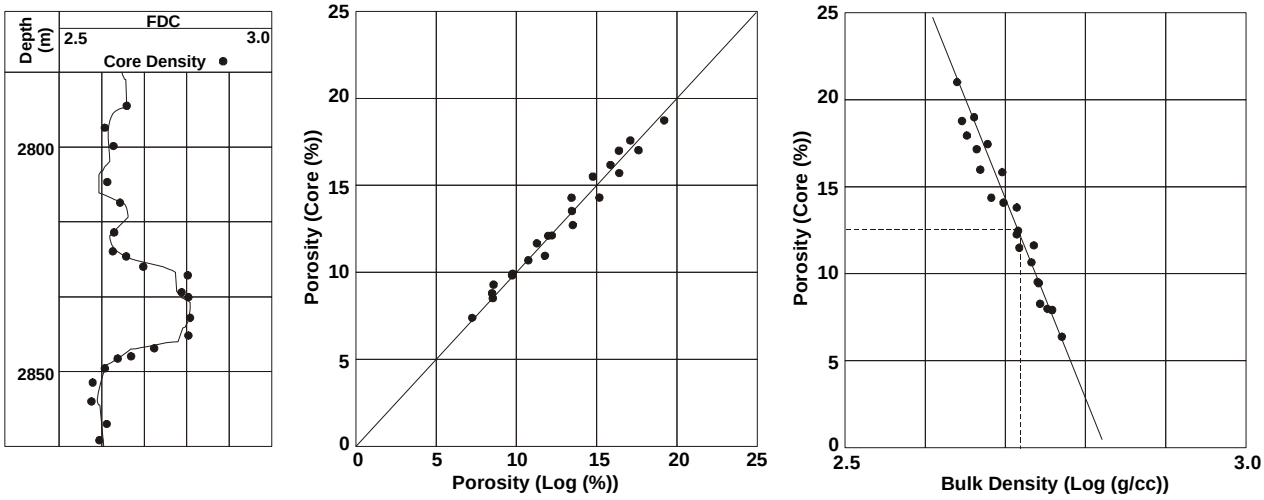

Figure 13.11 Calibration of the formation density tool against core porosities.

13.12.2 Acoustic Impedance

Density from the formation density log is often combined with acoustic velocity from the sonic log to calculate acoustic impedance down a well. The acoustic impedance can be used to create synthetic seismograms to help the interpretation of seismic data.

13.12.3 Identification of Lithology

When used alone, the density log is not a good tool for identifying most lithologies. This is because most rocks have a wide range of densities resulting from their varied mineralogical compositions and their variable porosities. For example, shales have bulk densities ranging from 1.8 to 2.8 g/cm^3 and have variable clay mineral densities. Sandstones, limestones and dolomites all have bulk density

ranges that overlap each other and that of shales (Fig. 13.12). However, when used with the neutron log, the combination is a very good lithological determination method (as described in Chapter 15).

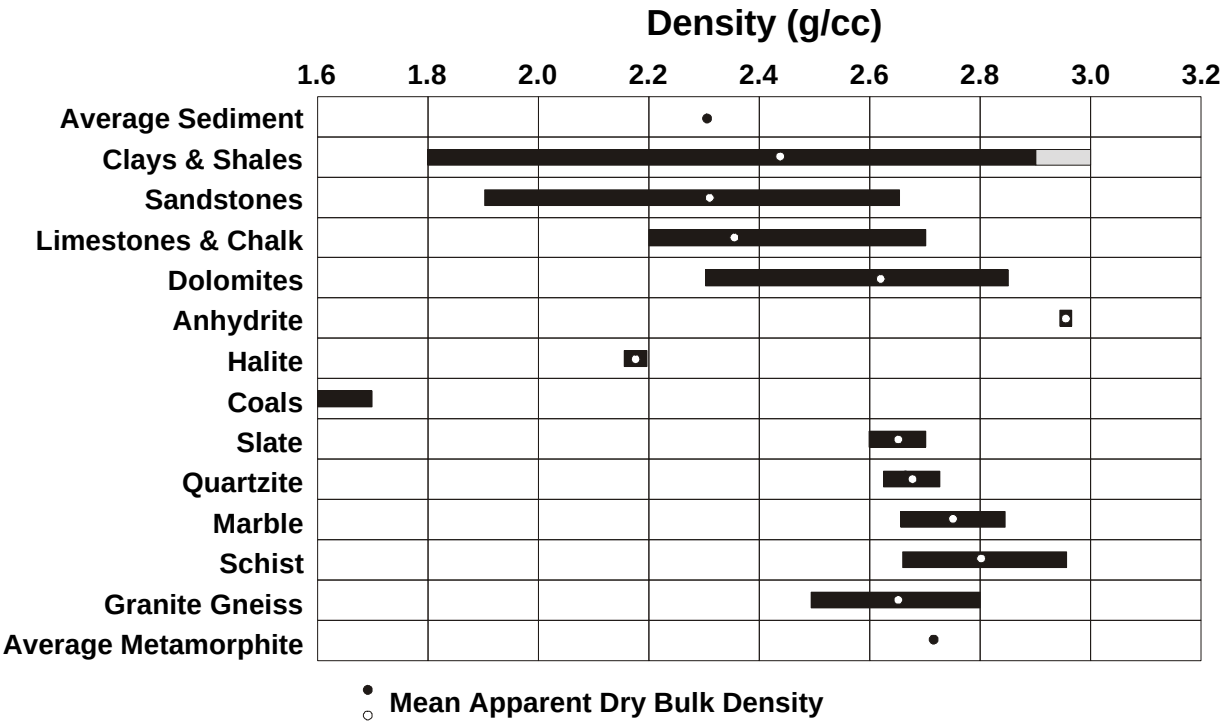

Figure 13.12 Density ranges of common lithologies.

13.12.4 Identification of Evaporites

Evaporites are often found in a very pure state, and have clearly defined densities. If evaporites are recognized within a log sequence, their type may be determined directly and unambiguously from the formation density log bulk density value. Table 13.1 gives data for some commoner evaporites.

13.12.5 Shale Compaction, Age, and Unconformities

Shale undergoes progressive compaction and increasing density with depth of burial and age. Occasionally, if the formation density data is plotted on a sufficiently small depth scale, the compaction trend may be noted by a steady but small rate of increase of density with depth (Fig. 13.13). It is a rule of thumb that the more compact shales are older (although this is not always the case).

If, within a given shale interval, there is a sudden change of density, the most likely explanation is that the formations above and below the change have been deposited in a completely different environment. The change is therefore an indication of a possible unconformity (Fig. 13.14).

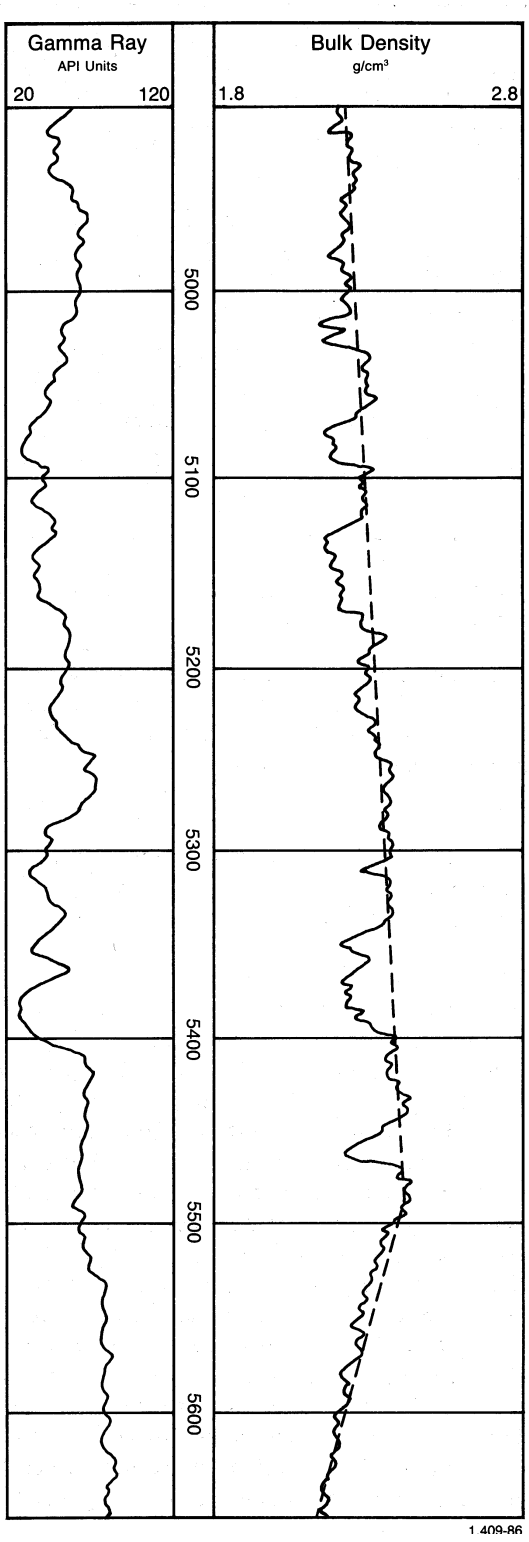

Figure 13.13 Recognition of shale compaction and overpressure in shale sequences using the formation density log.

13.12.6 Overpressure

Fluid overpressure works against any compaction trend caused by the overburden pressure. Hence, it is likely that overpressured zones will retain a greater porosity than normally pressured zones. If a normal compaction or no compaction is observed in a shale over some depth interval, and below it the bulk density begins to decrease (or the derived porosity begins to increase) without change in lithology, it is likely that one has entered a zone of overpressured fluids. In this zone the overpressured fluids keep the porosity open, stopping any compaction trend and reversing it (Fig. 13.13).

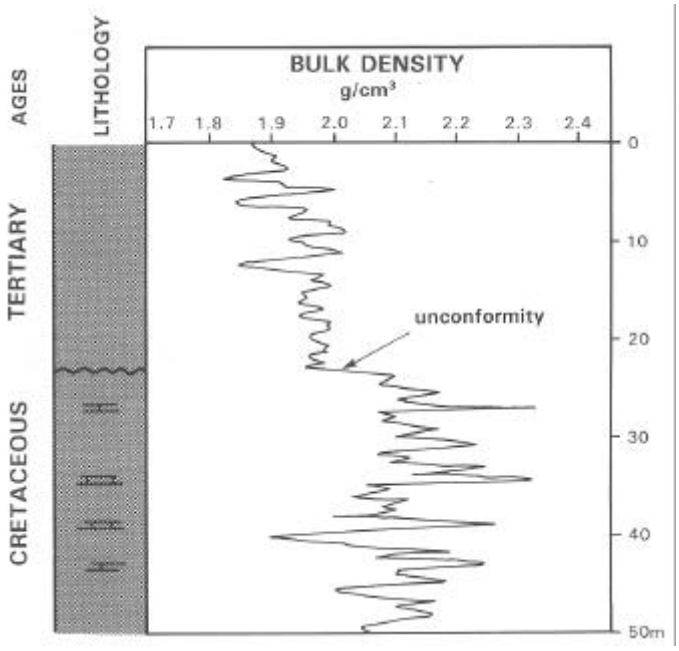

Figure 13.14 Recognition of unconformities in shale sequences using the formation density log.

13.12.7 Recognition of Accessory Mineralogies

Thin bands of anomalously high or low density within a single lithology, or a change in the character of the density log within a single lithology indicates that there are additional mineral present. Examples of this may be:

Thin bands of siderite in shales	Thin density peaks
Thin bands of carbonate nodules in shales or sandstones	Thin density peaks
Thin bands of carbonate in shales or sandstones	Thin density peaks
Thin bands of heavy or radioactive placer minerals	Thin density peaks
Dispersed micas in sandstones	Increased densities in affected zone

Mineralogies and lithologies that lower the density locally if present in thin bands include lignite, coal, anthracite or increased organic matter in a shale.

Mineralogies and lithologies that increase the density locally if present in thin bands include pyrite, siderite, basalt and gneiss.

13.12.8 Fracture Recognition

The density tool records the bulk density of the formation. The porosity derived from this will include all pores and fractures whether they are connected or not.

The sonic tool can also be used to measure the porosity of the formation. However, the sonic tool is not sensitive to fracture porosity.

Hence, the difference between the porosities derived from these two measurements can be used as an indicator of the extent of fracturing in a reservoir interval.

13.12.9 Organic Content of Source Rocks

The presence of organic matter can reduce the density of shales by up to 0.5 g/cm^3. It is possible to calculate the total organic carbon (*TOC*) content of a source rock from the change in bulk density. In practice this is done by calibrating the log with *TOC* determinations made on core samples from the well or nearby wells, then using the calibrated relationship to calculate *TOC* in the uncored intervals of the well.

14. THE LITHO-DENSITY LOG

14.1 Introduction

The *litho-density* log is a new form of the formation density log with added features. It is typified by Schlumberger's Litho-Density Tool (*LDT*). These tools have a caesium-137 source emitting gamma rays at 0.662 MeV, a short-spaced and a long-spaced detector in the same way as the basic formation density tool. However, the detectors are more efficient, and have the ability to recognize and to count separately gamma rays which have high energies (*hard gamma rays*: 0.25 to 0.662 MeV) and gamma rays which have low energies (*soft gamma rays*: 0.04 to 0.0 MeV).

The hard gamma rays are those that are undergoing compton scattering. The count rates of these gamma rays (in the energy window 0.25 to 0.662 MeV) are used in the conventional way to measure the formation density (Chapter 13). The final density value obtained is more accurate than the basic formation density tool because the harder gamma rays are less prone to attenuation by borehole effects, and there is a smaller spacing between the two detectors that has reduced statistical fluctuations in the count rates.

The soft gamma rays are those that are undergoing photo-electric absorption. This effect can be used to provide a parameter which is dependent upon the atomic number of the formation, and therefore immensely useful in lithological recognition.

14.2 Theory

14.2.1 Compton Scattering and Photo-Electric Absorption

Figure 14.1 shows the energy spectra of gamma rays as they are emitted from the source, and after travelling through various distances of the rock. At the radiation source, all gamma rays have a well defined energy of 0.662 MeV, represented by the sharp peak in Fig. 14.1. After travelling through the rock the gamma rays undergo compton scattering and loose energy, so the initially sharp peak moves to lower energies. Each of the gamma rays undergoes a different number of collisions dependent upon chance, and hence looses a different amount of energy. Thus the peak is not only moved to lower energies, but is also dispersed (becomes wider). In Fig. 14.1, Curve A represents the initial energy spectrum, Curve B represents the energy spectrum after the gamma rays have traveled a small distance through the rock, and Curve C represents the energy spectrum of the gamma rays after they have traveled an additional small distance through the rock.

However, some of the most scattered gamma rays now have energies close to 0.2 MeV. Once below the 0.2 MeV threshold, the gamma ray can be completely absorbed by the atoms in the rock, and there is a given probability that this will occur depending upon whether the soft gamma ray encounters an electron under the correct conditions. This is called photo-electric absorption, and is a completely different process from compton scattering. The result is that gamma rays attaining energies less than 0.2 MeV are eaten away from the energy distribution. Curve D in Fig. 14.1 shows the energies of the gamma rays after they have traveled another increment if distance through the rock, where some gamma rays have attained sufficiently low energies that they have been photo-absorbed. Curve E finally represents the energy distributions of gamma rays as they are detected by the tool. Note only the high energy tail of the distribution remains.

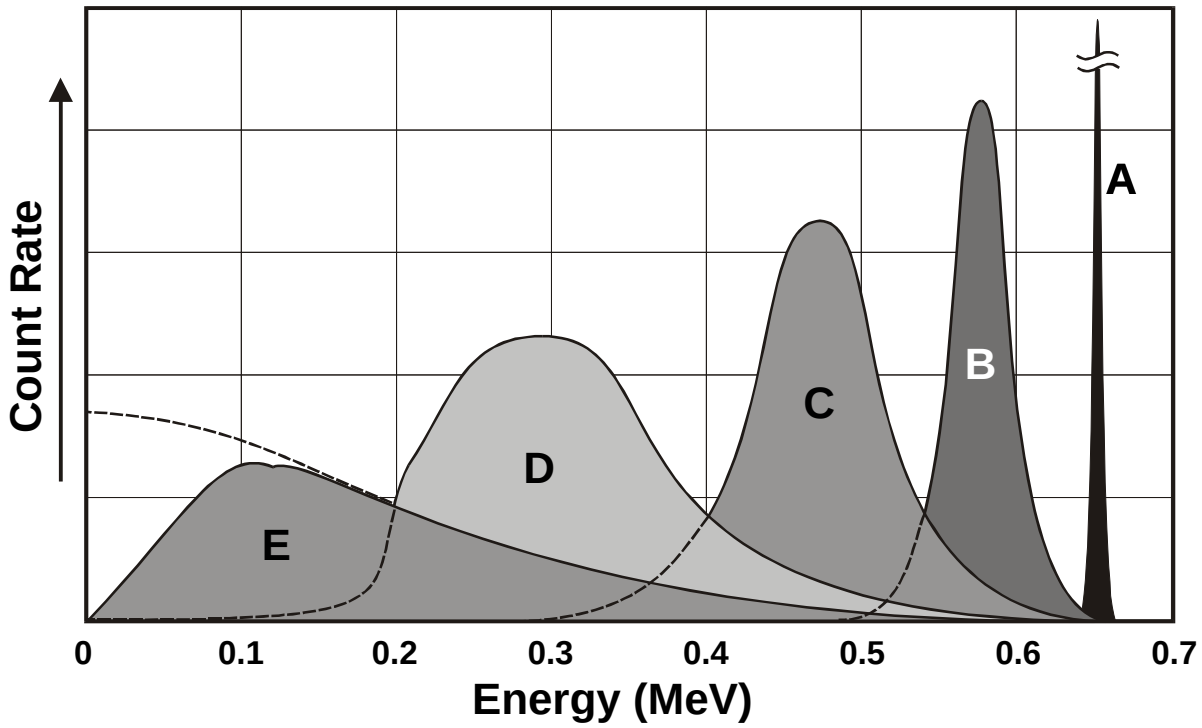

Figure 14.1 Gamma ray energy spectra.

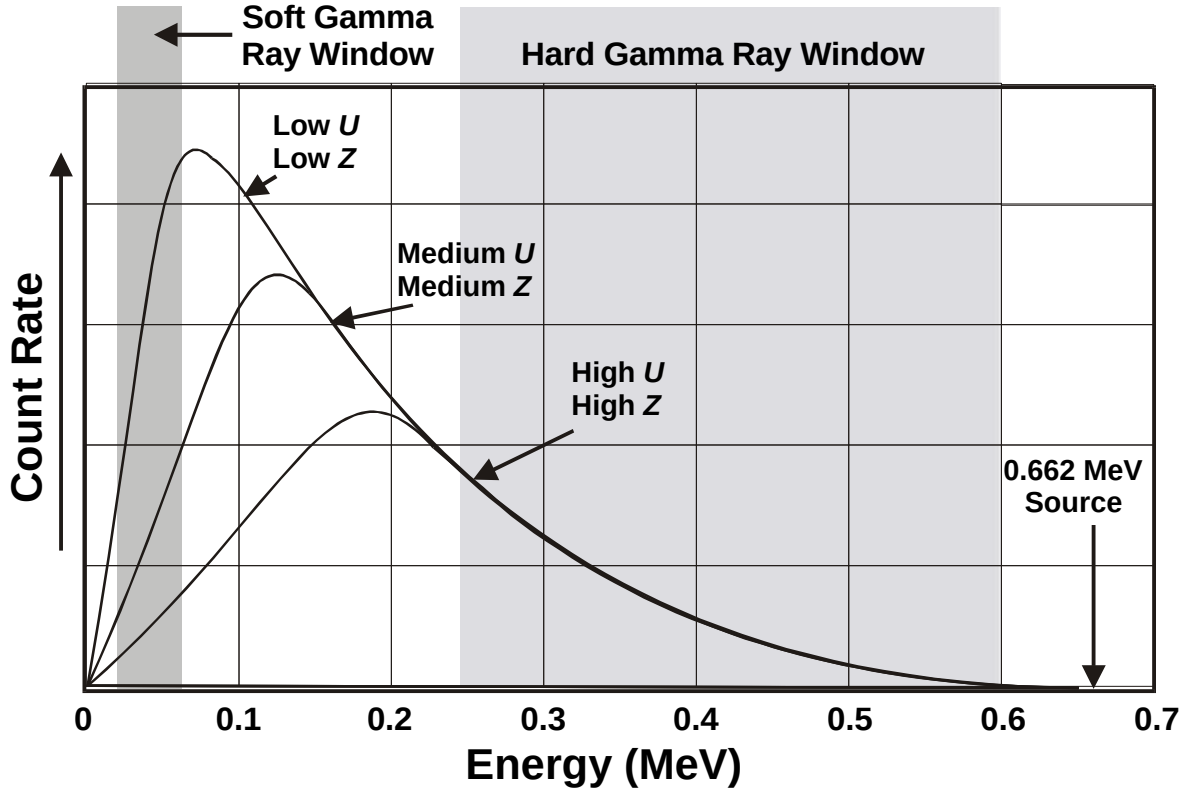

Figure 14.2 Gamma ray energy spectra and measurement windows.

Different materials have different abilities to photo-absorb gamma rays. Figure 14.2 shows the energy spectra of gamma rays after travelling to the detector through three media with low, medium and high photo-electric absorption indices.

We can use the count rates measured in the higher energy shaded window (for hard gamma rays) as a measure of compton scattering and hence the electron density of the material through which the gamma rays have passed. This gives information about the density of the formation in the same way as for the conventional formation density tool.

The count rate of the soft gamma rays in the lower energy shaded window in Fig. 14.2 is a measure of the density of the material (how many electrons there are available to take part in photo-absorption) and the rate of photo-absorption per electron. Hence, the number of gamma rays reaching the detector in the lower energy window depends upon the effective electron density of the rock as well as the photo-electric capture cross-section of the material.

14.2.2 Specific Photo-Electric Absorption Index

The probability that a gamma ray is adsorbed by the process of photo-electric absorption depends upon the characteristic cross-section of the process s_e. Characteristic cross-sections are measured in barns, where 1 barn=10^{-24} cm^2.

A *specific photo-electric absorption index* P_e is defined with the relationship

$$P_e \equiv \frac{1}{K}\frac{s_e}{Z} \qquad \textbf{(14.1)}$$

where: P_e = the photo-electric absorption index (barns/electron)
s_e = the photo-electric cross-section (barns)
Z = the atomic number (number of electrons)
K = a coefficient dependent upon the energy at which the photo-electric absorption is observed (no units).

The specific photo-electric absorption index P_e of a material describes the likelihood that a gamma ray will be photo-electrically absorbed per electron of the atoms that compose the material.

Both s_e and K depend upon energy, but since they do so in the same way, their energy dependencies cancel out, and P_e is therefore independent of energy. The photo-electric absorption index can be approximated by the empirical relationship

$$P_e = \left(\frac{Z}{10}\right)^{3.6} \qquad \textbf{(14.2)}$$

and values are given in Table 14.1.

14.2.3 Volumetric Photo-Electric Absorption Index

The Volumetric photo-electric absorption index *U* of a material describes the likelihood that a gamma ray will be photo-electrically absorbed per unit volume of the material. It can be written in terms of the specific photo-electric absorption index as

$$U = P_e \, r_e \qquad \textbf{(14.3)}$$

Table 14.1 Photo-electric data for common minerals and fluids.

Mineral	**Formula**	**Molecular Weight**	P_e	Z **(equiv.)**	r_b	r_e	r_a	U
Anhydrite	$CaSO_4$	136.15	5.055	15.69	2.960	2.957	2.977	14.93
Barite	$BaSO_4$	233.37	266.82	47.2	4.500	4.01		1070
Biotite			6.30				3.34	21.03
Calcite	$CaCO_3$	100.09	5.084	15.71	2.710	2.708	2.710	13.77
Dolomite	$CaCO_3$.$MgCO_3$	184.42	3.142	3.74	2.870	2.864	2.877	9.00
K Feldspar			2.86				2.62	7.51
Glauconite			5.32				3.95	21.00
Gypsum	$CaSO_4$.2 H_2O	172.18	3.420	14.07	2.320	2.372	2.350	9.37
Halite	NaCl	58.45	4.169	15.30	2.165	2.074	2.031	9.68
Haematite	Fe_2O_3	159.70	21.48	23.45	5.240	4.987		107
Limonite			13.00				3.59	46.67
Magnetite	$MgCO_3$	231.55	22.24	23.65	5.180	4.922		113
Muscovite			2.40				3.29	7.90
Pyrite	FeS_2	119.98	16.97	21.96	5.000	4.834		82.1
Quartz	SiO_2	60.09	1.806	11.78	2.654	2.650	2.648	4.79
Siderite	$FeCO_3$	115.86	1.69	21.09	3.940		3.89	55.9
Sylvite	KCl	74.6	8.510	18.13	1.984	1.916	1.862	15.83
Zircon	$ZrSiO_4$	183.31	69.10	32.45	4.560	4.279		311
Shale	-		3.42	14.07	2.650	2.645	2.642	
Shaly Sand	-		2.70				2.41	6.52
Anthracite	-		0.161	6.02	1.700	1.749	1.683	
Bituminous Coal	-		0.180	6.21	1.400	1.468	1.383	
Pure Water	H_2O	18.02	0.358	7.52	1.000	1.110	1.000	0.398
Salt Water	120,000ppm NaCl		0.807	9.42	1.086	1.185	1.080	0.850
Oil	$(CH_2)_n$		0.119	5.53	0.850	0.948	0.826	0.136× r_{oil}
Methane	CH_4	16.04	0.095	5.21	0.250		0.15	0.119× r_{gas}

Note the huge values for barite.

14.2.4 Factors Influencing the PEF Log

Mean Atomic Number of the Matrix. The *PEF* log is mainly controlled by the mean atomic number of the formation (Eq. (14.2)). Hence we can draw the following conclusions:

The higher P_e, the higher the mean atomic number of the formation. If there are isolated P_e peaks, this may indicate local deposits of heavy minerals especially those containing iron, or radioactive placer deposits (uranium and thorium). If there is a general high value for the P_e curve, this may indicate the presence of igneous or metamorphic rocks.

The lower P_e, the lower the mean atomic number of the formation. Thin bands of low P_e may indicate coal.

Formation Fluids. The porosity and fluid saturations of rocks vary, and so it would be expected that the measured P_e and U values might also vary with changing porosity and fluid saturation in the same way that many other logs do. However, the values of P_e and U for the fluids commonly found in rock are so low compared with the values for the matrix, that their influence is negligible. The one exception to this is perhaps highly saturated brines, which may have a significant P_e value. Figure 14.3 shows how little influence up to 35% porosity changes have on the P_e values for quartz, limestone and dolomite.

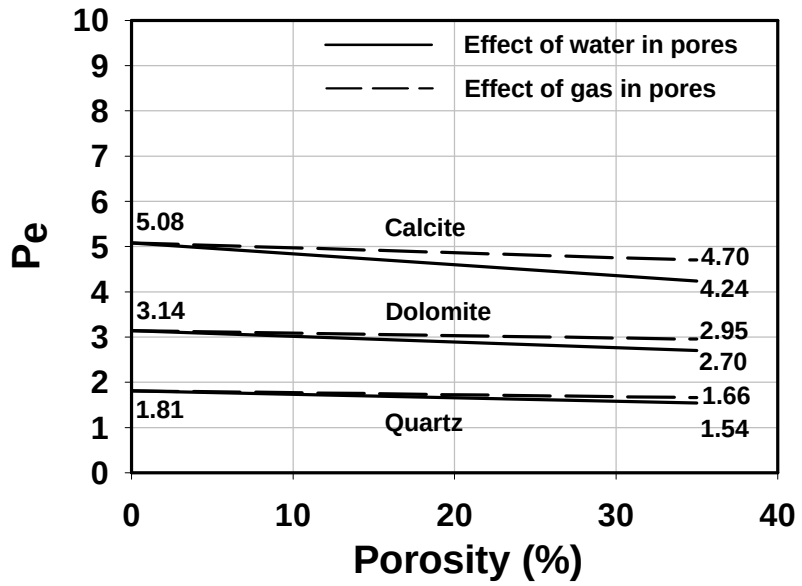

Figure 14.3 P_e as a function of porosity and fluid content.

The *PEF* log is therefore sensitive to differences in the mean atomic number of a formation without being sensitive to changes in the porosity and fluid saturation of that lithology. This combination makes the *PEF* log an extremely good indicator of lithology.

The ability of the *PEF* log to accurately indicate lithology is not impaired in gas-bearing zones, where the combination of the formation density and neutron logs may have difficulty distinguishing between lithologies.

14.3 Tool Operation

The tool is physically very similar to the formation density tool. It has enhanced detectors, and the distance between the long spacing and the short spacing detectors has been decreased. This decrease has increased the vertical resolution of the tool and improved its overall counting accuracy. The accuracy of the density measurement of the litho-density tool is approximately 0.01 to 0.02 g/cm^3, whereas that of the formation density tool is approximately 0.02 to 0.03 g/cm^3.

14.4 Log Presentation

The log is commonly referred to as the *photo-electric factor* log (*PEF*). It is shown in tracks 2 and 3 together with the formation density and neutron curves. Scales running from 0 to 10 or 0 to 15 or 0 to 20 barns/electron are most often used. As the *PEF* for most common rock forming minerals is low, this log usually sits to the left hand side of track 2.

This log is commonly run combined with the neutron log and a gamma ray log. The combination of the formation density log with the neutron log and the *PEF* log is very powerful in lithological assessment. The gamma ray log is run to aid depth matching with other logs. Figure 14.4 shows the typical layout of LDT-CNL-GR tool combination.

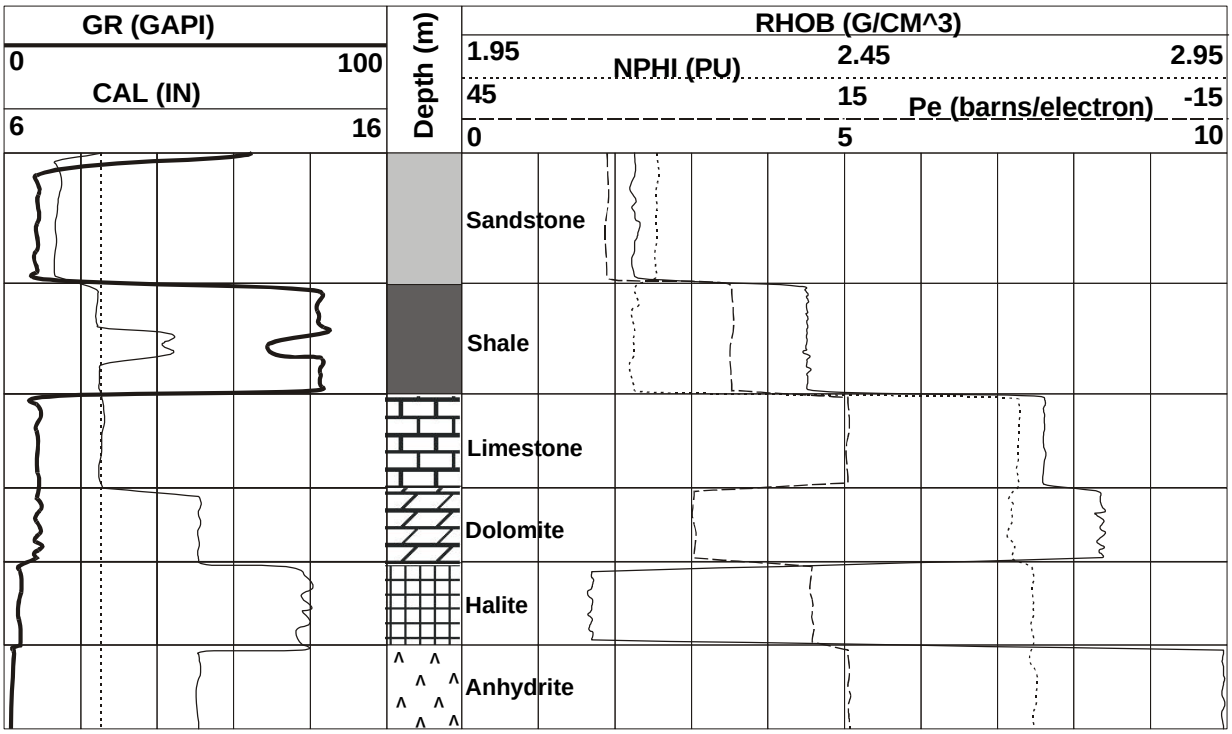

Figure 14.4 Layout of a typical LDT-CNL-GR tool run.

14.5 Depth of Investigation

The density and *PEF* measurement from the litho-density tool have a depth of investigation of 50 to 60 cm, defined by the distance of the long spacing detector from the short spacing detector.

14.6 Vertical Resolution

The density measurement from the litho-density tool has a vertical bed resolution of 50 to 60 cm, which is slightly better than the formation density tool. The enhanced vertical resolution results from the shorter distance between the short and the long spacing detectors.

The *PEF* measurement has a slightly better vertical resolution still. This is because the *PEF* log relies almost solely on the long spacing detector rather than both detectors. It has, therefore, a smaller 'footprint'.

As with the formation density log, it is possible o enhance the vertical resolution of this log by slowing down the logging speed and using modern digital data processing.

14.7 Borehole Quality

The litho-density suffers from the same borehole quality problems as the formation density tool, because of its similar borehole configuration (source and detectors pressed against the borehole wall).

14.8 Mud Type

The tool can be used with any muds except those that contain barite. Reference to Table 14.1 shows that the P_e for barite is 267 barns/electron compared with values of less than 6 barns/electron for most common lithofacies. Barite is such an efficient absorber of gamma rays that it reduces the levels of gamma rays to levels to low to be measured accurately. Hence, the litho-density tool cannot be used with barite muds.

14.9 Uses of the Litho-Density Log

14.9.1 Determination of Lithology

The litho-density log is one of the two most useful approaches to lithological determination downhole. This is because the tool is simply sensitive only to the mean atomic number of the formation, and at the same time is insensitive to changes in porosity and fluid saturation in the rock. Hence, the absolute P_e value may often be used to indicate directly the presence of a given lithology. This lithology may then be checked against the other tool readings for consistency. Figure 14.5 shows the response of the litho-density tool to common lithologies (also see Fig. 14.4).

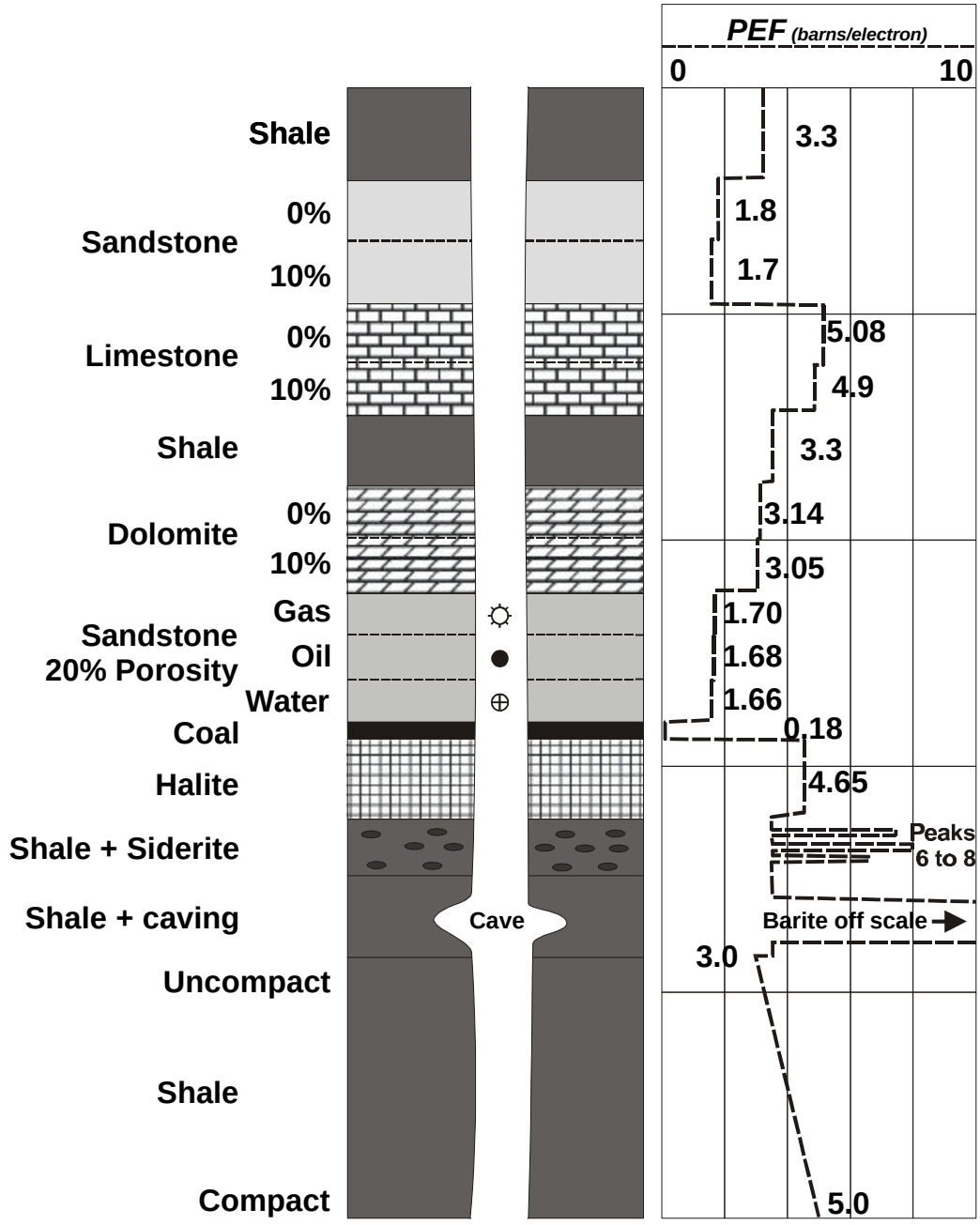

Figure 14.5 Measurements of the photo-electric absorption (*PEF*) litho-density log for common lithologies.

Note particularly that there are two common lithologies that cannot be distinguished by the gamma ray log easily. These are clean sandstones and clean limestones. It is clear from Figs. 14.4 and 14.5 that the *PEF* log can distinguish clearly and unambiguously between clean sandstones and clean limestones.

Also, it can be seen from Fig. 14.4 that limestone and anhydrite cannot be distinguished by the *PEF* log. However, anhydrite will always show up with little or no porosity on the neutron log, and will have a bulk density always above 2.9 g/cm^3, which compares with a maximum of 2.71 g/cm^3 possible with a clean limestone.

If there is a mixture of two mineralogies, for example a sandy limestone, a crossplot technique or a simple mixing rule can be applied to calculate the relative proportions of the two mineralogies.

In the crossplot technique, the P_e value is plotted on the *x*-axis against bulk density on the *y*-axis (Figure 14.6). The point lies between lines that indicate the relative proportions of three lithologies (sandstone, dolomite and limestone).

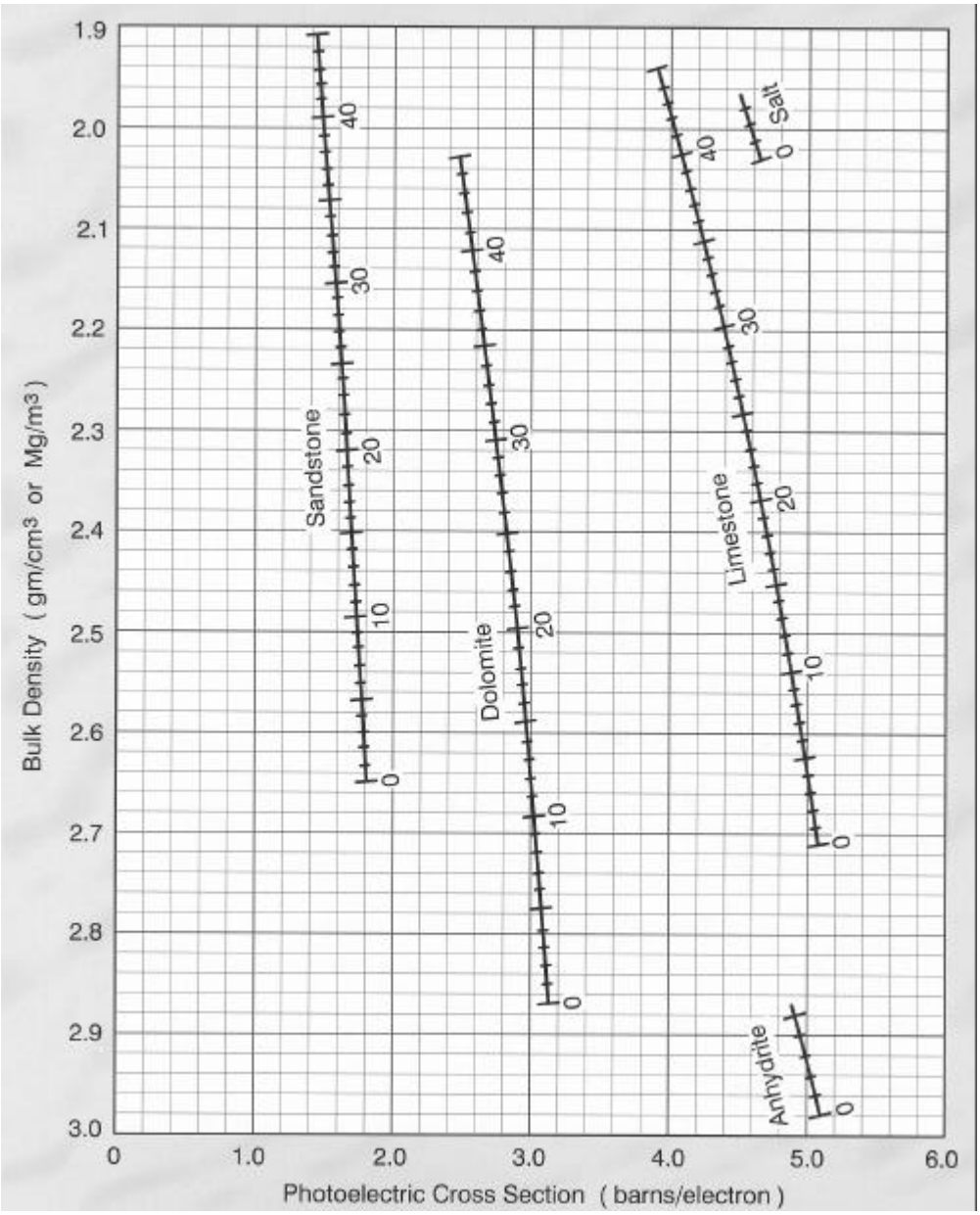

Figure 14.6 Matrix identification in a multi-mineral system using the *PEF* and density log data for a formation saturated with a fluid of density equal to 1.0 g/cm^3.

In the mixing rule method the relative proportions of two mineralogies may be calculated if one can obtain P_e values for each of the two pure mineralogies from fore-knowledge, standard values, or from log zones where each of the pure mineralogies are present. The mixing rule is simply

$$\left(P_e\right)_{\log} = c_1\left(P_e\right)_1 + \left(1 - c_1\right)\left(P_e\right)_2 \qquad \textbf{(14.4)}$$

where: $(P_e)_{\log}$ = the value of P_e measured in the zone of interest
$(P_e)_1$ = the value of P_e measured in mineralogy 1
$(P_e)_2$ = the value of P_e measured in mineralogy 2
c_1 = the volume fraction of mineralogy 1, where $c_1+c_2=1.0$.
$(1-c_1)$ = the volume fraction of mineralogy 2, where $c_1+c_2=1.0$.

When three minerals are present (plus porosity), the P_e log values are used together with the formation density log values. These two logs are multiplied to give the volumetric photo-electric absorption index U (according to Eq. (14.3)). The reason for this lies in the sensitivities of each of the parameters in Eq. (14.3). The P_e value is mass related and, as has been discussed, is sensitive to lithology but rather insensitive to porosities and fluid saturations. By comparison, the bulk density is sensitive to changes in porosity and fluid saturation. The product of the P_e values and the bulk density values gives a U value, which is sensitive to both the lithological composition of the formation, as well as any changes in porosity that are lithologically controlled.

The minerals are obtained from a cross-plot of the apparent bulk density r_{maa} of the matrix against the apparent value of U for the matrix U_{maa}. The apparent bulk density r_{maa} of the matrix is usually obtain from a density/neutron cross-plot (see Chapter 15). The matrix U_{maa} is obtained from

$$U_{maa} = \left(1-f\right)U_{ma} + f\,U_f \qquad \textbf{(14.5)}$$

where: U_{maa} = the apparent volumetric photo-electric absorption index of the formation of interest
U_{ma} = the volumetric photo-electric absorption index of the formation matrix
U_f = the volumetric photo-electric absorption index of the formation fluid
f = the fractional porosity of the rock.

The technique is very useful in complex carbonate-sand-evaporite systems where the porosity is controlled by the lithology, as is especially useful in gas-bearing zones, which do not alter significantly the P_e values. The technique is less useful in sand-shale sequences.

14.9.2 Detection of Heavy Minerals and Inter-Well Correlation

Heavy minerals give particularly high *PEF* and *U* values, and can be used to help their recognition in logs. For example, siderite is often found in dense bands in shales and in limestone/dolomites. These bands give peaks in the density log that may be 'lost' in the general variation due to varying porosity. However, the *PEF* log is insensitive to changes in porosity. In such a case the *PEF* log will be flat over the logging interval except at the siderite band, which will show up as a clear peak that is correlated to one of the peaks in the density log. The *U* value logs of heavy minerals give even higher peaks. This is because the heavy minerals have a high *PEF*, due to their high mean atomic number, as well as a high bulk density.

There are many heavy minerals which can be identified in small amounts on the *PEF* and *U* logs. The most common are, siderite, haematite, pyrite, glauconite and even biotite and muscovite micas.

These heavy mineral bands are not esoteric lithologies from the point of view of the reservoir petrophysicist, as heavy mineral bands with characteristic signatures can be very useful in the correlation of formations between wells.

14.9.3 Fractures

Most drilling fluids have very low *PEF* values. When this information is combined with he fact that the litho-density tool is pad mounted and pressed against the borehole wall, one can see that most types of drilling mud will not have a great effect on the *PEF* measurements. The exception is barite which has a huge *PEF* value and will swamp all other log responses if the tool sees barite drilling mud. Some people have used this to detect fractures. When there are fractures, the barite drilling mud will enter them, and the logged *PEF* value will saturate. While the hypothesis has been shown to work, it is not used in practice, since the barite drilling mud makes all other judgments from the log invalid. In practice *PEF* logs are not used in holes drilled with barite mud, and fractures are in general preferentially recognized by image logs.

15. THE NEUTRON LOG

15.1 Introduction

The *neutron* log is sensitive mainly to the amount of hydrogen atoms in a formation. Its main use is in the determination of the porosity of a formation.

The tool operates by bombarding the formation with high energy neutrons. These neutrons undergo scattering in the formation, losing energy and producing high energy gamma rays. The scattering reactions occur most efficiently with hydrogen atoms. The resulting low energy neutrons or gamma rays can be detected, and their count rate is related to the amount of hydrogen atoms in the formation.

In formations with a large amount of hydrogen atoms, the neutrons are slowed down and absorbed very quickly and in a short distance. The count rate of slow neutrons or capture gamma rays is low in the tool. Hence, the count rate will be low in high porosity rocks.

In formations with a small amount of hydrogen atoms, the neutrons are slowed down and absorbed more slowly and travel further through the rock before being absorbed. The count rate of slow neutrons or capture gamma rays in the tool is therefore higher. Hence, the count rate will be higher in low porosity rocks.

Figure 15.1 shows a typical neutron tool.

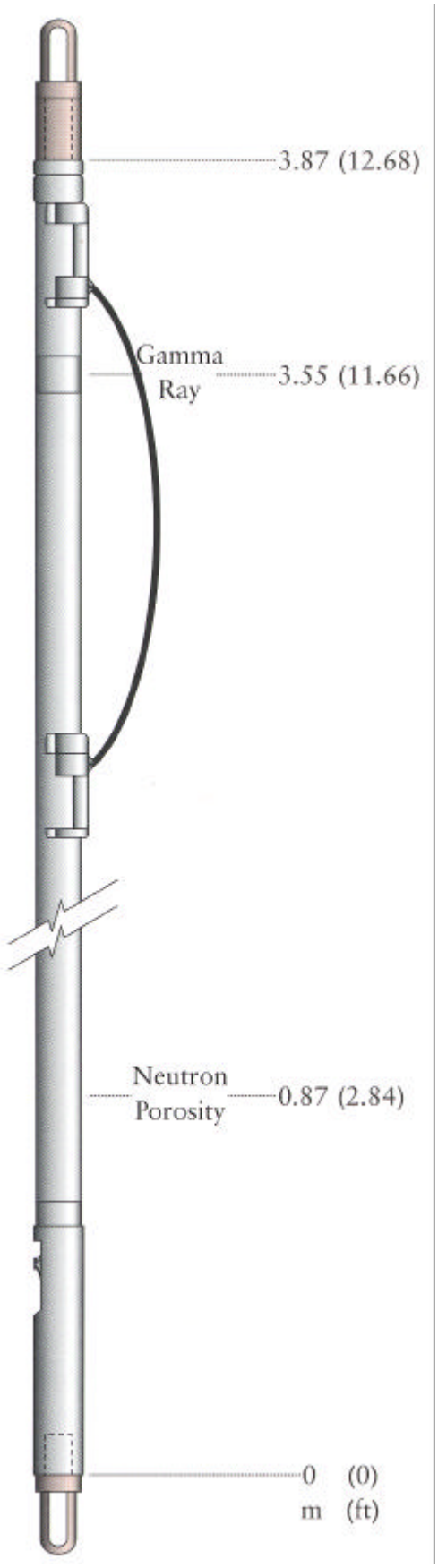

Figure 15.1 A typical neutron tool.

15.2 Theory

In neutron logging there are three processes of interest: neutron emission, neutron scattering and neutron absorption.

15.2.1 Neutron Emission

The neutron tool emits high energy (4.5 MeV) neutrons from a radioactive source. They move very fast, and their energy is related to their speed. They are called *fast neutrons*. The neutron sources used in logging are a mixture of two elements (i) a source of alpha radiation such as radium, plutonium or americium, and (ii) beryllium-9. The alpha particles from the radium, plutonium or americium interact with the beryllium-9 in an atomic reaction that produces carbon-12, a fast neutron and gamma rays.

$$ {}^{9}_{4}\mathrm{Be} + {}^{4}_{2}\mathrm{He} \Rightarrow {}^{12}_{6}\mathrm{C} + {}^{1}_{0}\mathrm{n} + g \qquad \textbf{(15.1)} $$

15.2.2 Neutron Scattering

The fast neutrons interact with the nuclei of atoms within the formation. The interaction is a form of elastic scattering involving the neutrally charged neutron and a stationary positively charged nucleus. At each interaction (collision) the neutron looses some energy and slows down, and the nucleus of the atom in the formation material gains energy. Such collisions occur with nuclei of *ALL* elements. However, the process of energy transfer (i.e., energy loss from the neutron) is most efficient when the masses of the neutron and the nucleus are the same, and becomes much less efficient when the nuclei of the formation material are more massive than the neutron. The neutron has approximately the same mass as hydrogen nuclei (the lightest element). Hence the neutrons lose energy by elastic scattering most efficiently by interaction with hydrogen nuclei, and lose energy much less efficiently by interaction with more massive nuclei such as silicon or oxygen. Figure 15.2 shows the efficiency of several elements in slowing down fast neutrons.

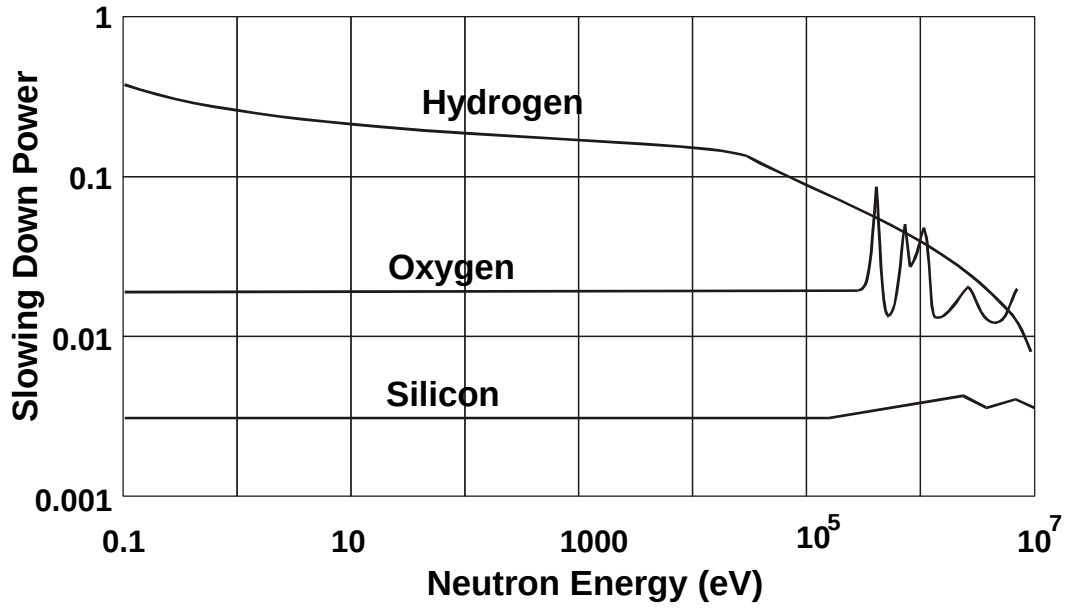

Figure 15.2 The fast neutron slowing efficiency of hydrogen, silicon and oxygen atoms as a function of neutron energy for a clean sandstone, f = 0.15.

The initially fast neutrons (>0.5 MeV) quickly lose their energy and become slower (Fig. 15.3), passing through stages called *intermediate neutrons* (10^2 to 10^5 eV), *epithermal neutrons* (0.1 to 100 eV), and finally *thermal neutrons* (<0.1 eV). In solid materials containing reasonable amounts of low atomic mass elements, this process can happen very quickly for a given neutron (of the order of micro-seconds). However, the time taken to slow down to a given energy will vary from neutron to neutron, depending on the chance collisions with nuclei. Thermal neutrons are so called because they have energies which are those that a particle has as a result of it existing a room temperatures. In other words, they only have the small energies associated with the random kinetic motion associated with room temperatures.

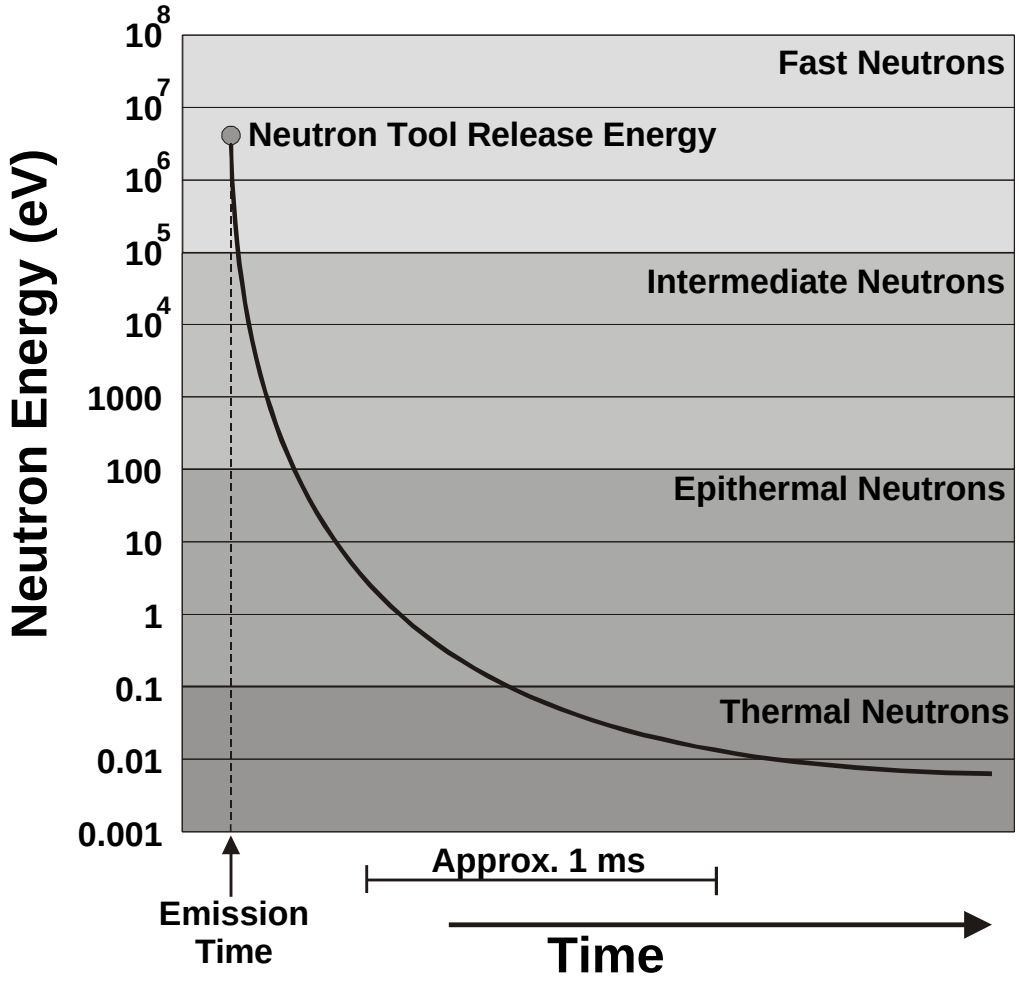

Figure 15.3 The slowing of fast neutrons with time by elastic collision with formation nuclei.

When the neutrons attain epithermal or thermal energies, collisions occur much less frequently because the neutrons are moving from nucleus to nucleus much more slowly. Within a few microseconds of being exposed to the fast neutron source, the formation has slowed the incoming neutrons down to epithermal and thermal levels, and a cloud of these thermal neutrons exists in the formation surrounding the source. Collisions continue resulting in little further loss of energy and the slow diffusion of the thermal neutrons from the zone around the detector. During this process the neutrons are absorbed by the formation nuclei.

15.2.3 Neutron Absorption

Thermal (and to some extent epithermal) neutrons can be absorbed by the nuclei of the formation atoms. The efficiency of neutron absorption varies from element to element. The only elements which exhibit significant neutron absorbing behaviour and exist is reasonable quantities in rocks are hydrogen and chlorine. The process of neutron absorption by hydrogen and chlorine are

$$ {}^{1}_{1}\mathrm{H} + {}^{1}_{0}\mathrm{n} \Rightarrow {}^{2}_{1}\mathrm{H} + g \qquad \textbf{(15.2)} $$

and

$$ {}^{35}_{17}\mathrm{Cl} + {}^{1}_{0}\mathrm{n} \Rightarrow {}^{36}_{17}\mathrm{Cl} + g \qquad \textbf{(15.3)} $$

In neutron logging, some tools measure the epithermal neutrons, some the thermal neutrons and some the gamma rays emitted when a neutron is absorbed.

15.2.4 Hydrogen Index

We can define a partial concentration of hydrogens per unit mass $(C_H)_{mass}$ of a material as the mass of hydrogen atoms in the material divided by the mass of all the atoms of all elements in the material.

$$ (C_H)_{mass} = \frac{n_H\, A_H}{\sum_i n_i\, A_i + n_H\, A_H} \qquad \textbf{(15.4)} $$

where: A_H = the atomic mass of hydrogen atoms in the material
A_i = the atomic mass of non-hydrogen element *i*
n_H = the number of hydrogen atoms in a molecule of the material
n_i = the number of non-hydrogen atoms of element *i* in a molecule of the material
Note: *i* is summed over every non-hydrogen element in the material.

Thus, for pure water (H_2O), where the atomic mass of hydrogen is 1.0 and the atomic mass of oxygen is 16.0, the partial concentration of hydrogen $(C_H)_{mass} = (2\times1.0)/(1\times16.0 + 2\times1.0) = 1/9$.

It is simple to obtain the partial concentration of hydrogens per unit volume $(C_H)_{vol}$, by multiplying the partial concentration of hydrogens per unit mass by the density of the material, $(C_H)_{vol} = \rho_b \times (C_H)_{mass}$. Hence, the partial concentration of hydrogens per unit volume $(C_H)_{vol} = \rho_{bwater}/9 = 1/9$, because the density of pure water is 1.000 g/cm^3.

Now, the *Hydrogen Index* of a material is defined as the partial concentration of hydrogens per unit volume *relative to water*. So, if the hydrogen index of water is constrained by the definition to be unity, and water has a partial concentration of hydrogens per unit volume of 1/9, the hydrogen index of a material *is*

$$ HI = \frac{9\, n_H\, A_H}{\sum_i n_i\, A_i + n_H\, A_H}\ \rho_b \qquad \textbf{(15.5)} $$

where: A_H = the atomic mass of hydrogen atoms in the material
A_i = the atomic mass of non-hydrogen element *i*

n_H = the number of hydrogen atoms in a molecule of the material
n_i = the number of non-hydrogen atoms of element *i* in a molecule of the material
Note: *i* is summed over every non-hydrogen element in the material.

Table 15.1 shows Eq. (15.5) in practice for a few minerals and fluids commonly found in reservoirs.

Table 15.1 Hydrogen index calculations for some reservoir minerals and fluids.

Compound	**Formula**	A_i	n_i	n_H	ρ_b	*HI*
Pure water	H_2O	16	1	2	1.000	1.000
Oil	$(CH_2)_x$	12	1	2	0.780	1.003
Methane	CH_4	12	1	4	ρ_m	$2.25\times\rho_m$
Gas	$C_{1.1}H_{4.2}$	12	1.1	4.2	ρ_g	$2.17\times\rho_g$
Quartz	SiO_2	28, 16	1, 2	0	2.654	0.000
Calcite	$CaCO_3$	40, 12, 16	1, 1, 3	0	2.710	0.000
Gypsum	$CaSO_4.2H_2O$	40, 32, 16	1, 1, 6	4	2.320	0.4855

Note the following:

- If the tool is in 100% water (a large tank of the stuff, say), the *HI* = 1.000. This is equivalent to a rock of 100% porosity saturated with water. So we have a fixed point that *HI* = 1 represents $\phi = 1$.

- If the tool is in a pure limestone rock with zero porosity, the *HI* = 0.000, because there are no hydrogen atoms in the solid matrix of calcite. So we have a second fixed point where *HI* = 0 represents $\phi = 0$.

- If the tool is in a pure limestone with a given porosity ϕ, the hydrogen index will be directly proportional to the amount of water in the formation. Hence *HI* = ϕ for completely water saturated limestones.

Thus the hydrogen index is a proxy measure of porosity if the solid minerals of the formation contain no hydrogen and if the pores are completely saturated with water. But, it is the hydrogen index that controls the count rate observed by the neutron tool. Hence we have a tool that can measure porosity in water saturated formations where the matrix minerals contain no hydrogen.

In practice, it is not only hydrogen that affects the passage of neutrons in a formation. As we can see from Fig. 15.2, other rock forming elements have an effect on the slowing down of neutrons in the formation, but their effect is small compared with hydrogen, and when it comes to neutron absorption, both chlorine and hydrogen have a part to play. The small errors that are introduced by assuming that it is just hydrogen that affects neutrons are overcome by calibrating the tool. The tool is calibrated in pure limestone, and hence does not give true porosities. Instead it gives equivalent porosities that would occur if the rock was measuring limestone. This will be discussed in further detail in Section 4.

The Hydrocarbon Effect. Note in Table 15.1 that the hydrogen indices of water and oil are approximately the same because the effect of their different compositions on the partial concentration of hydrogens per unit volume is approximately balanced by the difference in their density.

As with the formation density tool, the zone of investigation of the neutron tool is constrained to the flushed zone. Hence, the tool will measure the hydrogen index associated mainly with the mud filtrate,

together with whatever remains of the hydrocarbons and formation water in the formation. Imagine, for example that we are in an oil zone in a limestone, the mud filtrate almost completely replaces the formation fluids such that there is a saturation of mud filtrate S_{XO}, and a residual saturation of hydrocarbons (1- S_{XO}). The porosity read by the neutron tool is related to the actual porosity in the formation by

$$f_N = f\left[HI_{mf}\, S_{XO} + HI_{hc}\left(1-S_{XO}\right)\right] \quad \textbf{(15.5)}$$

If the hydrocarbon is oil, this equation reduces to $f_N \approx f$, because, as we have seen in Table 15.1 the hydrogen index of water and oils is similar; $HI_{mf} \approx HI_{hc}$. This is true whether the mud filtrate is oil-based or water-based.

$$f_N = f\left[1.00\times S_{XO} + 1.003\times\left(1-S_{XO}\right)\right] \approx f \quad \textbf{(15.6)}$$

If the hydrocarbon is methane gas with a density of 0.1 g/cm^3, the equation reduces to

$$f_N = f\left[1.00\times S_{XO} + 2.25\times 0.1\times\left(1-S_{XO}\right)\right] \quad \textbf{(15.7)}$$

If the saturation in the flushed zone S_{XO} = 0.7, Eq. (15.7) reduces to $f_N = 0.77\ f$. This is known as the *hydrocarbon effect in the neutron log*.

The Chlorine Effect. Some types of neutron tool measure the thermal neutrons and gamma rays produced during the capture of neutrons. There are only two elements that are found in reservoirs that contribute significantly to neutron absorption; hydrogen and chlorine. The presence of hydrogen in the fluids is what we want to measure, so this is not a problem.

However, if the drilling mud, mud filtrate or formation fluids contain a significant amount of dissolved chloride ions, as is often the case, the tool will measure a lower flux of neutrons and hence overestimate the porosity. This is called the *chlorine effect*, and is present in wells drilled or logged in the presence of drilling muds containing dissolved chlorine, or in formations where the formation waters are particularly salty.

The Shale Effect. Shale contain clays that have a significant amount of surface absorbed (bound) water. Hence shales can contain a significant proportion of hydrogens despite being low porosity. The apparent porosity read from the neutron tool in shale formations is therefore always significantly higher than it really is. This is called the *shale effect* or the *bound-water effect*, and will be discussed further later in this chapter.

15.3 Tool Operation

There are three main types of neutron tool, which are:

- The Gamma Ray/Neutron Tool (GNT)
- The Sidewall Neutron Porosity Tool (SNP)
- The Compensated Neutron Log (CNL)

15.3.1 Gamma Ray/Neutron Tool (GNT)

This tool has a neutron source and a single detector that is sensitive to high energy capture gamma rays and thermal neutrons and is non-directional. The tool can be run in either open or cased holes, and in both cases is run centered. A 3-3/8 inches diameter tool is used in open holes, and a 1-11/16 or 2 inch diameter tool is used in cased holes. The source to detector spacing varies between tool manufacturers, but is in the range 15.5 to 19.5 inches. Because the tool is centered, the detected neutrons and gamma rays have to travel through both mudcake and drilling mud. Hence, this tool is highly sensitive to changes in borehole quality, temperature, type of drilling mud, and mudcake thickness. Correction curves are available from the tool manufacturers to correct the log data for temperature, hole diameter, and the effect of drilling mud and mudcake.

Because the tool measures the thermal neutrons and the capture gamma rays, it is effected by the process of neutron capture by chlorine. Since drilling mud, mud filtrate and formation waters may contain significant amounts of dissolved chloride ions, the measurement can give erroneous values. Erroneous values take the form of overestimated porosities in formations either drilled with muds containing dissolved chloride ions, or salty formation fluids.

15.3.2 Sidewall Neutron Porosity Tool (SNP)

This tool is designed for use in open holes only. The tool has a source and a single detector with a 16 inch spacing, which are mounted on a skid that is pressed against the borehole wall. Often this will be the same carrier that holds the formation density source and detector. Because the tool is pressed against the borehole wall, the drilling mud does not affect the measurement, and the attenuation due to the mudcake is reduced. However rough holes can cause misalignment of the either the source of the detector with the borehole wall, and hence give erroneous readings.

The detector is sensitive to epithermal neutrons. These neutrons are not yet slow enough to take part in absorption reactions with hydrogen and chlorine. Hence, the SNP tool readings are unaffected by the presence of chlorine in high salinity muds and formation fluids.

15.3.3 Compensated Neutron Log (CNL)

This tool is designed to be sensitive to thermal neutrons, and is therefore affected by the chlorine effect. It has two detectors situated 15 in and 25 in from the source. The detector further from the source is larger to ensure that adequate count rates are observed. The critical measurement for this tool is the difference in the thermal neutron population, which results from neutron capture and neutron scattering. The tool readings are presented in limestone porosity units in the same way as the sidewall neutron porosity tool. The CNL tool has a very strong source of neutrons to ensure that the measured count rates are sufficiently high to obviate any significant errors associated with statistical fluctuations

in the count rate despite the longer source-detector spacing for this tool compared to the GNT and SNP tools. The stronger source permits a deeper depth of investigation as well as allowing the tool to operate in cased holes. The CNL tool is run eccentred in the hole by an arm which presses the tool against the side of the borehole. This means that the tool is insensitive to the type of mud in the hole, but implies that the readings are only for one portion of the borehole wall. The CNL log is shown in Fig. 15.4.

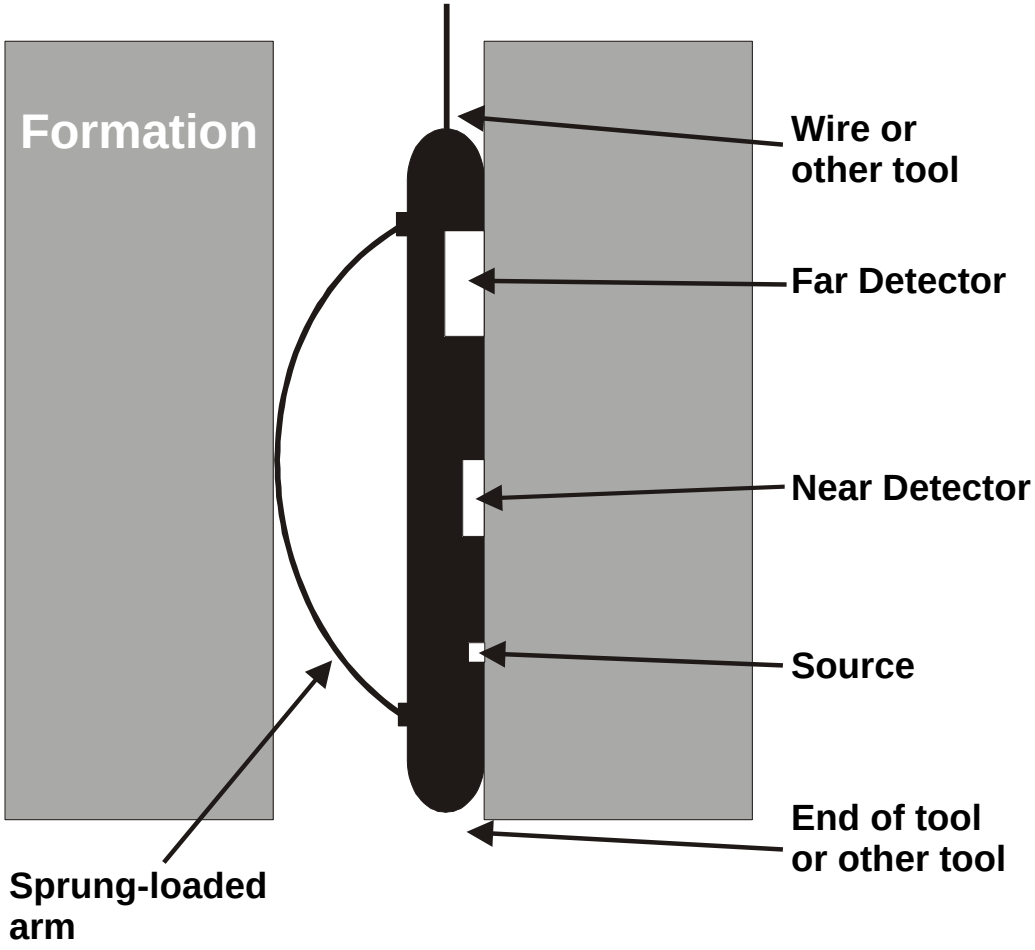

Figure 15.4 The CNL tool (Schlumberger).

15.4 Log Presentation

The data from all tool types are recorded in tracks 2 and 3.

The data from the GNT tool is given in API units as shown in Fig. 15.5.

The data from the SNP tool is given in equivalent limestone porosity units, with the scale running from approximately –10% to 30%, as shown in Fig. 15.6.

Data from the CNL tool is given in equivalent limestone porosity units, with the scale running from approximately –10% to 30%, as shown in Fig. 15.7.

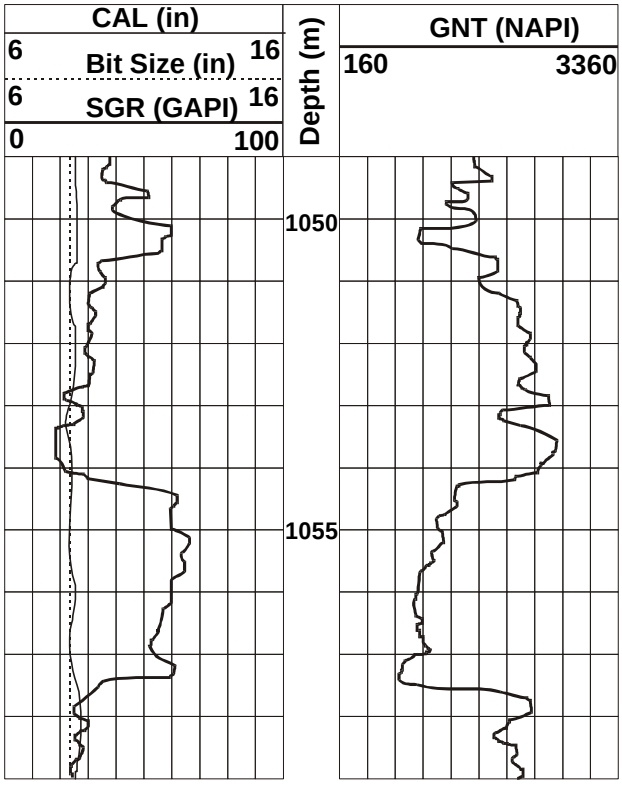

Figure 15.5 Log presentation for the GNT tool.

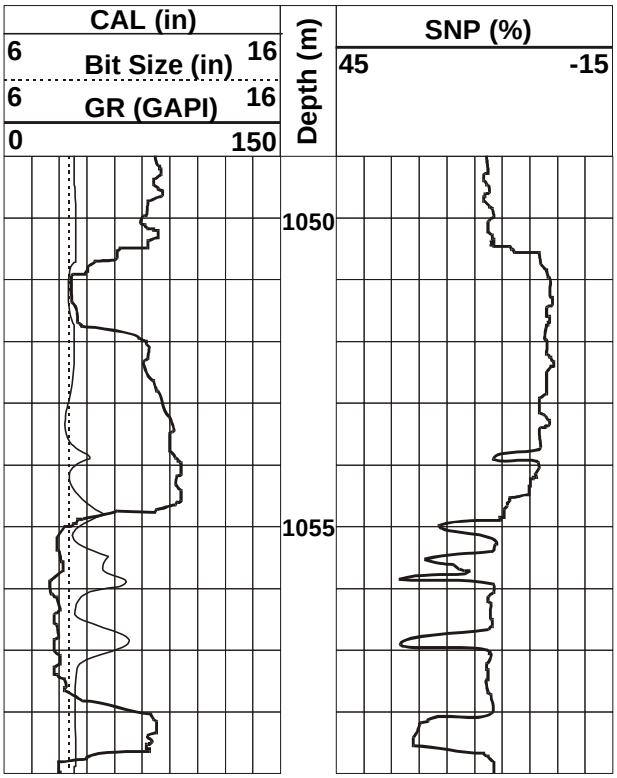

Figure 15.6 Log presentation for the SNP tool.

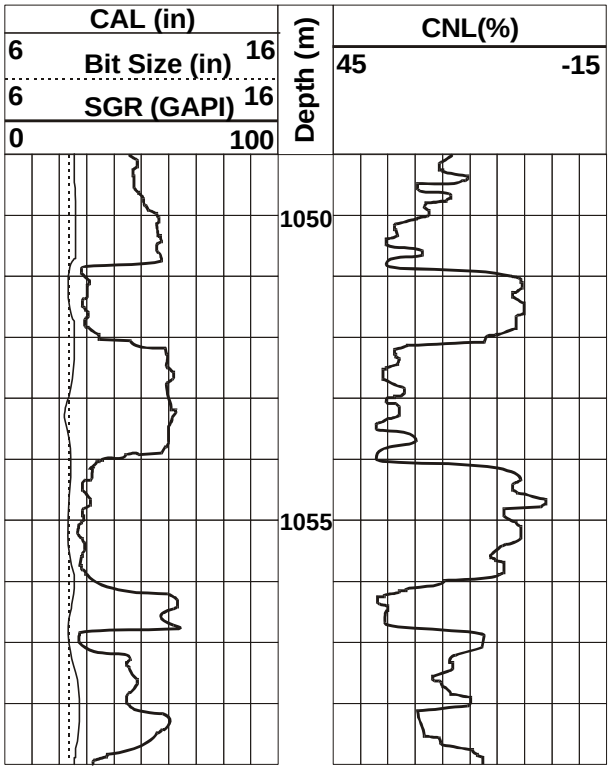

Figure 15.7 Log presentation for the CNL tool.

15.5 Calibration

15.5.1 The GNT Tool

The primary standard for this tool is the API Neutron Calibration Pit at the University of Houston. This pit contains three blocks of carbonate with accurately known porosities that are filled with fresh water that are drilled to accept a tool. The tool is calibrated in 19% porosity Indiana limestone, for which an API value of 1000 API neutron units is defined. The response of the tool is then checked in 1.9% Carthage Marble, 26 % Austin limestone, and 100% fresh water. A tool tested at Houston is used as a secondary reference for the calibration of other tools at the wireline company's workshops around the globe. A wellsite check on the calibration of a tool is also carried out before and after running the tool using a neutron source of accurately known radioactivity.

15.5.2 The SNP and CNL Tools

These tools are calibrated in blocks of limestone, sandstone and dolomite of high purity and accurately known porosity in test pits. The tools are calibrated, not to give readings in API neutron porosity units, but to give the porosity directly in percent. Limestone is chosen as the calibrating lithology, so the readings are given in limestone porosity units.

IMPORTANT The common use of limestone porosity units as the calibrating unit for these logs means that the reading of porosity in a limestone formation will be exact, but the reading of porosity in these units in any other formation lithology will need correction (Fig. 15.8).

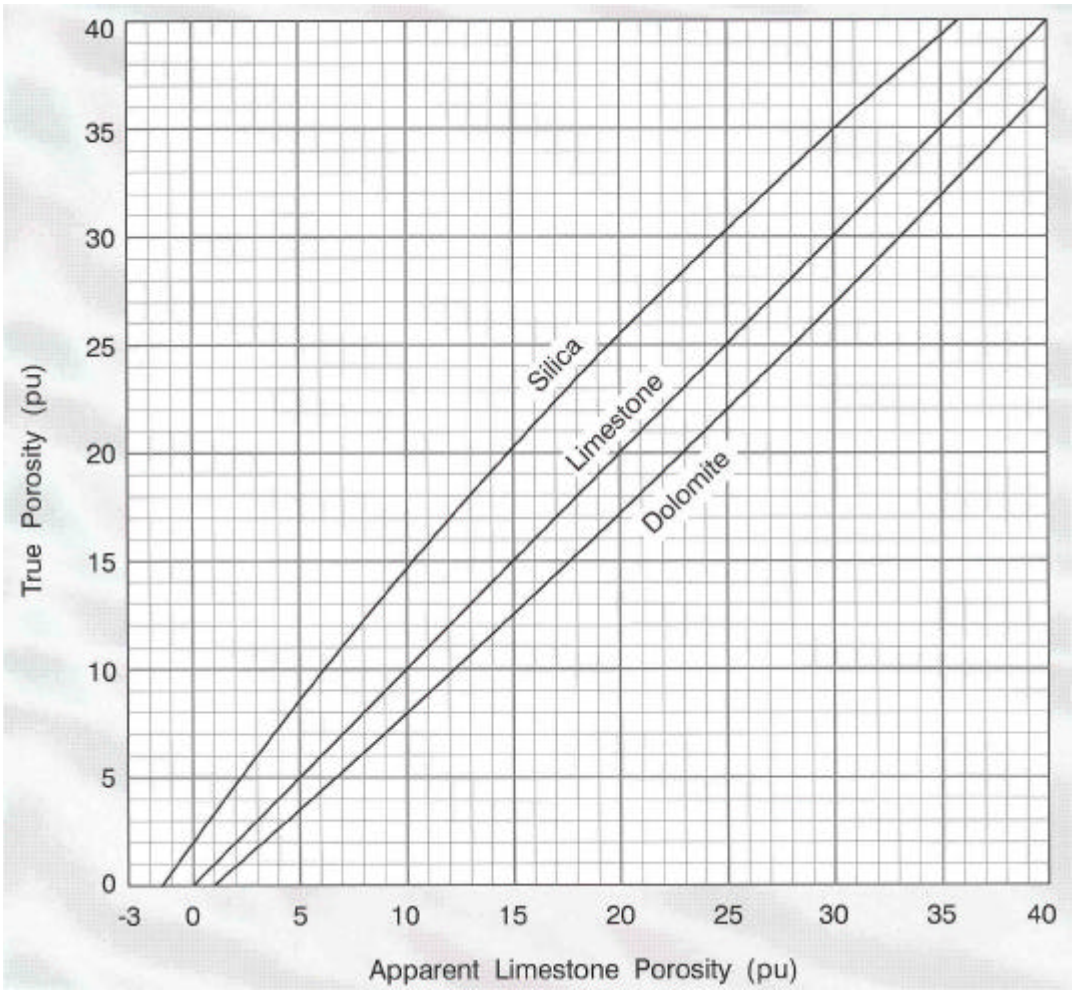

Figure 15.8 Correction chart for obtaining porosity values for lithologies other than limestone.

The SNP tool is calibrated at the wellsite uses a U-shaped polyethylene baffle (artificial formation) with a two position baffle, where the geometry of the block and baffle arrangements are known to result in readings equivalent to 11% porosity and 22% porosity.

The calibration of the CNL tool is checked at the wellsite before and after each logging run by the use of a neutron source of accurately known activity placed a standard distance from each detector.

15.6 Depth of Investigation

The depth of penetration of the tool readings depends directly upon the amount of hydrogens in the formation. Thus, for porous rocks that contain water or hydrocarbons (i.e., many hydrogens), there is much neutron scattering and absorption, and hence the depth of investigation is small. For low porosity rocks containing water or hydrocarbons, there are fewer hydrogens in the formation and the depth of investigation is larger.

The presence of gas in a formation increases the depth of investigation because, although the gas may contain hydrocarbons, the gas has a vary low density compared to liquid water and oil, and hence a very low hydrogen index.

The presence of shales decreases the depth of investigation because even low porosity shales contain many waters (i.e., hydrogen) that are bound to the surface of the clay crystals.

The depth of investigation of the CNL tool in a water saturated formation of 35% porosity is about 12 inches, and that of the SNP tool in the same formation is about 8 inches.

15.7 Vertical Resolution

As with most tools the vertical resolution is defined by the source detector spacing for single detector tools and the spacing between the two detectors for dual detector tools. The vertical resolution of neutron tools is a little greater than these spacings. For the GNT tool the vertical resolution is 16 inches or 20 inches depending upon which of the two source-detector spacings possible for this tool are used. The vertical resolution of the SNP tool is 16 inches, and for the CNL tool is 10 inches.

As usual, the true bed resolution (the thinnest bed for which the true neutron porosity reading in that bed is measured) is approximately three times the vertical resolution (i.e., 36 to 48 inches). Thinner beds will be noticed by the tool, but the apparent porosity will not be the same as the true porosity of the bed.

The measuring point for these tools is half way between the source and the detector for single detector tools, and half way between the two detectors for the dual detector tool.

15.8 Borehole Quality

The GNT tool is run centered in the borehole, and is therefore sensitive to the effect of caving and wash-out due to the attenuation of gamma rays and neutrons by the larger annulus of drilling mud around the tool. As the diameter of the borehole increases, more of the signal that the tool measures represents the borehole, and less comes from the formation. Clearly, there is a degree of caving where the signal measured by the tool is no longer representative of the formation, and then the tool cannot be used. This problem is accentuated by the presence of chloride ions in the drilling mud (i.e., a salt water-based mud), where attenuation by the drilling mud can lead to grossly erroneous porosity readings.

The SNP and CNL tools are run pressed up against the borehole wall. In this case, the roughness of the borehole wall due to caving or wash-out can result in the detectors or source not being pressed directly up against the borehole wall. This will cause erroneous porosity readings.

15.9 Mud Type

The tools can be used in most types of mud.

The GNT tool is sensitive to chloride-rich muds, and its results must then be corrected for the drilling mud, mudcake and mud filtrate.

The SNP tool is not sensitive to the chloride effect and is run pressed against the borehole wall. The mudcake tends to increase the apparent porosity because the mudcake has a high hydrogen index. This effect can be corrected for.

The detectors of the CNL tool are sensitive to the chloride effect. However, the tool is run pressed against the borehole wall so the effect of the drilling mud is not included in the measurement. Furthermore, the use of two detectors automatically compensates for the effect of chloride-rich mudcake and mud filtrate.

The density of the mud also affects the readings, because high density muds attenuate the radiation to a greater extent. This is usually only a problem for the GNT tool, where the effect can be compensated for using correction charts.

15.10 Uses of the Neutron Log

15.10.1 Determination of Porosity

The main use of the neutron log is to provide porosity information.

The tool is sensitive to the amount of hydrogens in the formation and to a less extent upon other elements. It is assumed that the contribution to the measurement by elements other than hydrogen is negligible, and that the contribution to the measurement from hydrogen comes entirely from the fluids fully occupying the pore space.

However, in real rocks elements other than hydrogen that exist in the rock matrix do contribute to the measurement (e.g., chlorine in formation water, mud filtrates and in some evaporite formations), and hydrogen is present in the matrix (e.g., bound water in shales).

The problem is partially overcome by calibrating the tool to give the porosity in limestone units. Pure limestone saturated with fresh water is chosen because it contains no elements which contribute significantly to the measured signal other than hydrogen.

The porosities that are read by the tool are accurate in limestone formations that contain fresh water.

The porosities that are read by the tool in other lithologies or with other fluids need to be corrected by a chart such as that shown in Fig. 15.8.

There are three effects that are not corrected for in the log data, that need to be briefly mentioned.

The Hydrocarbon Effect. The presence of hydrocarbon liquid (oil) does not effect the tool response as it has approximately the same hydrogen index as fresh water. Hydrocarbon gas, however, has a much lower hydrocarbon index resulting from its low density, and its presence will give rise to *underestimations* in porosity (Fig. 15.9).

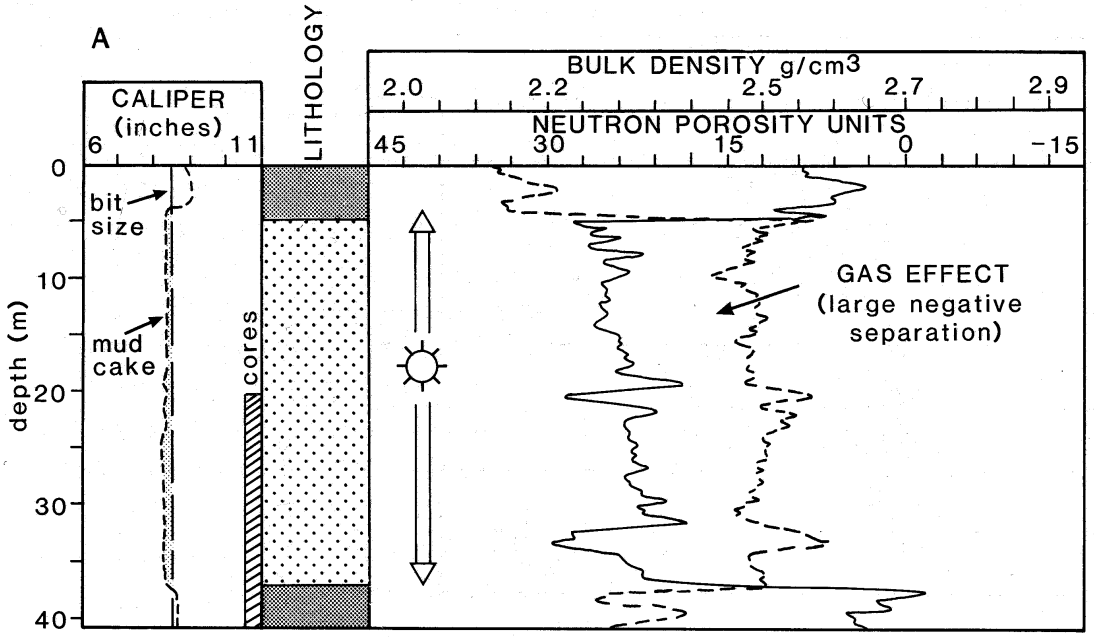

Figure 15.9 The Hydrocarbon gas effect in the neutron log.

The Shale Effect. Shale contain clays that have a significant amount of bound water molecules on their surfaces. This increases the hydrogen index of the formation. Even very low porosity shales can give erroneously high porosity readings due to the presence of these bound waters.

The Chloride Effect. Chlorine is a good absorber of neutrons, and can lead to overestimations of porosity if present either as formation fluid or mud filtrate.

15.10.2 Determination of Lithology

The direct use of the neutron log to identify lithologies depends upon the recognition of which lithologies may contain hydrogen atoms (Table 15.2).

Table 15.2 Lithological and fluid indicators for the neutron tool.

Type	Examples
Fresh and salt water	Formation water Drilling mud Mudcake Mud filtrate
Hydrocarbons	Gasses Oils Oil-based drilling mud Oil-based mud filtrate Oil-based mudcake Coal Organic-rich deposits
Bound water	Shales
Water of Crystallization	Evaporites
Hydrated minerals	Igneous and metamorphic rocks

Figure 15.10 shows typical log responses in common lithologies.

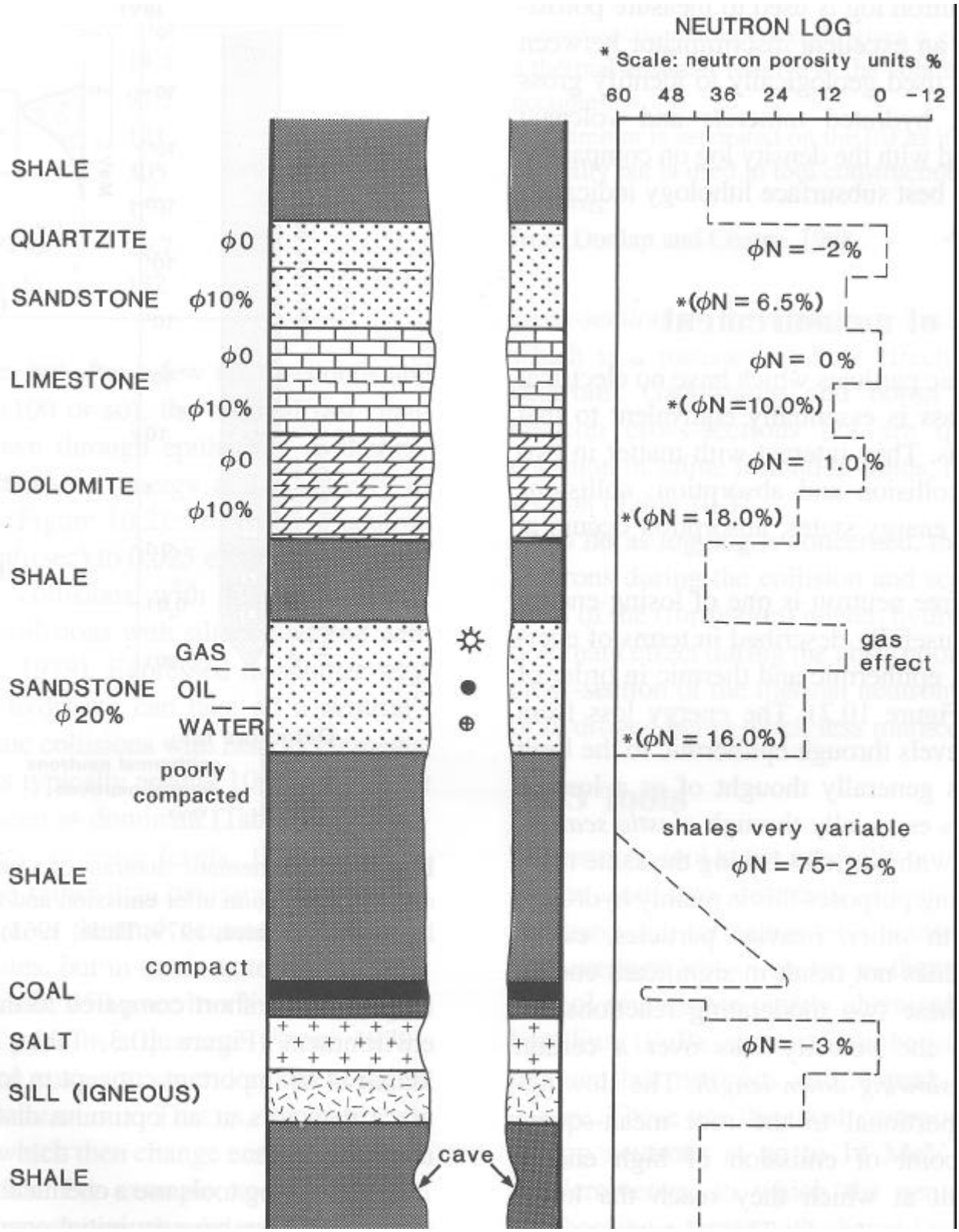

Figure 15.10 Typical neutron log responses in common lithologies.

The values of apparent porosity in shales varies considerably, but is usually higher than the apparent porosity in carbonate or sandstone rocks (i.e., 45 to 75%). This clearly high and unrealistic porosity is a partial indicator of shale, and can become diagnostic when combined with the gamma ray log. One may see a slight decrease in the apparent porosity in shales due to compaction, but only over large depth intervals.

The apparent neutron limestone porosity is affected by the amount of shale and sand, or shale and limestone in a mixture of the two. Hence we can recognize coarsening-up and fining-up sequences in the neutron log (Fig. 15.11). While one can calculate a shale volume from the neutron log directly, it is not recommended because of the effect of hydrocarbon gasses which may be present to disturb the log.

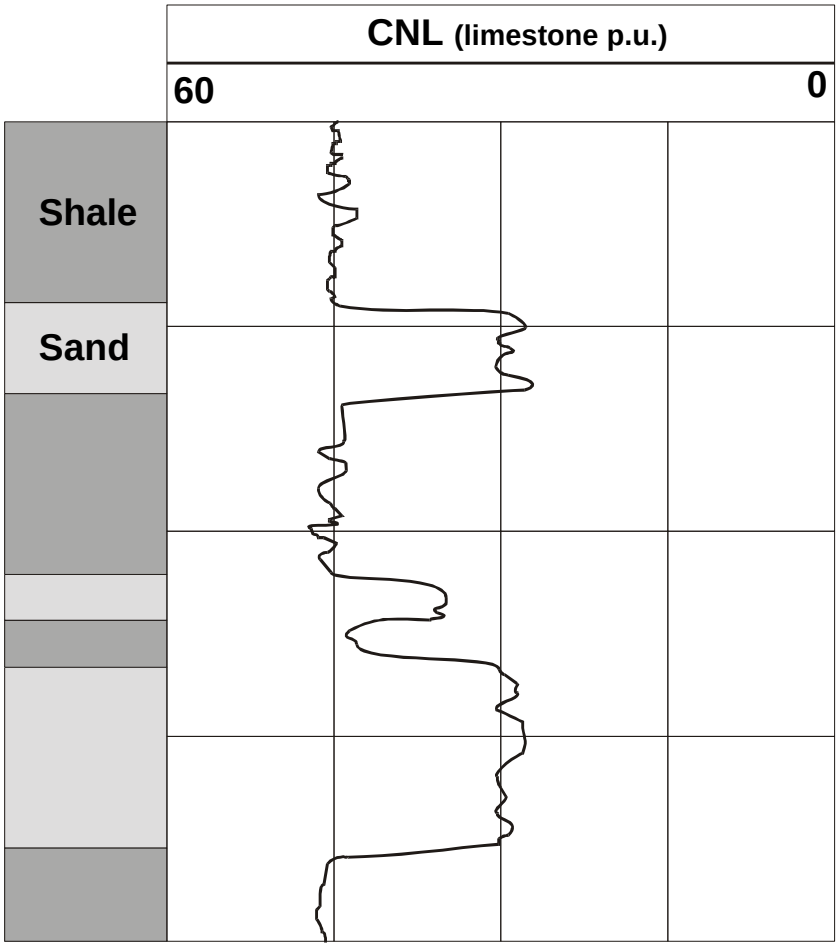

Figure 15.11 The neutron log response to mixtures of shales and sandstones.

Organic mater, often present in shales may cause an even higher apparent neutron limestone porosity than the bound water in the shales alone (Fig. 15.11).

The neutron log can detect evaporites by either their waters of crystallization. The most common example is gypsum ($CaSO_4.2H_2O$), but also include kainite, carnalite and polyhalite. The first three of these give apparent limestone porosities of about 60%, while polyhalite give about 25%. The apparent limestone porosities for halite, anhydrite, and sylvite are very low (-3, -2, and –3 respectively) as they contain no water. Note that there is no effect of the chlorine atom in halite or sylvite (Fig. 15.12).

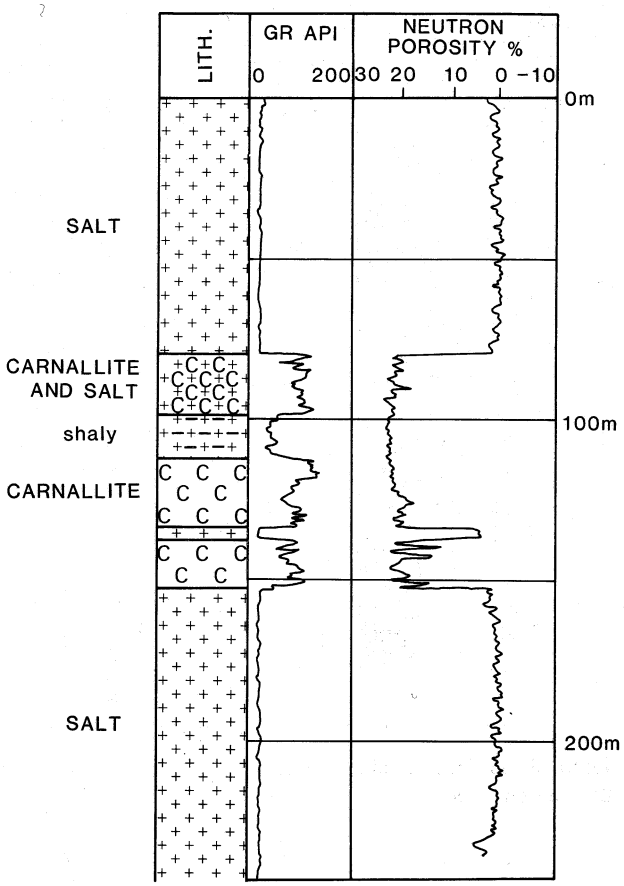

Figure 15.12 The neutron log response to evaporites (after Rider, 1997).

Hydrated minerals are not common in basins. The only occurrence is occasional chamosite in Liassic shales in the North Sea. Hydrated minerals may be seen in neutron logs used for non-hydrocarbon purposes, such as geothermal reservoir assessment in metamorphic and igneous provinces. However, volcanic and intrusive rocks show high apparent neutron porosities die to hydrated minerals, and these horizons in reservoirs can be very useful for correlation purposes.

15.11 Lithological Identification using the Neutron-Density Combination

15.11.1 Compatible Scales and the Density-Neutron Cross-plot

This is a hugely important technique, and together with the litho-density log forms the best downhole lithological identification technique available to the petrophysicist.

Both the formation density log and the neutron log give a direct measurement of TOTAL porosity. Hence, if they are plotted on compatible scales, they should overlie each other (Fig. 15.13).

Note that the compatible scale here is Density (1.95 to 2.95 g/cm^3) and Neutron (-15 to 45% limestone porosity units). This is the most commonly used scale range, although other wider or more restricted ones are possible.

Note also that good superimposition will ONLY occur for clean limestone formations 100% saturated with fresh water.

To construct a compatible scale we follow the following steps:

- For limestone with 0% porosity, the density log reads 2.71 g/cm^3 and the neutron log reads zero.
- For limestone with 100% porosity, the density log reads 1.00 g/cm^3 and the neutron log reads 100.

These two points can be plotted on a graph of density (from the density log) on the *y*-axis against neutron porosity (from the neutron log) on the *x*-axis. We can join up the two points with a straight line, and calibrate the line for porosity (Fig. 15.14). The graph is called the *density-neutron crossplot* and the line is called the *clean limestone line*.

The clean limestone line only works for clean limestones because of the effect of non-hydrogen elements in the matrix on the neutron porosity values, and the different grain densities. However, we can take account of the different densities and correct the neutron porosity units using Fig. 15.8, to obtain lines of the cross-plot for clean sandstones and clean dolomite, the *clean sandstone* and *clean dolomite* lines.

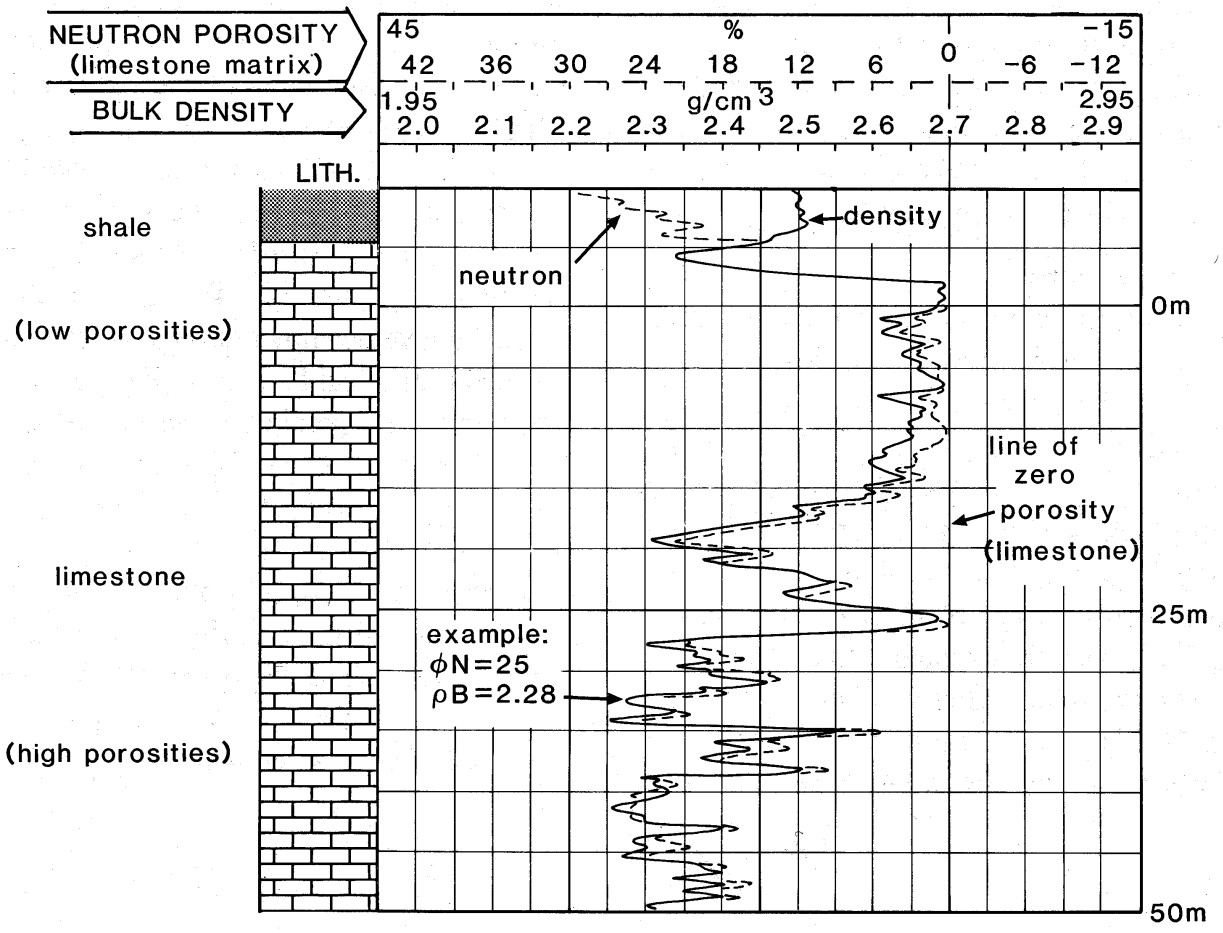

Figure 15.13 The density and neutron log responses for clean formations on a compatible scale (after Rider, 1997).

One can see from the cross-plot that for density and neutron logs plotted on compatible scales, there will be a *separation* of the density and the neutron logs for sandstone and dolomite, but no separation for limestone (Fig. 15.15). The sandstone separation is called *negative* and the dolomite separation is in the other direction and slightly larger, and is called *positive*.

The separations are caused by the relative positions of both logs.

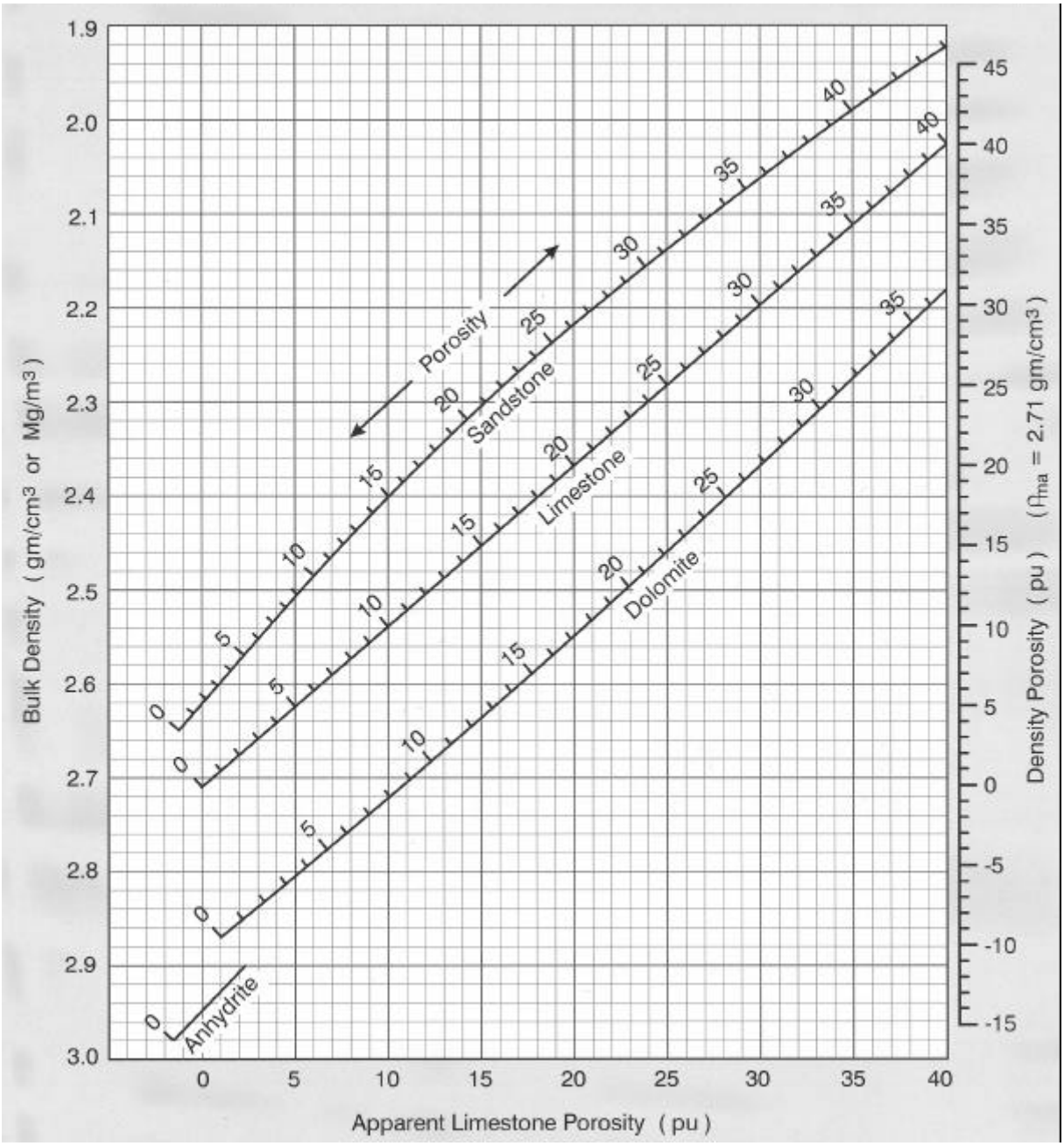

Figure 15.14 The density-neutron crossplot.

15.11.2 Clean Formations

- There is no separation for pure limestones, and the porosity value that the log gives is accurate.
- There is a small negative separation for clean sandstones.
- There is a moderate positive separation for pure dolomites.

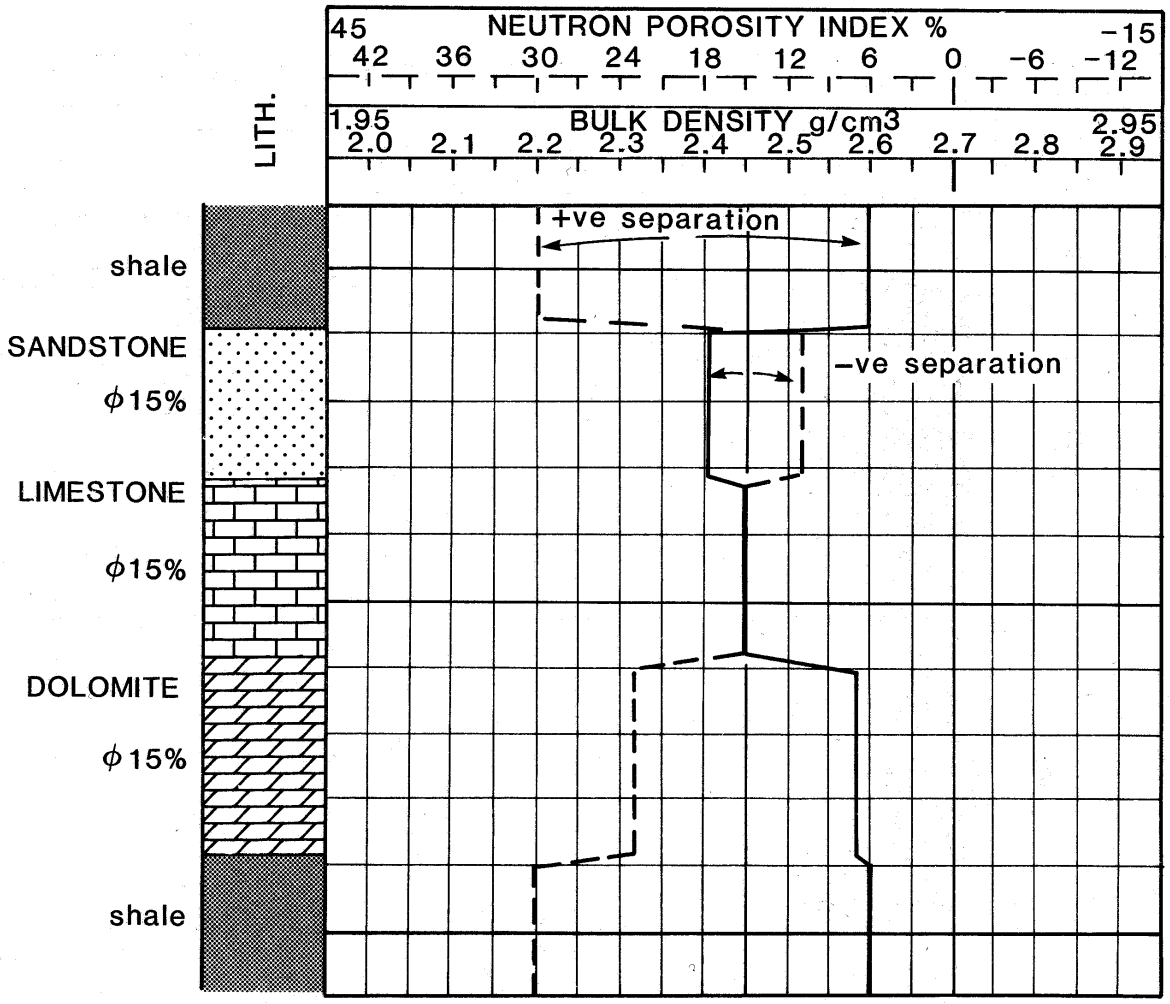

Figure 15.15 The density-neutron combination idealized responses.

15.11.3 Shaly Formations

If shale is present in the formation, the neutron log reads much higher porosities than it would otherwise do because of the effect of bound water. This gives a large positive separation.

This large positive separation is diagnostic of shales.

If the shale volume decreases due to the intermixture of sandstone, the large positive separation decreases, crosses-over and becomes eventually the small negative separation associated with pure sandstone.

Thus, a sequence of clearly defined sand and shale formations shows switching between positive and negative separations in the logs.

Often the beds will not be well defined, but coarsen-up or fine-up gradually. This can be seen by a gradual switch from one separation to another. Hence the characteristic patterns (reviewed in the chapter on the gamma ray log) can be recognized in the separations, and conclusions may be drawn concerning the depositional environment.

The size of the separation is actually THE BEST quantitative estimator or shale volume. It is better than the shale volume derived from the gamma ray log. We can write an equation for shale volume based on separations

$$V_{sh} = \frac{\Omega_{log} - \Omega_{sand}}{\Omega_{sh} - \Omega_{sand}} \quad \textbf{(15.8)}$$

where Ω stands for the separation measured in 100% sandstone, 100% shale, and at the point of interest in the log. Note that the separations may ALL be measured on the limestone porosity scale, ALL on the density scale, or ALL using a simple ruler on the log! Each is valid, but you must keep it consistent for the whole equation.

15.11.4 Distinctive Lithologies

Certain minerals have unusual combinations of density and neutron porosity. These unusual combinations can be used to identify them on a combination log. Examples are given in Fig. 15.16.

Coals are a good example of a distinctive combination of density and neutron porosity values. They have unusually low densities combined with unusually high apparent neutron porosity values associated with their hydrogen content.

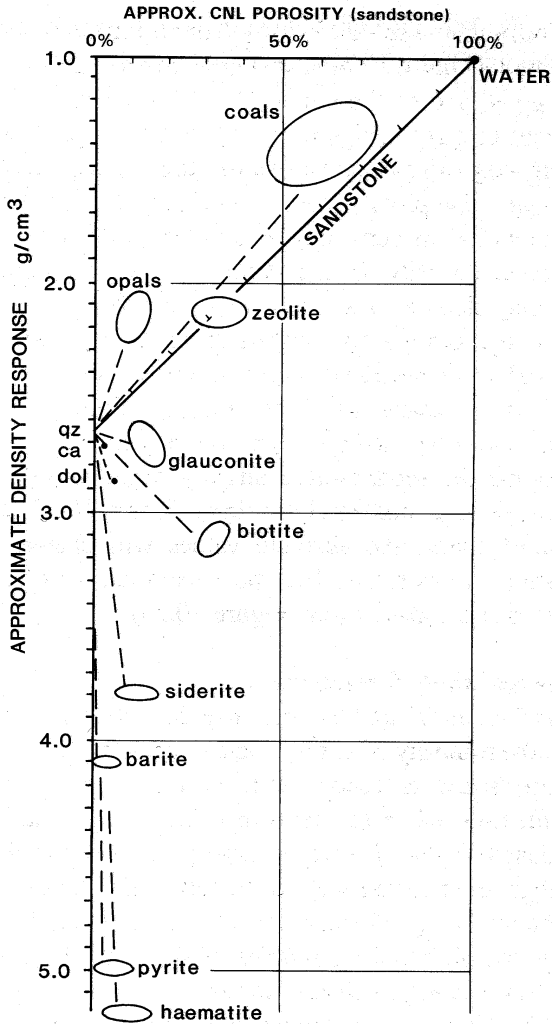

Fig 15.16 Distinctive minerals on a density-neutron log.

15.11.5 Evaporites

Remember from the section about the formation density tool that evaporites can often be recognized because their often pure nature leads to well constrained density values. Evaporites have apparent neutron porosity values which are either very high or very low. The combination of well constrained density values and very high or very low apparent neutron porosity values is a characteristic and diagnostic combination for evaporites (Fig. 15.17).

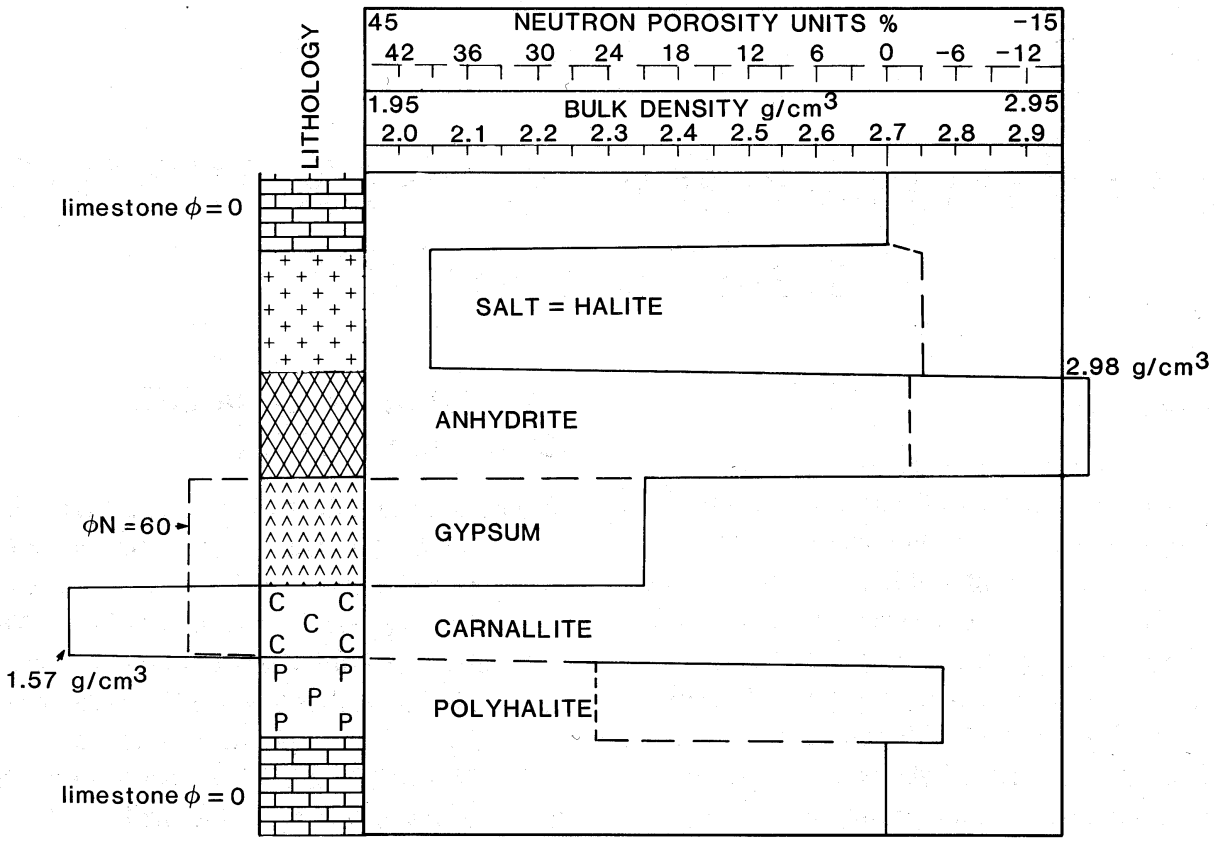

Fig 15.17 Distinctive evaporites on a density-neutron log.

16. THE SONIC OR ACOUSTIC LOG

16.1 Introduction

The *sonic* or *acoustic* log measures the travel time of an elastic wave through the formation. This information can also be used to derive the velocity of elastic waves through the formation.

Its main use is to provide information to support and calibrate seismic data and to derive the porosity of a formation.

The main uses are:

- Provision of a record of "seismic" velocity and travel time throughout a borehole. This information can be used to calibrate a seismic data set (i.e., tie it in to measured values of seismic velocity).
- Provision of "seismic" data for the use in creating synthetic seismograms.
- Determination of porosity (together with the FDC and CNL tools).
- Stratigraphic correlation.
- Identification of lithologies.
- Facies recognition.
- Fracture identification.
- Identification of compaction.
- Identification of over-pressures.
- Identification of source rocks.

The tool works at a higher frequency than seismic waves, therefore one must be careful with the direct comparison and application of sonic log data with seismic data.

16.2 Theory

16.2.1 Wave Types

The tool measures the time it takes for a pulse of "sound" (i.e., and *elastic wave*) to travel from a transmitter to a receiver, which are both mounted on the tool. The transmitted pulse is very short and of high amplitude. This travels through the rock in various different forms while undergoing *dispersion* (spreading of the wave energy in time and space) and *attenuation* (loss of energy through absorption of energy by the formations).

When the sound energy arrives at the receiver, having passed through the rock, it does so at different times in the form of different types of wave. This is because the different types of wave travel with different velocities in the rock or take different pathways to the receiver. Figure 16.1 shows a typical received train of waves. The transmitter fires at $t = 0$. It is not shown in the figure because it is masked from the received information by switching the receiver off for the short duration during which the pulse is transmitted. This is done to ensure that the received information is not too complicated, and to protect the sensitive receiver from the high amplitude pulse. After some time the first type of wave arrives. This is the *compressional* or *longitudinal* or *pressure* wave (*P-wave*). It is usually the fastest wave, and has a small amplitude. The next wave, usually, to arrive is the *transverse* or *shear* wave (*S-*

wave). This is slower than the P-wave, but usually has a higher amplitude. The shear wave cannot propagate in fluids, as fluids do not behave elastically under shear deformation. These are the most important two waves. After them come *Rayleigh waves*, *Stoneley waves*, and *mud waves*. The first two of these waves are associated with energy moving along the borehole wall, and the last is a pressure wave that travels through the mud in the borehole. They can be high amplitude, but always arrive after the main waves have arrived and are usually masked out of the data. There may also be unwanted P-waves and S-waves that travel through the body of the tool, but these are minimized by good tool design by (i) reducing their received amplitude by arranging damping along the tool, and (ii) delaying their arrival until the P-wave and S-wave have arrived by ensuring that the pathway along the tool is a long and complex one.

The data of interest is the time taken for the P-wave to travel from the transmitter to the receiver. This is measured by circuitry that starts timing at the pulse transmission and has a threshold on the receiver. When the first P-wave arrival appears the threshold is exceeded and the timer stops. Clearly the threshold needs to be high enough so that random noise in the signal dies not trigger the circuit, but low enough to ensure that the P-wave arrival is accurately timed.

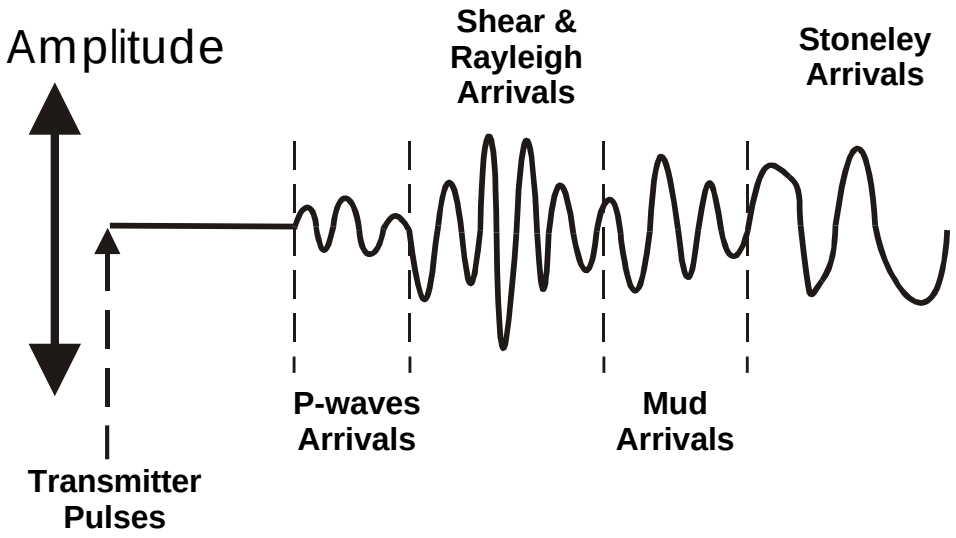

Fig. 16.1 The geophysical wavetrain received by a sonic log.

There are complex tools that make use of both P-waves and S-waves, and some that record the full wave train (*full waveform logs*). However, for the simple sonic log that we are interested in, only the *first arrival* of the P-wave is of interest. The time between the transmission of the pulse and the reception of the first arrival P-wave is the one-way time between the transmitter and the receiver. If one knows the distance between the transmitter (Tx) and the receiver (Rx), the velocity of the wave in the formation opposite to the tool can be found.

In practice the sonic log data is not presented as a travel time, because different tools have different Tx-Rx spacings, so there would be an ambiguity. Nor is the data presented as a velocity. The data is presented as a *slowness* or the travel time per foot traveled through the formation, which is called delta t (Δt or ΔT), and is usually measured in μs/ft. Hence we can write a conversion equation between velocity and slowness:

$$\Delta t = \frac{10^6}{V} \qquad \textbf{(16.1)}$$

where the slowness, Δt is in microseconds per foot, and the velocity, V is in feet per second.

The velocity of the compressional wave depends upon the elastic properties of the rock (matrix plus fluid), so the measured slowness varies depending upon the composition and microstructure of the matrix, the type and distribution of the pore fluid and the porosity of the rock. The velocity of a P-wave in a material is directly proportional to the strength of the material and inversely proportional to the density of the material. Hence, the slowness of a P-wave in a material is inversely proportional to the strength of the material and directly proportional to the density of the material, i.e.;

$$V \propto \frac{\text{Strength}}{r} \quad \text{and} \quad \Delta t \propto \frac{r}{\text{Strength}} \qquad \textbf{(16.2)}$$

The strength of a material is defined by two parameters (i) the bulk modulus, and (ii) the shear modulus.

The bulk modulus, *K* is the extent to which a material can withstand isotropic squeezing (Fig. 16.2a). Imagine an amount of material subjected to an isotropic pressure P_1. Now let the isotropic pressure increase to a pressure P_2. The material will compress from its initial volume v_1 to a new smaller volume v_2. The bulk modulus is then given by;

$$K = \frac{P_2 - P_1}{(v_1 - v_2)/v_1} = \frac{\Delta P}{\Delta v / v_1} \qquad \textbf{(16.3)}$$

where ΔP is the change in pressure, and Δv is the change in volume. Thus ΔP is the change in pressure that causes Δv change in volume.

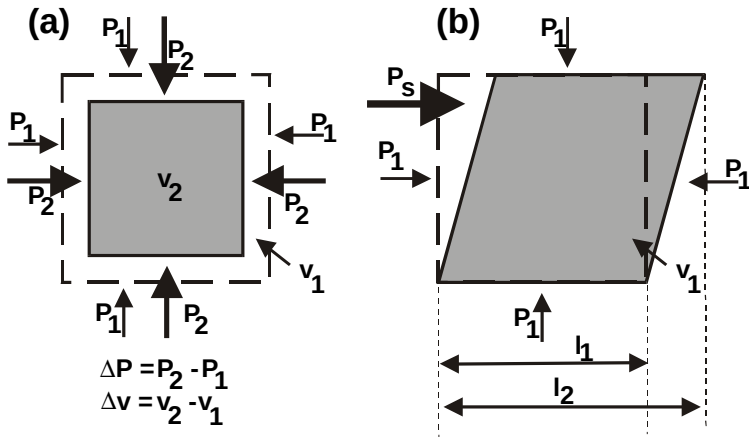

Fig. 16.2 The definition of bulk and shear moduli.

The shear modulus, μ is the extent to which a material can withstand shearing (Fig. 16.2b). Imagine an amount of material subjected to a isotropic pressure P_1. Now apply a shear stress (non-isotropic pressure) P_s to one side of the sample. The material will shear to the new shape, and its overall length will increase from its initial length l_1 to a new larger length l_2. The bulk modulus is then given by;

$$\mu = \frac{P_s}{(l_2 - l_1)} = \frac{P_s}{g} \qquad \textbf{(16.4)}$$

where g is the shear strain. The application of the shear stress P_s causes the development of a shear strain g.

Detailed analysis of the velocity and slowness of P-waves in a material shows that;

$$V_P = \sqrt{\frac{K + \frac{4}{3}\mu}{\rho}} \quad \text{for solids} \qquad \textbf{(16.5)}$$

$$V_P = \sqrt{\frac{K}{\rho}} \quad \text{for fluids} \qquad \textbf{(16.6)}$$

16.2.2 Reflection and Refraction

The transmitter emits "sound" waves at a frequency of about 20-40 kHz, in short pulses, of which there are between 10 and 60 per second depending on the tool manufacturer. The energy spreads out in all directions.

Imagine a pulse emanating from a Tx on a sonic tool. It will travel through the drilling mud and encounter the wall of the borehole. The P-wave travels well through the mud at a relatively slow velocity, V_m, as the mud has a low density. The S-wave will not travel through liquid mud. At the interface it is both reflected back into the mud and refracted into the formation. The portion of the P-wave energy that is refracted into the formation travels at a higher velocity, V_f, because the density of the rock is higher. This is depicted in Fig. 16.3. We can use Snell's law to write;

$$\frac{\sin i}{\sin R} = \frac{V_m}{V_f} \qquad \textbf{(16.7)}$$

and at the critical angle of refraction, where the refracted wave travels along the borehole wall, $R = 90^o$, so;

$$\sin i = \frac{V_m}{V_f} \qquad \textbf{(16.8)}$$

Hence, if the velocity of the elastic wave in the formation changes, the critical angle, i, will also change.

The velocity of the refracted wave along the borehole wall remains V_f. Each point reached by the wave acts as a new source retransmitting waves back into the borehole at velocity V_m.

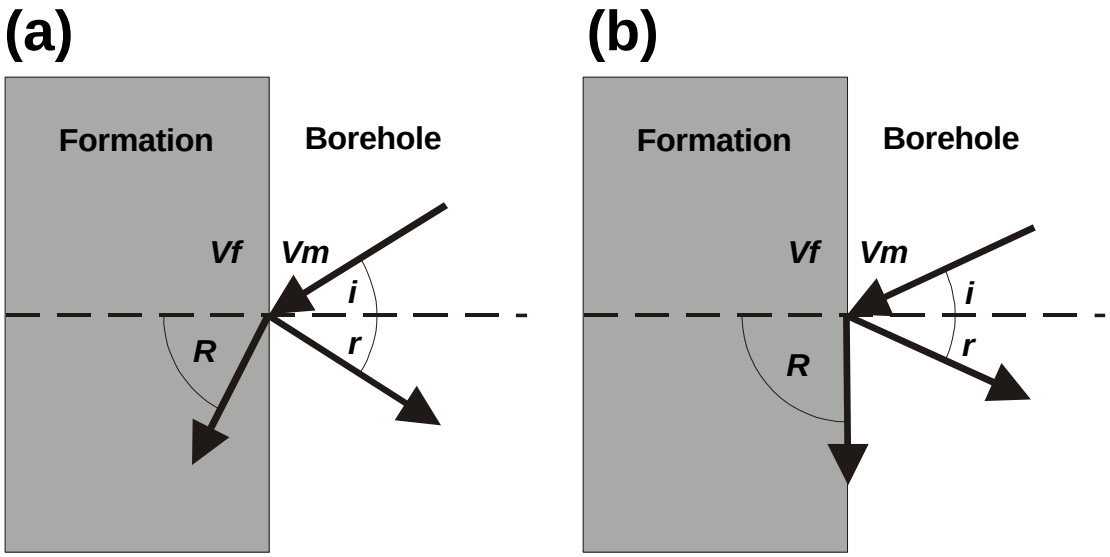

Fig. 16.3 Reflection and refraction at the borehole wall.

16.3 Sonic Tools

16.3.1 Early Tools

Early tools had one Tx and one Rx (Fig. 16.4). The body of the tool was made from rubber (low velocity and high attenuation material) to stop waves travelling preferentially down the tool to the Rx. There were two main problems with this tool. (i) The measured travel time was always too long because the time taken for the elastic waves to pass through the mud was included in the measurement. The measured time was A+B+C rather than just B. (ii) The length of the formation through which the elastic wave traveled (B) was not constant because changes to the velocity of the wave depending upon the formation altered the critical refraction angle.

16.3.2 Dual Receiver Tools

These tools were designed to overcome the problems in the early tools. They use two receivers a few feet apart, and measure the *difference* in times of arrival of elastic waves at each Rx from a given pulse from the Tx (Fig. 16.5). This time is called the *sonic interval transit time* (Δt) and is the time taken for the elastic wave to travel through the interval D (i.e., the distance between the receivers).

- The time taken for elastic wave to reach Rx1: T_{Rx1}= A+B+C
- The time taken for elastic wave to reach Rx2: T_{Rx2} = A+B+D+E
- The sonic interval transit time: $\Delta T = (T_{Rx2} - T_{Rx1})$ = A+B+D+E – (A+B+C) = D+E-C.
- If tool is axial in borehole: C = E, so $\Delta T = (T_{Rx2} - T_{Rx1})$ = D

The problem with this arrangement is that if the tool is tilted in the hole, or the hole size changes (Fig. 16.6), we can see that C ≠ E, and the two Rx system fails to work.

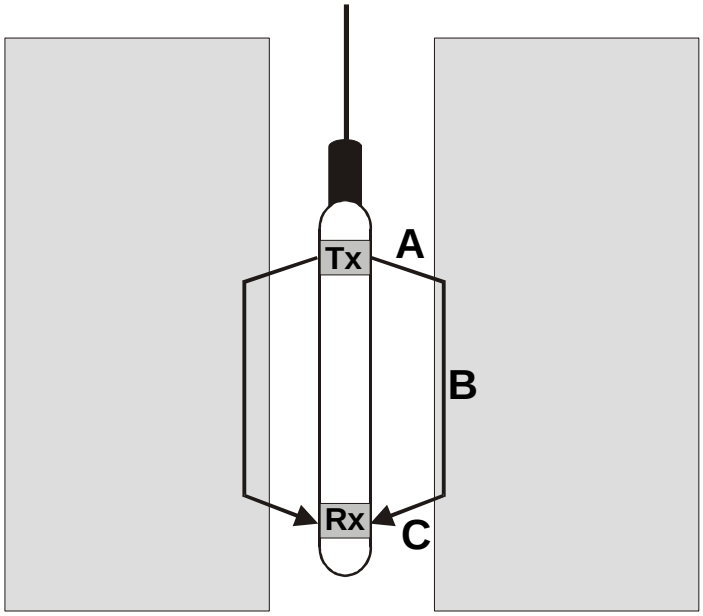

Fig. 16.4 Early sonic tools.

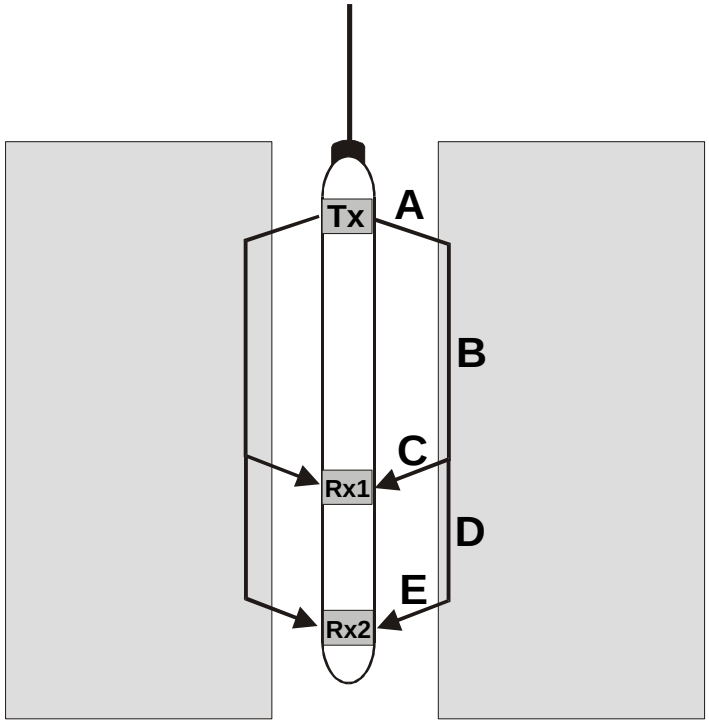

Fig. 16.5 Dual receiver sonic tools in correct configuration.

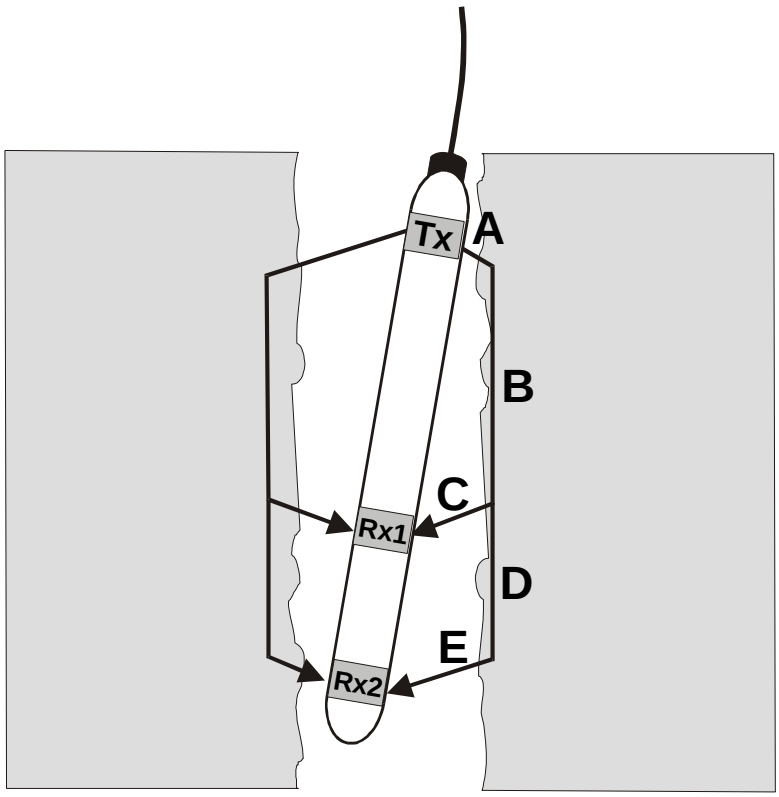

Fig. 16.6 Dual receiver sonic tools in incorrect configuration.

16.3.3 Borehole Compensated Sonic (BHC) Tool

This tool compensates automatically for problems with tool misalignment and the varying size of the hole (to some extent) that were encountered with the dual receiver tools. It has two transmitters and four receivers, arranged in two dual receiver sets, but with one set inverted (i.e., in the opposite direction). Each of the transmitters is pulsed alternately, and Δt values are measured from alternate pairs of receivers (Fig. 16.7). These two values of Δt are then averaged to compensate for tool misalignment, at to some extent for changes in the borehole size.

A typical pulse for the BHC is 100 μs to 200 μs, with a gap of about 50 ms, giving about 20 pulses per second. There are four individual Tx-Rx readings needed per measurement, so 5 measurements can be made per second. At a typical logging speed of 1500 m/h (5000 ft/h), gives one reading per 8 cm (3 inches) of borehole. Several versions of the BHC are available with different Tx-Rx distances (3 ft. and 5 ft. being typical), and the Rx-Rx distance between pairs of receivers is usually 2 ft.

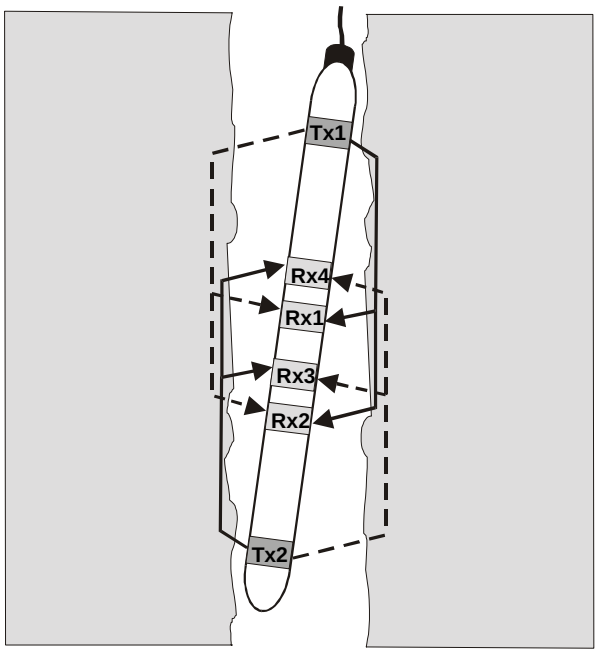

Fig. 16.7 Borehole compensated sonic tools.

16.3.4 Long Spacing Sonic (LSS) Tool

It was recognized that in some logging conditions a longer Tx-Rx distance could help. Hence Schlumberger developed the *long spacing sonic* (LSS), which has two Tx two feet apart, and two Tx also two feet apart but separated from the Tx by 8 feet. This tool gives two readings; a near reading with a 8-10 ft. spacing, and a far reading with a 10-12 ft. spacing (Fig. 16.8).

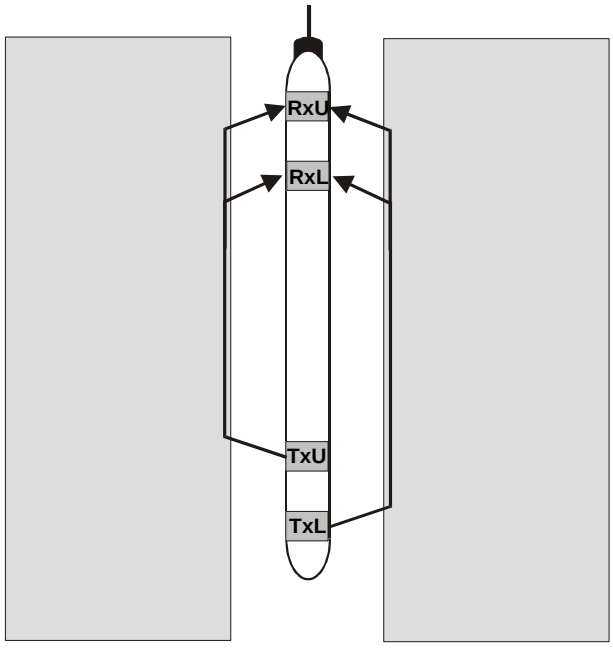

Fig. 16.8 Long spacing sonic tools.

16.3.5 Common Industry Tools

Table 16.1 shows the names and mnemonics of common industry sonic tools.

Table 16.1 The names and mnemonics of common industry sonic tools.

Tool	Mnemonic	Company
Compensated sonic sonde	CSS	BPB
Long spaced compensated sonic	LCS	
Borehole compensated sonde	BCS	Halliburton
Long spaced sonic	LSS	
Borehole compensated sonic	BHC	Schlumberger
Long spaced sonic	LSS	
Array sonic (standard mode)	DTCO	
Borehole compensated acoustilog	AC	Western Atlas
Long-spaced BHC acoustilog	ACL	

16.4 Calibration

The tool is calibrated inside the borehole opposite beds of pure and known lithology, such as anhydrite (50.0 μs/ft.), salt (66.7 μs/ft.), or inside the casing (57.1 μs/ft.).

16.5 Log Presentation

The interval transit time Δt is recorded on the log in microseconds per foot (μs/ft.). If the log is run on its own, the log takes up the whole of Track 2 and 3, if combined with other logs, it is usually put in Track 3 (Fig. 16.9). Most formations give transit times between 40 μs/ft. and 140 μs/ft., so these values are usually used as the scale.

The log will also show the *integrated travel time* (TTI). This value is derived simultaneously with the main measurement, and is the mean travel time in milliseconds. It is shown by pips on the right side of the depth column (in slightly different styles by different companies). The small pips occur every 1 millisecond and the larger ones occur every 10 milliseconds. The main advantage of this is that the average travel time between two depths can be found by simply counting the pips, which is really useful when comparing sonic logs to seismic sections. Likewise adding the pips together for a certain depth interval, and dividing by the thickness of the interval allows the mean velocity of the interval to be simply calculated. In the comparison it ***MUST*** be remembered that the pips give one-way travel time, and must be doubled to be compared to the two way travel time given in seismic data.

The accuracy of the travel time integrator can be checked on a log in a thick homogeneous formation. First, count the pips over the thickness of the interval to get the TTI value in milliseconds. Then read off the eyeballed mean Δt in the interval in microseconds per foot, multiply by the thickness of the interval and divide by 1000. The value should agree with the TTI reading.

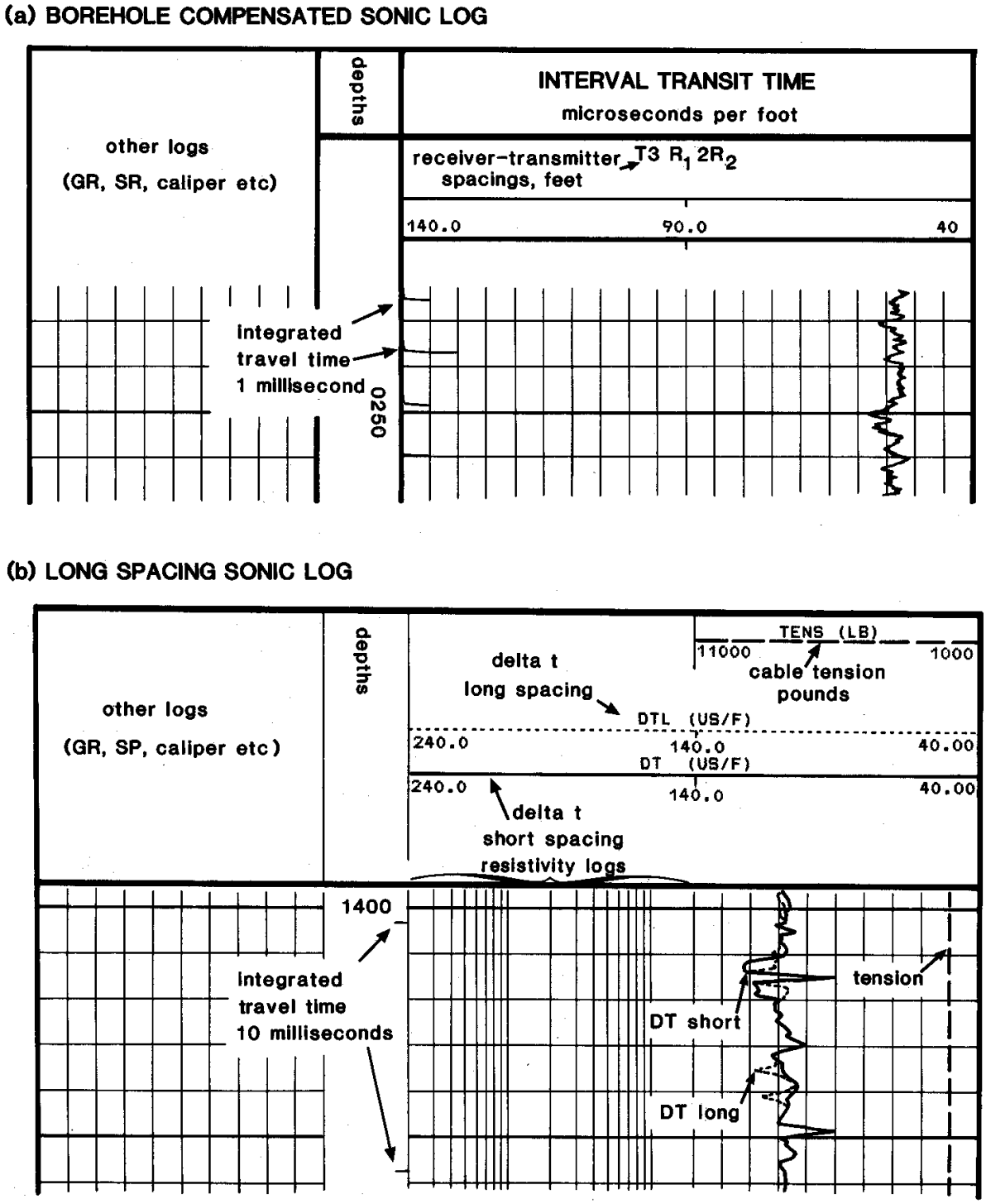

Fig. 16.9 Presentation of the sonic log. (a) BHC, (b) ISF-Sonic combination. (courtesy of Schlumberger and Rider)

16.6 Depth of Investigation

This is complex and will not be covered in great detail here. In theory, the refracted wave travels along the borehole wall, and hence the depth of penetration is small (2.5 to 25 cm). It is independent of Tx-Rx spacing, but depends upon the wavelength of the elastic wave, with larger wavelengths giving

larger penetrations. As wavelength $l = V/f$ (i.e., velocity divided by frequency), for any given tool frequency, the higher the velocity the formation has, the larger the wavelength and the deeper the penetration.

16.7 Vertical and Bed Resolution

The vertical resolution is equal to the Rx-Rx spacing, and hence is 2 ft. Beds less than this thickness can be observed, but will not have the signal fully developed. There are now some special tools which have an even better resolutions (e.g., ACL and DAC), but these are array sonic logs that will not be covered in this course.

16.8 Logging Speed

The typical logging speed for the tool is 5000 ft/hr (1500 m/hr), although it is occasionally run at lower speeds to increase the vertical resolution.

16.9 Logging Problems

16.9.1 Noise

Noise from stray electrical fields, the electronics package or derived from mechanically generated noise in rough holes can trigger the detection circuitry before the first arrival, causing a false (shorter) apparent first arrival. To limit this effect, all receiver circuits are disabled for 120 microseconds after the pulse. As the remaining time for the possibility of a noise spike occurring is greater for the far detector than the near one, most noise spikes occur for the far detector, which leads to values of Δt that are too small. These are seen as single data point spikes of low Δt in the log (Figs. 16.10 and 16.11).

16.9.2 D*t* Stretch

In heavily attenuating formations the value of Δt can be slightly too large due to the thresholding method employed by the detection circuitry. However, this problem is rarely significant, and is impossible to detect from the log.

16.9.3 Cycle Skipping

This is the occurrence of a failure in the thresholding to detect the first cycle of the wave's first arrival. Triggering may then occur at the second or even third cycle. This causes a marked and sudden shift to higher Δt values, followed by a shift back again to the correct value.

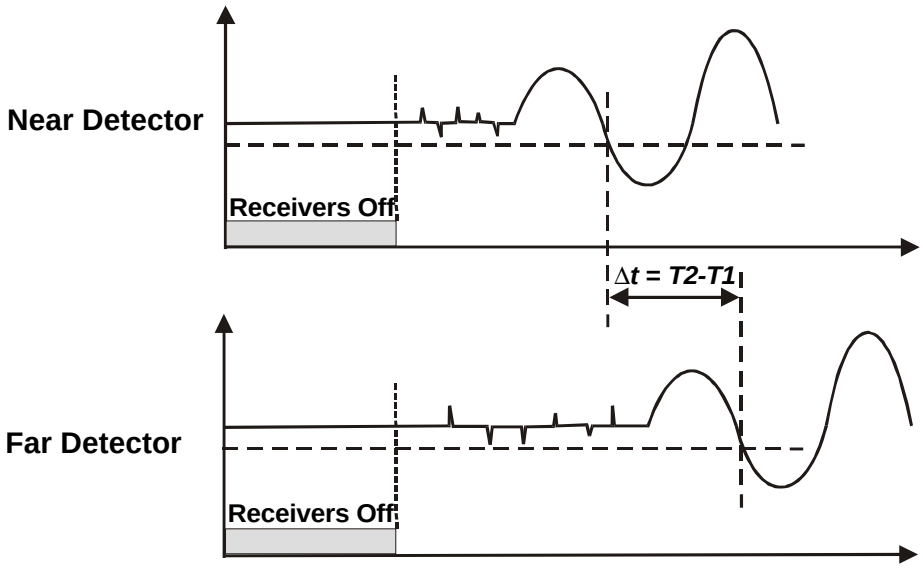

(a) Δt measured correctly

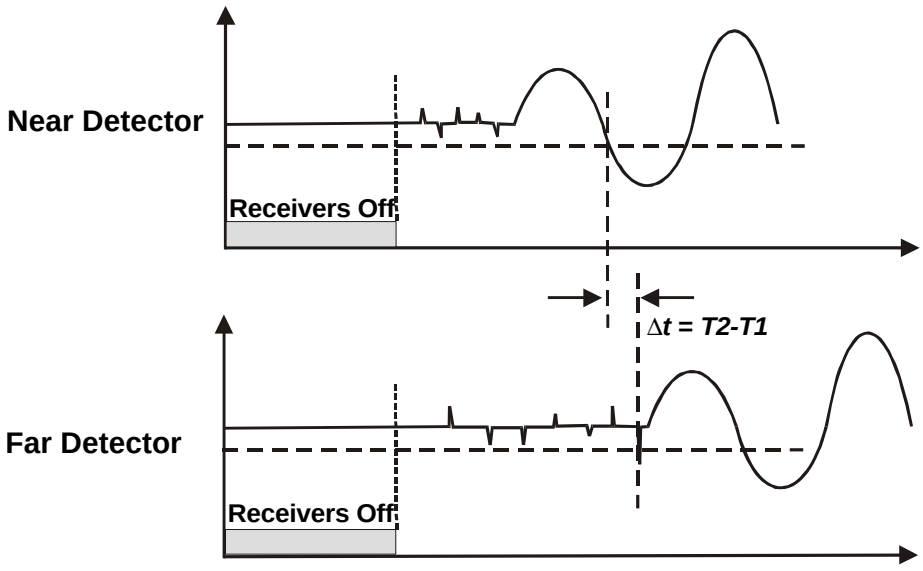

(b) Δt measured incorrectly (Δt is too small*)*

Fig. 16.10 The effect of noise spikes on thresholding.

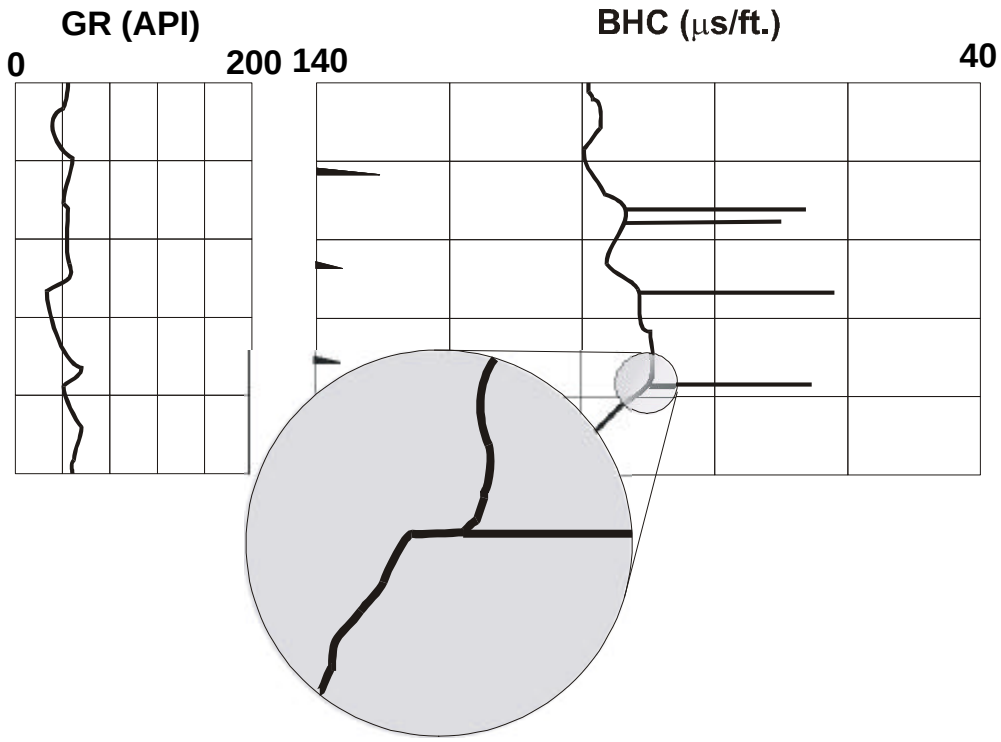

Fig. 16.11 How noise spikes occur in the log.

16.9.4 Mud Arrivals

Clearly the first arrival should be from a P-wave that has traveled through the formation. In some circumstances the P-wave that has traveled directly through the mud arrives first. This occurs if the Tx-Rx is smaller than a critical distance that depends upon the velocities of the P-wave through the formation and the mud, the diameter of the borehole and the diameter of the tool. Tools are designed to avoid this by making the Tx-Rx distance large enough for most applications. However, in some large diameter holes, the mud arrivals may come first. This leads to there being no structure in the sonic log response because the travel time through the mud is all that is being recorded. In these circumstances the tool may be run eccentred, but at the risk of picking up more noise spikes from the noise associated with the rough borehole surface.

16.9.5 Altered Zone Arrivals

The formation next to the borehole may not be typical of the rock. For example, it may be filled with solid mud and have a higher velocity than the virgin formation, or it may be fractured or altered and have a lower velocity. This is an analogous problem to the mud arrival problem.

If a low velocity altered zone exists, the Tx-Rx spacing must be large to ensure that the P-wave from the virgin formation arrives before that from the altered zone. In this case an LSS should provide better data than a BHC type log.

If a high velocity altered zone exists, there is no solution whatever type of log is used. The measured log value will be that for the altered zone.

A graph can be drawn to show the reliability of tools affected by mud and altered zone arrivals (Fig. 16.12). It is clear that the LSS has the better performance. However, the greater spacing means that arrival waves are weaker and therefore more prone to cycle skipping and noise spikes.

Figure 16.13 shows an example of altered zone arrivals affecting a BHC log but not an LSS log.

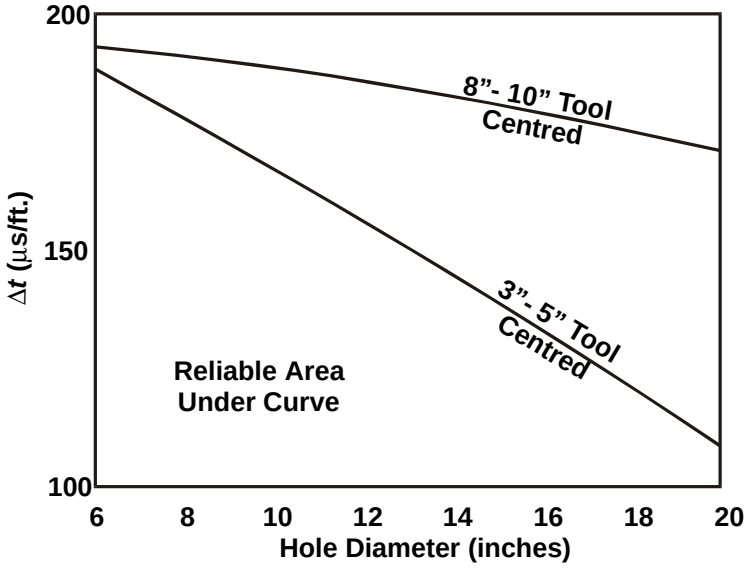

Fig. 16.12 Schematic reliability chart for Schlumberger tools (redrawn from Schlumberger data).

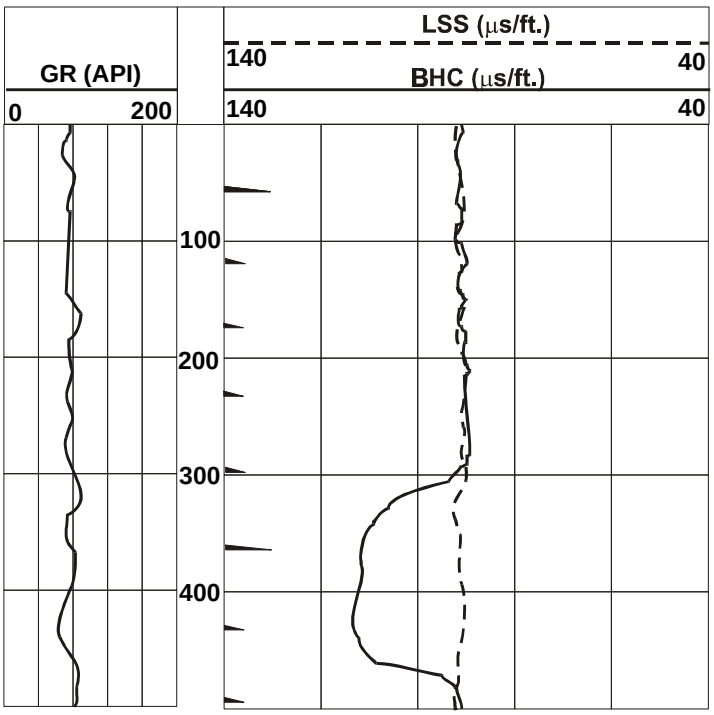

Fig. 16.13 Example of altered zone arrivals affecting the BHC log.

16.10 Uses of the Sonic Log

16.10.1 Seismic Data Calibration

The presence of a sonic log in a well that occurs on a seismic line or in a 3D survey enables the log data to be used to calibrate and check the seismic data. As the resolution of the sonic log is about 61 cm and that of the seismic technique is 10 m to 50 m, the sonic data must be averaged for the comparison to be made. However, the higher resolution of the sonic log may enable the log information to resolve indications of beds that are just beyond the resolution of the seismic technique.

It must be remembered that the sonic log gives a one-way travel time, and the seismic technique gives a two-way travel time.

16.10.2 Seismic Interval Velocities

The average sonic log interval velocity is obtained by counting the TTI pips over the interval concerned and dividing the thickness of the interval by this value.

A time-depth curve can then be obtained by taking a weighted sum of the interval velocities with depth, which will give the total time to a given depth and plotting this against depth. Figure 6.14 shows an example of such a curve, where the sonic interval transit time is given in parentheses next to the depth column.

The time-depth curve can then be compared against the velocity analyses from the seismic data, or can be used in place of velocity analyses in seismic processing.

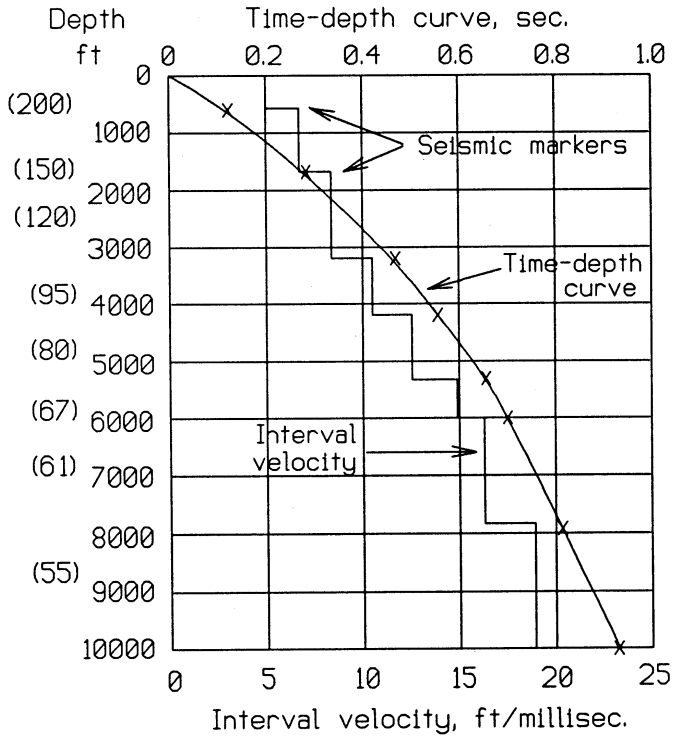

Fig. 16.14 Interval velocity and time-depth graphs.

16.10.3 Synthetic Seismograms

A synthetic seismogram is a seismic trace that has been constructed from various parameters obtainable from log information. It represents the seismic trace that should be observed with the seismic method at the well location. It is useful to compare such a synthetic seismogram with the seismic trace actually measured at the well to improve the picking of seismic horizons, and to improve the accuracy and resolution of formations of interest.

It should be remembered that the observed seismic trace is primarily a record of the ability of interfaces between formations to reflect elastic waves. This ability is called the reflection coefficient *R*. The reflection coefficient depends upon the properties of the rock either side of the interface, and in particular on its acoustic impedance. The acoustic impedance is the product of the seismic velocity and the density of the rock.

Thus, if we can derive the density and seismic velocity of a set of formations from logs, we can derive a synthetic seismogram. The procedure is as follows.

- Obtain a density log, $r(z)$, for the interval of interest. This is best obtained from a FDC log, but approximations can be made from the sonic log by using the sonic log to derive porosity, and then if the densities of the rock matrix and formation fluids are known, the density of the rock can be calculated.

- Convert the density log in depth to that against two-way time using the TTI information from the sonic log.

- Obtain the elastic wave velocity log, $V(z)$, from the sonic log using Eq. (16.1).

- Convert the elastic wave velocity log in depth to that against two-way time using the TTI information from the sonic log.

- Multiply these two values for each depth to give the acoustic impedance log, $AI = r(TWT)V(TWT)$.

- Calculate the reflection coefficient for each interface from the acoustic impedance log using;

$$R = \frac{AI_2 - AI_1}{AI_2 + AI_1} = \frac{r_2V_2 - r_1V_1}{r_2V_2 - r_1V_1} \qquad \textbf{(16.9)}$$

  where the subscript 2 refers to the formation below an interface, and the subscript 1 to the formation above it.

  Note that the reflection coefficient will only exist at interfaces, and is zero in between.

- Apply a multiplying factor to the reflection coefficient log to account for the fact that the seismic response will be attenuated with depth. This factor reduces with increasing two-way travel time (i.e., as depth increases).

- Convolve (multiply) the modified reflection coefficient with a chosen zero phase wavelet that represents the seismic data with which you wish to compare the synthetic seismogram.

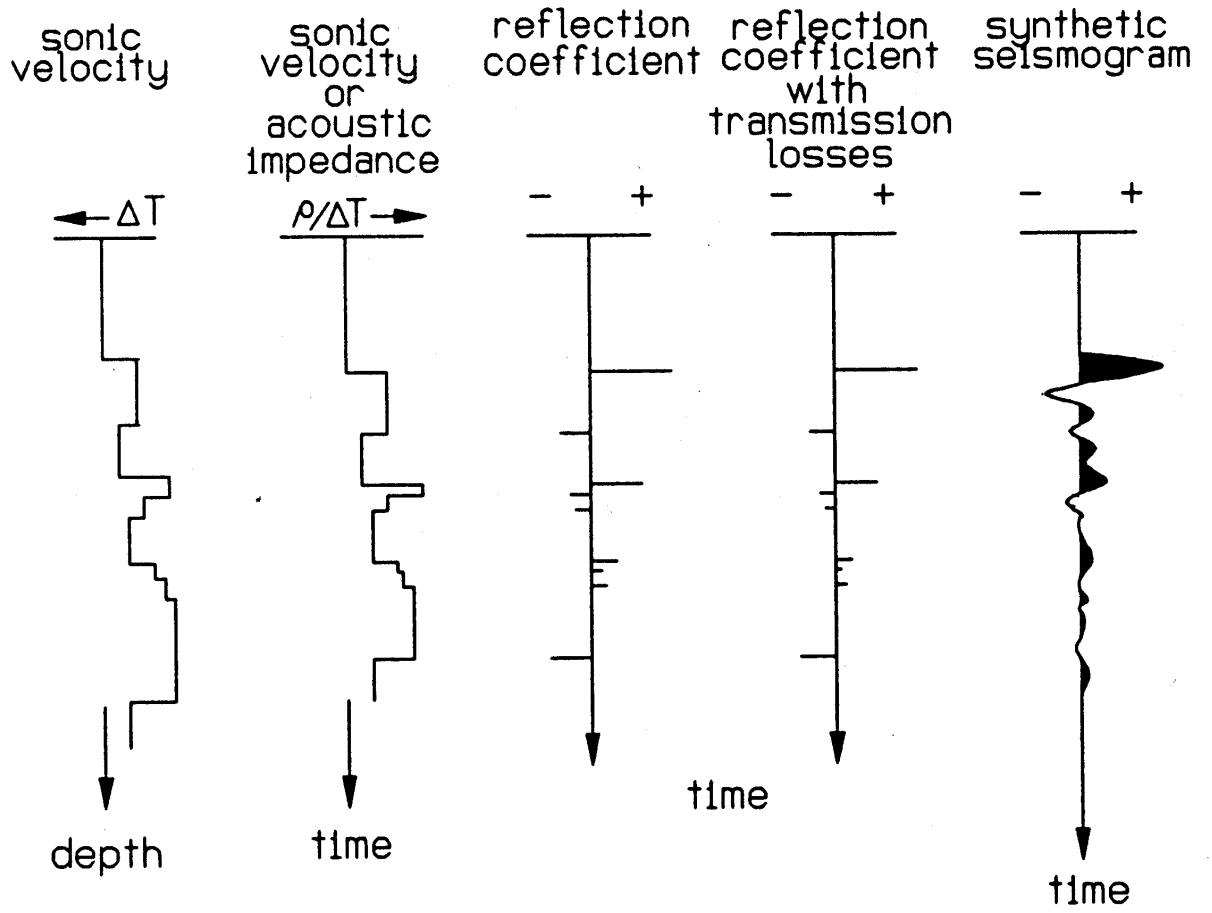

Fig. 16.15 The construction of a synthetic seismogram.

Note that the reverse procedure is also possible, and is used to obtain information about lithology and porosity (*via* density) (i.e., information about formation properties) from the seismic traces that are sensitive to the interfaces between formations. This is called *acoustic impedance inversion*, and is the domain of the geophysicist.

16.10.4 Porosity Determination

The sonic log is commonly used to calculate the porosity of formations, however the values from the FDC and CNL logs are superior.

It is useful in the following ways:

- As a quality check on the FDC and CNL log determinations.
- As a robust method in boreholes of variable size (since the sonic log is relatively insensitive to caving and wash-outs etc.).
- To calculate secondary porosity in carbonates.
- To calculate fracture porosity.

16.10.4.1 The Wyllie Time Average Equation

The velocity of elastic waves through a given lithology is a function of porosity. Wyllie proposed a simple mixing equation to describe this behaviour and called it the *time average equation* (Fig. 16.16). It can be written in terms of velocity or Δt:

$$\frac{1}{V} = \frac{f}{V_p} + \frac{(1-f)}{V_{ma}} \quad \textbf{(16.10)}$$

$$\Delta t = f\,\Delta t_p + (1-f)\Delta t_{ma} \quad \textbf{(16.11)}$$

Hence;

$$f_s = \frac{\Delta t - \Delta t_{ma}}{\Delta t_p - \Delta t_{ma}} \quad \textbf{(16.12)}$$

where Δt is the transit time in the formation of interest, Δt_p is that through 100% of the pore fluid, and Δt_{ma} is that through 100% of the rock matrix, f is the porosity, and the velocities are analogous. A list of input values to these equations for common lithologies and fluids is given as Table 16.2.

Table 16.2 Values for Δt and V for use in Wyllie's time average equation.

Material	**D*t* (ms/ft.)**	***V* (ft./s)**	***V* (m/s)**
Compact sandstone	55.6 – 51.3	18000 – 19500	5490 – 5950
Limestone	47.6 – 43.5	21000 – 23000	6400 – 7010
Dolomite	43.5 – 38.5	23000 – 26000	7010 – 7920
Anhydrite	50.0	20000	6096
Halite	66.7	15000	4572
Shale	170 – 60	5880 – 16660	1790 – 5805
Bituminous coal	140 – 100	7140 – 10000	2180 – 3050
Lignite	180 – 140	5560 – 7140	1690 – 2180
Casing	57.1	17500	5334
Water: 200,000 ppm, 15 psi	180.5	5540	1690
Water: 150,000 ppm, 15 psi	186.0	5380	1640
Water: 100,000 ppm, 15 psi	192.3	5200	1580
Oil	238	4200	1280
Methane, 15 psi	626	1600	490

The Wyllie time average equation gives porosities that are overestimated in uncompacted formations (indicated by the rule of thumb that adjacent shale beds have Δt values greater than 100 microseconds per foot). An empirical correction B_{cp} is then applied:

$$f_s = \frac{\Delta t - \Delta t_{ma}}{\Delta t_p - \Delta t_{ma}} \times \frac{1}{B_{cp}} \quad \textbf{(16.13)}$$

where B_{cp} is approximately equal to the value of Δt in the adjacent shales divided by 100.

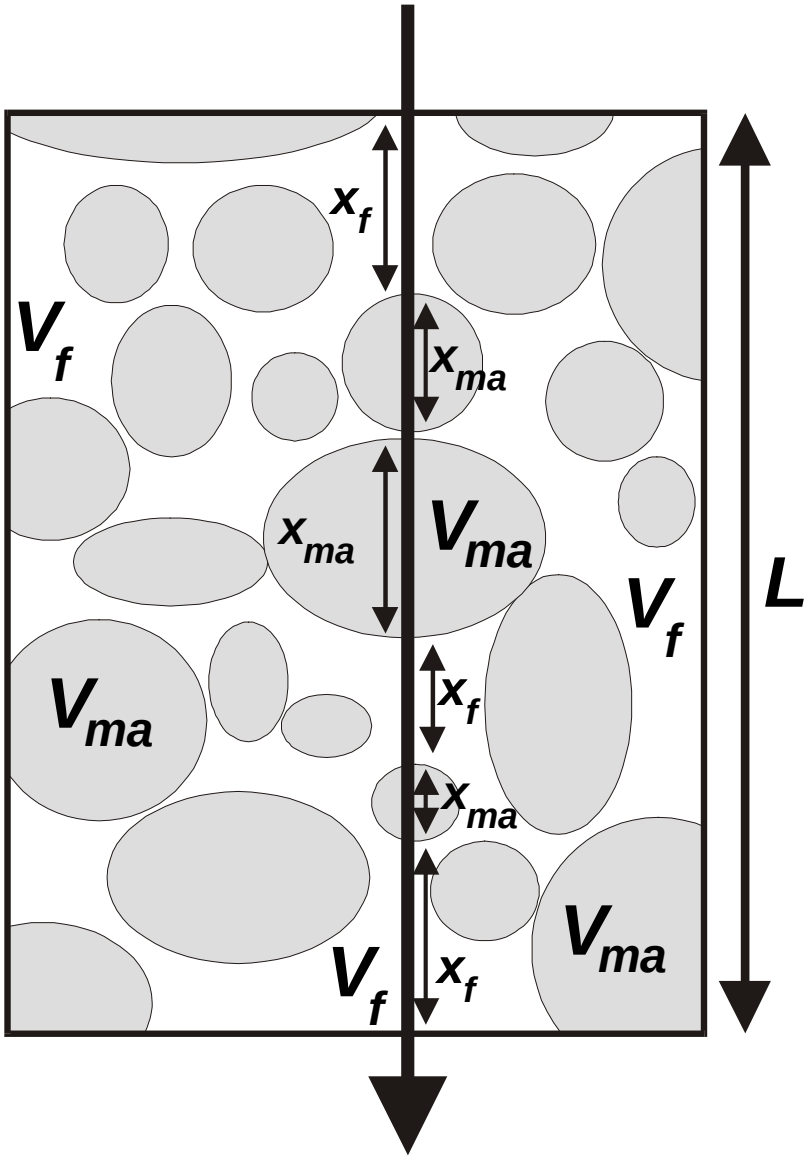

Fig. 16.16 The wave path through porous fluid saturated rocks.

The compaction correction factor can also be obtained from other logs:

- From the density log: A density-sonic cross-plot in clean water-bearing formations close to the zone of interest establishes a line that can be scaled in porosity units. But this is little better than using the density log to calculate the porosity directly.

- From the neutron log: The compaction factor is the ratio of the porosity from the uncorrected sonic log to that from the neutron log in clean water-bearing formations close to the zone of interest. Again, this is little better than using the neutron log directly to obtain the porosity.

- From the resistivity log: Obtain the porosity from the resistivity log in clean water-bearing formations close to the zone of interest using Archie's law and known values of its parameters. The compaction factor is then the ratio of the porosity from the sonic log to the porosity from the

resistivity log. Again, this is little better than using the resistivity log directly to obtain the porosity.

Even though these methods are not so useful to obtain a corrected sonic porosity, they are useful if one wants to calculate the correction factor for its own sake.

16.10.4.2 The Raymer-Hunt Equation

Another method for calculating the porosity from the sonic log was proposed by Raymer. This is expressed as:

$$\frac{1}{\Delta t} = \frac{f}{\Delta t_p} + \frac{(1-f)^2}{\Delta t_{ma}} \qquad \textbf{(16.14)}$$

This provides a much superior accuracy porosity over the entire range of geologically reasonable Δt. Figure 16.17 shows the Raymer-Hunt equation for some typical lithologies.

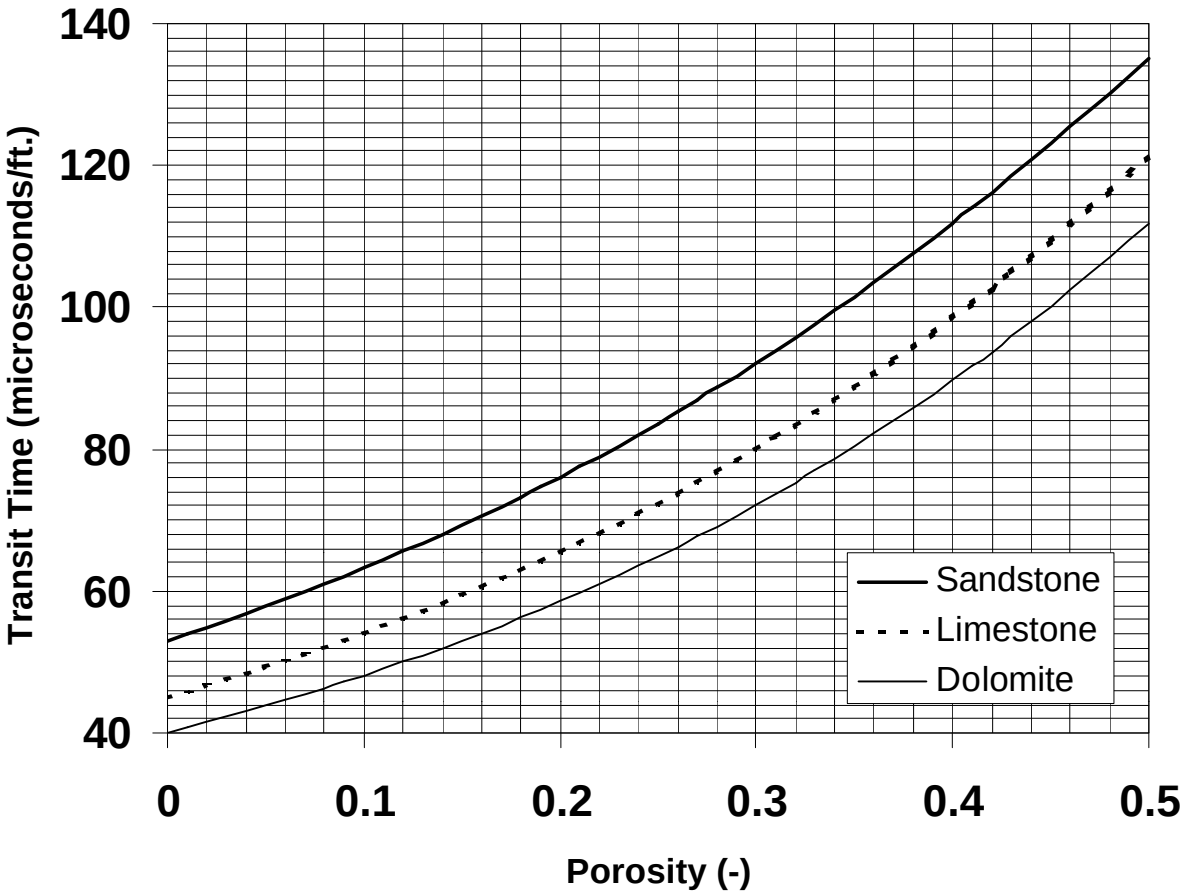

Fig. 16.17 The Raymer-Hunt equation for calculating porosity from transit time. Here the following data have been used: Δt = 53 (sandstone matrix), 45 (limestone matrix), 40 (dolomite matrix), 186 (fluid), all in μs/ft.

16.10.4.3 Calibration against Core

Occasionally, there is good core coverage in a well, so core porosities are available. If this is the case, it is useful to calibrate the sonic log against the core porosity. A cross-plot of core porosity against the transit time at the same depth should produce a straight line that can be extrapolated to the *x*-axis to give a value for the local matrix transit time Δt_{ma} (Fig. 16.18). This is best done for each obvious lithology in the well providing there are enough core determinations to ensure that the cross-plot for each lithology is worthwhile. Cross-plots can also be carried out between the core resistivity while 100% saturated with water, R_o, and the transit time from the sonic log. This should also give the local matrix transit time, and is a verification of the first plot.

The core porosity, sonic transit time cross-plot can also be used to calibrate the porosities derived from the sonic log between the cored points in a given well, but should not be extrapolated out of the cored interval or to other wells.

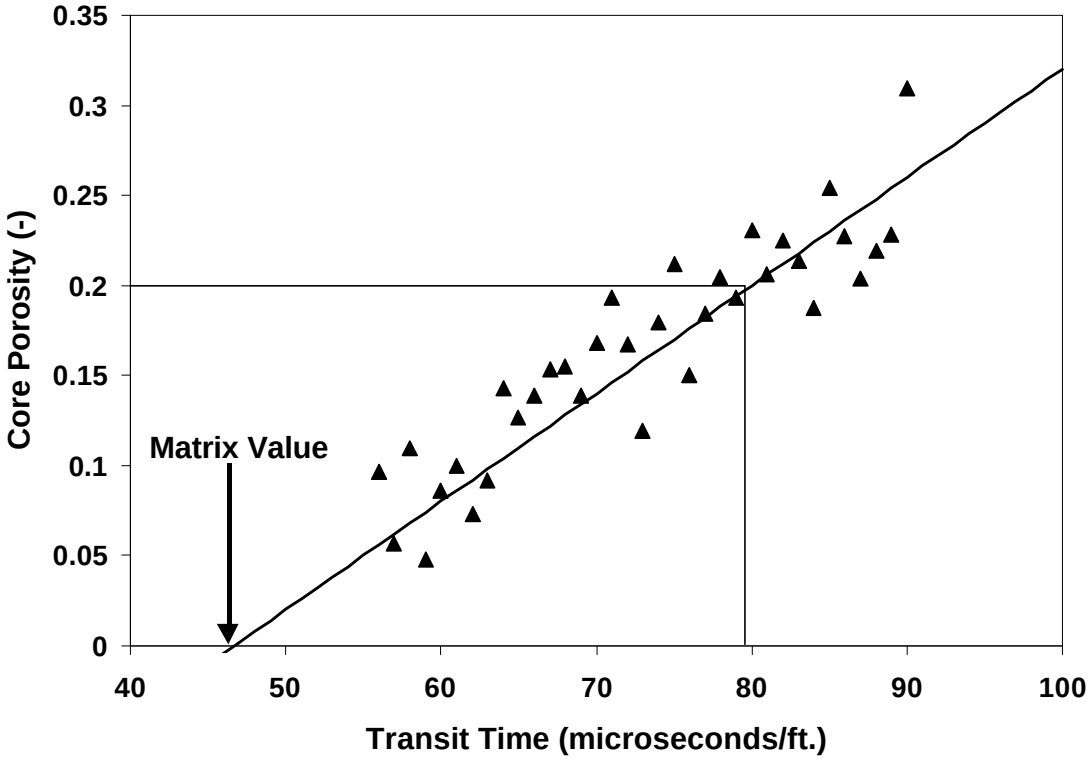

Fig. 16.18 Calibration against core porosities.

16.10.4.4 Secondary and Fracture Porosity

The sonic log is sensitive only to the primary intergranular porosity. By contrast, the density and neutron logs record the total porosity. The difference between the two measurements, therefore, can be used to calculate a value for the secondary porosity, whether it be isolated vugs in carbonates or fractures. This is called the *secondary porosity index* (SPI or f_2), and is defined:

$$f_2 = (f_N, f_D) - f_S \quad \textbf{(16.15)}$$

16.10.4.5 The Effect of Shale on the Sonic Derived Porosity

The effect of shales is very variable. This is because is depends upon the density of the shales, which varies a lot. Young shales are generally under-compacted and low density, tending to increase the transit times and hence give slightly higher sonic derived porosities. Exactly the opposite is the case for ancient compact shales with high densities, which give lower transit times and smaller porosities. The effect of shales on the porosity from the sonic log is not as great as the effect of gas.

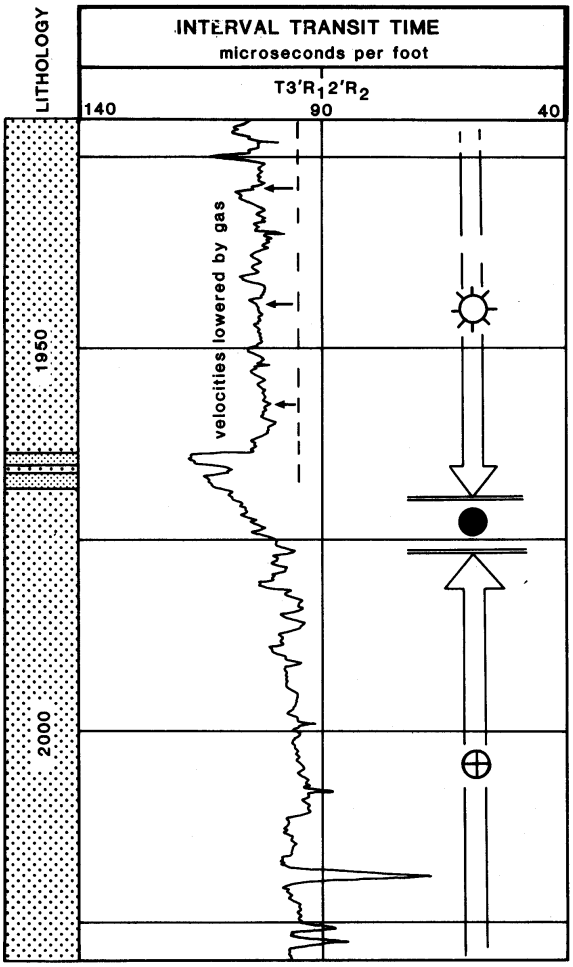

16.10.4.6 The Effect of Gas on the Sonic Derived Porosity

Gas has a low density, and hence decreases the apparent density of a formation if present. This causes an increase in the sonic transit time, and hence a porosity that is overestimated.

However, the sonic tool penetrates to shallow levels, and senses the flushed zone. Most gas, even in high porosity gas-bearing formations will be replaced by mud filtrate. The remaining 15% or so will still have an effect upon the measure sonic transit time and the sonic porosity because of the very low density of the gas. An example is given as Fig. 16.19.

Fig. 16.19 The effect of gas on the sonic log.

16.10.5 Stratigraphic Correlation

The sonic log is sensitive to small changes in grain size, texture, mineralogy, carbonate content, quartz content as well as porosity. This makes it a very useful log for using for correlation and facies analysis (Fig. 16.20).

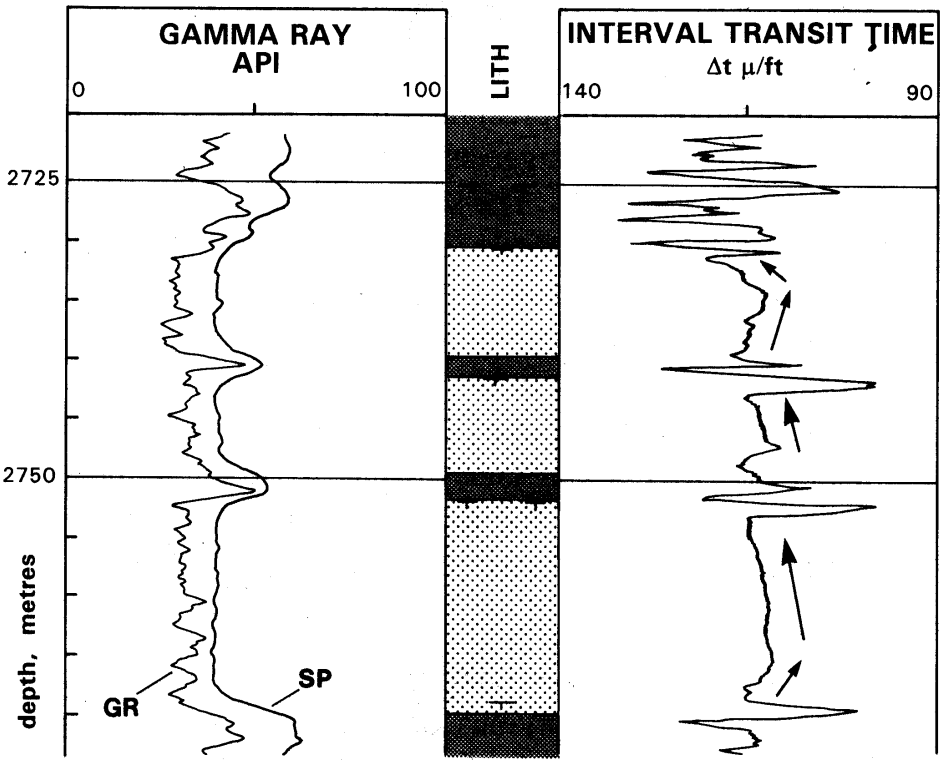

Fig. 16.20 Subtle textural and structural variations in deep sea turbidite sands shown on the sonic log (after Rider).

16.10.6 Identification of Lithologies

The velocity or interval travel time is rarely diagnostic of a particular rock type. However, high velocities usually indicate carbonates, middle velocities indicate sands and low velocities, shales.

The sonic log data is diagnostic for coals, which have very low velocities, and evaporites, which have a constant, well recognized velocity and transit time (see Table 16.2).

It is best to use the sonic log with other logs if lithological identification is important.

The main characteristics of the sonic log are shown in Fig. 16.21.

16.10.7 Compaction

As a sediment becomes compacted, the velocity of elastic waves through it increases. If one plots the interval transit time on a logarithmic scale against depth on a linear scale, a straight line relationship emerges. This is a compaction trend.

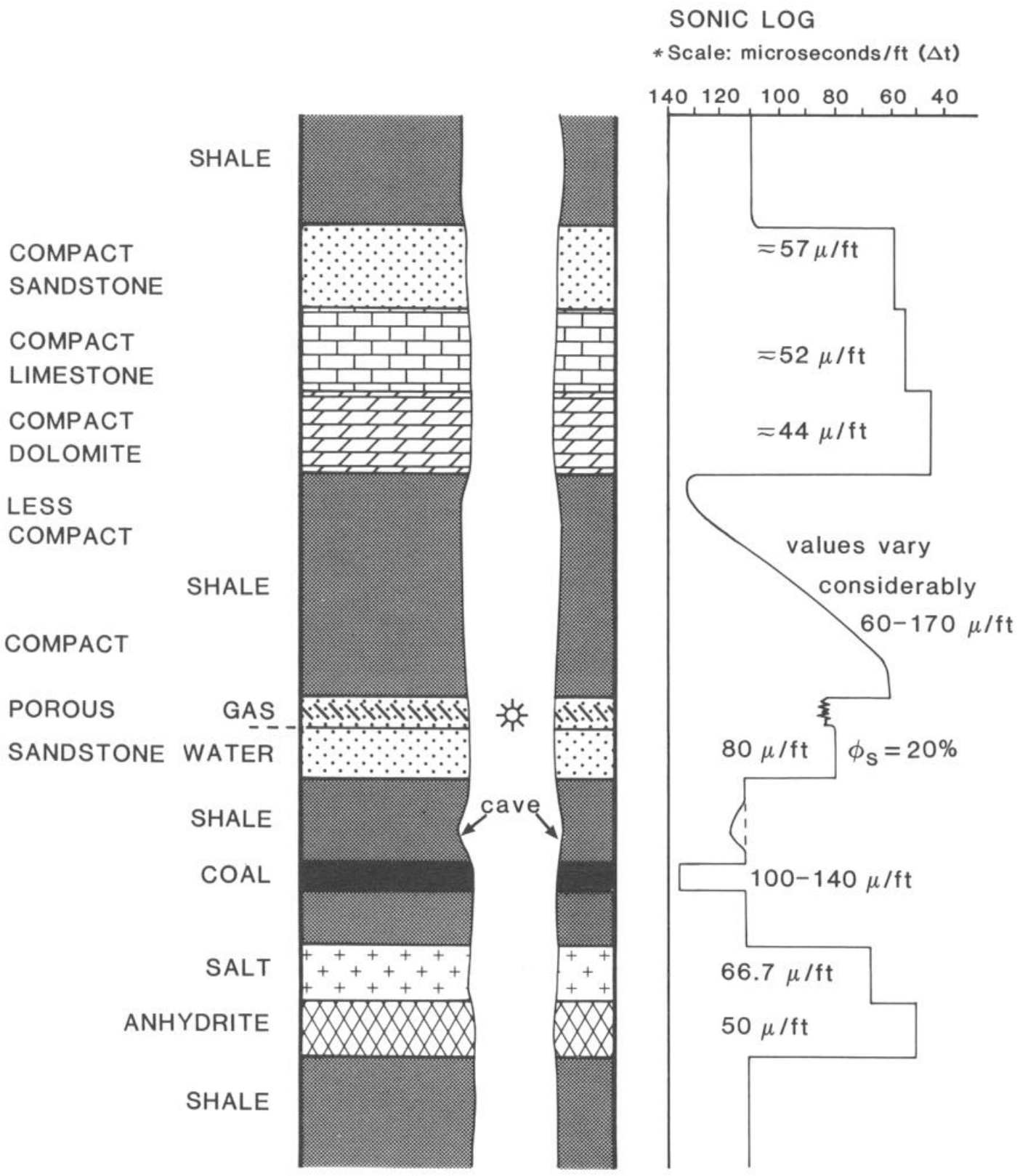

Fig. 16.21 Typical responses of the sonic log (courtesy of Rider).

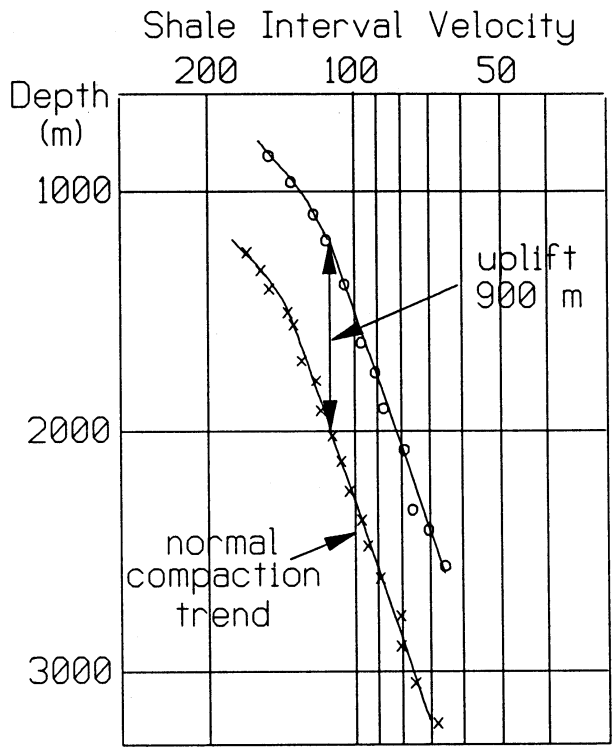

Compaction trends are constructed for single lithologies, comparing the same stratigraphic interval at different depths. It is possible to estimate the amount of erosion at unconformities or the amount of uplift from these trends. This is because compaction is generally accompanied by diagenetic changes which do not alter after uplift. Hence the compaction of a sediment represents its deepest burial.

Figure 16.22 compares the compaction trend for the same lithology in the same stratigraphic interval in one well with that in another well. The data from the well represented by the circles shows the interval to have been uplifted by 900 m relative to the other well because it has lower interval transit times (is more compact) but occurs at a shallower depth.

Compaction curves such as these may therefore be extremely useful, as they can indicate the amount of eroded rock at sudden breaks in the compaction curve that are associated with faults of unconformities.

Fig. 16.22 Uplift and erosion from compaction trends.

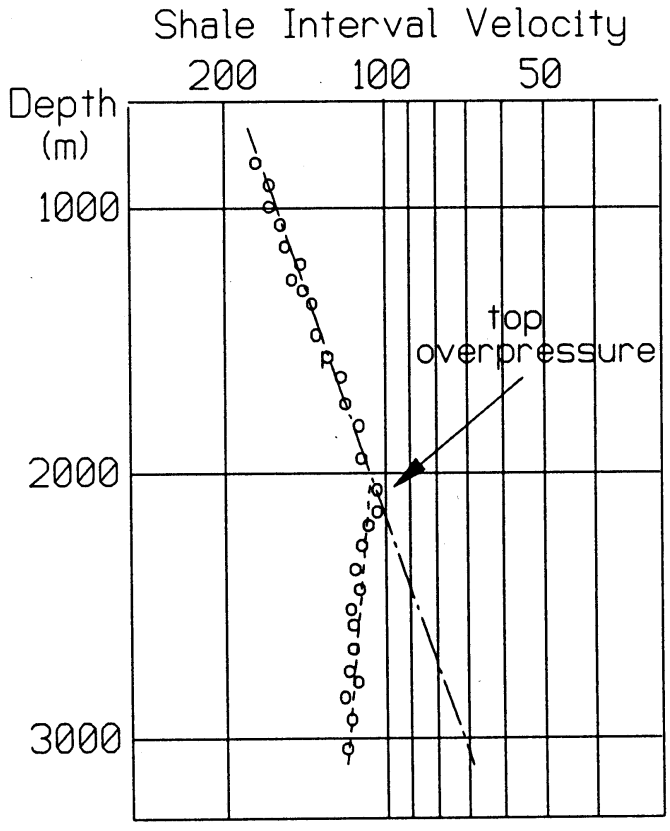

16.10.8 Overpressure

The sonic log can be used to detect overpressured zones in a well. An increase in pore pressures is shown on the sonic log by a drop in sonic velocity or an increase in sonic travel time (Fig. 16.23).

Plot interval transit time on a log scale against depth on a linear scale. In any given lithology a compaction trend will be seen. If there is a break in the compaction trend with depth to higher transit times with no change in lithology, it is likely that this indicates the top of an overpressured zone.

Fig. 16.23 An overpressured zone distinguished from sonic log data.

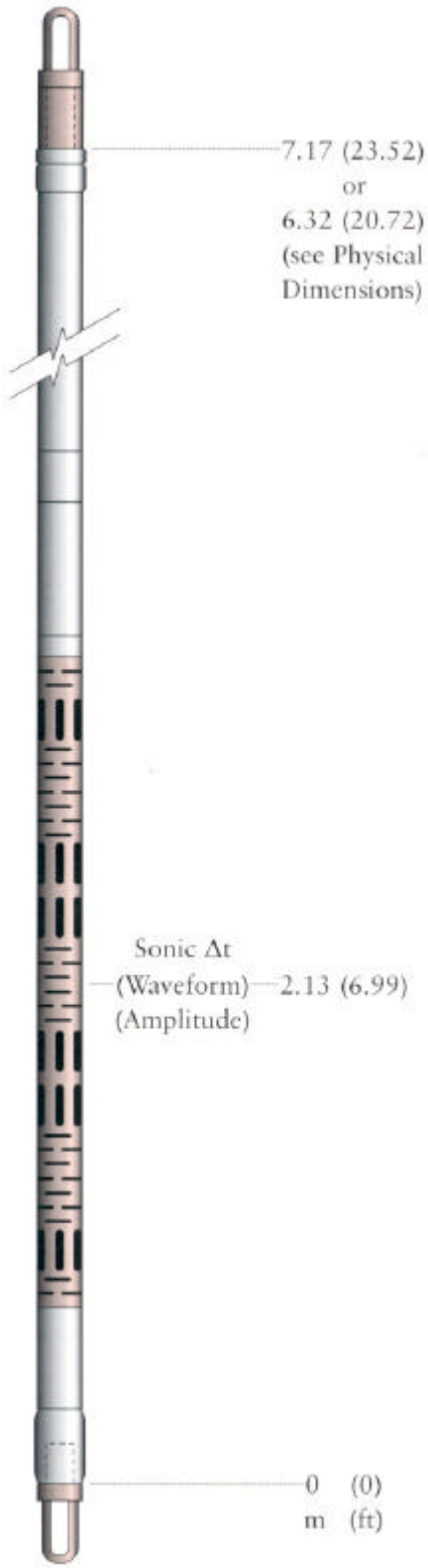

Fig. 16.24 The Compensated Sonic Sonde, CSS (courtesy of BPB Wireline Services).

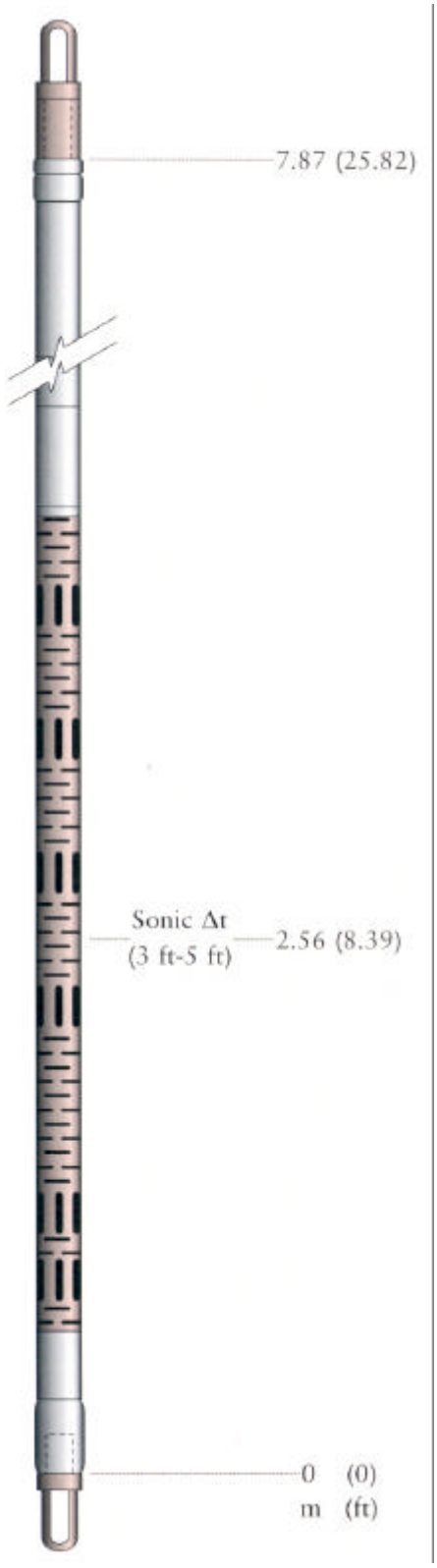

Fig. 16.25 The Long Spaced Compensated Sonic Sonde, LCS (courtesy of BPB Wireline Services).

17. RESISTIVITY THEORY

17.1 Introduction

The whole of resistivity logging is based upon a few very important equations which are introduced in this section. The equations, which are known as the Archie Equations, relate the resistivity of a formation to the resistivity of the fluids saturating a formation, the porosity of the formation and the fractional degree of saturation of each fluid present. As always, the story begins with Ohm's Law.

17.2 Basic Definitions and Ohm's Law

Ohm's Law states that the current flowing from point A to point B in a conductor I is proportional to the difference in electrical potential ΔE between point A and point B. The constant of proportionality is called the electrical conductance c. Current is measured in amperes (A), potential difference in volts (V), and conductance in siemens (S).

Hence, we can write

$$I = c\,\Delta E \tag{17.1}$$

We also define an electrical resistance r, which is the inverse of conductance.

$$r = \frac{1}{c} \tag{17.2}$$

Resistance is measured in ohms (Ω). Hence, we can rewrite Eq. (17.1) as

$$I = \frac{\Delta E}{r} \tag{17.3}$$

Thus, if we take a cylindrical rock sample with two flat faces A and B, and set a potential difference $\Delta E = E_A - E_B$ between its end faces, a current I will flow through the rock from face A to face B (Fig. 17.1). If we measure the current and the potential difference, we can calculate the resistance of the rock sample using Eq. (17.1).

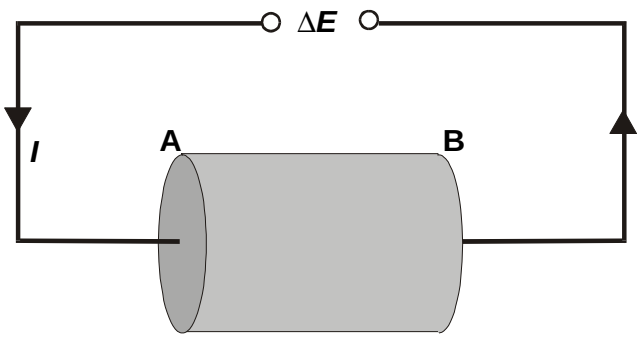

Figure 17.1 Ohm's Law for a rock sample.

- If the resistance is high, a given potential difference ΔE will only give a small current I.
- If the resistance is low, a given potential difference ΔE will give a high current I.

The value of resistance is a property of the material which describes how much the material resists the passage of a current for a given applied potential difference.

Imagine that the size of our rock sample now changes.

- If the length of the sample is doubled, one can see that the resistance of the sample to the passage of a current should also double.
- If the area perpendicular to the current flow doubles (the area of the end face in this example), there is twice the material for the current to pass through, the resistance of the sample to the passage of the current should therefore fall to a half of what is was before.

So the resistance (and therefore conductance) depend upon the size of the sample.

If we take the resistance per unit length and area, we can remove the effect of the dimensions of the sample. The value we obtain is then only a function of the property of the material and not its dimensions. The resistance per unit length and area is called the *resistivity R*, and can be expressed as

$$R = \frac{\Delta E}{I}\frac{A}{L} \qquad \textbf{(17.4)}$$

where: R = the resistance of the sample (Ωm or ohm.m)
ΔE = the potential difference across the sample (volts, V)
I = the current flowing through the sample (amperes, A)
A = the cross-sectional area of the sample perpendicular to the current flow (m^2)
L = the length of the sample (m).

Note that a conductivity C can also be defined as the reciprocal of the resistivity R, and therefore

$$C = \frac{1}{R} = \frac{I}{\Delta E}\frac{L}{A} \qquad \textbf{(17.5)}$$

where: C = the conductivity of the sample (S/m).

In petrophysical logging of electrical rock properties there are two main types of tool. One type measures resistivity directly, and the result is given in ohm.m (Ω.m). The other type measures conductivity directly, and the result is given in either siemens per metre (S/m), or more often in milli-siemens per metre (mS/m). The two measurements are, of course, measuring the same property of the rock, and can be interconverted using

$$C(\text{S/m}) = \frac{1}{R(\text{ohm.m})} \qquad \textbf{(17.6)}$$

$$C(\text{mS/m}) = \frac{1000}{R(\text{ohm.m})} \qquad \textbf{(17.7)}$$

17.3 Resistivity of Rocks

Reservoir rocks contain the following constituents

- Matrix material — High resistivity
- Formation waters — Low resistivity
- Oil — High resistivity
- Gas — High resistivity
- Water-based mud filtrate — Low resistivity
- Oil-based mud filtrate — High resistivity

All have a high electrical resistivity (*electrical insulators*) except the formation water and water-based mud filtrate, which are good *electrical conductors* and have a low electrical resistivity.

The resistivity of the reservoir rocks therefore depends only upon the water or water based mud filtrate occupying its pore space.

Uninvaded Formations. For uninvaded formations, the measured bulk resistivity of the rock depends only upon the amount of the aqueous formation fluids present in the rock, and the resistivity of those aqueous fluids. Since the amount of formation fluids depends both on porosity f and water saturation S_w, we can say that the resistivity of the formation R_t depends upon porosity f, water saturation S_w, and the resistivity of the formation water R_w. This resistivity is called the *true resistivity of the formation*. It is the resistivity of the formation in the uninvaded zone, where the rock contains some saturation of oil S_o, gas S_g, and water S_w, and where $S_o+S_g+S_w=1$.

The aim is to use knowledge of the resistivity of the formation, together with independent knowledge of the porosity and resistivity of the formation waters, to calculate S_w, and hence enable ourselves to calculate the STOOIP.

Typical values of R_t range from 0.2 to 2000 ohm.m (5000 to 0.5 mS/m).

The uninvaded zone of formations is commonly only measured directly by the most deeply penetrating electrical logging tools. The shallower investigating tools measure the invaded zone. Hence, if one wants a resistivity reading for use in STOOIP calculations, one should always chose the deepest penetrating electrical tool of those that have been run.

Invaded Zones. In most cases there is an invaded zone, where the formation fluids have been disturbed by the drilling fluid. The resistivity of the formation in this zone depends upon the resistivity of the mud filtrate R_{mf}, the resistivity of any remaining formation water R_w, the saturation of the mud filtrate S_{XO}, the saturation of the remaining formation water S_w (if any), and the porosity of the rock f.

If these values and the depth of invasion are known, the resistivity measured in the invaded zone can be corrected to account for the presence of the mud filtrate.

The symbols used in electrical logging in the invaded borehole environment are shown in Fig. 17.2.

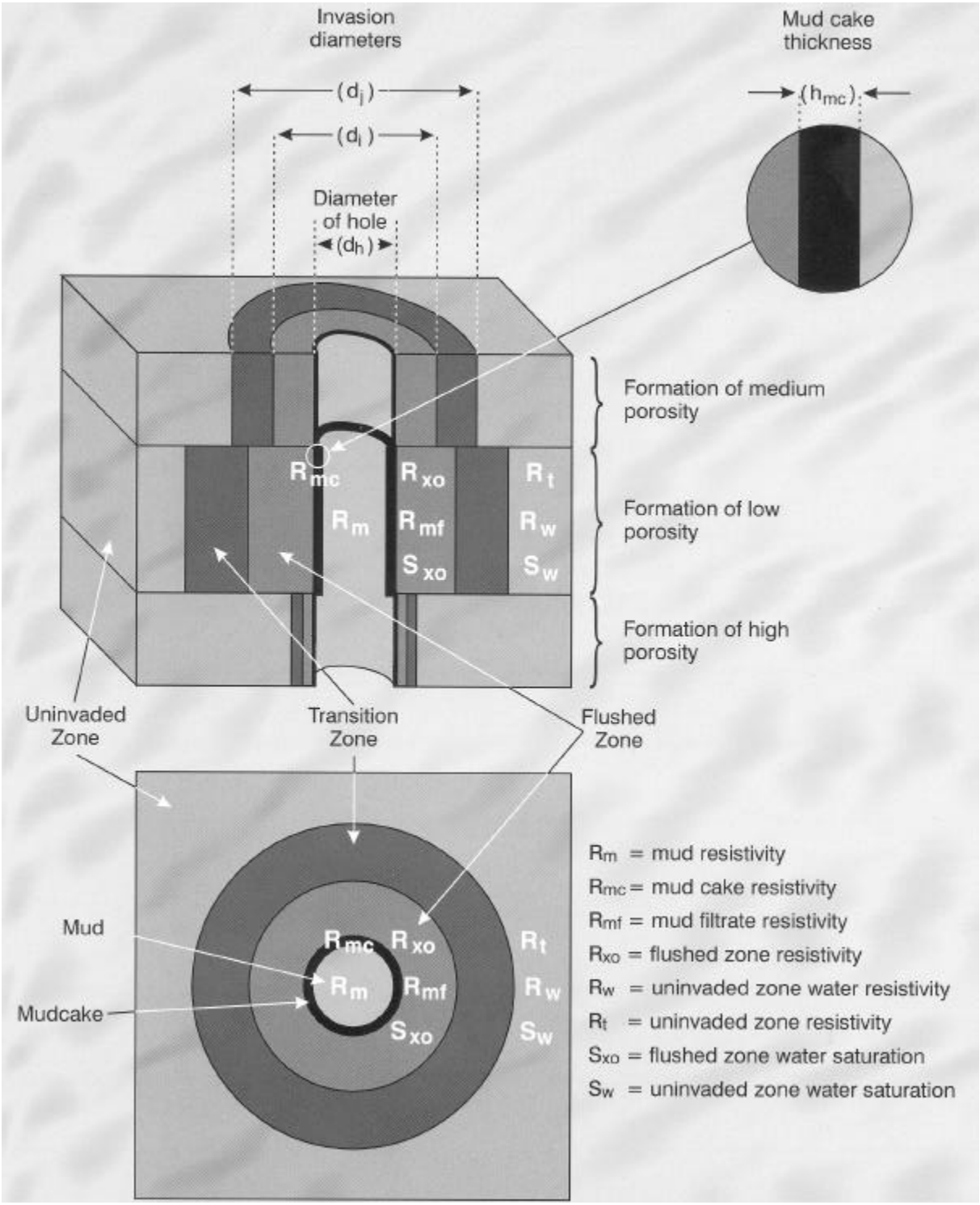

Figure 17.2 Borehole invasion, and the symbols used.

17.3 Temperature and Pressure

Calculating Formation Temperature. The resistivity of formation fluids and water-based drilling muds varies greatly with temperature, but little with pressure. The temperature in a borehole can be

found directly from modern Horner corrected temperature logs up the entire borehole, or more traditionally, from the geothermal gradient obtained from Horner corrected BHT measurements.

In the former case the temperature is given directly at a given depth. However, this is not used to calculate the mud resistivity as the newer temperature logs also measure directly the mud resistivity as it makes the temperature log.

In the latter, and more common, case the BHT allows us to calculate a mean geothermal gradient for the borehole. The formation temperature can then either be calculated directly, or obtained with a nomogram such as that given in Figure 17.3.

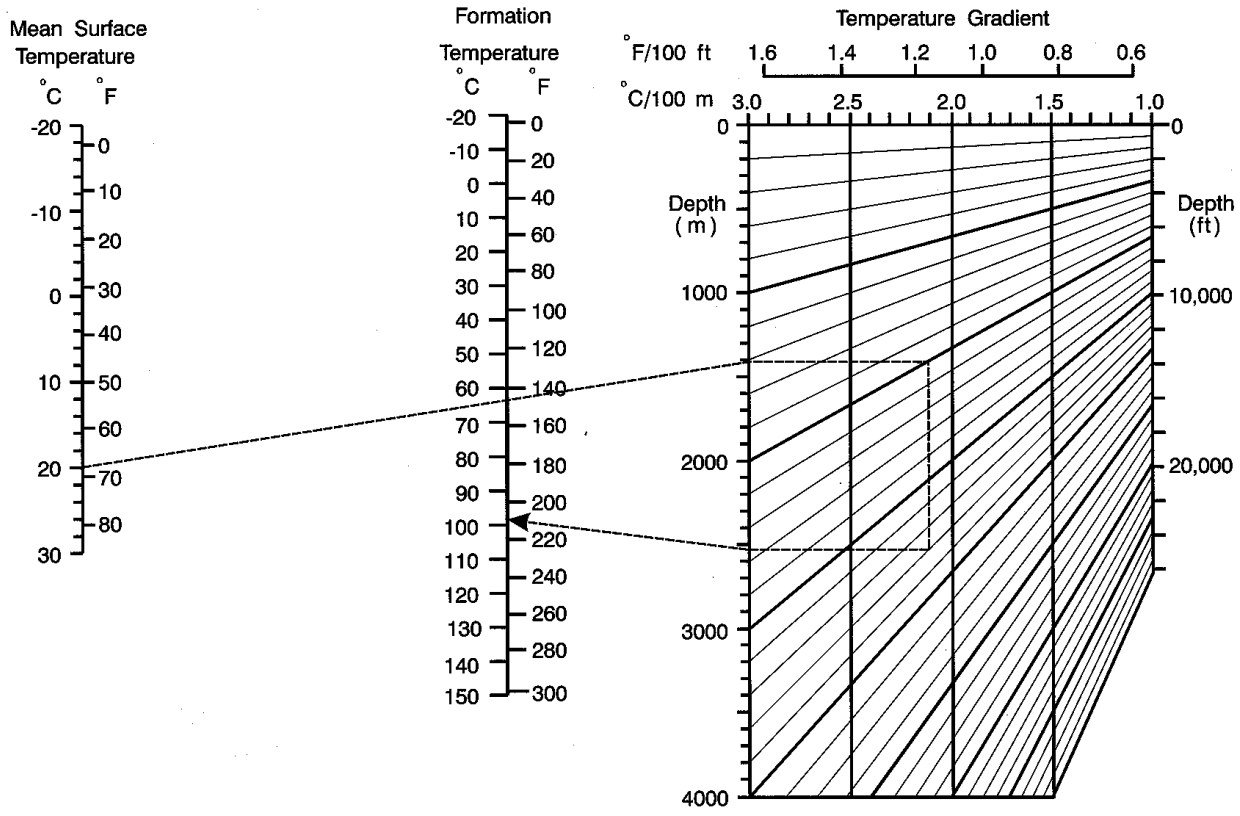

Figure 17.3 The formation temperature nomogram.

The Effect of Salt Composition. The resistivity of the formation fluids depends upon the concentration and type of salts dissolved in it. We know the concentration and type of dissolved solids in the formation water usually from chemical analysis of samples obtained by the RFT. The resistivity of this solution at a given temperature and pressure can be obtained by making up a synthetic brine to the recipe indicated by the chemical analysis of the RFT sample, or more often, by the use of equations relating the composition to the fluid resistivity.

For simplicity, we express the dissolved salts in a solution as an NaCl equivalent. Figure 17.4 shows a chart expressing multipliers *K* as a function of total concentration of solids for each individual ionic contributor to the salts in solution. We simply multiply the relevant multiplier by the solid

concentration for each component and sum the results. The sum is the total NaCl equivalent concentration in ppm, and this can be used to describe the concentration of the solution.

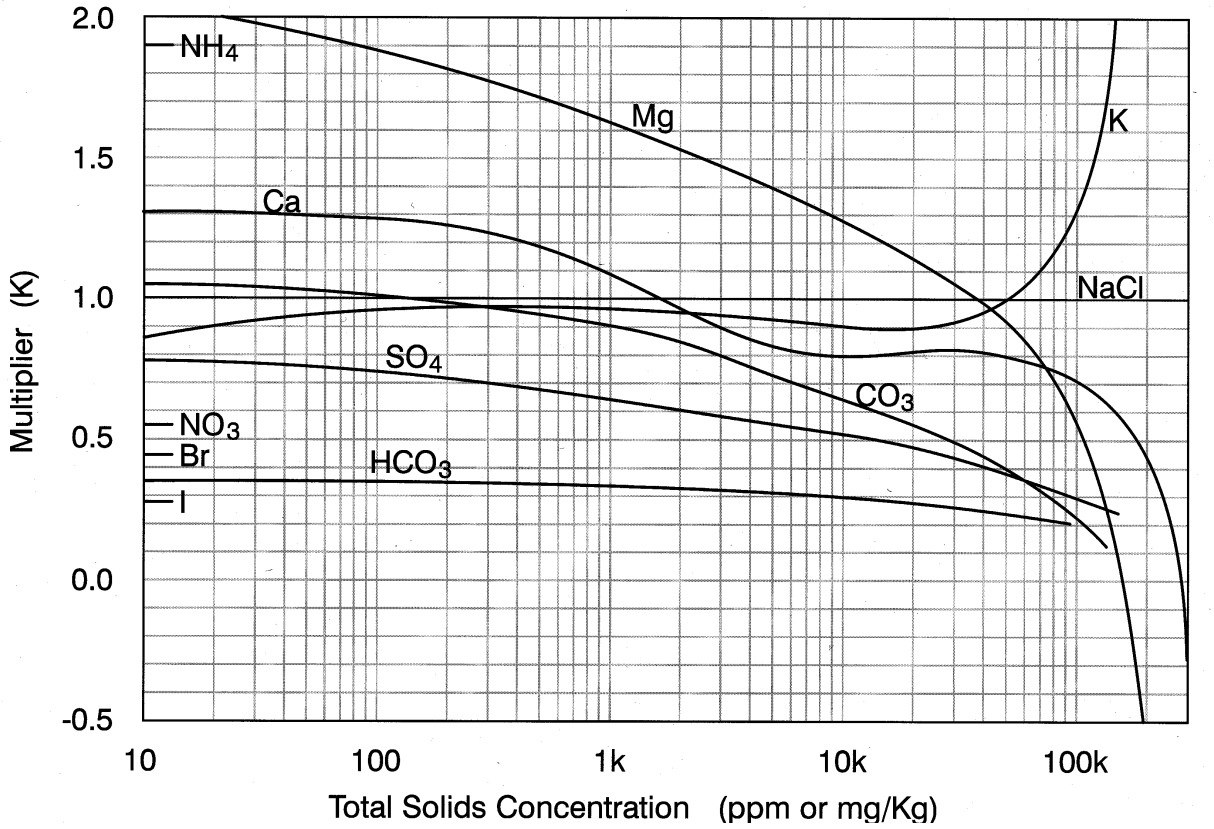

Figure 17.4 The NaCl equivalent plot.

For example, a solution contains 20,000 ppm NaCl, 10,000 ppm KCl and 1000 ppm $MgSO_4$. The multipliers are Na(1.00), Cl(1.00), K(0.9), Mg(1.63), SO_4(0.64). The total NaCl equivalent is 20,000×1+20,000×1+10,000×0.9+10,000×1+1000×1.63+1000×0.64 = 30,635 ppm NaCl.

The Variation of Formation Fluid Resistivity with Temperature. The resistivity of aqueous formation fluids varies significantly with temperature. The increase is approximately 4% per degree centigrade. Clearly, if the BHT is 200°C, the increase in the resistivity of the formation fluids can be as much as 800%. This will cause the resistivities measured with downhole tools to increase steadily down the borehole. To avoid this added complication all downhole resistivity measurements are corrected to read the resistivity they would read if the entire borehole was at some constant temperature (24°C/75°F is often used). To do this we need to convert the raw resistivity data. This is done automatically by the wireline logging company using a chart or an equation that represents the chart. Figure 17.5 shows a typical chart for this type of correction. It is based upon Hilchie's equation for the variation of the resistivity of aqueous fluids with temperature. Hilchie's equation relates the resistivity of an NaCl solution at one temperature to that at another.

$$R_{wT2} = R_{wT1}\left(\frac{T_1 + X}{T_2 + X}\right) \quad \text{where} \quad X = 10^{-(0.340396 \times \log_{10} R_{wT1} - 0.641427)} \qquad \textbf{(17.8)}$$

where: R_{wT1} = the resistivity of the fluid at temperature T_1
R_{wT2} = the resistivity of the fluid at temperature T_2
T_1 = the temperature T_1
T_2 = the temperature T_2

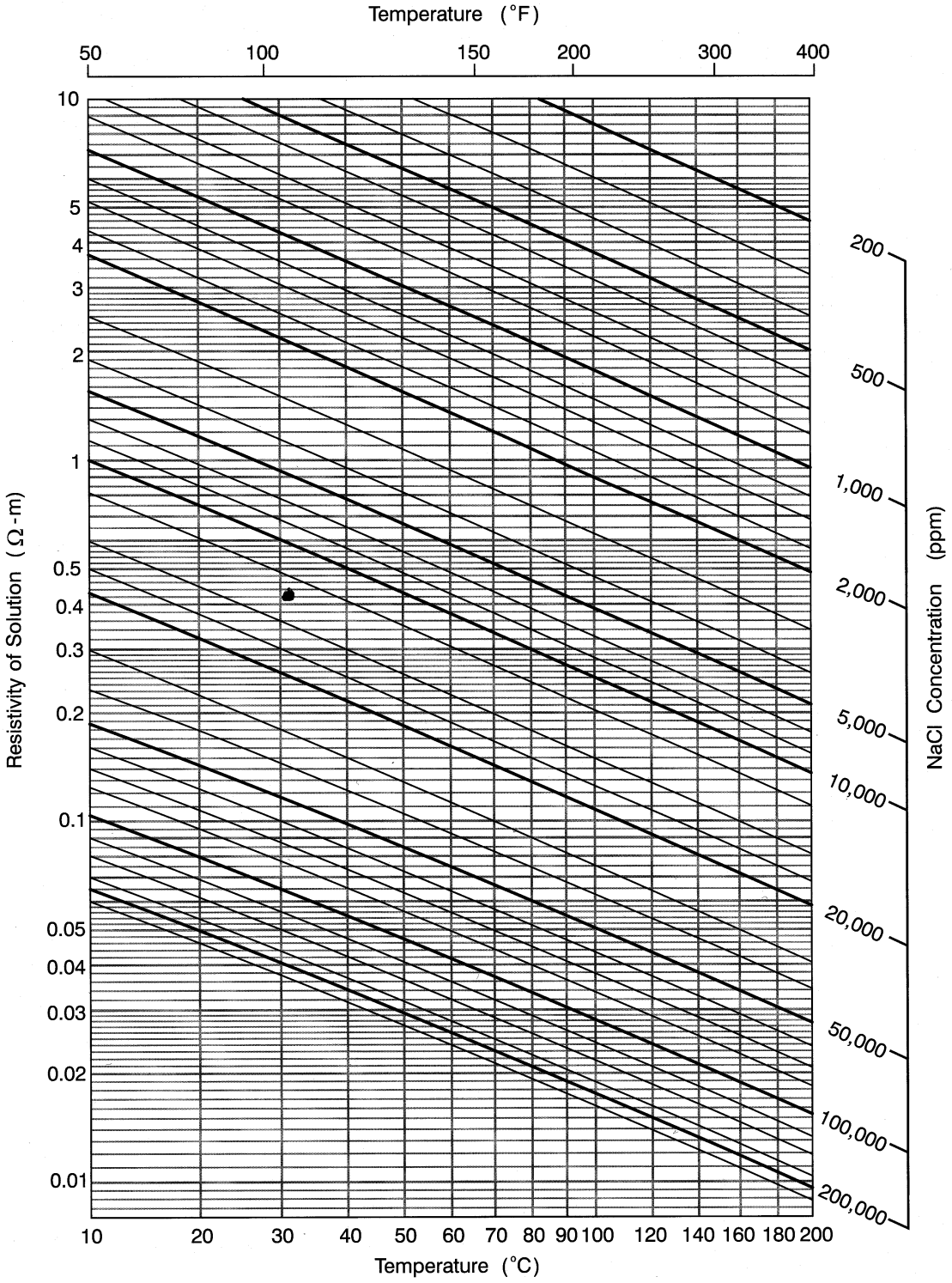

Figure 17.5 Resistivity of NaCl fluids as a function of temperature.

The Variation of Drilling Mud Resistivity with Temperature. The resistivity of the drilling mud is measured by many tools and is available directly for calculation at a given depth. Tools that measure the drilling mud resistivity include most resistivity tools, the newer temperature tools and some RFT tools.

The Variation of Mudcake and Mud Filtrate Resistivity with Temperature. The mud filtrate and mudcake resistivities may be obtained from the mud density (mud weight) and the resistivity of the drilling mud using the nomogram in Fig. 17.6. Note that this nomogram is valid for 24°C/75°F.

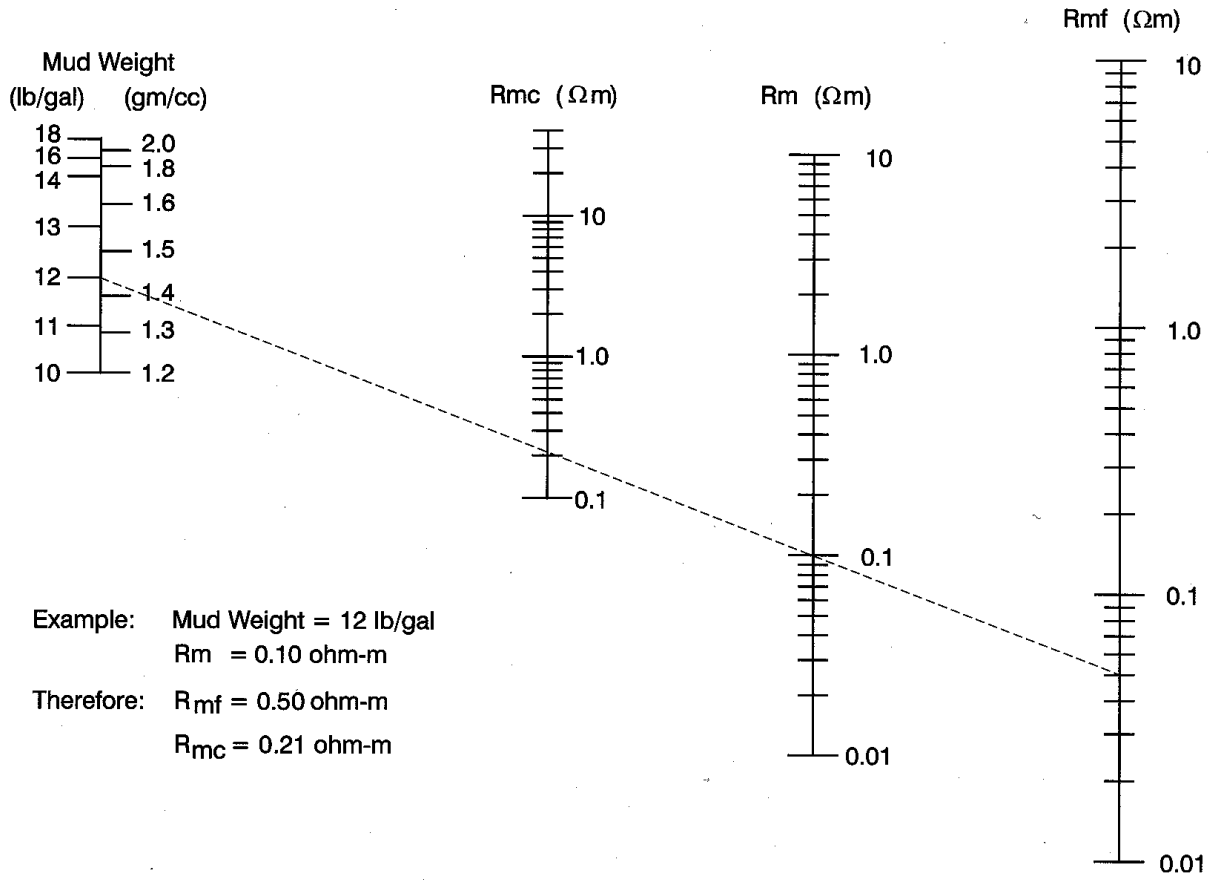

Figure 17.6 Mudcake and mud filtrate resistivity nomogram.

Once the various corrections for temperature have been carried out for the formation fluids and the mud-derived material, and the log is at 24°C/75°F equivalent, we can carry out calculations on the resistivity data along the borehole comparing the responses at different depths without regard to the fact that the formation fluids contain dissolved salts other than NaCl, and that the resistivity of the fluid is actually very sensitive to temperature (depth) changes.

17.4 Formation Factor (Archie's First Law)

In the late 1920s and early 1930s Archie carried out a series of experiments to analyze the relationship between the resistivity of rock samples saturated with various resistivity fluids. He used clean sandstones and carbonates which were 100% saturated with aqueous solutions of varying concentration and hence resistivity. His results are empirical (derived from experimental work on particular samples) and hence should not be assumed to have theoretical rigour. However, we are now beginning to see how the theory of the electrical properties of rocks can give rise to the Archie equations.

Archie observed that the bulk resistivity of a rock R_o fully saturated with an aqueous fluid of resistivity R_w is directly proportional to the resistivity of the fluid

$$R_o = F\ R_w \qquad \textbf{(17.9)}$$

The constant of proportionality F is called the *Formation Factor* and describes the effect of the presence of the rock matrix.

It can be immediately seen that F = 1.00 for a rock with 100% porosity, i.e., no matrix, just 100% fluid.

If we take 100% fluid and slowly add grains of rock, the porosity decreases. However, the insulating grains of rock have negligible conductivity (infinite resistivity) compared to the conducting fluid. Hence, R_o will increase, which implies that F is always greater than unity in a porous medium such as a rock. In real rocks F takes values usually between 20 and 500. Note that formation factor has no units because it is the ratio of two resistivities.

One way of interpreting the formation factor is therefore as a factor that describes the extent to which electrically insulating mineral grains 'dilute' the conducting fluid, making the bulk material more resistive than the fluid alone. The formation factor includes both the effect of the variable porosity and the effect of the tortuous pathways that the current is forced to take through the conducting fluid due to the presence of the insulating rock grains. It can be seen, therefore, that the formation factor is related to the porosity of the rock and the connectivity of the pore spaces. The natural complexity of pore systems in rocks means that the formation factor cannot be expressed simply as a function of porosity and connectivity in a theoretically rigorous way.

Archie examined the way that the formation factor changes from rock to rock, and noticed that the following rule commonly holds true

$$F = f^{-m} \qquad \textbf{Archie's First Law} \qquad \textbf{(17.10)}$$

where: m = the cementation index/factor/exponent (no units).

Equations (17.9) and (17.10) are often combined and called Archie's first law. The resulting equation is

$$R_o = R_w\ f^{-m} \qquad \textbf{(17.11)}$$

The cementation index is the factor that describes the increase in resistivity that results from the insulating mineral grains forcing the current to take tortuous pathways through the conducting fluid.

The cementation factor has a theoretical value of unity for uniform pores that penetrate the rock directly from one side of the sample to the other (i.e., direct tubes of pore space), and is zero for a rock with 100% porosity (i.e., no grains to get in the way of the fluid flow). No other values of the cementation factor are able to be defined in a purely theoretical way in rocks due to the complexity of the way that pore spaces are arranged.

In real rocks the cementation index usually varies between 1.0 and 3.0.

Values between 1.0 and 1.4 are associated with igneous and metamorphic rocks that contain fractures. Fractures are a form of porosity that is localized and well connected, and hence approximates to the situation where we had uniform tubes of porosity going through the sample.

Values between 1.4 and 2.0 are found in sandstones, with the higher values found in more consolidated sandstones, where the current flow paths are more tortuous.

Values between 2.0 and 2.6 are typical for carbonates, and represent a greater degree of tortuosity in the current flow that is found in carbonates because much of the porosity in carbonates is unconnected (e.g., vugs).

Both the formation factor and the cementation exponent can be measured on core plugs in the laboratory. This is done in the following way for a single plug.

- Clean and dry the rock sample.
- Measure the porosity of the rock sample with helium or with a fluid saturation technique.
- Saturate the rock with a conductive fluid if not already done in the porosity determination step.
- Measure the bulk resistivity of the rock saturated with the fluid.
- Measure the resistivity of the fluid that saturates the rock in a separate vessel.
- Rearrange and apply Eq.(17.9) to obtain the formation factor.
- Rearrange and apply Eq. (17.11) to obtain the cementation exponent.

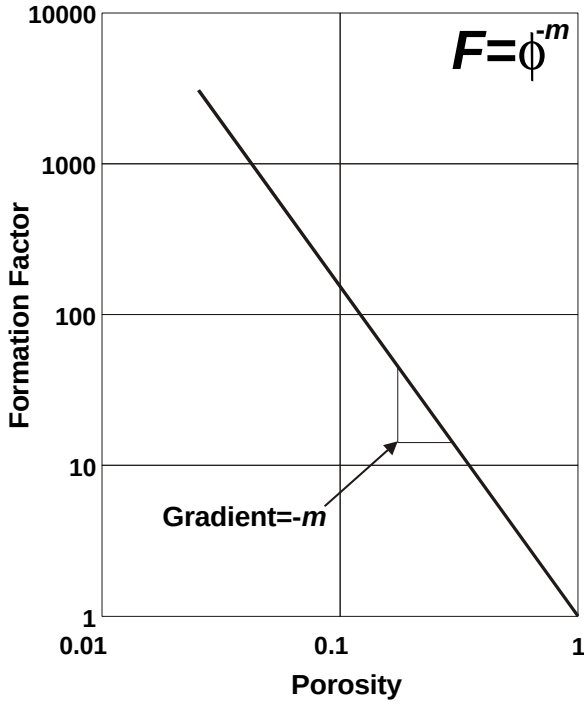

If there is a suite of such measurements from core plugs from a particular formation, a mean cementation exponent can be obtained graphically by plotting F against f on log-log graph paper, which gives a straight line for a given lithotype, which intersects F=1 when f=1, and with a gradient equal to $-m$. This is shown in Fig. 17.7.

Note that sometimes a constant 'a' is placed before the porosity term, and so $F=a$ when f=1. However, there is no physical justification for this term. It arises from applying a best fit engineering equation to F versus porosity data, and should be avoided.

Figure 17.7 Cementation exponent from a formation factor-porosity cross-plot.

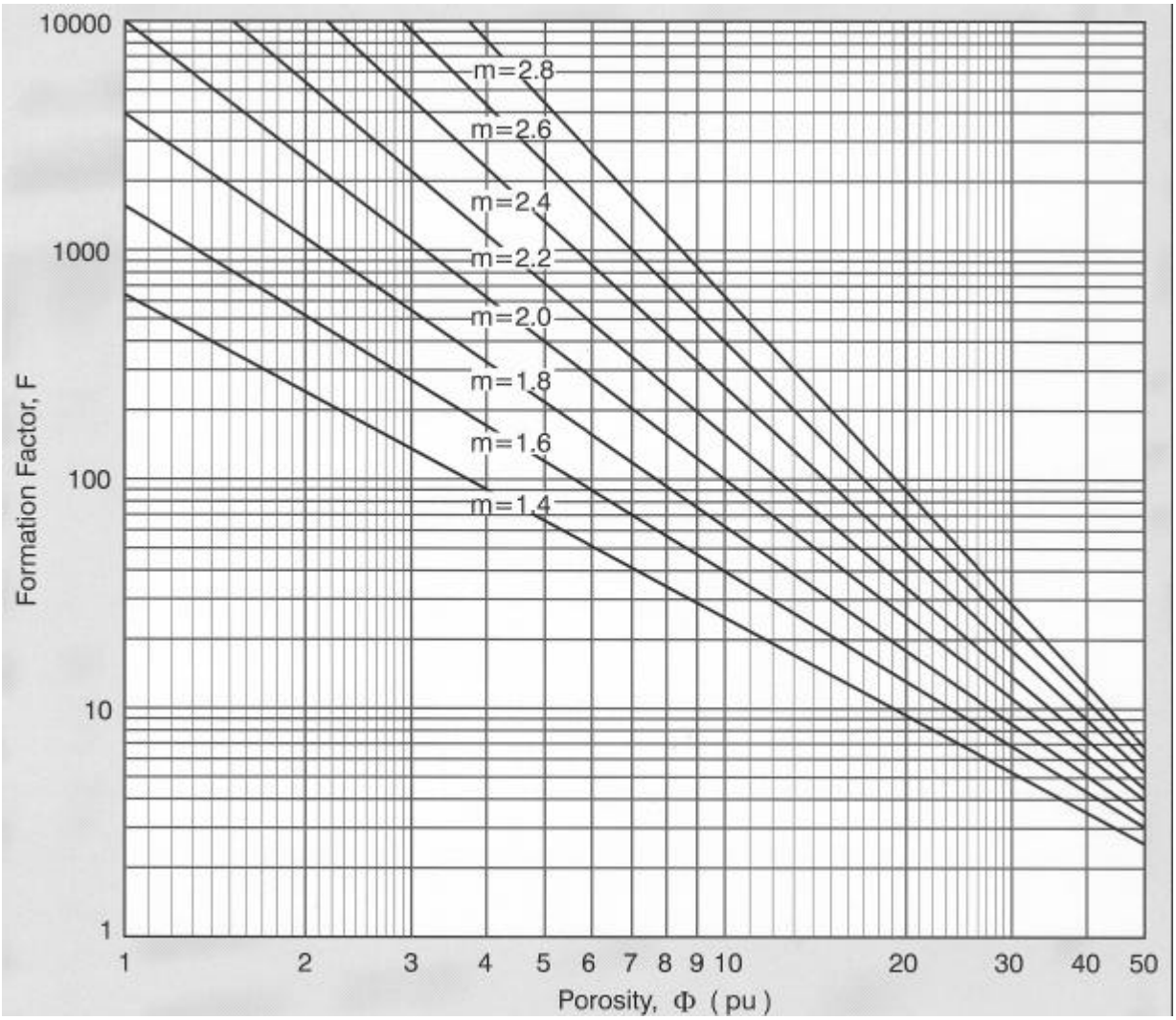

Figure 17.8 Cementation exponent from a formation factor-porosity cross-plot.

Figure 17.8 shows a formation factor-porosity cross-plot for various values of the cementation exponent.

It should be mentioned that there are a range of equations used in the oil industry to calculate the formation factor. Archie's equation is the most flexible, and the others are simply specific cases of it that have been shown to work empirically for a given type of rock. In all cases the equations have been derived from fitting a best line to a set of real data. The empirical relationships this provides, therefore includes values of a which are non-unity. Also, one should be extremely careful to only apply the equations when you are sure that they are valid. This often means going back to the original papers to see what type of rocks the equations have been derived from. By comparison the use of Archie's equation with known cementation exponent is more reliable, and should ALWAYS be used if the cementation exponent is known.

The Humble Formula. This is applied to soft formations and to clean sandstones with a sucrosic texture.

$$F = 0.62 \times f^{-2.15} \quad \textbf{(17.12)}$$

The Soft Formation Formula.

$$F = 0.81 \times f^{-2} \quad \textbf{(17.13)}$$

The Low Porosity Carbonate Formula. Valid for low porosity clean carbonates with no fracturing.

$$F = f^{-m} \qquad \text{where} \quad m = 1.87 + \frac{0.019}{f} \quad \textbf{(17.14)}$$

17.5 Partial Water Saturation (Archie's Second Law)

Archie also examined the work of other investigators who did experiments on the resistivity of partially saturated sandstones. He observed that the bulk resistivity of a rock R_t partially saturated with an aqueous fluid of resistivity R_w is directly proportional to the resistivity of the rock when fully saturated with the same fluid, i.e.,

$$R_t = I \; R_o \quad \textbf{(17.15)}$$

The constant of proportionality I is called the *resistivity index* and describes the effect of partial desaturation of the rock.

- If the rock is fully saturated, I=1.00.
- If the rock is full of dry air (i.e., not saturated with a conductive fluid), $I \rightarrow \infty$.

The resistivity index therefore varies between unity and infinity depending upon the degree of saturation of the rock.

Archie observed that the following relationship exists empirically for sandstones

$$I = S_w^{-n} \quad \textbf{Archie's Second Law} \quad \textbf{(17.16)}$$

where: S_w = the fractional water saturation of the rock
I = the resistivity index
n = the saturation exponent.

Again, the last two equations can be combined into a form which is usually referred to as Archie's second law

$$R_t = R_o \; S_w^{-n} \quad \textbf{(17.17)}$$

The saturation exponent normally has a range of values from 1.8 to 2.0, however much lower and much higher values have been found.

The value of the saturation exponent can be obtained from laboratory experiments on core samples. The procedure is as follows for a single core sample:

- Follow the procedure to measure the resistivity of a sample saturated completely with a conductive fluid as outlined in the last section.
- Replace in a step-wise manner some of the conductive fluid in the rock with a non-conductive fluid (e.g., gas) allowing for equilibrium to be attained at each step.
- Measure the resistivity of the sample when equilibrium is attained at the end of each step.
- Calculate from measurements of the evolved fluids and prior knowledge of the pore volume of the sample, the conductive fluid saturation in the sample at the end of each step.
- Rearrange and apply Eq. (17.15) to calculate the saturation index.
- Rearrange and apply Eq. (17.17) to calculate the saturation exponent.

These experiments are extremely time consuming as one has to wait a long time for the samples to come to equilibrium.

As before, a mean saturation exponent can be calculated from such measurements on a suite of cores. In this case the resistivity index I is plotted against the water saturation S_w, again on log-log paper (Fig. 17.9). The result is a straight line intersecting I=1 when S_w=1, and with a gradient equal to $-n$.

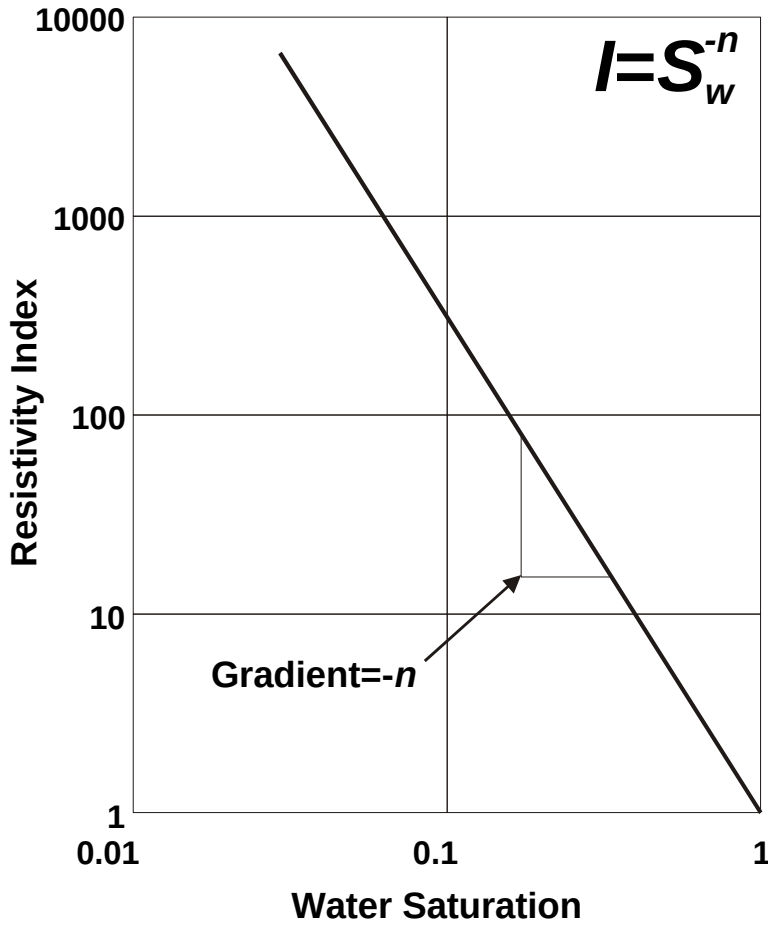

Figure 17.9 Saturation exponent from a resistivity index-water saturation cross-plot.

17.6 Combining Archie's Laws

The two equations for each of the Archie laws can be combined into one controlling equation. Combining Eq. (17.11) and (17.17) gives

$$R_t = R_w f^{-m} S_w^{-n} \tag{17.18}$$

We are ultimately interested in calculating the water saturation, S_w, so we rearrange the equation to give

$$S_w = \sqrt[n]{\frac{R_w f^{-m}}{R_t}} = \sqrt[n]{\frac{R_w F}{R_t}} = \sqrt[n]{\frac{R_o}{R_t}} \tag{17.19}$$

Table 17.1 summarizes the sources of the parameters that go into this equation to calculate the water saturation.

Table 17.1 Sources of data for calculation of water saturation.

Parameter	Source
R_t	• Deep investigation resistivity tool
R_w	• From SP log • Calculated from water zone • Measured on RFT sample
f	• Sonic tool • Formation density tool • Neutron tool
m	• Measured in laboratory • Guessed
n	• Measured in laboratory • Guessed

17.7 The Effect of Errors in Resistivity Calculations

The accurate determination of the water saturation is key to being able to calculate an accurate value for the amount of oil in place. Errors of a few percent in the determination of the water saturation result in errors worth billions of dollars when transferred into errors in the determination of STOOIP.

In attempting to reduce errors we ensure that the five parameters in Eq. (17.19) are measured using independent methods. Laboratory determined *m* and *n* values are the best ones to take, however early in a reservoirs life these are not available, and so guesses are used instead.

Table 17.2 shows the propagation of errors in Eq. (17.19) for the calculation of water saturation.

Table 17.2 Propagation of errors in water saturation calculations.

Data			
	-20%	Base Case	+20%
R_t	32	40	48
R_w	0.32	0.4	0.48
f	0.18	0.2	0.22
m	1.8	2	2.2
n	1.8	2	2.2
Saturations from changing individual parameters			
R_t	0.56	0.50	0.46
R_w	0.45	0.50	0.55
f	0.56	0.50	0.45
m	0.43	0.50	0.59
n	0.46	0.50	0.53
Saturations from changing combinations of *m* and *n* parameters			
	m-20%	m	m+20%
n-20%	0.39	0.46	0.55
n	0.43	0.50	0.59
n+20%	0.46	0.53	0.62
Saturations from changing combinations of resistivity parameters			
	R_t-20%	R_t	R_t+20%
R_w-20%	0.50	0.45	0.41
R_w	0.56	0.50	0.46
R_w+20%	0.61	0.55	0.50
Saturations from changing all parameters			
Worst Case Low	0.28		
Base Case	0.50		
Worst Case High	0.82		

Note that 20% underestimations and overestimations of m and n lead to an underestimation and overestimation of the water saturation by 0.11 and 0.12 respectively. These are huge errors when progressed through to the STOOIP calculation. Clearly there is a case here for doing m and n determinations on core.

Note also that the same degree of underestimation or overestimation in R_t and R_w leads to no further error as these errors cancel out.

The worst case scenarios for over and underestimation with 20% errors on the input parameters are 0.32 and 0.22 respectively. These errors will most probably be larger than the recoverable oil saturation in the reservoir. Clearly, the parameters that go to calculate the water saturation must be derived very carefully indeed.

17.8 The Hingle Plot

Theory. This plot is based on Eq. (17.18). The objective is to obtain a linear cross-plot of the R_t data measured by the resistivity tool and the f data measured by one of the porosity tools. To do this all of the exponents of Eq. (17.18) are multiplied by –1/m to give

$$R_t^{-1/m} = R_w^{-1/m} \; f \; S_w^{+n/m} \tag{17.20}$$

Because in any given reservoir we can take R_w, m and n as constant, and because we will apply the equation for selected values of S_w, Eq. (17.20) becomes

$$R_t^{-1/m} = Bf \tag{17.21}$$

where B is a constant. The Hingle graph paper is designed such that the y-axis represents $R_t^{-1/m}$ so that R_t can be entered directly in the plot. This implies that a different form of graph paper is needed for each value of m. The x-axis on the Hingle grid is porosity on a linear scale.

Figure 17.10 shows a Hingle plot.

Application. The use of the Hingle plot is as follows. For any given reservoir zone carry out the following steps:

- Construct the 100% water saturation (S_w=1) line. The first point on this line is automatically available, as R_t is infinite when f=0, and this point plots in the bottom left hand corner of the Hingle grid. The second point is calculated with knowledge of R_w for the reservoir. Equation (17.11) is used to calculate R_o knowing R_w for the reservoir, for the value of m relevant to the Hingle grid, and at any value of f (the higher the better for accuracy). For example, in Fig. 17.10, the m value is 2, and if R_w=0.4 ohm.m, we can say that at the arbitrary porosity of f =0.2, the value of R_o=10 ohm.m. The R_o, f point can be plotted on the grid and joined with the first point by a straight line. This is the water line, and represents how R_o varies with porosity when the rock is fully saturated with water.

- Other lines for partial water saturations can now be constructed. Their first point is always in the bottom left hand corner of the Hingle grid because R_t is always infinite when f=0 no matter what the water saturation. The second point is calculated from Eq. (17.17) at a given arbitrary porosity assuming or knowing the value of n and calculating R_t from the relevant R_o, which is available from the water line. For a particular partial saturation line (S_w=0.5, say) the R_t, f point can be plotted on the grid and joined with the first point by a straight line. This is the S_w=0.5 line, and represents how R_t varies with porosity when the rock is 50% saturated with water.

- A fan of partial saturation lines can be constructed in this way, say for every 10% increment in water saturation. A large number of porosity and R_t pairs are now extracted from the logs and plotted on the graph. It is immediately obvious how much water saturation is present on average, and the water saturation for particular points (relating to a particular depth) can be estimated from the graph by interpolation between the iso-saturation lines.

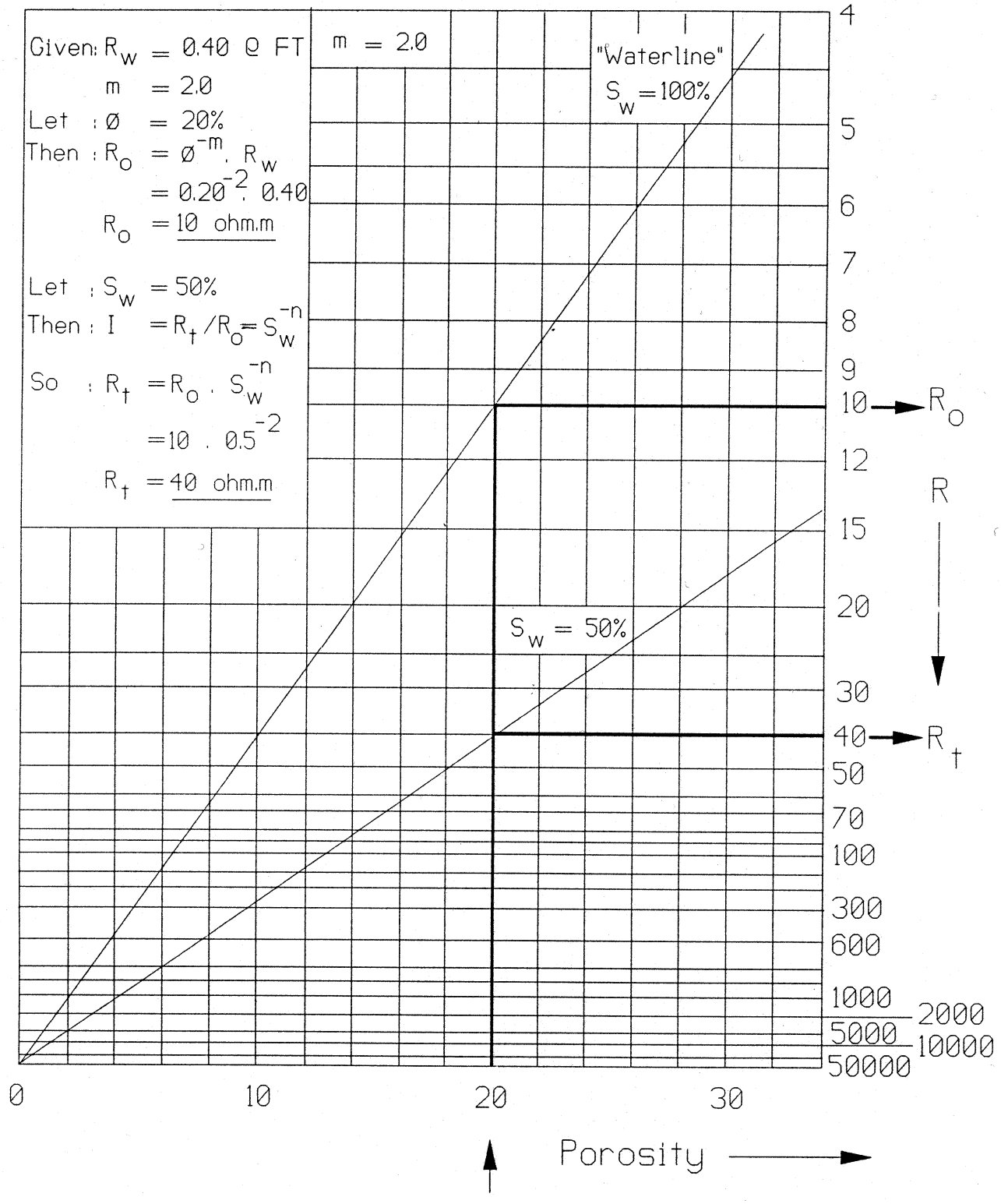

Figure 17.10 The Hingle plot.

17.9 The Pickett Plot

Theory. The Pickett Plot is also based on Eq. (17.18).

In a water-bearing formation we can write from Eq. (17.11)

$$R_o = R_w f^{-m} \tag{17.22}$$

which, when rearranged becomes

$$\log R_o = \log R_w - m \log f \tag{17.23}$$

So a plot of log R_o against log ϕ gives a straight line. The value on the *y*-axis is equal to log R_o when f=1, and the slope of the line is $-m$.

In a hydrocarbon-bearing formation we can write from Eqs. (17.11) and (17.15)

$$R_t = I R_o = I R_w f^{-m} \tag{17.24}$$

which, when rearranged, becomes

$$\log R_t = \log I + \log R_w - m \log f \tag{17.25}$$

which is the same straight line as described by Eq. (17.23), with the same gradient, but with a parallel shift equal to log *I*.

Application. The Pickett Plot plots the formation resistivity R_t against the porosity on a log-log scale. The data form straight lines with a gradient equal to $-m$. Hence, the cementation exponent can be calculated. If one has data in the water zone of the reservoir, Eqs. (17.22) and (17.23) hold true, and the value on the *y*-axis when the line intersects f=1, gives log R_w from which R_w can be calculated. The line is called the water line.

If one has data in the oil-bearing zone, and the value of *Rw* is known, the value on the *y*-axis when the line intersects f=1, gives log *I* + log R_w from which *I* can be calculated if R_w is known. If the saturation exponent is then known, we can use the *I* value to calculate the water saturation.

Alternatively, we can establish the water line and construct iso-saturation lines with the same gradient that are offset from the water line by values of log *I* that represent increments in water saturation. Plotting the formation resistivity and porosity values from logs on this plot then allows the mean saturation in the reservoir to be judged, and particular values of water saturation at a given depth can be calculated can be approximated by interpolation between the iso-saturation lines.

Figure 17.11 shows a Pickett plot example.

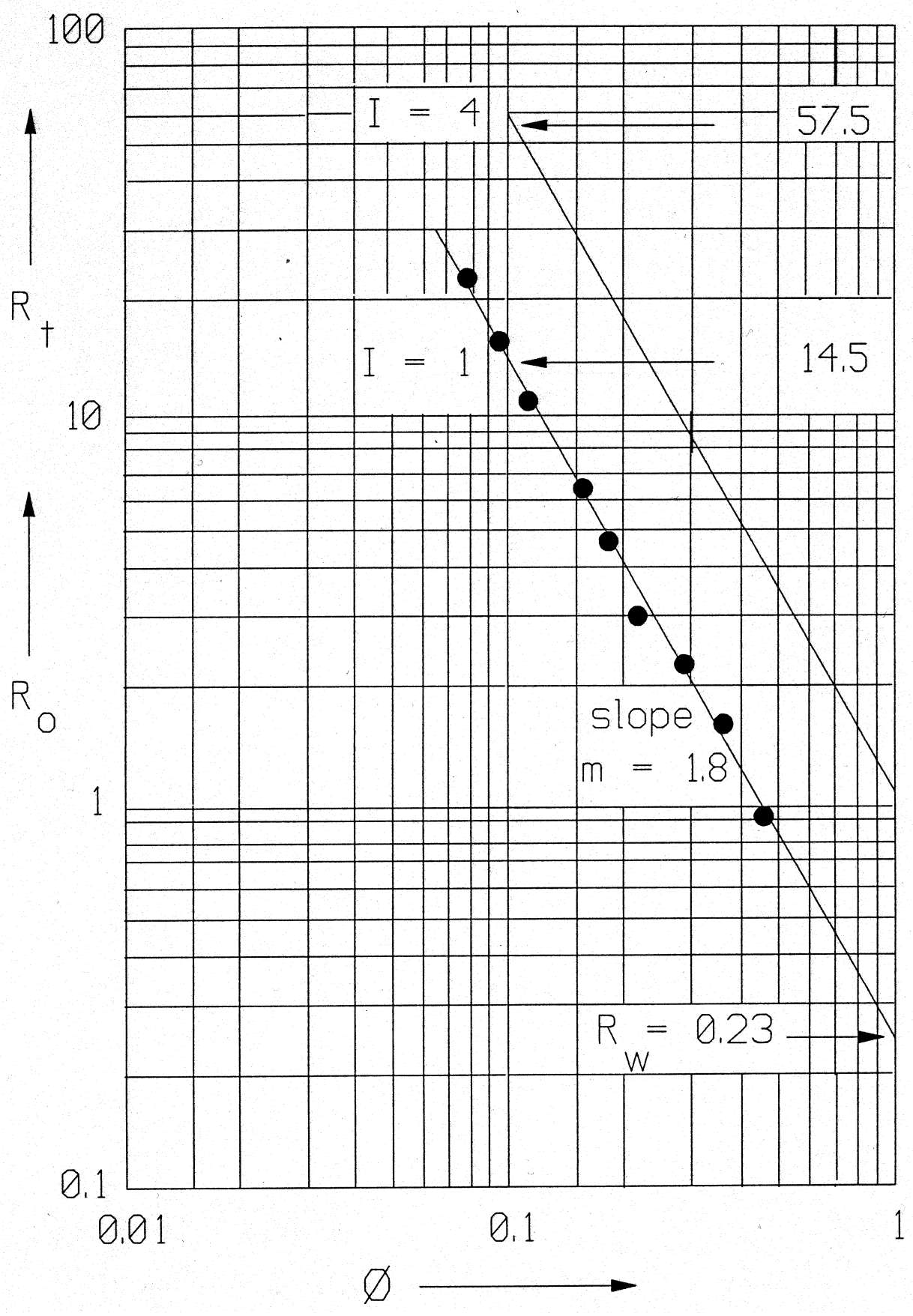

Figure 17.11 The Pickett Plot.

17.10 Saturation of Moveable Hydrocarbons

Equation 17.17 describes how the ratio of the resistivity of the formation containing partly non-conductive oil and partly conductive water to the resistivity when the formation contains 100% conducting water (I) is related to the saturation of water in the formation when it contains both fluids.

We apply this equation to the reservoir zone (i.e., the uninvaded zone deep in the formation) and can calculate the water saturation in the reservoir, and hence calculate the amount of oil in the reservoir.

However, we can also apply the equation in the flushed zone if we are using water based muds. Before invasion, we had a water saturation S_w and an oil saturation S_o. In the flushed zone after invasion, the water has been replaced with mud filtrate, and some of the oil has also been replaced by mud filtrate. The oil that has been replaced by mud filtrate is the *mobile oil*, i.e., that oil which was able to be pushed out of the way by the invading mud filtrate. We want to calculate the saturation of oil which the mud filtrate was able to push further into the formation, because if it was mobile enough to be moved in that way, the likelihood is that it will be mobile enough to be produced easily from the reservoir.

If we apply Eq. (17.17) in the flushed zone we get

$$R_{xoor} = R_{xomf}\ S_{xo}^{-n} \tag{17.26}$$

Hence,

$$S_{xo} = \sqrt[n]{\frac{R_{xomf}}{R_{xoor}}} \tag{17.27}$$

Here R_{xomf} is the resistivity of the formation flushed zone containing nothing but 100% mud filtrate, i.e., invasion has replaced all the oil and water, while R_{xoor} is the resistivity of the flushed zone containing residual oil.

The value S_{xo} is the saturation of water based mud filtrate in the invaded zone. Hence the saturation of oil that was moved by the invasion is $(S_{xo} - S_w)$, and the volume of moveable oil per unit volume of rock is $f\,(S_{xo} - S_w)$. We can use this modified value of moveable hydrocarbons in the reservoir to calculate a lower, and more accurate value for moveable STOOIP by inserting $(S_{xo} - S_w)$ in place of $(1 - S_w)$ in Eqs. (1.2) and (1.4).

18. THE SPONTANEOUS POTENTIAL LOG

18.1 Introduction

The *spontaneous potential* log (SP) measures the natural or *spontaneous potential difference* (sometimes called *self-potential*) that exists between the borehole and the surface in the absence of any artificially applied current. It is a very simple log that requires only an electrode in the borehole and a reference electrode at the surface. These spontaneous potentials arise from the different access that different formations provide for charge carriers in the borehole and formation fluids, which lead to a spontaneous current flow, and hence to a spontaneous potential difference. The spontaneous potential log is given the generic acronym SP.

The SP log has four main uses:

- The detection of permeable beds.
- The determination of R_w.
- The indication of the shaliness of a formation.
- Correlation.

The log has a low vertical resolution, is rarely useful in offshore environments, and is always recorded in the leftmost track of the log suite, together with the GR log.

It is very important to recognize that this log has no absolute scale – only relative changes in the SP log are important. This is reflected in the design of the log header, which shows only a bar that represents a change of, say, 10 mV.

18.2 Principles

There are three requirements for the existence of an SP current:

- A conductive borehole fluid (i.e., a water based mud).
- A sandwich of a porous and permeable bed between low porosity and impermeable formations.
- A difference in salinity between the borehole fluid and the formation fluid, which are the mud filtrate and the formation fluid in most cases. Note, however, that in some special cases an SP current can be set-up when there is no difference in salinity, but where a difference in fluid pressures occurs.

The origin of the spontaneous potential has four different components. These are shown in Fig. 18.1. The spontaneous potential is composed of contributions that are *electrochemical* (arise from electrical interactions between the various chemical constituents of the rocks and fluids), and *electrokinetic* (arise from the movement of electrically charged ions in the fluid relative to the fixed rock).

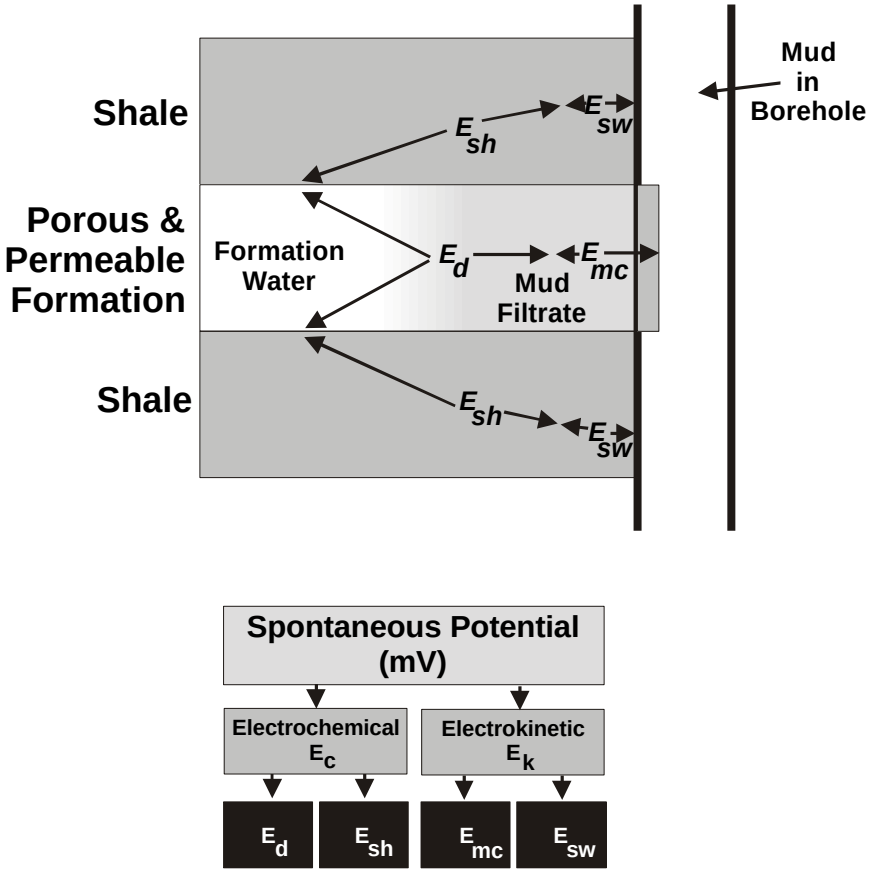

Figure 18.1 Electromotive components of the spontaneous potential.

18.2.1 Electrochemical Components

These components arise from the electrochemical interaction of ions in the mud filtrate and formation fluids.

The electrochemical contribution, itself, consists of two effects:

1. **The *diffusion potential* (sometimes called the *liquid-junction potential*).** This potential exists at the junction between the invaded and the non-invaded zone, and is the direct result of the difference in salinity between the mud filtrate and the formation fluid.

   Assume that the formation fluid is more saline than the mud filtrate for a moment, and that the only dissolved ions in the system are Na^+ and Cl^-, as NaCl. The chloride ions have a higher *mobility* than the sodium ions. When the two fluids come into contact across the interface between the invaded and non-invaded zones, diffusion will occur. Ions from the high salinity mud filtrate will diffuse into the invaded zone to try to balance the salinities out. The chloride ions are more mobile and so more of them diffuse into the invaded zone than sodiums. The net result is a flow of negative charge into the invaded zone, which sets up a charge imbalance (potential difference) called the diffusion potential. The diffusion potential causes a current to flow (from negative to positive) from the invaded zone into the non-invaded zone. This scenario is illustrated in Fig. 18.2 for an analogue system, and is applied to the borehole environment in Fig. 18.3.

Of course, if the mud filtrate has a higher salinity than the formation fluid, the same argument applies but in reverse, and leads to a reverse diffusion potential and current flow.

The same arguments also apply for more complex fluid compositions because some ions always have a greater mobility than others.

For NaCl solutions at 25°C, the diffusion potential, E_d, is given by; $E_d = -11.81 \times \log(R_1/R_2)$, where R_1 is the resistivity of the diluter solution, and R_2 is the resistivity of the more saline solution.

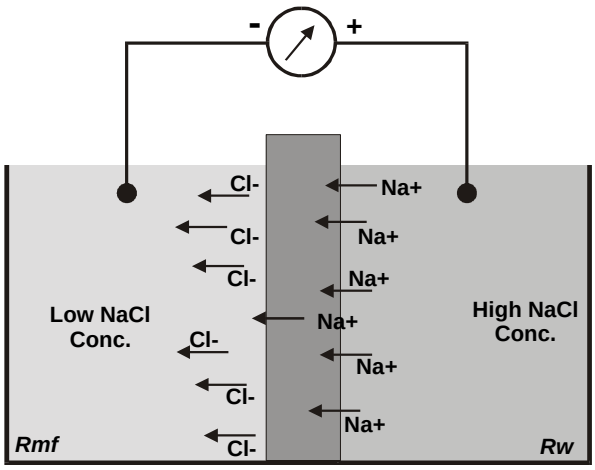

Figure 18.2 Laboratory demonstration of the diffusion potential.

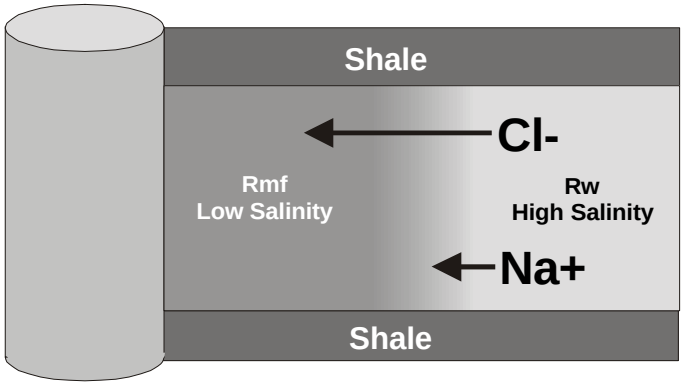

Figure 18.3 The diffusion potential in a borehole.

2. **The *membrane potential* (sometimes called the *shale potential*).** This potential exists at the junction between the non-invaded zone and the shale (or other impermeable rock) sandwiching the permeable bed. These beds are usually shale, and the argument that follows applies mainly to shales, but is also valid to a less extent for other low permeability rocks.

   Shales have the property that they can preferentially retard the passage of anions. This is called *anionic permselectivity* or *electronegative permselectivity* and is a property of *membranes*. It is due to an electrical double layer that exists at the rock-fluid interface, and that has the ability to exclude anions from the smaller pores in the rock (sometimes called *anion exclusion*). The

strength of this effect depends upon the shale mineralogy, the fluid concentration and the fluid pH. Most other rocks exhibit the same behaviour but to a lower degree for geologically feasible fluid concentrations and pHs, but cationic permselectivity is possible, if rare. Most subsurface shales are such efficient anionic permselecting membranes that they repel almost all anions (say, chloride ions). This results in the shale being more positive than the non-invaded zone, and hence there is an electrical membrane potential, which causes current to flow from the invaded zone into the shale (and hence borehole). This scenario is illustrated in Fig. 18.4 for an analogue system, and is applied to the borehole environment in Fig. 18.5.

For NaCl solutions at 25°C, the membrane potential, E_m, is given by; $E_d = 59.15 \times \log(R_1/R_2)$, where R_1 is the resistivity of the diluter solution, and R_2 is the resistivity of the more saline solution.

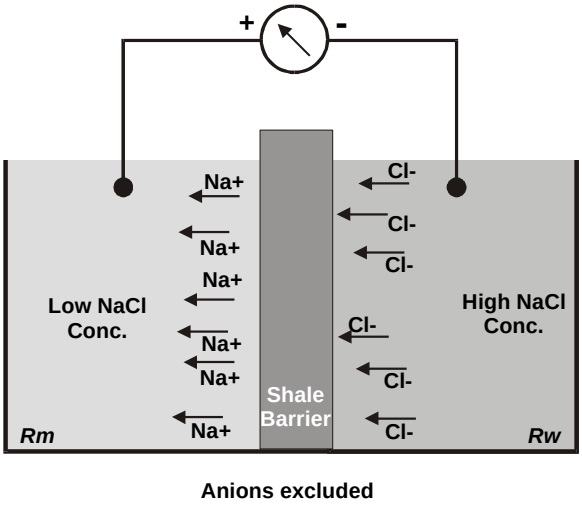

Figure 18.4 Laboratory demonstration of the membrane potential.

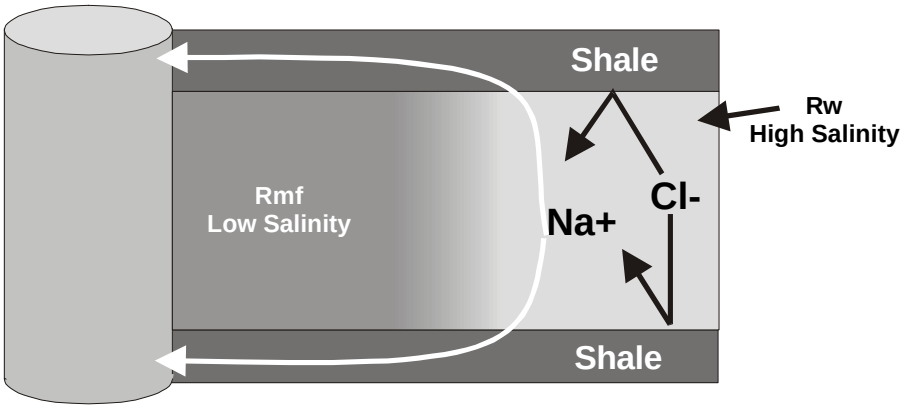

Figure 18.5 The membrane potential in a borehole.

The total electrochemical component of the SP at 25°C for NaCl solutions is therefore;

$$E_c = E_d + E_m = -11.81 \log\left(\frac{R_1}{R_2}\right) + (-)59.15 \log\left(\frac{R_1}{R_2}\right) = -71 \log\left(\frac{R_1}{R_2}\right) = -71 \log\left(\frac{R_{mf}}{R_w}\right) \quad \textbf{(18.1)}$$

for our situation where the mud filtrate is lower salinity than the formation fluid.

Equation (18.1) can be generalized by the formula;

$$E_c = -K \log\left(\frac{A_w}{A_{mf}}\right) \quad \textbf{(18.2)}$$

where; K is a coefficient that depends upon temperature, A_w is the activity of the formation water, and A_{mf} is the activity of the mud filtrate. This relationship breaks down for very saline solutions (R_{mf} < 0.08 Ωm), when corrected formation and mud filtrate resistivities must be obtained from charts. In this circumstance Eq. (18.2) is rewritten as

$$E_c = -K \log\left(\frac{A_w}{A_{mf}}\right) = -K \log\left(\frac{R_{mfe}}{R_{we}}\right) \quad \textbf{(18.3)}$$

where R_{mf} and R_{mfe} are corrected resistivities obtainable from charts.

18.2.2 Electrokinetic Components

These components arise from the movement of fluids containing conducting ions.

The electrokinetic contribution, itself, consists of two effects, which are usually very small and act in opposite ways such that they cancel each other out. These contributions depend upon fluid flow, and hence are larger when there is a substantial difference in pressure between the borehole and the formation. Thus, these contributions may be significant for depleted and under-pressured reservoirs where the differential pressure is high (>500 psi). The contributions also depend upon the development of an electrical double layer at mineral surfaces, which is larger for low salinity fluids. Hence, these contributions are also more important for fresh formation waters or mud filtrates.

1. **The *mudcake potential*.** This potential is produced by the movement of charged ions through the mudcake and invaded zone in a permeable formation. Its size depends upon the hydraulic pressure drop, and since most of this is across the low permeability mudcake, the great majority of electrokinetic potential is also generated across the mudcake, with an insignificant amount in the invaded zone.

   The surface of clay minerals carry a negative charge when in contact with fluids of pH and salinities that are geologically feasible. The surface negative charge attracts cations from the fluid, which become adsorbed to the surface and are fixed. The now apparent positive surface charge is balanced out by an excess of negative ions in the fluid close to the surface. This “layer” of excess negative fluid close to the surface ensures global charge balance and is mobile. If there is no fluid flow the situation is electrically balanced. However, if there is fluid movement due to passage of mud filtrate through the mudcake the mobile layer moves setting up a *streaming potential*. Since the mudcake is anionically permselective (like shales), the potential that arises is always negative, with current flowing from the borehole into the formation through the mudcake.

2. **The *shale wall potential*.** This potential is the same in origin to the mudcake potential, but applies to the flow of fluids from the borehole into shale formations. It is usually very small because the flow into impermeable shales is small. It also acts to set up a current flow into the formation. We will see how this tends to cancel out the mudcake potential.

The total electrokinetic potential is $E_k = E_{mc} + E_{sw}$, and because E_{mc} and E_{sw} have the same polarity, the value of E_k is the difference between their absolute values, i.e., $E_k = |E_{mc}| + |E_{sw}|$.

18.2.3 The Combined Spontaneous Potential Effect

Figure 18.6 shows the scenario with the formation water more saline than the mud filtrate. We will combine the previously described contributions to the SP step-by-step, which can be followed in both parts of the figure.

- First assume that point A in the borehole has some unknown potential relative to the surface E_o.
- The mudcake potential E_{mc} induces a current flowing into the formation through the mudcake. Therefore at point B, the potential is $E_o + E_{mc}$ and current has flowed from A to B.
- The diffusion potential E_d across the interface between the invaded and non-invaded zones induces a current flowing from the invaded zone into the non-invaded zone. Therefore at point C, the potential is $E_o + E_{mc} + E_d$ and current has flowed from A through B to C.

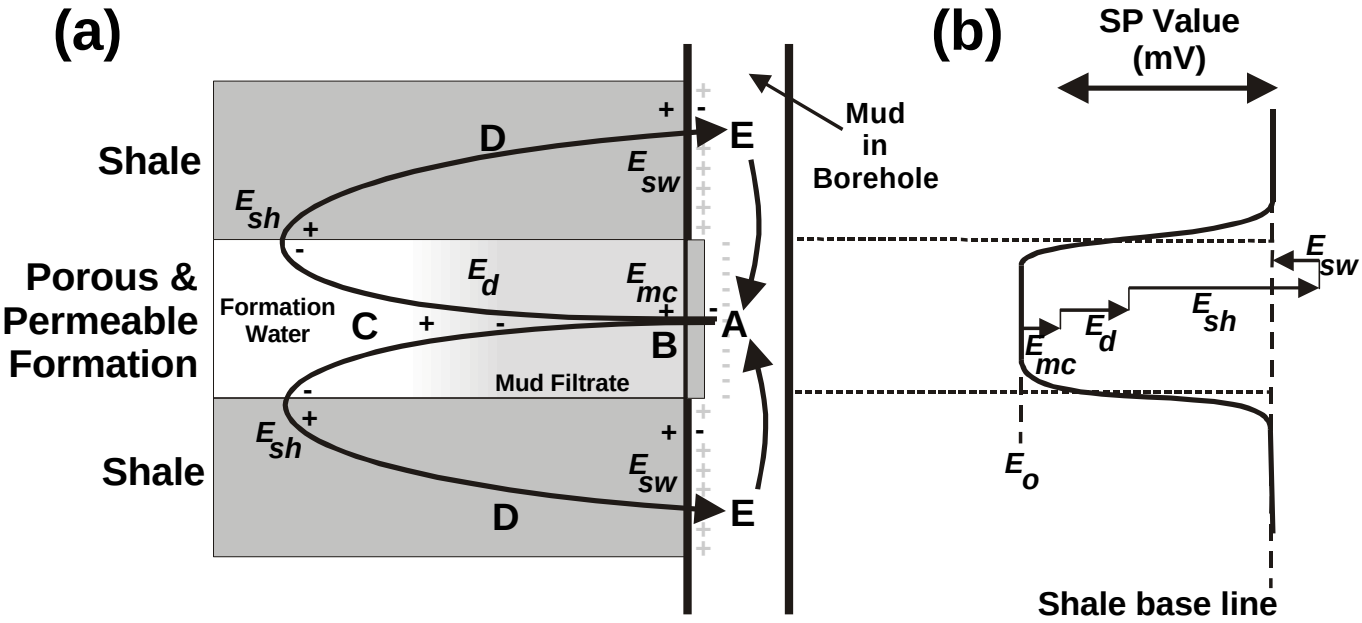

Figure 18.6 Combination of the electromotive components of the spontaneous potential for the formation water more saline than the mud filtrate.

- The membrane potential E_m across the interface between the permeable formation and the shale above it induces a current flowing into the shale from the non-invaded zone. Therefore at point D, the potential is $E_o + E_{mc} + E_d + E_m$ and current has flowed from A through B and C to D.

- The shale wall potential E_{sw} induces a current flowing into the shale from the borehole. This current counteracts the current flow set-up in the previous steps. Therefore at point E, the potential is $E_o + E_{mc} + E_d + E_m - E_{sw}$ and the current has flowed from A through B and C to D, and has been slightly reduced there by the small countercurrent due to the shale wall potential. The overall effect is for a net current to flow from A through B, C and D to E.

- The overall effect is for point E in the borehole opposite the shale wall to have a more positive potential than that at point A opposite the permeable formation. Hence there will also be a current flow in the borehole between the borehole opposite the shale beds and the borehole opposite the permeable bed to close the loop.

The arrows in Fig. 18.6a show the flow of currents and the black charge symbols indicate the local relative potential due to each of the contributions to the SP. The grey charge symbols indicate the overall potential set-up by the combined process. Figure 18.6b shows the summation of the potentials.

Note, since the value of E_o is arbitrary, there is no absolute value of spontaneous potential – what matters is the relative change in spontaneous potential.

So, is the SP opposite a permeable formation always less than that opposite the shale above (or below) it? ***NO***. This is for the particular case where the formation fluid is more saline than the mud filtrate.

If the formation fluid is less saline than the mud filtrate, the opposite applies, and the SP opposite the permeable formation is *GREATER* than that opposite the shale above (or below) it. This situation is shown in Fig. 18.7, and described in the step-by-step list below.

- First assume that point A in the borehole has some unknown potential relative to the surface E_o.

- The mudcake potential E_{mc} induces a current flowing into the formation through the mudcake. Therefore at point B, the potential is $E_o + E_{mc}$ and current has flowed from A to B. This is the same as in the previous case because nothing has changed locally. The mud filtrate is still passing through the mudcake and sets up the same potential difference.

- The diffusion potential E_d across the interface between the invaded and non-invaded zones now induces a current flowing from the non-invaded zone into the invaded zone (i.e., the opposite way to the previous case). Therefore at point C, the potential is $E_o + E_{mc} - E_d$ and current has flowed from C to B. Since this current is generally larger than that flowing from A to B in the opposite direction due to the mudcake potential, the net current flow is from C through B to A.

- The membrane potential E_m across the interface between the permeable formation and the shale above it now induces a current flowing out of the shale and into the non-invaded zone (i.e., again the opposite way to the previous case). Therefore at point D, the potential is $E_o + E_{mc} - E_d - E_m$ and the net current has flowed from D through C and B to A.

- The shale wall potential E_{sw} induces a current flowing into the shale from the borehole as it did in the previous scenario. This is because the local situation has not changed – mud filtrate is still flowing into the shale and setting op the associated streaming potential. This current now does not counteract the current flow, but contributes to it. Therefore at point E, the potential is $E_o + E_{mc} - E_d - E_m - E_{sw}$ and current has flowed from E through D, C and B to A, and has been slightly reduced by the small countercurrent due to the mud cake potential between B and A.

- The overall effect is for point E in the borehole opposite the shale wall to have a more negative potential than that at point A opposite the permeable formation. Hence there will also be a current flow in the borehole between the borehole opposite the permeable bed and the borehole opposite the shale beds to close the loop.

The arrows in Fig. 18.7a show the flow of currents and the black charge symbols indicate the local relative potential due to each of the contributions to the SP. The grey charge symbols indicate the overall potential set-up by the combined process. Figure 18.7b shows the summation of the potentials.

Note, if the mud filtrate and the formation fluids have the same or similar salinities, there is no change in the SP Log between shaly and permeable formations.

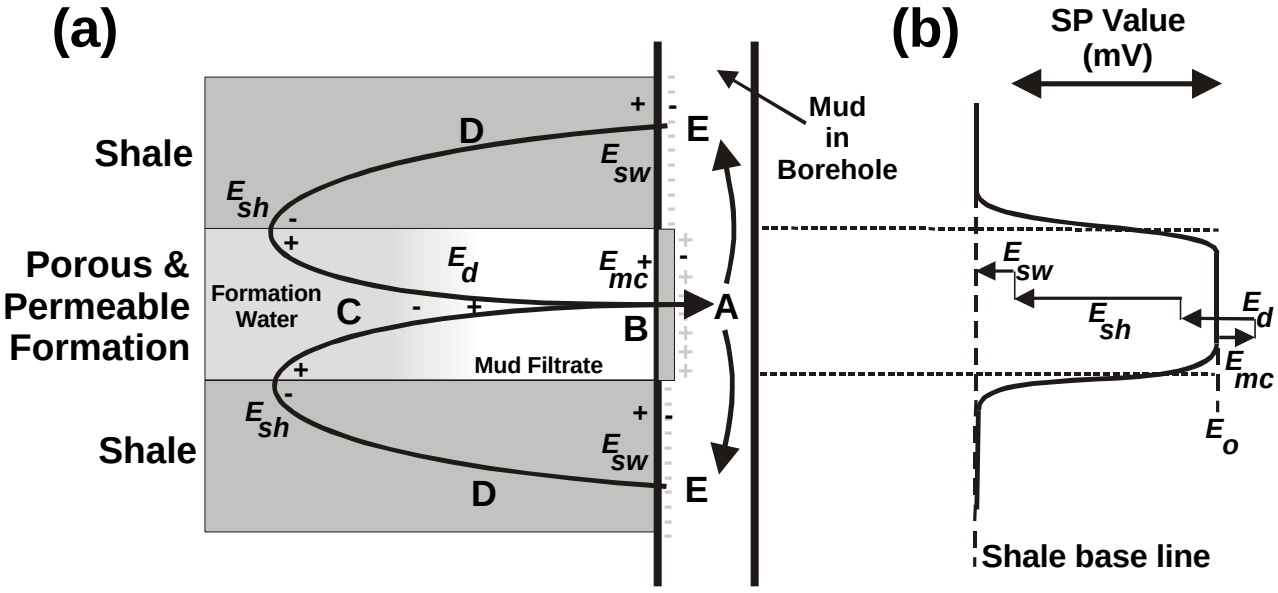

Figure 18.7 Combination of the electromotive components of the spontaneous potential for the formation water more saline than the mud filtrate.

18.3 Measurement Tools

The tool is extremely simple, consisting of a single electrode that is connected to a good surface earthing point *via* a galvanometer for the measurement of DC potential (Fig. 18.8). A small 1.5 V battery is also included commonly to ensure that the overall signal is measured on the correct scale. The simplicity of the log means that it is extremely cheap, and therefore give tremendous value for money.

Only relative changes in potential are measured because the absolute value of the SP is meaningless. Changes of the order of 50 mV are typical. For the log to be good, a good earth is necessary, which is often a metal spike driven 1 m into the ground.

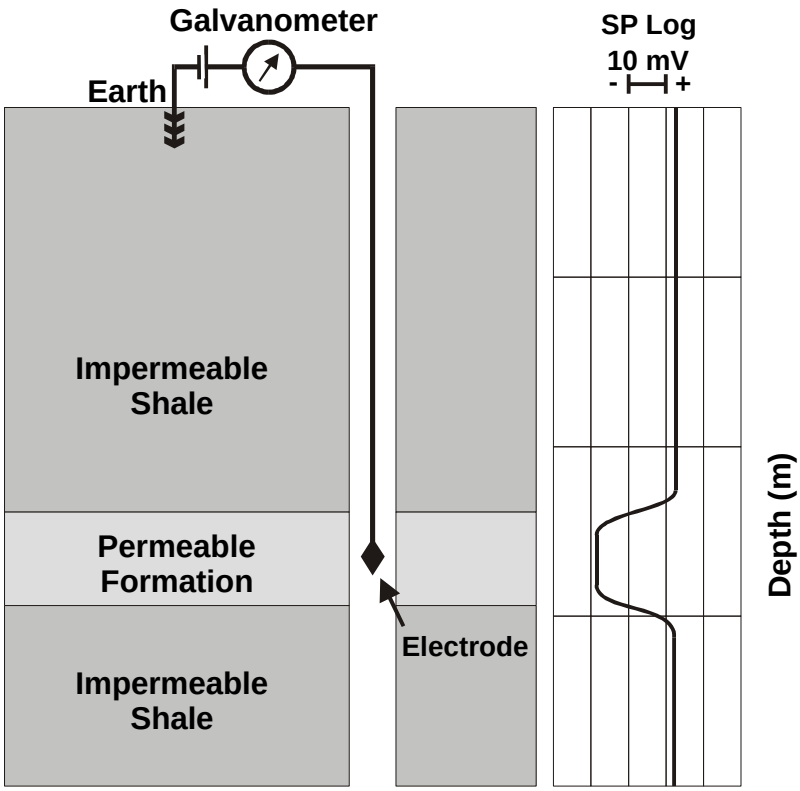

Figure 18.8 The SP tool arrangement.

The SP log is difficult to run offshore because (i) a good earth is difficult to find, and (ii) the amount of electrical noise on board a rig often causes problems for accurately measuring signals that commonly change by less than a millivolt. Sometimes the riser is used as the earth, but often the riser is in connection with the rig, and therefore a source of electrical noise. Sometimes the rig legs or an anchor chain are used, which is a big mistake because (i) the legs of oil platforms are given a specific electrical potential to help combat the effects of corrosion, and (ii) the operation of sea waves on the rig legs induces potentials in the rig legs that give rise to wavy patterns in the recorded SP log which cannot be removed.

18.4 Log Presentation

SP is shown in millivolts in Track 1, with negative deflections to the left and positive ones to the right (Fig. 18.9). Figure 18.9 shows the general presentation of the SP log, and Fig. 18.10 shows a schematic diagram of typical SP log responses.

In reading the SP log it is best to first define a *shale base line*. This is the typical SP level for shales and can be found by comparing the SP log with the GR log response. Permeable formations will then have excursions of variable intensity to the left or right of this line, depending upon the relative salinities of the formation water and the mud filtrate. It is useful to know the salinity or resistivity of the mud filtrate from the log header, if available, as this will indicate whether the formation water is likely to fall at a higher or lower salinity. For example, if the mud filtrate is known to be very fresh, the likelihood is that that the formation water will be saltier, and the SP will likely kick left.

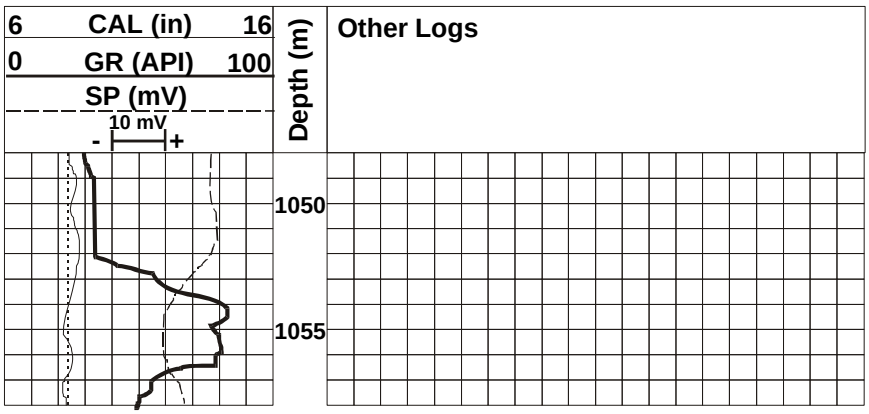

Figure 18.9 Presentation of the SP log.

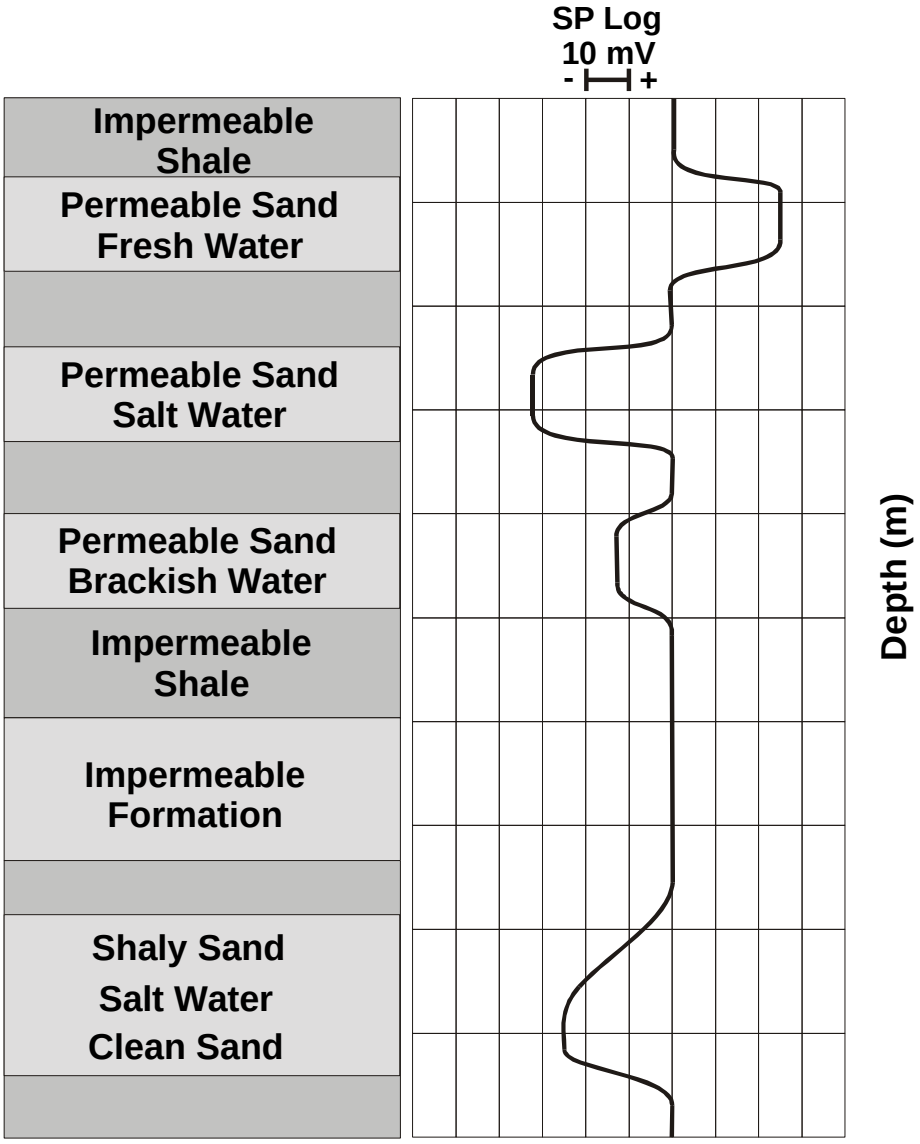

Figure 18.10 Typical responses of the SP log.

18.5 Vertical Resolution and Bed Resolution

The SP tool has a poor resolution. Although it can be used for correlation, it is best not to rely solely upon it. If it has to be used for defining a bed boundary, it is best to take the inflexion point in the SP change as the boundary depth.

Bed resolution is bad, and one would not expect it to show beds less than about 20 times the borehole diameter.

18.6 The Amplitude of the SP Deflection

Several factors govern the amplitude of the SP deflection opposite a permeable bed. This is because the size of the deflection and the change in the SP curve between beds depends upon the distribution of the current flux and the potential drops taking place in each part of the formation. The following parameters are important:

- The thickness of the permeable bed, h.
- The true resistivity of the permeable bed, R_t.
- The diameter of the invaded zone, d_i.
- The resistivity of the invaded zone, R_{XO}.
- The resistivity of the bounding formations.
- The resistivity of the mud, R_m.
- The diameter of the borehole, d_h.
- The relative salinities of the mud filtrate and the formation fluids.

The recorded SP log represents the potential drop in the borehole, only. To use the SP curve quantitatively, a value for the total potential drop around the circuit must be derived. This is called the *static spontaneous potential* (SSP). This value may be derived from correction charts. However, a direct reading of the SSP may be obtained directly from the SP log opposite *thick*, *clean*, *shale-free*, *100% water-bearing* formations. The SSP is the value in millivolts of the difference between the SP log at the shale base line and that in the centre of the thick clean formation, as shown in Fig. 8.11.

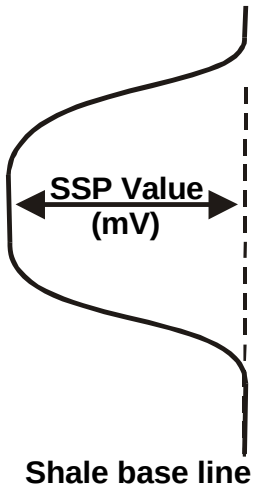

Figure 18.11 Definition of SSP.

The SP deflection obtained for homogeneous shaly formations or thin shaly beds after correction for bed thickness is called the *pseudo-static spontaneous potential* (PSP). The SSP is the value in millivolts of the difference between the SP log at the shale base line and that in the centre of the thick homogeneous shaly formation, or a thinner bed if a bed thickness correction has been carried out.

If there is a proportion of shale in the permeable bed, the SP deflection is reduced from what it would be if the bed were clean and contained the same fluids. Hydrocarbon saturation also decreases SP deflections.

The present understanding of the electrical effect of clays and shales in reservoir rocks depends largely upon the concept of *cation exchange capacity*, Q_v, which is the cation concentration in milliequivalents of exchange sites for sodium ions per cubic centimetre of pore volume. Laboratory investigations have used this concept to develop a method for calculating the formation water resistivity from SP log data in a way that takes account of the shaliness of a formation.

To use this method a value of Q_v is needed from the shale beds above or below the formation of interest, and a value of Q_v for the formation of interest. These values are normally obtained from standard chemical methods carried out in the laboratory upon cores or sidewall cores. More information concerning Q_v is given in Chapter 20.

18.7 Uses of the Spontaneous Potential Log

The main uses of this log are:

- The detection of permeable beds.
- The determination of R_w.
- The indication of the shaliness of a formation.
- Correlation.

18.7.1 Permeable Beds

The SP log is an extremely useful quick-look indicator of bed permeability. It is not quantitative, and opinions differ to the extent to which one can associate the size of the deflection with the degree of permeability. Given the large number of other parameters that might affect the SP log, I prefer to say that one should not associate very large permeabilities necessarily with large deflections and *vice versa*. However, the SP log is quite sensitive, and even a small deflection in the SP log indicates that the bed has reasonable permeability. It should be noted that some permeable beds might give no deflection, such as those where there is no difference in salinity between the formation fluids and the mud filtrate. These cases are rare however. Figure 18.12 shows an example of permeability recognition by SP log.

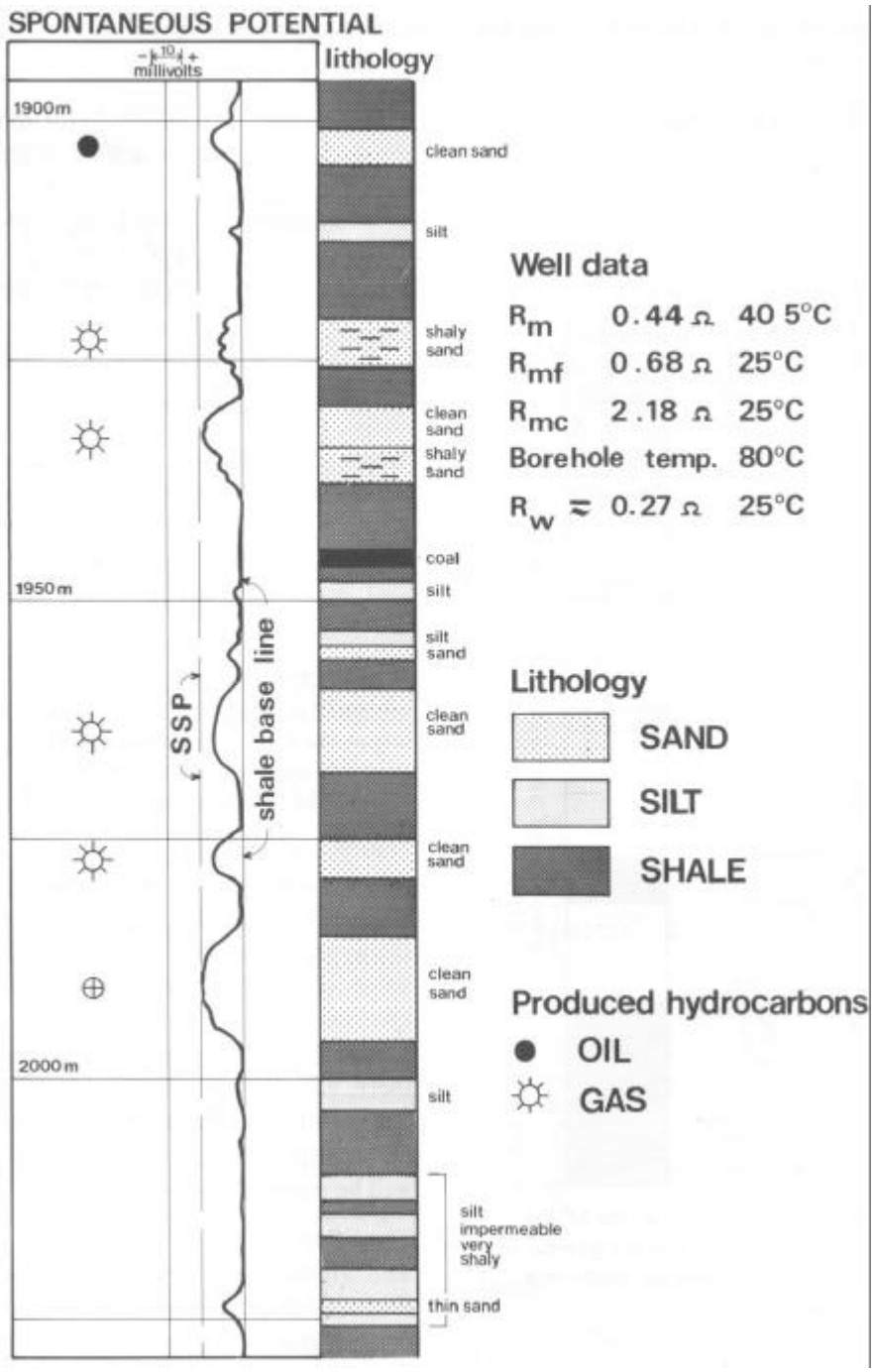

Figure 18.12 Permeability recognition by SP log.

18.7.2 Correlation and Facies

The SP log is sometimes a useful additional log to use in correlation, but is rarely used alone. If used, the wells should be close together and drilled with the same mud, and the salinities in the formations should be constant between wells.

The SP log can be used to follow facies changes. However, it has been largely replaced by the GR log, which has a higher resolution and is more reliable.

18.7.3 Mineral Recognition

Though not as good as some other logs, the SP log does react unusually to a few minerals and formations, and is therefore sometimes useful in mineral recognition. The most common occurrences are as follows, but are not reliable:

- Coals Large negative kick (or none at all!)
- Pyrite Very large negative kick.
- Rhyolite Large negative kick.
- Black shale Positive kick.

18.7.4 Calculation of R_w

This is one of two quantitative use of the SP log. However, it is extremely useful when no formation water samples or water-bearing sands are available to otherwise obtain R_w from during an analysis for OOIP.

There are three methods which will be described here.

18.7.4.1 The Quick-Look Method - Procedure

This is the quickest and most common method, and does not require knowledge of Q_v. As the method ignores the complicating effects of electrokinetic potentials and the possible presence of clay, it is to be used with caution as errors in R_w will translate into errors in OOIP that may represent tens of millions of dollars.

The following procedure is followed:

[1] Obtain mud resistivity at formation temperature. It will either be directly available, or given at some other temperature, such as at 75°C. If the latter is the case, use a resistivity-salinity-temperature correction chart, such as that shown in Fig. 18.13). [If the chart is used, enter the chart on the left *y*-axis with the value of mud resistivity at the starting temperature, and scan across to the point represented by that temperature. This may lie on a curve or between curves. At this point the equivalent salinity of the mud (which is constant) may be read off the chart. Now follow the curve (or parallel to the curves if lying between them) until the new temperature is reached. The value for the mud resistivity at this temperature can then be read off the right-hand *y*-axis.]

[2] Read off the difference in millivolts between the shale base line and the SP curve in the centre of the formation of interest.

[3] Correct the SP reading from [2] for bed thickness using the correction chart shown in Fig. 18.14. Enter the bed thickness, read off the correction factor, and multiply the correction factor by the reading from [2]. This gives the SSP for the depth concerned.

[4] Enter this value into the correction chart in Fig. 18.15 *x*-axis, and intersecting the relevant temperature curve, read off the value of the ratio R_{mfe}/R_{we} from the *y*-axis.

[5] Now go back to the initial data provided by the log header to find R_{mf} @ 75°F.

- If R_{mf} @ 75°F (24°C) > 0.1 Ωm, correct R_{mf} to the formation temperature using Fig. 18.13 as in [1], and use $R_{mfe} = 0.85 \times R_{mf}$
- If R_{mf} @ 75°F (24°C) < 0.1 Ωm, determine the value of R_{mfe} at the formation temperature using the correction chart shown in Fig. 18.13 as in [1].

[6] With the known value of R_{mfe} at the formation temperature, calculate the value of R_{we} at the formation temperature from the R_{mfe}/R_{we} ratio calculated in [4].

[7] Determine the value of R_w at the formation temperature from calculated R_{we} at the formation temperature using the correction chart shown in Fig. 18.16.

This is essentially the same method as described in Rider [1996].

18.7.4.2 The Quick-Look Method - Example

INPUT DATA	
Parameter	**Value**
Bed of interest	Shaly sand, homogeneous, 5ft thick
Bounding beds	Thick shale
Measured SP in centre of bed of interest	-25 mV
Formation temperature	200°F
Borehole diameter	8.75 inches
Diameter of invaded zone	20 inches
Mud resistivity, R_m @ 75°F	1.80 Ωm
Mud filtrate resistivity, R_{mf} @ 75°F	1.35 Ωm
Resistivity of invaded zone, R_{XO}	4.00 Ωm
True resistivity of formation, R_t	10.0 Ωm

[1] Mud resistivity, R_m @ 75°F = 1.80 Ωm. Therefore use Fig. 18.13 to give Mud resistivity, R_m @ 200°F = 0.68 Ωm.

[2] Value of SP log (difference between shale base line and value in centre of formation) = -25 mV.

[3] Find correct correction curve in available literature for your parameters. These are: (i) diameter of invasion ≈ 2×diameter of borehole, (ii) ratio of resistivity of surrounding beds (shale) to the resistivity of the mud (clay based), R_s/R_m = 1, (iii) borehole diameter = 8.75 inches. Then calculate the ratio of the resistivity of the invaded zone, R_{XO} (sometimes R_i) to the resistivity of the mud R_m; $R_{XO}/R_m \equiv R_i/R_m = 4/0.68 = 6$ in this case. The chart in Fig. 18.14 is close enough to these parameters to use reliably. Enter the plot from the appropriate *x*-axis, intersect the curve at the appropriate curve (or interpolated curve) for $R_i/R_m = 6$, and read off the correction factor on the *y*-axis. Correction factor = 1.2. Multiply this by the SP value gives the bed corrected SSP for the formation: SSP = 1.2 × –25 mV = -30 mV.

[4] Use the correction chart in Fig. 18.15 to obtain the value of R_{mfe}/R_{we} (on the *y*-axis) from input of the SSP into the *x*-axis by intersecting the appropriate formation temperature curve. This gives R_{mfe}/R_{we} = 2.1.

[5] We are given R_{mf} @ 75°F = 1.35 Ωm, which is > 0.1 Ωm. So, first correct the value of R_{mf} @ 75°F to that at 200°F using Fig. 18.12. This gives R_{mf} @ 200°F = 0.51 Ωm. The value of R_{mfe} @ 200°F can be calculated by simply multiplying this value by 0.85. So, R_{mfe} @ 200°F = 0.85 × 0.51 = 0.43 Ωm.

[6] As R_{mfe}/R_{we} = 2.1 and R_{mfe} @ 200°F = 0.43 Ωm, we can find R_{we} = 0.43/2.1 = 0.21 Ωm @ 200°F.

[7] Now this value of R_{we} = 0.21 Ωm @ 200°F can be entered into the correction chart shown in Fig. 18.16 to read off the value of R_w @ 200°F, by intersecting the appropriate temperature curve. Here R_w = 0.31 Ωm @ 200°F

This is the resistivity of the formation water in the formation at depth at the formation temperature.

18.7.4.3 The Single Chart Method - Procedure

This is a method used by Halliburton. It should be used with caution for the same reasons stated for the quick-look method. For more information see Silva *et al*. [1985]. The name indicates that a single chart is used for the main calculations, however all the input data need to be corrected for formation temperature and bed thickness. Hence, more than one chart is actually needed. The full procedure is given below.

The following procedure is followed:

[1] Read off the difference in millivolts between the shale base line and the SP curve in the centre of the formation of interest.

[2] Correct the SP reading from [1] for bed thickness using the correction chart shown in Fig. 18.14. Enter the bed thickness, read off the correction factor, and multiply the correction factor by the reading from [1]. This gives the SSP for the depth concerned.

[3] Now go back to the initial data provided by the log header to find R_{mf} @ 75°F.

- If R_{mf} @ 75°F (24°C) > 0.1 Ωm, correct R_{mf} to the formation temperature using Fig. 18.13 as in [1], and use $R_{mfe} = 0.85 \times R_{mf}$
- If R_{mf} @ 75°F (24°C) < 0.1 Ωm, determine the value of R_{mfe} at the formation temperature using the correction chart shown in Fig. 18.13 as in [1].

[4] Enter the known value of R_{mfe} at the formation temperature into the *x*-axis of the "single chart" (Fig. 18.17) and using the appropriate formation temperature curve, read off a value for apparent SSP on the *y*-axis.

- If the value of the true SSP calculated in [2] is positive, then leave the value of apparent SSP read off the chart also positive.

- If the value of the true SSP calculated in [2] is negative, then take the value of apparent SSP read off the chart as a negative number.
- If you are working with positive SSPs, add the real and apparent SSPs to give a modified SSP.
- If you are working with negative SSPs, subtract the real value of SSP calculated in [2] above from the apparent SSP to give the modified SSP.

[5] Take the value of the modified SSP on the *y*-axis and project across horizontally to the appropriate formation temperature curve, then read off on the *x*-axis the value of R_w at the formation temperature.

18.7.4.4 The Single Chart Method – Example

INPUT DATA	
Parameter	**Value**
Bed of interest	Shaly sand, homogeneous, 5ft thick
Bounding beds	Thick shale
Measured SP in centre of bed of interest	-25 mV
Formation temperature	200°F
Borehole diameter	8.75 inches
Diameter of invaded zone	20 inches
Mud resistivity, R_m @ 75°F	1.80 Ωm
Mud filtrate resistivity, R_{mf} @ 75°F	1.35 Ωm
Resistivity of invaded zone, R_{XO}	4.00 Ωm
True resistivity of formation, R_t	10.0 Ωm

[1] Value of SP log (difference between shale base line and value in centre of formation) = -25 mV.

[2] Find correct correction curve in available literature for your parameters. These are: (i) diameter of invasion ≈ 2×diameter of borehole, (ii) ratio of resistivity of surrounding beds (shale) to the resistivity of the mud (clay based), R_s/R_m = 1, (iii) borehole diameter = 8.75 inches. Then calculate the ratio of the resistivity of the invaded zone, R_{XO} (sometimes R_i) to the resistivity of the mud R_m; $R_{XO}/R_m \equiv R_i/R_m$ = 4/0.68 = 6 in this case. The chart in Fig. 18.14 is close enough to these parameters to use reliably. Enter the plot from the appropriate *x*-axis, intersect the curve at the appropriate curve (or interpolated curve) for R_i/R_m = 6, and read off the correction factor on the *y*-axis. Correction factor = 1.2. Multiply this by the SP value gives the bed corrected SSP for the formation: SSP = 1.2 × –25 mV = -30 mV.

[3] We are given R_{mf} @ 75°F = 1.35 Ωm, which is > 0.1 Ωm. So, first correct the value of R_{mf} @ 75°F to that at 200°F using Fig. 18.13. This gives R_{mf} @ 200°F = 0.51 Ωm. The value of R_{mfe} @ 200°F can be calculated by simply multiplying this value by 0.85. So, R_{mfe} @ 200°F = 0.85 × 0.51 = 0.43 Ωm.

[4] Take R_{mfe} @ 200°F = 0.43 Ωm from [3] and enter the single chart (Fig. 18.17) on the *x*-axis. Project vertically to the curve for formation temperature = 200°F, and then horizontally to read apparent SSP = -170 mV from the *y*-axis. Note that this axis looks positive, but we have taken the negative value, because the true SSP calculated in [2] is negative. If it were positive, we would have left the apparent SSP read from the graph as a positive value. Subtract the true SSP value from [2] from the apparent SSP just read off the graph, which gives a value of (-170) - (-30) = -140 mV. Enter this value back into the *y*-axis, project horizontally to the relevant temperature curve, and down to the *x*-axis, where the value of R_w @ 200°F can be read directly. In this case R_w @ 200°F = 0.19 Ωm.

18.7.4.5 The Smits Method – Procedure

This is a complex method that is the most accurate we have. It accounts for both electrokinetic potentials and the effect of the shaliness of the formation, but does not account for the possible presence of hydrocarbons.

[1] Read off the difference in millivolts between the shale base line and the SP curve in the centre of the formation of interest.

[2] Correct the SP reading from [1] for bed thickness using the correction chart shown in Fig. 18.14. Enter the bed thickness, read off the correction factor, and multiply the correction factor by the reading from [1]. This gives the SSP for the depth concerned.

[3] Determine the mudcake potential E_{mc} for your particular mud (Fig. 18.18).

[4] Determine the shall wall potential E_{sw} for the correct pressure differential between the borehole and the formation using $E_{sw} = \Delta P/100$, where the pressure difference is in psi.

[5] Derive the total electrokinetic contribution to the SP using $E_k = SSP + |E_{mc}| - |E_{sw}|$ at the appropriate formation temperature.

[6] Carry out the following temperature corrections:

- If the temperature is measured in °F, calculate E_k @ 77°F using the following relationship, where T_F is the formation temperature in °F: E_k @ 77°F = E_k @ $T_F \times 537/(460 + T_F)$.
- If the temperature is measured in °C, calculate E_k @ 25°C using the following relationship, where T_F is the formation temperature in °C: E_k @ 25°C = E_k @ $T_F \times 298/(273 + T_F)$.

[7] Obtain the mud filtrate salinity in g/l NaCl equivalent from the mud filtrate resistivity value.

[8] Select the correct "Q_v – shale" chart (Figs. 18.19 and 18.20) depending upon the value for your formation in meq/cm^3. Enter the mud filtrate resistivity on the *x*-axis, project vertically to intersect the appropriate Q_v reservoir curve, project horizontally to read the "*E*" value.

[9] If E_k is negative, subtract the absolute value of E_k calculated in [6] from the *E* value from [8].

[10] If E_k is positive, add the absolute value of E_k calculated in [6] to the *E* value from [8].

[11] Enter the new value into the *y*-axis of the chart, projecting horizontally to the appropriate Q_v reservoir curve and down to the *x*-axis again. read off the formation water salinity.

[12] Convert the formation water salinity to formation water resistivity using a chart (Fig. 18.13).

18.7.4.6 The Smits Method – Example

INPUT DATA	
Parameter	**Value**
Bed of interest	Shaly sand, homogeneous, 5ft thick
Bounding beds	Thick shale
Measured SP in centre of bed of interest	-25 mV
Formation temperature	200°F
Borehole diameter	8.75 inches
Diameter of invaded zone	20 inches
Mud resistivity, R_m @ 75°F	1.80 Ωm
Mud filtrate resistivity, R_{mf} @ 75°F	1.35 Ωm
Resistivity of invaded zone, R_{XO}	4.00 Ωm
True resistivity of formation, R_t	10.0 Ωm
Q_v shale	1 meq/ml
Q_v formation	0.04 meq/ml
Formation depth	5500 ft.
Mud pressure gradient	0.49 psi/ft.
Formation fluid pressure gradient	0.435 psi/ft.

[1] Value of SP log (difference between shale base line and value in centre of formation) = -25 mV.

[2] Find correct correction curve in available literature for your parameters. These are: (i) diameter of invasion ≈ 2×diameter of borehole, (ii) ratio of resistivity of surrounding beds (shale) to the resistivity of the mud (clay based), R_s/R_m = 1, (iii) borehole diameter = 8.75 inches. Then calculate the ratio of the resistivity of the invaded zone, R_{XO} (sometimes R_i) to the resistivity of the mud R_m; $R_{XO}/R_m \equiv R_i/R_m$ = 4/0.68 = 6 in this case. The chart in Fig. 18.14 is close enough to these parameters to use reliably. Enter the plot from the appropriate *x*-axis, intersect the curve at the appropriate curve (or interpolated curve) for R_i/R_m = 6, and read off the correction factor on the *y*-axis. Correction factor = 1.2. Multiply this by the SP value gives the bed corrected SSP for the formation: SSP = 1.2 × –25 mV = -30 mV.

[3] E_{mc} = -12 mV from Fig. 18.18 using the curves for untreated mud, R_m = 1.8 Ωm and a pressure difference of 303 psi, calculated below in [4].

[4] The pressure difference is 5500 × (0.49 – 0.435) = 303 psi. So E_{sw} = 303/100 = +3 mV.

[5] E_k @ 200°F = -30 + |-12| - |+3| = -21 mV.

[6] E_k @ 77°F = -21 × 537/(460 + 200) = -17 mV.

[7] As R_{mf} = 1.35 Ωm @ 77°F, use of Fig. 18.13 shows this to be for a solution of about 4 g/l NaCl equivalent.

[8] Chose the correct Q_v – shale chart (Fig. 18.19 in this case for Q_v – shale = 1 meq/ml). Read off an E = 57 mV for the input of a salinity of 4 g/l NaCl equivalent and a Q_v for the formation of 0.04 meq/ml.

[9] As E_k is negative, subtract the absolute value of E_k calculated in [6] from the E value from [8]. Hence the new E = 57 - |-17| = 40 mV.

[10] Entering this into Fig. 18.19 again, and using the Q_v = 0.04 meq/ml curve, gives a formation water salinity of 9.5 g/l NaCl equivalent.

[11] This corresponds to a water resistivity R_w @ 200°F = 0.23 Ωm , from using Fig. 18.13.

18.7.5 Calculation of Shale Volume

The shale volume is sometimes calculated from the SP log using the relationship:

$$V_{sh} = \left(1 - \frac{\text{PSP}}{\text{SSP}}\right) \qquad \textbf{(18.4)}$$

PSP = SP log read in a thick homogeneous shaly sand zone, SSP = SP log read in the thick clean sand zone.

This assumes a linear mixing relationship between the SP log and shale volume, and has no theoretical basis. It probably overestimates the shale volume.

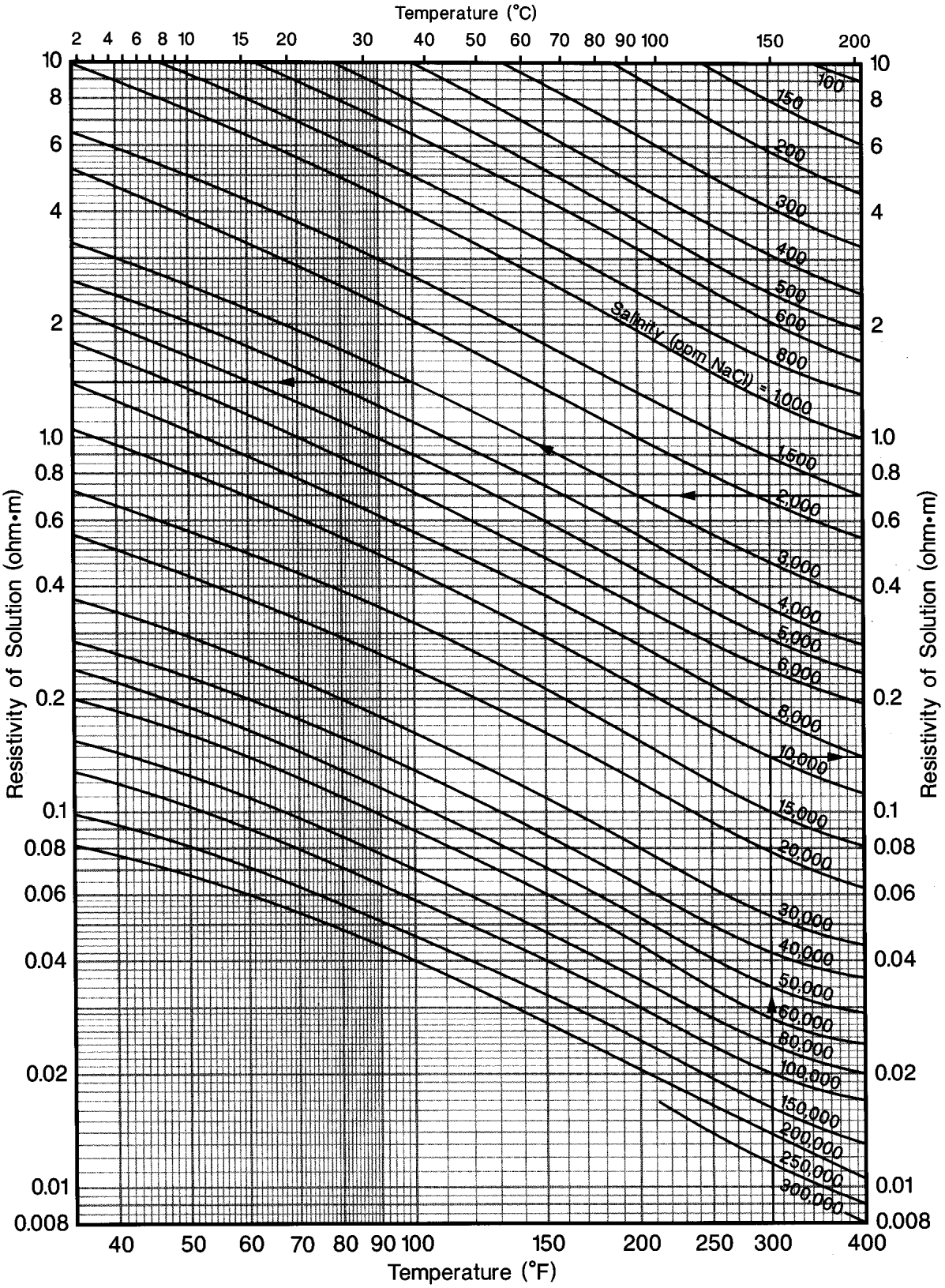

Figure 18.13 Correction chart for fluid resistivity-salinity-temperature.

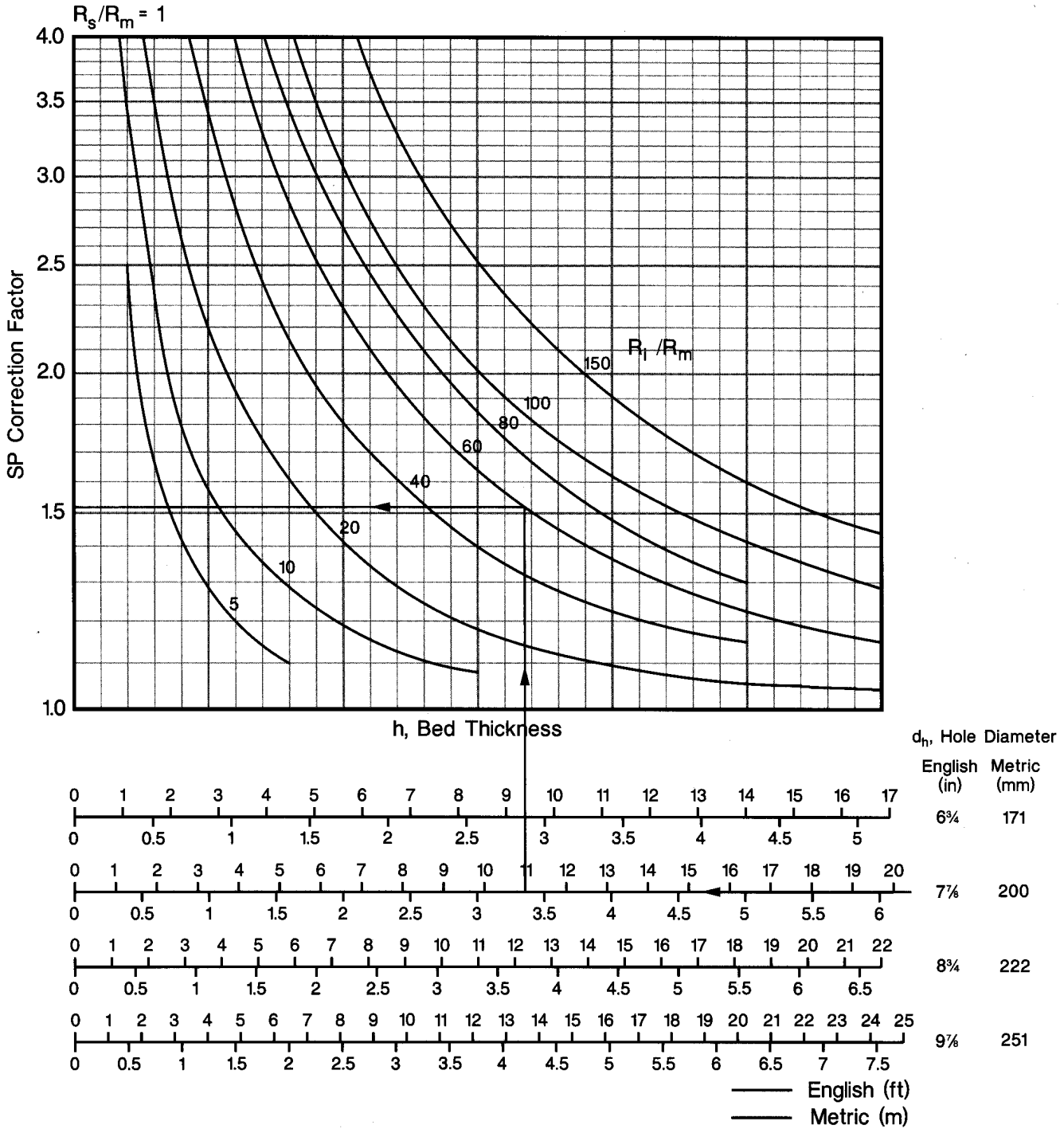

Figure 18.14 Correction chart bed thickness for diameter of invasion equals twice the borehole diameter.

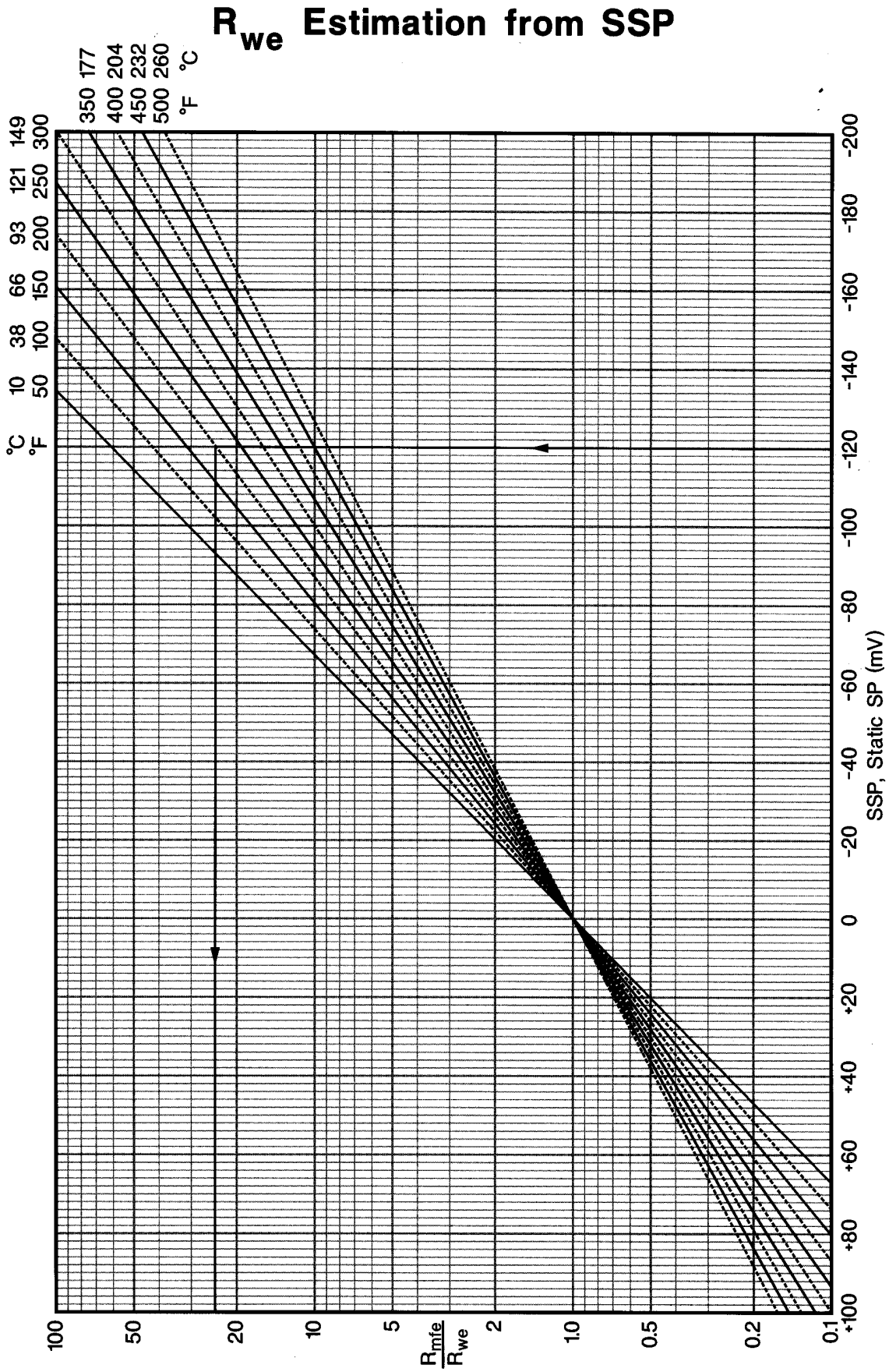

Figure 18.15 Correction chart for the R_{mfe}/R_{we} ratio from SSP for various formation temperatures.

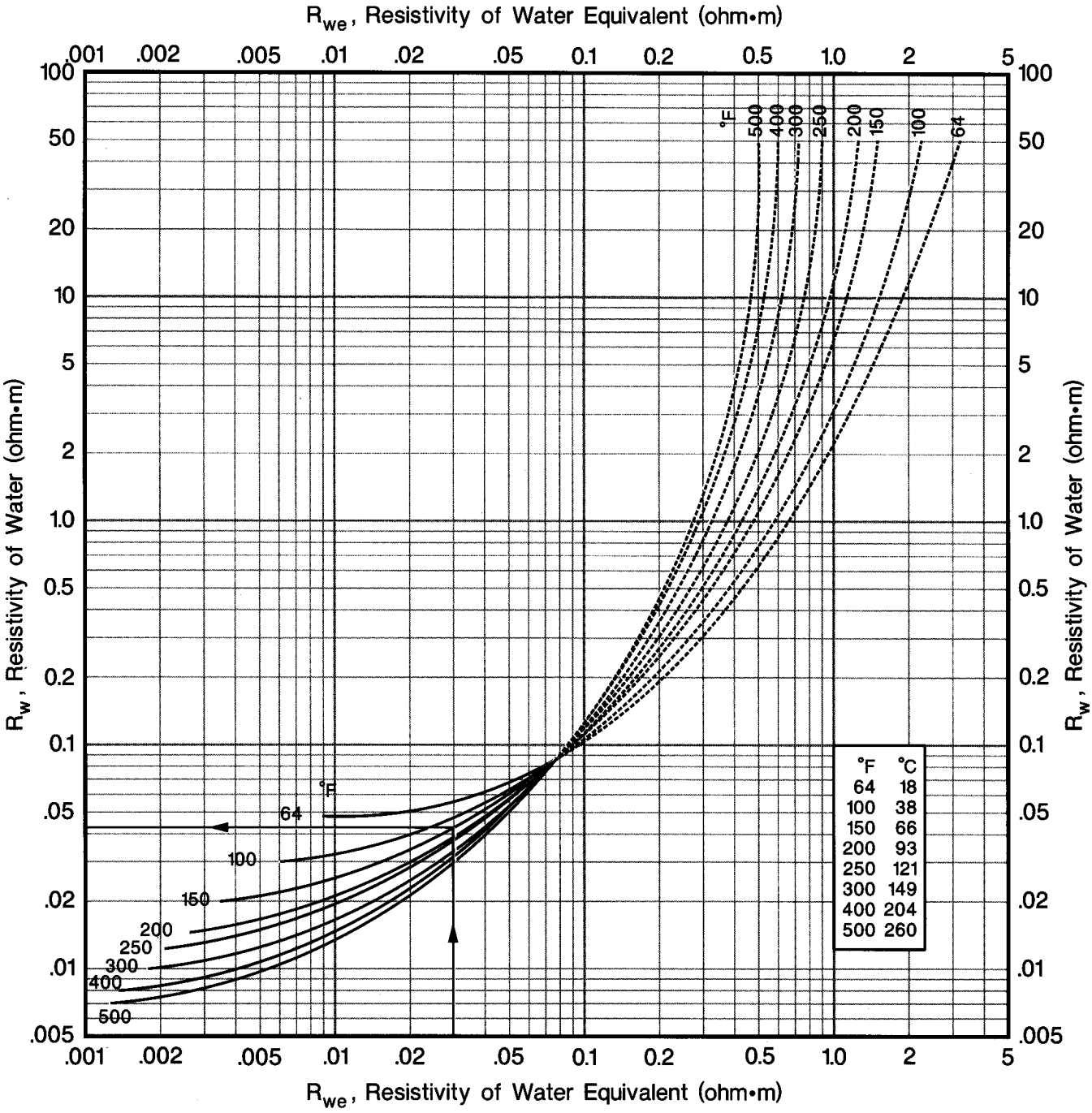

Figure 18.16 Correction chart for the R_w *from* R_{we} for various formation temperatures.

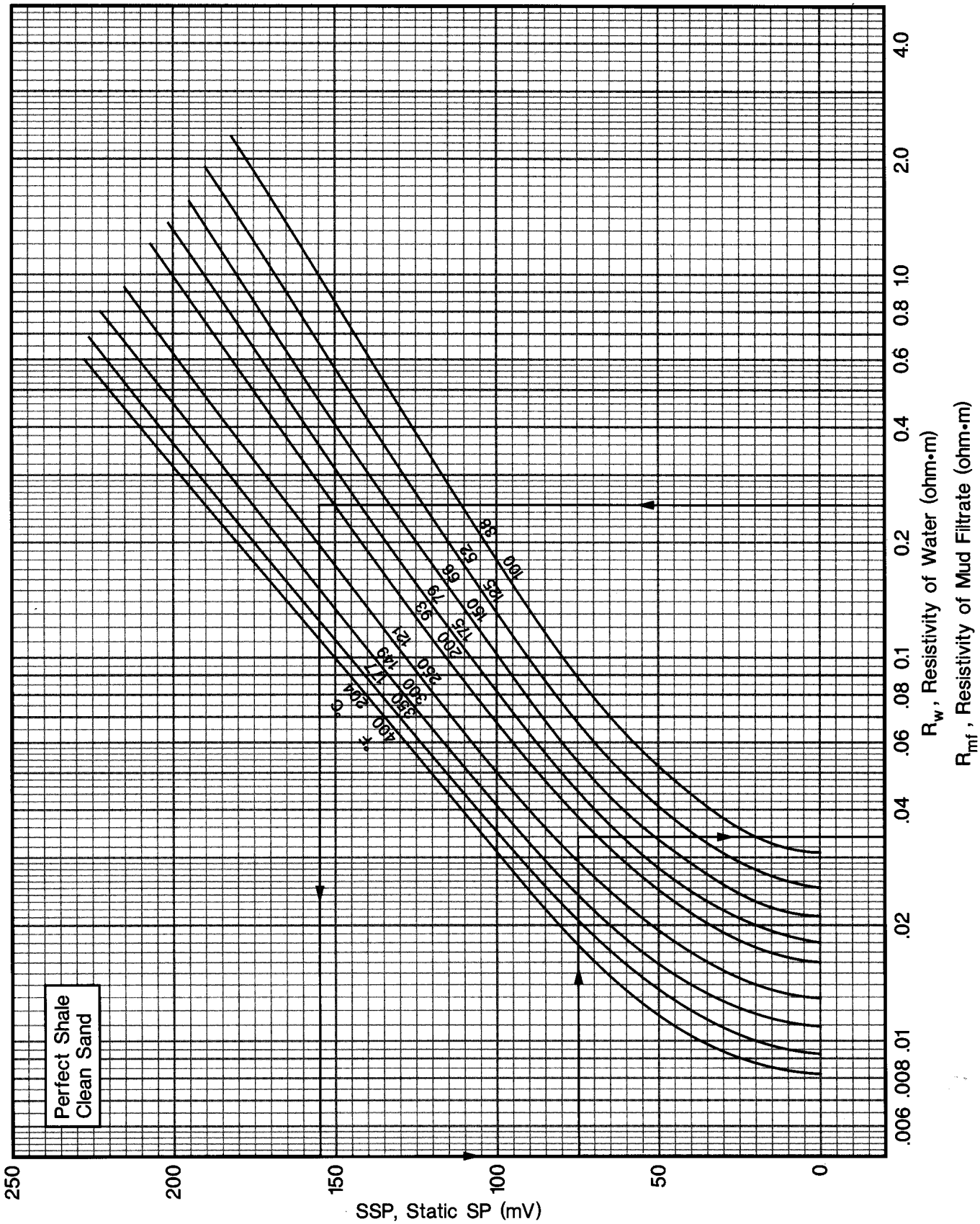

Figure 18.17 Single chart correction chart for obtaining water resistivity from SSP for various formation temperatures.

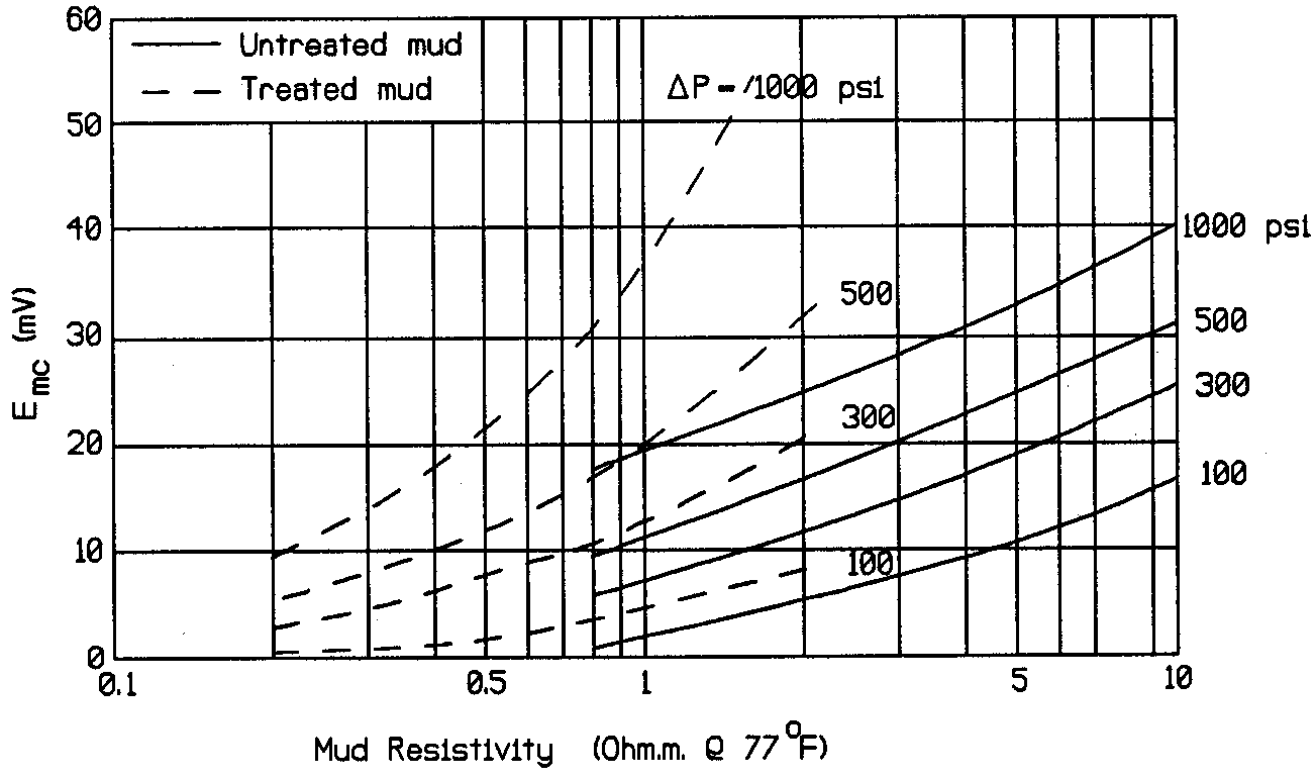

Figure 18.18 The electrokinetic mudcake potential for treated and untreated drilling muds as a function of mud resistivity for various fluid pressure differentials (mud pressure minus formation fluid pressure). This data has been derived from laboratory measurements.

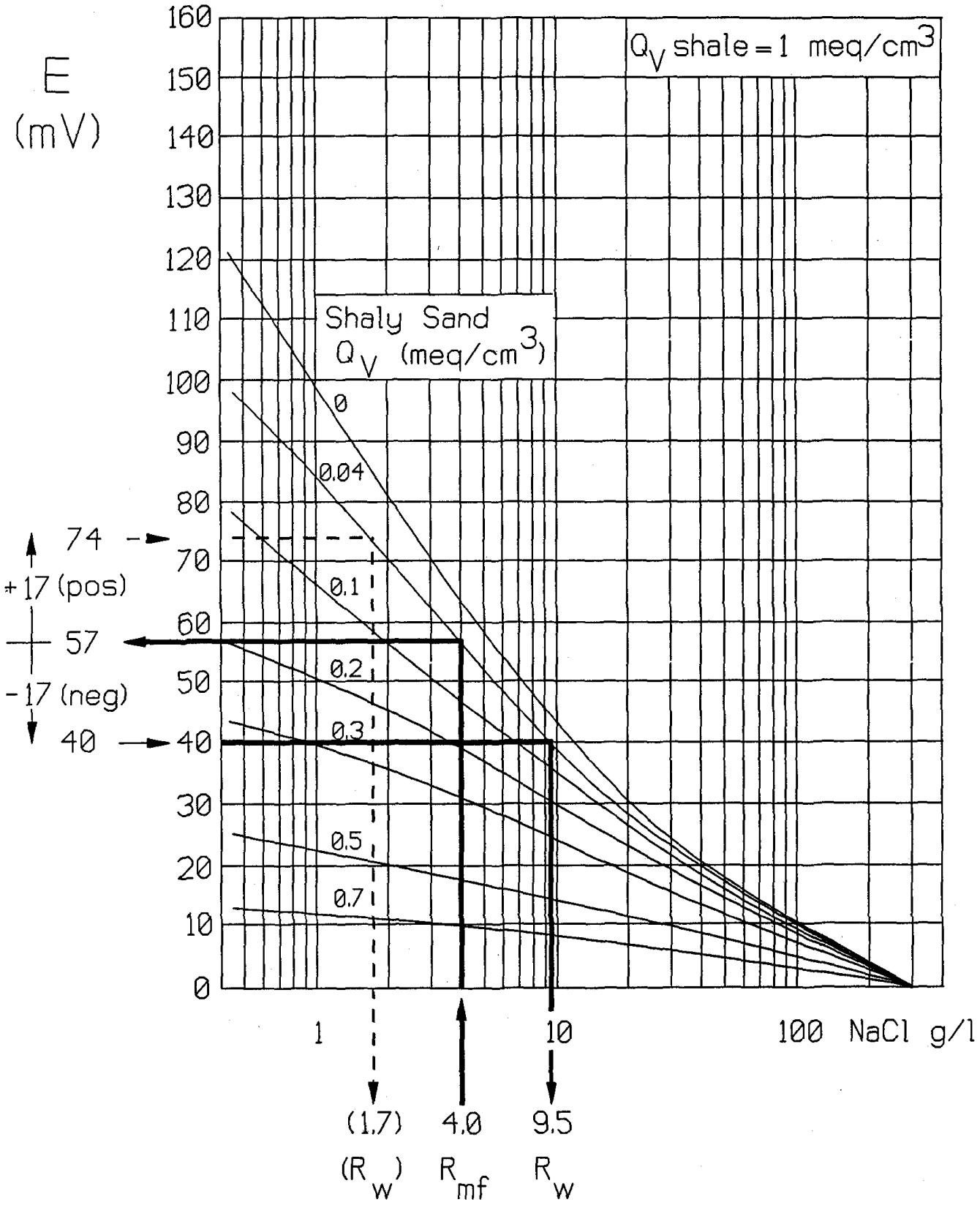

Figure 18.19 Smit method correction chart for obtaining water resistivity from SSP for various formation temperatures. This chart is for a shale Q_v = 1 meq/cm^3, and plots electrochemical potential against equivalent NaCl concentration in g/l.

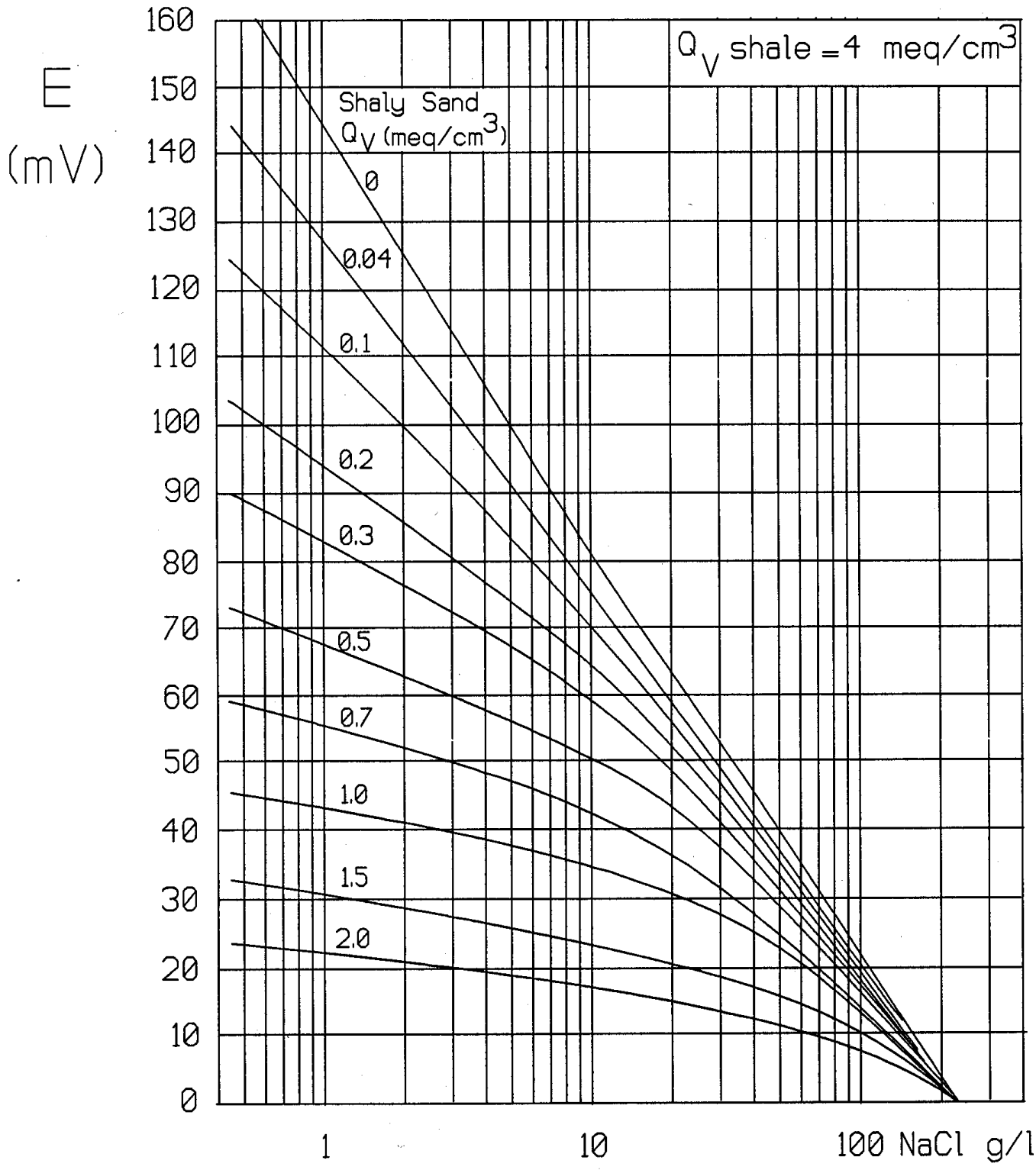

Figure 18.19 Smit method correction chart for obtaining water resistivity from SSP for various formation temperatures. This chart is for a shale Q_v = 4 meq/cm^3, and plots electrochemical potential against equivalent NaCl concentration in g/l.

19. ELECTRICAL LOGGING

19.1 Introduction

Electrical logs are perhaps the most important tools available to a petrophysicist. This is because they provide a method for calculating the water saturation, upon which calculations of STOOIP are based. They were also some of he first logs to be used, with Marcel and Conrad Schlumberger testing out an electrical log for the first time in 1927 in the Pechelbronn field, France.

These first measurements were continuous recordings using 2 or 3 electrodes and a direct current. It was discovered that high quality recordings of apparent resistivity could be obtained under favourable conditions of small diameter boreholes, high mud resistivities and shallow invasion in thick reservoirs. These early tools are called *electric logging tools*.

The development of electrical tools has henceforward been intense. There are now tools that can cope with extremely highly resistive muds (oil-based muds or gas as the borehole fluid), which rely upon electromagnetic coupling and an induced alternating current (*induction logs*). The induction log actually measures conductivity, and hence is sometimes called the *conductivity log*. The modern tool for measuring resistivity in high salinity (low resistivity) muds is the *laterolog*, which focuses its current into a thin sheet to improve vertical resolution and penetration depth. The laterologs measure resistivity in the conventional sense, and are usually referred to as *resistivity tools*. Both the induction logs and the laterologs come in different types, which are sensitive to different depths of penetration into the borehole. Hence resistivity determinations for the invaded, partly invaded and undisturbed rock zones can be measured. In addition, there is a range of smaller electrical devices (*micro-resistivity tools*), which are designed to measure the resistivity of mudcake. There are also *Array Logs*, which are state of the art tools, and electrical measurements are used at high resolutions (small scale) to image the interior of the borehole electrically.

19.2 Principle Uses of Electrical Logs

The main use of the electrical tools is to calculate the water saturation of a reservoir formation, and hence the STOOIP. Chapter 17 covered most of the important theory for this application, and Chapter 1 introduced the use of the derived values when calculating STOOIP.

The electrical tools also have a number of qualitative uses, principle of which are (i) indications of lithology, (ii) facies and electro-facies analysis, (iii) correlation, (iv) determination of overpressure, (iv) determination of shale porosity, (v) indications of compaction, and the investigation of source rocks.

19.3 Typical Responses of an Electrical Tool

Figure 19.1 shows the typical response of an electrical tool in a sand/shale sequence. Note the lower resistivity in shales, which is due to the presence of bound water in clays that undergo surface conduction. The degree to which the sandstones have higher resistivities depends upon (i) their porosity, (ii) their pore geometries, (iii) the resistivity of the formation water, (iv) the water, oil and gas saturations (oil and gas are taken to have infinite resistivity).

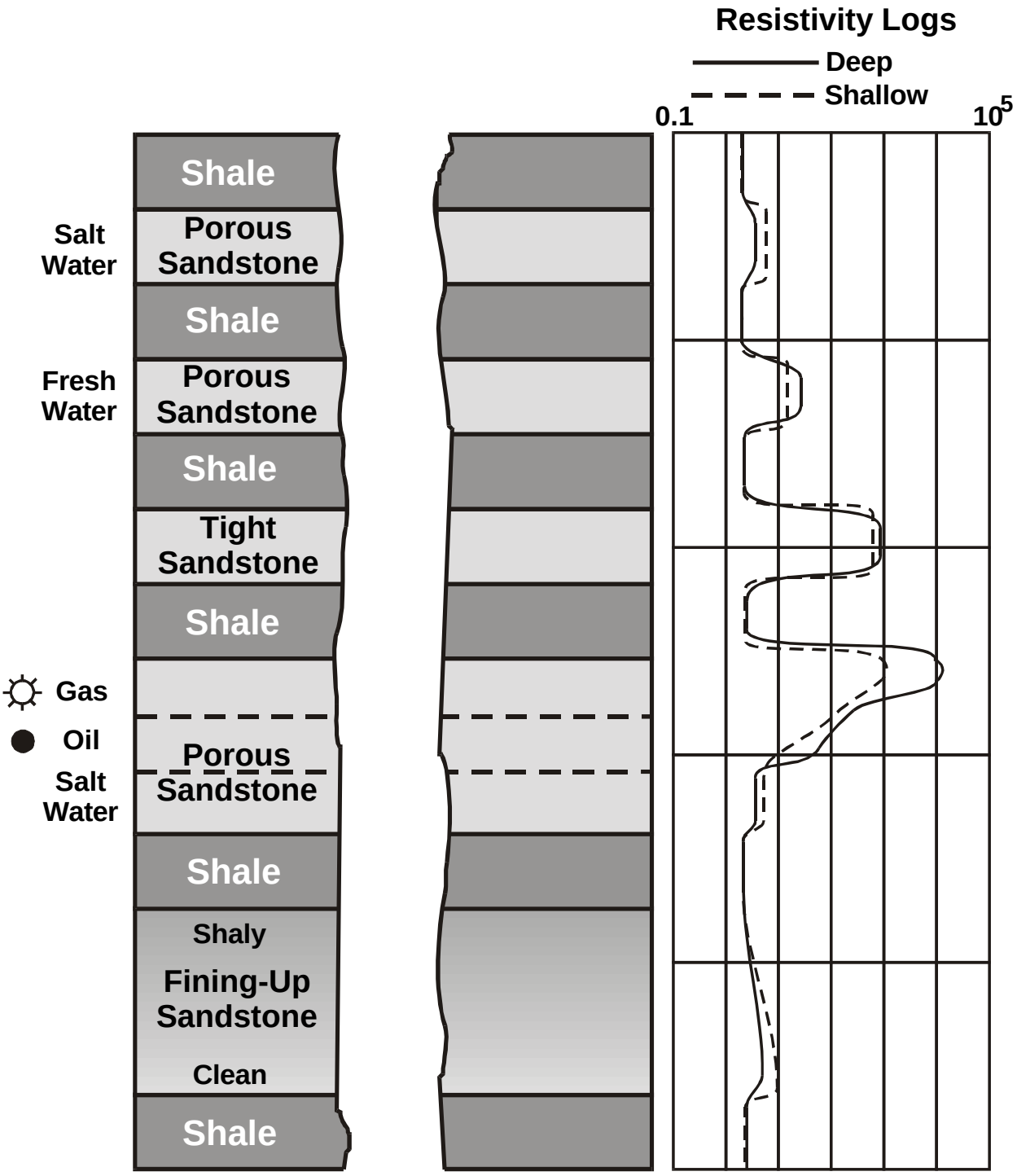

Fig. 19.1 Typical resistivity log responses.

19.4 Old Electrical Logs

These logs will be discussed briefly because data from them may still be encountered when reanalyzing mature fields.

Take an homogeneous and isotropic medium that extends to infinity in all directions. Now pass a current from an electrode A in the medium to another B infinitely distant. We take the potential of electrode A to be some value $V_A = V$, and that of electrode B to be zero, $V_B = 0$. The current will flow radially (Fig. 19.2), and generate spherical equipotential surfaces with electrode A at their centre. A third electrode M placed near A will lie on one of these equipotential surfaces, whose radius is r. If we connect electrode M to electrode B through a potential measuring device (voltmeter), it will show the value of the potential on the equipotential surface that passes through M, V_M. The resistivity of the material between A and M is the calculated as:

$$R = 4p\ r\ \frac{(V_A - V_M)}{I} = 4p\ r\ \frac{\Delta V}{I} \qquad \textbf{(19.1)}$$

Here: $\Delta V =$ the potential difference between A and M, the factor $4pr$ is defined by the geometry of the system (spherical symmetry), and it is assumed that A and M are close enough together for the current I to be constant, even though it is spreading out with distance.

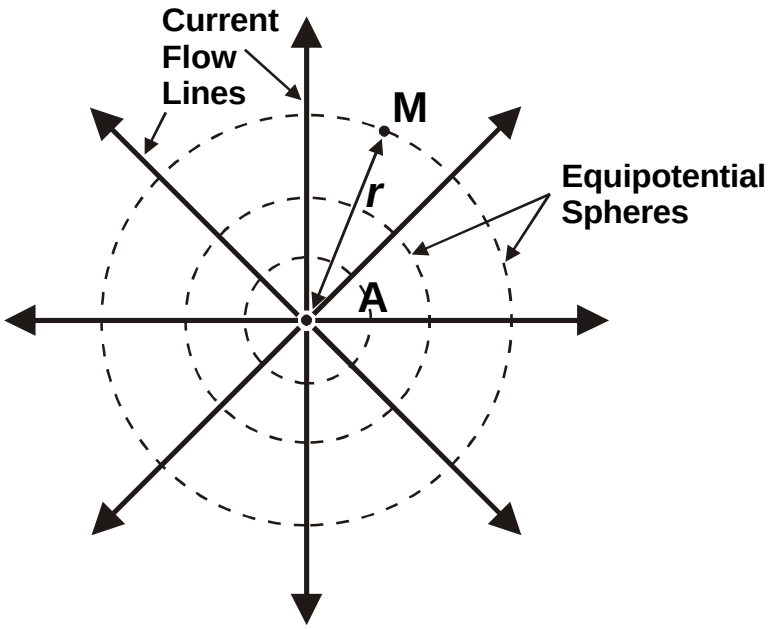

Fig. 19.2 Current flow in an homogeneous isotropic medium.

Different types of resistivity tool have different geometrical factors that depend on their electrode arrangements. These are calculated theoretically, and checked in tool calibration.

This theoretical scenario is the basis for the original tools: what are called the *normal* logging devices. The distance AM = r is called the *spacing*. Two spacings were commonly used, a *short normal spacing* equal to 16 inches, and a *long normal spacing* equal to 64 inches. The longer the spacing, the greater the depth of penetration of the current into the formation, but the lower its vertical resolution.

Although the theory is developed for 3 electrodes, and this is how the first measurements were made, a four electrode arrangement soon became standard. This allows the current flow circuit (the generator circuit in Fig. 19.3) to be separated from the potential sensing circuit (the meter circuit in Fig. 19.3), which provides better quality results. In this arrangement a constant known current is flowed from A to B (or B to A), and the potential is measured between M and N. Electrode B and N are kept at a long

distance from electrodes A and M to provide quasi-infinite reference points for the current and potential measurements.

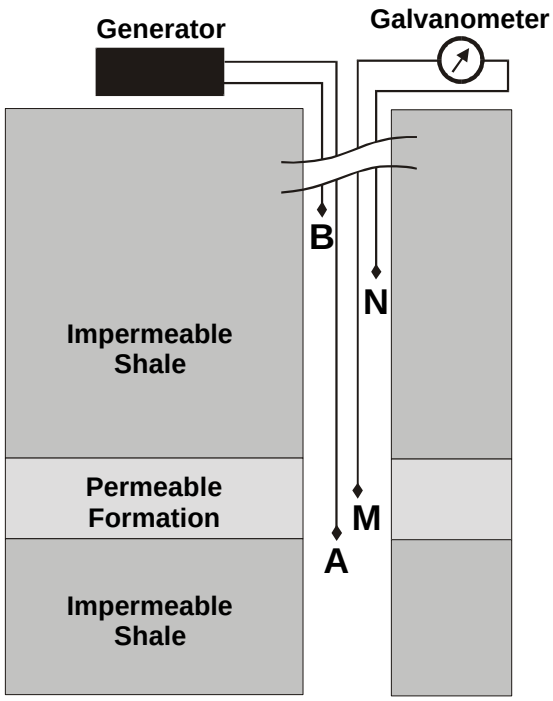

Fig. 19.3 The standard normal configuration.

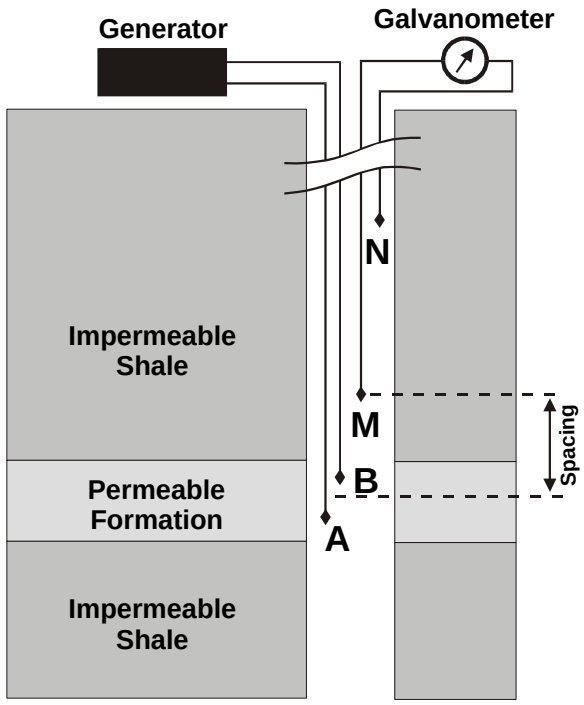

Fig. 19.4 The standard lateral configuration.

Another arrangement is possible, where electrodes A and B are placed close together with respect to the distance between A and M. This is shown in Fig. 19.4, and was called the *lateral configuration.*

19.5 Modern Resistivity Logs (Laterologs)

19.5.1 The Basic Laterologs

Figure 19.5 shows two of the earlier laterologs. Each have a number of electrodes. The LL3 has 3 current emitting electrodes. The middle one, which is 1 foot long emits the main current, while the 5 foot long electrodes either side of it emit a current that is designed to help keep the central current more focussed. This is called a *bucking current* and the electrodes are called *guard electrodes*. In this simple tool the bucking current is the same as that from the central electrode, and the potential of the central electrode is measured relative to the potential at infinity to give a potential difference. This potential difference and the known current from the central electrode are used to calculate the formation resistivity, using a known geometrical factor for the arrangement. The vertical resolution of the LL3 is 1 ft.

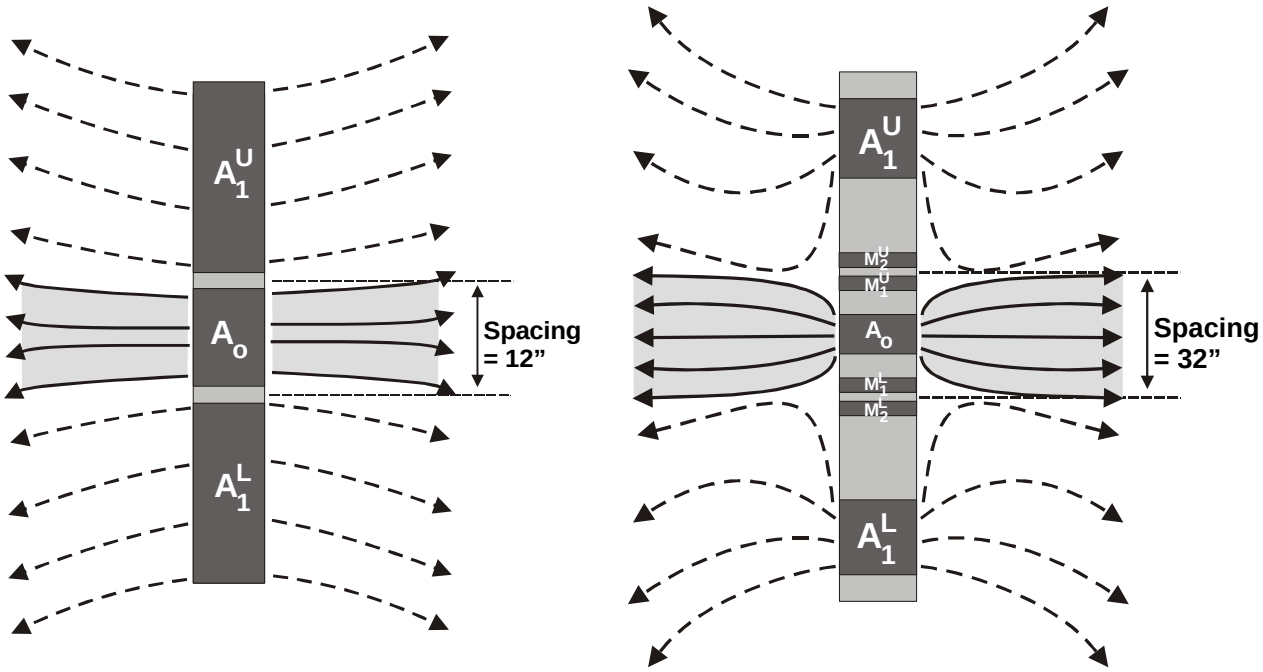

Fig. 19.5 The LL3 and LL7 tool electrode configurations.

The LL7 has 7 electrodes. A constant current is emitted from the centre electrode. A bucking current is emitted from the two far electrodes (80 inches apart), and is automatically adjusted such that the two pairs of monitoring electrodes are brought to the same potential difference. Then the current from the central electrode is focussed in a thin disk far out into the formation. The potential between one of the monitoring electrodes and the potential at infinity is then measured, and knowing the current from the central electrode allows the formation resistivity to be calculated providing the geometrical factor of the arrangement is known (calculated theoretically and tested in the calibration of the device). This electrode arrangement produces a thin disk of current that is confined between the two sets of measuring electrodes (32 inches apart). The strongly focussed beam is little affected by hole size, penetrates the invaded zone, and measures the resistivity of the virgin formation, R_t. The vertical resolution of the LL7 is 3 ft. and the sensitivity is 0.2 to 20,000 Ωm.

The LL8 is similar to the LL7, but has the current return electrode (which is not shown in Fig. 19.4 for the LL7 and LL3 because it is too far away) closer to the current emitting electrodes. This gives a current disk that does not penetrate as far into the formation before returning to the return electrode, and consequently the tool measures R_{XO} rather that R_t. The vertical resolution of the LL8 is about 1 ft and the sensitivity is 0.2 to 20,000 Ωm...

Corrections for all of these tools for borehole size, effect of invasion and thin beds are available in the form of charts from the logging companies. However, the first two of these corrections are usually minor.

19.5.2 The Dual Laterolog

The *dual laterolog* (DLL) is the latest version of the laterolog. As its name implies, it is a combination of two tools, and can be run in a deep penetration (LLd) and shallow penetration (LLs) mode. These

are now commonly run simultaneously and together with an additional very shallow penetration device. The tool has 9 electrodes, whose operation are shown in Fig. 19.6.

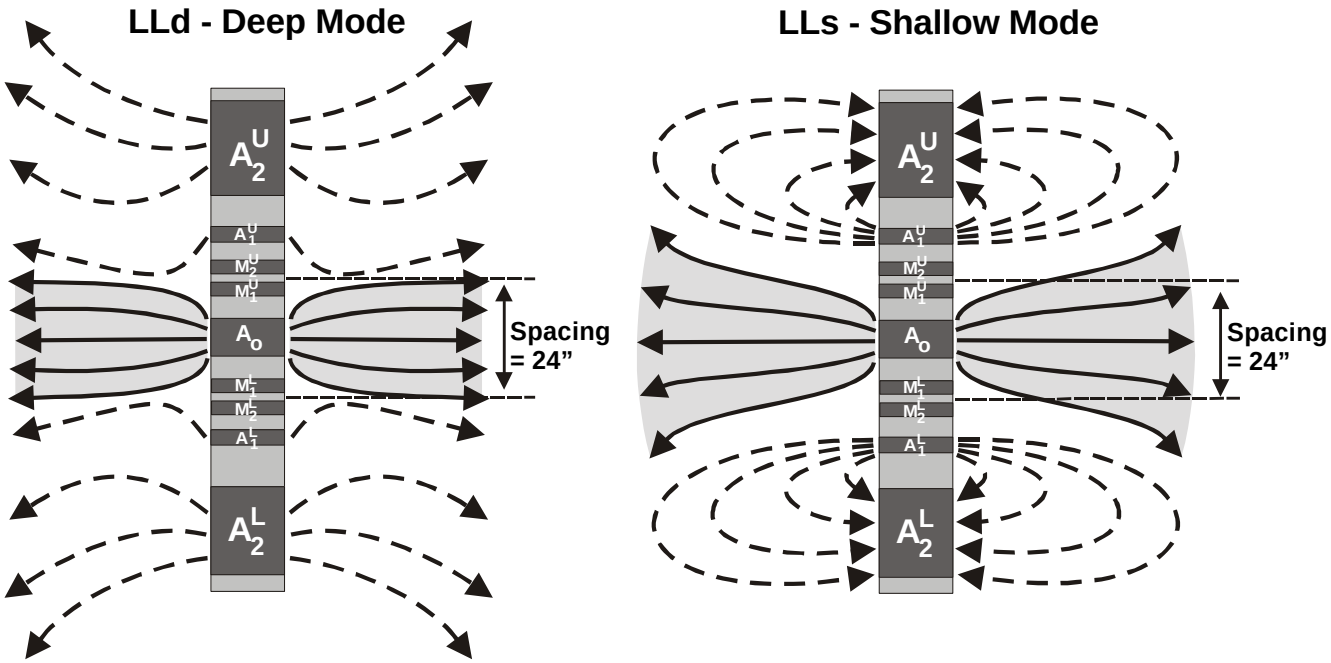

Fig. 19.6 The DLL electrode configuration in both the LLd and LLs modes.

In the LLd mode, the tool operates just like a LL7 tool but with the same bucking currents that are emitted from the A_1 electrodes also being emitted from the additional farthest electrodes, A_2. The result of this is to focus the current from the central electrode even more than was the case for the LL7.

In the LLs mode, the A_1 electrodes emit a bucking current as they did in the LL7 device, but the A_2 electrodes are set to sink this current (i.e., the bucking current comes out of A_1 and into A_2 electrodes). This means that the bucking current must veer away from the pathway into the formation, and back towards the tool A_2 electrodes, and hence cannot constrain (focus) the current being emitted from the central electrode as much. The overall result is that the central electrode current penetrates less far into the formation before it dies away.

Both modes of the dual laterolog have a bed resolution of 2 feet, and a sensitivity of 0.2 to 20,000 Ωm. To achieve this sensitivity both the current and voltage are varied during the measurement, keeping their product (the power) constant.

The dual laterolog is equipped with centralizes to reduce the borehole effect on the LLs. A micro-resistivity device, usually the MSFL, is mounted on one of the four pads of the lower of the two centralists. Hence, this tool combination examines the resistivity of the formation at three depths of penetration (deep, shallow, and very shallow).

The resistivity readings from this tool can and should be corrected for borehole effects and thin beds, and invasion corrections can be applied using the three different depths of penetration. An example of dual laterolog data is shown as Fig. 19.7.

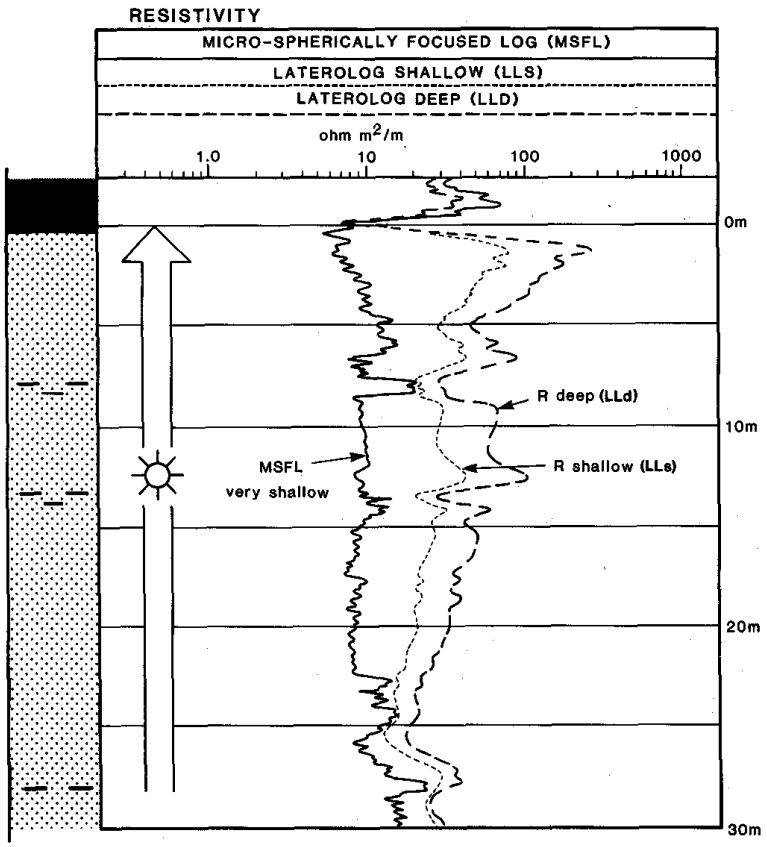

Fig. 19.7 An example of a DLL log. This shows good separation of the LLs and LLd from each other and from the MSFL, indicating the presence of a permeable formation with hydrocarbons (gas in this case in a formation of about 15% porosity). (Courtesy of Rider [1996]).

19.5.3 The Spherically Focussed Log

The *spherically focussed log* (SFL) has an electrode arrangement (Fig. 19.8) that ensures the current is focussed quasi-spherically. It is useful as it is sensitive only to the resistivity of the invaded zone.

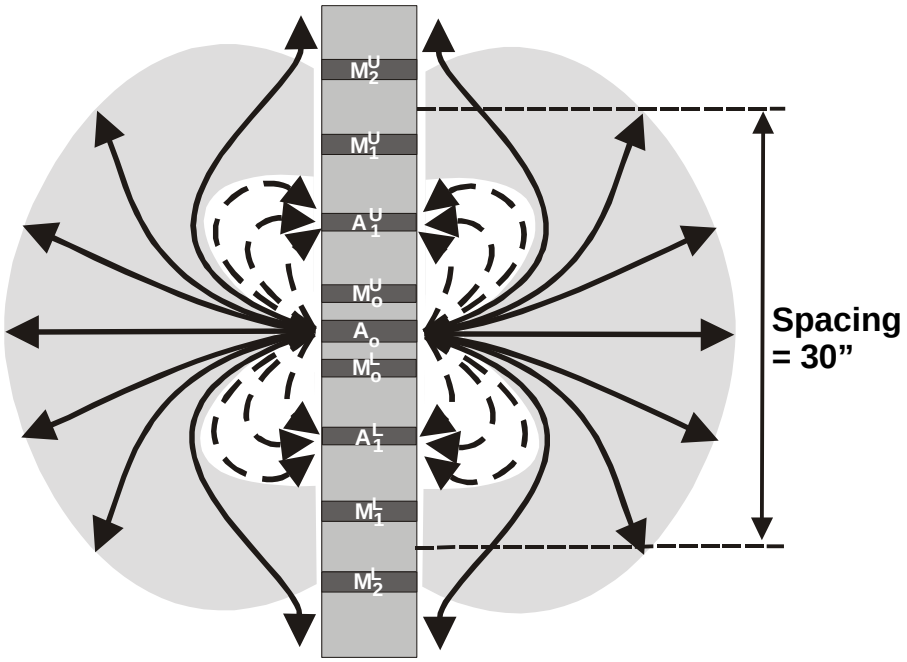

Fig. 19.8 The SFL electrode configuration.

19.6 Micro-Resistivity Logs

These are devices that often share the same sort of electrode arrangements as their larger brothers, but have electrode spacings of a few inches at most. Therefore, they penetrate the formation to a very small degree and most often do not penetrate the mudcake. They are all pad mounted devices that are pressed against the borehole wall, and often have the electrodes arranged coaxially. Combinations of these tools may be run together on the same sonde.

19.6.1 The Microlog

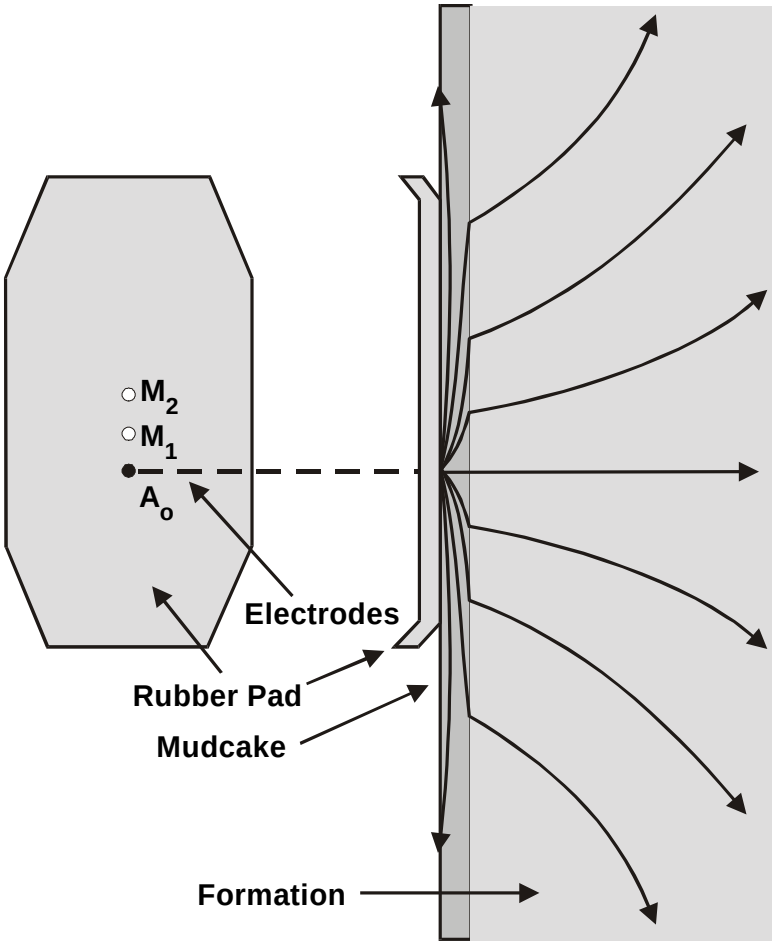

The *microlog* (ML) is a rubber pad with three button electrodes placed in a line with a 1 inch spacing (Fig. 19.9). A known current is emitted from electrode A, and the potential differences between electrodes M_1 and M_2 and between M_2 and a surface electrode are measured. The two resulting curves are called the *2" normal* curve (ML) and the *1½" inverse* curve (MIV). The radius of investigation is smaller for the second of these two curves, and hence is more affected by mudcake. The difference between the two curves is an indicator of mudcake, and hence bed boundaries. The ML tool is so good at this that it is used in making *sand counts*.

Fig. 19.9 The microlog electrode configuration.

The tool is pad mounted, and the distance across the pads is also recorded, giving an additional caliper measurement (the *micro-caliper* log). The arms of the caliper are kept in the fully collapsed state when inserting the tool into the hole. However, the microlog is recorded during this insertion to give a log of mud resistivity R_m with depth and at the BHT. Figure 19.10 shows an example of the *microlog-caliper* (MLC) showing beds clearly on both the microlog and the caliper traces.

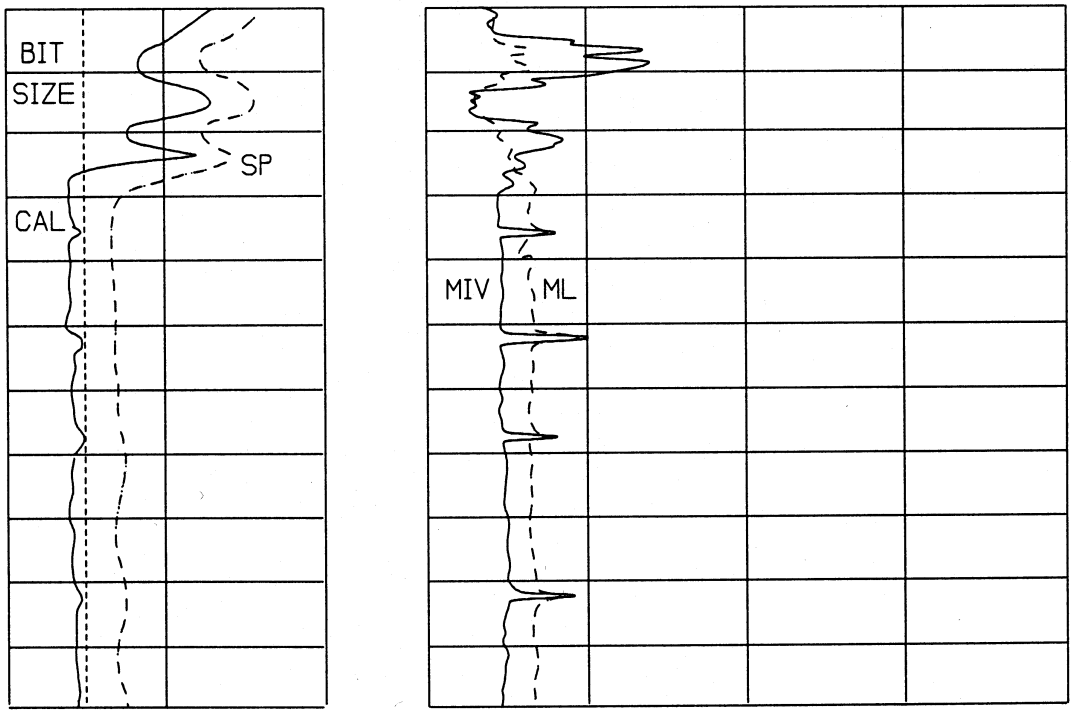

Fig. 19.10 An example of a MLC log showing mudcake from both the caliper and ML logs.

19.6.2 The Microlaterolog

The *microlaterolog* (MLL) is the micro-scale version of the laterolog, and hence incorporates a current focussing system. The tool is pad mounted, and has a central button electrode that emits a known measurement current surrounded coaxially by two ring-shaped monitoring electrodes, and a ring-shaped guard electrode that produces a bucking current as in the DLL (Fig. 19.11). The spacing between electrodes is about 1 inch.

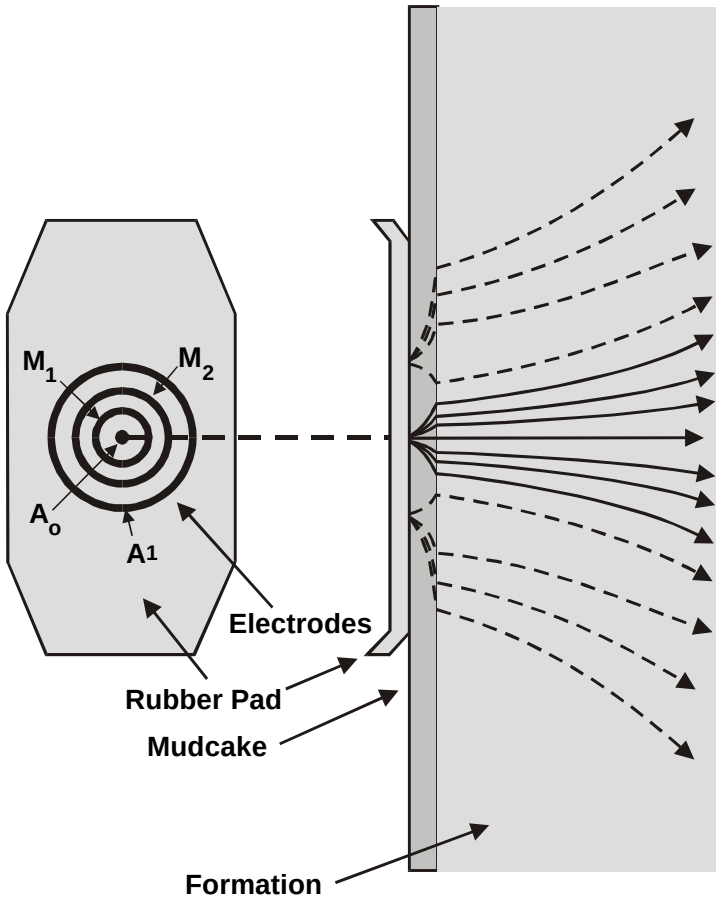

Fig. 19.11 The MLL electrode configuration.

The tool operates in the same way as the LL7. The focussed current beam that is produced from the central electrode has a diameter of about 1½ inches and penetrates directly into the formation. The influence of mudcake is negligible for mudcakes less than $^3/_8$" thick, and in these conditions R_{XO} can be measured. The depth of investigation of the MLL is about 4 inches.

19.6.3 The Proximity Log

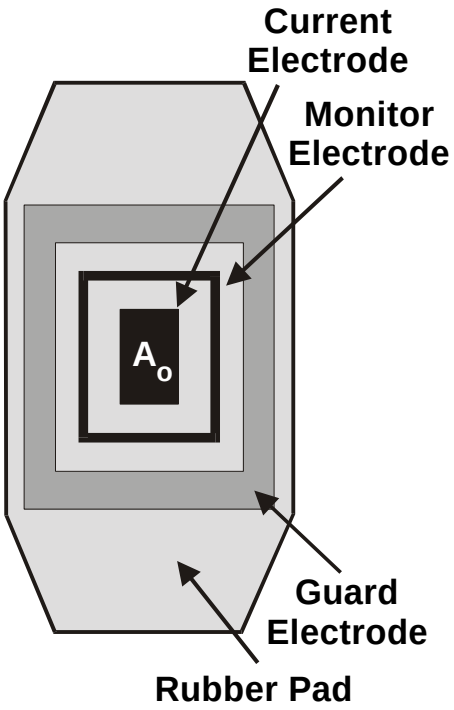

The *proximity log* (PL) was developed from the MLL to overcome problems with mudcakes over $^3/_8$" thick, and is used to measure R_{XO}. The device is similar, except that it is larger than the MLL and the functions of the central electrode and the first monitoring ring electrode are combined into a central button electrode. The device has a coaxial oblong shape (Fig. 19.12). The tool operates in a similar fashion to the LL3. It has a depth of penetration of 1½ ft., and is not affected by mudcake. It may, however, be affected by R_t when the invasion depth is small.

Fig. 19.12 The PL electrode configuration.

19.6.4 The Micro Spherically Focussed Log

The *micro spherically focussed log* (MSFL) is commonly run with the DLL on one of its stabilizing pads for the purpose of measuring R_{XO}. It is based on the premise that the best resistivity data is obtained when the current flow is spherical around the current emitting electrode (isotropic conditions). The tool consists of coaxial oblong electrodes around a central current emitting button electrode (Fig. 19.13).

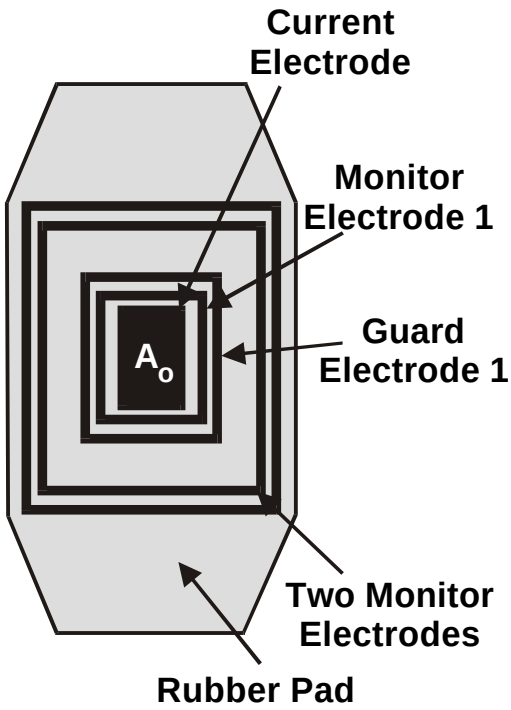

Fig. 19.13 The MSFL electrode configuration.

The current beam emitted by this device is initially very narrow (1”), but rapidly diverges. It has a depth of penetration of about 4” (similar to the MLL). The initial narrowness of the current beam means that its sensitivity to mudcake is somewhere between the MLL and the PL, and is not significantly affected by mudcake less than ¾” thick.

19.7 Induction Logs

These logs were originally designed for use in boreholes where the drilling fluid was very resistive (oil-based muds or even gas). It can, however, be used reasonably also in water-based muds of high salinity, but has found its greatest use in wells drilled with fresh water-based muds.

The sonde consists of 2 wire coils, a transmitter (Tx) and a receiver (Rx). High frequency alternating current (20 kHz) of constant amplitude is applied to the transmitter coil. This gives rise to an alternating magnetic field around the sonde that induces *secondary currents* in the formation. These currents flow in coaxial loops around the sonde, and in turn create their own alternating magnetic field, which induces currents in the receiver coil of the sonde (Fig. 19.14). The received signal is measured, and its size is proportional to the *conductivity* of the formation. Clearly there will be direct coupling of the transmitter coil and the receiver coil signals. This is removed by additional coils, which also serve to improve the vertical and depth of penetration focussing of the tool.

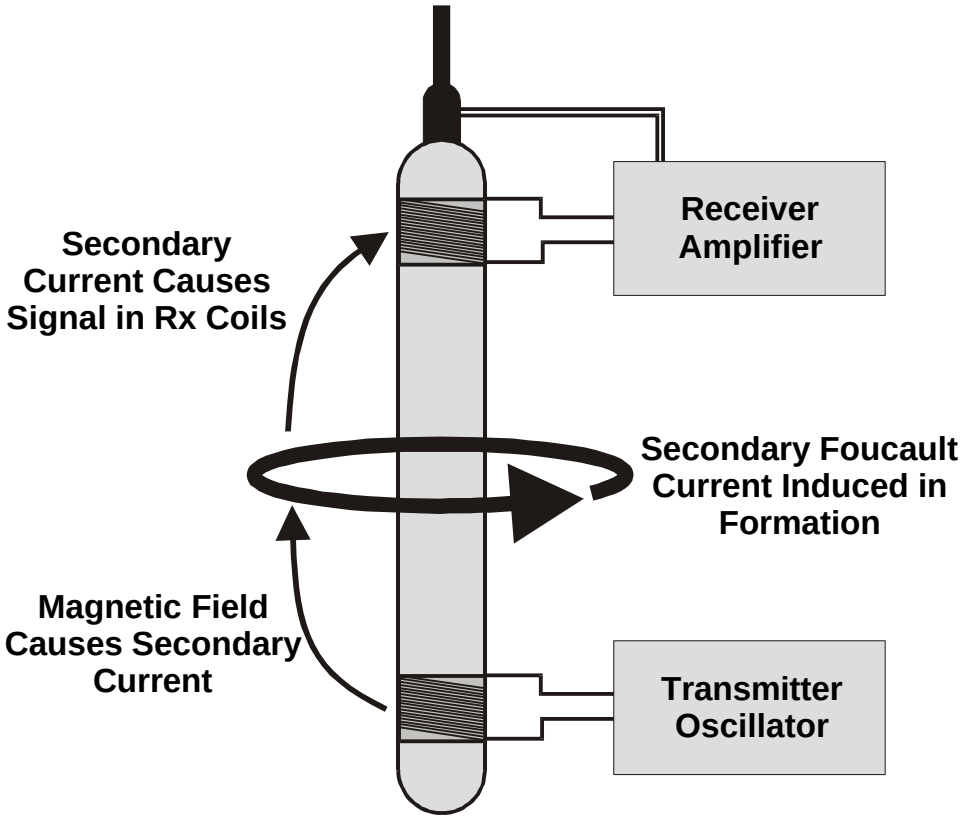

Fig. 19.14 The mode of operation of induction tools.

The intensity of the secondary currents generated in the formation depends upon the location in the formation relative to the transmitter and receiver coils. Hence there is a spatially varying *geometrical factor* to take into account. Figure 19.15 shows two ground loops of secondary current induced by the transmitter and sensed by the receiver. The actual signal recorded by the receiver will be the sum of all ground loops in the space investigated by the tool. Figure 19.16 shows the sensitivity map for this space for a homogeneous medium, showing that 50% of the total signal comes from close to the tool (borehole and invaded zone) between the transmitter and the receiver.

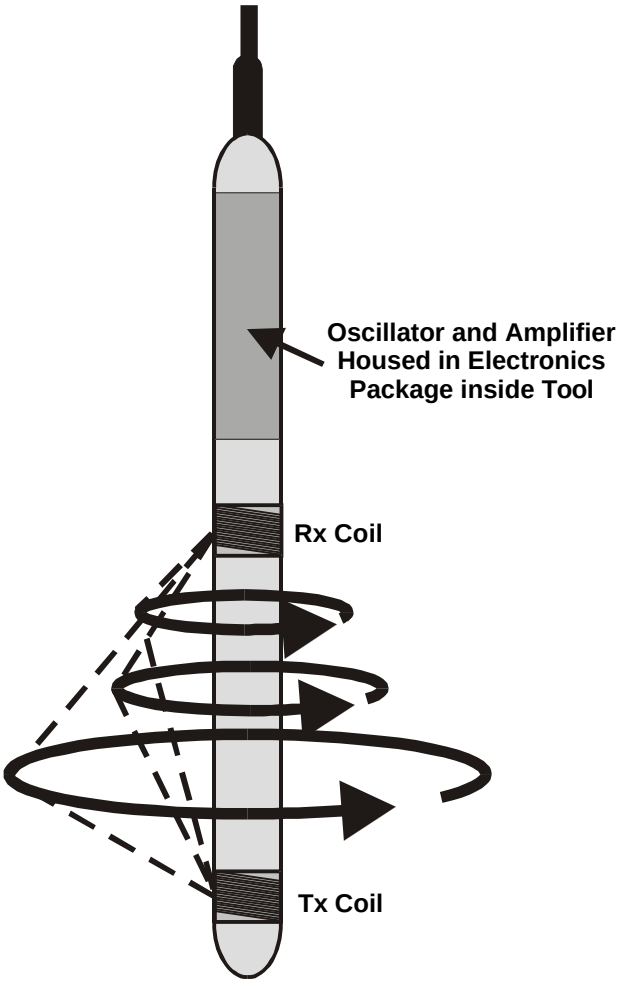

The *skin effect* is a problem that occurs with very conductive formations which results in the reduction of the signal. This is automatically corrected for during the logging run.

Induction logs are calibrated at the wellsite in air (zero conductivity) and using a 400 mS test loop that is placed around the sonde. The calibration is subsequently checked in the well opposite zero conductivity formations (e.g., anhydrite), if available.

Fig. 19.15 The integration of ground loop data in the construction of the received induction signal.

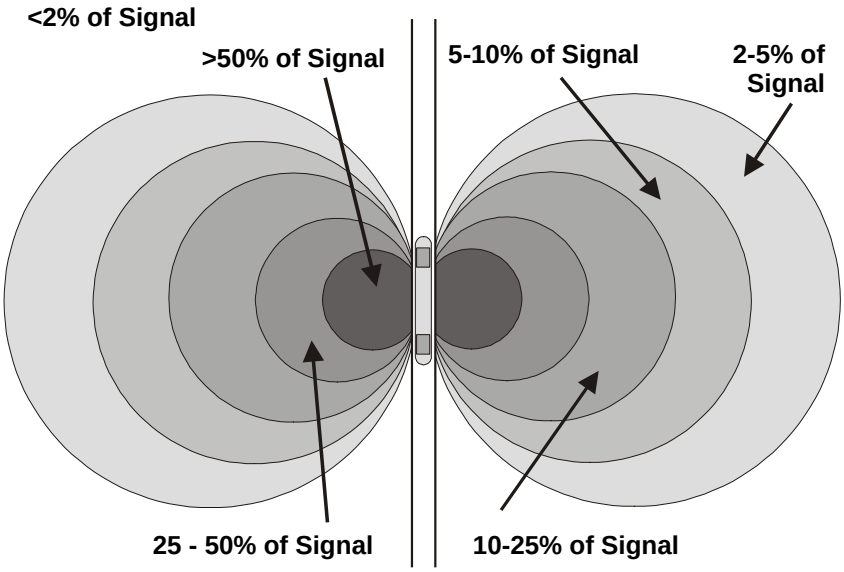

Fig. 19.16 Sensitivity map for induction tools.

The following tools are in common use today.

19.7.1 The 6FF40 Induction-Electrical Survey Log

The *6FF40 induction-electrical survey log* (IES-40) is a 6 coil device with a nominal 40 inch Tx-Rx distance, a 16 inch short normal device and an SP electrode. An example of its data is given as Fig. 19.17.

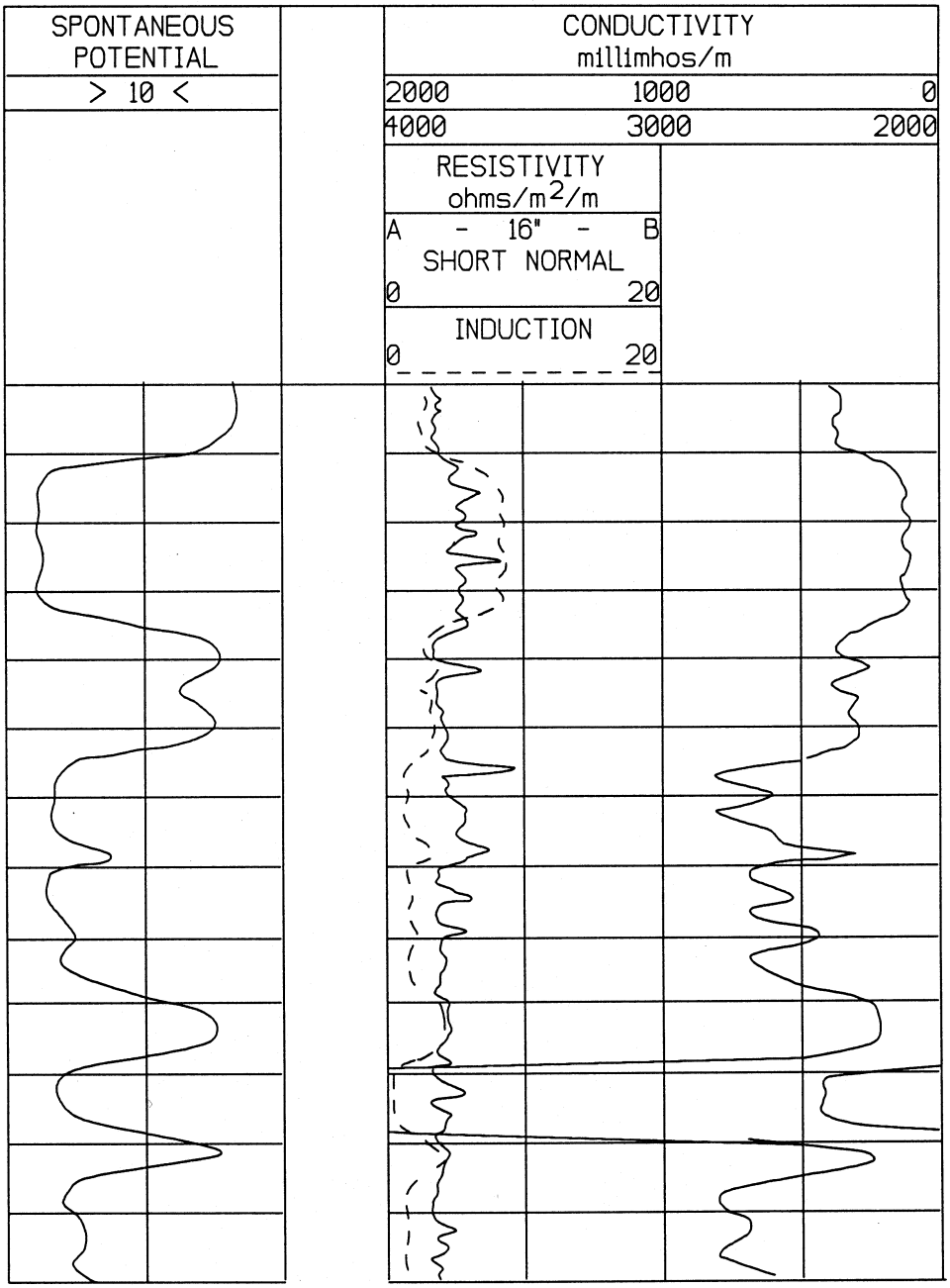

Fig. 19.17 An example of 6FF40 (IES-40) log data.

19.7.2 The 6FF28 Induction-Electrical Survey Log

The *6FF28 induction-electrical survey log* (IES-28) is a smaller scale version of the IES-40. It is a 6 coil device with a nominal 28 inch Tx-Rx distance, a 16 inch short normal device and an SP electrode.

19.7.3 The Dual Induction-Laterolog

The *dual induction laterolog* (DIL) has several parts: (i) a deep penetrating induction log (ILd) that is similar to the IES-40, (ii) a medium penetration induction log (ILm), a shallow investigation laterolog (LLs) and an SP electrode. The ILm has a vertical resolution about the same as the ILd (and the IES-40), but about half the penetration depth. An example of its data is given as Fig. 19.18.

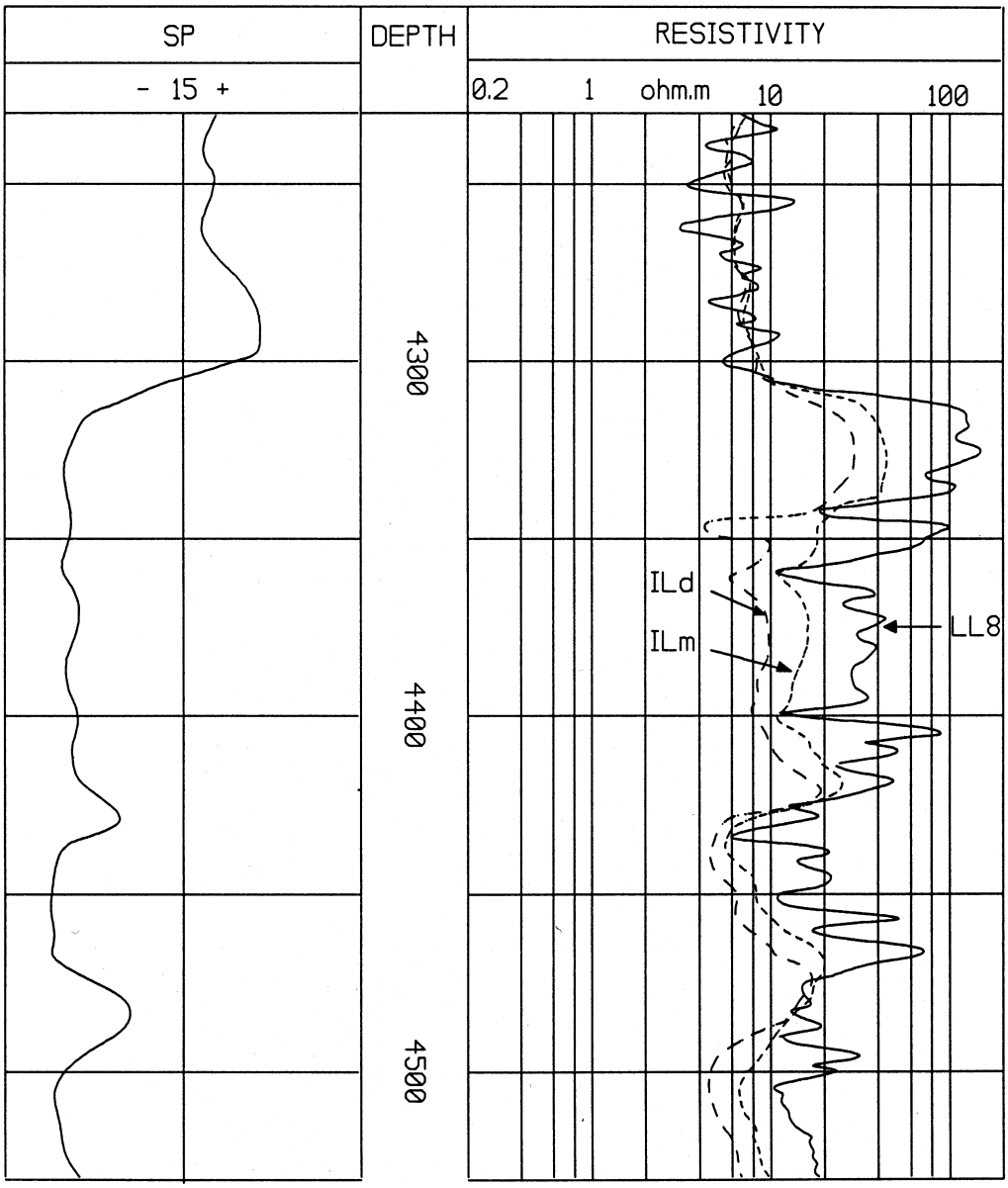

Fig. 19.18 An example of DLL log data.

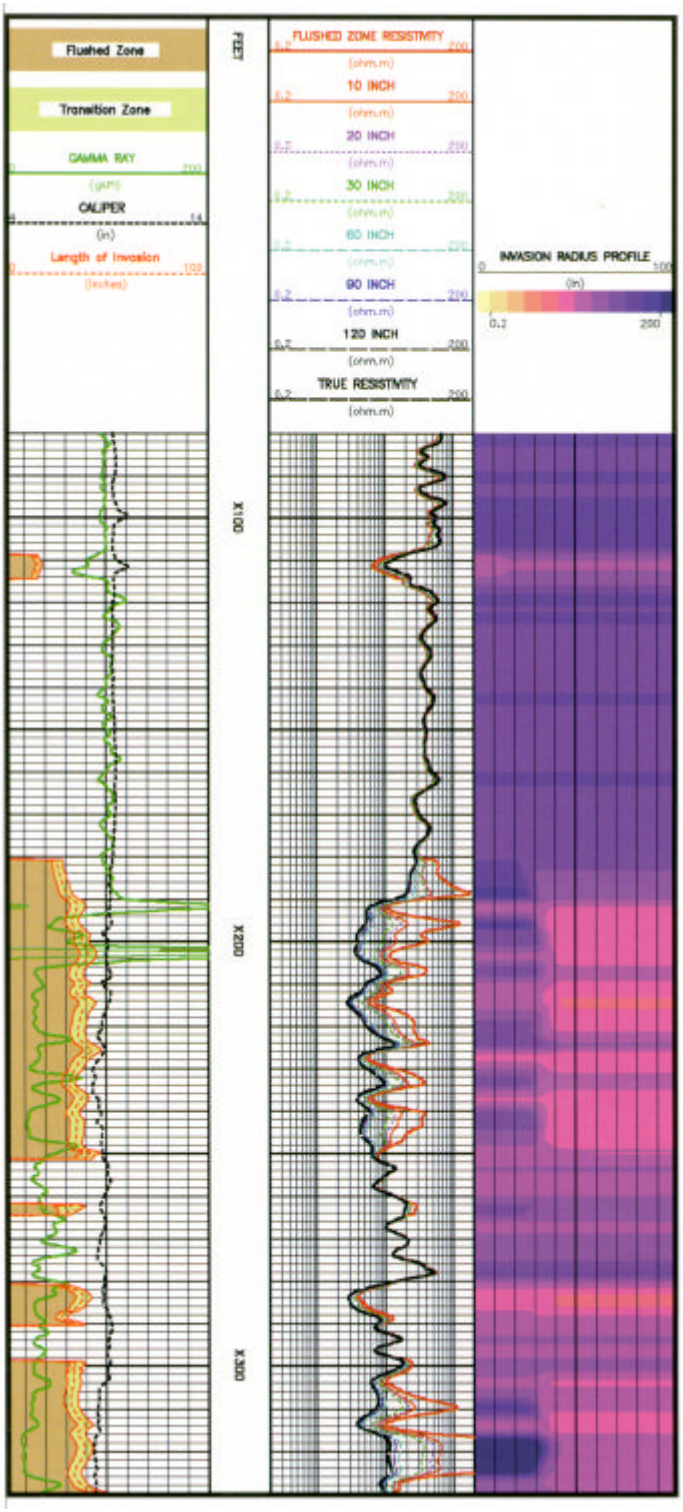

Fig. 19.19 An example of array induction log (HDIL) showing curves for different penetration depths as well as the calculated invasion profiles and extent of the flushed and transition zones in permeable beds (courtesy of Baker Atlas Ltd).

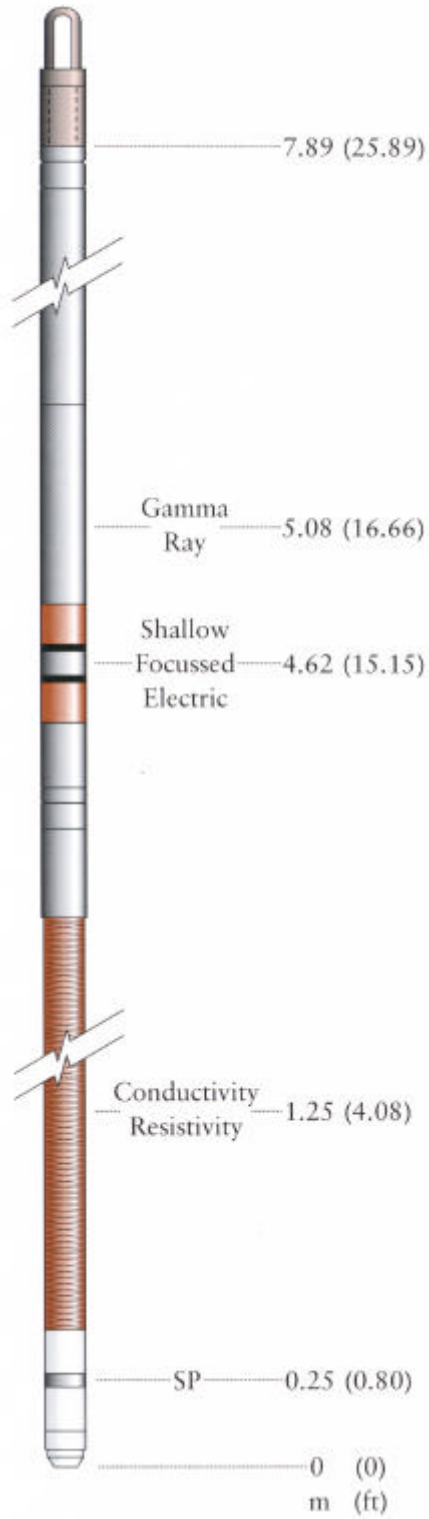

Fig. 19.20 The Array Induction data Sonde (AIS) of BPB Wireline Technologies Ltd. (BPB Wireline Technologies Ltd.).

19.7.4 The Induction Spherically Focussed Log

The *induction spherically focussed log* (ISF) combines (i) a IES-40, (ii) a SFL, and (iii) an SP electrode. It is often run in combination with a sonic log.

19.7.5 Array Induction Tools

The newest logs are *array induction logs* (AIS, HDIL). It consists of one Tx and four Rx coils. Intensive mathematical reconstruction of the signal enables the resistivity at a range of penetration depths to be calculated, which allows the complete invasion profile to be mapped. An example of array induction tool data is given as Fig. 19.19, while Fig. 19.20 shows a typical tool.

19.8 Comparing Laterologs and Induction Logs

At first sight it seems that induction logs and laterologs are complimentary:

- Induction logs provide conductivity (that can be converted to resistivity).
- Laterologs provide resistivity (that can be converted to conductivity).
- Induction logs work best in wells with low conductivity fluids.
- Laterologs work best in wells with low resistivity fluids.
- Both logs provide a range of depths of penetrations and vertical resolutions.

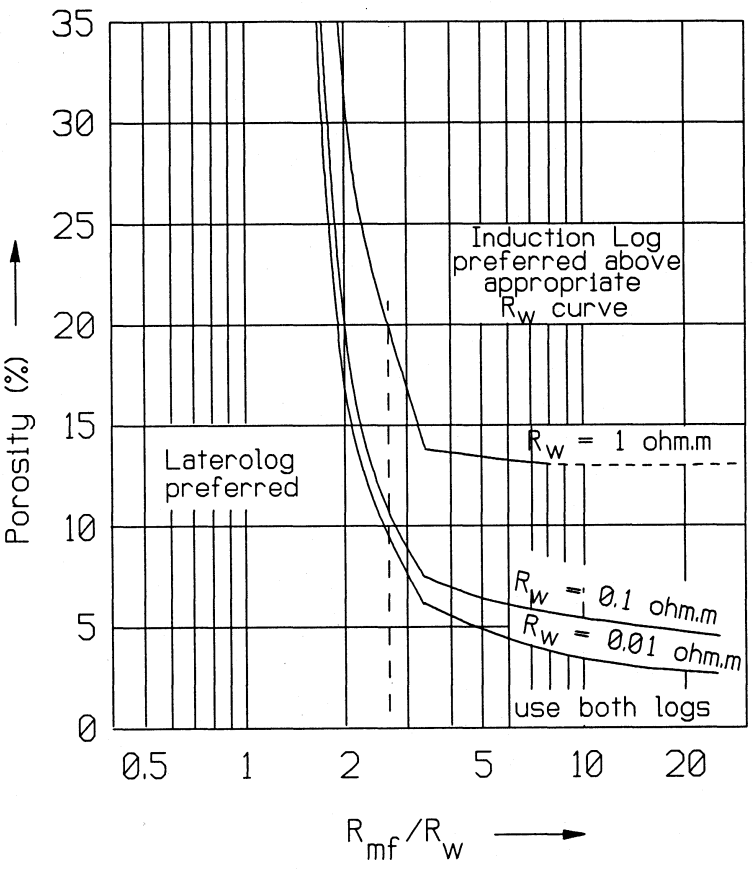

The decision to use one or the other depends upon the value of R_t/R_{XO} ratio, with the cut-off made at about 2.5 (Fig. 19.21).

Fig. 19.21 Chart showing the optimal tools to use as a function of R_w, R_{mf} and porosity.

19.9 Bed Resolution

The smaller the electrode spacing, the better the vertical and bed resolution. This is shown in Fig. 19.22. One should chose the tool for the purpose required, and this is related also to investigation depth. This is discussed further in the following section.

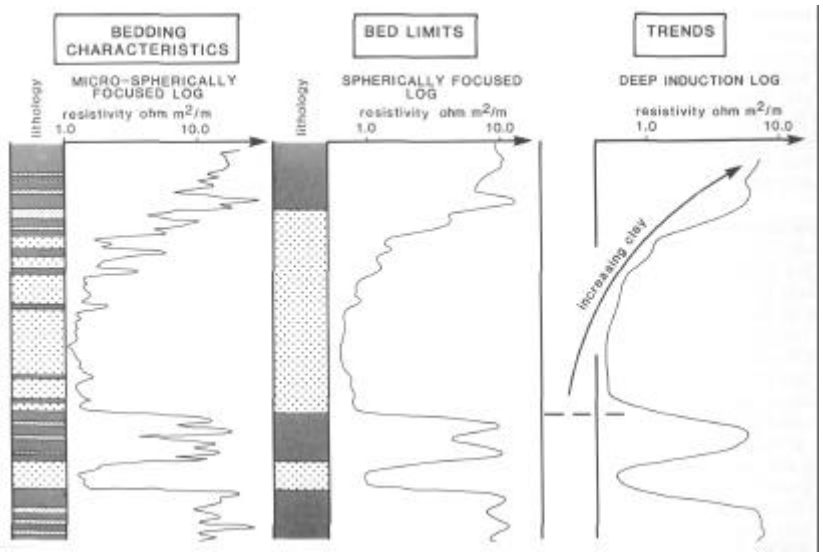

Fig. 19.22 Differences in bed resolution from different electrical tools (courtesy of Rider [1996]).

19.10 Investigation Depth

Figure 19.23 summarizes the depths of investigation of the various tools, and Table 19.1 summarizes the resistivity values commonly measured.

In general, the tool to use is that best suited for the purpose. If gross changes are needed, such as in certain types of correlation and shale compaction trends, the deeper looking tools should be used. If characteristics and values from formations which are relatively thin are needed, them a shallower looking tool with a better resolution should be used.

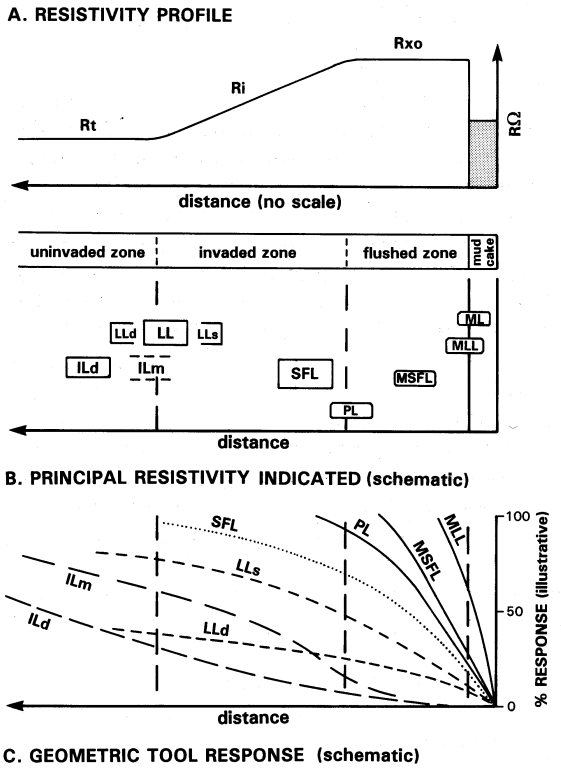

Fig. 19.23 Summary of the different depths of investigation for different electrical tools (courtesy of Rider [1996]).

Fine bed structure requires very shallow reading tools in order to obtain sufficient bed resolution. Changes in formation microstructure (texture) are best seen on logs that measure the invaded zone. This is because the texture of the rock is a significant parameter controlling the replacement efficiency of the formation fluids with the mud filtrate, and hence changes in the texture have a large effect on the degree of invasion, that is picked up by these medium depth penetration logs.

Table 19.1 Electrical tool penetration and resistivity measurements.

Tool	Mnemonic	Type	Commonly Measured	Possibly Measured
Laterolog3	LL3	Borehole	R_i	R_t
Laterolog7	LL7	Borehole	R_t	-
Dual Laterolog – deep	DLL-LLd	Borehole	R_t	-
Dual Laterolog – shallow	DLL-LLs	Borehole	R_i	R_t
Spherically Focussed Log	SFL	Borehole	R_i	R_t
Microlog - normal	ML	Pad	R_{mc}	R_{XO}
Microlog - inverse	MIV	Pad	R_{mc}	R_{XO}
Microlaterolog	MLL	Pad	R_{XO}	R_{mc}
Proximity Log	PL	Pad	R_{XO}	R_i
Micro Spherically Focussed Log	MSFL	Pad	R_{XO}	-
IES-40	IES-40	Borehole	R_t	-
IES-28	IES-28	Borehole	R_i	R_t
Dual Induction Log – deep	DIL-ILd	Borehole	R_t	-
Dual Induction Log - medium	DIL-ILm	Borehole	R_i	R_t
Induction Spherically Focussed Log	ISF	Borehole	R_t	-
Array Induction Tool	AIS, HDIL	Borehole	R_i to R_t	N/A

19.11 Log Presentation

Resistivity logs are presented in Track 2 or in Tracks 2 and 3 combined on a log scale. The units are Ωm, and sensitivity scales of 0.2-20 Ωm (3 log cycles) all the way up to 0.2 to 20,000 Ωm (6 log cycles) can be used. The scales are usually narrower if only Track 2 is used (e.g., 0.2-20 Ωm). A combination of deep, medium and shallow logs is usually available in the same track on the same scales so that a direct comparison can be made. It is possible to have data from both resistivity-type and induction-type tools shown together, and in this case it is usual to convert the conductivity readings from the induction devices to resistivities for display (although the opposite is also possible (converting resistivities to conductivities for display) it is rarely seen). If the conductivity from induction-type logs is displayed, the units are millimho per metre (mmho/m) and the scale is usually 0 – 2000 mmho/m (note the SI equivalent of mmho/m is millisiemens per metre, mS/m). The ML log is usually plotted in Track 2 over a range of 0 – 10 Ωm for both the micro-normal and micro-inverse curve. Array logs generally have six or seven curves, presented in terms of resistivity over an appropriate log scale. Figure 19.24 shows some typical log presentations for electrical logs.

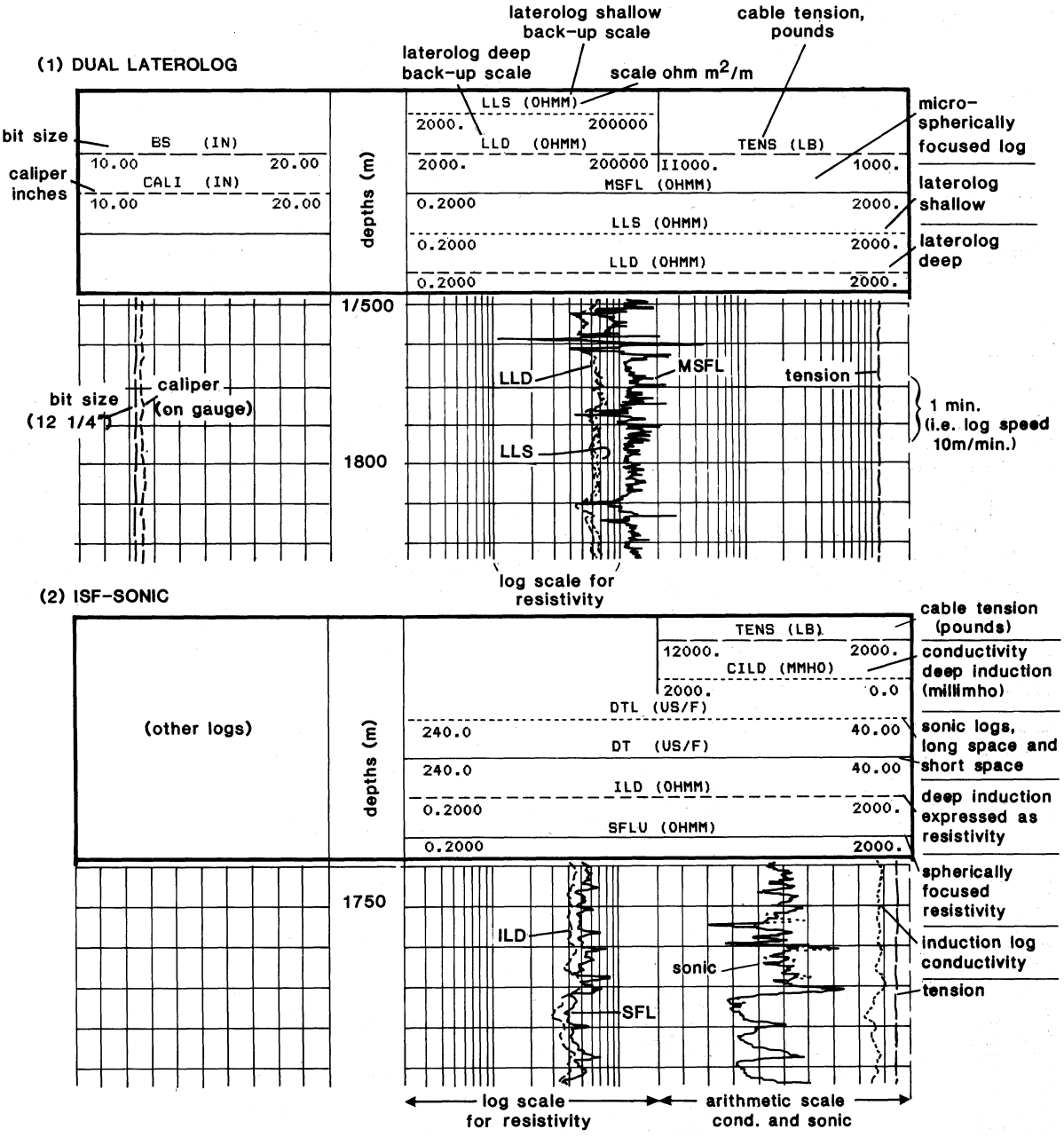

Fig. 19.24 The presentation of electrical logs (courtesy of Rider [1996]).

19.12 Uses of Electrical Logs

19.12.1 Recognition of Hydrocarbon Zones

Recognition of oil and gas in reservoir rocks is carried out by:

- Oil shows in the mud log.
- Noting a difference in the shallow, medium and deep resistivity tool responses.

Figure 19.25 shows the characteristics that are being looked for schematically.

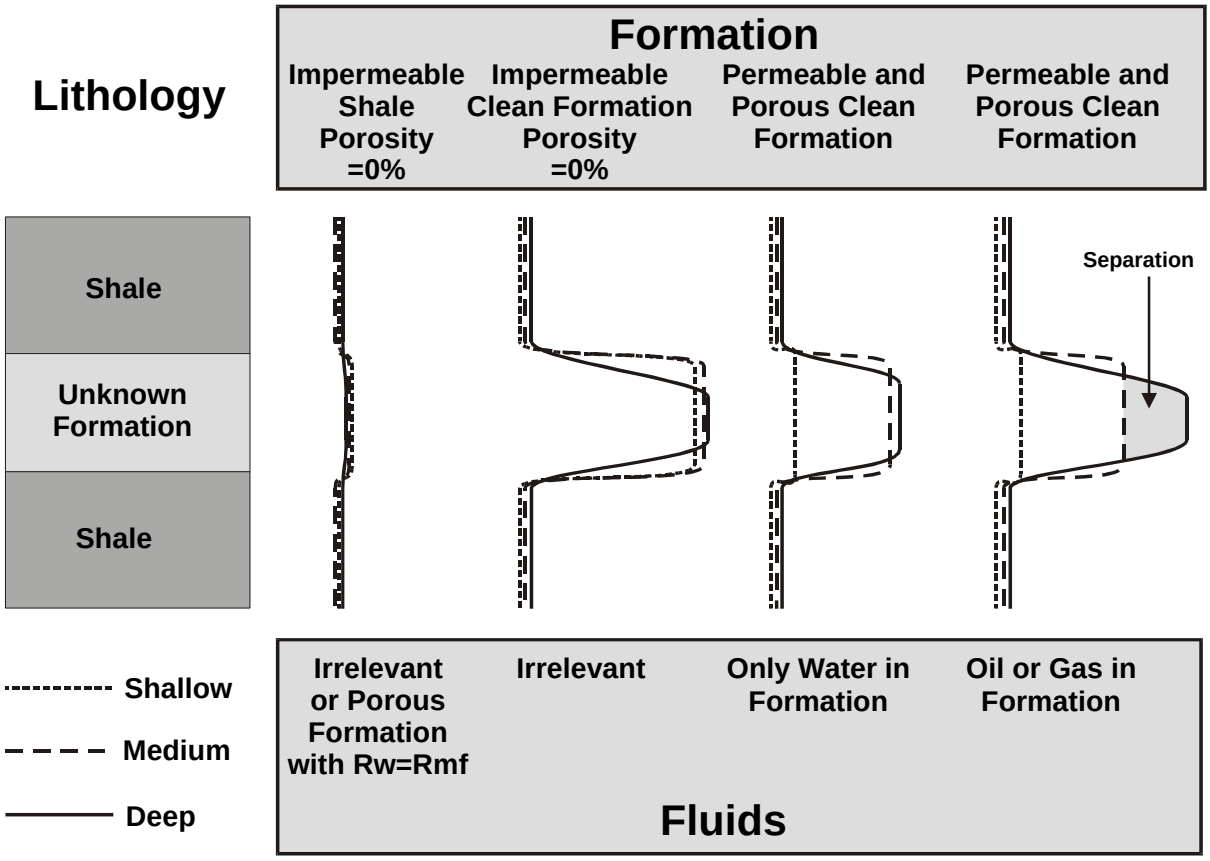

Fig. 19.25 The response of resistivity logs in formations with various fluids (recognition of hydrocarbon zones).

- If all three curves are low resistivity, and overlie each other, the formation is an impermeable shale, or, rarely, the formation is permeable and water-bearing but the mud filtrate has the same resistivity as the formation water.

- If all three curves are higher resistivity than the surrounding shales, and overlie each other, the formation is an impermeable cleaner formation (sandstone, limestone).

- If the shallow curve has low resistivity, but the medium and deep penetrating tools have a higher resistivity that is the same (they overlie each other), the formation is permeable and contains only formation water.

- If the shallow curve has low resistivity, the medium as a higher resistivity, and the deep one has an even higher resistivity (i.e., there is separation of the medium and deep tool responses), the formation is permeable and contains hydrocarbons.

Note 1: If the mud filtrate resistivity is constant, the effect is greater for formations with fresh formation waters than those for saline formation waters (Fig. 19.26), and in the case of extremely saline formation waters the deep resistivity in the formation can be smaller than that of the adjacent shale beds.

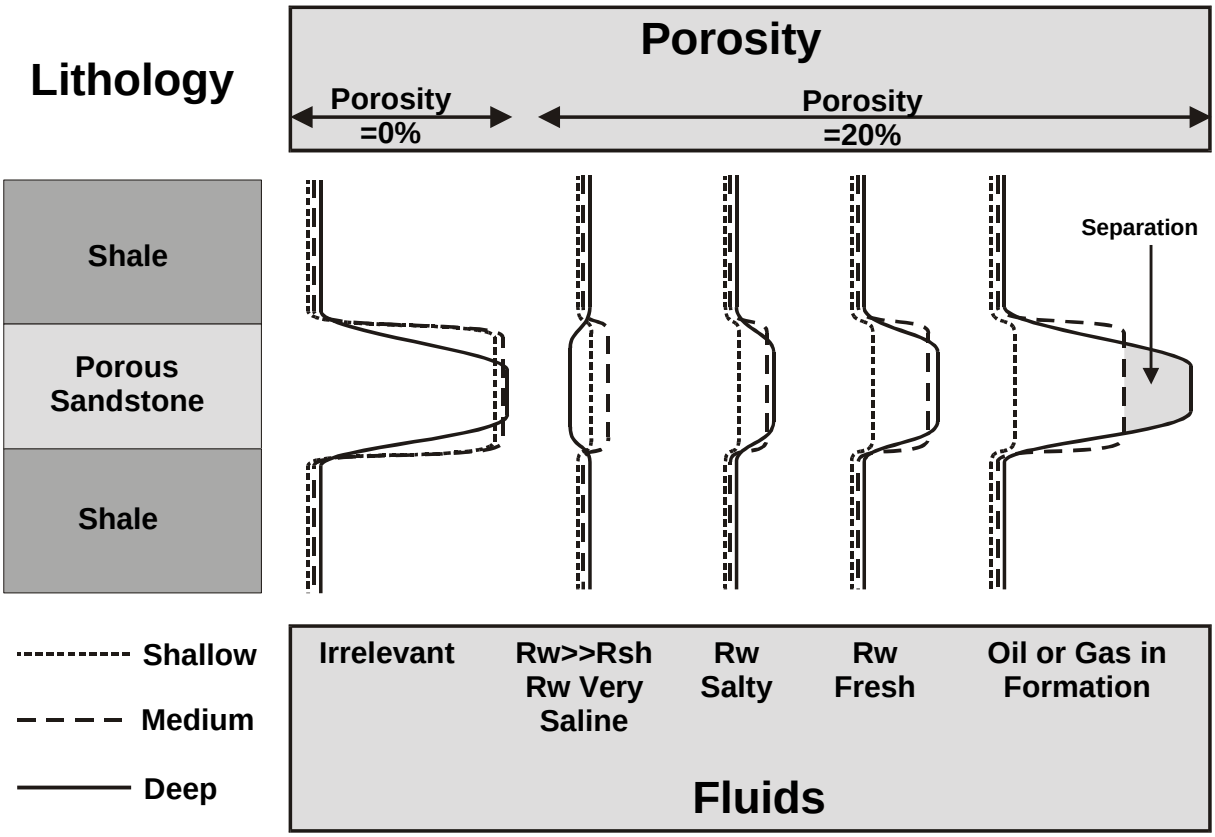

Fig. 19.26 The behaviour of the resistivity log responses for different formation water salinities.

Note that the effect is greater for oil-based drilling muds than fresh water-based muds and saline water-based muds in this order.

Some of the more advanced array type tools can now calculate the invasion profile of resistivity. An example of this is shown in Fig. 19.19, where the resistivity of the formation is shown as a function of depth into the formation in Track 3 as a colour coded map, and the interpreted flushed and transition zones are given in Track 1 for the permeable intervals.

Figures 19.25 and 19.26 are given as examples only. This is because there are too many variable parameters (mud filtrate resistivity, mudcake resistivity, formation water resistivity, water and hydrocarbon saturations, lithology and porosity etc.) to be comprehensive. In general, the best approach is to (i) see what type of tools have been used to create the logs, (ii) discover their penetration depths, (iii) discover the type of drilling mud and the resistivity of the mud filtrate used in the drilling, (iv) take account of information from other logs (caliper for mudcake, SP for permeable zones, gamma ray for shale volume, and sonic, neutron and density tools for porosity), and then interpret the resistivity curves from first principles!

19.12.2 Calculation of Water Saturation

The theory behind the calculation of water saturation from resistivity logs was given in Chapter 17 in detail. In summary, the resistivity log values for the deep tools R_t in reservoir intervals can be used with a reliable porosity f, the formation water resistivity R_w, and m and n values that are derived from laboratory measurements on core, to calculate the water saturation in the zone. This is combined with

information about the reservoir thickness, its area and porosity, and fluid compression factors in STOOIP calculations to calculate the amount of oil in the reservoir (Chapter 1).

19.12.3 Textures and Facies Recognition

The texture of a rock has a great effect upon its electrical response, all other factors being equal. This is because the electrical flow through the rock depends upon the tortuosity of the current flow paths, which is described by the formation factor *F*.

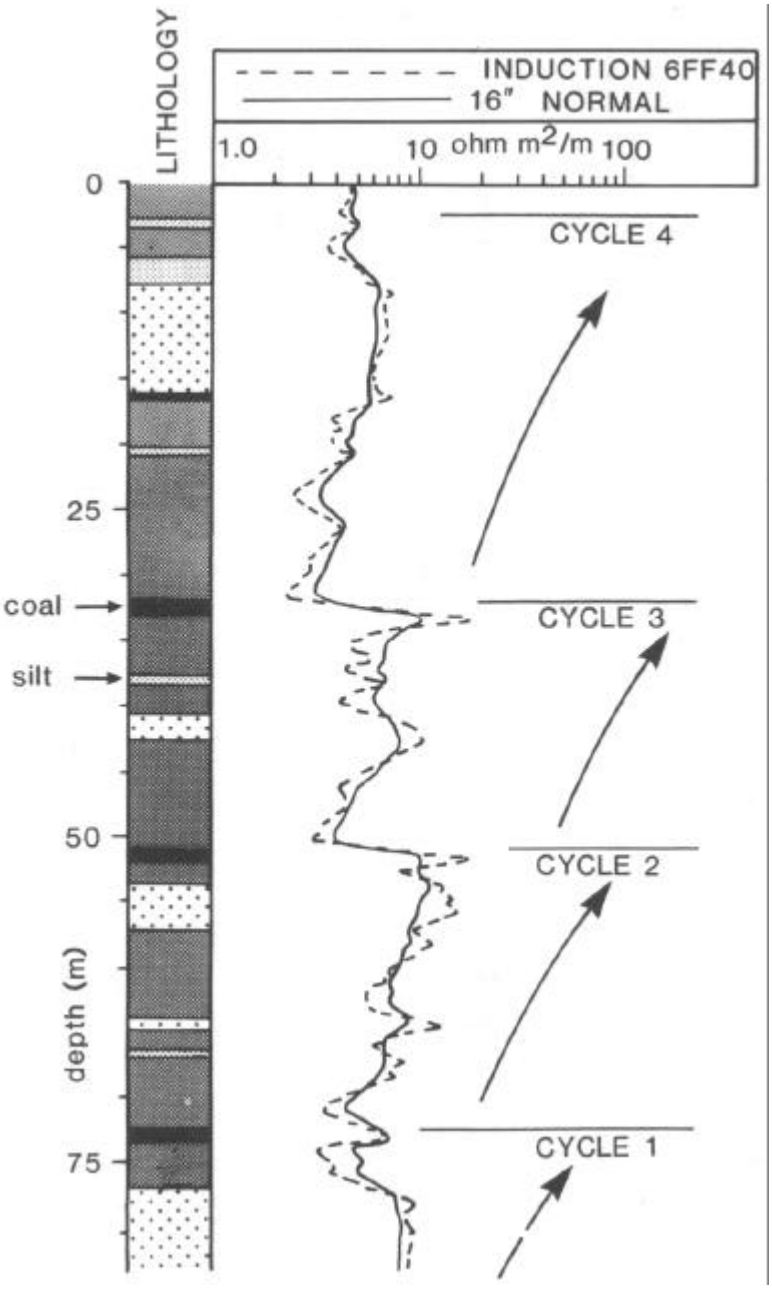

Fig. 19.27 Use of resistivity logs to track changes of lithofacies. In this case the log shows small scale deltaic cycles (courtesy of Rider [1996]).

However, we must always take into account the bed resolution and penetration depths of the various tools to understand how well we would expect the log to respond to changes in the log at various scales, as discussed in the sections above.

Figure 19.27 shows small scale deltaic cycles recorded by an IES-40.

The shapes electrical logs can be used to distinguish facies types as with other logs (e.g., sonic and gamma ray). These are sometimes called *electrofacies*, which are defined by Rider [1996] as "Suites of wireline log responses and characteristics sufficiently different to be able to be separated from other electrofacies.". Note, in general the wireline logs characteristics that define a particular electrofacies will also include data from wireline logs other than electrical logs.

19.12.4 Correlation

Electrical logs are often used for correlation. The deep logs (IES-40, ILd, LLd etc.) are the best to use, as they are sensitive to gross changes in the formations at a scale that is likely to be continuous with other wells. However, it must be noted that the resistivity of a formation also depends upon formation fluid pressure and formation water resistivity, which are non-stratigraphic variables, and changes in them from well to well may confuse correlations.

19.12.5 Lithology Recognition

Electrical logs are dramatically bad at indicating lithologies.

Sands shales and carbonates have no characteristic resistivity as their resistivities depend upon many factors including porosity, compaction, fluid resistivity, texture etc. However sequences of these rocks can usually be traced by using invariant characteristics from bed to bed, such as a similar resistivity reading as another set of beds or a characteristic roughness/smoothness of the curve within the bed. Thus if the basic lithologies can be defined from other logs, the electrical logs help progress them through the logged section. As the electrical logs are very sensitive to texture, they are extremely good at discriminating between lithologies of different types providing the types can be defined by some other log.

An example of this may include beds of shale separated by thin layers of siderite stringers and concretions. The shallow penetrating electrical tools will pick out each thin siderite bed as a sharp peak in resistivity.

However, electrical logs do provide characteristic responses for some lithologies (Fig. 19.28). The most common are:

- Gypsum – 1000 Ωm.
- Anhydrite – 10,000 - ∞ Ωm.
- Halite - 10,000 - ∞ Ωm.
- Coals – 10 –10^6 Ωm.
- Tight limestones and dolomites – 80 – 6000 Ωm.
- Disseminated pyrite - <1 Ωm (pyrite has a resistivity of 0.0001 – 0.1 Ωm.
- Chamosite - <10 Ωm.

19.12.6 Other Applications

Compaction of shales can be seen, as with other logs. In the case of electrical logs, the shale resistivity is seen to increase slowly but steadily in thick shale sequences. The deep tool should be used for this. Breaks in the compaction trend can then be used as indicators of unconformities and faults.

The beginning of *overpressure zones* can be seen by a sudden unexplained jump of the resistivity to lower values in a uniform lithology. This is best observed in shales and is associated with the higher porosity induced by the overpressure. Again, the best tools to use are the deep looking tools.

Source rocks may be recognized, and their maturity indicated by electrical logs. Immature sources have little effect upon electrical logs, but this effect grows with the degree of maturity. Hence, it

expected that it may be possible to calculate the TOC% from electrical logs under the correct conditions.

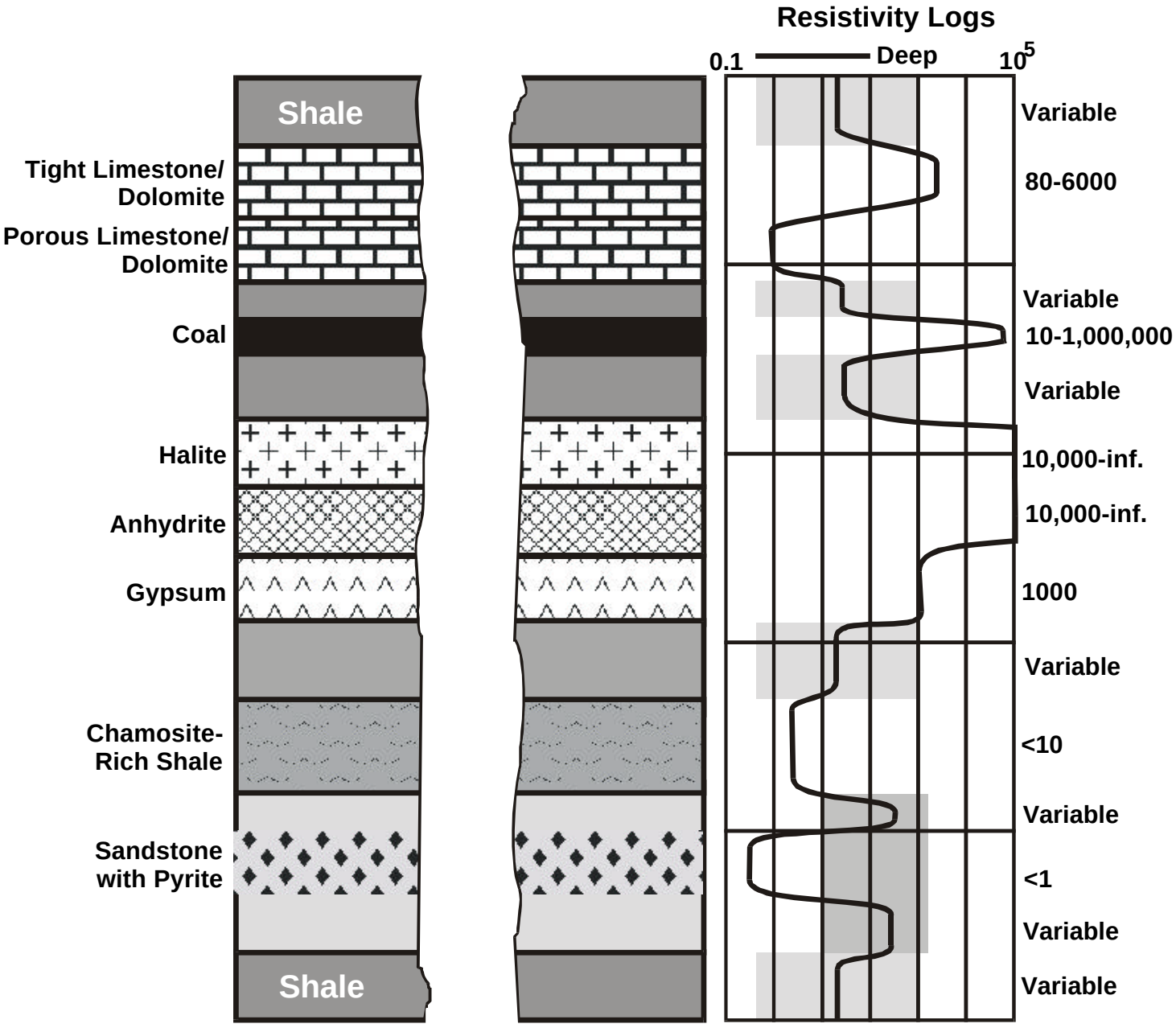

Fig. 19.28 Characteristic resistivities from various lithologies recorded by resistivity logs.

20. THE EFFECT OF CLAY ON POROSITY AND RESISTIVITY LOGS

20.1 Introduction

The presence of clay minerals or shale in porous formations presents problems from the interpretation of wireline logs. For most logs these problems have been discussed in the relevant chapter. The problem is, however, especially bad in the interpretation of resistivity data, and also affects the porosity logs. This is not only because the presence of clays and shale have a gross effect upon resistivity values, but because such data effects the final calculated STOOIP for a given formation. Even small amounts of clay can have a large effect, which is important because most reservoir sands contain some degree of shaliness.

Note: The terms clay and shale are used interchangeably by petrophysicists.

The distribution of clay within porous reservoir formations can be classified into three groups:

- Laminated – thin layers of clay between sand units.
- Structural – clay particles constitute part of the rock matrix, and are distributed within it. An example of this is coprolites.
- Dispersed – clay in the open spaces between the grains of the clastic matrix.

These are depicted schematically in Fig. 20.1.

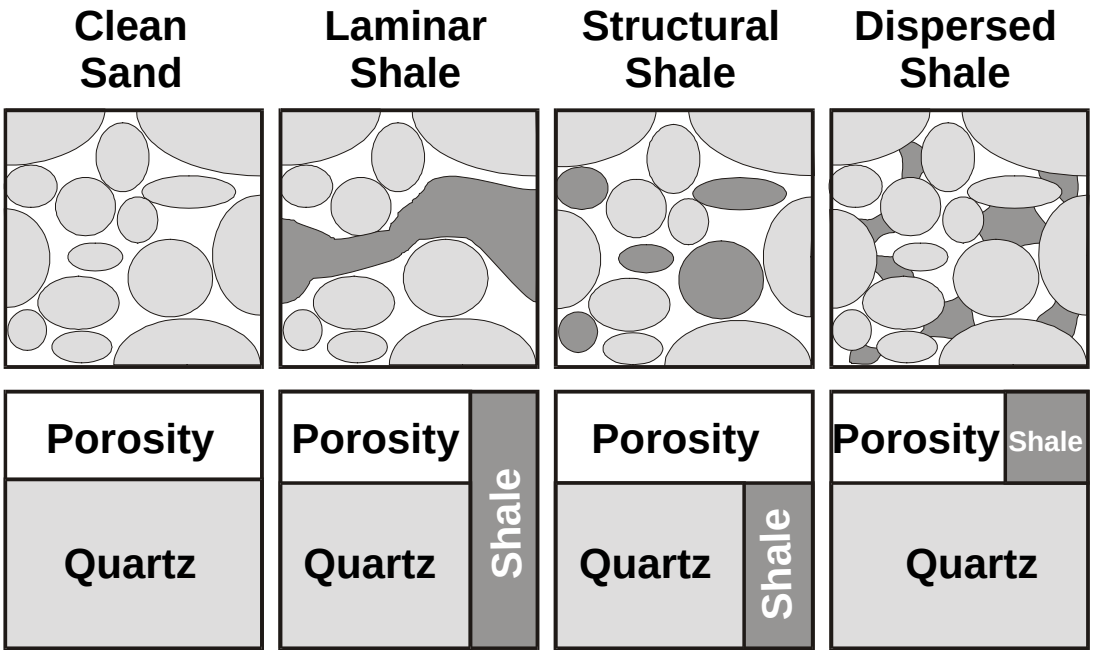

Fig. 20.1 Different modes of clay distribution in a reservoir.

The laminated and structural clays are part of the rock structure and are considered to have the same porosity (water content) as adjacent clay beds because they were subjected to the same overburden pressures. By contrast, the dispersed clays were only subjected to the formation fluid pressure, and therefore have a higher porosity and water content.

20.2 Porosity Logs

There are two different types of porosity that are relevant:

- Total porosity.
- Effective porosity.

These are illustrated in Fig. 20.2.

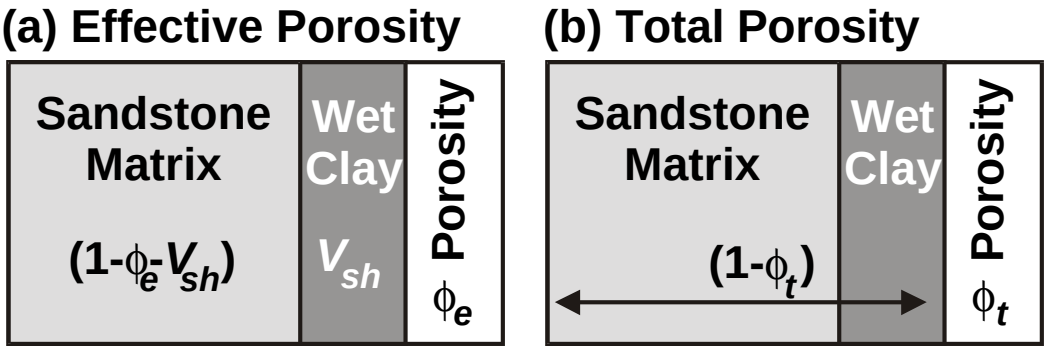

Fig. 20.2 Porosity models. (a) Total porosity. (b) Effective porosity.

20.2.1 Effective Porosity

The bulk volume of the rock is composed of a clastic/carbonate matrix fraction, a wet clay fraction (V_{sh}), and an "effective porosity", f_e. The matrix is therefore (1 - V_{sh} - f_e). This model is the basis for the density – neutron cross-plots, which is commonly used to assess f_e and V_{sh} in shaly formations, using the following equations:

$$r_b = \left((1 - f_e - V_{sh}) \times r_{ma}\right) + \left(f_e \times r_e\right) + \left(V_{sh} \times r_{sh}\right) \quad \textbf{(20.1)}$$

$$f_N = f_e + V_{sh} \times f_{sh} \quad \textbf{(20.2)}$$

Figure 20.3 illustrates this method graphically. The graph is a triangle, whose apices are at the following points:

- The clean matrix point: f_N = 0% r_b = 2.65 g/cm^3
- The fluid point: f_N = 100% r_b = 1.00 g/cm^3
- The clean matrix point: f_N and r_b obtained from an adjacent clay

The linear effective porosity scale is shown on the matrix-water side and the clay-water side. The iso-V_{sh} lines are drawn across the triangle. Each pair of f_N and r_b values obtained from the logs can be entered into the graph and the relevant effective porosity and V_{sh} can be read off. Alternately, a more accurate figure can be obtained by solving Eqs. (20.1 and 20.2).

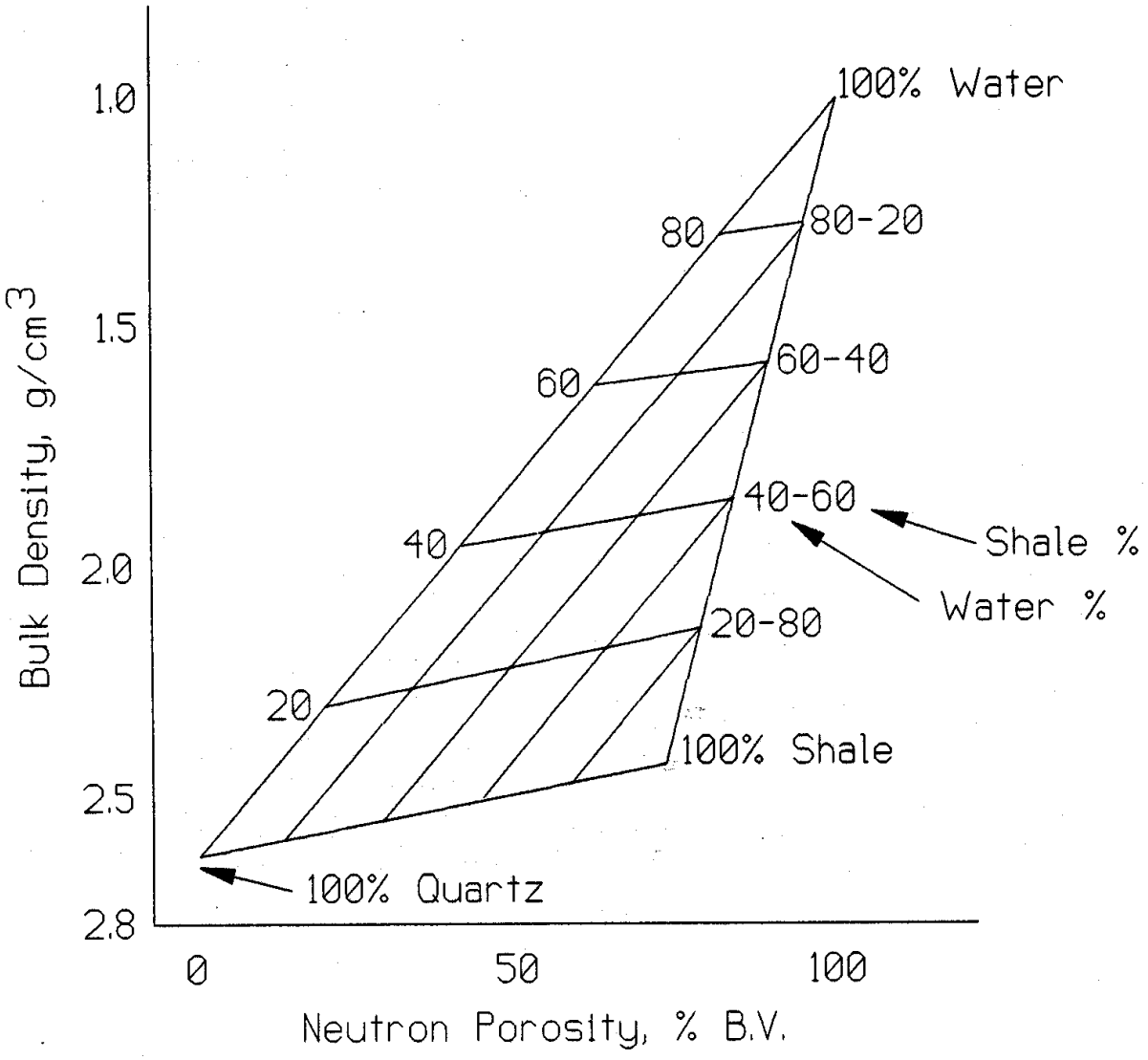

Fig. 20.3 Porosity- V_{sh} correction chart for the density – neutron log combination.

20.2.2 Total Porosity

In the total porosity mode, the clay grains/crystals are assumed to have a grain density equal to that of quartz. This is actually a good approximation for illite, kaolinite and montmorillonite. The model is composed of a sandstone matrix fraction, a clay crystal fraction (described as dry clay, i.e., without the clay bound water), and a so-called "total porosity" f_t. The matrix and dry clay fraction have a fraction (1 - f_t). The value of f_t can be derived directly from the density log.

The porosity obtained from routine core analysis is also the total porosity in the sense that the procedures used to prepare the cores ensure that all oil is extracted from the cores, and the core is then dried. Under these conditions all absorbed and interstitial water is removed from the clay. As a result, there is often good agreement between routine core porosities and density log derived porosity data. If there is a discrepancy, the core porosity is usually lower. This is because the methods used to measure the porosity of the cores uses imbibed fluids (water, mercury or gas), and these fluids can only access open pore spaces: there will always be some pore spaces that are isolated and cannot be accessed.

The difference between f_t and f_e is the fraction of water held by absorbing capillary forces in the clay fraction of the rock. This amount of water can be appreciable depending upon the type and distribution of the clay, and the salinity and pH of the formation fluid. The water is bound, and does not take part in fluid flow. It is common, therefore, to ignore this water fraction and to prefer to use f_e as a representative porosity for the rock. However, one must be cautious in using the effective porosity in calculations involving resistivity tools.

The NMR tool is sensitive to the difference between bound and free water (i.e., water associated with (f_t - f_e) and f_e, respectively), and can be used to derive these values directly, and then use them to predict the permeability of the rock.

20.2.3 Sand/Shale Modes

The effect on the effective porosity of the different clay modes is shown in Fig. 20.4. The clean water-bearing sand has an effective porosity of 30%, and is given by point Sd on the density-neutron crossplot (Fig. 20.4). If 10% shale is added to the sand, then the point will plot in slightly different places on the density-neutron crossplot depending upon the type of clay distribution (the mode of the shale).

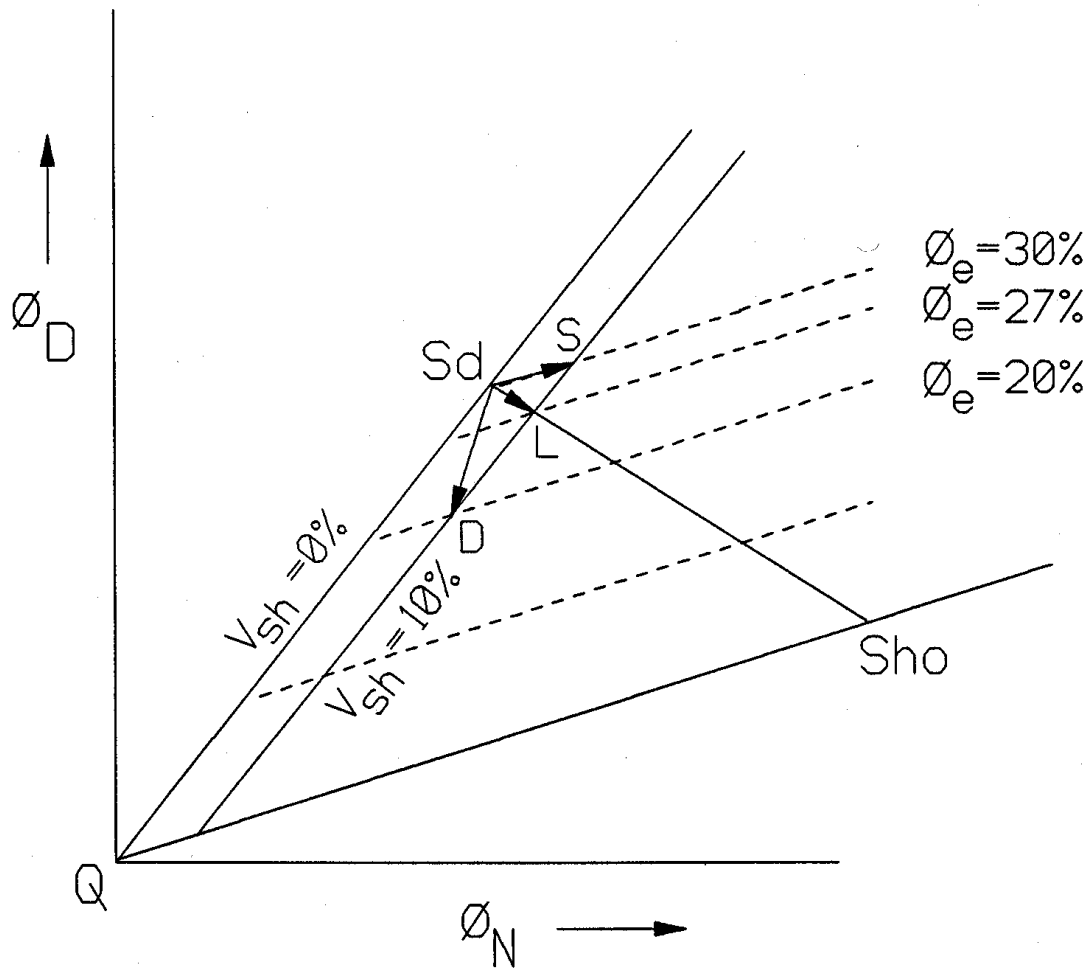

Fig. 20.4 Effect of shale/clay mode on the effective porosity of a shaly sand.

- If it is as a dispersed shale/clay, the 10% additional clays take the place of porosity, so the new effective porosity becomes 30 - 10 = 20%, and the point now plots at point D in the figure.
- If it is a laminated shale, the 10% additional clays reduce the overall effective porosity by 10%, so the new effective porosity becomes 30 – (30×10/100) = 27%, and the point now plots at point L in the figure.
- If it is a structural shale, the 10% additional clays replace volume for volume 10% of the original quartz grains, and the effective porosity is unchanged at 30%. Hence the new point plots at point S in the figure.

We can use these relationships to look at structural clay/shale distribution patterns on the density-neutron cross-plot.

Clay distribution patterns, indicating dispersed, laminated and structural shales can be analyzed with the density and neutron log data (Fig. 20.5). In this figure:

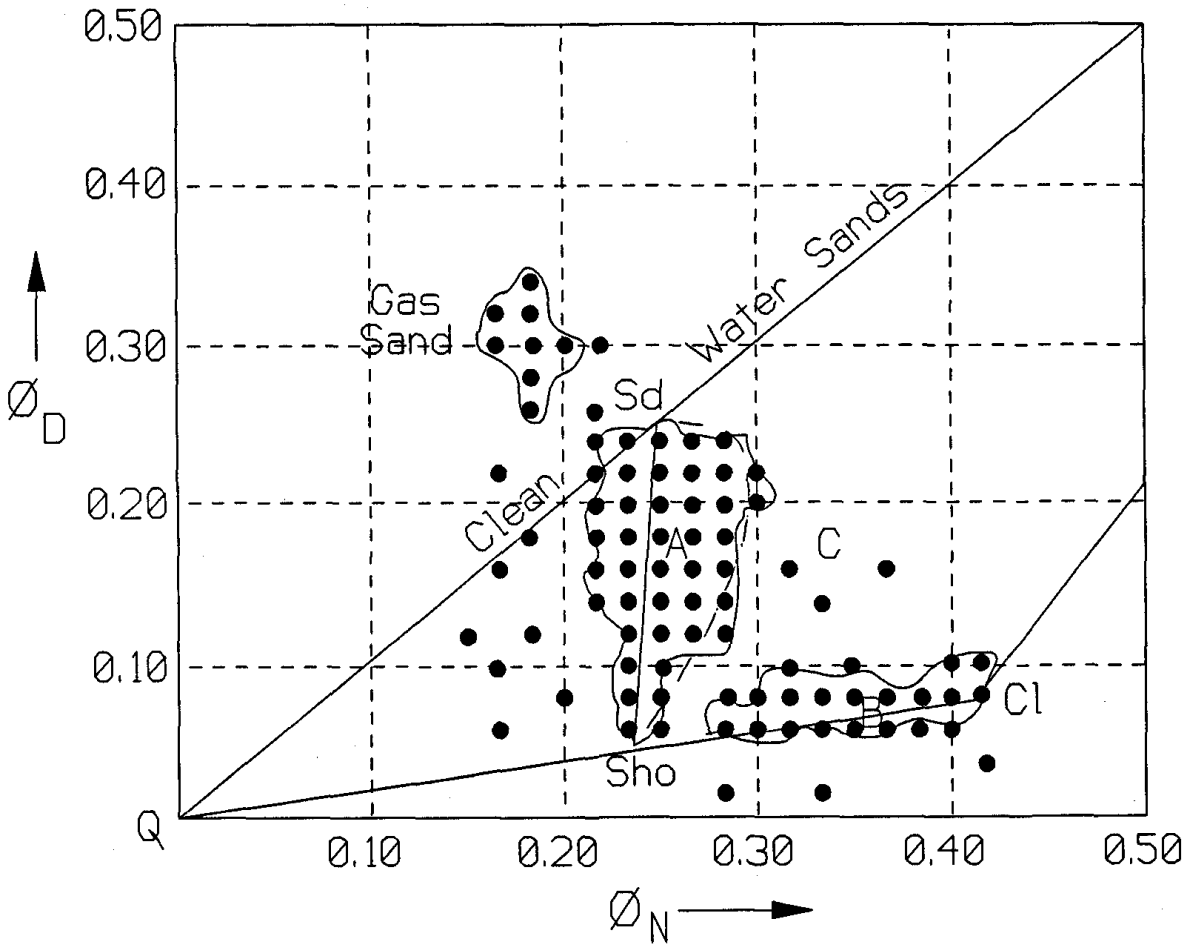

Fig. 20.5 Density-neutron crossplot showing characteristic points for shaly sands and shales.

- Cl is the "shale point" and indicates wet shale.
- The area A indicates sand and shaly sands. In area A, the samples range from clean sands at Sd to shales at point Sho.
- Laminar shales fall on the Sd-Sho line.
- Dispersed shales fall to the left of the Sd-Sho line.
- Structural shales fall to the right of the Sd-Sho line.
- The dashed line indicates the upper limit to shaly sands of laminated plus structural shale content.
- The area B indicates shales. The spread in this group is caused by the composition of the shales (composed of different clay minerals, silt and water). Pont Cl corresponds to shales which are relatively silt free, while point Sho represents shales that contain the maximum amount of silt.
- The area C indicates intermediate and ambiguous data.

If both the dry clay point and the wet clay point can be established, both the total and the effective porosities can be derived from the density and neutron log data. An example of this is shown in Fig. 20.6, which is a density-neutron cross-plot showing both the dry and wet clay points. In this case the dry clay density is assumed to be the same as that of quartz (2.65 g/cm^3) and the dry clay neutron porosity has been assumed (guessed). Both the density and the neutron porosity for the wet clay point have been taken from the log readings in adjacent good shales. Most dry clays have a density in the range 2.65 to 2.85 g/cm^3. Figure 20.9 can then be used to derive both the total and effective porosities from the density and neutron log readings in the formation of interest.

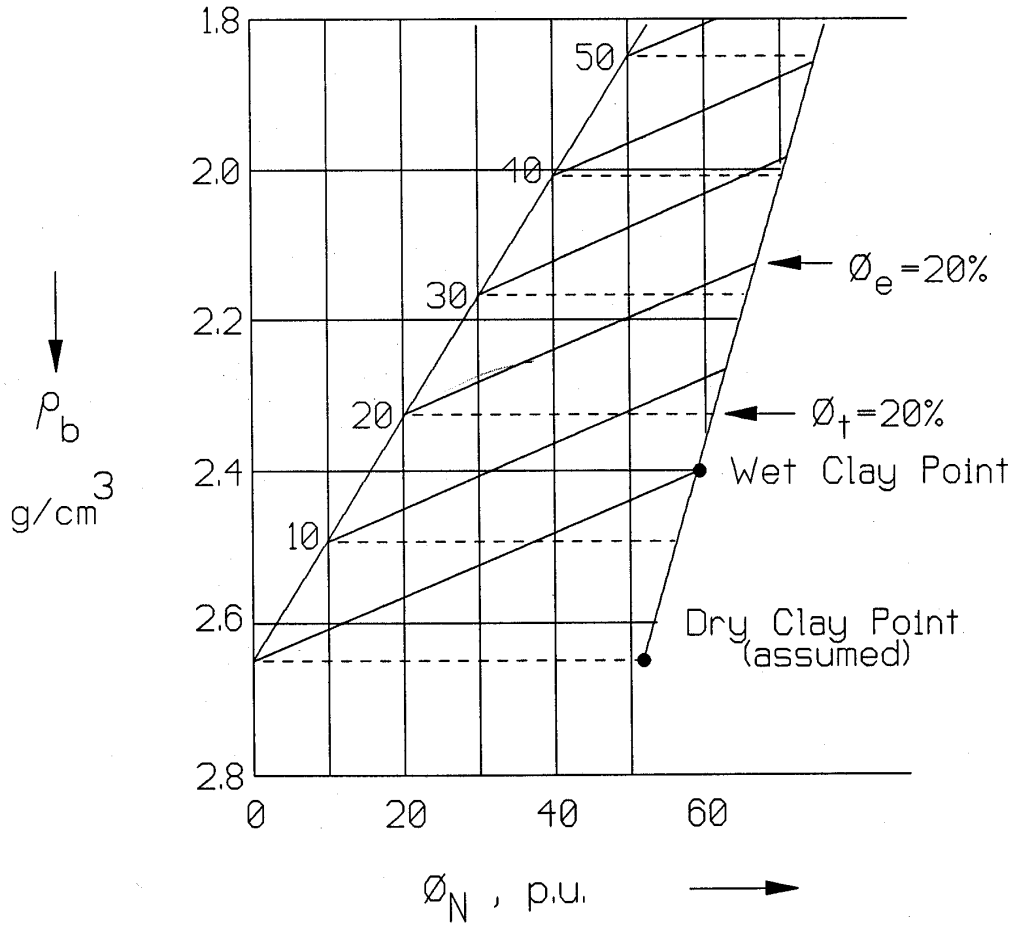

Fig. 20.6 The use of the density-neutron crossplot to calculate both total and effective porosities in shaly sands.

20.3 Resistivity Logs

The presence of clays reduce resistivity, and hence decrease the apparent hydrocarbon saturation. Their presence must be accounted for otherwise all our STOOIP calculations will be underestimated. The degree of effect that the presence of clays have depend on their amount (V_{sh}) and their distribution. Each of the tree different distributions of clay outlined above (laminar, structural, and dispersed) has a different effect upon the resistivity, SP, and sonic logs, and influences the permeability and water saturation in a different way. We can schematically illustrate the different modes of clay distribution in Fig. 20.1.

20.3.1 Laminar clays

These are thin streaks of clay deposited between units of reservoir rock. They do not change the effective porosity, the water saturation or the horizontal permeability of the reservoir layer, but destroy vertical permeability between reservoir layers.

The resistivity of the reservoir rock is the sum of the conductivities of the clean sand layers and the shale laminae:

$$C_t = C_{sand} + C_{sh} \tag{20.3}$$

or in terms of resistivity:

$$\frac{1}{R_t} = \frac{(1-V_{sh})}{R_{sand}} + \frac{V_{sh}}{R_{sh}} \tag{20.4}$$

where: R_t = log reading in the borehole corrected for bed thickness and invasion.
R_{sand} = resistivity of the clean reservoir rock ($R_{sand} = F_{sand}\, R_w\, S_w^{-n}$).
R_{sh} = resistivity of the clay.
V_{sh} = clay fraction.

Equation (20.4) can be written:

$$\frac{1}{R_t} = \frac{(1-V_{sh})\, S_w^n}{F_{sand}\ R_w} + \frac{V_{sh}}{R_{sh}} \tag{20.5}$$

which can be rearranged for water saturation:

$$S_w = \left[\left(\frac{1}{R_t} - \frac{V_{sh}}{R_{sh}} \right) \frac{F_{sand}\ R_w}{(1-V_{sh})} \right]^{1/n} \tag{20.6}$$

In practice the water saturation is found using an iterative method. The shale volume (V_{sh}) is derived from the GR or SP logs.

20.3.2 Dispersed Clays

These show very different properties from laminar shales. The permeability is significantly reduced because clays occupy the pore space and the water wetness of clays is generally higher than that of quartz. The result is an increased water saturation and a decreased fluid mobility.

There are many shaly-sand water saturation equations that have been proposed in the literature for dispersed clay systems. The most common is the Simandoux equation:

$$S_w = \left[A R_w f^{-m} \left(\frac{1}{R_t} - \frac{V_{sh}\ S_w}{R_{sh}} \right) \right]^{1/n} \qquad \textbf{(20.7)}$$

This equation is also solved iteratively.

20.3.3 Structural Clays

These have similar general properties to laminar clays, as they have been subjected to the same constraints. However, they behave more like dispersed clays in respect of their permeability and resistivity properties.

20.3.4 Waxman and Smits Equation

Clay-bearing rocks have a lower resistivity because clays have a low resistivity. This is caused partly by the presence of effective surface conduction processes on their surfaces, and partly because they generally have large surface areas upon which surface conduction can take place. Waxman and Smits used this to create an alternative way of analyzing the electrical resistivity of shaly sands.

[*Note: The Waxman and Smits method is an empirical one, and is therefore a local approximation. Recently, the physics behind the double layer conduction in rocks has been solved analytically, enabling this analysis to be carried out accurately now. However, the oil industry does not yet use this method because it is new and also strongly mathematical*.]

Waxman and Smit's equation relates the electrical resistivity of a water saturated shaly sand to the water conductivity and the cation exchange capacity per unit pore volume of the rock, Q_v (meq/ml). It is this last factor that partly controls the size of the surface conduction. The method is *independent* of clay distribution.

The conductivity of the shaly water-bearing sand is expressed by:

$$C_o = \frac{1}{F^*} \left(C_w + C_s \right) \qquad \textbf{(20.8)}$$

where: F^* = the formation factor in shaly sand (determined at high fluid salinities).
C_o = $1/R_o$
C_w = $1/R_w$
C_s = The specific surface conductance of the clay fraction.

The value of $C_s = B \times Q_v$, where B is the equivalent conductance of the counterions as a function of solution conductivity, C_w. The units of B are Ωcm/m.meq. Equation (20.8) is represented graphically in Fig. 20.7.

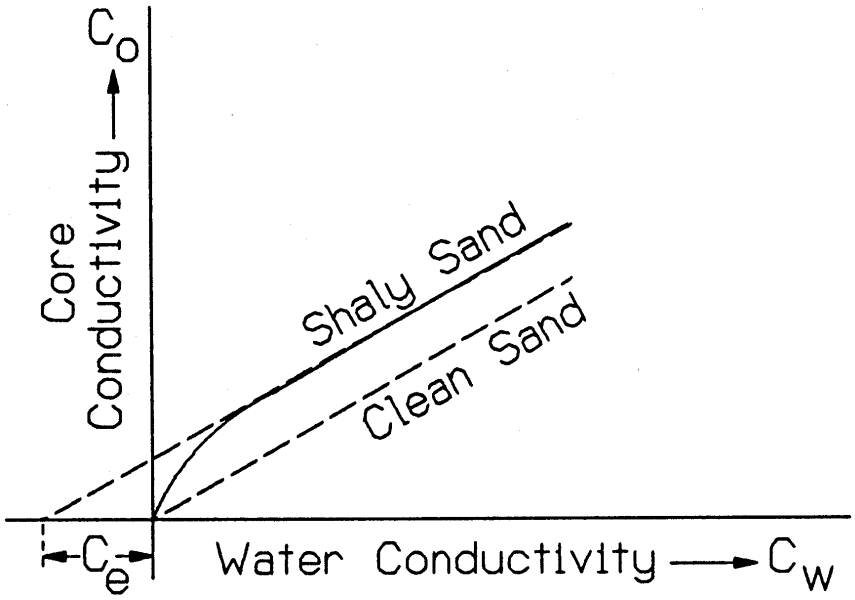

Fig. 20.7 The conductivity of a shaly sand as a function of formation water conductivity.

Since we can write $F^* = f^{-m}*$, Eq. (20.8) can be rewritten:

$$R_o = \frac{f^{-m^*}}{C_w + B Q_v} = \frac{R_w f_t^{-m^*}}{1 + R_w B Q_v} \qquad \textbf{(20.9)}$$

in which formula the triple product $R_w B Q_v$ is dimensionless.

This equation was developed and tested in the laboratory using the total porosity, and hence it should be restricted to use with total porosity.

The concentration of clay counterions as defined by Q_v can be determined in the laboratory on material from core by a titration/conductivity method. This is done on crushed samples, so there is some concern that the value may not be relevant for whole rocks. Clearly there will be more exchangeable counterions possible in crushed samples, which have a higher surface area for reactions. Some whole rock measurements exist, but are uncommonly used in the oil industry.

It has been noted that there exists in some areas a relationship between Q_v and f_t. If this is noted in a reservoir (Fig. 20.8), the Q_v value may be determined from the total porosity from log data. In shaly sands Q_v usually ranges between 0.01 and 2 meq/ml.

Empirical relationships between B and R_w have been established at different temperatures. between 50°C and 200°C (120 – 390°F) the product BR_w is not dependent upon temperature, and can be represented as a function of water salinity alone, as illustrated in Fig. 20.9.

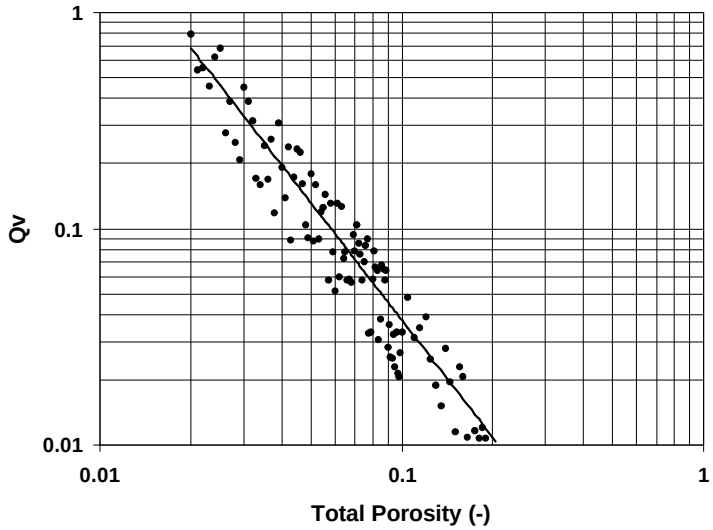

Fig. 20.8 Typical Q_v - f_t for reservoir intervals. Here Qv = $0.0006 \times f_t^{-1.8}$.

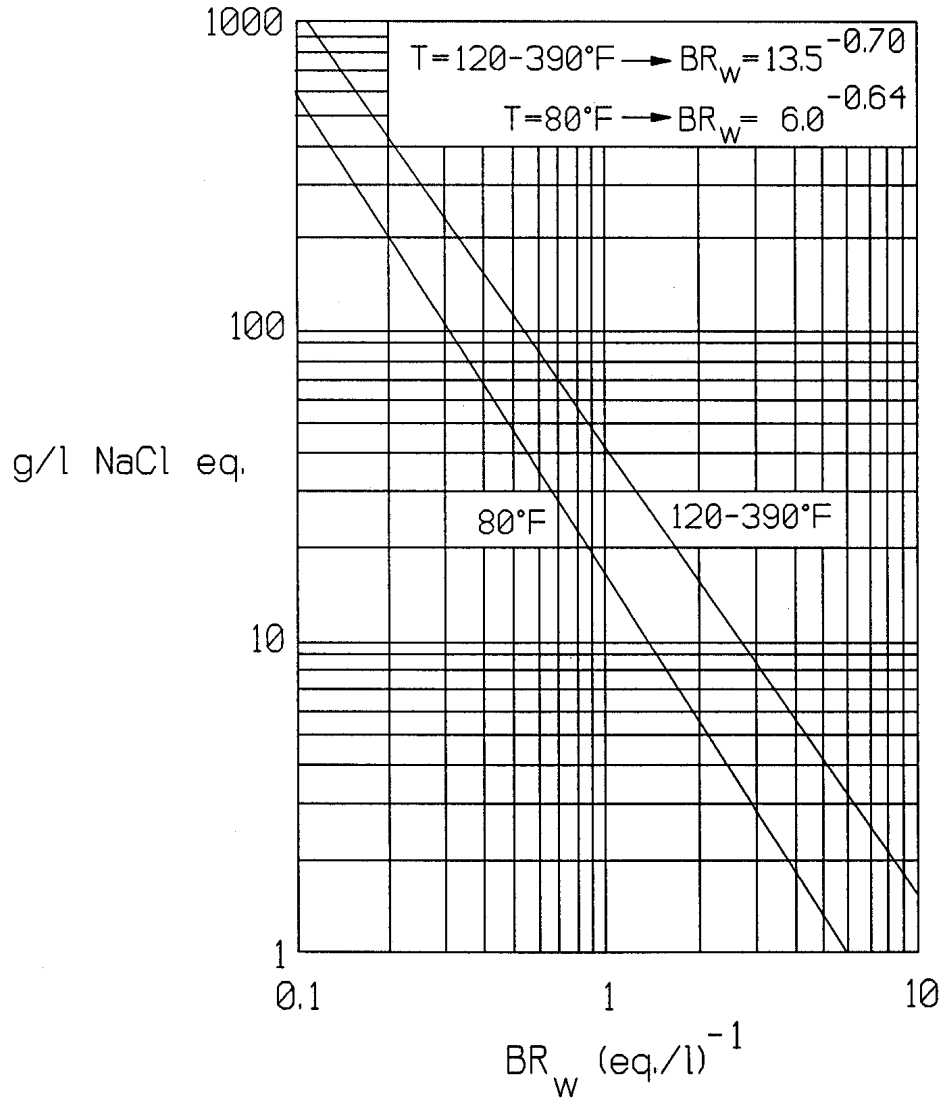

Fig. 20.9 The BR_w – Salinity relationship.

In hydrocarbon-bearing formations the exchange ions associated with the clay become more concentrated in the remaining pore water. This concentration Q_v' is related to Q_v and the water saturation S_w by $Q_v' = Q_v / S_w$.

The conductivity of the counterions is BQ_v/S_w (Ωm), hence:

$$C_t = \frac{1}{G^*}\left(C_w + \frac{B\,Q_v}{S_w}\right) \qquad \textbf{(20.10)}$$

Here, C_t = the conductivity of a partially water saturated sand.
G^* = a geometric factor, which is a function of the porosity, water saturation and pore geometry, but independent of Q_v.

Dividing Eq. (20.8) by Eq. (20.10) gives:

$$S_w^{-n^*} = \frac{G^*}{F^*} = \frac{R_t}{R_o}\cdot\frac{C_w + B\,Q_v/S_w}{C_w + B\,Q_v} = \frac{R_t}{R_o}\cdot\frac{1 + R_w\,B\,Q_v/S_w}{1 + R_w\,B\,Q_v} \qquad \textbf{(20.11)}$$

where, n^* is the saturation exponent for shaly sand.

The equation is solved for S_w using an iteration process, computationally. A quick manual solution can be obtained from the graph shown in Fig. 20.10, which is valid for the saturation exponents, n^*=1.8 and 2.0.

This is derived from the relationship:

$$\frac{R_t}{F^*\,R_w} = S_w^{-n^*}\left[\frac{1}{1 + R_w\,B\,Q_v}\right] \qquad \textbf{(20.12)}$$

where, F^* = $F\,(1 + R_wBQ_v)$, and R_w and B are the values at 77oF.

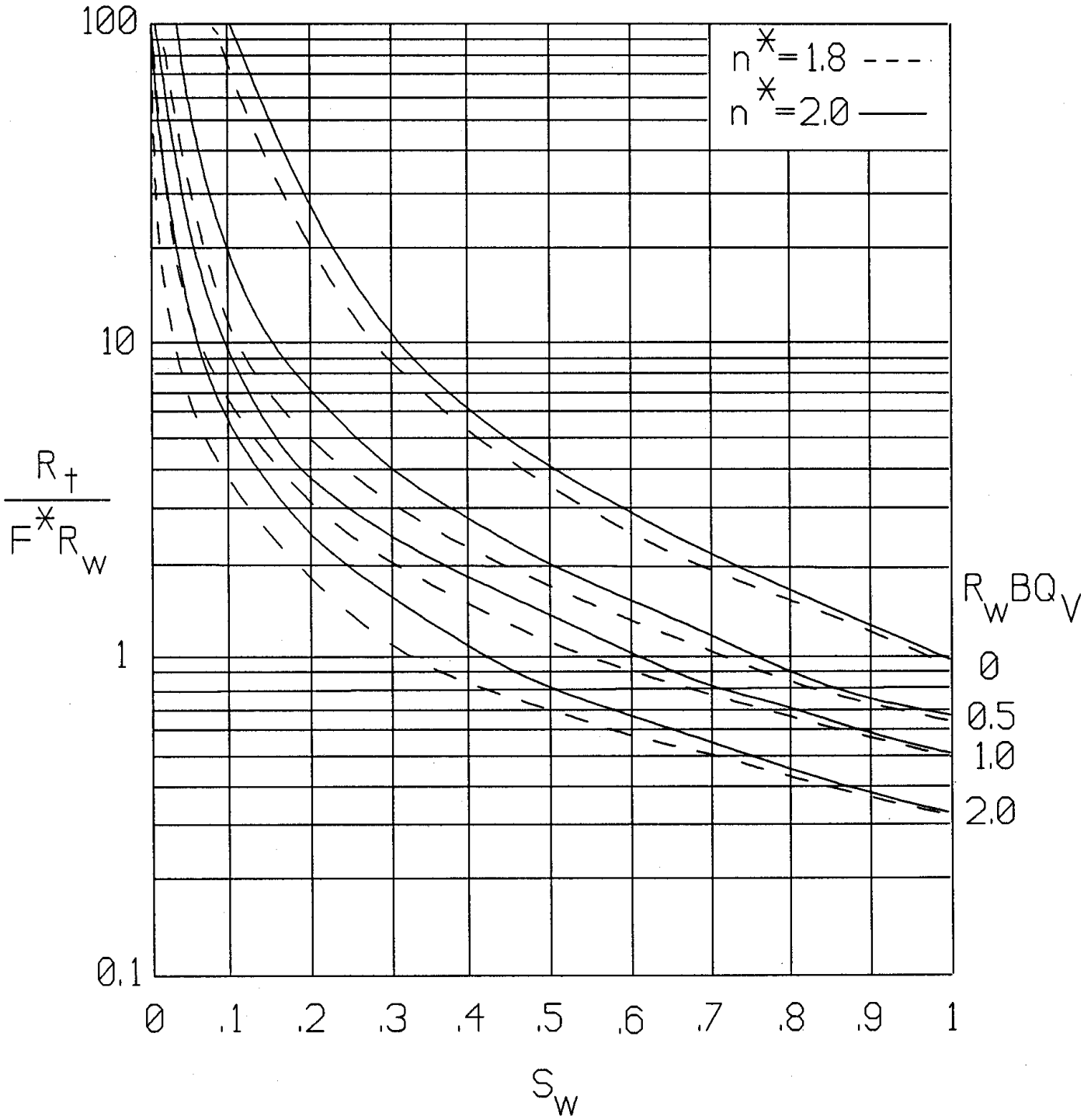

Fig. 20.10 Quick-look Waxman and Smits S_w solution chart.

Exercises

INTRODUCTORY EXERCISE – STOOIP CALCULATIONS

OIL FIELD CASE 1

You are provided with the following data:

Area of oil field	4500 acres
Thickness of reservoir formation	25 m
Porosity of formation	19% for top 7 m
	22% for middle 12 m
	12% for bottom 6 m
Water saturation	20% for top 7 m
	15% for middle 12 m
	35% for bottom 6 m
Oil formation volume factor	1.5 bbl./bbl.

(a) Calculate the OOIP.

(b) Calculate the STOOIP.

Give your results in Mbbl. to one place of decimals.

OIL FIELD CASE 2

You are provided with the following data:

Area of oil field	4900 acres
Thickness of reservoir formation	20 m
Porosity of formation	20%
Water saturation	15%
Oil formation volume factor	1.65

Give your results in Mbbl. to one place of decimals.

(c) Calculate the STOOIP.

(d) Calculate the two resulting values of STOOIP if there is an error of ±20% in the area of the oil field.

(e) Calculate the two resulting values of STOOIP if there is an error of ±20% in the thickness of the formation.

(f) Calculate the two resulting values of STOOIP if there is an error of ±20% in the porosity of the formation.

(g) Calculate the two resulting values of STOOIP if there is an error of ±20% in the water saturation of the formation.

(h) Calculate the two resulting values of STOOIP if there is an error of ±20% in the oil formation volume factor for the oil field.

(i) Summarise the results in the table below.

Case	-20%	Base Case	+20%
Error in area			
Error in thickness			
Error in porosity			
Error in water saturation			
Error in oil formation volume factor			
Give values in Mbbl. and as a percentage of the base case in parentheses (e.g., 55 Mbbl. (-13%))			

GAS FIELD

You are provided with the following data:

Area of gas field	6400 acres
Thickness of reservoir formation	30 m
Porosity of formation	22%
Water saturation	28%
Gas formation volume factor	0.0035 cu.ft./cu.ft.

Give your results in millions of cu.ft. to one place of decimals.

(j) Calculate the GIP.

(k) Calculate the STGOIP.

(l) Calculate the two resulting values of STGOIP if there is an error of ±20% in the area of the gas field.

(m) Calculate the two resulting values of STGOIP if there is an error of ±20% in the thickness of the formation.

(n) Calculate the two resulting values of STGOIP if there is an error of ±20% in the porosity of the formation.

(o) Calculate the two resulting values of STGOIP if there is an error of ±20% in the water saturation of the formation.

(p) Calculate the two resulting values of STGOIP if there is an error of ±20% in the gas formation volume factor for the oil field.

(q) Summarise the results in the table below.

Case	-20%	Base Case	+20%
Error in area			
Error in thickness			
Error in porosity			
Error in water saturation			
Error in gas formation volume factor			
Give values in Mcu.ft. and as a percentage of the base case in parentheses (3000 Mcu.ft. (-15%))			

POROSITY EXERCISE

(a) Calculate the porosity of a formation composed of uniform spherical grains of radius 100 μm in a *cubic* packing arrangement.

(b) What would be the porosity of the formation if it were composed of uniform spherical grains of radius 10 μm in a cubic packing arrangement instead?

(c) Calculate the porosity of a formation composed of uniform spherical grains of radius *r* in a *hexagonal* packing arrangement.

(d) Calculate the porosity of a formation composed of uniform spherical grains of radius *r* in a *tetragonal* packing arrangement.

(e) A new spherical particle requires to be less than a maximum size for it to fit through the pore throat created by the particles in the cubic cell matrix and into the central space. Calculate the porosity of a formation composed of uniform spherical grains of radius *r* in a cubic packing arrangement if a single smaller particle of the maximum possible size squeezes inside the unit cell and stays there without projecting beyond the confines of the unit cell.

(f) Calculate the porosity of a formation composed of uniform spherical grains of radius *r* in a cubic packing arrangement, when the central space is occupied by the largest possible sized spherical particle. Such a particle could not squeeze inside the cell between the other particles, but must have been placed there during initial rock deposition.

PERMEABILITY EXERCISE

Many of the following exercises relate to a fictional field called the Elysian Field. The following data has been collected from cores from this field.

WATER PERMABILITY

Well: 24-1X
Depth: 3100 m

An experiment has been carried out where formation brine was pumped through a core plug obtained from this depth. The core plug was placed in a rubber sleeve in a pressure vessel. A confining pressure was placed on the sleeve using gas. Initially a single measurement was made with the sleeve pressure set to 500 psig. Subsequently permeability measurements were carried out at a range of higher sleeve (confining) pressures. For each permeability measurement, the fluid pressures at each end of the sample were measured, and the flow rate was also determined.

The following data were collected:

General Data	
Sample Length (average of 10 caliper readings)	7.8 cm
Sample Radius (average of 10 caliper readings)	1.905 cm
Sample Weight (saturated with dry air at 25^{o}C)	186.15 g
Water Viscosity (at the temperature and pressure at 3100 m)	1.007 cP

Flow Data

Sleeve Pressure (psig)	**Input Press. (psig)**	**Input Press. (atma)**	**Output Press. (psig)**	**Output Press. (atma)**	**Flow Rate (cm^3/min)**	**Perme ability (mD)**	**Norm. Perm. (-)**	***f*** **(-)**	**Norm. *f* (-)**
500	101		30		20			0.21	
1500	121		31		19.27			0.197	
2500	116		33		14.50			0.190	
3500	111		32		12.51			0.188	
4500	107		30		11.5			0.185	
5500	108		33		10.565			0.184	

Note the following conventions:

- psi = pressure unit, pounds per square inch.
- atm = pressure unit, atmospheres.
- To convert psi to atm **divide** by 14.7 psi because there are 14.7 psi in one atmosphere at standard conditions at sea level.
- Postscript ‘g’ means gauge. Mechanical gauges read relative to the atmospheric pressure on the day.
- Postscript ‘a’ means absolute, which is the pressure relative to a perfect vacuum. Values for the calculation must be in atmospheres absolute.
- To convert pressure in psig to psia **add** 14.7 psi, which is the standard mean atmospheric pressure at sea level.

- To convert pressure in atmg to atma **add** 1.00 atm, which is the standard mean atmospheric pressure at sea level.
- To convert pressure in psig to atma **add** 14.7 psi, which is the standard mean atmospheric pressure at sea level, then **divide** the result by 14.7 psi.
- The above calculations can be carried out using the measured value of the atmospheric pressure in psi on the day of the experiment. The results are then marginally more accurate.

(a) Calculate the relevant pressures in atma and insert them into the table.

(b) Calculate the permeability of the core plug at each of the sleeve (overburden) pressures.

(c) Calculate the normalised permeability (permeability at a given sleeve pressure divided by the permeability at 500 psig).

(d) Calculate the normalised porosity (porosity at a given sleeve pressure divided by the porosity at 500 psig).

(e) Draw a graph of normalised permeability and porosity (y-axis, linear scale 0 to 1) against sleeve (overburden) pressure (x-axis, linear scale 0 to 6000 psig).

(f) Why does permeability decrease with increasing overburden pressure?

(g) Why does porosity decrease with increasing overburden pressure?

(h) Why is the effect of overburden pressure greater on permeability than on porosity?

(i) The calculated values of permeability at increasing overburden pressures are actually slightly wrong. What causes this, and infer whether these calculated values are slightly over-estimating or slightly under-estimating the true values.

Graph paper for part (e)

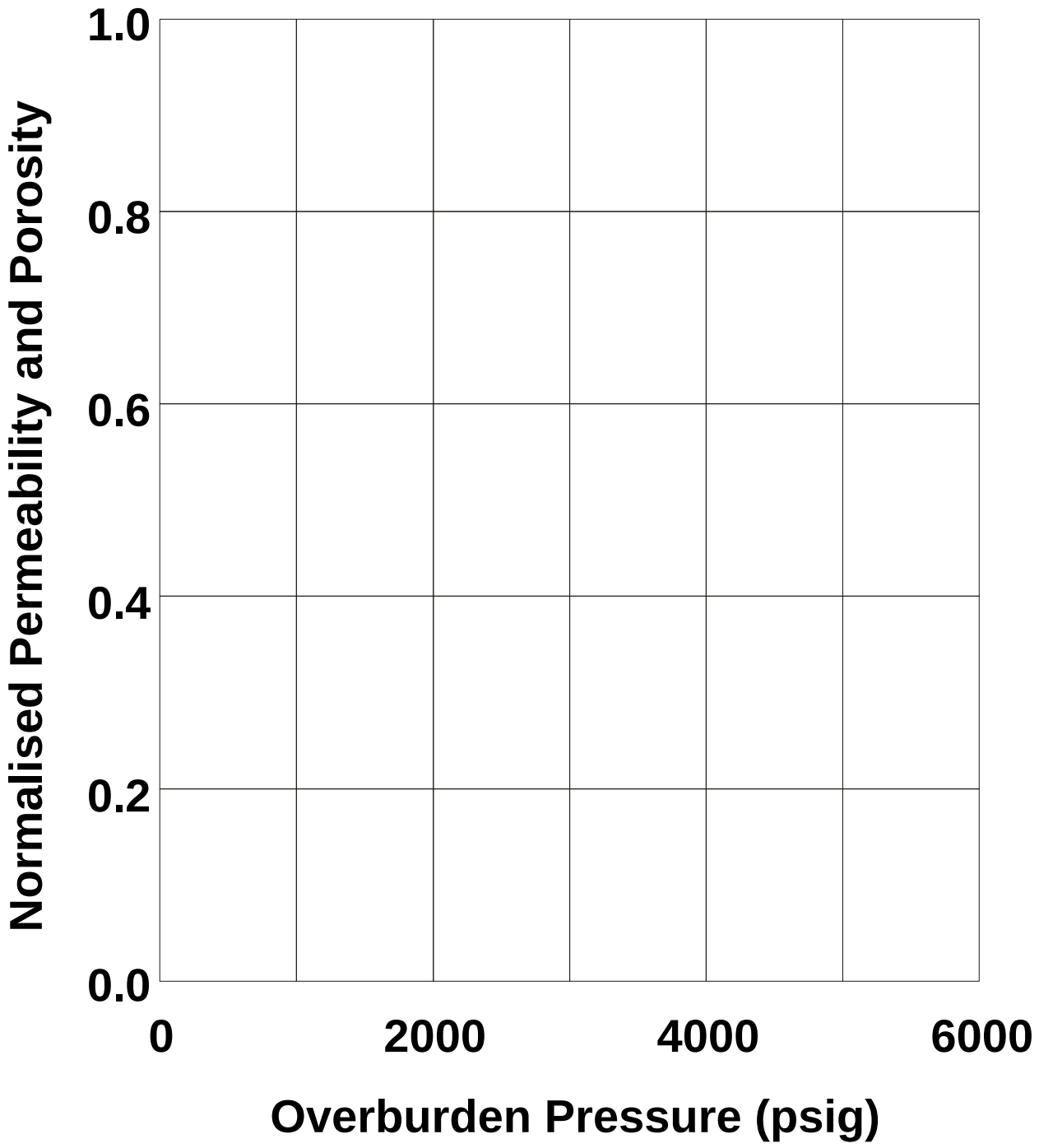

GAS (KLINKENBERG) PERMABILITY

Well: 24-1X
Depth: 3050 m

An experiment has been carried out where *nitrogen* gas was passed through a core plug obtained from this depth. The core plug was placed in a rubber sleeve in a pressure vessel and a single confining pressure of 500 psig was used throughout the entire experiment. The input gas pressure and output gas pressure were measured together with the volume of gas passing through the core plug for six different values of input gas pressure.

The following data were collected using nitrogen gas:

General Data	
Sample Length (average of 10 caliper readings)	7.8 cm
Sample Radius (average of 10 caliper readings)	1.905 cm
Sample Weight (saturated with dry air at 25^{o}C)	186.15 g
Nitrogen Gas Viscosity	0.0176 cP

Flow Data

Sleeve Press. (psig)	**Input Press. (psig)**	**Input Press. (atma)**	**Output Press. (psig)**	**Output Press. (atma)**	**Flow Rate (cm^3/min)**	**N_2 Permea-bility (mD)**	**Mean Press. (atma)**	**$1/P_{mean}$ ($atma^{-1}$)**
500	2		0.2		3.27			
500	4		0.3		7.02			
500	8		0.5		15.47			
500	16		0.9		36.12			
500	32		1.5		92.18			
500	64		3.1		265.56			

Note the following conventions:

- psi = pressure unit, pounds per square inch.
- atm = pressure unit, atmospheres.
- To convert psi to atm **divide** by 14.7 psi because there are 14.7 psi in one atmosphere at standard conditions at sea level.
- Postscript ‘g’ means gauge. Mechanical gauges read relative to the atmospheric pressure on the day.
- Postscript ‘a’ means absolute, which is the pressure relative to a perfect vacuum. Values for the calculation must be in atmospheres absolute.
- To convert pressure in psig to psia **add** 14.7 psi, which is the standard mean atmospheric pressure at sea level.
- To convert pressure in atmg to atma **add** 1.00 atm, which is the standard mean atmospheric pressure at sea level.
- To convert pressure in psig to atma **add** 14.7 psi, which is the standard mean atmospheric pressure at sea level, then **divide** the result by 14.7 psi.
- The above calculations can be carried out using the measured value of the atmospheric pressure in psi on the day of the experiment. The results are then marginally more accurate.

(j) Calculate the relevant pressures in atmospheres absolute, and update the table.

(k) Calculate the apparent permeability for each set of input pressure, output pressure and flow rate, using the viscosity of nitrogen and filling in the table as you go.

(l) Calculate 1/Mean Pressure for each set.

(m) Draw a Klinkenberg Plot by plotting the apparent permeability (y-axis, scale linear) against 1/Mean Pressure (x-axis, scale linear from zero).

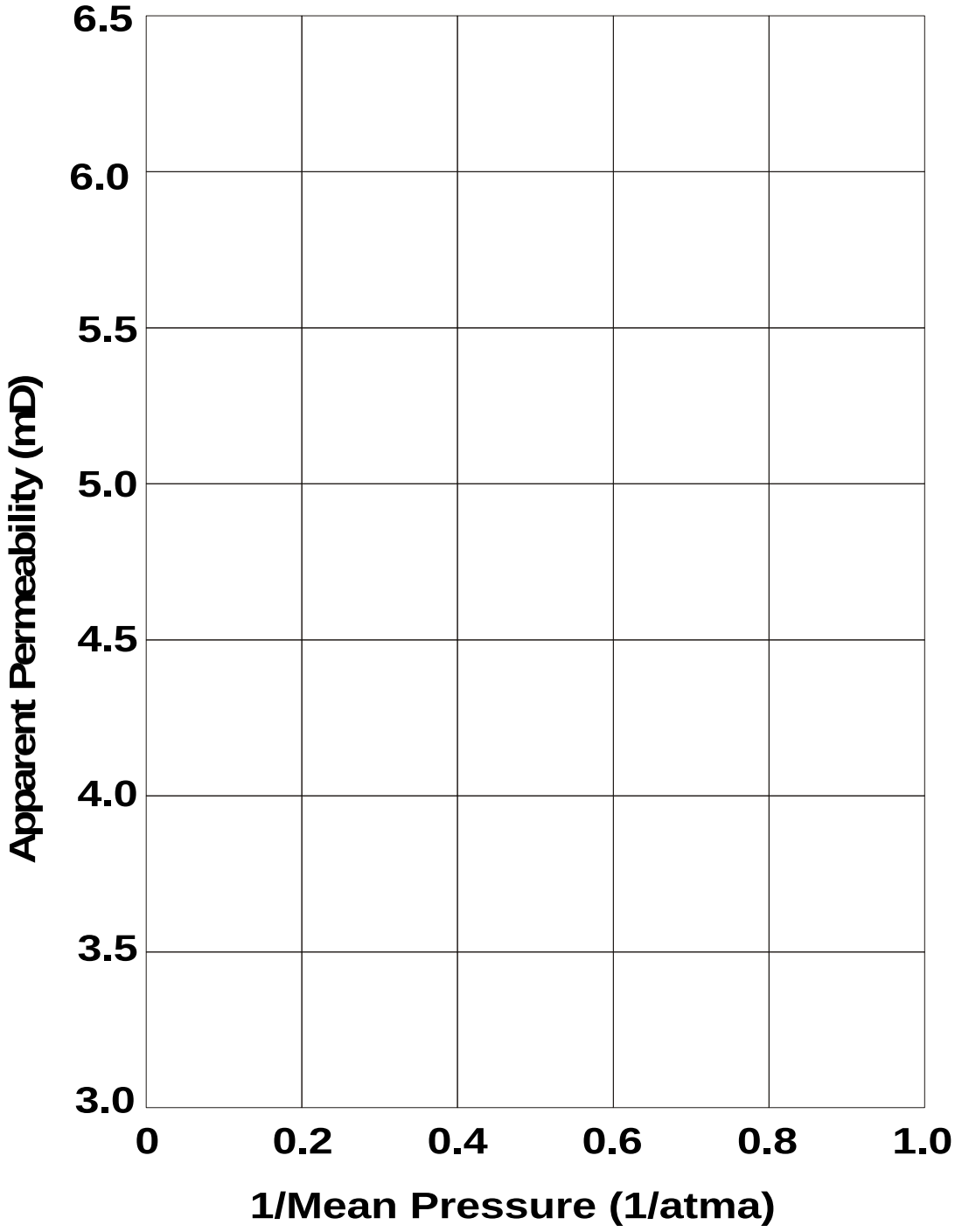

(n) Determine the Klinkenberg Permeability (K_L). Comment upon the accuracy of the determination.

(o) Determine the Slip Factor α, where $K_{app}=K_L(1+\alpha/P_{mean})$. Note that this is the gradient of the line divided by K_L. Remember to include the units.

(p) The values of the apparent permeabilities are different if a different gas is used in place of nitrogen. Recalculate all apparent permeabilities if either helium or dry air were used instead of nitrogen. Plot these on the Klinkenberg plot too.

The following data were collected using dry air:

General Data	
Sample Length (average of 10 caliper readings)	7.8 cm
Sample Radius (average of 10 caliper readings)	1.905 cm
Sample Weight (saturated with dry air at 25°C)	186.15 g
Dry Air Viscosity	0.0184 cP

Flow Data

Sleeve Press. (psig)	**Input Press. (psig)**	**Input Press. (atma)**	**Output Press. (psig)**	**Output Press. (atma)**	**Flow Rate (cm^3/min)**	**Dry Air Permea-bility (mD)**	**Mean Press. (atma)**	**$1/P_{mean}$ ($atma^{-1}$)**
500	2		0.2		3.52			
500	4		0.3		7.53			
500	8		0.5		16.45			
500	16		0.9		37.88			
500	32		1.5		95.50			
500	64		3.1		267.44			

The following data were collected using helium gas:

General Data	
Sample Length (average of 10 caliper readings)	7.8 cm
Sample Radius (average of 10 caliper readings)	1.905 cm
Sample Weight (saturated with dry air at 25°C)	186.15 g
Helium Gas Viscosity	0.0196 cP

Flow Data

Sleeve Press. (psig)	**Input Press. (psig)**	**Input Press. (atma)**	**Output Press. (psig)**	**Output Press. (atma)**	**Flow Rate (cm^3/min)**	**He Permea-bility (mD)**	**Mean Press. (atma)**	**$1/P_{mean}$ ($atma^{-1}$)**
500	2		0.2		3.68			
500	4		0.3		7.84			
500	8		0.5		16.99			
500	16		0.9		38.69			
500	32		1.5		95.97			
500	64		3.1		263.68			

(q) Clearly, the apparent permeabilities depend upon the type of gas used. Determine the klinkenberg permeabilities and slip factors for the klinkenberg permeability measurement using helium and dry air. Do the Klinkenberg Permeability (K_L) and slip factor depend on the type of gas used?

(r) List four advantages of the klinkenberg permeability method over a single measurement of gas permeability at an arbitrary input gas pressure.

CAPILLARY PRESSURE EXERCISE

This exercises uses data from the Elysian Field.

Well: 24-1X
Depth: 3100 m
Lithology: Slightly shaly sandstone (90%sandstone, 10% shale)

A mercury injection capillary pressure experiment has been carried out on a core plug from well 24-1X of the Elysian Field at a depth of 3100 m.

The following data were collected:

Cap. Press. (Hg-Air) @25°C (psi)	**S_{Hg}**	**S_{Air}**	**S_w**	**S_o**	**Cap. Press. (Oil-Water) @ 25°C (psi)**	**Cap. Press. (Oil-Water) @ Reservoir Temp. (psi)**	**Height above FWL (m)**	**Change in Hg Satura-tion**	**Pore Throat Radius (mm)**
1.00	0	1					0.16		106.72
2.00	0	1							
4.00	0	1							
7.00	0	1							
9.00	0.05	0.95							
9.03	0.12	0.88							
11.70	0.25	0.75							
17.00	0.38	0.62							
24.00	0.46	0.54							
37.50	0.50	0.50							
57.89	0.55	0.45							
84.50	0.61	0.39							
114.00	0.70	0.30							
154.00	0.77	0.23							
200.00	0.81	0.19							
270.00	0.85	0.15							

Fluid System	**Interfacial Tension (dynes/cm)**	**Wetting Angle (degrees)**
Mercury-Air	368	0
Oil-Water @ 25°C	35	0
Oil-Water @ Reservoir Conditions	28	20

In the following calculations use values for interfacial tension and wetting angles given in the table above.

(a) Convert the mercury-air capillary pressure to oil-water capillary pressure at 25°C and fill in the table.

(b) Fill in the appropriate values for water saturation and oil saturation that apply to the data calculated in (a).

(c) Convert the oil-water capillary pressure at 25°C to oil-water capillary pressure at reservoir conditions and fill in the table.

(d) Draw a graph of the capillary pressures for both the oil-water at 25°C and the oil-water capillary pressure at reservoir conditions (y-axis, linear 0 to 30 psi) against the saturation of the wetting phase (air or water) (x-axis, linear 0 to 1.00).

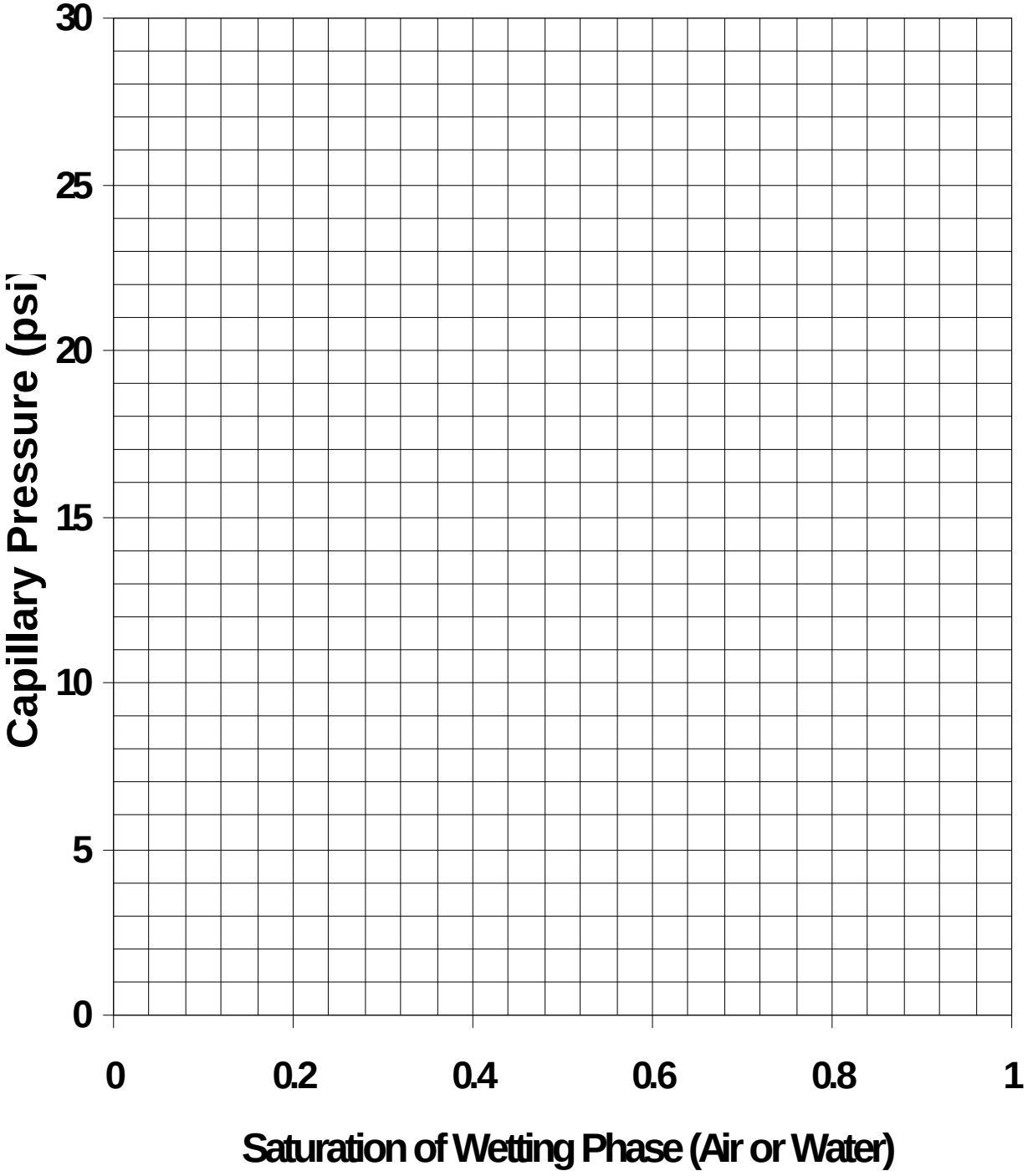

(e) Given that the reservoir interval contains both water and oil, and that the fluid pressure gradient in the oil leg is 1.015 psi/m, and in the water leg is 1.45 psi/m, calculate the height above the free water level for each value of capillary pressure, and insert the data into the table.

(f) Given that the free water level exists at 3120 m, draw a graph of water saturation (x-axis, linear 0.0 to 1.0) against depth (y-axis, linear 3060 m at top to 3130 m at bottom).

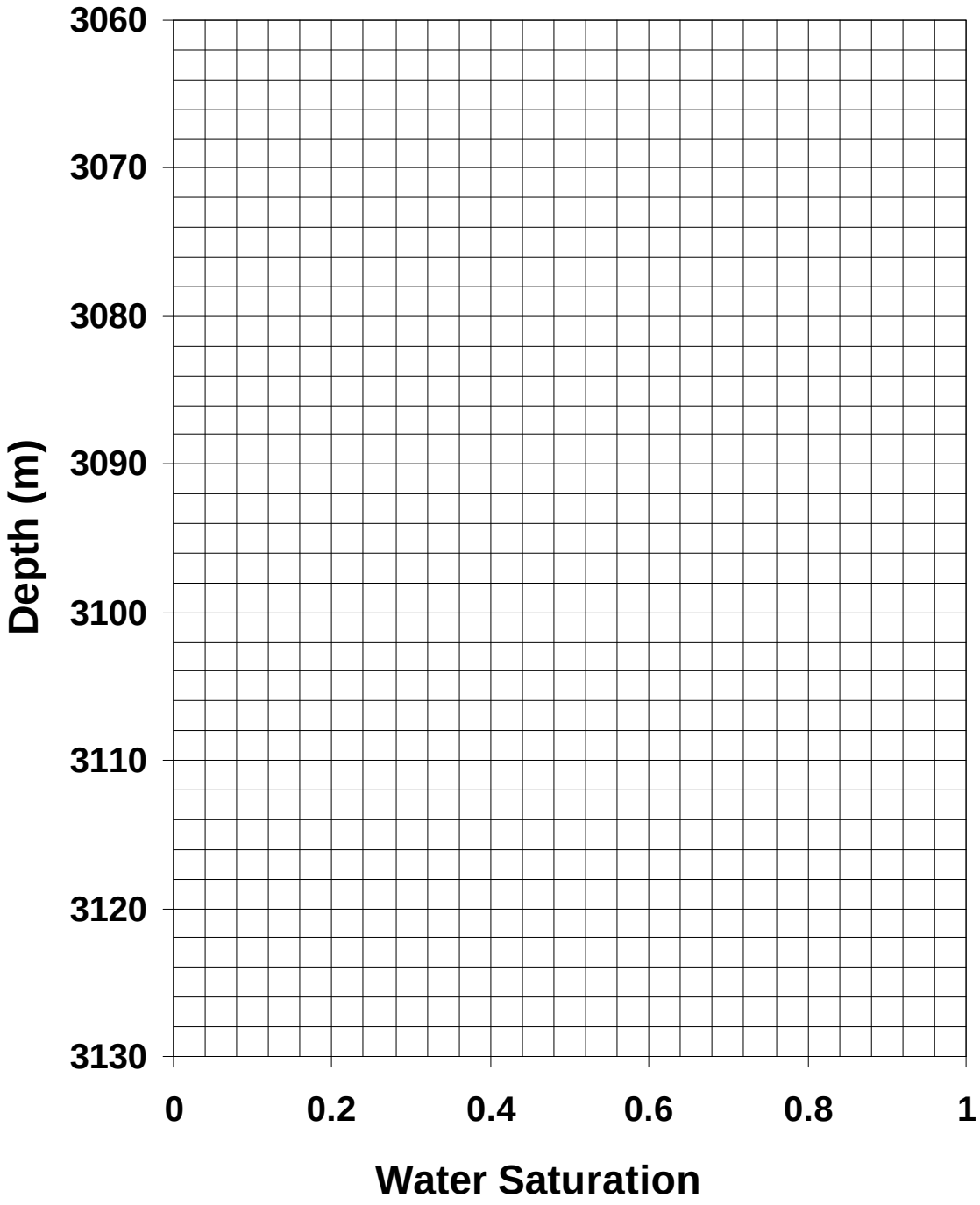

(g) Mark the free water level on the graph.

(h) At what depth is the oil-water contact (*OWC*), and mark it on the graph?

(i) What are the water and oil saturations at the following depths: 3125 m, 3119 m, 3110 m, 3090 m?

(j) What, approximately, is the value of the irreducible water saturation?

(k) If the rock sample had a greater percentage of shale, would you expect a higher or a lower value of S_{wi}, and why? Draw on the graph created in part (f) an example of the curve that would be produced if the lithology was a sandy shale (say, 40% sandstone, 60% shale).

(l) Equation (4.4) in the notes relates capillary pressure to interfacial tension, wetting angle and the radius of the aperture in which the fluid interface exists. This equation is for capillary pressure in dynes/cm^2, interfacial tension in dynes/cm, wetting angle in degrees, and radius in cm. If you multiply the right hand side of the equation by 0.145, the equation is valid for capillary pressure in psi, interfacial tension in dynes/cm, wetting angle in degrees, and radius in microns.

Rearrange this modified equation to calculate the radius of the aperture (in microns) from the mercury-air capillary pressure (in psi).

Calculate the aperture values for each value of mercury-air capillary pressure, and insert the results into the table. Note that these apertures represent the radii of pore throats in the rock.

(m) Calculate the incremental increase in mercury saturation for each row of the table, and insert the results into the table.

(n) Draw a graph of incremental increase in mercury saturation (y-axis, linear 0.0 to 0.14) against the calculated radius (x-axis, logarithmic 1000 to 0. 1).

(o) Write a brief paragraph interpreting the physical meaning of this graph.

(p) Given that the graph calculated in (n) is for the rock sample at 3100 m, which is a sandstone with a small amount of shale (say 90% sandstone, 10% shale), draw freehand on the graph constructed in (m) the likely curve for a sandy shale (say 40% sandstone, 60% shale).

(q) Justify your choice of curve in (o).

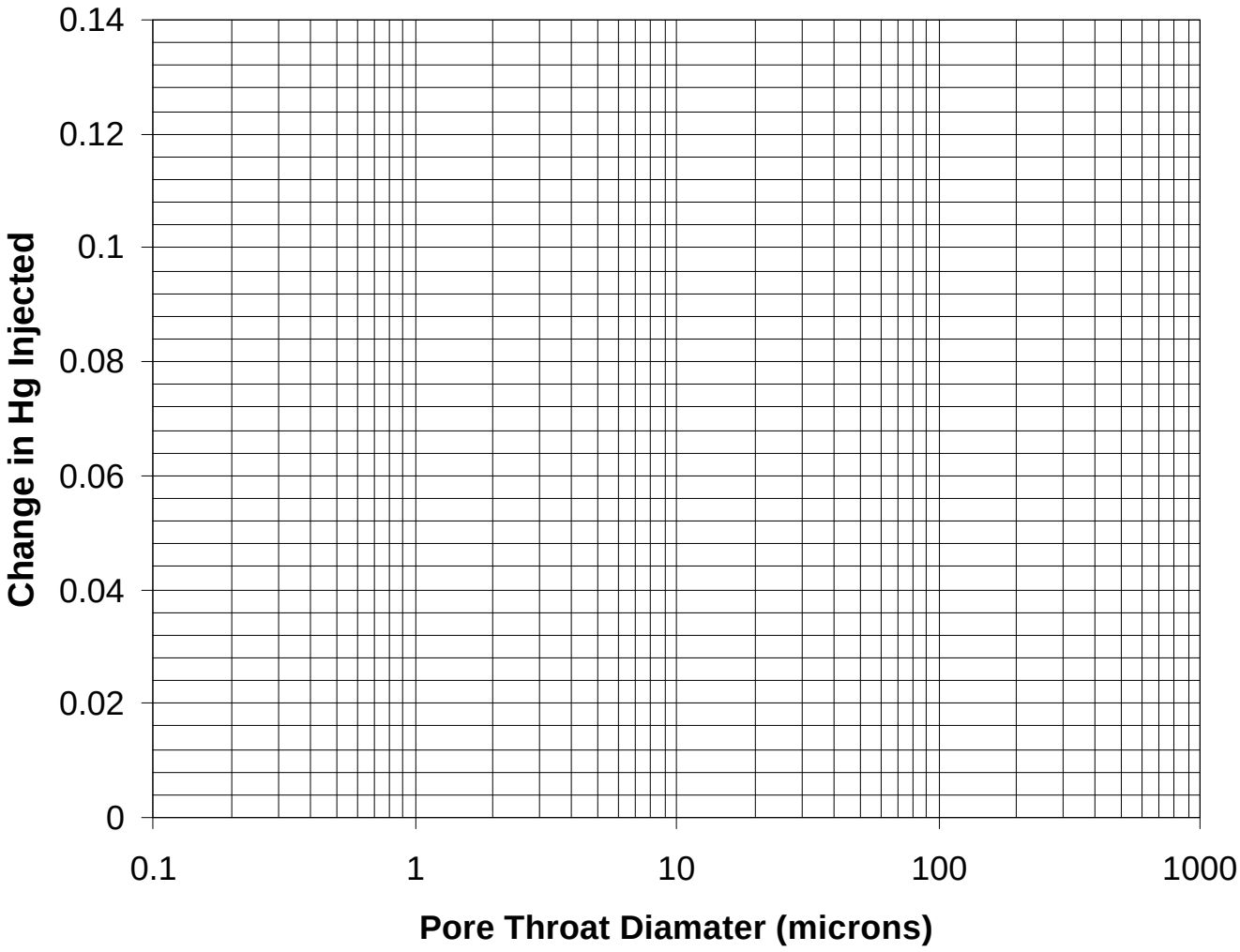
0.14
0.12
0.1
0.08
0.06
0.04
0.02
0
Change in Hg Injected
0.1
1
10
100
1000
Pore Throat Diamater (microns)

FLUID PRESSURE EXERCISE

This exercises uses data from the Elysian Field.

Well: 24-1X
Depth Range: 2980 – 3160 m
Lithology: Variable

An RFT log has been run in the reservoir section of well 24-1X of the Elysian Field between depths of 2990 m and 3145 m.

The following data were collected:

Depth (m)	Lithology	Fluid	Fluid Pressure (bar)	Water-Oil Capillary Pressure (psi)	Gas-Oil Capillary Pressure (psi)
2980-2985	*Shale*	*No sample*	*No measurement*		
2990	Sandstone	Gas	7.2981		
2995	Sandstone	Gas	7.2986		
3000	Sandstone	Gas	7.2991		
3005	Sandstone	Gas	7.2996		
3015	Sandstone	Oil	7.6501		
3020	Sandstone	Oil	8.0001		
3025	Sandstone	Oil	8.3501		
3028	Sandstone	Oil	8.5601		
3035-3075	*Clean sandstone at 3075 m fining up gradually until a shale is reached at 3035 m*	*No sample*	*No measurement*		
3082	Sandstone	Oil	12.3401		
3085	Sandstone	Oil	12.5501		
3090	Sandstone	Oil	12.9001		
3095	Sandstone	Oil	13.2501		
3100	Sandstone	Oil	13.6001		
3105	Sandstone	Oil	13.9501		
3110	Sandstone	Oil	14.3001		
3125	Sandstone	Water	15.5000		
3130	Sandstone	Water	16.0000		
3135	Sandstone	Water	16.5000		
3140	Sandstone	Water	17.0000		
3145	Sandstone	Water	17.5000		
3150-3160	*Shale*	*No sample*	*No measurement*		

(a) Draw a graph of depth (y-axis, linear, 2980 to 3160 m increasing downwards) against fluid pressure (x-axis, linear, 0 to 20 bar).

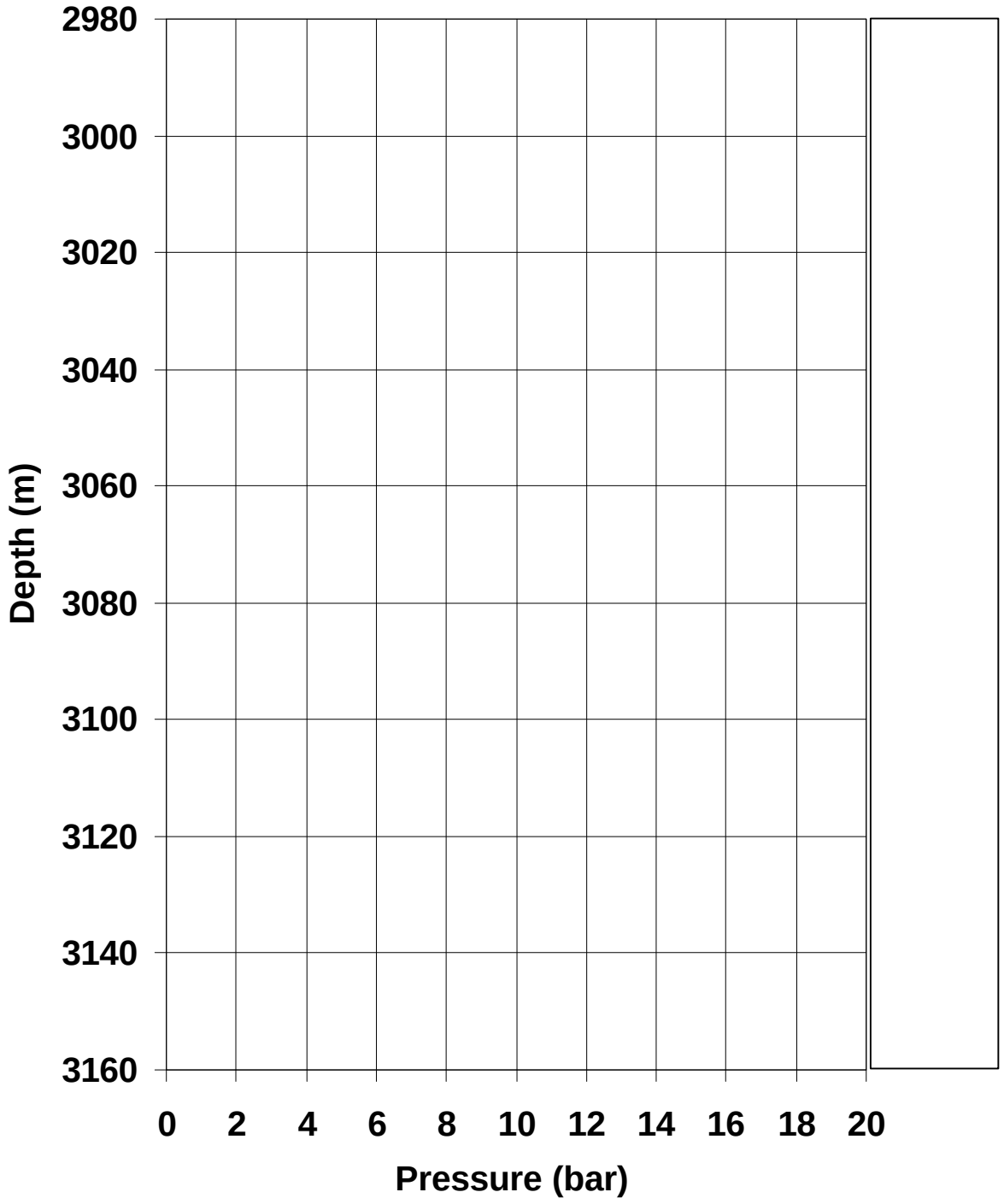

(b) Shade the column to the right of the plot with the appropriate lithology.

(c) Mark on the graph and measure the depth of (i) the free water level (*FWL*), (ii) the likely gas-oil contact (*GOC*).

(d) The graph also indicates a possible gas-water contact (*GWC*). Mark it on the graph. Why does this not exist in reality?

(e) Is the gas and oil in the sandstone formation between 2990 and 3028 m in communication with the oil and water in the sandstone formation between 3082 and 3145 m? Why do you reach this conclusion? What inference can you make about the composition of the oil in each formation?

(f) Calculate the density of each of the fluids (gas, oil and water) in g/cm^3 using the gradients of the fluid lines. Note that to convert bars to pascals (Pa) multiply the value in bars by 10^5. Note also that the acceleration due to gravity, $g = 9.81\ ms^{-2}$.

(g) Calculate the gradient of the gas, water and oil lines in psi/m (1 bar/m = 14.50 psi/m).

(h) Calculate the water-oil and gas-oil capillary pressures in psi, and insert the results into the table.

(i) Obtain the water saturation at each depth in the interval 3015 – 3145 m, and plot it on a graph of depth (y-axis, linear 2980 – 3160 m increasing downwards) against water saturation (x-axis, linear 0.0 to 1.0).

(j) Comment upon the relative reliability of this water saturation curve in the depth intervals 3015 m to 3035 m, 3035 m to 3082 m, 3082 m to 3145 m. If the curve is unreliable in any of these intervals indicate whether the water saturation is under- or over-estimated and by approximately how much. How does the fining-up sequence influence the water saturation?

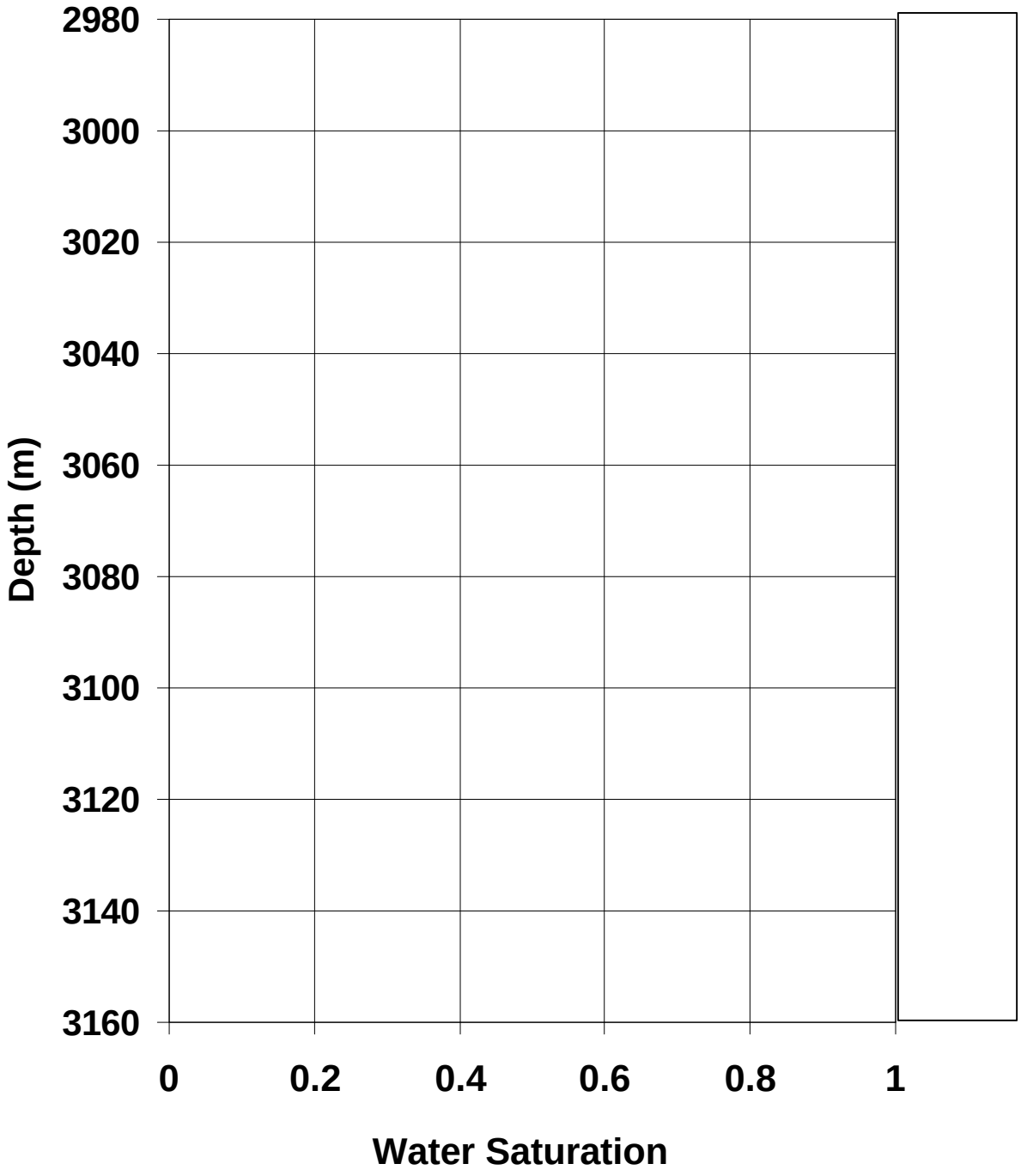
2980
3000
3020
3040
3060
3080
3100
3120
3140
3160
Depth (m)
0
0.2
0.4
0.6
0.8
1
Water Saturation

TEMPERATURE EXERCISE

This exercises uses data from the Elysian Field.

Well: 24-1X
Depth Range: 2900 – 3300 m
Lithology: Variable

Several logs have been run in well 24-1X of the Elysian Field between depths of 2900 m and 3300 m (the bottom of the borehole).

The following data were collected:

	Process	**Depth (m)**	**Temp. (^{o}F)**	**Time & Date**	***T* (hours)**	**(*t*+*T*)/*T***
	Drilling Stopped	3300	-	22:00/15th	-	-
	Mud Circulation Stopped	-	-	04:00/16th	-	-
1	DIL log	3300	241	12:15/16th		
2	FDC log	3300	257	15:00/16th		
3	SNP log	3300	266	17:30/16th		
4	Dipmeter	3300	273	20:30/16th		

(a) Calculate the mud circulation time, *t*, in hours $t =$

(b) Calculate the recovery time, *T* (hours), for each logging run and fill in last but one column. Note: remember to use decimal time in hours.

(c) Calculate (*t*+*T*)/*T*, and fill in the table.

(d) Make a Horner plot of temperature on the y-axis (linear, 230 to 310^{o}F) against (*t* + *T*)/*T* on the x-axis (linear 1.0 to 2.0).

(e) What is the true formation temperature at 3300 m in ^{o}F and in ^{o}C? (Note that to convert ^{o}F to ^{o}C subtract 32, divide the result by 9, and then multiply by 5.)

(f) Given that the mean annual temperature of the sea-floor is 10^{o}C and that the sea-floor is 300 m below the logging depth measurement point, calculate the mean temperature gradient in the well in ^{o}C/m and in ^{o}F/m.

(g) What is the temperature in ^{o}F and in ^{o}C at 3100 m?

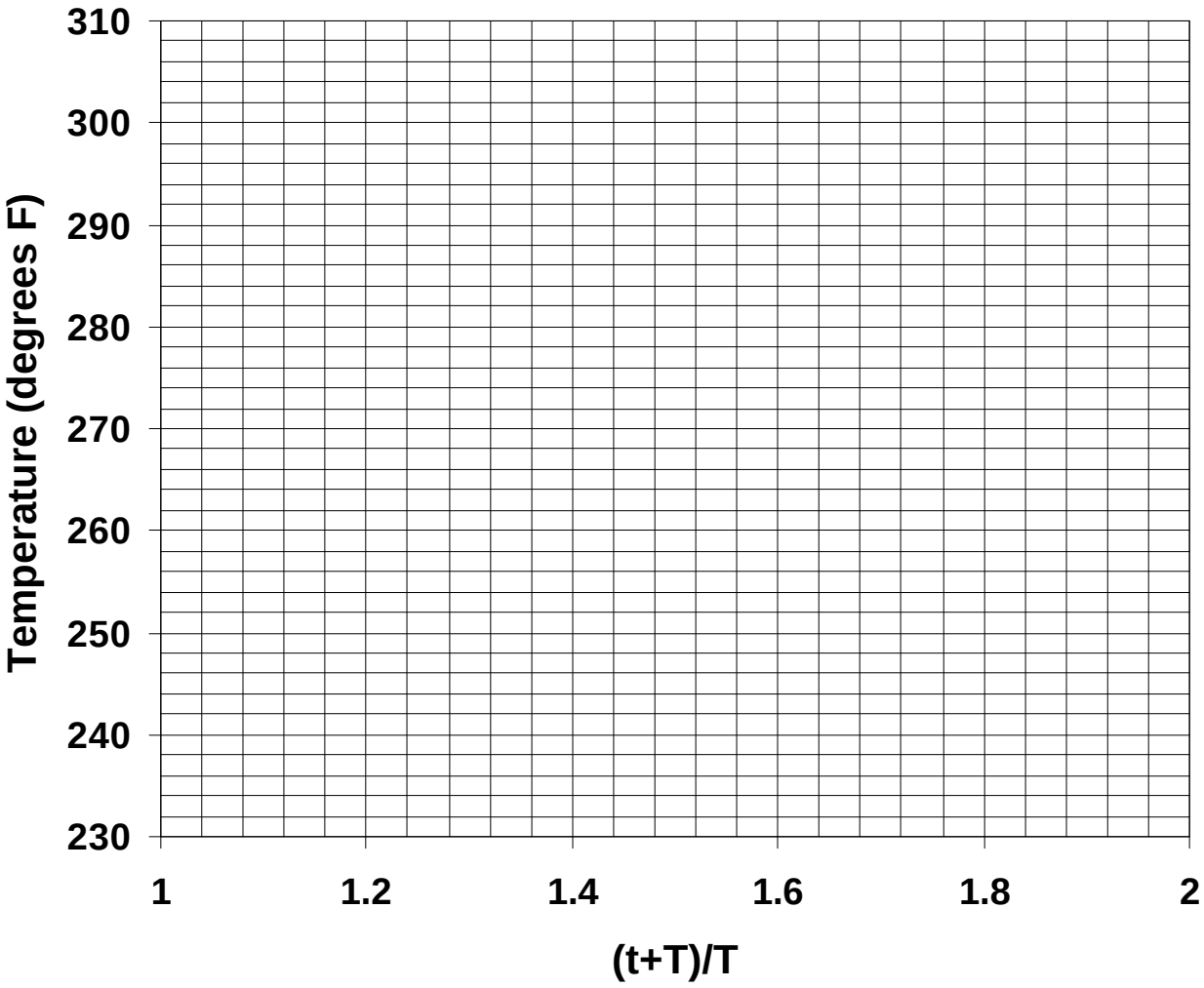
310
300
290
280
270
260
250
240
230
Temperature (degrees F)
1
1.2
1.4
1.6
1.8
2
(t+T)/T

CALIPER EXERCISE

This exercises uses data from the Elysian Field.

Well: 24-1X
Depth Range: 2900 – 3250 m
Lithology: Variable

The enclosed log sheet shows the results from a simple two arm caliper tool.

(a) Indicate where likely mud-cake occurs by shading between the caliper and the bit size curves.

(b) Divide the log into sections which you believe to be of the same, or approximately the same lithology.

(c) Indicate the possible lithologies down the right hand side of the log. Indicate the most likely lithology of those you have indicated for each lithology section.

(d) Indicate, if present, zones of (i) caving, (ii) sloughing, (iii) marl creep.

(e) What is the mean mud-cake thickness in the intervals 2980 m to 3035 m, and 3082 m to 3145 m?

(f) What is the approximate borehole volume in the intervals 2900 m to 3250 m in litres?

(g) What is the cement volume required to complete the borehole between 2900 m and 3250 m with a 7 inch diameter casing liner in litres?

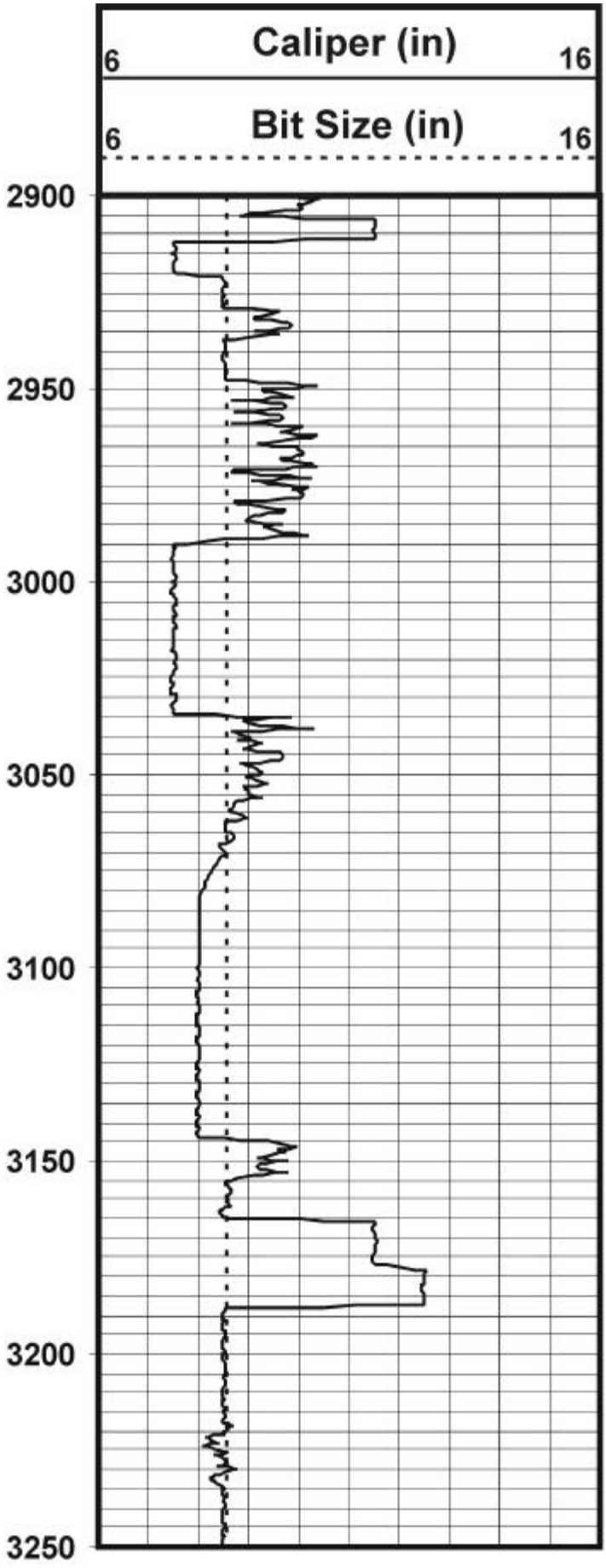
Caliper (in)
6
16
Bit Size (in)
6
16
2900
2950
3000
3050
3100
3150
3200
3250

TOTAL GAMMA RAY LOG EXERCISE

GENERAL DATA EXERCISE

The enclosed pseudo-log sheet shows the lithologies in a pseudo-well.

(a) Draw in the log as a schematic representation of the total gamma ray that you might expect from each of the 100% shale and clean sandstone lithologies. Assume that all 100% shales have the same GR value, which is 120 API. Make the sandstone with an API value of 40 API. These are your relative points.

(b) Indicate the effect on the gamma ray log of the caving in the shale.

(c) Extend the log to include the sandy shale (V_{sh}=0.75) and shaly sandstone (V_{sh}=0.375).

(d) Add the additional effect that is to be expected from:

- The heavy mineral glauconite band, that is represented by *.
- The presence of feldspars in the arkose sandstone.
- The presence of significant mica in the micaceous sandstone.

(e) Draw in the shale line and sand lines.

(f) Extend the log to the bottom including typical values for the remaining lithologies.

(g) Draw in a possible shape for the GR log in the finning-upwards shaly sandstone.

When complete, you should have a log that is typical of the various lithologies occurring in the exercise.

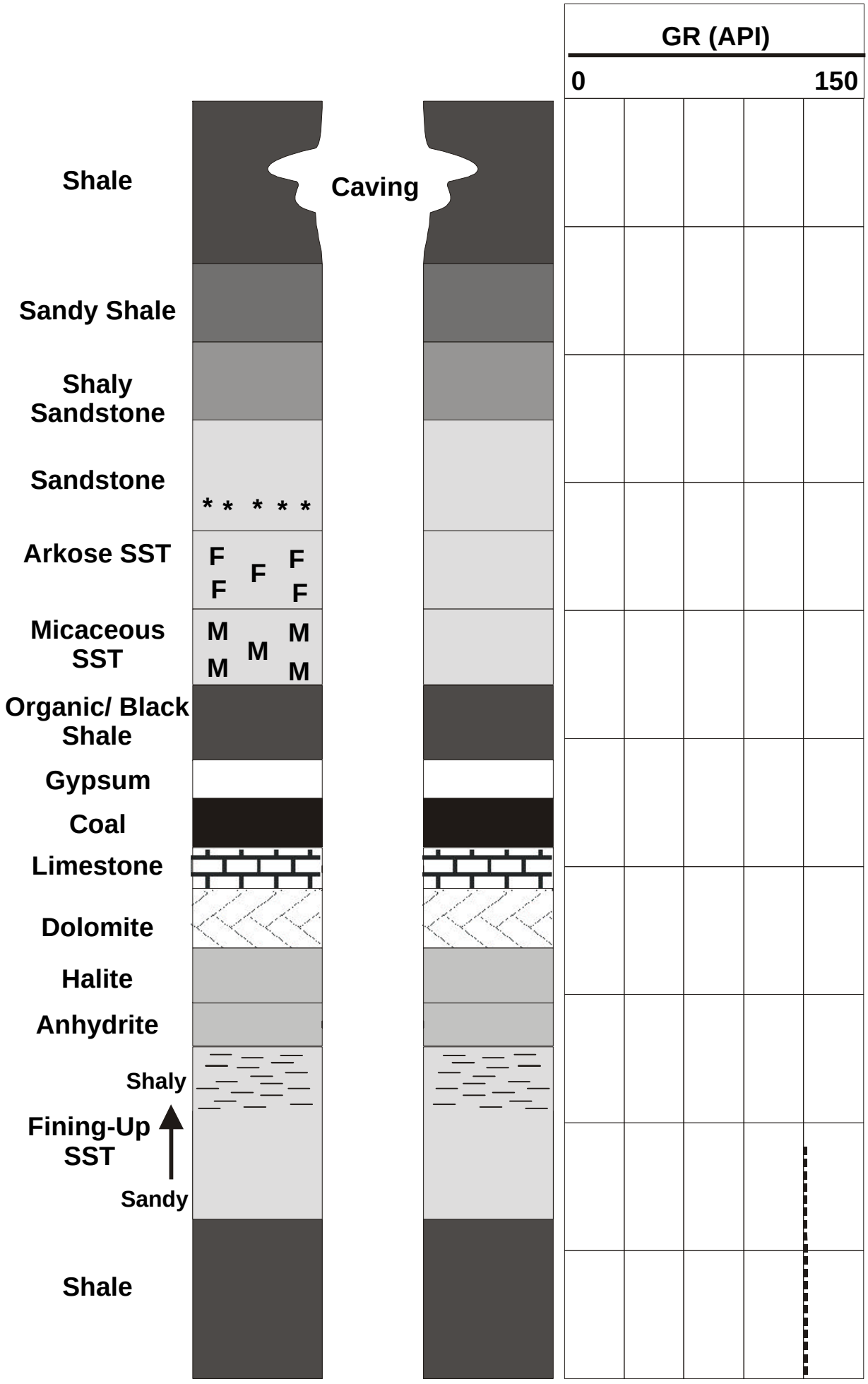
GR (API)
0
150
Shale
Caving
Sandy Shale
Shaly Sandstone
Sandstone
Arkose SST
F
F
F
F
F
Micaceous SST
M
M
M
M
M
Organic/ Black Shale
Gypsum
Coal
Limestone
Dolomite
Halite
Anhydrite
Shaly
Fining-Up SST
Sandy
Shale

NORTH SEA EXAMPLE

The next few pages show a toal gamma ray log from the North Sea. It begins in the Upper Kimmeridge Clay on the 9 – 150 API scale (i.e., no wraparound). The log contains, predominantly sequences of sands and shales of varying shale volume, but also contains, in part, micaceous sandstones, carbonate cemented sandstones, a thin heavy mineral bed associated with a marine transgression, and some organic-rich shales.

The order of the formations in the log (downward) are:

- Upper Kimmeridge Clay
- Lower Kimmeridge Clay
- Heather formation?
- Tarbet formation
- Ness formation
- Etive formation
- Rannoch formation
- Dunlin formation

A literature survey may help you with this exercise.

(a) Divide the log into large scale units that you believe to be of similar lithology, or indicate packages (i.e, a fining-up sequence).

(b) Indicate to the right-hand side of the log, your interpretation of the likely lithology of these units.

(c) Revisit the log at a finer scale to attempt to find areas where there are small scale disturbances to the overall pattern within the units and attempt to find a reason for these disturbances.

(d) Analyse the log for facies and the sedimentary environment, indicating all possible finning-up and coarsening-up sequences, marine transgressions and maximum flooding surfaces etc. , if present, and mark on the log.

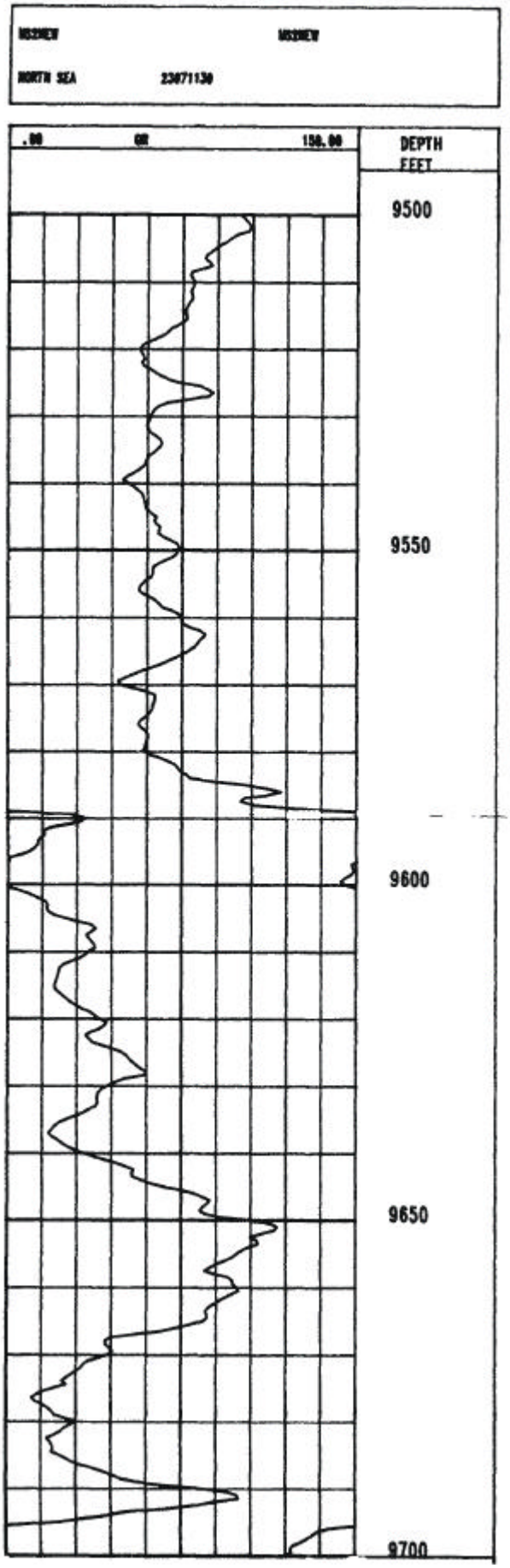
NORTH SEA
23071130
.00
GR
150.00
DEPTH
FEET
9500
9550
9600
9650
9700

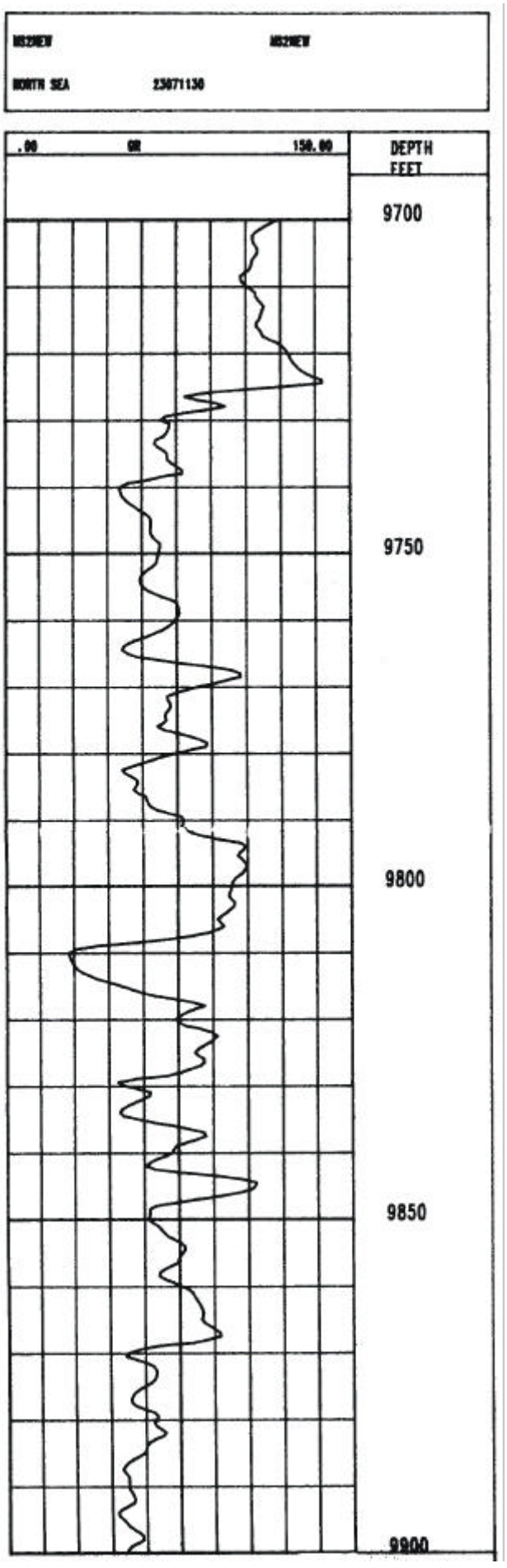
NORTH SEA
23071130
.00
GR
150.00
DEPTH
FEET
9700
9750
9800
9850
9900

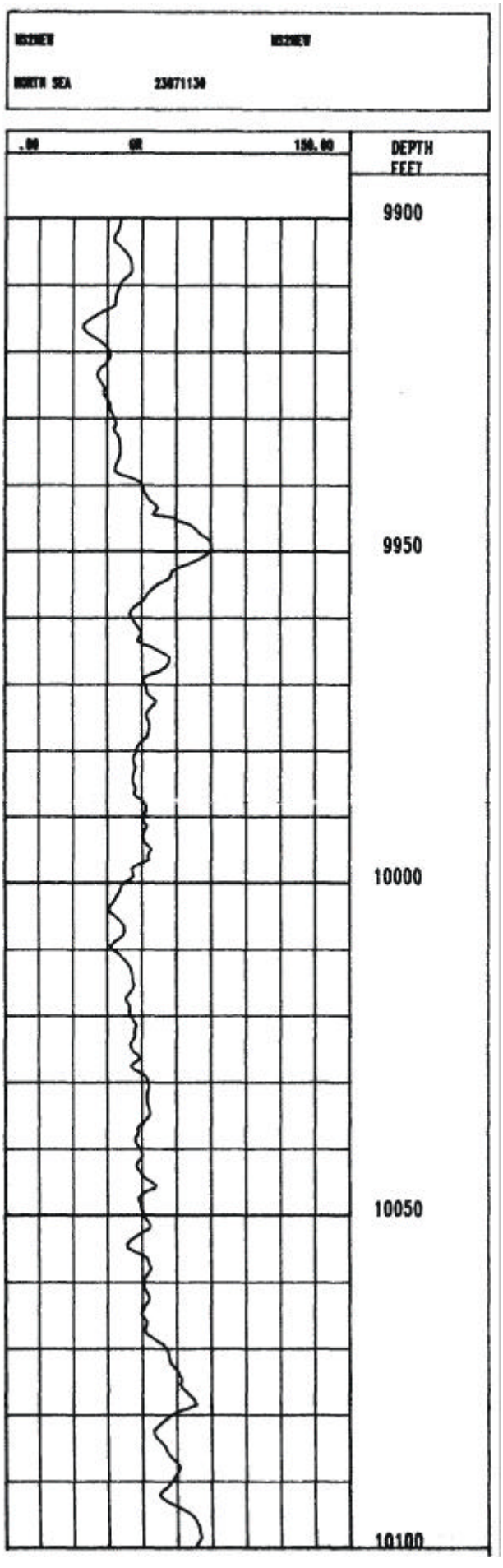
NORTH SEA
23071130
.00
GR
150.00
DEPTH
FEET
9900
9950
10000
10050
10100

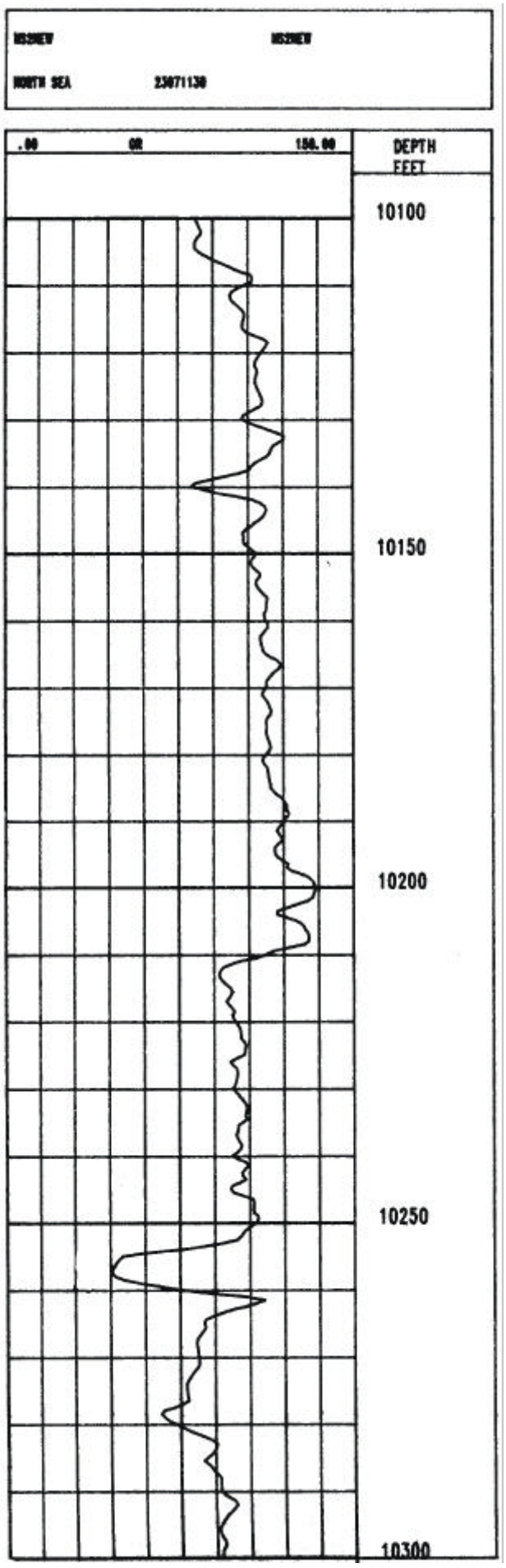
NORTH SEA
23071130
.00
GR
150.00
DEPTH
FEET
10100
10150
10200
10250
10300

COMBINED EXERCISE 1

You are provided with a set of logs from a reservoir sequence in the UKCS of the North Sea and a neutron-porosity crossplot.

- The drilling mud was saline water-based and contained no KCl or barite.
- The depth scale is in metres.

Answer the following questions marking the logs with construction lines where appropriate and showing full working for numerical questions.

(a) Identify the main lithologies throughout the log, marking explicitly any fining-up or coarsening-up sequences. Shade the depth scale with the standard colour or pattern for each lithology. (***Hint:*** *You may find carrying out parts (b) and (c) below first help you in this process.*)

(b) Shade the difference between the caliper log and the bit size for:

- Intervals where Caliper<BS and there is mudcake.
- Intervals where Caliper>BS and there is caving.

(c) Shade the intervals of (i) negative separation, and (ii) positive separation on the neutron-density log (track 2).

(d) Comment briefly upon the likely cause of the shape of the gamma ray log in the interval 2635 m and 2645 m.

(e) Why is a similar effect noted on the density log, but not on the neutron or resistivity logs?

(f) Calculate the mud-cake thickness at 2590 m.

(g) Calculate the shale volume (V_{sh}) at 2550 m from the gamma ray log.

(h) Calculate the shale volume (V_{sh}) at 2550 m from the neutron/density separation.

(i) Given that the section between 2560 m and 2609 m is 100% saturated with water (r_f = 1.0 g/cm^3), calculate the porosity at 2590 m.

(j) Repeat the porosity assessment at 2590 m by plotting the appropriate point on the neutron-density crossplot, supplied.

(k) Given that at 2590 m the Archie '*m*' exponent equals 1.86, calculate the resistivity of the water occupying the pores in the rock using the porosity calculated in part (j).

(l) Use the cross-plot method (part (j) above) to calculate the mean porosity in the interval 2505 m to 2531 m.

(m) Given that the water resistivity, R_w, in the interval 2505 m to 2531 m can be assumed to be the same as that calculated in part (k), and that the Archie exponents are m = 1.86

and $n = 2$, use the combined Archie equation to calculate the mean fractional water saturation, S_w, and mean fractional oil saturation, S_o, in the interval.

(n) Given that the reservoir has an area of 5050 acres and that the oil formation volume factor $B_o = 1.45$, calculate the oil in place in Mbbl. to 2 places of decimals.

(o) Given that 30% of this oil is producible, and the mean selling price of Brent crude in 1997 was 19.26 $/bbl., calculate the value of the reserves in the field at that time in millions of dollars.

(p) This was good news for the oil company, and they perforated the interval and completed the well. In order for the well to produce, they committed themselves to an investment of $200,000,000 for a rig to produce the well. The new rig was due to come on-stream on 1st January 1999.

However, by 1998 the mean selling price of Brent crude was 13.52 $/bbl.

Furthermore, additional drilling had confirmed that (i) the earlier values for the reservoir area, reservoir thickness, and porosity were actually only 90% of the original estimates, (ii) the water saturation was 10% higher than originally thought, and (iii) the fraction of producible oil in the reservoir was only 20%.

Additionally, the rig will cost $5000 per day to run in maintenance and salaries.

The current tax regime indicates that the government will take 55% of the value of all oil produced (i.e., 55% of the value of all your revenue from selling the oil).

Reservoir modelling calculations indicate that a steady mean production of 10,000 bbl./day oil will be produced over the lifetime of the field.

The transport costs of getting the oil from the rig to the refinery (laying a pipeline and operating it) will be $0.1 per barrel.

The costs of drilling the initial well, carrying out logging, appraisal of the data, reservoir modelling and administration and management of the field throughout its lifetime must also be taken into account, and come to 50 million dollars for both scenarios.

There is now a decision to be made – what to do! The following questions are relevant, but you may consider other factors as well:

- How much were the reserves worth in 1997, and how much are they worth in 1999?
- How much tax will be paid over the lifetime of the field at 1997 and 1998 costings?
- How much nett revenue will the company have left over at 1997 and 1998 costings?
- How much will this be after rig construction costs and oil transport costs have been taken into account?
- How many days (years) is the field expected to produce for using the 1997 and 1998 data?
- What therefore is the likely rig operating costs over the lifetime of the field using the 1997 and 1998 data?

- Taking all the factors into consideration, what will be the final nett revenue from the field over its lifetime using the 1997 data and then using 1998 data. This is the profit from the field after you have taken into consideration (i) the new estimates for the reservoir parameters, (ii) the revenue lost to tax, (iii) the cost of the rig, (iv) the cost of the transport of the oil, (v) the running costs of the rig, and (vi) the analysis and administration costs.

If it was your decision would you let the field start producing? Give reasons for your decision, backed-up by robust figures to illustrate your point. Remember (i) you have a responsibility to your shareholders and (ii) you have a responsibility to your own pension fund!

At approximately what value of the price of Brent crude does the field become a nett loss to the company?

HELPFUL EQUATIONS

Shale Volume from the gamma ray log: $V_{sh}=\frac{GR_{\log}-GR_{sand}}{GR_{shale}-GR_{sand}}$

Shale Volume by neutron /density separation: $V_{sh}=\frac{Separation\ at\ given\ depth-Separation\ for\ sand}{Separation\ for\ shale-Separation\ for\ sand}$

Porosity from the density log: $f_D=\frac{r_{ma}-r_b}{r_{ma}-r_w}$

Porosity from the sonic log: $f_S=\frac{\Delta t_{ma}-\Delta t_b}{\Delta t_{ma}-\Delta t_w}$

Archie's First Law: $R_t=R_w f^{-m}$ therefore $R_w=R_t f^m$

Archie's Combined Law: $R_t=R_w f^{-m} S_w^{-n}$ therefore $S_w=\sqrt[n]{\frac{R_w}{R_t\ f^m}}$

Stock Tank Oil In Place: $STOOIP=\frac{25453\ A\ hf\ \ (1-S_w)}{B_o}$

where: reservoir area, A is measured in acres, and reservoir zone thickness, *h*, is measured in metres.

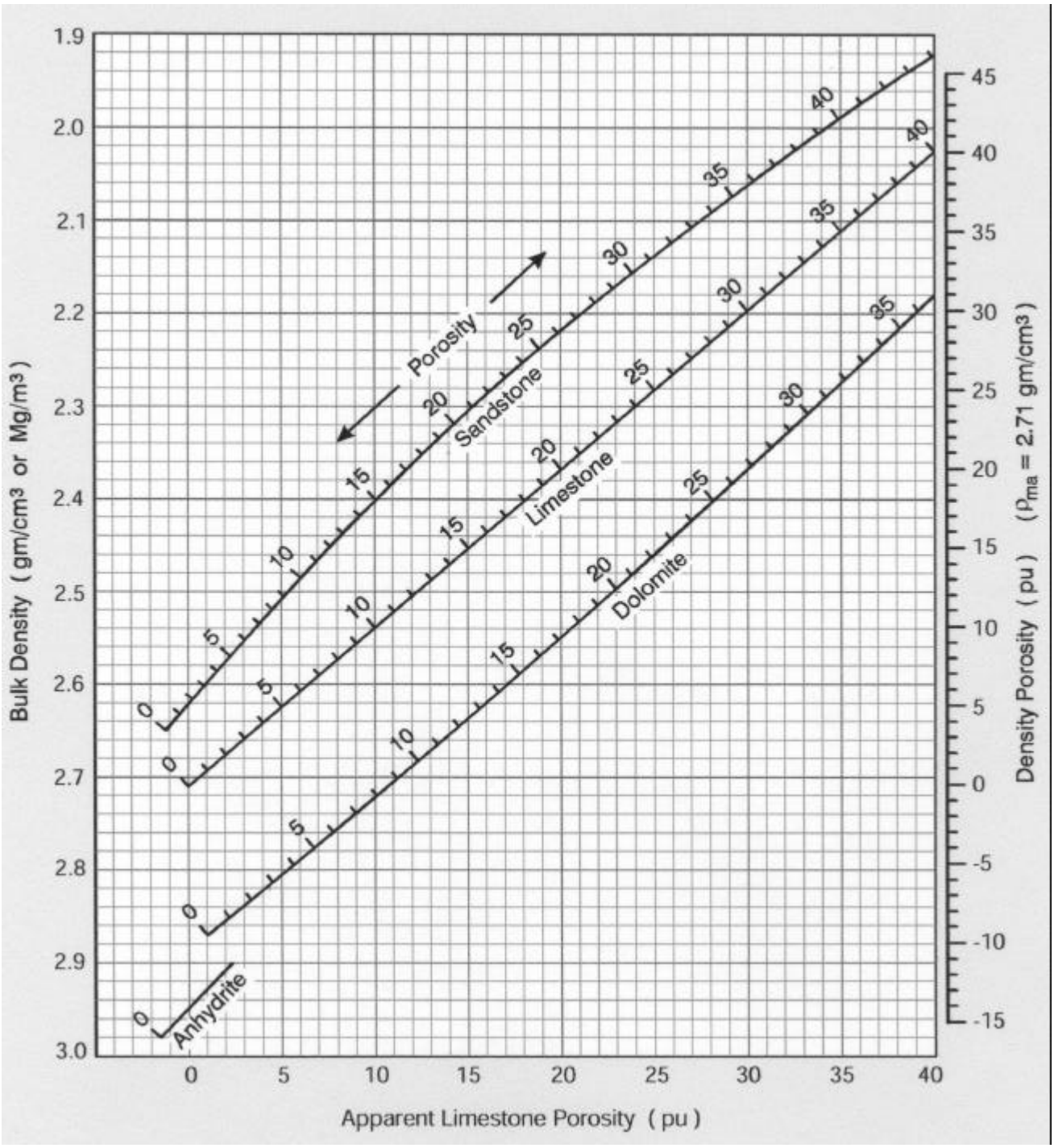

Neutron-Density-Porosity-Lithology Cross-plot for a fluid density of 1.0 g/cm^3. (Courtesy of Reeves Wireline Ltd.)

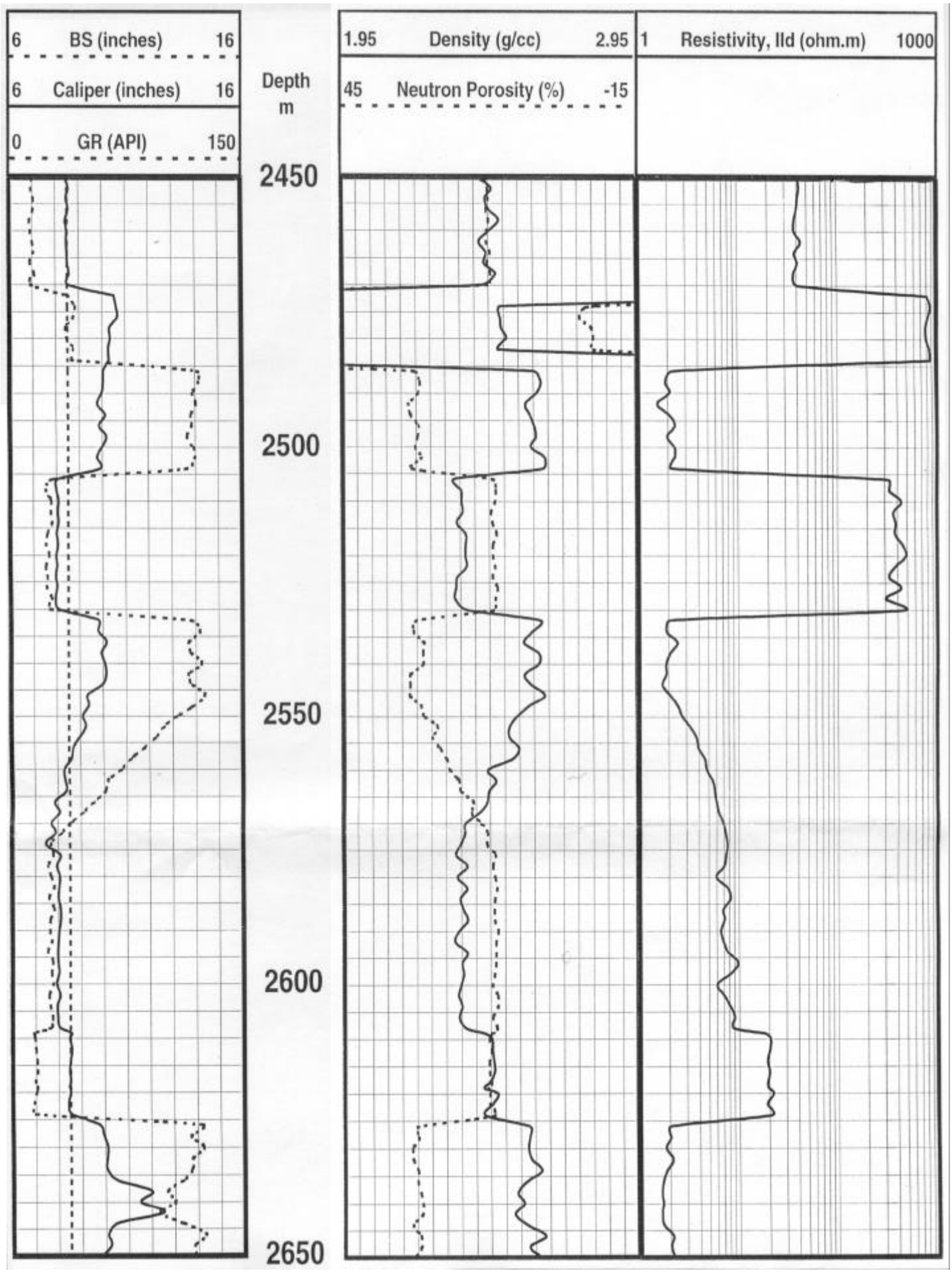
6 BS (inches) 16
6 Caliper (inches) 16
0 GR (API) 150
Depth m
2450
2500
2550
2600
2650
1.95 Density (g/cc) 2.95
45 Neutron Porosity (%) -15
1 Resistivity, lld (ohm.m) 1000

COMBINED EXERCISE 2

Objectives

Your task is to produce an interpretation of the reservoir succession penetrated by a single well. To do this you will need to include:

1. An analysis of the various lithologies present, marking the major stratigraphic boundaries.
2. An analysis of the geological depositional environment.
3. Zonation of the well for reservoir calculation purposes.
4. Calculation of STOOIP and STGOIP if relevant.
5. Produce a short summary report for management, including (a) very briefly the methods used, (b) clearly stated equations that you have used, (c) clearly stated input parameters for the equations, (d) logical structure, (e) key geological characteristics of the reservoir succession, and (f) a balanced assessment of the oil reserves in place, giving approximate error bounds in the calculation.

Resources

You are provided with:

1. A log suite for a single well in the northern North Sea that intersects a Middle Jurassic reservoir. Two copies are given such that one can be used as a rough copy. Note that the gamma ray log is reading slightly low in depth so you may have to take this into account in the assessment of the logs, and use the depths from the neutron-density log for readings of absolute depth to a given lithology boundary.
2. The trap in this reservoir is a tilted fault block.
3. Both the seal and the likely source of the oil in an unconformable Upper Jurassic Kimmeridge Clay formation.
4. Seismic analysis of the area reveals off-lapping horizons that suggest the reservoir sequence may be part of a progradational delta.
5. Seismic analysis also reveals that the best approximation currently to the extent of the reservoir is 2023.5 ha.
6. PVT tests in the laboratory reveal that the oil formation factor B_o = 1.65.
7. The mean price of Brent crude in 1996 and 1998 was 20.16 and 13.42 $/bbl., respectively.

Deliverables

1. The annotated logs for the well indicating clearly all useful parameters and construction lines. This includes (i) a shaded depth scale for lithology, (ii) if present, shaded mudcake, caving, washout, neutron-density separation (positive and negative), (iii) GR sand and shale lines, (iv) Neutron and Density sand and shale lines, (v) the position and coding of your zonation of the well together with codes for their fluid content and indication qualitatively of their permeability, (vi) facies information including fining-up (FU) and coarsening-up (CU) profiles, (vii) the depth of main

fluid interfaces (i.e., at least an OWC), (viii) boundaries between the main depositional environments.

2. A separate diagram summarizing the lithologies penetrated with an indication of likely grain sizes and grain size changes (i.e., a sedimentary log).
3. Tables: (i) The first, identifying all zones and calculating the respective physical parameters therein contained, and (ii) the second, which takes only the reservoir zones and progresses the calculations to a final value of OOIP.
4. A summary report including: (i) A brief description of the methods that you have used, including equations where appropriate, and indicating the type of mud used and the type of formation waters present, and the values of the various cut-offs and sand and shale lines that you have used. (ii) The key geological characteristics of the reservoir succession including an interpretation of the depositional environments present (quote depths and reference to the wireline logs and your drawn sedimentary log to illustrate the points you make). (iii) An assessment of oil reserves in place, including the net-to-gross ratio for (a) sands and (b) all lithologies, (iv) an assessment of the gross worth of extractable oil in the reservoir in 1996 and then in 1998. Do not comment upon the economic viability of the field.
5. Ensure that your name appears on every item submitted, and informally bind the document in a holder or docket.

Suggested Procedure

- Do a basic lithology interpretation and qualitatively locate porous and permeable intervals and reservoir fluid type. Shade the depth scale for the lithologies, and place codes for the qualitative porosity, permeability and hydrocarbon content in the right-hand margin (e.g., +, ++, and +++ for permeability; 0, L, H, VH for the porosity; and the symbols for water oil and gas for the fluid content). Mark on the relevant log obvious FU or CU sequences with arrows. Work from obvious large packages of rock to smaller ones. Highlight with shading (i) positive neutron-density separations, negative separations, (iii) between the medium and deep resistivity tools where deep resistivity > medium resistivity, (iv) mudcake etc. Note that; (a) small +ve neutron-density separations indicate shaly sand not shale, (b) where medium resistivity ≈ deep resistivity, but greater than the MLL (very shallow resistivity) you have an interval of high permeability but NO hydrocarbons.
- Locate the mudstones on the gamma ray log, and use a 30% cut-off to separate the shaly sandstones (which you will ignore in any reservoir oil calculations as not productive) from the cleaner sandstones (which you will keep). To define the shale line use values in the interval 9760’ to 9880’ in the upper part of the log, and values in the interval 10050’ to 10140’ in the lower part of the log. The sand line definition is the same throughout the log. Choose to switch between the two shale lines at some appropriate depth in the middle of the log at a lithology boundary. Use a 80% cut-off to locate the depths at which good shales occur.
- Zone the log. Define depth zones for what is reservoir and non-reservoir rock. Give each zone a code (e.g., A, B, C, D etc) in the left-hand margin with lines to indicate the depth extent of each zone (so that you can easily measure their thicknesses later). Every depth in the log should be in a single zone or exactly on an interface between two zones. You will use some of these zones as reservoir zones later, so we must take into account various properties in carefully defining them. In the zoning process, therefore, take account of :

    1. The lithology (e.g., good shales ($V_{sh} > 0.8$) and evaporites are not reservoir rock).

2. The shale volume (rock with $V_{sh} < 0.3$ (in this exercise) is not reservoir rock).
3. The presence of hydrocarbons (rock with no hydrocarbons is not reservoir rock).
4. The permeability (rock with low permeability is not reservoir rock).
5. No zone should be thinner than 5 ft.

Note that: (i) ALL of the above need to be good for the zone to be a reservoir zone, but non-reservoir zones will exist and have a code, where the points above are only partially fulfilled. (ii) Your zones may differ from that of your colleagues (petrophysical interpretation is petrophysicist-dependent). (iii) It is also possible to implement a cut-off on porosity by also saying that porosity must be greater than 5%, say, for a reservoir zone. I have not asked you to carry out this procedure in this exercise as it does not affect the final zonation greatly.

Zonation hint: Start with the obvious shales on the neutron density log, check against the gamma ray log. Then find major clean sandstones from the neutron-density and gamma ray logs. Then find indications of fluid type and permeability from the caliper, resistivity and SP logs. What is left is shaly sand or other lithologies. Iterate back and forth, finding progressively thinner units until a minimum thickness of about 5 feet, then stop. Adjust the zones to ensure that the remaining intervals less than 5 feet are included in other zone, such that the log is completely zoned. If in doubt in a particular interval, leave it and come back to it later.

[In this log there is only one small interval below the OWC that may be not shaly sand, clean sand or shale. You can give this a zone of its own if you like, but it is irrelevant to the main purpose of the analysis as it is below the OWC. We do not know the lithology of this zone, but its recognition and analysis may be useful for correlation with other wells.]

- Construct a sedimentary log on a separate sheet of paper (at a scale of 1" to 100' or 2 cm to 100') showing interpreted approximate grain size (e.g., sand-silt-clay), marking on your interpreted zone codes. Work out the depositional environment by thinking about the nature and variation in the packages of sediment, and remembering that this is a progradational delta sequence. Group the zones where the depositional environment is consistent with a given depositional sequence. Boundaries between these groups show where the depositional environment has changed suddenly by a large amount, and may indicate unconformities. Expect about 4 or 5 groups. Each group is a well defined depositional environment.
- Complete Worksheet 1 for every coded zone.

1. **Depths and Thicknesses.** Note that the gamma ray log is reading slightly low in depth so you should take this into account in the assessment of the logs, and hence use the depths from the neutron-density log for readings of absolute depth to a given lithology boundary.
2. **Hole Condition.** Comment; OK, dodgy, bad. These are highly technical assessments!
3. **Lithology.** SST, SH-SST, or SH is sufficient.
4. **Neutron Porosity.** Correct the neutron porosity read from the log (f_N) to that valid for sandstone for all depths (f_{Ncorr}) using the correction chart supplied.
5. **Density Porosity.** Read the porosity from the density log (r_b), then calculate the porosity (f_D) from this value. Use $r_{ma} = 2.65$ for quartz throughout, $r_f = 1.10$ for water in a water zone and $r_f = 0.81$ for oil in a hydrocarbon-bearing zone. The porosities obtained will not give exactly the same porosity as that corrected from the neutron log. Why not? It is possible to back-calculate from the resistivity logs a value for S_w and S_h to allow the two fluid densities to be linearly mixed to give a value closer to the actual mean fluid density. Do not attempt to do this, as it is long-winded and boring, and will overcomplicate the exercise.

6. **Sonic Porosity.** Ignore the "Sonic" columns in the table.
7. **Resistivity.** Write down the value of R_t for each zone.
8. **Gamma Ray Log.** Write-down the gamma ray value for each zone, and calculate the shale volume for each zone using the relevant sand and shale lines.
9. **Fluid Type.** Indicate the type of fluid originally present in the virgin zone.

- Complete Worksheet 2 for only those zones that are reservoir zones (i.e., fulfill the lithology, permeability, fluid type, shale volume, and thickness criteria given during the zoning step above. The resistivity log in this particular example has not been corrected to 24°C/75°F, therefore we must either correct every value from the log value to that at 24°C/75°F, or correct the water resistivity from the value given to that at reservoir temperature. We will do the easier, latter, process.
  1. Calculate the reservoir temperature in °F using:

$$T_{res}(^{o}\text{F}) = 227 + (\text{mid.-depth} - 10{,}000) \times 0.01975$$

  2. Calculate the water resistivity at reservoir temperature using:

$$\log_{10}(R_w) = 1.2245 - 0.9492 \times \log_{10}(T_{res})$$

  3. Copy R_t from Worksheet 1, and use mean porosity of f_{Ncorr} and f_{D}.
  4. Calculate the formation factor using the Humble equation:

$$F = 0.62 \times f^{-2.15}$$

  5. Calculate the water saturation using the Archie equation:

$$S_w^{\,2} = (F \times R_w)/R_t$$

- Calculate the OOIP for each zone. Sum them up to give an OOIP for the reservoir. Calculate the STOOIP for the reservoir. Give all answers in Mbbl. to two places of decimals.
- Given that the producible fraction of the oil is 0.20, calculate the gross value of the reserves in the field in 1996 and in 1998.

Name: ..... **Detailed log interpretation - pore fluids worksheet 1**

Zone No.	Top Depth	Base Depth	Thick-ness	Hole Cond.	Lithology	Neutron		Density		Sonic		LLD	Gamma-ray		Fluid type
					Sst/Sh.Sst	ϕN	ϕN_{corr}	ρ_b	ϕD	δt	ϕ	R_t	γ_{log}	V_{sh}	O/W/G

Name: ..... **Detailed log interpretation - water saturation worksheet**

Zone no.	Mid-point Depth (ft)	Temp-erature °F	Calculated R_w	R_t from worksheet 1	Porosity: average of ϕN_{corr}, ϕD, ϕ	Formation Factor, F (Humble)	Calculate S_w
E	9907	225.16	0.0981	100	0.265	10.7749	0.1028

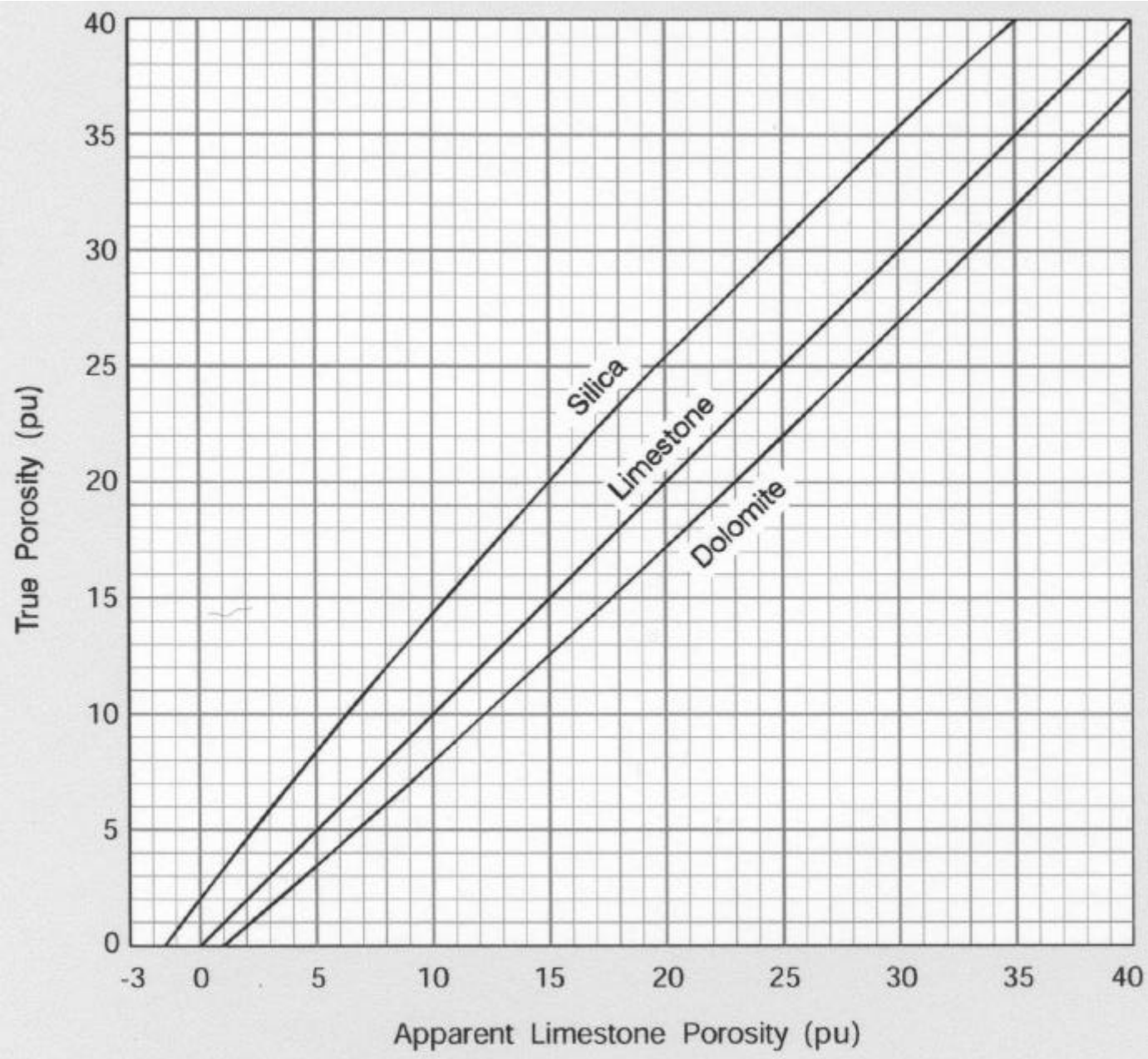
True Porosity (pu)
Apparent Limestone Porosity (pu)
Silica
Limestone
Dolomite
40
35
30
25
20
15
10
5
0
-3
0
5
10
15
20
25
30
35
40